

MICROPHYTOBENTHIC DIVERSITY AND FUNCTION IN ESTUARINE SOFT SEDIMENT

Birgit Weinmann

A Thesis Submitted for the Degree of PhD
at the
University of St Andrews



2012

Full metadata for this item is available in
St Andrews Research Repository
at:

<http://research-repository.st-andrews.ac.uk/>

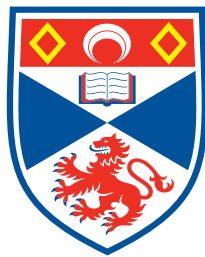
Please use this identifier to cite or link to this item:

<http://hdl.handle.net/10023/3664>

This item is protected by original copyright

Microphytobenthic diversity and function in estuarine soft sediment

Birgit Ellen Weinmann



University of
St Andrews

600
YEARS

A thesis submitted in partial fulfilment of the
requirements for the degree of Doctor of
Philosophy, at the University of St Andrews

School of Biology
University of St Andrews
August 2012

“I love deadlines. I like the whooshing sound they make as they fly by.”

Douglas Adams

English humorist & science fiction novelist (1952 - 2001)

Acknowledgements

I would like to thank the following people.

I would like to thank my supervisors David Paterson, Kevin Laland, and Rupert Perkins. For the much needed support over the past 5 years I am indebted to Thomas Edwards, Margot and Günter Weinmann, Sinead Murphy, and Alice Mackay. I would also like to thank my now and past colleagues at SERG (in particular Melanie Chocholek, Rauhan Wan Hussein, Christina Wood, Rebecca Aspden, Irvine Davidson, Frederik Larson, Helen Lubarsky, Emma Defew, Cedric Hubas, Claire Gollety, Bryan Spears, Nikki Khanna, Pam Cramb, Kirstie Dyson, Natalie Hicks, Julie Hope, and Kate Wade) and in the Laland Lab (especially William Hoppitt for his generosity and patience in helping me with various R and stats problems, and also Laurel Fogarty, Mike Webster, Katherine Meacham, and Tom Pike). The technical and clerical staff of the Biology department who helped me along the way (Murray Coutts, Keith Haynes, Jane Williamson, Joyce Strachan, Katrina Gaterum, Iain Johnston, and Pete Baxter). I also owe my gratitude to those who have lent me a hand (Meredith Wouters), lab equipment (Ian & Vera Johnston, Ronnie & Annie Glud, and Martin & Jasmin Solan), and their much needed statistical and R expertise (Mike Lonergan, Monique McKenzie, Debbie Russell, Marjolaine Caillat). Finally, I would like to thank Inez Campbell, Claire Brett, and Roberta Weber for being around!

Contents

Acknowledgements

Contents

List of Abbreviations

Abstract

Chapter 1: General Introduction	1
1.1 Ecosystem engineering, classical evolutionary theory and niche construction	3
1.2 The physical environment of the estuaries	7
1.2.1 Estuarine morphology, salinity, and tidal range	7
1.2.2 Sediment dynamics.....	9
1.2.3 Zonation	11
1.3 Nutrient cycles and estuaries	11
1.3.1 The carbon cycle	12
1.3.2 The nitrogen cycle	13
1.3.3 Other important cycles	15
1.3.4 Nutrient status.....	17
1.4 Residents of temperate estuaries.....	18
1.4.1 Eubacteria.....	18
1.4.2 Primary producers	20
1.4.2.1 Protists.....	20
1.4.2.2 Macrophytes and angiosperms.....	26
1.4.3 Invertebrates	26
1.4.3.1 <i>Corophium volutator</i>	29
1.3.4 Vertebrates	33

1.5 Ecosystem functions in soft sediments	33
1.5.1 Carbon fixation and degradation.....	33
1.5.2 Oxygenation uptake of sediment.....	34
1.5.3 Nutrient release from sediment to overlying water.....	35
1.5.4 Benthic – pelagic sediment exchange	36
1.6 Aims of this thesis.....	38
 Chapter 2: General Methods.....	38
2.1 The field site.....	42
2.2 Sediment sampling and characterisation.....	47
2.2.1 Sediment sampling	47
Macrofauna cores	47
Contact cores	47
Mini-cores	47
2.2.2 Grain size.....	47
2.2.3 Sediment organic and inorganic content	48
2.3 Nutrients	48
2.4 Measuring microphytobenthic biomass	49
2.4.1 Chlorophyll-a quantification by acetone extraction and spectrophotometry ..	49
2.4.2 Chlorophyll-a estimation by fluorescence proxy.....	51
2.4.2.1 A brief summary of photosynthesis.....	51
2.4.2.2 Fluorescence, non-photochemical quenching (NPQ), photoinhibition and photoacclimation	55
2.4.2.3 Fluorescence measurements and calculation of Photosynthetic parameters	60
2.4.2.4 Fluorometers	63

2.4.2.4. Limitations of fluorescence	65
2.5 Microphytobenthic assemblage description	67
2.5.1 Sampling.....	67
2.5.2 Fixed “live” assemblages	67
2.5.3 Acid cleaned assemblages.....	68
2.6 Natural abundance and biomass of macrofaunal assemblage at Paper Mill	
site	69
Collection.....	69
2.7 Statistical analysis	70

Chapter 3: Ecosystem engineering effect of *Corophium volutator* (pallas) on microphytobenthic assemblage composition and biomass..... 73

Abstract.....	73
3.1 Introduction.....	75
3.2 Materials & Method.....	81
3.2.1 Experimental design	81
3.2.2 Experimental mud, biofilms and macrofauna	83
3.2.3 Set up and sampling	84
3.2.4 Measurements.....	85
3.2.4.1 Temperature and light intensity.....	85
3.2.4.2 Turbidity & nutrients in overlying water	79
3.2.4.3 Fluorescence measurements	86
3.2.4.4 Chlorophyll a, water, and organic content of sediment.....	86
3.2.4.5 Microphytobenthic assemblage	86
3.2.5 Statistical analysis	88

3.3 Results	90
3.3.1 Light and temperature	90
3.3.2 Turbidity	92
3.3.3 Nutrients	95
3.3.3.1 Ammonium	95
3.3.3.2 Nitrate	95
3.3.3.3 Phosphate	96
3.3.4 Sediment water and organic content	98
3.3.5 Sediment chlorophyll-a content	99
3.3.6 Surface biomass (F0)	101
3.3.7 MPB assemblage	108
3.3.7.1 Proportion Live cells	108
3.3.7.2 Taxa richness	109
3.3.7.3 Live assemblage diversity	110
3.3.7.4 Live assemblage comparison	110
3.4 Discussion	112
3.4.1 The effects of <i>C. volutator</i> on sediment and overlying water column	112
3.4.2 Effects of <i>C. volutator</i> on MPB biomass	118
3.4.3 Effects of <i>C. volutator</i> on MPB assemblage structure	122
3.4.4 General comments	125
3.5 Conclusion	126

Chapter 4: Ecosystem engineering effect of different bioturbators on microphytobenthic biomass and assemblage composition	129
--	-----

Abstract	129
-----------------	-----

4.1 Introduction	137
4.2 Materials & Method	137
4.2.1 Experimental design	137
4.2.2 Set up and sampling	138
4.2.3 Measurements	140
4.2.3.1 Temperature and light intensity	140
4.2.3.2 Turbidity, suspended sediment, light attenuation and nutrients in the overlying water	140
4.2.3.3 Fluorescence measurements	141
4.2.3.4 Chlorophyll a, water, and organic content of sediment	141
4.2.3.5 Microphytobenthic assemblage	142
4.2.4 Analysis	143
4.3 Results	146
4.3.1 Light and temperature	146
4.3.2 Turbidity, suspended sediment, and light attenuation	147
4.3.2.1 Turbidity	147
4.3.2.2 Suspended sediment	150
4.3.2.3 Light attenuation	150
4.3.3 Nutrients	151
4.3.3.1 Ammonium	151
4.3.3.2 Nitrite + Nitrate	151
4.3.3.3 Phosphate	152
3.3.4 Sediment properties	152
3.3.5 Sediment chlorophyll-a content	155
3.3.6 Surface biomass (F_0^{15})	156

3.3.7 MPB assemblage.....	161
3.3.7.1 Taxa richness	162
3.3.7.2 Assemblage diversity	162
4.4 Discussion.....	163
4.4.1 The effects of Corophium, Hediste, and Macoma on sediment and overlying water column.....	163
4.4.2 The effects of Corophium, Hediste, and Macoma on MPB biomass	166
4.4.3 The effects of Corophium, Hediste, and Macoma on MPB assemblage composition.....	169
4.4.4 Biodiversity and ecosystem function of MPB	171
4.5 Conclusions	173
 Chapter 5: Ecosystem engineering effect of <i>Corophium volutator</i> Pallas on the water column: daily and tidal time spans.....	 175
Abstract.....	175
5.1 Introduction.....	177
5.2 Materials and Method	179
5.2.1 Set up	179
5.2.2 Sampling regime	179
5.2.3 Sample analysis	182
5.2.3.1 Nutrient analysis.....	182
5.2.3.2 Sediment composition.....	182
5.2.3.3 Light attenuation through a 10 cm water column	182
5.2.3.4 Suspended sediment	182
5.2.3.5 Deposition.....	183

5.3 Results	183
5.3.1 Sediment	183
5.3.1.1 Sediment grain size, water and organic content	183
5.3.1.2 Ammonium	186
5.3.1.3 Combined nitrite and nitrate	186
5.3.1.4 Phosphates	186
5.3.2 Water column	187
5.3.2.1 Turbidity	187
5.3.2.2 Suspended and deposited sediment	187
5.3.2.3 Light penetration through water column	188
5.3.2.4 Ammonium	188
5.3.2.5 Combined nitrite + nitrate	189
5.3.2.6 Phosphate	190
5.4 Discussion	195
5.4.1 Sediment grain size, water & organic content	195
5.4.2 Sediment resuspension, turbidity, and light attenuation	195
5.4.3 Dissolved inorganic nitrogen dynamics	198
5.4.3 Phosphate dynamics	201
5.5 Conclusions	201
 Chapter 6: Investigating the effects an overlying water column on microphytobenthic migration and productivity	203
Abstract	203
6.1 Introduction	205
6.1.1 Rationale	194

6.1.2 Previous migration studies	206
6.1.3 Using Fluorescence to monitor migration	210
6.1.4 Hypotheses.....	211
6.2 Materials and Methods	212
6.2.1 Biofilm collection and treatment.....	212
6.2.2 Experimental set up	212
6.2.3 Light intensity at emersion and immersion	213
6.2.3 Measurements and tidal rythmns.....	215
6.2.5 Calibration measurements.....	219
6.2.6 Analysis	220
6.3 Results	223
6.3.1 Sediment grain size and microphytobenthic assemblage	223
6.3.2 Calibrations	223
6.3.3 MPB bulk migration over tidal periods	226
6.3.3.1 Run 1.....	226
6.3.3.2 Run 2.....	229
6.3.3.3 Run 3.....	231
6.3.3.4 Summary of results of bulk migration over tidal period.....	233
6.3.4 MPB migration over different levels of irradiation within tidal periods	233
6.3.5 Photosynthetic efficiency over the tidal cycle	237
6.3.5.1 Run 1.....	237
6.3.5.2 Run 2.....	238
6.3.5.2 Run 3.....	238
6.3.5.3 Summary of maximum photosynthetic efficiencies over tidal cycle.....	240
6.3.7 Are photosynthetic parameters ($rETR_{max}$, α , E_k) a response to tide,	

exposure time, or light intensity?	241
6.3.7.1 Maximum relative photosynthetic rate (rETR _{max})	241
6.3.7.2 Initial slope (α)	244
6.3.7.3 Saturation light coefficient (E_k)	244
6.4 Discussion	247
6.4.1 Migratory response of MPB (F0) to diurnal and tidal cycles and light variation.....	247
6.4.2 Vertical migration and maximum light utilization efficiency	251
6.4.3 Are photosynthetic parameters (rETR, rETR _{max} , α , E_k) a response to tide, exposure time or irradiance?	253
6.4.4 For further investigation	257
6.5 Conclusion	258
 Chapter 7: General Discussion	259
7.1 Bioturbation modifies the overlying water column and resource flow to MPB	261
7.1.1 Suspended sediment, turbidity and light attenuation	262
7.1.2 Nutrient release	262
7.2 The effect of macrofaunal feeding and bioturbation on MPB biomass	264
7.2.1 Trophic effect	264
7.2.2 Effect of increased turbidity and nutrient release	264
7.3 <i>C. volutator</i> feeding and bioturbation does not affect MPB assemblage composition	267
7.4 Biodiversity and ecosystem function in MPB	267
7.5 Can <i>C. volutator</i> bioturbation be considered positive niche construction?	268

References.....	271
Glossary of terms.....	303
Appendix I: Cleaned Valve Catalogue.....	AI.1
Appendix II: Live: Dead Cell ID, Chapter 3 Categories.....	AII.1
Appendix III: Live: Dead Cell ID, Chapter 6 Categories.....	AIII.1

Abbreviations

α	In a photosynthetic context, α denotes the initial gradient of increase of photosynthetic output per unit of light.
anova	R function to perform an F-statistic on factors in a previously specified “lm”, “glm”, or “lme” model, or to perform a hypothesis (F-stat of log likelihoods) test on a pair of nested models.
β	1. In statistical context it denotes regression parameters where β_0 represents the general intercept and β_1, \dots, β_p represent regression estimates for explanatory variables x_1, \dots, x_p . 2. In a photosynthetic context it denotes photoinhibition.
BST	Biomass specific turbidity (turbidity generated by 1g <i>C. volutator</i>).
Chl <i>a</i>	Chlorophyll- <i>a</i> concentration
Cv, Cvol	Factor indicating <i>Corophium volutator</i> presence/absence in Chapter 3 or treatment in Chapter 4.
cPAR	Centralised values of PAR (see PAR) within the experimental or treatment context.
cTemp	Centralised values of temperature within the experimental or treatment context.
D or (SD)	Simpson’s diversity index
ΔF_0	The % change in F_0 from starting measurement at each core in Chapter 6.
ΔNH_4^+	Change in ammonium concentration (overlying water) over a specified period in Chapters 3, 4, and 5.
ΔPO_4^{3-}	Change in phosphate concentration (overlying water) over a specified period in Chapters 3, 4, and 5.
E_k	The light level (in PAR) at which the increase in photosynthetic output per unit PAR ceases to be linear.
E_s	The light level (in PAR) at which the maximum photosynthetic output per unit PAR occurs.
fBm	Feeding biomass of <i>C. volutator</i> in the MP treatments in Chapter 3
fID	Identity of macrofauna actually present in the tank in Chapter 4.
F or F’	Minimum fluorescence of non-dark adapted cells (see Glossary or Chapter 2.4.2.3 for further explanation).
F_0, F_0^{15}, F_0^5	Minimum fluorescence (general) or specifically after 15 or 5 minutes dark adaption (see Glossary or Chapter 2.4.2.3 for further explanation). Normally the first one is used because dark adaptation times usually explained in text of each chapter
F_m, F'_m	Maximum fluorescence of dark adapted material or non-dark

	adapted material (See Glossary or Chapter 2.4.2.3 for further explanation).
$F_v/F_m, \Delta F/F_m$	Genty factor or maximum photosynthetic efficiency (made at the same dark adaptation time as specified for the corresponding F_0 measurement) and ambient photosynthetic efficiency of non-dark adapted material, respectively (See Glossary or Chapter 2.4.2.3 for further explanation).
$\varepsilon \sim N(\mu, \sigma^2)$	Errors (from statistical model) follow a normal distribution
$\varepsilon \sim N(\mu, \sigma^2 * V)$	Errors (from statistical model) follow a normal distribution adjusted by a variance-covariance to account for non-independence or non-homogeneity (see “V”)
GB	Shorthand for Guardbridge fieldsite
glm	R function for “Generalized Linear Model”
gls	R function for “Generalized Least Squares Model”
hr	hour
ID	Macrofauna treatment (factor) in Chapter 4.
i	Primary index describing a change in data record. Meanings defined for all models in the summary of models table in statistical analysis section of each chapter.
Intcpt	Intercept in statistical regression
j	Secondary index describing a change in data record. Meanings defined for all models in the summary of models table in statistical analysis section of each chapter.
lm	R function for “Linear Model”
lme	R function for “Linear Mixed Effects Model”
-lnD	The negative log of the Simpson diversity index
HD	<i>Hediste diversicolor</i>
mnNH ₄ ⁺	Mean phosphate concentration in an experimental unit (overlying water) over experimental period in Chapters 3 and 4
mnPO ₄ ³⁺	Mean ammonium concentration in an experimental unit (overlying water) over experimental period in Chapters 3 and 4
mnTurb	Mean turbidity in an experimental unit (overlying water) over experimental period in Chapters 3 and 4
MA	Macrofauna absent treatment in Chapters 3 and 4.
Mb	<i>Macoma baltica</i>
MP	Macrofauna presence treatment (factor and level within factor) in Chapters 3 and 4.
ntu	Nephelometric turbidity units
OW	Overlying water column
p	Index describing a change in PAR (chapter 6 only)

PAR	Photosynthetically active radiation measured in $\mu\text{mol photons m}^{-2} \text{ s}^{-1}$, where photons are of $\lambda = 400 - 700$ energy.
PM	Paper mill field site
%LA	Proportion of light attenuation (light loss, Chapter 4) between incident light at top of water column and at the sediment bed.
%Live	Proportion of cells alive in fixed live assemblage counts
%PAR	Proportion of incident light to water surface penetrating to sediment
PW	Porewater
s	second
SW	Seawater
SR	Species richness (number of taxa)
t	Index describing a change in time of record. Meanings defined for all models in the summary of models table in statistical analysis section of each chapter.
tempAM/tempPM	Temperature in overlying water in morning and evening.
rETR, rETR _{max}	Relative electron transport rate or maximum relative electron transport rate (See Glossary or Chapter 2.4.2.3 for further explanation).
RLC	Rapid light curve described by 3 parameter (a, b, and c) non-linear equation (See Glossary or Chapter 2.4.2.3 for further explanation).
V	In statistical context, variance-covariance matrix, meaning any modification to overall variance (σ^2), including correlations, random effects, or weights (as factors or covariates).

Abstract

Corophium volutator (Pallas) fit the criteria of 'ecosystem engineers' as defined by Jones and colleagues (1994, 1997): they are widely distributed within and across North Atlantic estuaries, are often present in intertidal soft sediment in vast numbers, and build semi-permanent burrows in the sediment matrix, which they irrigate continuously. Previous studies have demonstrated that *C. volutator* burrowing and feeding not only modifies the sediment biogeochemistry but can also modify the overlying water biogeochemistry (during immersion). *C. volutator* activities have also been shown to be detrimental to microphytobenthic (MPB) biofilms in the immediate vicinity of the burrows. As MPB are the stabilizing force in the estuary, the decimation of biofilm destabilizes the habitat for all the organisms colonising it. However, several aspects of *C. volutator* ecology remain unclear. First, previous studies on the effect of *C. volutator* on local (within burrow proximity) MPB diversity have not presented a clear signal as to whether they increase or decrease biodiversity or established whether there is preferential survival amongst MPB taxa with certain cell shapes and sizes or lifestyles. Second, as it has been established that *C. volutator* have the potential to change the water column, it is possible for them to effect MPB populations remotely (outwith burrow proximity). It is therefore of interest to determine the effects they have, whether such an effect can be achieved within a tidal period, and whether these effects can change MPB biomass, behaviour or diversity over time.

A series of controlled mesocosm experiments were carried out to quantify those effects of *C. volutator* on the water column which were likely to impact MPB survival, to determine whether those effects were specific to *C. volutator* or common to deposit-feeding bioturbators, to determine to what degree they could be achieved within a single immersion period, and to separate the effects of *C. volutator* on MPB bulk (chlorophyll-*a* in top 5 mm) and photosynthesizing (fluorescing) biomass and

diversity both 'locally' and 'remotely'. The results of the first 3 experiments consistently showed that *C. volutator* substantially increased the resuspension of sediment to the overlying water column and that the resulting turbidity could reduce light penetration to the sediment by as much as 50% within one immersion period. Results of nutrient fluxes were less consistent and clear within and between experiments but there was some suggestion that increased bioirrigation increased inorganic nitrogen flux to the overlying water column in accordance with previous studies. The effects of *C. volutator* on local and remote MPB biomass (bulk and surface) and diversity varied between experiments but, broadly speaking: (1) bulk biomass was unaffected, reduced locally, or increased remotely; (2) surface biomass was reduced both locally and remotely; and (3) community diversity (Simpson's diversity index) was consistently unaffected, both locally and remotely. Because increased water column turbidity is the most distinctive calling card of *C. volutator* but is only likely to affect the photosynthetically active (surface) MPB biomass during immersion, a controlled laboratory experiment was designed to examine the extent to which turbidity could influence MPB migratory behaviour and photosynthetic activity. MPB bulk migration was shown to be driven by site-specific, entrained rhythms of light availability and spatial variation in light availability only drove micro-cycling in the photic zone during the immersion period. So, in the absence of *C. volutator*, or any other turbidity producing phenomenon (deep water columns, high flow rates, physical disturbance, etc.), MPB will remain at the surface to photosynthesize during immersion and the productivity during this period is determined by total light intensity and exposure hours (or 'light dose'). Therefore, the proximity and size of *C. volutator* populations to a site is likely to be influential in determining local productivity patterns of MPB. In addition, differences in MPB assemblage composition were shown to influence the biofilm productivity but what drives changes in MPB assemblage composition is still unclear and requires further investigation.

Chapter 1: General Introduction

Chapter 1: General Introduction

The primary aim of this thesis is to determine whether the engineering activities of bioturbating sediment-dwelling invertebrates have resource modifying consequences that can potentially exert natural selective pressure on the primary producers of mud and sandflats – microphytobenthic (MPB) organisms – and thereby, ultimately, back on themselves. Evidence of the potential for selection will be sought from ecological consequences only – there will be no genetic component to this work and no attempt at measuring an evolutionary response. As a result of this investigation the relationship between MPB biomass and diversity will also be examined.

1.1 Ecosystem engineering, classical evolutionary theory and niche construction

The ever accelerating rates of species loss from the biosphere in the last century has made “does biodiversity matter?” the most important and pressing questions for ecologists to answer (Wilson 1992). Wilson answered with a resounding ‘yes’ primarily for the reason that we evolved within a biotic matrix and it is this matrix to which we are suited and on which our lives depend; in his words “...our bodily functions are finely adjusted to the idiosyncratic environment already created” (Wilson 1992). Everything from the oxygen we breathe to the soil we need to grow our food is a biological construct. While we like to imagine that we can recreate this matrix by simply re-engineering it to suit our needs. However, the reality of this happening is still distant, whilst our ability to destroy the mechanisms that already exist and that we do not fully understand is considerable. Therefore, ecologists over the past two decades have pragmatically focused on elucidating (1) the ecosystems that exist and the fundamental mechanisms or processes by which they operate, (2) what parts of those processes are biotic and abiotic, (3) what organisms perform the biotic

functions within each ecosystem, and (4) to price these functions as ecosystem services that humans currently receive “for free” but that would be lost if an ecosystem process collapses. This fourth objective is the most important and one on which ecologists and economists have had to co-operate in order to present ecology in the language and framework to which voters, consumers and policy-makers respond (i.e. economics). However, in order to achieve this ultimate objective, ecologists must lay the foundations specified by the first three objectives.

The realization that biota do not just inhabit the environment but help create it is not new: in his last published book, Darwin (1881) described how earthworms did not just live in soil but helped create it by digesting and excreting plant debris. However, this idea did not become part of the classical evolutionary framework until Dawkins (1982) argued that a change of physical habitat, which is brought about by an organism’s physiology and behaviour, and as such is genetically guided as either of those organismal characteristics, is, by logical extension, part of the engineering species’ phenotype. But even though endorsed by both Darwin and Dawkins, neither niche construction nor the extended phenotype became core aspects of ecological theory for another decade. Ecologists already inherently understood that biodiversity was fundamental to ecosystem stability and resilience (Townsend *et al* 2000; McCann 2000). However, because their theoretical models conceptualized only the trophic portion of the ecosystem and lacked the engineering and habitat creating aspect of biological life, evaluation of the stability of those models did not corroborate those beliefs (Gardner & Ashby 1970; May 1972; McCann 2000). Instead, mathematical evaluation of the stability of trophic ecosystem models determined that complex ecosystems were less stable than simple ones (Gardner & Ashby 1970; May 1972).

The gap between ecologists' belief in ecosystem stability and resilience increasing with increasing complexity and the lack of stability demonstrated by mathematical evaluation, as well as the gap between evolutionary theory and ecological theory, is partly due to the fact that the ecosystem functions of species were not included in conceptual frameworks of ecosystems (McCann 2000; Odling-Smee 2003?). Jones et al (1994, 1997) drew attention to the paucity of ecological research studying how organisms modulate flows of energy and matter, and create habitat, for other organisms, which they called 'ecosystem engineering', but it is only recently that ecologists have started to consider whether ecosystem engineering might have evolutionary consequences (e.g. Loreau, 2010). So Odling-Smee and colleagues (2003) have reformulated the classical evolutionary model so that instead of just emphasizing genetic inheritance, by which genes successful in a given the environment continue in the gene pool, it also emphasizes 'ecological inheritance', whereby the environmental conditions wrought by organisms like earthworms are inherited by subsequent earthworm generations as well as by all the other soil-dwellers (Figure 1.1).

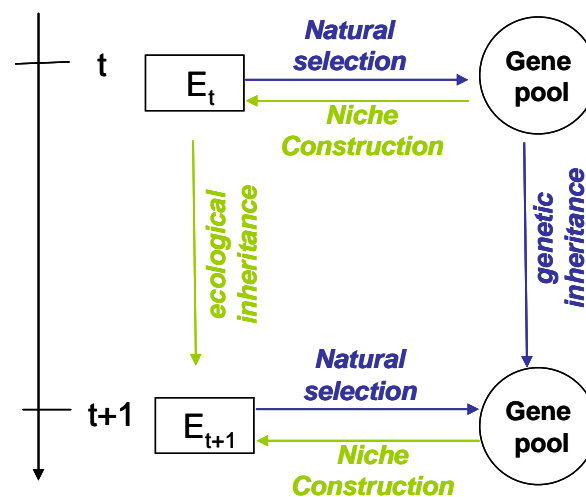


Figure 1.1: How the concept of Niche Construction modifies classical evolutionary theory by binding genetic and ecological inheritance (redrawn with authors' permission from Odling-Smee *et al* 2003)

In a nutshell, by modifying environmental resources or building physical structure, organisms can construct their own environmental niches where none existed, or modify them, and can thereby transform the pattern of natural selection on other organisms in their environment.

Ecological inheritance has important evolutionary and ecological ramifications, and thereby important ramifications for conservation science. In analyses of the temporal dynamics of two hypothetical diallelic loci, one which influences the niche-constructing ability of the organism with respect to a resource and the other of which confers fitness with respect to the same resource, it was demonstrated that, at least theoretically, niche-constructing genes can generate selection that can oppose the external source of selection (Laland *et al* 1999). So the selective pressure exerted by the engineered resource (by the niche-constructing gene) can counteract and overcome the pressure exerted by the non-engineered resource on the fitness-conferring gene so that the one gene is effectively altering the selection of the other, thereby influencing the rate and direction of the population's evolution (Laland *et al* 1999). Applying this niche-construction modelling concept to symbiotic nitrogen-fixation in plants, Kylafis & Loreau (2008) demonstrated that niche constructing genes influencing the attraction of symbionts allowed the persistence plants that would otherwise have gone extinct in a nutrient poor environment. The ecological importance of niche construction is underpinned by many empirical studies (Thayer 1979; Shachak *et al* 1987; Jones & Shachak 1990; Irlandi & Peterson 1991; Seabloom & Richards 2003; Lill & Marquis 2003). In one such study an animal which played no vital trophic role in its environment nevertheless had a profound impact of the assemblage composition in its environment (Lill & Marquis 2003). A combined empirical and modelling examination of benthic marine assemblages demonstrated that the loss of an active bioturbator from a habitat would result in a cascade of local extinctions of other taxa (Solan *et al* 2004). Based on the evidence from these and other studies, Boogert and colleagues (2006) argue that

the important ecological concept of “keystone” species should be reformulated to include not just taxa that are vital to the trophically important in a system, but also the dominant habitat creator or resource modifier of that ecosystem. Criteria by which important ecosystem engineers can be identified are: (1) the amount of time the taxa engages in the engineering activity is large, (2) the average high population density of the taxa is high, (3) the distribution of the taxa is extensive, (4) their longevity (as a population) in the areas they colonize is long, (5) the durability of their constructs is relatively long, and (6) the number of resource flows that their activity modulates is high, as is the number of other species these resource flows affect (Jones *et al* 1994, 1997). These factors scale up to determine the impact of ecosystem engineering.

1.2 The physical environment of the estuaries

Estuaries are not stable environments and, in geological terms, they are not long-lived (Dyer 1997). Rather they are constantly changing in morphology and shifting their position in the landscape due to constant deposition, erosion, and resuspension of sediment, changing water flows from land to sea, weather patterns, and changes in sea level (Dyer 1997). In addition to being unstable, estuaries are environments of extremes: huge gradients in salinity (5 – 35 psu), exposure (fully immersed to fully exposed), sedimentology (clay to boulders) and nutrient availability (nutrient poor overlying seawater to nutrient rich sediment, riverine input, and runoff) occur over relatively small geological temporal and spatial scales (seconds – years and mm to km) (McLusky 1971; Dyer 1997).

1.2.1 Estuarine morphology, salinity, and tidal range

The morphology of an estuary is forged by a combination of the volume and flow rate of the river, the geology and topography of the land through which it cuts, and the wave and tidal currents of the surrounding ocean (Dyer 1997; Brown *et al* 1999). There are three general types of estuaries: “drowned river

valleys”, flooded during the Flandrian transgression, have large width:depth ratios and are V-shaped in topography and cross-section; “fjords” are steep, rocky, and have very small width:depth ratios and are rectangular in topography and cross-section; “bar-built estuaries” are drowned river valleys where ocean currents have deposited so much sand at the mouth of the river that the mid-sections of these estuaries tend to be shallow with low flow rates and extensive sand- and mudflats and marshes (Dyer 1997 and references therein). Additional estuary types are intermediates or combinations of these. Deltas are river valleys where the river has such a high volume and sediment load that it overcomes the marine processes (inundation and sedimentation). Estuaries and deltas are thought to evolve into one another over time depending on whether progradation processes (land accretion due to fluvial sediment and organic content) or transgression processes (land submersion due to sea encroaching) dominate (Dyer 1997 and references therein).

Estuaries are also classified by their salinity structure: highly stratified salt wedge estuaries, fjords, partially mixed estuaries, and well-mixed estuaries (Dyer 1997; Brown *et al* 1999). Salinity structure is affected by topography and by the dominance of river flow to tidal flow. Vertical structure is created by density differences between fresh river water and seawater: less dense river water flows downstream over more dense seawater (Dyer 1997). Horizontal structure is created by the Coriolis force: in the northern hemisphere river water runs towards the right which pushes the seawater to the left (Dyer 1997). The more river flow dominates the tidal flow (as in deltas) and the deeper the estuary (as in fjords), the more stratification there will be in the water column (Dyer 1997; Brown *et al* 1999). The more tidal flow dominates over river flow the more mixing will occur in the water column (Dyer 1997). Tidal flows increase the energy within the estuarine system, which is dissipated by friction against surfaces, which in turn causes turbulent eddies, which act as ‘mixers’. The difference between a partially mixed and fully mixed (homogenized) estu-

ary is mostly determined by the magnitude of tidal range relative to water depth (Dyer 1997). So smaller, shallower rivers will have more mixed water columns than larger, deeper rivers given the same tidal range. Global patterns of water movement, caused by lunar cycles interacting with centrifugal force due to the Earth's rotation, and the Earth's land-sea bulks, determine the volume of the tidal standing wave that pushes seawater up the estuary against the riverine flow (Brown *et al* 1999). In the UK, the South and West tend to have the highest tidal ranges (> 3 m), the tidal ranges along the eastern seaboard from Aberdeen to Norfolk facing the North Sea are in the 3 m vicinity, and tidal ranges in northern Scotland and N. Ireland are about 2 m (Brown *et al* 1999). Most UK coasts experience semi-diurnal tides: there are roughly 2 high tides and 2 low tides within a 24 hour period whose maximum ranges vary with neap (smallest) and spring (largest) tides (when the Moon is furthest and nearest from that point on Earth, respectively). Localized variations in tidal heights occur due to the interaction between tidal range in the area and the topography of the estuary (Dyer 1997; Brown *et al* 1999).

1.2.2 Sediment dynamics

As mentioned above, a water column consists of different layers and there is friction between different moving fluid layers (e.g. layers of water with slightly different densities, or a layer of water over a solid surface). This friction is also called 'shear stress' and is enacted on each surface by the layer moving directly above it (Dyer 1997; Brown *et al* 1999). Laminar flow is like a vector (i.e., it has a single direction) that is horizontal to sediment bed and streamlines around particles within it (Brown *et al* 1999). Turbulent flow contains a vertical component which creates movement in multiple directions (in 3 dimensions) at multiple velocities within the net direction of flow (Brown *et al* 1999). Shear stress is highest at the sediment bed and, as its effect diminishes through successively higher layers of water. The interaction of the flowing water with the bed results in bed shear stress which represents the friction of the flow against the bed. The

maximum layer of water (measurable reduction in velocity) affected by bed shear stress is called the 'boundary layer'. Because the sediment bed is not a perfectly flat and solid surface, the horizontal component of flow can push sediment particles that are higher than mean sediment surface along the sediment bed and the vertical component can cause the lifting of particles off the sediment bed. The amount shear stress required to shift a sediment particle off its position on the sediment bed is called 'critical shear stress' and the mean velocity in boundary layer required to generate critical shear stress is the 'critical shear velocity'. Mean critical shear velocity varies with sediment composition.

Individual sediment particles are characterized by their mean diameter (in addition to substance and shape). From largest to smallest these size groups are: boulders ($> 256 \text{ mm}$), gravel ($2 - 256 \text{ mm}$), very coarse ($< 2 \text{ mm}$) to very fine ($> 63 \mu\text{m}$) sand, silt ($2 - 63 \mu\text{m}$) and clay ($< 2 \mu\text{m}$) (Wentworth 1922). Bulk sediment is often can be characterized by its sand:silt:clay ratio; it is referred to as 'mud', 'muddy sand', 'sandy mud' or 'sand' with decreasing clay and increasing sand content (Folk 1954). Clay is probably the most important element because it is cohesive: individual particles of clay stick together to due a combination of electrostatic attraction and surface tension (Brown *et al* 1999). Therefore, sediment with $> 5 - 10 \%$ clay is called 'cohesive sediment' and requires much higher critical shear stress to displace than non-cohesive sediment (Brown *et al* 1999). The movement of sediment from its position in the sediment bed is the process of erosion. Erosion is not linear with velocity, it increases (non-linearly) with increasing grain size but decreases (non-linearly) with increasing clay content (Brown *et al* 1999). Sediment rolling along the sediment bed is known as bed load, and sediment no longer in contact with the sediment bed is known as suspended load (Brown *et al* 1999).

Once suspended, larger grain sizes sediment out of the water column more readily (in slower mean velocity) than smaller grain sizes. This sedimentation

is also known as deposition. Finally, in still water, where no erosion is occurring, sediment within the bed begins to sink under its own weight, this process, by which the sediment is effectively 'de-watered', is known as 'compaction' (Brown *et al* 1999).

1.2.3 Zonation

The biological component of soft sediment changes with shore height which determines local exposure time. In estuaries, shore height is determined both by distance from the central channel and distance from the coast. However, these two variables do not just determine exposure time but also determine salinity and nutrient levels in the pore water and overlying estuarine water which are very important to all organisms. Another structuring feature in estuaries is distance from rivulets of run-off that run directly into the estuary, often perpendicular or oblique to the central channel. Salinity decreases and nutrient levels generally increase with distance from the shore while the reverse is true for distance from river or rivulets. River water generally has much higher nutrient loads than seawater due to run-off from fertilized agricultural land, gardens and golf courses so distance from rivers and rivulets affect nutrient status of the pore water. Distance from the shore and central channel also largely determines grain size as sand tends to be imported from the sea, and is therefore more abundant in the outer reaches of the estuary, and silt and clay is imported from the land via the river and is therefore, more abundant nearer the river and the coast. However, patterns in sediment grain size across the estuary vary depending upon local hydrodynamics (Chocholek 2012). Grain size is an important assemblage defining factor for both benthic invertebrate communities (Meadows 1964; Green 1968) and benthic diatom communities (Ribeiro 2010).

1.3 Nutrient cycles and estuaries

Life on earth is comprised of six major elements, hydrogen, carbon, nitrogen, oxygen, sulphur, and phosphorus, and the biogeochemical cycles of the first 5

of these elements are linked via electron transfer (redox) reactions that occur in the biological component of the earth's chemistry (Falkowski & Godfrey 2008). The C, N, S, and P cycles, and the role of estuaries in them, are briefly described below. H and O cycles are not discussed separately, as H and O are the drivers of the C, N and S cycles by being the sources of protons and electrons for the redox reactions. Finally, because a large part of this thesis is concerned with diatoms, the silicon cycle is also briefly discussed.

1.3.1 The carbon cycle

There are 4 reservoirs of carbon in the global carbon cycle: the atmosphere, the hydrosphere, the terrestrial biosphere and the lithosphere (Holmen 1992). In the non-biogenic 'slow carbon cycle', which existed prior to the evolution of life, carbon cycled between only 3 reservoirs: CO₂ from the atmosphere dissolved in the oceans and over millennia becomes carbonate mineral in rocks which was eventually re-released into the atmosphere following volcanic eruptions (Purves *et al* 1992; Falkowski & Godfrey 2008). This cycle still occurs but movement of carbon between reservoirs is accelerated by the fixation of organic carbon by primary producers, movement through the food chain and deposition in terrestrial and marine sediment thereafter. With the evolution of oxygenic photosynthesis, estimated at 3.8 bya, atmospheric carbon from CO₂ became a vital resource (Holland 2006; Buick 2008). The proliferation of primary producers in the hydrosphere made carbon levels increase, while carbon levels in the atmosphere decreased between 2.45 – 1.85 bya (Holland 2006; Buick 2008; Kasting & Siefert 2010). When the terrestrial biosphere began to form at around 0.5 – 0.3 bya, carbon from the atmospheric and hydrological reservoir (Strother *et al* 2010). Today it is estimated that global net primary production of organic carbon is about 104.9 petagrams C yr⁻¹ of which approximately half is of marine origin and the other half is terrestrial (Field *et al* 1998). However, while all the organic carbon in the terrestrial environment is respired, a tiny proportion (1 %) of the carbon fixed in the oceans does not get respired, sinks to the

ocean floor, and eventually is locked in the lithosphere (until released in volcanic eruptions or fossil fuel burning). Therefore, it is marine photosynthesis that has generated the surplus in O_2 that has maintained modern O_2 levels and it is the lithosphere that is the greatest carbon sink even though it does not sequester carbon and fluxes from the other three compartments are tiny (Holmen 1992; Falkowski & Godfrey 2008; Bendall *et al* 2008; Kasting & Siefert 2010). It is uncertain what proportion of global marine carbon fixation originates in estuaries but coastal and estuarine areas are some of the most productive in the oceans so it is likely to be a substantial proportion (Field *et al* 1998). Global MPB carbon fixation has been estimated at $0.34 - 0.5$ petagrams $C\ yr^{-1}$ (Cahoon 2006) which is only a tiny fraction of total global estimate (above) and yet it supports an ecosystem vital to the rest of the ocean as well as the terrestrial biosphere (Costanza *et al* 1997).

1.3.2 The nitrogen cycle

Dissolved inorganic nitrogen is one of the most important nutrients required by primary producers. The nitrogen cycle (Figure 1.2) begins with inorganic nitrogen (ammonium – NH_4^+) fixation from inert atmospheric N_2 by specialized nitrogen fixing bacteria, a reaction which requires anoxic conditions (Dexter Dyer 2003). Most nitrogen is fixed by specialized cells called heterocysts, containing the catalysing enzyme nitrogenase, in cyanobacterial colonies (Kasting & Siefert 2002). However, dissolved inorganic nitrogen also enters the estuary from agricultural and urban run-off and sewage discharge (Herbert 1982). NH_4^+ tends to build up in anoxic regions of the sediment (Nealson 1997) because under oxygenic conditions nitrifying bacteria (aerobes) oxidize ammonium to nitrite (NO_2^-) (Dexter Dyer 2003). In addition, NH_4^+ becomes adsorbed to clay particles in the sediment (which has a slight negative charge) and becomes buried over time (Rysgaard *et al* 1999) but increased salinity in incoming seawater causes the desorption of NH_4^+ whereupon it dissolves into the porewater or overlying water.

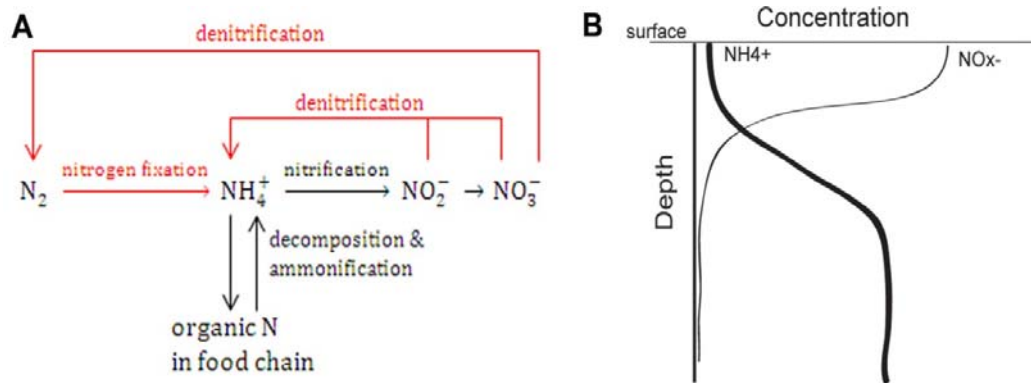


Figure 1.2 **A:** A simplified version of nitrogen evolution where anoxic reactions are drawn in red and oxic reactions in black (drawn from Dexter Dyer 2003 and Herbert 1982). **B:** Generalized schematic of NH_4^+ and NO_x^- distribution with depth in the sediment

NO_2^- is further oxidized to nitrate (NO_3^-) by other nitrifying bacteria. NO_2^- and NO_3^- (referred to together as NO_x^-), and NH_4^+ can all be used as nutrients by primary producers, although it has been suggested that they prefer NH_4^+ because they tend to block the release of NH_4^+ from the sediment more than NO_x^- (Sundbäck & Graneli 1988; Andersen & Kristensen 1988; Rizzo 1990; Feuillet-Girard *et al* 1997). Therefore, NO_x^- is more readily available in oxygenic parts of the estuary, surface sediment and overlying water column, especially in winter (Herbert 1982; Henriksen *et al* 1980, 1983; Rysgaard *et al* 1995; Nealson 1997; Sundbäck *et al* 2000; SEPA 2006) and is less toxic to animals. Denitrification is the process by which anaerobic bacteria (although some can perform nitrate reduction in oxygenic conditions) reduce NO_3^- is reduced to N_2 and while it is facilitated by anaerobes, it takes place along the border with oxygenated sediment (Nealson 1997; Pelegri *et al* 1994). NO_x^- and NH_4^+ are taken up by primary producers and converted into organic nitrogen (in amino and nucleic acids) and it is organic forms of nitrogen that enter the animal food chain. Thus animal excreta are nitrogenous as are the remains of all dead organisms; benthic invertebrates excrete nitrogen as NH_4^+ (Henriksen *et al* 1980). Following decomposition (of dead organisms), organic nitrogen is recycled back into dissolved inor-

ganic nitrogen ($\text{DIN} = \text{NO}_x^-$ and NH_4^+) by ammonifying (nitrate reducing) bacteria (Herbert 1982; Dexter Dyer 2003). Primary producers generally use DIN as nitrogen source although, at least in freshwater, they have been shown to be able to utilize organic nitrogen (urea and amino acids) as well (Berman & Chava 1999). So by recycling biological nitrogen and bypassing the reduction to N_2 the nitrogen cycle is shortened. However, even with the biogenic sub-cycling of DIN within a system, nitrogen remains the most limiting nutrient to primary production in marine systems (Ryther & Dunstan 1971; Herbert 1982; Malcolm & Sivy 1997).

1.3.3 Other important cycles

Three other important nutrients to primary producers are phosphates, sulphates and silicon. The sulphur cycle is similar to the nitrogen cycle in that it has solid, aqueous, and gaseous phases in its cycle, it is transformed from its various different forms by the redox reactions in bacterial photosynthesis and respiration, and one common form can be toxic to animals. Like nitrogen, sulphur is also an abundant element and but unlike nitrogen, its required state (SO_4^{2-}) for primary producers is abundant relative to requirement so it is unlikely to ever be a limiting nutrient (Purves *et al* 1992). It is released to the crust by volcanic eruptions, is absorbed by terrestrial and marine primary producers following precipitation or gaseous absorption by the ocean, and is returned to the earth sediment by sedimentation of inorganic and organic molecules (Purves *et al* 1992). Its importance in estuarine ecology is that primary producers require an oxidised version sulphate (SO_4^{2-}) while the reduced version (H_2S) is toxic to animals in high concentrations. H_2S is produced by sulphate reducing bacteria (SRB) living in the anoxic depths of the sediment which use sulphate as a terminal electron acceptor to respire organic carbon (Dexter Dyer 2003). Similarly to NH_4^+ , H_2S concentration increases with depth in the sediment but some drifts up the concentration gradient towards the surface layers where it is used by purple and green sulphur bacteria as a proton source for

non-oxygenic photosynthesis, thereby re-oxidizing it to SO_4^{2-} , which is also used by oxygenic photosynthesizers at the surface (Dexter Dyer 2003).

Phosphorous is vital to all organisms as it is required for both ATP and NADPH- H^+ , the energy releasing molecules of all living cells. Phosphorous exists in mineral form bound to rocks and sediment, especially with iron oxides, and does not go through a gaseous stage in its cycle (Purves *et al* 1992; Malcolm & Sivyer 1997). It is released from terrestrial and marine rocks by physical erosion and becomes dissolved in the water in the form of phosphate ions (PO_4^{3+}) which will re-associate with sediment particles (especially clay) under oxic conditions (Malcolm & Sivyer 1997) unless sequestered by primary producers. Attached to sediment particles or within organic material, it becomes buried by sedimentation and sediment compaction, which will lead to its eventual remineralization. However, under anoxic conditions in the lower sediment, some PO_4^{3+} becomes desorped from sediment particles and dissolves in pore water (Malcolm & Sivyer 1997). Disturbance of the sediment is thought to release dissolved phosphate from the sediment (Malcolm & Sivyer 1997) and thus phosphates are also cycled biogenically with all systems. However, while phosphate is considered the primary limiting factor to photosynthesis in freshwater systems, in estuarine and marine systems, while still present in only very low quantities ($< 4 \mu\text{mol L}^{-1}$), it is comparatively abundant to the amount required by living organisms (Ryther & Dunstan 1971).

Finally, silicon is an extremely abundant element in the earth's crust and is found various different kinds of silicates such as quartz or, more commonly, in conjunction with aluminium, or in its dissolved form silicic acid. As with phosphates, the weathering of terrestrial and marine rocks releases silicates into water and it does not have a gaseous component in its cycle: following sedimentation out of the water column, it either re-dissolves in porewater and fluxes out of the sediment along the concentration gradient or is buried (Mal-

colm & Sivyver 1997). Silicates, like phosphates, are replenished in oceanic surface waters by upwelling (Malcolm & Sivyver 1997). Again, the recycling of biogenic silica (opal from diatom frustules) by-passes this larger cycle and means that silicon stores become temporarily localized within a system (Carbonell *et al* 2009). Dissolution of biogenic silicon occurs faster in higher salinities and following removal organic material (Roubeix *et al* 2008) so estuarine diatoms, which are regularly immersed in seawater and grazed upon by all estuarine deposit feeders, are not likely to become silicate limited prior to becoming CO₂ or DIN limited.

1.3.4 Nutrient status

While nutrients are important and necessary for primary production, excess nutrient tend to have a deleterious effect on MPB diversity and animal biomass and diversity (Smith *et al* 1999). Oligotrophic, mesotrophic and eutrophic refer to the nutrient status of an estuary (or any body of water): oligotrophic refers to low dissolved nutrient in overlying water, thought to be 'normal' for more pristine, pre-industrial habitats, and eutrophic refers to very high (~10 fold higher than oligotrophic) dissolved nutrient levels in overlying water (Smith *et al* 1999; Hessen 1999). Eutrophication is the process by which waters become more nutrient rich (generally in terms of N and P concentration) due to external loading, usually due to human activity (Smith *et al* 1999). The trend for increased fertilisation of the land due intensification of agriculture has led to a 10 fold increase of anthropogenic N input into the North Atlantic (Haworth *et al* 1996 Smith *et al* 1999). The deleterious effects of eutrophication are that fecund, fast growing, species of micro- and macrophytes 'bloom' at the expense of general diversity in primary producers (Smith *et al* 1999; Paerl 2006). In marine systems, phytoplanktonic blooms have the unfortunate characteristic that they often involve species that produce toxins harmful to other marine life (Smith *et al* 1999; Paerl 2006). Common macroalgal indicators of eutrophication are *Enteromorpha* species which form deep and extensive mats on intertidal sand- and

mudflats, and tend to smother the MPB and some invertebrates underneath (Raffaelli 2000). A knock-on effect caused by gluts of organic carbon availability is that they are followed by an increase in bacterial decomposition within the sediment, and the increased respiration in the sediment means oxygen levels in the overlying water and surface sediment are rapidly depleted leading to mass die offs in invertebrate infauna and vertebrate water inhabitants (Smith *et al* 1999; Paerl 2006). These types of problems have been reported from coastal marine and estuarine ecosystems worldwide (Howarth *et al* 1996; Smith *et al* 1999; Paerl 2006; and references in each).

1.4 Residents of temperate estuaries

Dyer (1997) speculates that estuaries have been crucial environments in the evolution of life: the environments where organic life and the subsequent oxygenation of the atmosphere began and where marine animals evolved into the earliest terrestrial forms. However, animal diversity is relatively low in temperate estuaries and McLusky (1971) suggests that this is partially due to the fact it is still relatively early in their evolutionary history – today's estuaries are not likely to be more than 3000 years old. Also, very few animals from the surrounding marine and terrestrial environments would have been able to colonize estuaries due to the extreme range of environmental conditions that must be tolerated (McLusky 1971). Nevertheless, there is huge biodiversity in estuaries but it is mostly in the form of prokaryotes and protists.

1.4.1 Eubacteria

Of all organisms only the Eubacteria (bacteria hereafter) are traditionally described by their hugely diverse physiology and function rather than by their morphology (Nealson 1997; Dexter Dyer 2003). They are the original and ultimate ecosystem engineers and responsible for the Earth's oxygenated atmosphere and they still control most biogeochemical cycles (Falkowski *et al* 2008). Estuarine sediment bacteria are gram negative and non-pathogenic, and, with

the exception of cyanobacteria and green sulphur bacteria, which are each in their own phylogenetic group, they are all proteobacteria (α , β , γ , and δ) (Dexter Dyer 2003). The major functional groups of bacteria in an estuarine sediment column are like those that can be seen in a Winogradsky column: phototrophs, chemotrophs, nitrifiers (ammonia oxidisers), denitrifiers (nitrate reducers), sulphur oxidizers, and sulphate reducers (Nealson 1997; Dexter Dyer 2003). However, it should be noted that bacteria display a remarkable functional plasticity in their metabolisms (Nealson 1997). For example purple non-sulphur bacteria will photosynthesize when light is available but can become heterotrophic in the absence of light (Nealson 1997).

Cyanobacteria are not only the oxygenic phototrophs of the estuarine system but are also the nitrogen-fixers (Dexter Dyer 2003). They live in the photic zone at the sediment surface and when present in large quantities can be recognized by a blue-green colouration of the sediment and common estuarine genera are *Merismopedia*, *Oscillatoria*, and *Lyngbya*. Also in the photic zone are the sulphide oxidizers, purple (γ -proteos) and green sulphur bacteria which are photosynthetic but use H_2S rather than H_2O as proton source, evolving SO_4^{2-} , and prefer anaerobic conditions (Dexter Dyer 2003). Common genera of purple and green sulphur bacteria in estuarine mud are *Chromatium* and *Chlorobium*, respectively, and *Chromatium* are especially easy to distinguish due to their distinctive magenta colouring (Dexter Dyer 2003). GSB are often found in deeper layers than the purple because they prefer high H_2S concentrations (Dexter Dyer 2003). Purple (α - or β -proteos) non-sulphur bacteria have the same colouring as PSB but oxidize organic molecules rather than H_2S for protons; *Rhodobacter* (α) and *Rhodocyclus* (β) can be found in anoxic estuarine mud (Dexter Dyer 2003). Finally, there are chemolithoautotrophic (they use chemical bond energy rather than sunlight) sulphur-oxidizing bacteria such as *Beggiatoa* which can be distinguished as a white dust or long white filaments near the PSB (Dexter Dyer 2003); *Beggiatoa* do not oxidize H_2S into SO_4^{2-} but into elemental S. Heterotro-

phic bacteria include nitrifying bacteria (β -proteos) like *Nitrosomonas* (NH_4^+ oxidized to NO_2^-) and *Nitrobacter* (NO_2^- oxidized to NO_3^-), which use nitrogenous compounds as energy sources to respire organic carbon (Nealson 1997; Dexter Dyer 2003). Anoxic denitrifying bacteria like *Aeromonas*, *Vibrio*, and *Klebsiella* reduce nitrates back to NH_4^+ or N_2 by using nitrates as final electron acceptor instead of oxygen (Herbert 1982). Anaerobic sulphate reducing bacteria (δ -proteos) on the other hand use SO_4^{2-} as terminal electron acceptors and their field marks are the black, sulphurous mud frequently found in areas with very small grain size (Dexter Dyer 2003). In addition to these main groups there are also Fe, Mn, and CH_4 oxidizers and reducers (Nealson 1997).

1.4.2 Primary producers

In addition to cyanobacteria, oxygenic photosynthesis in estuaries is carried out by protists, algae, and marine angiosperms. Although only 7 - 15 % of global primary production is carried out in estuarine and coastal areas, these ecosystems are vital to oceanic primary and secondary production (Gattuso *et al* 1998; Field *et al* 1998).

1.4.2.1 Protists

Single-celled photosynthesising eukaryotes include chlorophytes, rhodophytes, heterokontophytes, haptophytes, dinophytes, and euglenophytes (van den Hoek *et al* 1995). They live in the water column (phytoplankton), attached to solid substrata (epiliths) or plants (epiphytes), and in surface sediment (phytobenthos) (van den Hoek 1995; Round 1981). This thesis is primarily concerned with the latter category, which, together with cyanobacteria, are grouped as “microphytobenthos” (MPB). Mud- and sand-dwelling MPB mostly consist of cyanobacteria, diatoms (Division Heterokontophyta, Class – Bacillariophyceae) and Euglenids (Division Euglenophyta). MPB, benthic microalgae, and biofilm are blanket terms which include a huge diversity of different organisms of different biologies and ecologies which is perhaps why such a wide variety of dif-

ferent, and often contradictory, behaviour and physiology are described for them (Admiraal 1984; Underwood 2005).

All oxygenically photosynthesizing organisms are thought to have evolved from a single endosymbiosis event where a heterotroph engulfed a cyanobacterial cell which became the progenitor of green and red algae and land plants (Armbrust 2009). The main photosynthetic pigment of this cyanobacteria, and all its descendents, is green chlorophyll-*a* but the main accessory pigment in a species can change the colour of the cells (van den Hoek *et al* 1995). In cyanobacterial cells the main accessory pigments are phycobilins which are blue and give cyanobacteria their characteristic blue-green colour. In chlorophytes (green algae) it is chlorophyll-*b* which is also green, and in rhodophytes (red algae) it is phycoerythrin, which is red, and also phycobilins (van den Hoek *et al* 1995). A secondary endosymbiotic event is thought to have occurred in which a red algal cell (and perhaps also a green algal cell) was engulfed by a different heterotroph and became the progenitor of the brown algae such as diatoms (Armbrust 2009). The brown colour comes from the accessory pigment fucoxanthin and a diatom biofilm on the sediment surface looks brown or olive, depending on the relative abundance of diatoms:cyanobacteria:euglena (chlorophyll-*a* + -*b*) (Figure 1.3).



Figure 1.3: MPB blooms on the sediment surface. On the left, evolved O₂ bubbles can be seen on the surface of the biofilm.

Diatom cells are housed within a glass basket of hydrated silicate ($\text{SiO}_2 \cdot n\text{H}_2\text{O}$) constructed of two halves (valves), similar to the two halves of a petri dish, but

bound together into a case by several girdle bands (see Glossary). According to a molecular clock analysis, the first diatoms evolved 240 – 135 mya and centric diatoms are thought to have evolved before pennate diatoms (Figure 1.4) as they appear first in the geological record (Medlin 2006). Nomenclatural rankings vary from source to source, i.e.. sometimes diatoms are a division and sometime they are a class but it is the structural order within this grouping that is important rather than the nomenclatural order (van den Hoek *et al* 1995; Round *et al* 1990; Medlin 2006). Originally, the Bacillariophyceae were thought to have two clades, the centric (Coscinodiscophyceae) and pennate, and the pennates were further subdivided into the araphid (Fragilariophyceae) and raphid (class Bacillariophyceae) diatoms (Round *et al* 1990). However, current molecular evidence points to 3 clades rather than 2 clades, where radial centrals (Coscinodiscophyceae) are separated by one further clade from the raphid, araphid and the bi- or multipolar centrals (Medlin 2006). Most centric diatoms live in the water column, so the majority of phytoplankton in the oceans consists of centric diatoms. However, with the exception of a few benthic Coscinodiscophycidae like *Melosira* spp. and sedimented phytoplankton, microphyto-benthos come from the grouping – the Pennales (order) – containing raphid and araphid pennates. Araphid pennates were likely the earliest descendents of centric groups, however, it is unclear whether monoraphid or biraphid pennates evolved first.

Pennate valves are organised around a central (or marginal) sternum which either has a raphe slit or not (Figure 1.4). The raphe slits are used to exude strand of mucus of extracellular polymeric substances (EPS) that stick onto sediment particles and allow the diatom to slide along the central axis (Admiraal 1984; van den Hoek *et al* 1995; Round *et al* 1990; Consalvey 2005). Alternatively, exudate is used to create mucilage sheaths which diatoms can slide up and down in. Therefore, diatoms with raphes on both valves (biraphid) are mobile, monoraphid diatoms are semi-mobile, and araphid diatoms are immobile. Mo-

bile diatoms are generally free-living in the sediment matrix and are referred to as 'epipellic', whereas semi- or non-motile diatoms live attached to sediment particles (epipsammic), or macrophytes and plants (epiphytic) or rocks (epilithic) (Round *et al* 1981, 1990).

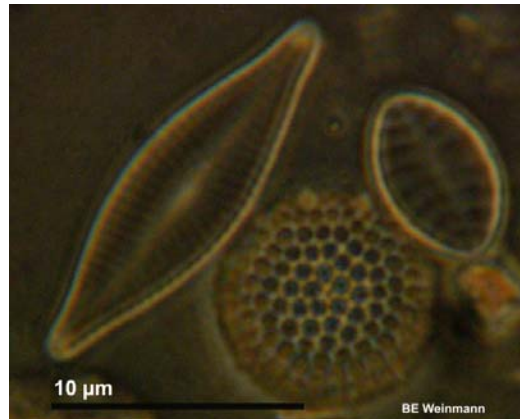


Figure 1.4: 3 Cleaned diatom valves at 1250x (LM) magnification. The centric valve (centre) is from a *Thallasiosira* sp., the pennate raphid (top left) is a *Navicula*, and the rapheless valve (top right) is from the pennate monoraphid genera *Achmanthes*. The raphe is hardly visible on the *Navicula* but the central and terminal nodules (see Appendix 1) indicate its presence.

Mobility was an important innovation to diatoms living in the estuarine intertidal as the movement of water with the tides inevitably resuspends sediment and muddy sediment is indicative of low flow rates and the lower the flow in the overlying water, the more sediment is deposited at the surface if the suspended load is high (Brown *et al* 1999). In addition, the finer the sediment the more light attenuates with depth and therefore the narrower the photic zone (MacIntyre *et al* 1995). It is therefore hardly surprising that muddy sediments (where flow is slowest and sedimentation highest) are dominated by epipellic diatoms whereas sandy areas are dominated by epipellic diatoms (Admiraal 1984; Round *et al* 1981; MacIntyre *et al* 1995). All photosynthetic organisms have polysaccharide storage and in diatoms this is the major reserve but both cyanobacteria and diatoms can also store energy in lipid form and droplets of oil can be seen inside living cells (van den Hoek *et al* 1995). However, in addition to motility and energy storage, another adaptation to living in light-limited

environments is that several diatom species have evolved the ability to grow in the dark by feeding heterotrophically on organic substances and these heterotrophic capacities are most frequent among the mud-living species where organic content is high but the photic zone is narrow (Admiraal & Peletier 1979).

Pelagic and benthic diatoms account for 20 % world carbon fixation (Armbrust 2009), so it is important to understand their ecology and how they respond to changes in resource availability. Studies on freshwater benthic and pelagic communities and marine phytoplanktonic communities, which are more numerous than benthic estuarine and marine studies, have shown that changing limiting nutrient and turbidity levels changes microalgal biomass and composition (Grover 1989; Pan & Lowe 1994; Smith 1996; Naymik *et al* 2005; Passy 2007, 2008; Finkel *et al* 2009; Licurzi & Gomez 2009; Duarte *et al* 2000; Vidal & Duarte 2000). Increased availability of DIN and phosphate, adsorbed on the surface of sediment particles, in turbid systems can compensate for the loss of light and benefit smaller, epipsammic species of diatoms that inhabit the understory of benthic biofilms (Burkholder 1996). From a theoretical point of view, bioturbation could be interpreted as a source of intermediate disturbance, which could increase niche availability and thereby increase species diversity (Townsend *et al* 2000), although there is so far no empirical evidence for this from either fresh water or marine MPB communities.

It is not unusual for intertidal diatoms to be tolerant of a very broad range of light, salinity, and nutrient ranges (Underwood & Provot 2000; Defew *et al* 2002, 2004). However, although they exhibit large tolerances to salinity, it has been shown that differences in salinity can induce morphological changes within taxa, so that assemblages at different salinities may look different even if they are not taxonomically different (Leterme *et al* 2010). Some controlled experiments on intertidal MPB biofilms maintained under different nutrient regimes have not demonstrated profound changes in MPB assemblage composition

(Sundbäck & Snoeijs 1991; Hagerthey *et al* 2002), but others have found that some species are negatively affected by increased nutrient concentration (Underwood *et al* 1998). However, the effect of nutrients on assemblage composition can be idiosyncratic to starting conditions: the effect of nutrients on assemblage structure can vary depending on whether the assemblages had come from eutrophic or oligotrophic assemblages (Hagerthey *et al* 2002). Field studies, have shown differences in assemblage compositions along nutrient gradients. A coastal study in Sylt (Germany) larger diatoms dominated eutrophic areas and smaller semi-motile diatoms dominated oligotrophic areas (Agatz *et al* 1999) and an estuarine study in SE England demonstrated clear differences in taxa abundances at different salinity and nutrient levels (Underwood *et al* 1998). Comparisons of bottom-up (nutrients) / top-down (grazer) effects on MPB assemblage diversity have demonstrated that the effects of grazers are not necessarily consistent at different nutrient levels (Hagerthey *et al* 2002; Hillebrand *et al* 2000). Also, the effect of grazers on MPB community composition appears to depend on the grazer: general deposit feeders do not appear to feed preferentially, therefore dominant species are removed more so than rare species (Smith *et al* 1996; Hagerthey *et al* 2002) whereas gastropods preferentially graze on upright species, leaving the prostrate species thereby enhancing survival of small epipsammic species and slightly increasing overall diversity (Hillebrand *et al* 2000; Hagerthey *et al* 2002). With respect to light levels, diatoms have been shown to be able to last for well over a week in complete darkness due to their ability to hoard nitrates and use them for nitrate respiration (Kamp *et al* 2011). However, a shift to smaller diatoms has also been found to accompany a shift of natural populations to oligotrophic and lower light conditions of a tidal, laboratory system (Defew *et al* 2002). Intuitively, the decreased energy input should decrease overall biomass and favour motile diatoms, which can migrate fastest to the sediment surface but they found it had no effect on biomass or species richness, although there was decreased diversity due

to a shift to smaller sized diatoms following 2 weeks of incubation in the laboratory (Defew *et al* 2002). This suggested that smaller cell sizes were more competitive in situations of lower light and nutrient availability (Defew *et al* 2002). In a follow-up experiment, they (Defew *et al* 2004) found that the response of MPB assemblage diversity was temperature dependent: at lower temperatures (10 °C and 18 °C) species richness, evenness, and diversity were higher after three weeks at low light than at high light whereas the reverse was true at high temperatures (25 °C). As there are so few estuarine and coastal benthic studies, and the data is highly variable and noisy, there is as yet no clear understanding of diatom ecology.

1.4.2.2 *Macrophytes and angiosperms*

Unlike oceanic photosynthesis, which is carried out almost entirely by microphyte, estuarine and coastal areas also have large and important macroalgal, halophyte and sea grass constituents (Gattuso *et al* 1998). Multicellular brown and green algae such as *Fucus*, *Ulvae*, *Enteromorpha* spp. are very common in north Atlantic estuaries. *Fucus* and *Ulvae* are generally found in rocky or mussel-dominated areas as they require holdfasts, whereas *Enteromorpha* are found in small quantities all over estuaries but found in large quantities on eutrophic mud flats (Raffaelli 2000). The most important grasses commonly found in estuarine and coastal zones are eel grass (*Zostera* spp.), which grow in beds on mud and sand flats (Wilkie 2011), and salt-marsh angiosperms (*Spartina* and *Puccinellia* spp.), which are a particularly important habitat type and provide food and shelter for other plants, like the succulent halophytes *Salicornia* spp. (marsh samphire), but also for terrestrial animals like insects (Boorman 2003, O'Connor *et al* 2011).

1.4.3 Invertebrates

Most of the adult animal inhabitants of the mud flat are invertebrates: nematodes, oligochaetes, polychaetes, gastropods, bivalves, and crustaceans. Inver-

tebrates that can be sieved out of the sediment through a 0.5 mm² mesh are referred to as 'macrofauna' to distinguish them from 'meiofauna', which cannot be sieved out through a 0.5 mm² mesh (eg. nematodes and larva or juvenile individuals of any species). Body sizes of macrofauna vary substantially from the tiny gastropods *Hydrobia ulvae*, which have approximately 1 mm body lengths, to bivalves *M. baltica*, which vary between 1 – 7 cm, and large polychaetes like *Hediste diversicolor*, which can have a body length of up to 20 cm in Eden estuary specimens (Figure 1.5).



Figure 1.5: *H. diversicolor* surrounded by *H. ulvae*, and *M. baltica* (from marLIN web page).

While a few species, such as the common mussel *Mytilus edulis* and the mud snail *H. ulvae* are mostly surface dwellers, most species burrow into the sediment thereby changing the sediment structure (Jones & Jago 1993). Burrowing styles are classified as: biodiffuser, gallery diffuser, regenerator, upward-conveyer, downward conveyer, and bio-irrigator (Jones & Frid 2009). Biodiffusers (*M. baltica* and other bivalves, *C. volutator*, *H. diversicolor*) move sediment around in a random directions and in small increments whereas bio-irrigators (eg. *C. volutator*) and gallery diffusers (eg. *H. diversicolor*) actively irrigate a burrows by drawing surface water through it (Jones & Frid 2009). The distinction between bio-irrigators and gallery diffusers are that bio-irrigators, like *C. volutator*, maintain a single burrow (U-shaped burrows in Figure 1.6) whereas gallery-diffusers like *H. diversicolor*, maintain a network of burrows (Figure 1.6) (Jones & Frid 2009). Upward-and downward- conveyers are animals which are either ori-

ented head-up or head-down in the sediment and therefore deposit sediment from the head area to the other end (Jones & Frid 2009). Regenerators also move sediment from lower depths to the sediment surface (eg. *Arenicola marina*) but do not necessarily have stationary orientation like upward-conveyors (Jones & Frid 2009). Burrowing depths also vary substantially from 2 mm (*H. ulvae*) to 20 cm (*H. diversicolor*).

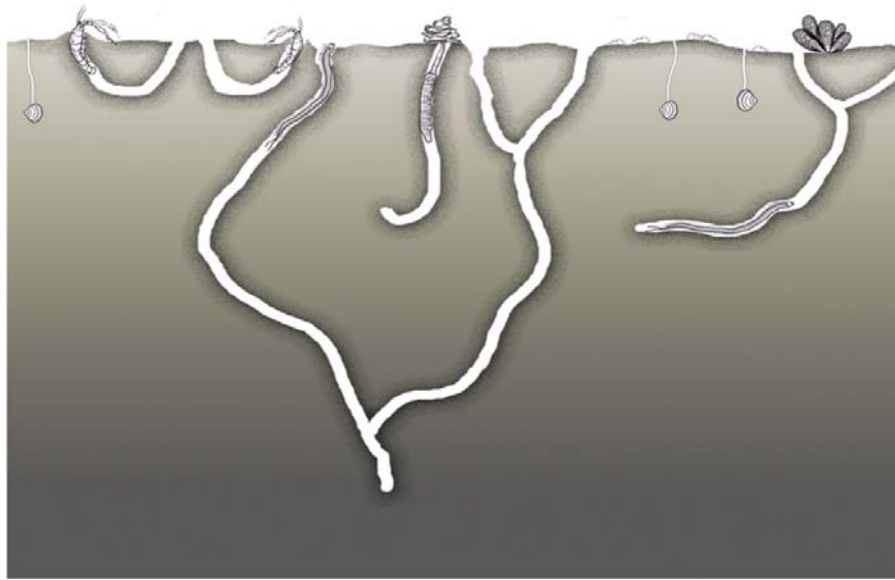


Figure 1.6: A macrofauna assemblage of *M. baltica*, *C. volutator*, *H. diversicolor*, *A. marina*, *H. ulvae*, and *M. edulis* (from left to right). Different burrowing depths are approximate and not to scale. Maximum depth of *H. diversicolor* is about 20 cm.

Feeding mode classifications include: deposit-feeder, active suspension feeder, passive suspension or 'filter' feeder, scavenger, predator (Jones & Frid 2009). Deposit feeders ingest sediment whole and extract organic molecules from them, thereby effectively 'cleaning' the sediment (*C. volutator*, *H. ulvae*, *H. diversicolor*, *M. baltica*). Active and passive suspension feeders remove particles from the water column, digest the organic content and deposit the remains at or near the sediment surface; active suspension feeders generate their own currents to move water through their feeding apparatus (eg. *C. volutator* and *H. diversi-*

color), whereas passive suspension feeders require water flow to trap particles (eg. *M. edulis*). Scavengers and predators eat either dead animals in the sediment or actively hunt other animals, respectively. Many species exhibit multiple feeding modes; for example *H. diversicolor* can feed as a deposit- and active suspension feeder, scavenger, and predator. Additional information is given below on *C. volutator* biology and ecology due to its prominence in this thesis.

1.4.3.1 *Corophium volutator*



Figure 1.7: Clockwise from top left: *C. volutator* male (with long 2nd antennae, front and centre) with female to the right (similar body length but short 2nd antennae), large columnar “chimneys” built under deoxygenated conditions, single *C. volutator* in U-shaped burrow in dried sediment, and *C. volutator* in invading another’s burrow

Corophium volutator (Pallas) is one of the most ubiquitous and abundant organisms living on North Atlantic estuarine mudflats throughout the year (Green 1968; McLusky 1968; Henriksen *et al* 1980; Hylleberg & Henriksen 1980; Murdoch *et al* 1986; de Deckere 2000, Gerdol & Hughes 1994b, Møller & Riisgård, 2006). They are patchily distributed throughout most estuaries and have a very wide substratum and salinity tolerance, although the highest concentrations are generally found around the mid-shore, 5 – 30 ‰ salinity, and in finer sedi-

ment types (muddy sand, sandy mud, mud) which have higher water and organic content and are less well oxygenated (Meadows 1964; McLusky 1968, 1970; Murdoch 1986). Abundance of *C. volutator* fluctuates drastically over the year in all studies but the months in which lowest and highest abundance occur are particular to each estuary; they generally increase when annual MPB and plankton blooms occur and in some estuaries decrease dramatically when migratory birds arrive to feed in the summer (Murdoch *et al* 1986; Daborn *et al* 1993; personal observations 2008 – 2009). Peak estimates of 10,000 – 100,000 of individuals m^{-2} have been reported at various North Atlantic locations but overwintering populations often drop down to one to five thousand m^{-2} (McLusky 1968; Henriksen *et al* 1980; Hylleberg & Henriksen 1980; Murdoch *et al* 1986; Daborn *et al* 1993; Gerdol & Hughes 1994b; de Deckere 2000; Møller & Riisgård 2006). Average abundance (in individuals m^{-2}) at the Guardbridge site in the Eden estuary tends to be highest in late spring, early summer when eggs have hatched but flocks have not yet arrived: ~9200 (32.5 g) in early May and ~2000 (7.8 g) in late July (from 2008, Table 2.3).

C. volutator build permanent narrow, U-shaped burrows to about 5 cm sediment depth through which they keep a steady flow of overlying water circulating, by rhythmic beating of their pleopods (Meadows & Reid 1967, Gerdol & Hughes 1994a, Møller & Riisgård 2006). This current is not only required to pass oxygenated water over the gills but also facilitates feeding: sediment scraped into the burrow from the surface is resuspended in the burrow along with phytoplankton from the overlying water column and flows through a makeshift basket, formed by the bristles on the setae of the 1st and 2nd gnathopods, which filters out particles greater than 4 – 7 μm (Meadows & Reid 1967; Nielsen & Kofoed 1982, Icely & Nott 1985 and references therein). If these particles, organic and inorganic, are between 4 (or 7) and 63 μm they are ground by the mandibles and swallowed (Nielsen & Kofoed 1982, Icely & Nott 1985 Murdoch 1986). Particles larger than 63 μm are manipulated differently: diatoms, bacteria and

EPS are scraped off the surface with the bristles on the setae of the gnathopods and passed to the mouthparts, a feeding style known as 'epipsammic browsing' (Nielsen & Kofoed 1982). This makes *C. volutator* quite versatile: they can filter feed during immersion if concentrations of phytoplankton are sufficiently high and switch to deposit feeding (i.e., scraping sediment off the surface) during emersion or if phytoplankton concentrations during immersion are low (Gerdol & Hughes 1994a; Møller & Riisgård 2006). The actual nutritional content from the sediment and phytoplankton is thought to be predominantly from diatoms and EPS although bacteria are also readily consumed and assimilated but probably do not account for a large percentage of the energy budget (Gerdol & Hughes 1994a and references therein). While it has been suggested that *C. volutator* probably gets some of its nutrition from plant detritus in the sediment (Icely & Nott 1985, Murdoch 1986, Stuart *et al* 1985), physiological experimental evidence shows that cellulase concentrations in *C. volutator* guts is negligible and that survival rates of animals on a *Spartina* diet are very low compared to those on diatom diet (Agrawal 1963; Bärlocher 1988; Stuart *et al* 1985). In addition, field experiments have shown that *C. volutator* abundance decreases with increasing macroalgal mat coverage (Raffaelli 2000 and references therein), and heterogeneous microcosm experiments (Dyson *et al* 2007) have shown that *C. volutator* avoids sediment containing macroalgal pigment (powdered *Enteromorpha*). *C. volutator* are probably forced to avoid macroalgal mats not only because they provide little sustenance but also interfere with the amphipod's feeding apparatus (Rafaelli 2000 and references therein). From their laboratory feeding experiments, Gerdol and Hughes (1994a) estimated that adult amphipods feeding on surficial biofilms consumed an average of approximately 4000 diatoms an hour. Møller and Riisgård (2006) investigated suspension feeding in *C. volutator* and found that pumping rate increased with body size and temperature and filtration rates varied between $0.9 - 19.4 \text{ m}^3 \text{ m}^{-2} \text{ d}^{-1}$. Feeding is more or less continuous and coarse material is ejected in the faeces within 4 – 24

minutes of ingestion but fine material not until 24 – 48 hours (Icely & Nott 1985). Researchers have not found many diatom frustules in either *C. volutator* gut contents nor faeces from which they surmised that diatoms were ground down by the mandibles prior to ingestion (Murdoch *et al* 1986; Icely & Nott 1985; Gerdol & Hughes 1994a). Therefore, when faeces and detritus expelled from the burrow by the ventilation current it should be low in organic content.

Individuals crawling across the mud surface at emersion are usually adult males either looking for an empty burrow or a female to mate with (Meadows & Reid 1966). Sexually mature individuals are generally between 5 and 12 mm and males can usually be recognised by exceptionally long 2nd antennae which can make up half their body length (Meadows & Reid 1966;). Unlike most crustaceans, *C. volutator* do not have different body forms at different live stages or a pelagic dispersal phase; fertilized eggs are maintained in a brood pouch in the female from which offspring crawl out as miniature versions of adults and burrow immediately nearby (Neal & Avant 2006). However, given their voracious feeding rate, dispersal is a necessity to avoid competition between closely related individuals. From their study in the Ythan estuary Lawrie and Raffaelli (1998) found that while very few *C. volutator* were found in the water column during the majority of immersion tides the few that were caught were usually large males; however, on the occasional nocturnal intermediate tide large numbers of juveniles (≤ 4 mm) were caught in plankton nets. They reasoned that the swimming activity of large males is probably for reproduction with unrelated females but that it is the mass movement of juveniles that maintains the patchiness of *C. volutator* distributions within estuaries. Meadows (1964, 1967) showed that *C. volutator* will repeatedly sink out of the water column to examine sediment and will generally choose to settle in fine sand or mud which is better burrowing material and where MPB reach higher densities reach much higher concentrations than in coarse sand.

1.3.4 Vertebrates

Estuaries are important nursery grounds for many coastal fish – 90 % of world fish catch is from estuarine and coastal zones (Gattuso *et al* 1998). They are also important feeding grounds for migratory birds which feed on invertebrate in-fauna (reference). Abundance of plankton, fish, and invertebrates also attract marine mammals (Figure 1.9). Finally most remains of the earliest human civilizations are found around estuaries (McLusky 1971; Dyer 1994) and to this day 37% world population within 100 km of an estuary or coast (Gattuso *et al* 1998).

1.5 Ecosystem functions in soft sediments

While organisms inhabiting soft sediments in estuarine and coastal systems perform many vital ecosystem functions, below are brief introductions to four that are important in this thesis.

1.5.1 Carbon fixation and degradation

Carbon fixation in estuarine mudflats is carried out by MPB. Estuaries and coastal zones account for 14 – 30 % of oceanic primary productivity (Gattuso *et al* 1998), which represents approximately half of global carbon fixation (Field *et al* 1998). However, it is compartmentalized between very different microsystems (grasses, macrophytes, MPB and phytoplankton) and determining which compartments contribute most to net ecosystem productivity (NEP) is complex (Gattuso *et al* 1998). MPB on estuarine and coastal mud- and sandflats are estimated to contribute less net primary productivity than phytoplanktonic, macrophytic- and plant-dominated (salt-marsh) systems (Underwood & Kromkamp 1999; Gattuso *et al* 1998), in fact net primary production from estuarine mudflats is negative (Gattuso *et al* 1998). However, at the same time, in shallow estuarine areas, MPB production can account for 30 – 70 % of total estuarine primary production (Gazeau *et al* 2005) and MPB biomass specific productivity is more temporally stable and overall higher in mudflats than salt marshes

(Pinckney & Zingmark 1993a). Most primary production is consumed *in situ* by bacteria and primary consumers. Many invertebrates (eg. *C. volutator*, *H. diversicolor*, and *M. baltica*) have multiple feeding modes and will feed alternately on phytoplankton and sediment MPB and detritus depending on which is more available (Budd 2008; Budd & Rayment 2001; de Goij & Luttikhuisen 1998; Green 1968; Meadows & Reid 1966; Møller & Riisgård 2006). Deposit-feeding bioturbators are important to decomposition and mineralization of organic compounds (Hylleberg & Henriksen 1980; Andersen & Kristensen 1991; Aller & Aller 1998) and it is estimated that 90 % of sedimentary re-mineralization of nutrients occurs in relatively shallow coastal water (Gattuso *et al* 1998). In addition, invertebrate grazers in intertidal areas are an important food source for fish and shore birds (Green 1968; Raffaelli & Milne 1987; Gattuso *et al* 1998).

1.5.2 Oxygenation uptake of sediment

Primary producers are the ecosystem engineers that generate O₂ but often this penetrates the sediment no deeper than 2 mm (Kristensen 2000; Glud 2008) beneath which anoxic bacteria sequester organic carbon often producing waste products that, in high concentrations, are toxic to animals (Nealson 1997; Dexter Dyer 2003). Burrowing infauna increase the oxygen uptake of the sediment for two reasons: (1) they must bring oxygen down from the surface to breathe, and (2) their feeding activity redistributes sediment and the mixing action also increases O₂ concentrations (Kristensen 2000; Jones & Frid 2009). The depth to which O₂ penetrates the sediment varies with the burrowing style, depth and intensity of the organism (Kristensen 2000). Gallery diffusers such as *H. diversicolor* (Figure 1.8) tend to oxygenate the sediment most, followed by bio-irrigators like *C. volutator*, whereas biodiffusers such as *M. baltica* oxygenate the sediment the least (Andersen & Kristensen 1988; Andersen & Kristensen 1991; Pelegri *et al* 1994; Rysgaard *et al* 1995; Kristensen 2000; Mermillod-Blondin *et al* 2004; Michaud *et al* 2005).

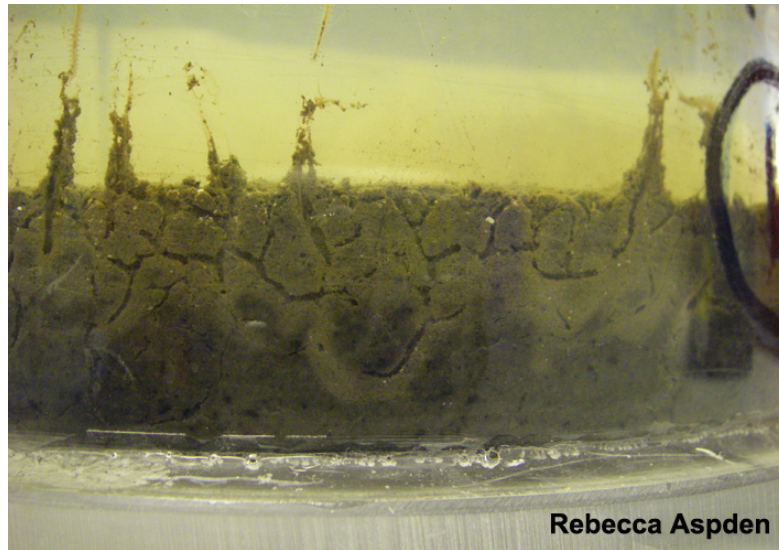


Figure 1.8: This mesocosm contained sieved mud and *H. diversicolor*. Oxygenated sediment is generally lighter in colour than anoxic sediment, the black specs are from Fe reactions with H_2S and indicate the presence of SRB. Individuals can be seen shooting out of their burrows to feed on fish food placed at the water surface.

Meiofauna and less mobile or active burrowers depend on ecosystem engineering of active bioturbators to create suitable habitat, so the loss of certain key bioturbators can result in a cascade of species losses in the affected area (Solan *et al* 2004).

However, O_2 uptake of the sediment is also increased, predominantly by bio-irrigators and gallery diffusers, because they increase bacterial activity (Hargrave 1970; Mermillod-Blondin *et al* 2004, 2005) including processes such as nitrification and denitrification (Sørensen J 1978; Henriksen *et al* 1980; Pelegri & Blackburn 1994; Pelegri *et al* 1994, 1995; Rysgaard *et al* 1995; Michaud *et al* 2006) and ammonification (Aller & Aller 1998).

1.5.3 Nutrient release from sediment to overlying water

As NH_4^+ and PO_4^{3-} are more concentrated in the sediment than in the overlying water, they diffuse along their concentration gradient into the overlying water but can be blocked in light conditions as they are sequestered by photosynthesizing MPB at the sediment surface (Henriksen *et al* 1980, 1983; Andersen &

Kristensen 1988; Sundback & Graneli 1988; Rysgaard *et al* 1995; Rizzo 1990; Feuillet-Girard *et al* 1997). However, gallery diffusers, bio-irrigators and feeding macrofauna tend to increase the release of these nutrients to the overlying water (1) because they are depleting the MPB biomass at the sediment surface by feeding on them, (2) because they disturb the sediment surface which means NH_4^+ and PO_4^{3-} tends to become desorped from sediment particles either due to higher salinity or due to the disturbance itself (Malcolm & Sivy 1997; Rysgaard *et al* 1999), and (3) because increased sediment – water interface of the burrows increases the diffusive surface area (Henriksen *et al* 1980, 1983; Andersen & Kristensen 1988; Rysgaard *et al* 1995; Emmerson *et al* 2001; Mermillod-Blondin *et al* 2004; Michaud *et al* 2006; Ieno *et al* 2006; Bulling *et al* 2010). However, total DIN fluxes to the overlying water can also decrease and become negative due to increased nitrification and denitrification within the sediment (Pelegri & Blackburn 1994; Pelegri *et al* 1994, 1995).

1.5.4 Benthic – pelagic sediment exchange

While sediment exchange is largely due to physical processes such as fluvial and marine deposition and physical erosion, ecosystem engineers make very important contributions to this and can vastly increase and decrease the deposition, accretion, resuspension and erosion of sediment (Widdows *et al* 2000, 2004; Widdows & Brinsley 2002; Wood & Widdows 2002). Broadly speaking, primary producers increase sediment stability and thereby accelerating progradation and primary consumers decrease sediment stability by increasing resuspension and erosion, thereby accelerating transgression (Paterson 1989; Daborn *et al* 1993; Daborn *et al* 1993; Jones & Jago 1993; Dyer 1994; Gerdol & Hughes 1994b; Paterson *et al* 1999, 2000; Tollhurst *et al* 1999, 2006; Christianson *et al* 2000; de Deckere *et al* 2000, 2001; Biles *et al* 2002; Maynard *et al* 2011). However, passive and active suspension feeders can also increase sediment accretion (Luckenbach 1986; Jones & Jago 1993; Murray *et al* 2002).

MPB organisms produce EPS, which binds sediment particles together and decreases its erodibility (Paterson 1989; Daborn *et al* 1993; Paterson *et al* 1999, 2000; Tollhurst *et al* 1999, 2006). However, in addition to the “armouring” the sediment against eroding water flow, EPS also increases the stickiness of the sediment thereby has the potential to increase sediment accretion (Lubarsky 2011). Marine grass beds tend to increase sediment accretion by slowing down flow rates in overlying water, thereby increasing particle deposition and their root systems help anchor accumulated sediment to prevent it being dragged back out to sea with the ebbing tide (Christianson *et al* 2000; Maynard *et al* 2011; Wilkie 2011). On the other hand grazers not only increase the erodibility of the sediment surface because they remove the biofilm but also by active resuspension (Daborn *et al* 1993; Jones & Jago 1993; Gerdol & Hughes 1994b; de Deckere *et al* 2000, 2001; Biles *et al* 2002). However, invertebrates who aggregate in beds above the sediment surface (eg. *M. edulis*, *Lanice conchilega*) act similarly to grasses in that they increase sediment accretion by reducing overlying water flow rates, remove particles from the water column, digest the organic content and deposit the remaining sediment particles on the sediment surface which, in the case of *M. edulis*, are anchored by byssus threads (Figure 1.9) (Jones & Jago 1993; Saurel 2008; Murray *et al* 2002). However, animal tubes can also have the opposite effect, i.e. they can increase erodibility of sediment depending on the density of the aggregation (Luckenbach 1986; Murray *et al* 2002).



Figure 1.9: Mussel mounds in the Eden central channel (with harbour seals and swans in the foreground).

1.6 Aims of this thesis

1. To determine whether *C. volutator* has significant engineering effects on the overlying water column which can modify resources to MPB and therefore affect MPB biomass and/or assemblage composition.

Chapter 3 (Experiment 1) hypotheses:

H₀3.1: *C. volutator* has no significant effect on the water column at any biomass.

H₀3.2: *C. volutator* has no significant effect on MPB biomass, locally or remotely.

H₀3.3: *C. volutator* has no significant effect on MPB assemblage composition, locally or remotely.

2. To determine whether macrofauna with different bioturbation and feeding modes (*C. volutator*, *H. diversicolor*, *M. baltica*) have similar engineering effects on the overlying water column and therefore differentially modify resources to MPB and thereby changing MPB biomass and/or assemblage composition.

Chapter 4 (Experiment 2) hypotheses:

H₀4.1: Bioturbation by *Corophium*, *Hediste*, and *Macoma* produces similar modifications to the overlying water column.

H₀4.2: *Corophium*, *Hediste*, and *Macoma* feeding and bioturbation only effects MPB biomass in the sediments in which they are present and cannot remotely affect MPB biomass remotely via resource modification in the water column.

H₀4.3: *Corophium*, *Hediste*, and *Macoma* feeding and bioturbation only effects MPB assemblage composition in the sediments in which they are present and cannot remotely affect MPB biomass remotely via resource modification in the water column.

H₀4.4: There is no relationship between MPB biomass and biodiversity.

3. To determine whether significant changes to the overlying water column can be achieved within a single immersion and how the effects therefore differentially modify resources to MPB and thereby changing MPB biomass and/or assemblage composition.

Chapter 5 (Experiment 3) hypotheses:

H₀5.1: Turbidity created by *Corophium* in one average tidal period is a simple proportion (6/168 h) of what is generated over a week.

H₀5.2: DIN release from sediment modified by *Corophium* in one average tidal period is a simple proportion (6/168 h) of what is released over a week.

H₀5.3: Phosphate release from sediment modified by *Corophium* in one average tidal period is a simple proportion (6/168 h) of what is released over a week.

H₀5.4: Surface compaction is not modified by *Corophium*.

4. To determine whether differences in water column turbidity can effect MPB migration and productivity.

Chapter 6 (Experiment 4) hypotheses:

H₀6.1: MPB bulk migration is triggered by changes in tidal state

H₀6.2: MPB bulk migration is triggered by changes in irradiance

H₀6.3: MPB productivity is negligible during emersion

Chapter 2: General Methods

Chapter 2: General Methods

2.1 The field site

The Eden estuary (Figure 2.1) was the source of all sediment, fauna and microphytobenthos for the experiments undertaken in this PhD project. It is a small estuary and lies just north of St Andrews, Fife, in southeast Scotland. Downstream of Guardbridge the estuary contains about 6.3 km² of sand- and mudflats along the central channel (average depth at high spring tide is 3 – 4 m, maximum depth of 9 m), small patches of salt marsh along the northern and southern mean high water line, mussel bed mounds along the central channel, as well as small eel grass beds dispersed across the estuary (Chocholek 2012). The Eden is a mesotidal, bar-built estuary with an average tidal range of about 3.3 m (Brown *et al* 1999; Chocholek 2012). As it is a bar-built estuary (see Chapter 1.2.1), most of the estuary (except the outermost region between the out head and Rere's Wood) is shallow with low flow rates and rarely experiences wave crash conditions. Sediment grain size and organic content generally change inversely to each other: the larger the grain size of the sediment the poorer it is in organic content. The general sediment trend in the Eden is of grain size decrease with distance from the coast and, therefore, a concomitant increase in organic content; however, there are patches of mud in sandy areas and as well as sandbanks located as far upstream as the Guardbridge due to local hydrological patterns. Salinities all along the estuary during immersion are more or less 33 – 35 psu, although porewater salinities can be substantially lower (at paper mill ~ 15 – 25 psu) but vary greatly over the tidal period and with rainfall. Unfortunately, there is no published information on the flow rates over the mudflats during immersion although they are expected to be low (Biles 2002).

Area in 2000 and because they are also a popular haul out site for common seals, *Phoca vitulina*, they are designated as a Special Area of Conservation (Scottish Natural Heritage 2006). SPAs and SACs are part of the Europe-wide 'Natura sites' threatened habitat and species protection scheme. Management of both sites are ultimately under Scottish Natural Heritage but they actually locally managed; the Eden estuary is managed by the Eden Estuary Management Committee which is a consortium made up of local government, surrounding land owners, and interest groups.

The outer Eden estuary (as presented in Figure 2.1) is flanked by golf course fairways and agricultural and pasture land on the south shore, has a paper mill and Guardbridge village on its western shore and RAF Leuchars airbase on its northern shore. Effluents from fertilized fairways, agricultural land and pastures, and the human populations are likely to increase nitrate and phosphate input into the estuary, and indeed most MPB blooms found in the Eden are seen along the rivulets of run-off or along the central channel at low tide (personal observation). Marine systems have been shown be limited by nitrates rather than phosphates and hence are far more sensitive to nitrate pollution (Ryther & Dunstan 1971). The 2005 report for the European Framework Water Directive (SEPA 2005) states that while direct discharge of effluent generally declined across the UK in the 1990s with improved sewage treatment (SEPA 2005), the Eden estuary had "exceptionally high" riverine nitrate concentrations but due to the low residence time and high dilution factor during immersion tide the Eden estuary (sediment and overlying water) is not classified as a "Nitrate Vulnerable Zone". The NVZ classification criteria are vague because nitrate pollution levels that are not as well studied and understood as phosphate pollution levels in freshwater; so NVZ assessment criteria are a combination of measured nitrate levels and observed possible primary and secondary response to nitrate increase (such as chlorophyll-a levels and dissolved oxygen levels, re-

spectively). In Scotland, only the Ythan estuary is classified as a NVZ although most large rivers and most of the East coast ground water is considered of NVZ status. The only other source of pollution (with the exception of noise pollution from the RAF base) to the Eden estuary is the Guardbridge paper mill which, while operational, had a treatment plant to mitigate residues, and shut down several years ago, prior to which it was only sporadically active for a several years. Paper mill effluent is a mixture of many substances (carbohydrates, lignins, organic acids, boiler ash, etc) whose presence in the water column reduces the photosynthetic output due to shading and whose bacterial breakdown increases the biochemical oxygen demand (BOD) and in the sediment and water column and results in overall depleted oxygen levels, and, in addition, they release to the chlorinated organic substances (AOX) which have been shown to be toxic to marine and freshwater life in many studies (Colodey and Wells 1992). While there are multiple studies on the damage to life due to working mills, the length of time taken for recovery from the sum of environmental impacts following mill closure is sketchy and largely unknown (Colodey and Wells 1992).



Figure 2.2: The two field sites used in this project: the Paper mill site (PM) on the north shore of the estuary (looking towards the shore) and the Guardbridge site (GB) on the southeast shore of the Eden estuary.

Experimental sediment and organisms were collected at two sites: the paper mill site, for experiments Chapters 3 – 5 and the Guardbridge site for experiments in Chapter 6 (labeled PM & GB, respectively, in Figure 2.2). The mid-shore at the paper mill site had a deep mud layer (~15 cm) covering rock and debris which is likely to have very high level of bioturbation as the light grey oxidised sediment layer was usually about 5 cm deep and was dominated by *Corophium volutator* with some *Nereis diversicolor* and *Macoma baltica* but hardly any *Hydrobia ulvae*. The midshore was very flat and MPB blooms were seen only in sporadic patches.

The low shore slopes quite steeply (4% incline) towards the central channel and, in the first 2 years of this project, was dominated by dark, rich MPB biofilms and had a sparse macrofauna population, and had a very thin (≤ 1 cm) pale layer covering black, sulphurous mud beneath. At the end of the summer 2009 these blooms on the lower shore ceased and have not been encountered in anything like their previous abundance since. Blooms are now more patchy and sporadic, although the oxidized sediment layer is still not as deep as on the flatter mid-shore. During immersion the mid shore is covered with approximately 2 - 3 m of turbid water (Chocholek 2012; personal observation). The Guardbridge site, on the southeast bank of the Eden has a very shallow, ≤ 3 cm, mud layer covering rocks and debris and interspersed with boulders and patches of *Fucus* sp. This site is dominated by *N. diversicolor*, with a moderate population of *H. ulvae* and very few *C. volutator*. MPB blooms are patchy and are visible first on top and around the bases of rocks (with < 2 mm layers of fine mud on them) and around the outlines *Fucus* patches and, later in the tide, along the exposed sediment. During immersion, the flow at this site is moderate and the water is calm, less than a meter deep, and quite clear.

2.2 Sediment sampling and characterisation

2.2.1 Sediment sampling

Macrofauna cores

Sediment cores (SA = 84 cm², depth = 15 cm) for macrofaunal biomass estimation in a 20 x 20 m quadrat at the paper mill site.

Contact cores

Contact cores are taken by inserting a bicompartamental stainless steel cup (Ford & Honeywill 2002) onto the sediment surface, pouring liquid nitrogen into the top compartment which then freezes the sediment in the bottom compartment (SA = 25 cm², depth = 2 mm).

Mini-cores

The tips were removed from plastic syringes with flat plastic plungers (Becton-Dickson Discardit™ II) to create mini-corers for sediment sampling for subsequent organic and inorganic content, chlorophyll-a extraction, microphytobenthic assemblage descriptions, or pore-water sampling (Table 2.1, 20, 2, 5, and 20 ml syringes, respectively).

Table 2.1: Sampling syringe sizes for sediment mini-cores

Syringe volume (mL)	Syringe diameter (mm)	Surface Area (mm ²)
20	20	314
5	12	113
2	8.5	57

2.2.2 Grain size

Grain size was determined by Coulter Counter LS20 which gives the percent distribution of particles in 92 bins (increasing in 10% increments) of particle diameters from 0.345 to 2000 µm. Particle diameter bins can be characterized either as clay (0.5 – 3.9 µm), silt (3.9 – 62.5 µm), or sand (62.5 – 2000 µm) accord-

ing to the Wentworth scale (Wentworth 1922). Percent volume in each bin was summarized to the total percentage of clay, silt, and sand in the sediment, although it should be noted that as all sediments were sifted through a 500 mesh to remove macrofauna prior to all experiments so the largest sand particle could only be 500 μm (or medium sand).

2.2.3 Sediment organic and inorganic content

To determine the water and organic content of sediment a sample was collected, usually, with a known surface area and, preferably, with a starting weight of at least 2g). The sample was weighed (wet weight), dried either by freeze drier (≥ 12 h) or oven (≥ 48 h at $\sim 60^\circ\text{C}$), reweighed (dry weight), combusted in a muffle furnace (≥ 12 h at 450°C), and reweighed (ash-free dry weight). Water and organic contents are calculated equations 2.1 and 2.2, respectively.

$$\text{water content} = \frac{\text{wet wt} - \text{dry wt}}{\text{wet wt}} * 100$$

Equation 2.1

$$\text{organic content} = \frac{\text{dry wt} - \text{ashfree dry wt}}{\text{dry wt}} * 100$$

Equation 2.2

These proportions can then be used to calculate the water or organic content per area sediment. This protocol follows standardized methods from HIMOM (2005).

2.3 Nutrients

Nutrient analysis was performed with a FIA star 5010 analyser by Analytical Services, University of Aberdeen, Scotland. Water column samples were fil-

tered through a 0.45 μm syringe filter (Nalgene) and all samples were immediately stored at -80°C . All samples were analysed for nitrogen from ammonium ions ($\text{NH}_4^+\text{-N}$), nitrogen from combined nitrate and nitrite ($\text{NO}_x^-\text{-N}$), and phosphorous from orthophosphate ($\text{PO}_4^{3-}\text{-P}$). Silicate analysis was not possible. Spectrophotometer readings were translated to parts per million (ppm) by comparison to a calibration with standard solutions with the salinities at the same level as the samples being measured. A standard was run after every tenth sample to account for machine drift. The ppm is then recalculated as to $\mu\text{g L}^{-1}$, $\mu\text{mol L}^{-1}$, or $\mu\text{mol hr}^{-1} \text{m}^{-2}$ for comparison with the literature.

2.4 Measuring microphytobenthic biomass

Microphytobenthic biomass in a surface area can be enumerated as a count of cells per surface area and a protocol for such a count was described by Eaton and Moss (1966). However, this is laborious and not time efficient for large numbers of samples even with their suction method it is impossible to know whether the same depth of sediment is sampled over a range of samples. As all microphytobenthic organisms contain chlorophyll-*a*, chlorophyll-*a* content is generally used as a proxy for photosynthetic biomass. Chlorophyll-*a* content can be measured in a variety of ways but in this thesis chlorophyll-*a* content per volume of sediment is estimated by acetone extraction followed by spectrophotometric measurement, and comparative chlorophyll-*a* content at the sediment surface is measured by the proxy of chlorophyll-*a* fluorescence (Serôdio *et al* 2001; Honeywill 2002).

2.4.1 Chlorophyll-*a* quantification by acetone extraction and spectrophotometry

Chlorophyll-*a* was extracted from sediment cores with a known surface area and depth following the protocol described in “Chapter 20: Pigment analysis using Spectrophotometry” in HIMOM (2005) and the procedure was conducted under minimum possible light conditions to avoid pigment degradation during

processing. Sediment samples were weighed (wet weight), freeze-dried overnight to facilitate cell lysis, and reweighed (dry weight). A recorded weight (3 - 5 mg) of the ground-up freeze-dried sample was deposited in an amber 1.5 ml eppendorf tubes and vortexed with 1.5 ml of 90% acetone as the pigment extractant. Following sonication in seawater for 90 minutes, to further separate pigment from cells and sediment, the samples were thoroughly mixed and stored at -80°C for 2 days (thoroughly mixing each day). Samples were removed from the freezer, thoroughly shaken one last time, and then centrifuged to separate the sediment from the acetone. The acetone from each sample was poured into a quartz cuvette and placed in a spectrophotometer (Biomate 5, Thermo Fisher Scientific Inc) and absorbance measured at four wavelengths (λ = 750, 664, 647, 630). Absorbances at each wavelength was used to calculate chlorophyll-*a* g^{-1} sediment using Equation 2.3

$$chl a \ g^{-1} = \frac{(11.85 * (E_{664} - E_{750}) - 1.54 * (E_{647} - E_{750}) - 0.08 * (E_{630} - E_{750})) * V_e}{X}$$

Equation 2.3

where

$E_{664}, E_{750}, E_{647}, E_{630}$ = absorbances at $\lambda_{664}, \lambda_{750}, \lambda_{647}, \lambda_{630}$

X = weight of the sample (g)

V_e = the extraction volume (ml)

As it is usually more intuitively useful to have a biomass per unit area of sediment, the quantity of chlorophyll-*a* per gram of sediment is transformed to a quantity of chlorophyll-*a* per square meter by Equation 2.4.

$$\text{Chl}a (\text{mg m}^{-2}) = \frac{\text{chl}a(\mu\text{g})}{g} * \frac{A}{B} * \frac{1}{1000}$$

Equation 2.4

where,

Chl-*a* = in the sediment sample (μg/g) from Equation 2.3

A = the dry weight of the whole core (in g)

B = surface area of the whole core (in m²)

2.4.2 Chlorophyll-*a* estimation by fluorescence proxy

A second method of estimating biomass is by using the emission of low energy photons by photosystem I and II of chloroplasts under illumination.

2.4.2.1 A brief summary of photosynthesis

By the process of photosynthesis, chloroplasts are able to harness the sun's energy to strip protons and electrons from water molecules (hydrolysis) to use them to reduce inorganic carbon CO₂ to organic carbon molecules (e.g. glucose C₆H₁₂O₆), generating O₂ as a waste product (summarized in Table 2.2 and Figure 2.3).

The process occurs in two separate steps: the cascade of reactions required to convert light energy into chemical bond energy (ATP, NADPH-H⁺) are jointly known the light-dependent (or just 'light') reactions (Equation 2.6) and the reactions involved in the reduction of CO₂ to a 3-Carbon sugar (and ultimately the 6C sugar glucose) are the light-independent (or 'dark') reactions. Chemical notation for photosynthesis (Equation 2.5), the light reaction (Equation 2.5), and the dark reaction (Equation 2.7) are given below (Stöcker & Dietrich 1996).

Table 2.2: The main reactions in the light and dark phases (colour coded in the left hand column) of photosynthesis (summarised from Whitmarsh & Govindjee 1999 and Falkowski & Raven 1999)

Phase	Reaction	Structures	Description
	1. Photon harvest at PSII	Antenna complex, stroma side of PSII, PSII-Rx Ctr	Light strikes the PSII antenna complex and a photon is eventually passed down to a particular chlorophyll-a molecule in the PSII-Rx Ctr called P680 which boosts $1e^-$ in its orbit to a higher energy level P680 \rightarrow P680*
	2. Photonic oxidation of water	Oxygen Evolving Complex, lumenal side of PSII-Rx Ctr	Water is oxidized by the 4Mn 'oxygen evolving complex' as it is oxidized by photon: $2H_2O \rightarrow 4H^+ + 4e^- + O_2$ The H^+ ions remain on the lumenal side of PSII. The $2e^-$ oxidize tyrosine (Y_z)
	3. Charge separation	PSII-Rx Ctr	The P680* almost instantly loses its electron to Pheophytin creating P680⁺/Pheo⁻ .
	4. Production of ATP		
	4a. Replacement of P680 e^-	PSII-Rx Ctr	The missing electron at P680 is replaced by one from Y_z (P680 is reduced).
	4b. PQ oxidizes Pheo ⁻	PSII-Rx Ctr	A quinone (Q_A) molecule binds the e^- from Pheo ⁻ and transfers it to another plastoquinone molecule (PQ_B) which can bind $2e^-$. Once PQ_B has $2e^-$, it picks up $2H^+$ molecules at the stroma and the reduced molecule (PQH_2) disengages from the PSII-Rx Ctr and floats freely in the intermembrane space until it encounters a PSII binding site.
	4c. PQ_B transfers $2e^-$ to Cyt-bf	Cyt-bf, lumenal side	PQH_2 encounters a binding site on the lumenal side of Cyt-bf in the intermembrane space and is oxidized by a FeS compound. The loss of the $2e^-$ releases the $2H^+$ into the lumenal side of the thylakoid membrane, and releases PQ from the binding site.
	4d. Electrochemical gradient	Lipid bilayer	H^+ build up in lumen from oxidized H_2O & PQH_2 creates electrochemical gradient (lumenal side $pH \approx 6$, stroma side $pH \approx 8$) across the thylakoid membrane.
	4e. $ADP + P \rightarrow ATP$	ATP Synthase	Passive H^+ flow from lumen to stroma through ATP Synthase releases enough energy for ATP Synthase to catalyse the reaction: $ADP + P \rightarrow ATP$.
	5. Production of NADPH-H^+		
	5a. Photon harvest at PSI	Antenna complex, stroma side of PSI	Light strikes the antenna complex of PSI and when it reaches chlorophyll-a pigment P700 in PSI-Rx Ctr it boosts an $1e^-$ up to a much higher energy level P700 \rightarrow P700*
	5b. Redox series	PSI-Rx Ctr	The high energy e^- from P700 is passed in a series of reduction-oxidation reactions from P700 $\rightarrow A_0 \rightarrow A_1 \rightarrow FeSx \rightarrow FeSa \rightarrow FeSb \rightarrow$ Ferredoxin (Fd)
	5c. Replacement of P700 e^-	PSI-Rx Ctr	The e^- lost from P700 is replaced by the e^- (released from P680*) that has transferred from Cyt-bf to PSI-Rx Ctr by the molecule plastocyanine (PC).
	5d. $NADP^+ + 2H^+ \rightarrow NADPH-H^+$	PSI-Rx Ctr	The e^- from P700* is carried by Ferredoxin to an enzyme called Ferredoxin-NADP ⁺ Reductase (FNR) which catalyses the reaction $NADP^+ + 2H^+ \rightarrow NADPH-H^+$ using the energy released from the e^- once it is bound to $NADP^+$.
	6. Reduction of $CO_2 \rightarrow G3P$		
	6a. CO_2 bound to RuBP	Stroma	The enzyme Rubisco binds a CO_2 molecule to a pre-existing 5C sugar (ribulose biphosphate, RuBP) creating a 6C sugar which immediately splits into 2 x 3C sugars (3-Phosphoglycerate)
	6b. G3P formed	Stroma	The newly formed 3C sugar is phosphorylated by an ATP (1,3-Bisphosphoglycerate) and then reduced by NADPH to Glyceraldehyde-3-phosphate (G3P).
	6c. Regeneration of RuBP	Stroma	The Calvin cycle begins with a 5C sugar so only 1 out every 6 CO_2 molecules fixed becomes a net gained G3P, the other 5 requires 3 ATPs to be reduced back to RuBP.

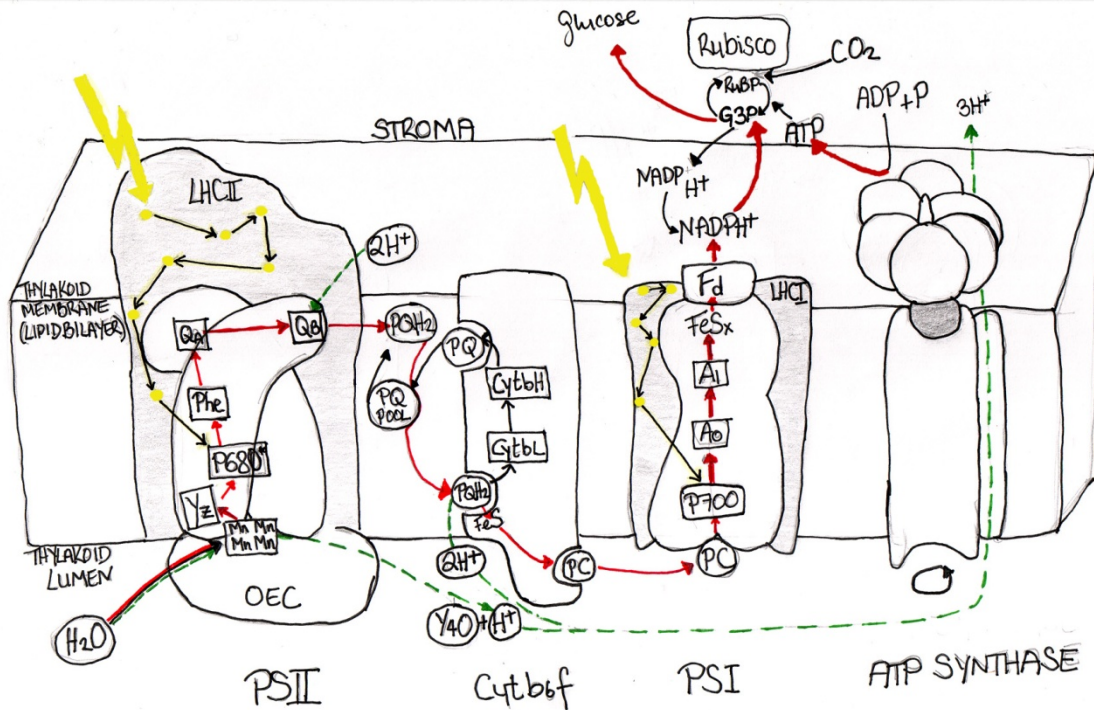
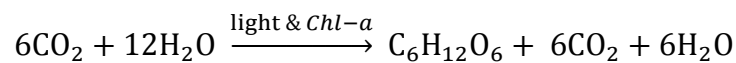
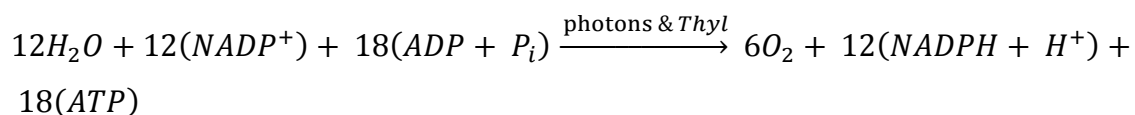


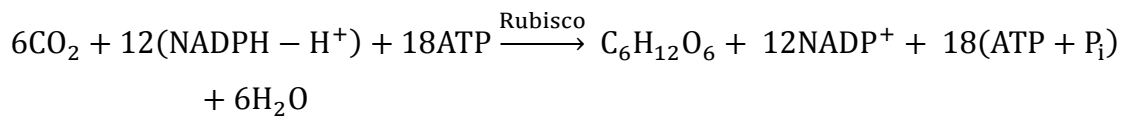
Figure 2.3: A schematic of the thylakoid membrane showing all the major macromolecules and processes in photosynthesis (redrawn from Falkowski & Raven 2007, Whitmarsh & Govindjee 1999, and Allen *et al* 2011). Photons are in yellow, electron paths are in drawn in red and H^+ paths are in green. Photosystem II (PSII) comprised of the light harvesting complex (LHCII), a reaction center, and the oxygen-evolving-complex (OEC). Chlorophyll P680 (charge separation site); Pheophytin-*a* (Pheo); first quinone electron acceptor (Q_A); second quinone electron acceptor (Q_B); plastoquinone (PQ) and reduced (PQH_2) from the PQ pool; Cytochrome-*b/f* (Cyt-*bf*); plastocyanin (PC); photosystem I (PSI) comprised of a, light harvesting complex (LHCI) and a reaction centre with chlorophyll P700 site of charge separation; electron acceptors in PSI: A_0 , A_1 , FeS, ferredoxin (Fd); Rubisco, which catalyses the synthesis of a 3C sugar (G3P) from CO_2 and ribulose-1,5-bisphosphate (RuBP) using light reaction energy stored in NADPH and ATP molecules.



Equation 2.5



Equation 2.6

**Equation 2.7**

The apparatus involved in the light and dark reactions are the vesicular thylakoid membrane and the enzyme Rubisco, respectively, both found in chloroplast. They are very similar across cyanobacteria, photosynthetic protists (including diatoms), and plants because all eukaryotic photosynthetic organisms are presumed to have arisen from a single oxygenically photosynthesizing cyanobacterial ancestor (Falkowski & Raven 2007; Martin *et al* 2003; Yoon *et al* 2004; Armbrust 2009). Inside the chloroplast, stacks of thylakoid vesicles are surrounded by fluid, stroma, in which the enzymatic reactions catalysed by the enzyme Rubisco take place. The membranes of the thylakoid vesicles have a lipid bilayer membrane studded with an extraordinary and unique compliment of macroproteins which enables a non-cyclic electron transport chain (ETC) of the photosynthetic light reactions (Figure 2.3). All photosynthetic organisms use photopigments to transform radiation in the visible light range of 400 – 700 nm wavelengths into electrical potential energy in the form of ATP and NADPH⁺-H; hence this range of wavelengths is referred to as ‘photosynthetically active radiation’ (PAR) and is measured in $\mu\text{mol PAR photons m}^{-2} \text{ s}^{-1}$. Different photopigments are capable of absorbing light quanta of different energies (expressed in wavelengths): chlorophylls absorb energy between 400 – 500 nm and 630 – 700 nm, carotenes absorb energy between 440 – 500 nm and phycobiliproteins can absorb energy between 500 – 580 nm.

Photorespiration and chlororespiration are deviations from the normal photosynthetic pathway. Photorespiration occurs when, in high light conditions, the system is limited by CO₂ depletion and Rubisco begins to bind O₂ instead of CO₂ to RuBP.

This alternate pathway uses up O_2 and produces CO_2 without generating any ATP or 3C compounds that can make sugar or regenerate RuBP. It is considered an evolutionary legacy as Rubisco evolved when there was hardly any O_2 and high CO_2 in the atmosphere so no affinity preferences evolved in the molecule (Campbell & Reece 2005). Chlororespiration is defined as a respiratory ETC taking place within the photosynthetic ETC machinery (Peletier & Cournac 2002). The first model was proposed by Bennoun in 1982 because of two observations that were contrary to the standard photosynthetic model: (1) Transmembrane potentials detected in darkness, and (2) changes in the redox state of the PQ pool detected in darkness (Bennoun 2002). It has since been established that PQ from the PQ pool is reduced by NADPH- H^+ in the stroma and is then re-oxidized by O_2 in the thylakoid lumen (Peltier & Cournac 2002). Chlororespiration is especially important because it commonly occurs in estuarine biofilms (Serôdio *et al* 2005) and interferes with one of the most important fluorescence measurements for estimating productivity (see below).

2.4.2.2 Fluorescence, non-photochemical quenching (NPQ), photoinhibition and photoacclimation

Because pigments are light sensitive, they must have means of channelling light energy or they are damaged by it (Consalvey *et al* 2005). Energy not carried away by non-cyclic electron transport must be dissipated in some other way. So in addition to photosynthesis, there are three other ways by which pigment molecules can dissipate energy: by emitting low-energy photons (predominantly from PSII), which is known as fluorescence, by passing energy to other molecules, and by vibration (energy released as heat) (Consalvey *et al* 2005). These pathways are competitive so an increase in energy dissipation by one pathway means a proportional

decrease by the other pathways (Consalvey *et al* 2005). Of these, fluorescence is the most easily measurable response.

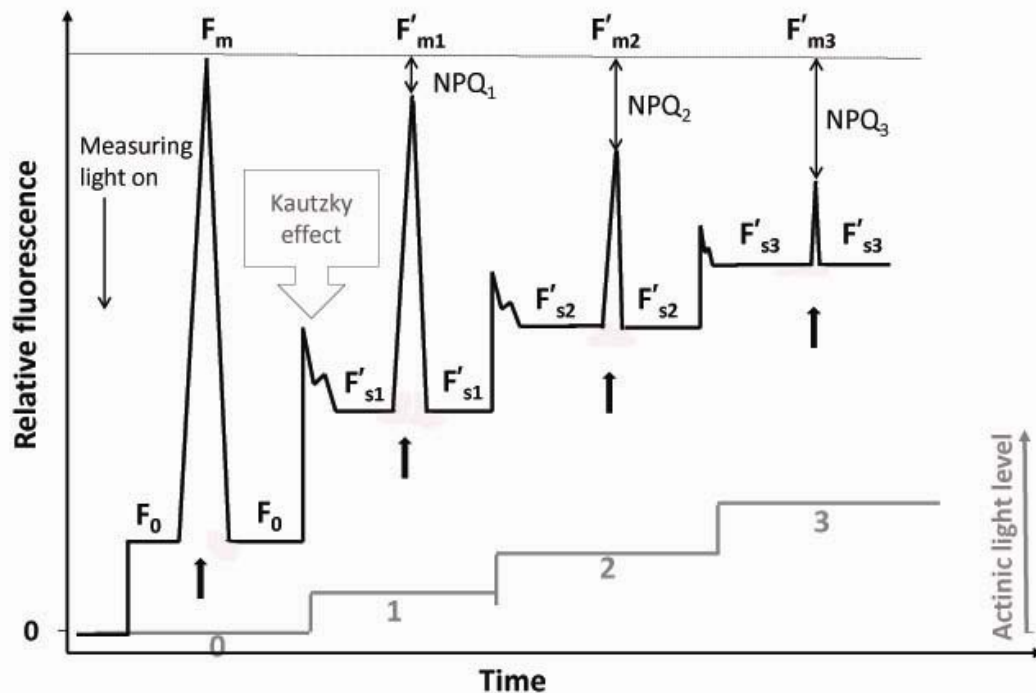


Figure 2.4: Schematic of fluorescence measurements (redrawn from Consalvey *et al* 2005). Actinic light steps are represented in grey and the thick black arrows represent a 'saturating' flash of light which closes all reaction centres.

Non-cyclical electron flow rates are limited by the number of PSII reaction centers available to receive a photons; once PSII has been oxidized by a photon it cannot receive another photon until Q_A has been re-oxidized by Q_B (this is thought to be the rate limiting step) and the reaction centre is 'closed' (Maxwell & Johnson 2000; Consalvey *et al* 2005). In the dark, all the reaction centers are 'open' but as soon as the material is illuminated with actinic light and photons start striking the reaction centers and they begin to close which causes a concurrent increase in fluorescence emission which rapidly peaks but eventually decreases and reaches a steady state

which is designated F_s (see Figure 2.4) as equilibrium is reached between the different routes of energy dissipation (Maxwell & Johnson 2000; Consalvey *et al* 2005). The change in fluorescence at steady PAR was first described by Kautzky and co-workers in 1960 (Maxwell & Johnson 2000) and, in fluorescence terms, steady state fluorescence (F_s) occurs when the quenching of fluorescence by competition with the other energy pathways, photochemical (pQ) and non-photochemical (NPQ) quenching, and eventually, reaches equilibrium. NPQ is in effect an expression of a combination of the last two energetic pathways, energy is passed to a nearby pigments and dissipating it as heat (Maxwell & Johnson 2000; Consalvey *et al* 2005). NPQ is carried out by specialized pigments in the LHCs called xanthophylls (Falkowski & Raven 2007). Xanthophylls are carotenoid pigments and have various forms which can be interconverted by means of epoxidation/de-epoxidation. When diatoms are exposed to high light, the decrease in pH in the luminal thylakoid triggers the de-epoxidation of the epoxidated form, diadinoxanthin (DD), into diatoxanthin (DT) which has a higher capacity to lose energy by heat (Lavaud & Kroth 2006, Falkowski & Raven 2007). Whereas normally carotenoid pigments pass energy to chlorophyll-*a*, high pH gradients across the thylakoid membrane (by the build up of H^+ on the luminal side of the thylakoid membrane during non-cyclic electron transport), photons are diverted to the de-epoxidated carotenoid forms which effectively reduces its absorptive cross section for photosynthesis (Lavaud & Kroth 2006; Falkowski & Raven 2007).

Photosynthetic response to changing light levels is described by a P-E curves (photosynthesis-energy, or photosynthesis-irradiance, P-I, curve, Figure 2.5). When the actinic light level increases, energy removal through all synthetic pathways also increases. The initial slope is linear (α) but becomes asymptotic as a maximum photosynthetic rate (P_{max}) is reached at a saturating light level (E_s).

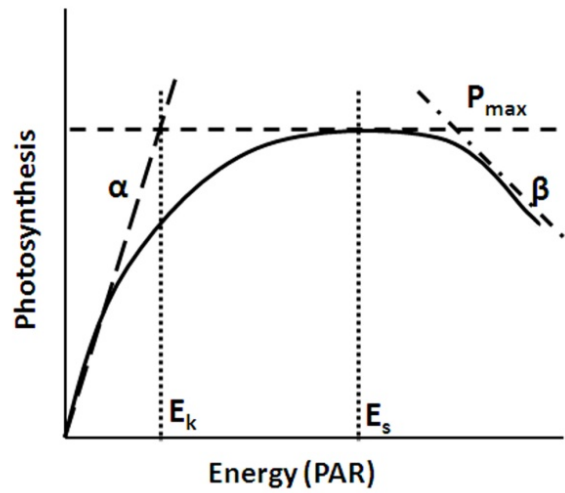


Figure 2.5: A photosynthesis-energy curve with photosynthetic parameters: α is the initial linear, rate of increase, P_{\max} is a maximum photosynthetic rates, E_k and E_s are both measures of the irradiance, β is the rate of photoinhibition (redrawn from Consalvey *et al* 2005).

At this point light level where the linear slope ceases (E_k) the two other energy pathways begin to outcompete the photosynthetic pathway, and if light levels continue to increase beyond E_s , then energy dissipated by the photosynthetic pathway actually begins to decrease and this is known as photoinhibition (β). Eilers & Peeters (1988) defined a model that expresses photosynthetic output as a proportion of light intensity using a set of 3 parameters (a , b , c). These three parameters cannot be solved for analytically. Hence, the photosynthetic rate curve (Figure 2.5) can only be estimated statistically by applying the model (Equation 2.8) to empirical data (measured efficiency at known light intensity), which allows calculation of the photosynthetic parameters by according to Equations 2.9 – 2.11 (Eilers & Peeters 1988).

$$rETR = \frac{E}{(a * E^2) + (b * E) + c}$$

Equation 2.8

Where,

rETR = relative electron transport rate

$E = \mu\text{mol PAR m}^{-2} \text{ s}^{-1}$

a, b, c = photosynthetic parameters

$$ETR_{max} = \frac{1}{b + (2 * \sqrt{a * c})}$$

Equation 2.9

$$\alpha = \frac{1}{c}$$

Equation 2.10

$$E_k = \frac{ETR_{max}}{\alpha}$$

Equation 2.11

The photosynthetic parameters of interest are: maximum photosynthetic rate (ETR_{max} , Equation 2.9), the initial (linear) rate of increased photosynthesis per unit light (α , Equation 2.10), and the light energy at the maximum point of linear gradient (E_k , Equation 2.11).

Photoinhibition can be caused by CO_2 or nutrient limitation but can also be caused when NPQ takes over as an energy dissipation pathway when irradiances are very high (Maxwell & Johnson 2000; Consalvey *et al* 2005). In conditions of prolonged high irradiance PSFs become ‘photoacclimated’ which is a long term acclimation to irradiance by a change in photopigments expressed in the LHCs (Falkowski & Raven 2007). However, the term is also used to describe adjustments made by MPB within a biofilm (NPQ or vertical migration) in response to light levels during a 3 – 5 minute rapid light curve (Perkins *et al* 2006). If irradiance persists at levels that

cannot be dissipated by NPQ or migration, photodamage can occur where highly reactive singlet oxygen is formed and damages molecules in the thylakoid membrane (Consalvey *et al* 2005).

Photosynthetic rate can be measured by photosynthetic products, organic carbon and oxygen, or by proxy of fluorescence and methodologies have been reviewed by Underwood and Kromkamp (1999). Measurement of organic carbon production are made by ^{14}C isotope from a sediment slurry and, therefore, the sediment cannot be studied in situ, and must be sampled destructively to extract organic ^{14}C compounds. O_2 production can be measured in situ and non-destructively by microelectrode (Glud 2008). However, the O_2 profiles are quite time consuming, and microelectrodes are extremely delicate making them difficult to use for inexperienced users. Fluorescence measurements on the other hand are extremely rapid and easily carried out regardless of environment.

2.4.2.3 Fluorescence measurements and calculation of photosynthetic parameters

Fluorescence accounts for less than 5% of the absorbed light and is mostly (> 95%) emitted from the antenna complex of PSII rather than PSI (Krause & Weis 1991). As there can be no fluorescence without a light input but actinic light 'closes' reaction centres, the 'measuring beam' of a fluorometer gives off a very low intensity (<1 $\mu\text{mol PAR m}^{-2} \text{s}^{-1}$) high frequency modulated signal, which allows measurement of the returned fluorescence only from its own signal, i.e. it can filter out the fluorescence from any other light sources. The minimum amount of fluorescence that can be measured, F_0 , is the returned fluorescence from the measuring beam in the absence of actinic light (FMS2 & Diving-PAM manuals). Traditionally dark adapted samples (all reaction centres open) are used for this measurement and it has been shown to correlate well to actual chlorophyll-a abundance in the sedi-

ment over a variety of temperatures, pHs and irradiances (Serôdio *et al* 1997; Honeywill 2002) and so are generally used as a biomass indicator. Photic depths (of downwelling light) of intertidal muddy sediments have been variously estimated at 0.27 mm (Serôdio *et al* 1997) and 0.4 mm (Consalvey 2002). Upwelling distance of fluorescence from photosynthetic cells has been estimated at 0.15 mm (Kromkamp *et al* 1998). Although there is obviously uncertainty around the actual depth of measurement fluorescence signal is measuring in each biofilm, it is clearly only the biomass that is at the very surface of sediment that is being included in the measurement. Hence F_0 is regarded as a relative measure of 'photosynthetically active biomass' (PAB) or 'productive biomass', as cells migrate to the surface to photosynthesize (Guarini *et al* 2000a, 2000b, Serôdio *et al* 2001).

Following F_0 measurement, the maximum fluorescence, F_m , is the fluorescence detected when all the reaction centres are closed due to the application of a saturating flash (generally $> 6000 \mu\text{mol photons m}^{-2} \text{s}^{-1}$). Krause and Weis (1991) estimated that F_0 and F_m emit about 0.6 % and 3 % of absorbed light. Variable fluorescence, F_v , is the difference between the maximum and minimum fluorescence and the scaled difference, F_v/F_m , is used as an indicator of the maximum efficiency with which PSII converts light into chemical energy (Genty *et al* 1989).

$$\text{PSII max. efficiency} = \frac{F_m - F_0}{F_m} = \frac{F_v}{F_m}$$

Equation 2.12

Variable fluorescence is greatest in the absence of actinic light because it is when F_0 is at its lowest and F_m is at its highest (Figure 2.4), as the probability of a photon reaching an open reaction centre is maximized. Once the sample is exposed to actinic light, some of the reaction centres start to close so more energy is expended as fluorescence and the fluorescence signal, F' , rises and falls and eventually reaches a

stable state, F_s , that is higher than F' (see Figure 2.4). Another fluorescence measurement is made during another saturating pulse and F'_m , is slightly lower than the first because some PSII units are already closed. This efficiency, F'_v/F'_m (or $\Delta F/F'_m$), is the actual photosynthetic efficiency at a particular actinic light level and can be multiplied by ambient PAR/2 ($\mu\text{mol m}^{-2}\text{s}^{-1}$) to estimate electron transport rate, ETR, or relative electron transport rate, rETR (Consalvey *et al* 2005).

$$\text{PSII efficiency at PAR}_x = \frac{F'_m - F'}{F'_m} = \frac{F'_v}{F'_m} = \frac{\Delta F}{F'_m}$$

Equation 2.13

$$\text{ETR} = \frac{\Delta F}{F'_m} * \frac{\text{PAR}}{2} * a$$

Equation 2.14

$$\text{rETR} = \frac{\Delta F}{F'_m} * \frac{\text{PAR}}{2}$$

Equation 2.15

If the coefficient of light absorption ($\text{m}^2 \mu\text{g chl-a}^{-1}$), a , is known then ETR can be turned into an absolute measurement of photosynthetic rate ($\mu\text{mol e}^- (\text{mg chl-a})^{-1} \text{s}^{-1}$) but because it is difficult to determine in a benthic biofilm (Perkins 2002a, Consalvey *et al* 2005) it is usually omitted and only rETR is calculated, which can only be used as a comparative measure. Half the light input is used as only PSII is involved in fluorescence measurements and the other half of the light is presumably absorbed by PSI.

F'_m is expected to be lower than F_m due to NPQ and increases with increasing actinic light levels (Maxwell & Johnson 2000; Consalvey *et al* 2005) (Figure 2.4). However, this is not always the case in MPB biofilms where F'_m at low light levels (~ 5% of ambient) is often higher than F_m due to the onset of chlororespiration in the dark (Bennoun 2002; Serôdio *et al* 2005). Due to F' being higher than F_0 and F'_m being lower than F_m , photosynthetic efficiency of PSII decreases with increasing light levels (Maxwell & Johnson 2000; Consalvey *et al* 2005). A rapid light curve (RLC) is a series of $\Delta F / F'_m$ measurements made at increasing actinic light levels applied by the fluorometer; it can be made with prior dark adaptation, in which case the first measurement is F_v / F_m (the maximum efficiency), or without prior dark adaptation. The efficiencies can be used to calculate rETR (Equation 2.15). Finally, the rate of NPQ at increasing light steps can also be calculated from RLCs (Equation 2.16).

$$\text{NPQ} = \frac{F_m - F'_m}{F'_m}$$

Equation 2.16

2.4.2.4 Fluorometers

All fluorescence measurements in this thesis were made with either an FMS2 (Hansatech Ltd, UK) or a Diving-PAM (Heinz Walz GmbH, Germany) fluorometer both of which both use a multiple turnover flash method. The FMS2 has a blue measuring light, $\lambda = 470$ nm, which considered optimal for diatom dominated biofilms (Yentsch & Yentsch 1979; Honeywill *et al* 2002) and the Diving-PAM has an amber measuring light, $\lambda = 650$ nm. The Diving-PAM requires calibration against 0 fluorescence standard (clean aluminium foil on the lab bench) and it subtracts the measured value, i.e. “noise”, from its subsequent measurements. It has a threshold of 130 below which Walz warns there is increased uncertainty and increased likelihood of overestimating efficiency. In the FMS2, measurements on any non-

photosynthesizing surface or even in mid-air are always 0, so do not require ‘zeroing’; nevertheless F' of F_0 measurements below 100 are considered to have increased uncertainty and while they can still be used to compare surface biomasses they should not be used to compare efficiencies or rETRs (Honeywill 2001; Mouget & Tremblin 2011). Fluorescence measurements lower than 130 or 100, in PAM and FMS2, respectively, can be used to compare surface biomass but should not be used to track efficiency changes (Mouget 2011, personal communication).’

Measurement with the FMS2 follows Honeywill (2001): covers approximately 120 mm² of sediment and is measured at a distance of 4 mm from the surface (using a “foot” as described by Honeywill 2001) with FMS2 settings of gain 99, modulation frequency level 3 (32 x 1.8 μ s measurements averaged for one data point), minimum fluorescence duration 2.8s, saturation intensity level 100 ($\sim 6900 \mu\text{mol m}^{-2} \text{s}^{-1}$) and saturation intensity pulse width of 1.0 s. Measurements were made following 10 minutes of low light adaptation.

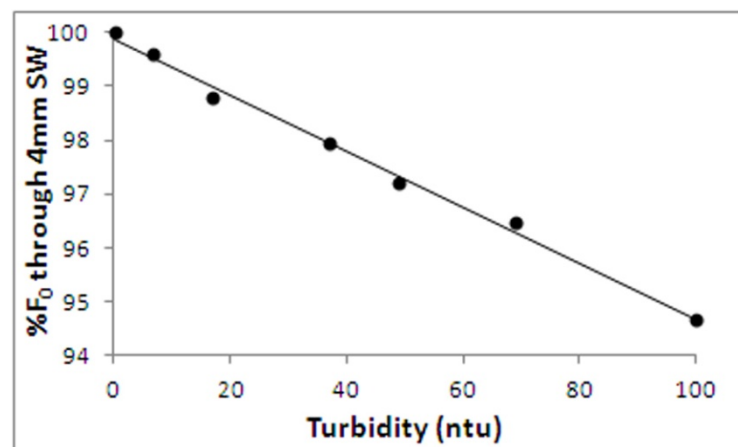


Figure 2.6: Calibration of signal loss (%) in FMS2 F_0 over 4mm over a range of turbidities ($y = -0.05x + 100$, $R^2 = 0.992$)

As measurements on sediment with the FMS2 made with the through an overlying water column of varying turbidity, the effect of water column turbidity on F_0 was

measured using calibration solutions, made up with seawater and mud from the PM site ($100\% < 63\mu\text{m}$ particle diameter), to 0.35, 7, 17, 37, 49, 69, and 100 ntu (Figure 2.6).

2.4.2.5 Limitations of fluorescence

The benefits of fluorescence measurements are clear: fast, multiple measurements on intact biofilms means that a high number of replicate measurements can be made within samples and across samples. Being able to make repeated measurement within a sample not only allows for observation of change within the same biofilm but can also reduce the number of replicate biofilms required per treatment (as long as repeated measurements are accounted for statistically). However, there are also problems associated with fluorescence measurements that need to be borne in mind when discussing fluorescence data.

1. O_2 or ^{14}C measurements give empirical values of photosynthetic biomass and so can be compared across studies whereas F_0 only gives a relative values and can only used to compare biofilms within a study. F_0 can be only be used to elucidate patterns in surface biomass according to measurement time or treatments. Efficiencies and rETRs can, however, can usually be compared across studies.
2. Different sediments have different light transmission depths (*Serôdio et al* 1997; Consalvey 2002; Kromkamp *et al* 1998) due sediment characteristics such as grain size, water and organic content (*Consalvey et al* 2005). Light penetration (actinic and measuring light) depth measurement is not a straight forward and is, therefore, not carried out routinely as part of most fluorescence studies. So again, there is probably variation in the actual sediment volume measured between samples and certainly between studies,

whereas biomass estimations made from extractions are made from known volumes of sediments.

3. Similarly, the stratification of biomass within the sediment is usually unknown and the weakness of the measuring light results in under estimation of biomass, F_0 , at the lower sediment levels (Serôdio *et al* 2001) but not during F_m measurements, as the saturating light is much higher up- and downwelling, meaning that efficiencies, F_v/F_m or $\Delta F/F'_m$ are overestimated (Perkins *et al* 2011 and references therein).
4. Migration is a major adaptation to light levels (Perkins *et al* 2010) and interferes with standard fluorescence measurements that were designed for higher plants with fixed chloroplasts. Migration can occur during both dark adaptation (Jesus *et al* 2006) and during a RLC (Perkins 2006) and hence both biomass and photosynthetic parameters, derived from P-E curve fit following Eilers & Peeters (1988), can be over- or underestimated depending on the direction of migration. In addition, it means that F_s (Figure 6.4) cannot be achieved during a light curve so rapid light curves, with 10 – 60 seconds instead of 5 – 15 minute light steps and F' instead of F_s , are generally used to establish photosynthetic parameters in MPB biofilms.
5. Serôdio and colleagues (2005) demonstrated that F'_m can actually be higher than F_m due to NPQ that persists in darkness less so in low light conditions. For this reason and because of migratory responses to light, Jesus and colleagues (2006) recommended low light adaptation for 5 minutes rather than the more traditional 15 minute dark adaptation. However, actual PAR meant by 'low light' conditions will vary depending on ambient levels the biofilms are acclimated to; in the Serôdio study low light meant 125 – 250 $\mu\text{mol m}^{-2} \text{s}^{-1}$, which is quite a high light level but probably low by Tagus es-

tuary standards, but Jesus *et al* (2006) defined low light as 5 % of ambient light.

2.5 Microphytobenthic assemblage description

2.5.1 Sampling

Lens tissue or syringe core samples were immediately fixed in a 4% glutaraldehyde in seawater solution. The lens tissue method follows the HIMOM (2005) protocol 26 which is modified from Eaton & Moss (1966): 2 sheets of lens tissue are placed on top of each other on the sediment surface and left for 2 - 6 hours to collect epipelagic diatoms as they migrate upwards, the top sheet is then collected and fixed in glutaraldehyde solution. The lens tissue method is useful as it means sampling from a known surface area and most of what is collected in the top sheet is live, unless the top sheet becomes completely saturated and diatoms are drawn up by capillary action. However, this sampling method is biased towards epipelagic diatoms which are the most migratory. A syringe core collects all of the sediment in a certain volume and therefore indiscriminately collects the entire assemblage, epipelagic and epipsammic, live and dead cells.

2.5.2 Fixed “live” assemblages

Fixed samples were diluted 9:1 in filtered water to allow penetration of microscope illumination and then 300 cells or colonies (for cyanobacteria) were counted, and the proportion of live to dead diatom frustules calculated (cyanobacteria are only seen live). For Chapter 3 samples were examined under Leitz large universal research light microscope under a 40x lens (400x magnification, bright field) and for Chapter 4 and 6 samples were examined under a 63x lens with a 1.25x optivar (788x magnification, phase 2). As identification of species according to most of the literature requires acid cleaned frustules in order to be able to see valve morpholo-

gy more clearly, identification of intact frustules was limited to size and shape taxa which were not necessarily single species groups; Cox (1996) and Kelly *et al* (2005) were helpful in separating taxa based on plastid arrangement. Taxa from Chapters 3 and 6 are presented in Appendix 2 and 3, respectively.

2.5.3 Acid cleaned assemblages

By oxidizing the MPB sample, mini-core or lens tissue, all the organic content of the cells and sediment is removed and the only the siliceous diatom skeletons remain (for diatom morphology descriptions see Appendix A1). Without organic material the various components of the diatom frustules come apart and the two valves are more likely to fall face up or down rather than on the side (with a few exceptions such as *Roicosphenia*) which allows inspection of valve morphology. Only valves, not girdle components, are identified and counted, and as each frustule has two valves a 300 valve count is actually just a 150 cell count but as only relative proportions of taxa are of interest here, this is generally ignored. It is not possible in this state to distinguish between valves that were live or dead prior to collection. All the species encountered in this project are described in Appendix A1 with morphological terminology following Hendey (1964), Barber & Haworth (1981), and Kelly *et al* (2005), with, where possible, the source of identification.

Oxidation, acid-cleaning and mounting of sediment samples onto slides followed HIMOM protocol (2005). Either the lens tissues were washed thoroughly into fresh water and spun down or 50 μ l aliquot of each sediment sample was added to 1 ml of saturated potassium permanganate solution in a centrifuge tube and left to oxidize for ~ 12 hours with frequent mixing. The KMnO_4 was neutralized the following day by adding concentrated hydrochloric acid (Fisher Scientific, Loughborough, UK, ~36%) until the mixture ceased to bubble and then the reaction was allowed to continue in an oven at 70°C until all solutions turned from dark maroon

to pale yellow. The reagents were washed off the sediment samples by repeated (7x) centrifuging (1300 g for 6 minutes), discarding the supernatant and resuspending the pellet in ultrapure water. The final pellet was resuspended in 5 ml of ultrapure water, mixed thoroughly and 400 µl pipetted from the centre of the tube onto an acetone-cleaned coverslip (Menzel-Gläser, Braunschweig, Germany, 20 x 20 mm, thickness Nr.1). Coverslips were left to dry in the fume cupboard overnight and when dried they were mounted onto a glass slide (Menzel-Gläser, Germany, 76 x 26 x 1 mm, Ground edges 90° /double frosted 20 mm) with a large drop of Naphrax Diatom Mountant (Brunel Microscopes Ltd, UK). Slides were investigated under a Leitz light microscope using a phase 3, 100x lens and a 1.25 optivar (1250x total magnification) photographs were taken with a mounted Olympus SP-500UZ camera.

2.6 Natural abundance and biomass of macrofaunal assemblage at Paper Mill site

Collection

A 20 x 20 meter quadrat was marked out on the North Shore of the Guardbridge. Seven and five cores were taken during May and July 2008, respectively, and were then treated following HIMOM (2005). First the core was sieved through a 500 µm mesh into a lidded container so it could be fixed in formaldehyde for 48 hours, the formaldehyde was then poured off and the remaining fumes allowed to evaporate in a fume cupboard before the sample was re-immersed in formalin with a tiny amount of Rose Bengal to dye animal cells pink. The sample was then picked through under the dissection microscope to remove macrofauna from the rest of the debris. Macrofauna (and whatever meiofauna was still in the sample) were collected in separate glass vials per sample for subsequent enumeration and

weighing. The total biomasses were summed (Table 2.3) for a per area bulk macrofauna abundance in the sediment so that mesocosm experiments would have reasonably representative macrofaunal biomasses.

Table 2.3: Mean abundance (head count) and mean biomass (g, damp weight) of macrofauna m⁻² at the paper mill site quadrat.

	<i>C.vol</i>	<i>N. div</i>	<i>M. bal</i>	Other	Total g m ⁻²
May					
abundance	9,235	884	85		
biomass	32.5	15.5	13.6	11.8	73.4
July					
abundance	1,954	881	95		
biomass	7.82	29.25	17.35	9.4	63.82

2.7 Statistical analysis

All experimental data was investigated graphically prior to any statistical tests. Normally or approximately normally distributed data were investigated with linear models (“lm” function in the “stats” package in R). To determine violations of model assumptions (general linear and general least squares models) the standardized residuals and fitted values were examined graphically (following Crawley 2002; Mackenzie 2006; Zuur *et al* 2007, 2007b, 2010) with scatterplots (covariates), boxplots (factors), or histograms (response variables) as follows (y-axis ~ x-axis):

1. Constant variance:

- Standardized residuals ~ fitted values
- Random residuals from Normal distribution ~ fitted values
- Standardized residuals ~ each variable in the model separately

2. Independence:

- Standardized residuals ~ relevant order in samples or measurements (temporal, spatial)
3. Linearity (when relevant)
 - Residuals ~ each covariate (as above)
 4. Normality
 - Histogram of standardized residuals and/or
 - Standardized residuals ~ random residuals from normal distribution

Non-linear models were modeled either by categorical variables or by using a non-linear regression (“nls” in “stats” package in R). Patterns in the residuals plots (as opposed to a random spread) suggests that one or more assumptions are likely to have been violated and an error structure may be required. Error structures were fitted following the proposed method of Zuur and colleagues (2007b, 2010) detailed below. The model is specified with the maximum contingent of fixed effects in “REML” (restricted maximum likelihood estimation) mode using generalized least squares (“gls” from “nlme” package in R) and was then compared by residuals plots (above) and AICc comparison to the same model with various error structures using either a mixed effects model (“lme” in “nlme” package in R) or another GLS. The model with the lowest AICc was then selected from a subset of all models with no latent trends in their residuals plots. Once the error structure was selected the model was reformulated with ML and the fixed parameters of the maximum model were selected by stepwise parameter removal again using lowest AICc and least-patterned residuals plots as selection criteria. As it was possible for appropriate error structure to change as fixed factors are removed, each full model with different error structures, specified in ML, was also run through an automated model selection tool in R (the “dredge” function in “MuMIn” package in

R) and model with lowest AICc compared to the “minimum adequate model” selected by the Zuur method (Crawley 2002) was in fact the one with the lowest AICc.

The final, minimum adequate, model is reported by either model output (covariate regressions) or by table of estimates and confidence intervals (for factorial models) and by a model visualisation. The “gls” function does not include confidence interval predictions for pooled regressions, only on the estimated parameters, so estimated parameters from the final model were bootstrapped using the multivariate normal distribution (“rmvnorm” function, “MASS” package, 10000 replications) and the predicted means and confidence intervals plotted against the main covariate, with other covariates kept constant. Occasionally, for models with multi-level categorical variables, only the results of F-tests performed (Pinheiro & Bates 2000)

Chapter 3: Ecosystem engineering effect of *Corophium volutator* (Pallas) on microphytobenthic assemblage composition and biomass

Abstract

This experiment was designed to investigate what the net effect of increasing biomass of *Corophium volutator* (Pallas) on MPB biomass and diversity both ‘locally’ (within burrow proximity) and ‘remotely’ (outwith burrow proximity). Previous studies have demonstrated that *C. volutator* feeding and bioirrigation behaviour can have both deleterious and regenerative effects on MPB biomass and diversity. The remote effects are of interest because the immersion of sediment during high tide can transmit both the deleterious and regenerative effects of *C. volutator* beyond its immediate habitat to the wider estuarine ecosystem, in which MPB is the main stabilizing component.

A 7-day laboratory mesocosm experiment was carried out in which 32 tanks, each containing homogenized mud and biofilm and a 7 cm seawater column, were divided into 16 experimental units in which one tank each contained either 0, 0.5, 1.0, 2.0 g *C. volutator* and water columns were circulated between two tanks (~ 1 hr turnover of tank water). Temperature, light intensity, turbidity, DIN, DIP, MPB bulk biomass (Chlorophyll-*a* in top 5 mm sediment) and surface (fluorescing) biomass, and ‘live’ MPB assemblage diversity in sediment were analysed to determine whether *C. volutator* had any effect on MPB biomass and diversity locally (‘macrofauna present’ tanks) or remotely (‘macrofauna absent’ tanks). While no significant

relationship was found between *C. volutator* and DIN or DIP release to the overlying water column ($p > 0.05$, though there was a slightly positive linear relationship between both), a significant positive linear relationship was found between *C. volutator* biomass and turbidity ($p < 0.001$). While effect of increasing *C. volutator* biomass on MPB bulk biomass was unresolved, surface biomass declined significantly ($p = 0.002$) with increasing *C. volutator* biomass both locally and remotely due to the linear increase in turbidity. No effect was found on the *C. volutator* biomass on MPB diversity either locally or remotely. This suggests that the net effect of *C. volutator* in the estuary is to decrease MPB productivity, a consequence of which is likely to be an overall destabilizing effect.

Chapter 3: Ecosystem engineering effect of *Corophium volutator* (Pallas) on microphytobenthic assemblage composition and biomass

3.1 Introduction

Jones and colleagues (1994) stipulate that while all organisms are ecosystem engineers to some extent, organisms are more likely to be important engineers in an ecosystem if: (1) they spend a large amount of time engaging in the engineering activity, (2) they have a high population density, (3) they are widely distributed, (4) they live in colonized areas over long periods of time, (5) their constructs are durable, and (6) the number of resource flows that their activity modulates and the number of other species these resource flows affect is high. *Corophium volutator* (Pallas) are ubiquitous and extremely abundant in North Atlantic estuarine mudflats. Although their distributions within the estuaries are patchy, they have a wide tolerance of salinity, grain size, and nutrient levels (Meadows & Reid 1966; Meadows 1967; McLusky 1968) and so can live in most areas of the estuary, and their numbers may vary between 1,000 and 20,000 individuals m⁻² but maximum abundances of 100,000 individuals m⁻² have been reported (McLusky 1968; Henriksen *et al* 1980; Murdoch *et al* 1986; Raffaelli & Milne 1987; Gerdol & Hughes 1994b; de Deckere 2000; Møller & Risgård 2006). Although abundances fluctuate widely throughout the year (references as previous) they can be usually be found in the same general area throughout the year unless driven away by macroalgal mats (Raffaelli 2000) or by competition from *Arenicola marina* (Beukema & Flach 1995). *C. volutator* build U-shaped burrows to about 5 cm depth whose walls are cemented with mucus (Meadows & Reid 1966;

Meadows *et al* Hussain 1990). Their burrows are considered to be semi-permanent because abandoned burrows remain intact and are often re-inhabited by other individuals (Meadows & Reid 1966). They maintain a steady current through their burrows by beating their pleopods rhythmically, which is necessary for respiration as well as feeding (as discussed in Chapter 1.4.3.1) and also acts to shunt faecal pellets and grazed sediment out of the burrow, into the overlying water column. This burrowing and irrigating activity begins as soon as the hatchlings leave the parental burrow and is maintained more or less continuously throughout the animals' life (Gerdol & Hughes 1994a; Møller & Riisgård, 2006). *C. volutator* shows functional plasticity and can both filter and deposit feeders. They deposit feed by scraping off surface biofilm from around their burrows and then digesting the diatoms, bacteria and EPS. In this manner, *C. volutator* can be voracious deposit feeders – Gerdol and Hughes (1994a) estimated that an adult would consume an average of 4000 diatoms an hour and showed that within a month would completely destroy the MPB biofilm in the area they inhabited (1994b). When suspension feeding, they can equally efficiently clear the water column of diatoms – Forster-Smith estimated a pumping rate for a single adult of $63 \pm 36 \text{ ml h}^{-1}$ and Møller and Riisgård (Møller and Riisgård 2006 and references therein) demonstrated that, at *in situ* population densities ($3,100 - 20,000 \text{ ind m}^{-2}$) a sublittoral *C. volutator* population in a shallow fjord would pump between $0.9 - 19.4 \text{ m}^3 \text{ m}^{-2} \text{ d}^{-1}$ of overlying water through their burrows resulting in phytoplankton half-lives of $14.5 - 0.7$ hours in the water column (Møller and Riisgård 2006).

Apart from their importance in the estuarine food chain, the feeding and burrow irrigating of *C. volutator* results in a number of important resource-modifying ecosystem functions. Firstly, one the effect of *C. volutator* deposit-feeding is a loss of biofilm, which has three knock on effects: (1) the prevention of sediment accretion

and lamination and increased erodibility of the sediment, and (2) the dissolution and recycling of nutrients, and (3) decreasing the organic content of the sediment. Secondly, the effect of *C. volutator* burrowing and maintaining the irrigation current also has several knock on effects: (4) the resuspension of sediment into the overlying water column, (5) the release of nutrients from the sediment, (6) the extension of the sediment-water boundary, and (7) increased sediment porosity and water content. The first resource pathway that *C. volutator* modifies, according to Gerdol & Hughes (1994b), is the prevention of sediment accretion and lamination due to the loss of biofilm resulting a loss of elevated stable sediment bases for plant colonisation preventing sea grasses and salt marsh plants from taking root and then encouraging further sediment accretion. In addition to lowering of the critical erosion threshold of the sediment (Paterson 1989; Gerdol & Hughes 1994b; Daborn 1993; de Deckere *et al* 2000), *C. volutator* actively flings sediment and faecal pellets into the water column through their burrow irrigation at immersion, thereby increasing sediment load in the overlying water (de Deckere *et al* 2000; Biles *et al* 2002). This increases the turbidity at immersion potentially decreases the sunlight received by MPB, phytoplankton, and macroalgae by reducing light transmission and further reducing organic carbon production. The third resource that *C. volutator* modifies (actually multiple resources) is inorganic nutrients, in particular inorganic nitrogen (NH_4^+ , NO_3^- , NO_2^-), phosphates, and dissolved silicates. By digesting biofilms, *C. volutator* facilitates the regeneration of dissolved nutrients in the porewater (Henriksen *et al* 1980; Henriksen *et al* 1983; Gerdol & Hughes 1994a; Roubéix *et al*, 2008). Burrow irrigation not only releases these nutrients from the porewater into the surface or overlying water (Henriksen *et al* 1980; Henriksen *et al* 1983; Biles *et al* 2002; Emmerson *et al* 2001; Bulling *et al* 2010), but also extends the sediment-water boundary interface, which releases ammonium from the deeper sediment where concentrations are higher and this in-

creases nitrification and denitrification (Pelegri & Blackburn 1994; Pelegri *et al* 1994; Mermillod-Blondin *et al* 2004). Finally, the consumption of organic carbon by macrofauna means less availability for burial and which can mean less sulphate reduction to H₂S by sulphate reducing bacteria (Mermillod-Blondin *et al* 2004).

Because *C. volutator* grazing has a detrimental effect on local MPB, they may, in time, reduce the availability of food resources, changing their locality into an unsuitable habitat for subsequent generations, which will potentially have to find other pastures. While *C. volutator* locally reduces total MPB biomass, they can potentially increase the assemblage diversity by preferentially grazing on dominant, mid-sized, free-living motile cells like *Navicula* over very large (> 200 µm length), heavily silicified, or epipsammic cells (Smith *et al* 1996; Hagerthey *et al* 2002). In addition, bioturbation could be interpreted as a source of intermediate disturbance, which could increase niche availability and thereby increase species diversity (Townsend *et al* 2000), although there is no empirical evidence for this theory in MPB communities. Theoretically, *C. volutator*'s multiple potential effects on the water column could have both beneficial and detrimental effects on MPB biomass and diversity, and this study aims to examine the net effect. The net effect of CV activity on MPB will be determined by which of the physicochemical properties of the overlying water column is changed most drastically and exerts the greatest selective pressure on MPB assemblages. For example, assemblages from a eutrophic estuary may not necessarily respond to increased nutrient availability in the overlying water column, but may respond drastically to changes in light level, or increased sedimentation and the opposite could be true for assemblages in an oligotrophic estuary.

One effect on MPB biomass and assemblage composition could be that diatoms resuspended into the overlying water could increase biomass and diversity where they

settle out of the water column. Another potential effect is that increased availability of nitrates and phosphate, adsorbed on the surface of sediment particles, might compensate for the loss of light, a phenomenon previously described in freshwater systems and shown to benefit smaller, epipsammic species of diatoms that inhabit the understory of benthic biofilms (Burkholder 1996). The other source of nutrients are the increased dissolved nutrients fluxes to the overlying water column due to bioturbation and bioirrigation, which are likely to increase MPB biomass, but the effect on assemblage composition appears to be particular to the specific system. Hagerthey and colleagues (2002) found that estuarine MPB populations maintained *ex situ* in tidal systems with high nutrients had a higher biomass than those with low nutrients regardless of whether they originated from eutrophic or oligotrophic estuary. However, the effect of nutrients on assemblage structure varied depending on the whether the assemblages had come from eutrophic or oligotrophic assemblages: species richness, evenness and diversity of assemblages from eutrophic assemblages were higher in the low nutrient treatment than the high nutrient treatment, whereas the reverse was true for assemblages from oligotrophic estuaries. Agatz and colleagues (1999) found that along a nutrient gradient from a sewage outflow on a North Sea sandflat, MPB biomass increased with increasing nutrients, but diversity maximized at intermediate nutrient concentrations and that smaller epipsammic diatoms dominated oligotrophic areas and non-local and large, motile, local diatoms dominated eutrophic areas. On the other hand, working on phosphate-limited freshwater chemostats, Grover (1989) predicted and found that larger elongate diatoms (almost all MPB diatoms are elongate or 'pennate' rather than centric) were more competitive than smaller ones and so should dominate assemblages that are nutrient limited. Finally, *C. volutator* turbidity generation can remotely affect MPB communities by reducing light intensity. Intuitively, the decreased energy input

should decrease overall biomass and favour motile diatoms, which can migrate fastest to the sediment surface. However, Defew and colleagues (2002) found that removing diatoms from the field into the laboratory as well as applying different shading levels to them once in the laboratory (> 1000 , and 164 and $77 \mu\text{mol m}^{-2} \text{s}^{-1}$ in field and laboratory, respectively) had no effect on chlorophyll *a* content of the sediment between initial and final values (2 weeks) for either treatments, or on surface biomass (F_0) between treatments. In terms of assemblage structure, Defew and colleagues (2002) found no change in species richness, but a decrease in diversity due to a shift to smaller sized diatoms following 2 weeks of incubation in the laboratory. They surmised that smaller cell sizes were more competitive in situations of lower light and nutrient availability. In a follow-up experiment, Defew and colleagues (2004) found that the effect of light intensity on MPB biomass was temperature dependent and at 18°C rather than 10°C , biomass (chlorophyll *a* and F_0) did increase with light intensity but species richness, evenness, and diversity were higher after three weeks under shaded, rather than unshaded, light conditions (70 and $350 \mu\text{mol m}^{-2} \text{s}^{-1}$) at both temperatures. The lowest diversity was exhibited by unshaded treatments at 18°C and cyanobacteria became more plentiful in the assemblage under stressful conditions (temperature $> 25^\circ\text{C}$, low nutrients, and low light).

By allowing a *C. volutator* modified water column to circulate over both grazed and ungrazed sediment, it should be possible to distinguish a pure engineering effect from the combined trophic and engineering effect on MPB biomass and assemblage structure and to determine whether effects are amplified by increasing *C. volutator* biomass. The combined trophic and engineering effect would be observed in the grazed sediment and the 'remote' effect, via the engineered water column, would be observed in the ungrazed sediment. More specifically, this experiment was designed to test the following hypotheses:

H₀2.1: *C. volutator* has no significant effect on the water column at any biomass.

H₀2.2: *C. volutator* has no significant effect on MPB biomass, locally or remotely.

H₀2.3: *C. volutator* has no significant effect on MPB assemblage composition, locally or remotely.

3.2 Materials & Method

3.2.1 Experimental design

An experimental unit consisting of two “paired” tanks was designed to allow two discrete tanks of sediment to share the same overlying water column (see Fig. 1). Thirty-two rectangular acrylic tanks (20 cm long x 14 cm wide x 12 cm high) were made into 16 independent experimental units. Each tank had two holes drilled into the narrow ends which were fitted with rubber O-rings and nylon tank connectors (Williamson Pumps Ltd, 3 mm internal diameter, 5 mm external diameter) and connected into pairs by 16 small peristaltic pumps (Williamson Pumps Ltd, UK, 200 Series Peristaltic Pump, 30 r/min, 230v AC, 5.0 mm Silicone Tubing, catalogue number 200-030-230-050) and silicone tubing (5.0 mm internal diameter). The peristaltic pumps pumped water from tank 1 into tank 2 at a rate of 35.4 ml min⁻¹, which then flowed passively from tank 2 back to tank 1, meaning that the total volume of seawater in the tank was exchanged every 47 minutes.

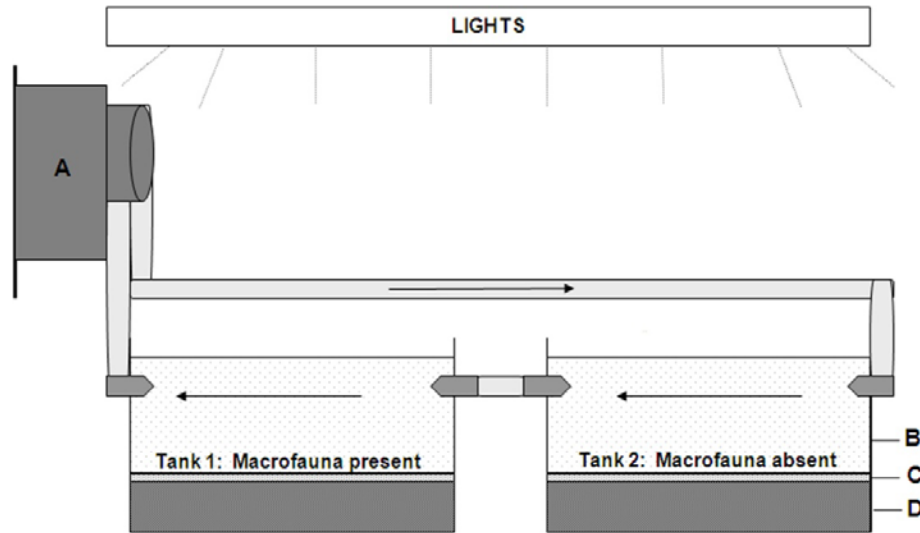


Figure 3.1: One experimental unit consisted of two tanks connected with peristaltic pump (C), tanks connectors and silicone tubing that circulated overlying water (D) from between tanks at a rate of 35.4 ml⁻¹ min⁻¹. Tanks were filled with a 50 mm layer of sifted sediment (B) topped with a 5mm layer of biofilm slurry (A).

Each of the 32 tanks contained sieved mud and microphytobenthos. Tanks were lined up in 2 rows of 16 experimental unit (for schematic see Fig. 3.2) and in each experimental unit tank 1 (the grazed tank) contained different biomass levels of *C. volutator*, hitherto referred to as the “macrofauna present (MP) tank”, and tank 2 containing no *C. volutator*, “macrofauna absent (MA) tank”, containing none. Four replicate units each of 4 experimental treatment groups containing 0, 0.5, 1.0, or 2.0 g damp weight of *C. volutator* in the grazed tank which corresponded to roughly 0.5x, 1x and 2x the *in situ* total macrofaunal biomass in 280 cm² sediment. The control group where the tank 1 contained 0 g *C. volutator* is still be referred to as an “MP” tank in the context of comparing treatment groups.

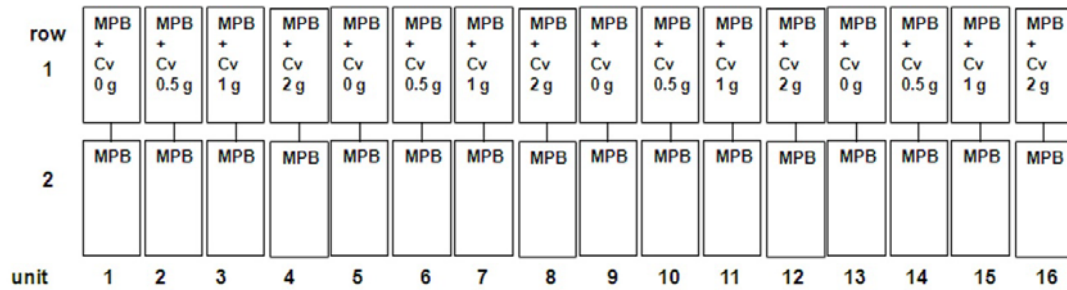


Figure 3.2: A total of 32 tanks, arranged as 16 units (above), distributed amongst 4 four *C. volutator* biomass treatments of either 0, 0.5, 1, or 2 grams, and 2 *C. volutator* presence/absence treatments.

The thermostat of the aquarium was set to 12°C. Two lighting arrays consisting of ten four foot fluorescent 36 watt full daylight spectrum tubes (F36W/72 Activa 172 Full Spectrum Daylight Tubes, 6500K colour temperature, Newey & Eyre (Hagemeyer) UK Ltd, UK, with Arcadia ULTRA SEAL waterproof (IP67) lamp leads (T8, 25 mm) with 36/38W twin lamp controllers from Arcadia, UK) at 5 cm intervals were hung side by side so that array 1 covered units 1 to 8 and array 2 covered units 9 to 16. . Lights were set to a 14:10 light: dark cycle and daylight began at 8 am and ended at 10 pm. Tanks were aerated for the duration of the experiment (2 × Resun 9908 24 W eight outlet air pumps (GuangDong Risheng Group Co. Ltd., China) with an Algarde 2 way gang valve per unit (Algarde Enterprises Ltd., Colwick, UK) and stone diffusers).

3.2.2 Experimental mud, biofilms and macrofauna

Mud and *C. volutator* were all collected from the 400 m² quadrat on the North Shore of the Eden estuary at the Guardbridge paper mill (Chapter 2: General Methods) in late July 2008. Mud was collected to about 15 cm depth and sifted through 0.5 mm² mesh into filtered seawater (35 psu) over several days and aerated. *C. volutator* specimens that had been picked out from the mesh were kept in aerated tanks with mud and fed microphytobenthic biofilm. Prior to adding them to the tanks, they

were sifted out of their interim tanks and damp weighed into 4 batches each of 0.5 g, 1.0 g, and 2.0 g corresponding to approximately 0.5x, 1x, and 2x the *in situ* total macrofaunal biomass for 280 cm². Surface mud (approximately top 0.5 cm) with microphytobenthic biofilm was collected from just below the quadrat a few hours before it was added to the tanks. The biofilm was sifted through a 0.5 mm mesh into seawater upon return to the laboratory, homogenized and sampled.

3.2.3 Set up and sampling

A time line of the experiment is presented in Figure 2.3. A day prior to the start of the experiment each tank was filled to 5 cm with (1400 mL) of mud, topped up with 6 cm of filtered (0.64 µm²) seawater, and finally 140 ml biofilm-seawater slurry (collected that day) was added to each tank to create an 5 mm layer. The microalgae were given 24 hours to establish a surface biofilm and then the overlying seawater was changed in order to remove the initial nutrient flush from sediment and biofilm slurries (Ieno *et al* 1996). The following day, the samples were taken from overlying water and surface sediment to measure starting values ("day 1") for turbidity, nutrients levels, water and organic content of sediment, MPB biomass by fluorescence and chlorophyll-*a* content of sediment, and MPB assemblage diversity in each tank. *C. volutator* were added on the evening of day 2 and pumps were switched on the following morning (day 3) after turbidity and benthic fluorescence were recorded. On day 4, 2 units were found to have blocked tank connectors which had led the second tanks to flood and a depleted water level on one side; as the damaged units were from different treatment groups, one set of replicates was dropped from the experiment. Biomass and turbidity were again recorded on the morning of day 6. On the morning of Day 8 (after 6 days of *C. volutator* presence) the pumps were switched off and the tanks disconnected from each other and a full set of samples and measure-

ments, as on day 1, were taken. Sediment samples were taken from pre-determined quadrats within each tank to avoid resampling the same location on days 1 and 8.

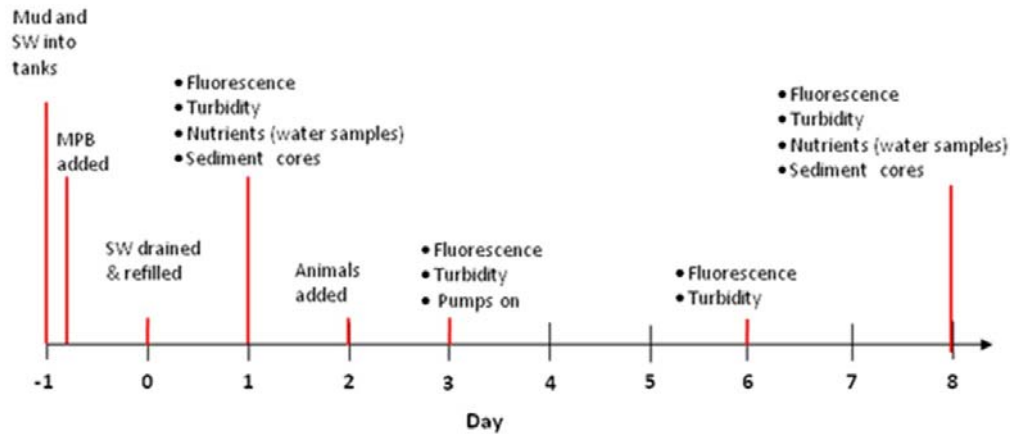


Figure 3.3: A timeline of the experiment.

3.2.4 Measurements

3.2.4.1 Temperature and light intensity

Although the thermostat of the cold room was set to 12°C, the actual temperature varied due to energy input from the lights, so temperature was measured just before the lights came on in the morning and before the lights went out at night. Incident light to the top of each tank was measured, in triplicate, with a photometer (LI-189, LI-COR inc, P.O. Box 4425/4421, Superior St, Lincoln, Nebraska 68504, U.S.A.) in two conditions: with and without the experimental lights on (only the room lights) reflecting the fluorescence measurements.

3.2.4.2 Turbidity & nutrients in overlying water

Turbidity was reported in nephelometric turbidity units (ntu) using a Eutech Instruments Turbidimeter TN100. The unit was calibrated using standards at 0.02, 100, and 800 ntu, followed by measurement of filtered seawater. Water from each tank

was measured in triplicate and a mean taken; filtered seawater was measured after each unit was measured to determine whether there was machine drift and recalibration was required. 40 ml water samples were collected from each tank, analysed for $\text{NH}_4^+\text{-N}$, $\text{NO}_3^-\text{-N}$, and $\text{PO}_4^{3-}\text{-P}$ as described in section 2.3, and quantities are reported as $\mu\text{mol L}^{-1}$.

3.2.4.3 Fluorescence measurements

F_0 is a proxy for surface biomass (section 2.4.2) and measurements were made in the mornings (~ 9 am) in randomized (Urbaniak & Plous 2008) orders following 15 minutes of dark ($< 4 \mu\text{mol m}^{-2} \text{s}^{-1}$) adaptation. An FMS2 fluorometer (Hansatech Instrument Ltd, UK) was used (with settings as per section 2.4.2.4) with the probe tip was fixed in a specialised housing 4 mm from sediment surface. Four measurements were made within each tank and means calculated.

3.2.4.4 Chlorophyll *a*, water, and organic content of sediment

Sediment cores for chlorophyll *a* and water and organic content were collected and immediately immersed in liquid nitrogen and stored at -80°C . Three $57 \text{ mm}^2 \times 2 \text{ mm}$ sediment cores for measurement chlorophyll *a* (expressed in $\mu\text{g cm}^{-1}$) were processed as described in section 2.4.1. Two $314 \text{ mm}^2 \times 2 \text{ mm}$ sediment cores for measurement of water and organic content were processed as described in section 2.2.3, with 48 hours of oven drying, and results expressed as relative percentages.

3.2.4.5 Microphytobenthic assemblage

For the description of microphytobenthic assemblages, three $50 \text{ mm}^2 \times 2 \text{ mm}$ cores were collected and combined into a 15 ml centrifuge tubes containing a 5 ml of 4% Glutaraldehyde (Sigma-Aldrich, Germany, 25% Glutaricdialdehyde in water) in filtered, autoclaved seawater. Samples were obtained from the starting slurry and

from each tank on day 8. 300 cells or colonies were counted and classified as cyanobacteria, diatom or euglenid and as live, if the plastids were intact, or dead, if the cell contained a desiccated or no plastid. As many diatoms can only be, at best, identified to species from the literature from their silicate which require acid-cleaning to allow close observation, fixed cells/colonies were divided into 63 different size and shape taxa, which were readily identifiable under low magnification (4000 \times , bright field) light microscopy suitable for wet mounts and are described in Appendix 2. In addition, a sample from the original slurry was acid-cleaned and 300 valves identified as far as possible from the literature (taxa descriptions of all acid cleaned valves presented in Appendix 1). The identifications from Appendix 1 were then used to infer likely species making up the size and shape taxa of Appendix 2. Some of the taxa in Appendix 2, such as taxa 14, 15, 23, 41, represent a single species (*Cylindrotheca closterium*, *C. gracilis*, *Gyrosigma fasciola*, and *Tryblionella apiculata*, respectively) as they are very distinctive but others, such as taxa 33, 34, and 35 could individually represent several species (*Navicula gregaria* and *Navicula phyllepta* morphotype I) and as a group different sized specimens of the same species. Also, the shape of diatom frustule dictates the aspect it is likely to present for microscopic examination on a glass slide: whereas some species are more likely to fall in valve view (face) or girdle (side) view, others are shaped so that they may lie in either view (such as many *Navicula* sp.) and often cannot be readily identified to species. There were 9 taxa in girdle view, 2 of which were likely to also fall in valve view. From these identifications the percentage of live cells, the species richness (total live taxa) in each sample, and Simpson's diversity index were calculated for comparison between treatment groups and statistical analysis.

3.2.5 Statistical analysis

All measurements are presented graphically against treatment groups and group means are presented with ± 1 standard error. Statistical analysis was carried out on response variables which included changes in the overlying water column (turbidity and nutrient levels) and ultimately the effects of these changes on the MPB biomass and community response variables – chlorophyll *a*, F_0 , % live cells, species richness, and negative log transformed Simpson diversity(D). Model selection procedures are as described in Chapter 2.7. As the two tanks within the same experimental unit were not independent of each other, this was accounted for in the error structure by applying either “unit” as variance category, either as a weight, (using a “glms” function, “nlme” package in R) or as a fixed factor (in “lme” function, “nlme” package in R). However, if fitting unit into the error structure did not improve the model AICc, residuals plots, or change the fixed portion of the model in any substantial way then it was not retained in the final model. The effects of *C. volutator* treatments on the overlying water column were investigated by regression models where *C. volutator* biomass could be treated as either a covariate or a categorical variable and so it was applied on a best fit basis (according to AICc and residuals plots) for each response variable. For covariate regressions the model outcomes are presented as a table with estimates, and p-values from t-tests but where regressions were categorical, model outputs are presented as F-tests (following Pinheiro & Bates 2000, using the “anova” function in “nlme” package in R).

Table 3.1: Summary of statistical models in Chapter 3: i = index for tank number; j = index for unit number; Y = the response variable; Bm = *C. volutator* biomass treatment; Cv = the *C. volutator* presence/absence treatment; FBm = feeding biomass (g *C. volutator* in tank); $cPAR$ = centralised PAR; $cTemp$ = centralised evening temperature; $mnTurb$ = mean turbidity in each tank by day 8. ε = errors; V = a variance-covariance matrix; gls = generalized least squares; lm = linear model (least squares) in R; lme = linear mixed effects model.

Model Nr	Response variable	Day	Fixed effects (maximum model)	Error	R Funct
3.1.1	Turbidity	all	$Y_i \sim Bm_i * \text{factor}(Cv_i) * \text{factor}(\text{Day}) + \varepsilon_i$	$\varepsilon_i \sim N(\mu, \sigma^2 * V)$	gls
3.1.2	Unit Turbidity	all	$Y_j \sim Bm_j * \text{factor}(Cv_j) + \varepsilon_i$	$\varepsilon_i \sim N(\mu, \sigma^2 * V)$	gls
3.1.3	Δ Turbidity	all	$Y \sim \text{Day} + \varepsilon_i$	$\varepsilon_i \sim N(\mu, \sigma^2)$	gls
3.2.1a	NH_4^+	8	$Y_i \sim \text{factor}(Bm_i) * \text{factor}(Cv_i) + \varepsilon_i$	$\varepsilon_i \sim N(\mu, \sigma^2 * V)$	gls, anova
3.2.1b	PO_4^+	8	$Y_i \sim \text{factor}(Bm_i) * \text{factor}(Cv_i) + \varepsilon_i$	$\varepsilon_i \sim N(\mu, \sigma^2 * V)$	gls, anova
3.2.2a	ΔNH_4^+	8-1	$Y_j \sim Bm_j + \varepsilon_j$	$\varepsilon_i \sim N(\mu, \sigma^2)$	gls
3.2.2b	ΔPO_4^+	8-1	$Y_j \sim Bm_j + \varepsilon_j$	$\varepsilon_i \sim N(\mu, \sigma^2)$	gls
3.3	% organic	8	$Y_i \sim \text{factor}(Bm_i) * \text{factor}(Cv_i) + \varepsilon_i$	$\varepsilon_i \sim N(\mu, \sigma^2 * V)$	gls, anova
3.4	Chl- <i>a</i>	8	$Y_i \sim \text{factor}(Cv)_i + mnTurb_i + FBm_i + cTemp_i + cPAR_i + [mnNH_4^+]_i + [mnPO_4^{3+}]_i + mnTurb_i : \text{factor}(Cv)_i + mnTurb_i : cPAR_i + \varepsilon_i; \varepsilon_i \sim N(\mu, \sigma^2 * V)$	$\varepsilon_i \sim N(\mu, \sigma^2 * V)$	gls
3.5	F_0	8	$Y_i \sim \text{factor}(Cv)_i + mnTurb_i + FBm_i + cTemp_i + cPAR_i + (mnNH_4^+)_i + mnPO_4^{3+}_i + mnTurb_i : \text{factor}(Cv)_i + mnTurb_i : cPAR_i + \varepsilon_i; \varepsilon_i \sim N(\mu, \sigma^2 * V)$	$\varepsilon_i \sim N(\mu, \sigma^2 * V)$	gls
3.6	% Live	8	$Y_i \sim \text{factor}(Cv)_i + mnTurb_i + FBm_i + cTemp_i + cPAR_i + (mnNH_4^+)_i + mnPO_4^{3+}_i + mnTurb_i : \text{factor}(Cv)_i + mnTurb_i : cPAR_i + \varepsilon_i; \varepsilon_i \sim N(\mu, \sigma^2 * V)$	$\varepsilon_i \sim N(\mu, \sigma^2 * V)$	lme
3.7	Species Richness	8	$Y_i \sim \text{factor}(Cv)_i + mnTurb_i + FBm_i + cTemp_i + cPAR_i + (mnNH_4^+)_i + mnPO_4^{3+}_i + mnTurb_i : \text{factor}(Cv)_i + mnTurb_i : cPAR_i + \varepsilon_i; \varepsilon_i \sim N(\mu, \sigma^2 * V)$	$\varepsilon_i \sim N(\mu, \sigma^2 * V)$	lme
3.8	$-\ln D$	8	$Y_i \sim \text{factor}(Cv)_i + mnTurb_i + FBm_i + cTemp_i + cPAR_i + (mnNH_4^+)_i + mnPO_4^{3+}_i + mnTurb_i : \text{factor}(Cv)_i + mnTurb_i : cPAR_i + \varepsilon_i; \varepsilon_i \sim N(\mu, \sigma^2 * V)$	$\varepsilon_i \sim N(\mu, \sigma^2 * V)$	lme

3.3 Results

Measurements for days 6 and 8 were only made on units 1 – 12 (24 tanks); pump failure due to hose blockages meant that two tanks had to be dropped from the experiment, so, in order to keep replicate numbers consistent between treatment groups two further units were dropped. No *C. volutator* were seen in the MA tanks during the experiment or found in the sediment at the end of the experiment.

3.3.1 Light and temperature

Morning temperatures did not vary substantially between the two rows of tanks but by the evening quite a large difference had built up between the front and back rows (Figure 3.4, Table 3.2). Light intensity was not found to be consistent across the bench, (Figure 3.5): tanks under the centre of the tubes had higher light intensities than tanks under the ends of the tubes so overall mean light intensities varied substantially (Table 3.2). The temperature difference between evening and morning did not correlate with the light intensity for that tank (Figure 3.6).

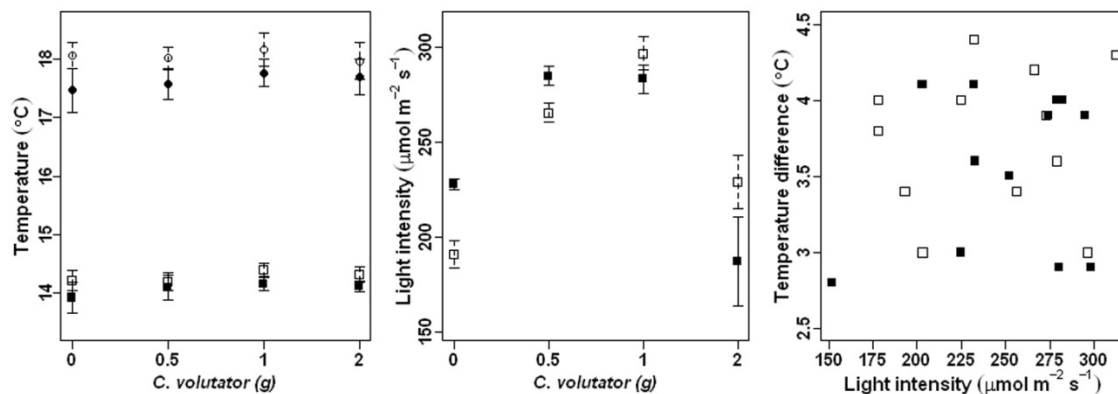


Figure 3.4: Mean temperatures measured in the morning (squares) and evening (circles) in MP tanks and MA tanks (left). **Figure 3.5:** Mean light intensity in MP tanks and MA tanks (centre). **Figure 3.6:** Temperature difference between morning and evening in the tanks plotted against incident light intensity in (right). In each plot, MP tanks and MA tanks are represented by open and closed symbols, respectively.

Table 3.2: Mean measurements for all 8 treatment groups (± 1 standard error): incident light intensity ($\mu\text{mol m}^{-2} \text{s}^{-1}$), temperatures ($^{\circ}\text{C}$), turbidity (ntu), $\text{NH}_4\text{-N}$ and $\text{PO}_4^{3+}\text{-P}$ ($\mu\text{mol L}^{-1}$), sediment water and organic content (%), chlorophyll *a* ($\mu\text{g cm}^{-2}$), F_0^{15} (arbitrary units), percent live cells (% Live), species richness (# taxa), and Simpson diversity index (*D*).

Biomass	0 g		0.5 g		1 g		2 g	
Presence	MP	MA	MP	MA	MP	MA	MP	MA
TempAM	14.2 \pm 0.17	13.9 \pm 0.27	14.2 \pm 0.15	14.1 \pm 0.21	14.4 \pm 0.12	14.7 \pm 0.12	14.3 \pm 0.13	14.1 \pm 0.09
TempPM	18.1 \pm 0.22	17.5 \pm 0.37	18.0 \pm 0.18	17.6 \pm 0.26	18.2 \pm 0.28	17.8 \pm 0.23	18.0 \pm 0.32	17.7 \pm 0.31
Light int.	265 \pm 5.0	227 \pm 2.7	265 \pm 5.0	285 \pm 5.1	296 \pm 8.8	283 \pm 7.5	229 \pm 14.2	187 \pm 23.5
Turb d1	3.0 \pm 0.5	2.1 \pm 0.3	2.0 \pm 0.4	2.2 \pm 0.2	2.9 \pm 0.6	3.0 \pm 0.6	2.0 \pm 0.2	2.3 \pm 0.4
d3	3.64 \pm 1.3	3.10 \pm 0.2	7.9 \pm 0.5	3.1 \pm 0.6	12.1 \pm 0.6	3.1 \pm 0.5	21.5 \pm 1.0	4.0 \pm 1.39
d6	1.8 \pm 0.31	1.9 \pm 0.2	6.4 \pm 1.1	5.05 \pm 0.56	8.8 \pm 0.5	7.8 \pm 0.4	13.5 \pm 1.0	12.1 \pm 0.8
d8	1.7 \pm 0.2	1.5 \pm 0.04	8.2 \pm 2.0	9.4 \pm 0.56	13.6 \pm 2.0	14.0 \pm 0.23	25.9 \pm 4.7	27.1 \pm 4.7
NH₄⁺ d1	17.4 \pm 0.46	17.9 \pm 0.61	9.8 \pm 3.56	10.8 \pm 5.15	43.3 \pm 31.3 12.3 \pm 6.8	9.9 \pm 5.80	10.9 \pm 3.61	10.0 \pm 3.95
d8	23.4 \pm 3.58	9.3 \pm 3.83	12.1 \pm 6.09	13.8 \pm 3.78	12.3 \pm 6.23	16.2 \pm 5.11	18.3 \pm 7.24	16.5 \pm 9.70
PO₄³⁺ d1	2.9 \pm 0.57	2.3 \pm 0.55	2.5 \pm 0.74	2.4 \pm 1.42	2.5 \pm 0.19	2.0 \pm 0.25	2.8 \pm 0.08	3.2 \pm 0.65
d8	3.9 \pm 0.87	2.9 \pm 0.39	3.9 \pm 0.65	3.6 \pm 2.01	2.9 \pm 0.26	4.8 \pm 1.50	3.4 \pm 0.72	4.2 \pm 1.44
% H₂O d1	56.9 \pm 0.96	61.80 \pm 0.98	57 \pm 1.2	58.37 \pm 4.0	60.1 \pm 2.8	58.45 \pm 2.8	59.4 \pm 2.3	66.49 \pm 4.4
d8	68.90 \pm 4.5	63.14 \pm 0.35	62.01 \pm 1.3	62.12 \pm 2.3	68.75 \pm 2.5	66.07 \pm 1.7	66.41 \pm 1.1	64.52 \pm 3.1
% Org d1	3 \pm 0.02	3.0 \pm 0.39	2.7 \pm 0.13	2.9 \pm 0.2	2.9 \pm 0.11	3.0 \pm 0.14	3.0 \pm 0.05	2.8 \pm 0.04
d8	2.5 \pm 0.57	3.2 \pm 0.09	2.8 \pm 0.13	3. \pm 0.41	3. \pm 0.29	4.1 \pm 0.94	2.8 \pm 0.21	3.6 \pm 0.98
Chl-<i>a</i> d1	87.5 \pm 13.4	171.6 \pm 50.3	134.3 \pm 18.1	128.4 \pm 28.4	143.7 \pm 14.5	145.8 \pm 29.7	175.8 \pm 19.4	171.2 \pm 48.8
d8	87.3 \pm 4.6	115.9 \pm 27.7	91.7 \pm 17.2	87.2 \pm 8.6	77.8 \pm 7.2	83.2 \pm 14.5	76.4 \pm 5.2	95.5 \pm 10.3
F₀¹⁵ day 1	173 \pm 19	207 \pm 29	183 \pm 31	205 \pm 38	174 \pm 3	233 \pm 11	181 \pm 9	228 \pm 20
day 8	110 \pm 4	112 \pm 9	55 \pm 13	73 \pm 5	40 \pm 8	95 \pm 26	23 \pm 3	82 \pm 10
% Live	42.1 \pm 14.0	39.8 \pm 13.3	33.0 \pm 11.0	35.7 \pm 11.9	34.1 \pm 11.4	37.7 \pm 12.6	32.3 \pm 10.8	30.7 \pm 10.2
# Taxa	23 \pm 8	22 \pm 7	23 \pm 7	21 \pm 7	21 \pm 7	23 \pm 8	21 \pm 7	23 \pm 8
D	0.19 \pm 0.06	0.22 \pm 0.07	0.18 \pm 0.06	0.22 \pm 0.07	0.25 \pm 0.08	0.20 \pm 0.07	0.22 \pm 0.07	0.19 \pm 0.06

3.3.2 Turbidity

The mean turbidities for each treatment group over the 8 days are presented (Figure 3.7, Table 3.2). Differences in turbidities between treatments were tested with a GLS (Model 3.1, Table 3.3). On day 1 mean turbidity levels were slightly higher than the average for filtered seawater, $0.5 (\pm 0.15)$ ntu, across all units as there was still residual sediment in the water column from setting up but all treatments had a similar starting turbidity level (Figure 3.7). However, there were no significant differences over biomass treatments in either group (MP slope = -0.53 ± 0.51 , $p = 0.310$; MA slope = 0.40 ± 0.73 , $p = 0.210$). By day 3, approximately 16 hours after *C. volutator* were added to the MP tanks, turbidities had diverged markedly: turbidity in the MP tanks increased with biomass (slope = 10.1 ± 0.73 , $p = 3.2 \times 10^{-24}$), and were therefore significantly different from the MA tanks where there was no relationship with biomass (slope = -0.74 ± 1.0 , $p = 1.2 \times 10^{-16}$). Following the day 3 measurements, the pumps were switched on and turbidities in the paired tanks equalized, temporarily reducing the turbidity in the MP tanks. There was no significant difference between MP and MA treatments (6.96 ± 0.73 and 5.14 ± 1.0 , respectively, $p = 0.082$) showing that the pumps had equalized the turbidity of the water in the paired tanks. By day 8 there was no significant difference between MP and MA treatments (12.9 ± 0.73 and 12.5 ± 1.0 , respectively, $p = 0.724$).

To determine how much turbidity is generated by *C. volutator* the turbidities in the two units were combined (Figure 3.8) Model 3.1.4 (Table 3.3, Model 3.1.2) shows that whereas the turbidity in the control tanks (0 g *C. volutator*) did not change significantly over days 3, 6, 8, ($p = 0.75, 0.50, 0.29$, respectively), the turbidity per gram of *C. volutator* increased significantly over subsequent days ($p = 5.2 \times 10^{-5}, 9.1 \times 10^{-7}$,

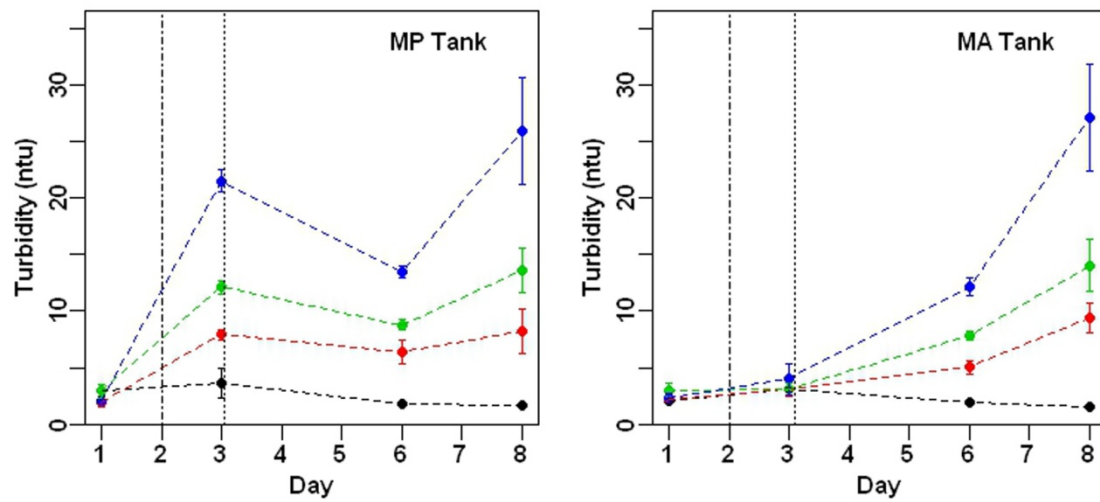


Figure 3.7: Mean turbidity in each treatment (macrofauna present, MP, and macrofauna absent, MA) and *C. volutator* biomass level (0g = black, 0.5 g = red, 1 g = green, 2 g = blue) where error bars represent 1 standard error. The dot-dash line represents the time the animals were added and the dotted line represents the time at which the pumps began cycling water between the two tanks in the units.

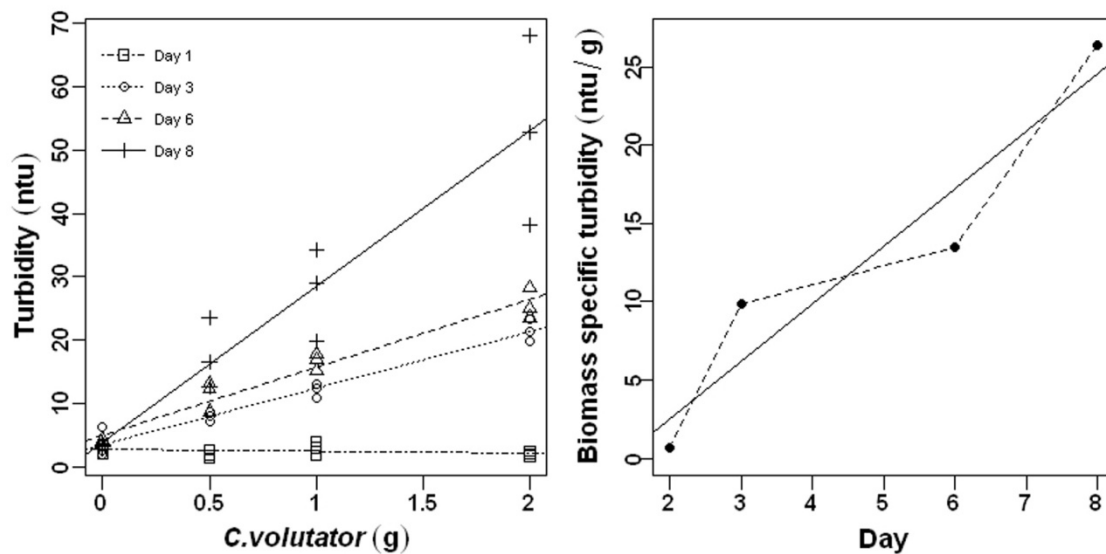


Figure 3.8: Total turbidity generated by each treatment of *C. volutator* biomass on days 1, 3, 6 & 8 (left). For days 1 and 3 only the Tank 1 treatments were used, whereas for days 6 and 8 the sum of the two tanks was used (see text for explanation). **Figure 3.9:** Biomass specific turbidity (estimates from Model 3.1.4) over each day with the LM superimposed (right).

2.2×10^{-14} , respectively). The turbidity per gram estimates from days 1, 3, 6, and 8 from Model 3.1.4, 0.7, 9.9, 13.5, 26.4, respectively, are regressed against day (Figure 3.9) which demonstrated a significant linear relationship (Model 3.1.3: Res/Tot DF = 2/4, $R^2 = 0.849$) in which the turbidity $\text{g}^{-1} \text{day}^{-1}$ is estimated at $3.5 (\pm 0.82, p = 0.05)$.

Table 3.3: Regression results for models with turbidity as response variable. BST represents the daily biomass specific turbidity (ntu g^{-1}).

Model Nr / Response variable	Res/Tot DF	Variable	Est	Standard error	p-value
3.1.1 Turbidity, all days Error structure includes biomass as a variance co- variate and unit as variance cate- gory	68/96	Intcpt (MP, 0)	3.64	3.5×10^{-5}	2.8×10^{-313}
		factor(Cv)	-1.3	5.0×10^{-5}	3.5×10^{-277}
		Bm	-0.53	0.51	0.310
		factor(Day)-3	-0.96	5.0×10^{-5}	6.3×10^{-268}
		factor(Day)-6	-1.85	5.0×10^{-5}	4.3×10^{-291}
		factor(Day)-8	-2.30	5.0×10^{-5}	1.2×10^{-298}
		fact(Cv) : Bm	0.92	0.727	0.210
		fact(Cv):fact(Day)-3	1.84	7.1×10^{-5}	7.4×10^{-279}
		fact(Cv):fact(Day)-6	1.16	7.1×10^{-5}	7.9×10^{-263}
		fact(Cv):fact(Day)-8	1.44	7.1×10^{-5}	2.4×10^{-270}
		Bm:fact(Day)-3	10.6	0.727	3.2×10^{-24}
		Bm:fact(Day)-6	7.48	0.727	2.6×10^{-16}
		Bm:fact(Day)-8	13.4	0.727	1.6×10^{-30}
		Bm:fact(Cv):fact(Day)-3	-10.8	1.03	1.2×10^{-16}
		Bm:fact(Cv):fact(Day)-6	-1.81	1.03	0.082
		Bm:fact(Cv):fact(Day)-8	-0.36	1.03	0.724
3.1.2 Turbidity (unit total), all days Error structure included a within unit tem- poral autocorre- lation and bio- mass was used as a variance- covariate	37/48	Intcpt (Day 1)	2.8	0.87	0.002
		factor(Day 3)	-0.50	1.56	0.749
		factor(Day 6)	0.76	1.13	0.504
		factor(Day 8)	1.3	1.23	0.294
		Bm	0.7	2.03	0.557
		Bm (D3)	9.2	2.03	5.2×10^{-5}
		Bm (D6)	12.8	2.20	9.1×10^{-7}
		Bm (D8)	25.7	2.21	2.2×10^{-14}
3.1.3 BST	3/4	Intcpt	-5.0	4.35	0.369
		Day	3.5	0.82	0.05

3.3.3 Nutrients

3.3.3.1 Ammonium

Of the 24 samples, one (from MP at 0 g on day 1) was an incorrect measurement and one (from MP at 1 g on day 1) was an extreme outlier ($3 \times$ the third quantile of overall distribution on day 1). The error value was dropped from the data set and the data was plotted and analyzed with and without the outlier. $\text{NH}_4^+\text{-N}$ values were quite low across all treatments, overall average without the outlier was $13 \mu\text{mol L}^{-1}$ (1.9 mg L^{-1}) (Figure 3.10). $\text{NH}_4^+\text{-N}$ levels should have been relatively consistent across treatments at the start, however the tanks for the 0 g treatment seem to have had higher starting values. F-tests (Table 3.43, Model 3.2.1a), found no significant differences between $\text{NH}_4^+\text{-N}$ levels in *C. volutator* presence treatments ($p = 0.909$) or biomass treatments ($p = 0.275$) or their interaction ($p = 0.372$); no patterns were found between the residuals and the starting values (day 1). As the water columns in each unit were pooled during the experiment, to estimate $\text{NH}_4^+\text{-N}$ flux ($\Delta\text{NH}_4^+\text{-N}$) starting mean values per unit were subtracted from final unit means, so positive values represented flux out of the sediment and negative values represented flux into the sediment. Regression of $\Delta\text{NH}_4^+\text{-N}$ against *C. volutator* biomass (Figure 3.11, Model 3.2.2a) shows a slightly positive trend with and without the outlier (2.9 ± 6.7 or 3.9 ± 2.8 , respectively) but the relationships were not significant either with or without the outlier ($p = 0.670$ or $p = 0.205$, respectively).

3.3.3.2 Nitrate

Of the 48 samples analysed, 34 were measured as 0 and the overall mean value was $0.36 \mu\text{mol L}^{-1}$ ($5 \mu\text{g L}^{-1}$) so further graphics and analysis were not carried out.

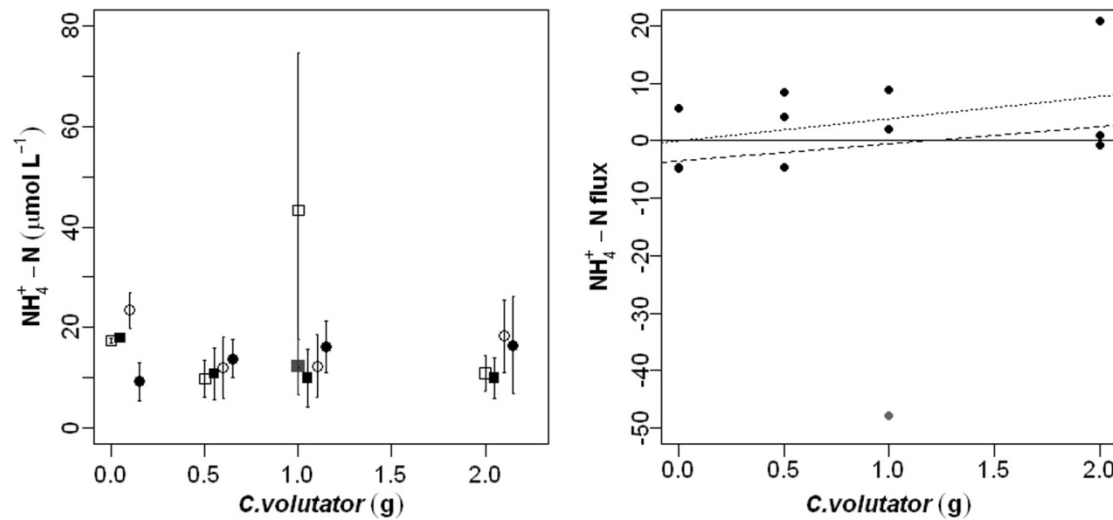


Figure 3.10: $\text{NH}_4^+ - \text{N}$ levels at the start (day 1, squares) and end (day 8, circles) across *C. volutator* presence (MP = open symbols; MA = closed symbols) and biomass treatments. The mean in the absence of the outlier is marked in grey. **Figure 3.11:** $\Delta\text{NH}_4^+ - \text{N}$ in each unit against *C. volutator* biomass. Dashed line represents the linear model with (Model 3.2a) the outlier (slope = 2.9; $p = 0.67$) and the dotted line represents the regression without the outlier (slope = 3.9; $p = 0.21$).

3.3.3.3 Phosphate

Mean phosphate levels across treatments, tended to be higher on day 8 than day 1 (Figure 3.12): mean $\text{PO}_4^{+} - \text{P}$ levels on day 1 and 8 were 2.6 and $3.7 \mu\text{mol L}^{-1}$ (or 79.8 and $114.3 \mu\text{g L}^{-1}$), respectively. There was no significant difference between the relationship of $\text{PO}_4^{+} - \text{P}$ and *C. volutator* biomass either in the MP ($p = 0.474$) or in the MA tanks ($p = 0.348$) Model 3.2.1b (Table 3.3). Phosphate flux per unit ($\Delta\text{PO}_4^{+} - \text{P}$), calculated as for $\text{NH}_4^+ - \text{N}$ above, indicated that flux was generally positive, i.e. phosphates were leaching from the sediment into the water column (Figure 3.13). While flux was generally positive (Table 3.4, Model 3.2.2a, estimate = 1.15 ± 0.49 , $p = 0.042$) it did not increase with increasing *C. volutator* biomass (estimate = -0.04 ± 0.43 , $p = 0.930$).

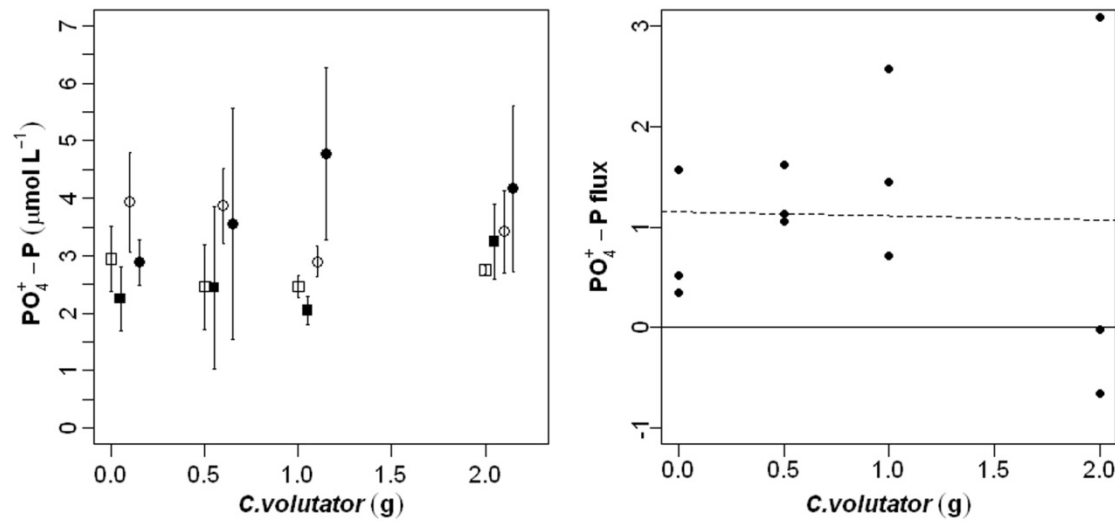


Figure 3.12: PO₄³⁻-P levels at the start (day 1, squares) and end (day 8, circles) across *C. volutator* presence (MP = open symbols; MA = closed symbols) and biomass treatments (left). **Figure 3.13:** ΔPO₄³⁻-P within each unit against *C. volutator* biomass (right). Dashed line represents the linear model (Model 3.2b).

Table 3.4: Regression results from Models 3.2.1 and 3.2.2

Model Nr / Response variable	Res/Tot DF	Variable	Est (DF)	St Error (F-stat)	p-value
3.2.1a	14/24	Intercept	1	46.5	<.0001
NH ₄ ⁺ -N		factor(Cv)	1	0.180	0.909
day 8		factor(Bm)	3	0.275	0.275
Biomass as variance- covariate		factor(Cv):factor(Bm)	3	0.372	0.372
3.2.1b	20/24	Intercept	3.8	0.49	1.8*10 ⁻⁷
PO ₄ ³⁺ -P		Bm	-0.31	0.43	0.474
MP/MA as variance		factor(Cv)	-0.53	1.15	0.647
categories		factor(Cv): Bm	0.97	1.00	0.348
3.2.2a	10/12	Intercept	-3.55	7.6	0.653
ΔNH ₄ ⁺ -N		Bm	2.93	6.7	0.670
without outlier	9/11	Intercept	-0.10	3.3	0.976
		Bm	3.91	2.9	0.205
3.2.2b		Intercept	1.15	0.49	0.042
ΔPO ₄ ³⁺ -P		Biomass	-0.04	0.43	0.930

3.3.4 Sediment water and organic content

One set of the two replicate samples from each tank were discarded as a batch was clearly insufficiently dried prior to incineration and therefore had been found to be unusually high (mean = 24 %) organic content. Mean percentages of water and organic content of the sediment across treatments are presented (Figures 3.14 and Figures 3.15). Pearson correlations between final and starting values (correlation = 0.264, DF = 22, t-value = 1.28,) were investigated prior to model fitting and found not to be significant in either case (% water: DF = 22, t-value = -0.629, p-value = 0.536. % organic: DF = 2, t-value = 1.28, p-value = 0.213) nor were any patterns found in the residuals over starting values. Percentage water content of sediment on day 8 was generally higher than on day 1, with the exception of MA tanks in the 2 g treatment group which were slightly higher on day 1 (Table 3.2, Figure 3.14). There were no effects of either the presence or the biomass of *C. volutator* on the water content of the sediment (Figure 3.14). Percentage organic content of sediments in all tanks on both days were more or less consistent with the exception of MA tanks in the 1 g and 2 g treatment groups which were much higher on day 8. Although there were high values for organic content in the MA tanks on day 8, F-tests (on Model 3.3, Table 3.1, Res/Tot DF = 14/24, fitted values as variance-covariate) showed that neither *C. volutator* presence, (DF = 1/16, F-value = 2.14, p-value = 0.163), or biomass (DF = 3/16, F-value = 0.323, p-value = 0.809), or their interaction (DF = 3/16, F-value = 0.091, p-value = 0.964) had a significant effect on the organic content of the sediment.

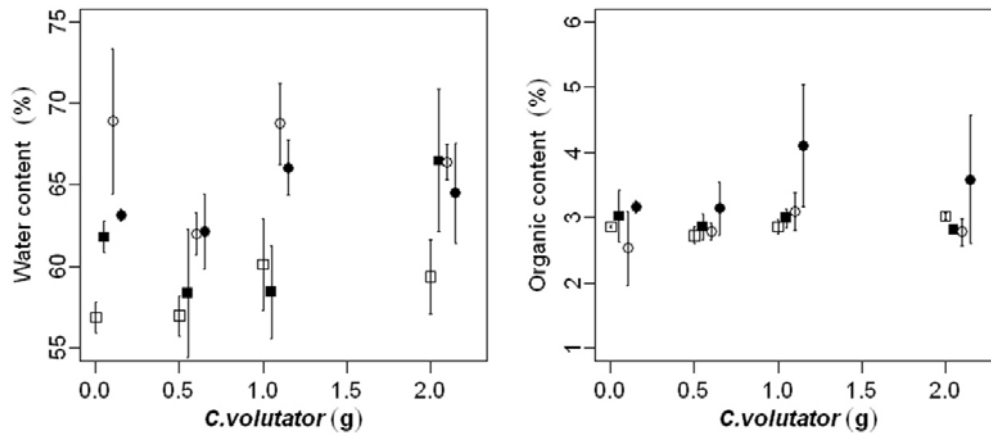


Figure 3.14: Mean water content of the sediment in each treatment. **Figure 3.15:** Mean sediment organic content, in each of the 8 treatments on day 1 and day 8 (right). Day 1 (squares); day 8 (circles); MP (open symbols); MA (closed symbols); Error bars represent ± 1 standard error.

3.3.5 Sediment chlorophyll-*a* content

Chlorophyll - *a* concentration of sediment on day 8 was generally higher than on day 1, with the exception of MA tanks in the 2 g treatment group which is slightly higher on day 1 (Table 3.2, Figure 3.16). There were no clear patterns between chlorophyll *a* concentrations and treatment groups, neither is there a correlation between final and starting values ($\text{cor} = -0.07$, $p = 0.747$). While there is no relationship between chlorophyll *a* concentrations against incident light intensity there is a significant correlation ($p = 0.025$) between chlorophyll *a* concentration evening temperatures (Figures 3.19 E and F, respectively). There are no significant correlations between chlorophyll *a* concentrations mean turbidity unit ammonium concentrations, and unit phosphate concentrations (Figures 3.20 D, E, and F, respectively).

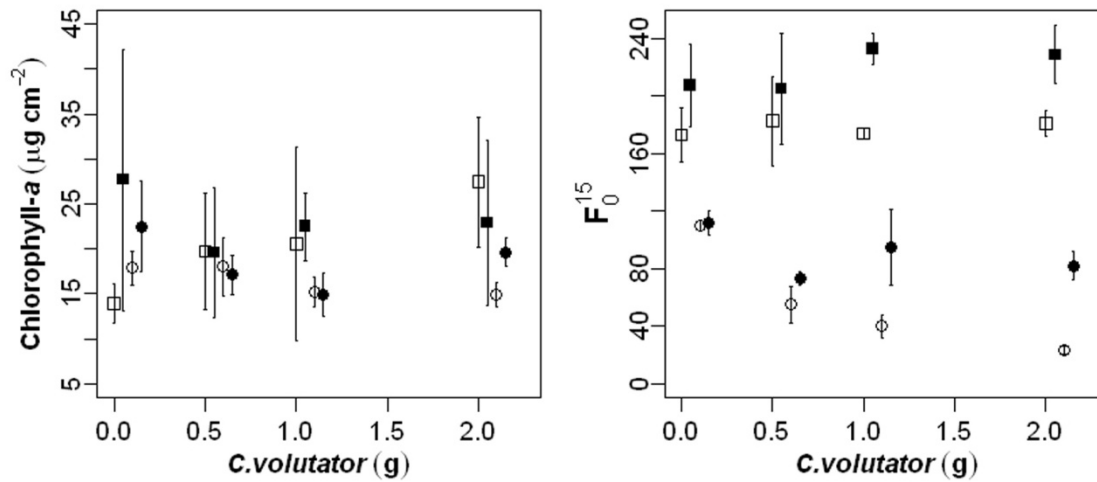


Figure 3.16: Mean chlorophyll-a (in $\mu\text{g cm}^{-2}$ of sediment ± 1 standard error) over all biomass levels on day 1 (squares) and day 8 (circles) in MP (open circles) and MA (closed circles). **Figure 3.17:** F_0^{15} on day 8 against *C. volutator* biomass with MP tanks as open symbols and MA tanks as closed symbols.

Statistical analysis of final chlorophyll *a* concentrations included the five environmental variables (above) as covariates, as well as the feeding biomass (FBm) in the tanks (i.e. 0 for all MA tanks) as a covariate and *C. volutator* presence as a factor. Temperature and light intensity were centralised. There was no covariation between any of the covariates except feeding biomass and mean turbidity (0.74, $p = 2.9 \times 10^{-5}$). As there are only 24 data points it is not possible to fit a full interaction model so only the two most relevant 2-way interactions were chosen *a priori*: the interaction between incident light and turbidity (reflecting actual light intensity at the sediment bed) and the interaction between *C. volutator* presence and turbidity. The final model is presented in Table 3.4. While neither factor(Cv):mnTurb interaction nor the *C. volutator* presence main effect had a significant on chlorophyll *a* concentrations ($p = 0.077$ and $p = 0.244$, respectively) the model AICc increased with their removal. Chlorophyll *a* content was estimated to decrease by $2.5 \mu\text{g cm}^{-1}$ with each unit of turbidity ($p = 0.001$) and decrease by $-0.04 \mu\text{g cm}^{-1}$ with each additional $\mu\text{mol m}^{-2} \text{s}^{-1}$ of light intensity ($p = 8.5 \times 10^{-9}$). Chlorophyll *a* content was estimated to increase by 3.8

$\mu\text{g cm}^{-1}$ with each additional $\mu\text{mol L}^{-1}$ phosphate and, strangely, by $13.8 \mu\text{g cm}^{-1}$ with each additional gram of *C. volutator*. No latent patterns were found in the residuals with regard to starting values. Bootstrapped slopes and 95% confidence intervals plotted against turbidity (in Figure 3.22). In the full model, at low phosphate levels and 1 g *C. volutator* the estimates and lower confidence intervals at high turbidities become negative, which is impossible for chlorophyll *a* values. However, as none of the fitted values from the model (without bootstrap) are negative and these are only a few extreme cases it did not necessitate use of a more complex distribution.

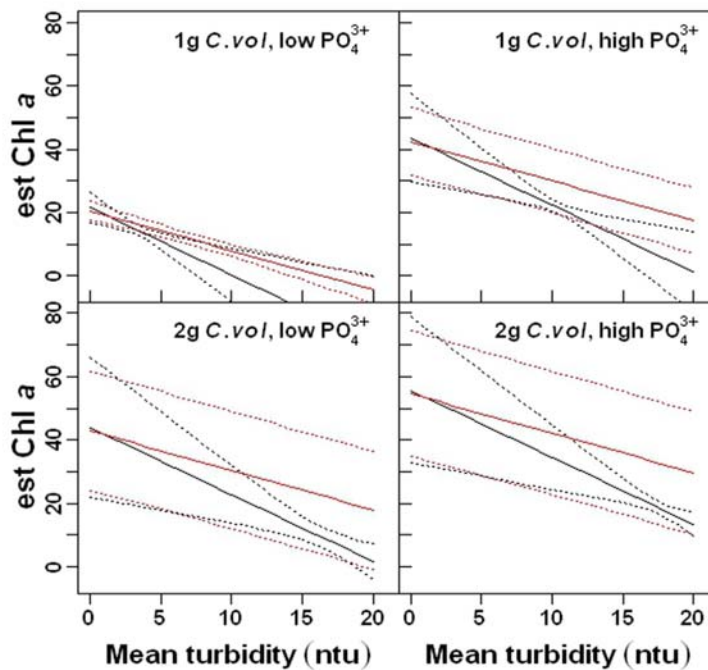


Figure 3.18: Bootstrapped 95% confidence intervals over the full range of mean turbidity (Model 3.4) at mean temperature and light intensities, where *C. volutator* were present (black lines) and absent (red lines).

3.3.6 Surface biomass (F_0)

Fluorescence signal strength at 4 mm probe height was calibrated over a turbidity range of 0.35 (seawater) to 100 ntu to determine whether fluorescence measurements needed to be adjusted for signal loss at increasing turbidity. The maximum turbidity

measured, 35 ntu, corresponded to < 2% signal loss so fluorescence values were not adjusted. While fluorescence values below 100, in the FMS2, are not considered reliable enough for photosynthetic efficiency measurements they are acceptable for biomass comparisons (Mouget 2011, personal communication) provided that the measurement of a non-fluorescing material is 0.

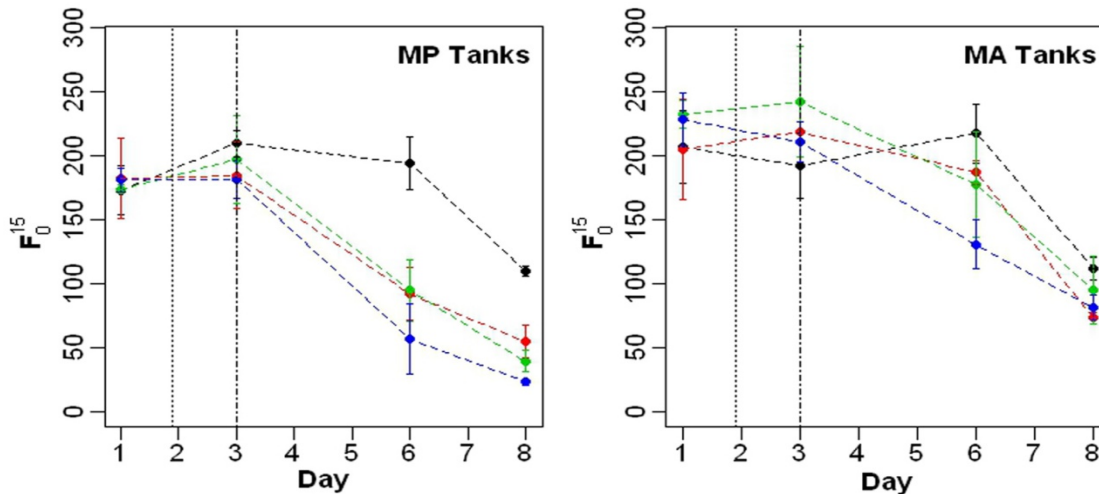


Figure 3.19: Average microphytobenthic biomass measured by minimum fluorescence (F_0^{15} , arbitrary units) in each treatment: *C. volutator* biomass treatments are: black (0 g), red (0.5 g), green (1.0 g), and blue (2.0 g).

F_0 in the *C. volutator*-MA tanks were lower than in the control-MA tanks (Figure 3.18). Day 1 F_0 values plotted against incident light intensity (Figure 3.19 A) and evening temperatures (Figure 3.19 B) suggested that it is temperature, not incident light, that is likely to have created the variation between treatment groups. There was no correlation between F_0 and chlorophyll *a* values from each tank either on day 1 or day 8 (see Figure 3.23 A and B, respectively). Surface MPB biomass on day 8 in both the MP and MA tanks clearly declines with increasing *C. volutator* biomass and that this decline was more pronounced in the MP tanks (Figure 3.18). Figures 3.19 C and D shows that on day 8 a negative trend between had emerged between incident light intensity and surface biomass while the earlier negative trend with increasing eve-

ning temperatures was absent. There was a significant negative correlation ($p = 8.5 \times 10^{-5}$) between turbidity and surface biomass (Figure 3.20 A) while there was a slight but not significant increase in surface biomass with increasing mean ammonium and phosphate levels in the overlying water (Figures 3.20 B and C).

The minimum adequate model (Table 3.4, Model 3.5) retained only mean turbidity: each extra unit of turbidity decreased surface biomass by 3.9 (arbitrary units) and the presence of *C. volutator* in the tank decreased surface biomass by another 42.4. Contrary to plotted patterns (Figure 3.19 D), a 1°C increase in temperature (full range 1.6°C) was estimated to increase surface biomass by 23.9, whereas a $1 \mu\text{mol m}^{-2} \text{s}^{-1}$ increase in light intensity was estimated to decrease F_0 by only 0.7. However, whereas both increased incident light and increased turbidity decreased F_0 , their effect was slightly tempered by a positive interaction between the two covariates; while this interaction is borderline in terms of significance ($p = 0.056$), removing it from the model increases the AICc and skews the residuals. The opposite effects of light and turbidity are due to the fact that the tanks with the most disparate levels of incident light (152 and $312 \mu\text{mol m}^{-2} \text{s}^{-1}$) had very similar average turbidities (11.4 and 10.2 ntu) and the one with the lower light had a higher final F_0 (63 vs. 49). Finally, higher mean phosphate levels in the overlying water corresponded to higher F_0 ($p = 0.05$). The final model has an outlier (residual = 3 st. dev) which was from the 1.0 g *C. volutator* MA treatment, and has high mean phosphate value and temperature.

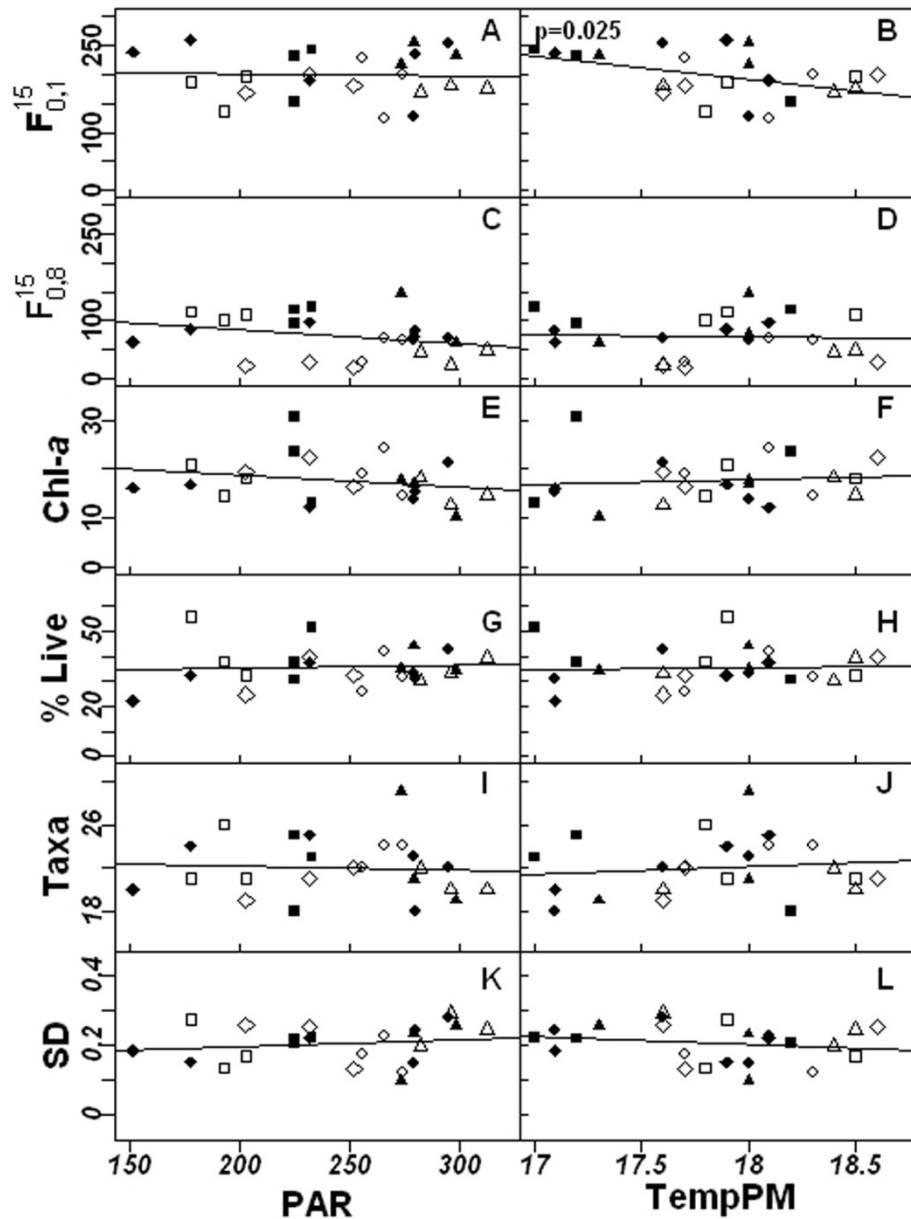


Figure 3.20 A – L: MPB biomass (F_0 , Chlorophyll *a*) and assemblage (% live cells, number of live taxa, and Simpson's diversity index) measurements on day 8 (and day 1 for F_0) against light intensity (PAR, $\mu\text{mol m}^{-2} \text{s}^{-1}$) in the left column (A, C, E, G, I, K) and evening temperatures ($^{\circ}\text{C}$) in the right-hand column (B, D, F, H, J, L). Trend lines represent Pearson correlations with only the significant p-values given. Open and closed symbols represent MP and MA tanks, respectively, and biomass treatments are represented in numeric order by squares, circles, triangles, and diamonds.

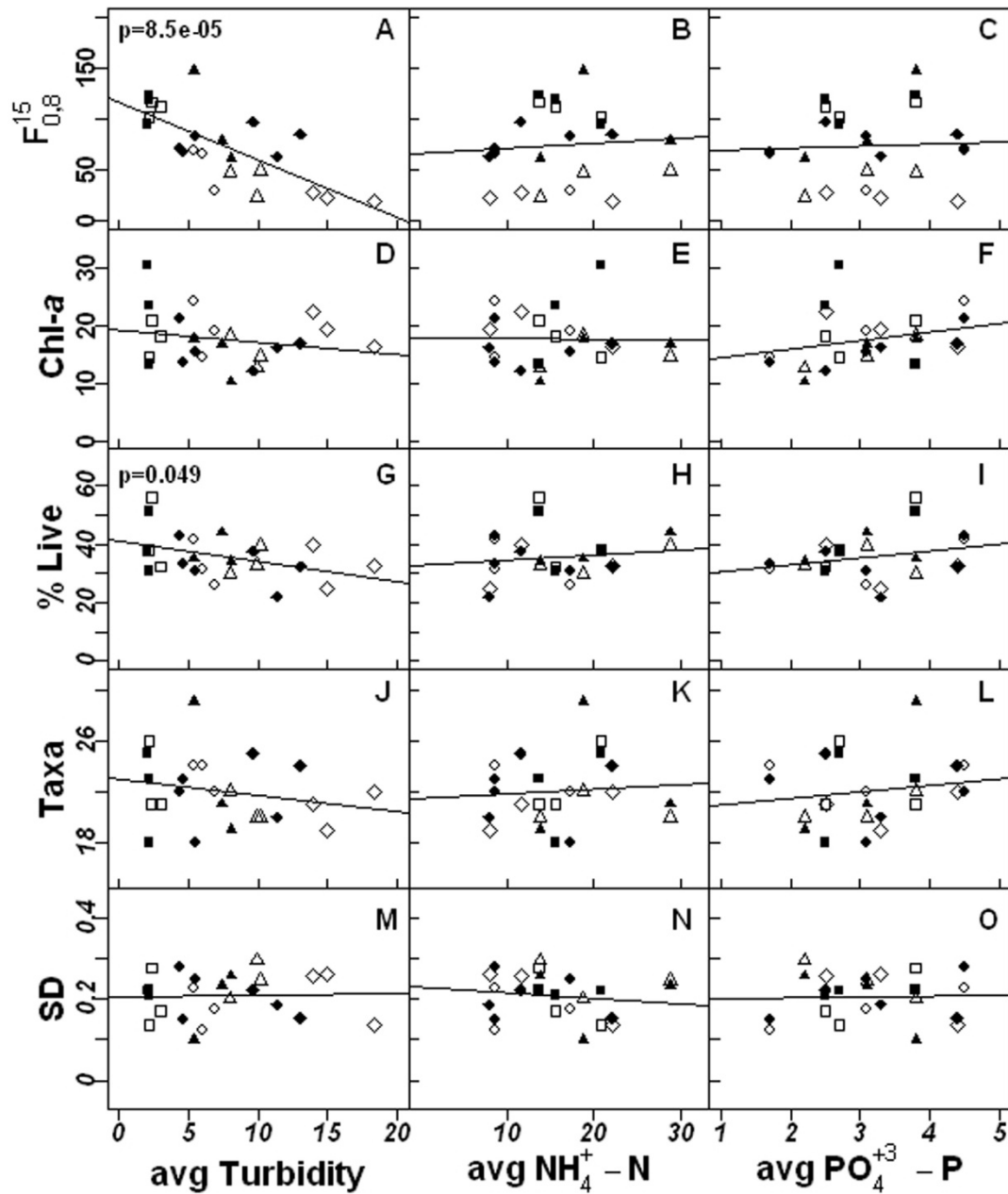


Figure 3.21 A – O: MPB biomass (F_0 , Chlorophyll *a*) and assemblage (% live cells, number of live taxa, and Simpson's diversity index) measurements on day 8 against the average turbidity in each tank and mean NH₄-N and PO₄-P in each unit over the experimental period. Open and closed symbols represent MP and MA tanks, respectively, and biomass treatments are represented in numeric order by squares, circles, triangles, and diamonds. Trend lines represent Pearson correlations and p values are presented only where correlations are significant ($p < 0.05$).

Table 3.5: Summary table for Model 3.4 on Chlorophyll *a* ($\mu\text{g cm}^{-1}$) and Model 3.5 F_0 (arbitrary units).

AICc	resDF/ totDF	Parameter for	EST	Std Error	p-value
159.3	13/24	Chl <i>a</i> _{<i>i</i>} ~ mnTurb _{<i>i</i>} + factor(Cv) _{<i>i</i>} + FBm _{<i>i</i>} + cTemp _{<i>i</i>} + cPAR _{<i>i</i>} + (mnNH ₄ ⁺) _{<i>i</i>} + mnPO ₄ ³⁺ _{<i>i</i>} + mnTurb :factor(Cv) _{<i>i</i>} + mnTurb :cPAR _{<i>i</i>} + ε_i ; $\varepsilon_i \sim N(\mu, \sigma^2 \cdot V)$; V= fitted values as variance-covariate			
122.4	15/24	Chl <i>a</i> _{<i>i</i>} ~ mnTurb + factor(Cv) + cPAR + mnTurb *factor(Cv) + mnPO ₄ + ε_{ij} ; $\varepsilon_{ij} \sim N(\mu, \sigma^2 \cdot V)$			
		Intercept	17.1	1.4	5.5*10 ⁻¹⁰
		factor(Cv) - MA	-2.0	1.7	0.244
		mnTurb	-2.5	0.6	0.001
		FBm	13.8	4.5	0.007
		cPAR	-0.04	0.004	8.5*10 ⁻⁹
		mnPO ₄	3.8	0.4	9.6*10 ⁻⁹
		factor(Cv):mnTurb	1.1	0.60	0.077
237.3	13/24 12/23	F_{0i} ~ mnTurb _{<i>i</i>} +factor(Cv) _{<i>i</i>} + FBm _{<i>i</i>} + cTemp _{<i>i</i>} + cPAR _{<i>i</i>} + (mnNH ₄ ⁺) _{<i>i</i>} + mnPO ₄ ³⁺ _{<i>i</i>} + mnTurb :factor(Cv) _{<i>i</i>} + mnTurb : cPAR _{<i>i</i>} + ε_i ; $\varepsilon_i \sim N(\mu, \sigma^2 \cdot V)$; V = light intensity as a variance-covariate			
219.2	16/24 15/23	F_0 ~ mnTurb + factor(Cv) + cTemp + cPAR + mnTurb: cPAR + mnPO ₄ + ε_{ij} ; $\varepsilon_{ij} \sim N(\mu, \sigma^2 \cdot V)$			
		Intercept	53.8	17.3	0.0064
			61.1	13.0	0.0002
		factor(Cv)	42.4	9.2	0.0003
			37.1	7.0	7.0*10 ⁻⁵
		mnTurb	-3.9	1.1	0.0017
			-3.7	0.8	0.0003
		cTemp	23.9	8.4	0.0108
			19.0	6.3	0.0085
		cPAR	-0.699	0.2	0.0080
			-0.75	0.2	0.0005
		mnPO ₄	9.0	4.3	0.0504
			6.2	3.3	0.0780
		mnTurb:cPAR	0.056	0.03	0.0560
			0.058	0.02	0.0110

Model visualisations (Figure 3.23) of bootstrapped slopes and 95% confidence intervals were plotted against mean turbidity at low, high, and no phosphate (from the minimum model without the outlier). In the full model, at low phosphate levels, estimates and lower confidence intervals at high turbidities become negative, which is of course not possible for fluorescence values and is due to the normal distribution being used. Removing the outlier from the model (Table 3.4, values in grey) removes the significance of phosphate from the model ($p = 0.078$, $\Delta\text{AICc} = -0.2$) and reduced the effect of temperature and *C. volutator* presence, and increased the effect of light intensity and the significance of the light intensity-turbidity interaction ($p = 0.011$).

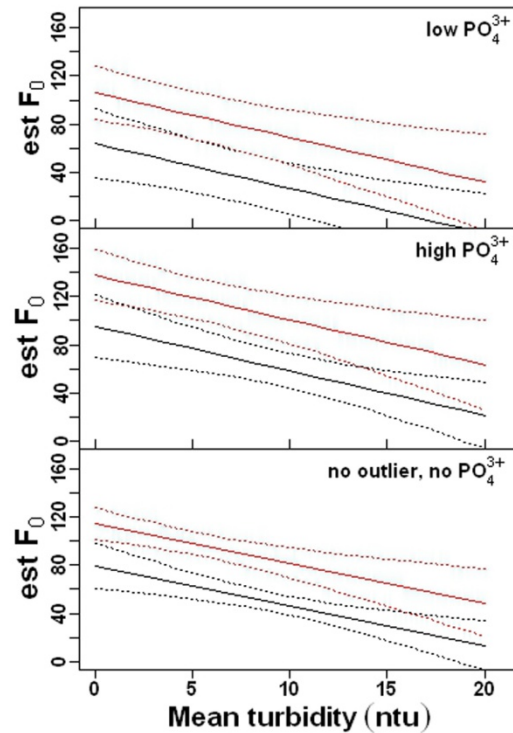


Figure 3.22: Bootstrapped predictions and 95% confidence intervals (Model 3.5) over the full range of mean turbidity in the presence (black lines) and absence (red lines) of feeding *C. volutator* at mean temperature and light intensities.

3.3.7 MPB assemblage

The original assemblage in the biofilm slurry contained $70 (\pm 3)$ % live cells distributed across 26 size and shape taxa. At $49 (\pm 4)$ %, small *Navicula* ($\leq 30 \mu\text{m}$ length) contributed the largest proportion of live cells, and these groups were composed *N. gregaria* and 2 morphotypes of *N. phyllepta* (see Appendix 1 & 2), *Gyrosigma fasciola* made up $21 (\pm 2)$ %, and *Cylindrotheca closterium* and *gracilis* combined made up $7 (\pm 1)$ %, and, finally, several species of cyanobacteria (*Merismopedia*, *Oscillatoria* and *Spirulina* sp) made up $9 (\pm 2)$ % of the live assemblage.

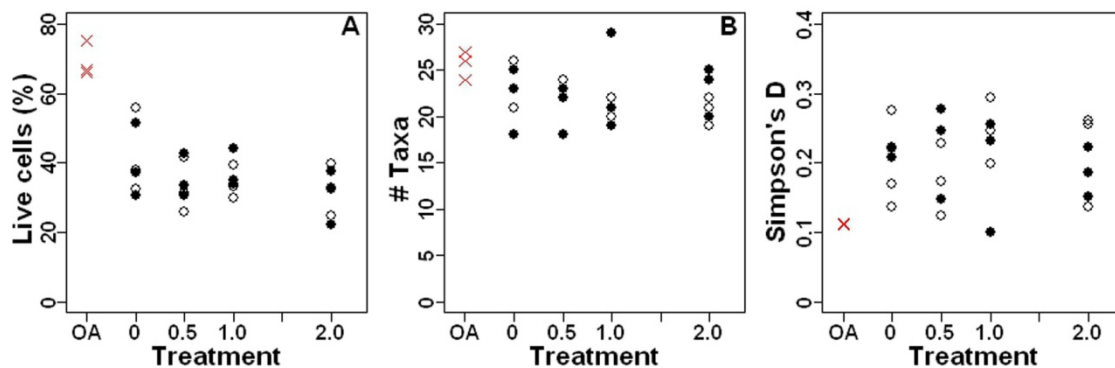


Figure 3.23 A – C: % Live cells (A), species richness (live taxa, B), and transformed Simpson diversity (C) against *C. volutator* biomass treatment with MP tanks as open symbols and MA tanks as closed symbols. The original assemblage (OA) values are marked with red crosses.

3.3.7.1 Proportion Live cells

The proportion of live cells in the sediment had declined from $70 (\pm 3)$ % to $37 (\pm 4.5)$ % by day 8; there also appeared to be a slight decline in % live cells with increasing biomass but no difference with *C. volutator* presence or absence (Figure 3.23 A). There was no significant correlation between % live cells against incident PAR or evening temperatures (Figures 3.19 G & H) but there was a significant decline in % live cells with increasing turbidity (Figure 3.20 G, Pearson correlation coefficient of -0.41 , $DF = 22$, $t = -2.1$, $p = 0.05$), but no significant change with increasing $\text{NH}_4^+\text{-N}$ and $\text{PO}_4^{3-}\text{-P}$ fluxes (Figures 3.20 H & I). However, in the regression of % live cells

against environmental variables in each tank (Model 3.6) there were no residual significant effects of any of the measured variables, including mean turbidity (Table 3.4). The proportion of live cells corresponds significantly with F_0 on day 8 ($\text{cor} = 0.417$, $t = 2.2$, $\text{df} = 22$, $p\text{-value} = 0.043$) but not with chlorophyll *a* content of the sediment on day 8.

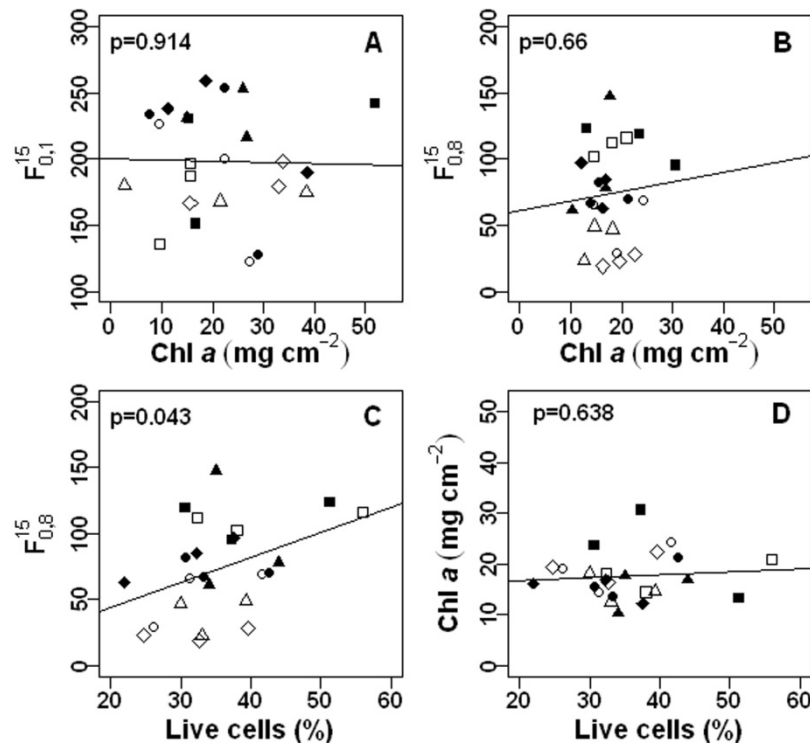


Figure 3.24: Comparison of biomass measurements: F_0 against sediment chlorophyll *a* on Day 1 (A) and day 8 (B), and F_0 (C) and chlorophyll *a* (D) against % live cells. Open and closed symbols represent MP and MA tanks, respectively, and biomass treatments are represented in numeric order by squares, circles, triangles, and diamonds. Probabilities from Pearson product moment correlations are presented on each plot.

3.3.7.2 Taxa richness

The number of size and shape taxa in the samples declined from $26 (\pm 1)$ to an overall average of $22 (\pm 1.5)$ by day 8 (Figure 3.24 B) but the difference was not significant ($\text{DF} = 8/18$; $F\text{-test} = 0.976$, $p = 0.484$). There was no correlation between number of

taxa against incident PAR or evening temperatures (Figures 3.19 I & J) and while mean F_0 (Figure 3.20 J) declined slightly with increasing turbidity and increased slightly with increasing $\text{NH}_4^+\text{-N}$ and $\text{PO}_4^{3-}\text{-P}$ fluxes (Figures 3.20 K & L), none of these correlations were significant ($p > 0.05$). The regression of taxa number against environmental variables in each tank (Model 3.7) required unit as a random factor and there were no significant effects of any of the measured variables (Table 3.4).

3.3.7.3 Live assemblage diversity

Simpson's index of diversity for the original assemblage was 0.111 (± 0.0003), meaning there was a 11.1% probability that two individuals picked at random from the population would be from the same taxa, and increased to an average of 0.207 (± 0.03) across all tanks by day 8 (Figure 3.24 C). There were no correlations between diversity and light intensity or temperature (Figures 3.19 K and L), or mean turbidity, ammonium and phosphate quantity in the overlying water column (Figure 3.20 M, N, and O). Consequently, the regression of negative log transformed diversity (Magurran 2004) against any of these variables (Model 3.8, with unit as random factor) showed no significant covariation (Table 3.4).

3.3.7.4 Live assemblage comparison

An MDS plot with the Bray-Curtis similarity indices for each treatment (including the original assemblage) shows that the final assemblages were different from the starting values but there are no clusters between the experimental treatments suggesting that neither *C. volutator* feeding or water column modification exerted any selective pressure on MPB assemblage.

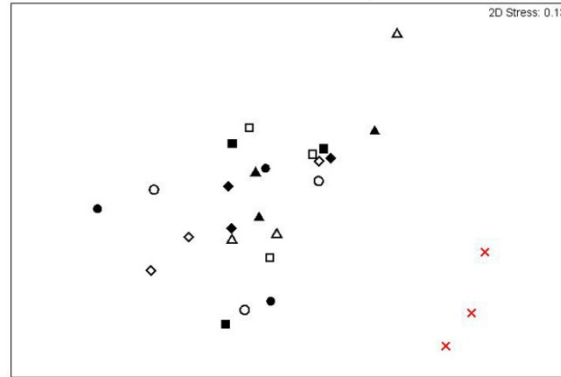


Figure 3.25: MDS plots of Bray-Curtis similarity indices from each MPB sample. Open and closed symbols represent MP and MA tanks, respectively, and biomass treatments are represented by squares (0g), circles (0.5g), triangles (1g), and diamonds (2g), original assemblage samples are represented by a red x.

Table 3.6: Summary table for Models 3.6 – 3.7 for % live cells, species richness, and $-\ln D$, respectively.

AICc	resDF/ totDF	Parameter for	EST	Std Error	p-value
180.1	12/24	$pLive_i \sim mnTurb_i + factor(Cv)_i + FBm_i + cTemp_i + cPAR_i + (mnNH_4^+)_i + (mnPO_4^{3+})_i + mnTurb_i : factor(Cv)_i + mnTurb_i : cPAR_i + \epsilon_i; \epsilon_i \sim N(\mu, \sigma^2 * V); V = \text{"unit" as variance category,}$			
150.3	21/24	$pLive_i \sim intercept + \epsilon_{ij}; \epsilon_{ij} \sim N(\mu, \sigma^2 * V)$			
		Intercept	35.7	2.2	0.006
155.8	12/24	$SR_i \sim mnTurb_i + factor(Cv)_i + FBm_i + cTemp_i + cPAR_i + (mnNH_4^+)_i + (mnPO_4^{3+})_i + mnTurb_i : factor(Cv)_i + mnTurb_i : cPAR_i + \epsilon_i; \epsilon_i \sim N(\mu, \sigma^2 * V)$			
119.8	21/24	$SR_i \sim intercept + \epsilon_{ij}; \epsilon_{ij} \sim N(\mu, \sigma^2 * V)$			
		Intercept	22.0	0.63	$1.9 * 10^{-13}$
47.5	12/24	$-\ln D_i \sim mnTurb_i + factor(Cv)_i + FBm_i + cTemp_i + cPAR_i + (mnNH_4^+)_i + (mnPO_4^{3+})_i + mnTurb_i : factor(Cv)_i + mnTurb_i : cPAR_i + \epsilon_i; \epsilon_i \sim N(\mu, \sigma^2 * V)$			
12.9	21/24	$-\ln D_i \sim intercept + \epsilon_{ij}; \epsilon_{ij} \sim N(\mu, \sigma^2 * V)$			
		Intercept	1.6	0.07	$2.7 * 10^{-11}$

3.4 Discussion

3.4.1 The effects of *C. volutator* on sediment and overlying water column

Turbidity increased linearly with *C. volutator* biomass on all three days (see Figure 3.8. day 3: 9.2 ± 2.0 , $p < 0.0001$; day6: 12.8 ± 2.2 , $p < 0.0001$; day 8: 25.7 ± 2.2 , $p < 0.0001$) and turbidity g^{-1} also increased linearly with day (Figure 3.9, $-0.5 + 3.5 \cdot \text{day}$, $p=0.05$). In similar experiments with increasing *C. volutator* biomasses in aquaria without flow, de Deckere and colleagues (2000) found an exponential increase in suspended sediment with increasing *C. volutator* biomass ($y = 50 + 0.43x^{0.45}$), whereas Biles and colleagues (2002) found a sigmoidal relationship, where the suspended sediment in the 1 g biomass group (surface area same as in this experiment) hardly varied from 0 g biomass group but the 2 g treatment was 8 fold higher than the 1 g treatment. However, both studies had much higher maximum biomasses than this one (5x and 4x, respectively), so possibly, had this experiment included a 8 or 10 g group, the relationship would eventually no longer have been linear but flattened off. With respect to the *C. volutator* presence/absence treatments in this experiment, the pumps distributed the overlying water effectively as there were no significant differences in turbidity between the tanks within each unit after they were switched on (see Table 3.2, Model 3.1.1: on days 6 & 8 p-values = 0.082 & 0.724, respectively). Lastly, if *C. volutator* pumping rate increases with temperature (as per Møller & Riisgård 2006) then turbidity should also increase with temperature, however, the 1.6 °C range in evening temperatures did not correlate with turbidity on any day (Pearson correlations day 3, 6, and 8, respectively: -0.044, 0.168, and 0.294; p-values: 0.608, 0.431, and 0.162). This suggests that a temperature difference of < 2 °C is not sufficient to initiate any behavioural change in *C. volutator*.

In contrast to multiple studies, on both laboratory reconstructed sediment microcosms and in the field, which have demonstrated *C. volutator* presence increasing ammonium flux from the sediment to the overlying water column (Henriksen *et al* 1980; Henriksen *et al* 1983; Emmerson *et al* 2001; Biles 2002; Mermillod-Blondin *et al* 2004, Bulling *et al* 2010), in this study the ammonium flux to the overlying water column did not significantly increase with increasing biomass (Figure 3.11 and Table 3.3, Model 3.2.2a, slope = 2.9 ± 6.7 , $p = 0.670$). There are several possible reasons why there was not much distinction in ammonium levels in the overlying water. First, coupled nitrification-denitrification could have simultaneously depleted ammonia and nitrate levels leading to lower ammonium levels in the overlying water column. The source of the increased ammonia is partially *C. volutator* excretion and partially ammonia release from lower depths in the sediment, due to bioturbation, where ammonia concentrations are higher (Henriksen *et al* 1980, 1983). However, in conjunction with the release of ammonium, there can also be an increase in nitrification, mediated by aerobic bacteria, and denitrification mediated by anaerobic bacteria living along in the oxic-anoxic boundary – the surface areas of both of these habitats are increased substantially by burrow building and irrigation (Pelegri & Blackburn 1994; Pelegri *et al* 1994; Rysgaard *et al* 1995). In Pelegri and Blackburn's experiment (1994) ammonium from overlying water fluxed into the sediment but ammonium levels in the sediment also decreased and this was due to enhanced coupled nitrification-denitrification in the sediment with *C. volutator* burrows. However, it has also been shown that coupled nitrification-denitrification increases with increasing nitrate levels in the overlying water column (Pelegri *et al* 1994; Rysgaard *et al* 1995) and as nitrate levels were almost nil from the start of this experiment, coupled nitrification-denitrification probably was not the reason for the lack of relationship between *C. volutator* biomass and ammonium in the overlying water column. Second, MPB

biofilms themselves influence biogeochemical fluxes: phosphate and dissolved inorganic nitrogen release tends to be low or negative (going into the sediment) in the light, when photosynthesis is presumably sequestering resources, and becomes more positive when in the dark or with increased respiration in the sediment (Henriksen *et al* 1980; Andersen & Kristensen 1988; Rizzo 1990) whereas others have found that nitrogen dynamics are seasonal and whereas slight nitrate uptake prevails in spring ammonium release prevails in summer (Feuillet-Girard *et al* 1997). As each tank containing a *C. volutator* biomass treatment was coupled to a tank containing only sediment and MPB and measurements were only made from single samples from each tank on days 1 and 8 it is impossible to tell which tank had a stronger effect on the overlying water column and whether a negative or positive flux of one tank could have cancelled out the negative or positive flux in the other tank. This uncertainty would have been avoided by measuring the fluxes within the two tanks of each unit independently of each other: stopping the pumps, plugging the tanks, and then sampling the water immediately, at 3 hours, and at 6 hours before draining the water. Daily net fluxes could have then been calculated for each day to establish (independent) trends for *C. volutator* presence and biomass treatments. Finally, it is possible that ammonium was flushed from the mud because, due to a delay in starting the experiment, mud previously collected, sifted, and stored outdoors had to be aerated to prevent it from becoming completely anoxic prior to starting the experiment – water was poured off every 3 days and fresh oxygenated seawater stirred in. Not only could this have washed away porewater nutrients but it is also possible that the sediment had not stabilized by day 1, hence the large outlier (see Figure 3.10). Experiments on nutrient fluxes by other researchers have allowed mesocosms to be established from anywhere from 2 – 9 weeks before making flux measurements (Henriksen *et al* 1980; Henriksen *et al* 1983; Andersen & Kristensen 1988; Pelegri &

Blackburn 1994; Emmerson *et al* 2001; Mermillod-Blondin 2004), although there have been experiments where significant differences in fluxes between treatments have been found after just 5 – 7 days and with a similar setting-up procedure (Biles *et al* 2002; Bulling *et al* 2010). Also, the variability in nutrient levels is quite large so possibly a larger sample size was required to detect relatively small differences. A power analysis by Ieno and colleagues (2006) concluded that a minimum sample size of 5 was required to detect a significant nutrient release from sediments bioturbated by different macrofauna, although Biles and colleagues (2002) found significant differences with only 3 replicates. Phosphates fluxes between days 1 and 8 also did not vary significantly between *C. volutator* biomass treatments (Figure 3.13 and Table 3.3, Model 3.2.2b, slope = -0.04 ± 0.43 , $p = 0.930$). The reasons are probably similar to those discussed for ammonium release above. However, interestingly phosphate was released (fluxes from day 1 to 8 are mostly positive) across all treatments, including the control, which suggests that phosphate flux is either purely diffusive or that it is mediated by MPB rather than macrofauna. As water samples for flux measurements were taken in the morning after only maximum 2 hours of light, it is possible that it is simply the release of phosphate in the dark as described by previous authors (Henriksen *et al* 1980; Andersen & Kristensen 1988; Rizzo 1990) that is being detected.

Water content over the top 2 mm of sediment varied substantially within and between *C. volutator* treatments (on both days) but no relationship was apparent because while water contents on day 8 were mostly higher than on day 1 this was also true for the control treatment (see Figure 3.14). Meadows and Tait (1989) found a significant negative correlation between sediment water content and *C. volutator* biomass in their laboratory cores, which they reasoned was due to burrows providing increased drainage from surface sediment, whereas Gerdol and Hughes (1994b) and de Deckere and colleagues (2001) in field experiments in which *C. volutator* and

other infauna were excluded from patches of sediment found that water content increased in the presence of burrowing infauna. In contrast one would expect the organic content in the top 2 mm of sediment to decrease with increasing *C. volutator* density because they feed on MPB as well as EPS. However, although while there were no real differences in sediment organic content between *C. volutator* presence and biomass treatments, organic content in the MA treatments of the 1 and 2 g treatments were higher than those in the corresponding MP treatments by 1 and 0.8 % (Figure 3.15). De Deckere and colleagues (2000) found lower organic content in sediment where *C. volutator* was present (but found no further decreasing relationship at increasing densities) and higher percentages of organic content in the suspended sediment, which increased with increasing *C. volutator* density. It is possible that suspended sediment with organic content from the MP tanks settled on the surface in the MA tanks whereas it was more likely to remain suspended in the MP tanks. However, if that were the case, then the organic contents in the MA tanks should be correspondingly lower, which they were not. For both sediment assays, larger samples or pooling of sample cores from the same tanks instead of measuring them separately could possibly have reduced the variance within tanks and within treatments. Also freeze drying rather than oven drying is a more accurate as it is immediately apparent when there is moisture remaining after the standard drying time. Slight variations in residual moisture content in the samples following drying and prior to incineration would lead to both inaccurate estimation of water and organic content.

3.4.2 Effects of *C. volutator* on MPB biomass

There were differences in light and temperature across the bench: temperatures were generally higher in the back row (Figure 3.26) and light intensities were higher under the middle of each light array than near the edges. Unfortunately, tanks were placed

in such a way that meant that light and temperature differences were confounded with *C. volutator* presence and biomass treatments: MP tanks had higher temperatures than MA tanks and the 0.5 and 1 g biomass treatments had, on average, up to $100 \mu\text{mol m}^{-2} \text{s}^{-1}$ more light than the 0 and 2 g treatment.

As with other sediment assays, cores for chlorophyll *a* extraction probably had too small a surface area (57 mm^2) and should have been pooled prior to assaying to provide a more accurate measure of chlorophyll *a* content of sediment. Chlorophyll *a* values also varied greatly within treatment (though more so on day 1) and did not present any obvious patterns with *C. volutator* presence or biomass treatments (Figure 3.16). However, when regressed against the environmental variables in each tank (Table 3.4, Model 3.4), both turbidity and incident light intensity had a significant negative effect on chlorophyll *a* concentration ($-2.5 \pm 0.6 \mu\text{g cm}^{-2} \text{ntu}^{-1}$, $p = 0.001$ and $-0.04 \pm 0.004 \mu\text{g cm}^{-2} \mu^{-1}$, $p = 8.5 \times 10^{-9}$, respectively), while phosphate in the water column and, oddly, the biomass of feeding *C. volutator* in the tank both had a significant positive effect on chlorophyll *a* concentration ($3.8 \pm 0.4 \mu\text{g cm}^{-2} \mu\text{mol}^{-1}$, $p = 0.007$ and $13.8 \pm 4.5 \mu\text{g cm}^{-2} \text{g}^{-1}$, $p = 9.6 \times 10^{-9}$, respectively). Turbidity was certainly caused by *C. volutator* and reduced light penetration to sediment and this seemed to deplete MPB biomass. Phosphate flux is discussed in conjunction with F_0 model below. The effects of light intensity and *C. volutator* feeding, though, are counter-intuitive and slightly suspect: one would expect increased light intensity to have a positive effect on photosynthetic biomass rather than a negative one and *vice versa* for *C. volutator* feeding. Bootstrapped predictions and confidence intervals of chlorophyll *a* concentration over the mean turbidity range (Figure 3.21) shows that while significant effects are predicted by the model, the confidence intervals on the predictions for each scenario (low biomass – low phosphate, low biomass - high phosphate, high biomass – low phosphate) are so wide that in fact there is no convincing difference either be-

tween *C. volutator* presence and biomass treatments or between the maximum and minimum turbidity. The only variable for which the model predicts a marked difference on chlorophyll levels, where the confidence levels of the predictions for high and low levels do not overlap, is phosphate. It is likely that the large uncertainty in chlorophyll *a* estimation is caused either by too small a sample area or interference of chlorophyll degradation products such as pheophytin *a* and pheophorbide *a* in the chlorophyll *a* signal as measured by fluorescence (Lorenzen 1967). Some studies have shown that these pigments increase with grazing of sediment biofilms (Lucas & Holligan 1999; Cartaxana *et al* 2003) although other studies have found a decrease in pheopigments in grazed sediment and do not recommend inference of grazing intensity from phaeopigment quantification (Ford & Honeywill 2002). Concentration of pheopigments in a solution can be detected by acidification of the pigment solution (Lorenzen 1967) and this step should probably be performed as a caution for interpreting chlorophyll *a* content of grazed sediment.

Minimum fluorescence (F_0) is an estimation of surface biomass by proxy of the fluorescence emissions by pigments in the LHC complexes of chloroplasts in response to light. F_0 has been demonstrated to correlate with chlorophyll *a* content as they are both proportional to biomass (Serôdio 2001; Honeywill *et al* 2002). However, that was not the case in this study (Figure 3.23 A & B), where there was no significant correlation between these two biomass estimators at either the start or the end of the experiment ($p = 0.914$ and $p = 0.660$, respectively). This is more likely due to inaccuracy in chlorophyll *a* quantification, discussed above, rather than inaccuracy in F_0 measurement. Surface biomass clearly declined once *C. volutator* was added to the tanks (Figure 3.18); the only treatments where there was an overall decline before *C. volutator* were added were the 2nd tanks (MA) of the 0 and 2 g treatments which had low mean light levels (Figure 3.5) although it should be noted that the 1st tanks in the 0 g

treatment (MP) had the lowest light and their biomass increased in this time. The fact that decline also occurred in all 0 g treatments between days 6 and 8 suggests that laboratory conditions were not suitable in the long term; perhaps this was because MPB were from intertidal populations that were permanently submerged in the laboratory. Defew and colleagues (2004) found that healthy biofilms could be maintained in a tidal system in the laboratory for almost 3 weeks at 10 and 18 °C and 70, 175 and 350 $\mu\text{mol m}^{-2} \text{s}^{-1}$ light, whereas Dyson and colleagues (2007), using permanently submerged systems, also found a decline in F_0 after 7 days even in the absence of grazers, and also found no correlation between chlorophyll *a* biomass and F_0 (Dyson 2008, personal communication). It should also be noted that F_0 measures only chlorophyll *a* biomass within about 100 - 150 μmol of the sediment surface and are therefore measuring only the proportion of the total productive biomass in the sediment that is currently photosynthesising (Serôdio *et al* 2001). Diatoms migrate during the tidal cycle and their *in situ* migratory rhythm is maintained for up to a week in the laboratory in the absence of light and tidal stimuli (Consalvey *et al* 2004 and references therein); so even though F_0 measurements were made at the same time each day (9 – 10 am), they would not have been made at similar times in the *in situ* tidal cycle. However, F_0 measurements were made at the start of the low tide on day 1 (when migration to the surface should be at peak levels), during high tide (when most diatoms should be buried below 200 μm) on days 3 and 6, and towards the end of the low tide (where diatoms should be migrating downwards) on day 8, so it is unlikely that the low levels on day 8 are due to migratory rhythms. Since all MPB assemblages in all tanks came from the same slurry, biomass levels across tanks on the same day are still be comparable. On the final day of the experiment, there was a clear pattern of surface biomass levels across treatments (Figure 3.17, round symbols): while there was no difference between control tanks of MP/MA treatments,

where *C. volutator* was present (MP) had substantially lower biomasses than tanks where *C. volutator* was absent (MA) and tanks that shared a water column with *C. volutator* had much lower surface biomass than control tanks (with the exception of one outlier in the 1 g – MA treatment). Overall, the pattern of decline was exponential in both treatments, with the rate of decline decreasing with increasing biomass, but with a steeper decline in the tanks where *C. volutator* was feeding. De Deckere and colleagues (2001) also found an exponential decrease in their aquaria experiment with increasing *C. volutator* biomass.

In the regression of F_0 against all the environmental variables measured for each tank (Table 3.4, Model 3.5), turbidity, incident light intensity, and feeding *C. volutator* presence (but not biomass) had a significant negative effect on surface biomass (-3.9 ± 1.1 units ntu^{-1} , $p = 0.002$; -0.699 ± 0.2 units μmol^{-1} , $p = 0.008$; -42.4 ± 9.2 units g^{-1} , $p = 0.0003$). That *C. volutator* feeding on diatoms reduced the biomass comes as no surprise and the fact that there was no increased MPB biomass loss with increased *C. volutator* presence suggests that to some degree feeding rate is density dependent (although the 2 g), which is also a common ecological phenomenon. The increase of turbidity in the overlying water column is clearly linked to increased *C. volutator* abundance and clearly reduced MPB biomass. However, light intensity also has a negative effect on MPB biomass which would counteract the effect of turbidity; the reason for this is to the fact that the biggest difference in light intensities occurred in two tanks that had very similar turbidities, and the one with the lower light intensity had a higher F_0 . The significant positive interaction between turbidity and light intensity reduces both effects slightly. The bootstrapped predictions of the model over the full range of turbidity, assuming mean temperature and light intensity, shows that at low turbidities presence of *C. volutator* is more pronounced than at high concentrations (Figure 3.22).

Finally, it is interesting that the models for both biomass measurements estimated a positive response to increasing phosphate levels in the overlying water (for F_0 9.0 ± 4.3 units $\mu\text{mol P} \cdot \text{L}^{-1}$, $p = 0.050$) and neither model estimated any significant effects of increasing ammonium fluxes. The effect is significant in the F_0 model due to the fact that a positive outlier in the 1 g MA tank (std. res = 3.1) is from a unit with a high phosphate content in the overlying water column; when the outlier is removed from the model, phosphate no longer has a significant effect (Table 3.4, $p = 0.078$) and can be removed from the model without AICc increase (AICc with = 197.66, without = 197.44). It is unlikely that higher phosphate in the overlying water caused higher MPB levels for two reasons: (1) MPB is more likely to be DIN limited, and (2) if higher phosphate levels did encourage MPB proliferation, then MPB biomass should correlate positively with day 1 levels and negatively with day 8 levels, i.e. flux should have been into the sediment rather than out of it, which is the exact opposite of what happened. The first point was made clear by Ryther and Dunstan (1971) who demonstrated that coastal phytoplankton are far more likely to be limited by DIN because while Redfield's 15:1 N:P ratio may be true over oceanic spatial and geological time scales, it certainly is not true in coastal and eutrophic waters where the ratios of 0:0.25 prevail but the atomic content in photosynthetic cells is, on average, 10:1. Phosphorus regenerates more rapidly in seawater than nitrogen and nitrogen fixation is inefficient in the short term so there is generally a constant, if low, amount of phosphate available in the water column and no DIN (Ryther & Dunstan 1971). The range of mean unit total DIN: phosphate ratio in the overlying water on day 8 in this experiment lay between 2 and 9.4, the mean was 5.4 ± 0.4 , which suggests that while DIN was in reasonably high supply compared to coastal seawater it was probably still below the average cell content (although this was not measured) and hence MPB were more likely to be nitrogen limited. As far as the second point

goes, several studies have shown that sediments with MPB release phosphates at night or in the summer, which is probably related to lower redox potentials in the sediment at these times (Henriksen *et al* 1980; Andersen & Kristensen 1988; Rizzo 1990; Feuillet-Girard *et al* 1997) but so far there are no reports of increased phosphate release linked to increased MPB biomass. However, that appears to be the only reasonable conclusion here: that increased phosphate flux to the overlying water does not increase MPB biomass, but rather the reverse – MPB increase phosphate flux to the overlying water.

The last biomass estimator, live: dead diatom frustule count can be considered an indicator of mortality independent of predation, as *C. volutator* they have been shown to grind up diatom frustules prior to ingestion (Gerdol & Hughes 1994a). So the mortality indicated by the decline in live cells from the initial slurry to day 8 (Figure 3.24A) was likely caused by something other than grazing, such as natural mortality or loss of light. The plot of live counts against turbidity shows that live counts decreased significantly with increasing turbidity (Figure 3.27G; $\text{cor} = -0.41$, $t = -2.1$, $\text{df} = 22$, $p = 0.049$). However, the regression of proportion of live cells against environmental variables failed to detect any significant covariation (Table 3.5, Model 3.6) with turbidity or any other variable. The fact that live counts correlate significantly with F_0 (Figure 3.23C, $\text{cor} = 0.42$, $t = 2.2$, $\text{df} = 22$, $p = 0.043$) is probably due to the fact that both decrease with turbidity and increase slightly with increasing ammonium and phosphate fluxes (Figures 3.20G & E) although there is no difference in live counts with *C. volutator* presence or absence.

3.4.3 Effects of *C. volutator* on MPB assemblage composition

There were no differences in either species richness (3.24B) or diversity (3.24C) with *C. volutator* presence or biomass treatments; species richness varied between 19 and

28 taxa per tank and diversity varied between 0.1 and 0.3. Neither responses correlated significantly with either light intensity and temperature (Figures 3.19I – L) or turbidity, ammonium and phosphate flux (3.20J – O), although species richness did exhibit the same patterns of responses to turbidity and nutrient fluxes as % live cells and F_0 , i.e. a slight decrease in total live taxa with increasing turbidity and an increase in total live taxa with increasing nutrient release from sediment. Regression of both species richness and transformed Simpson's diversity (Table 3.4, Model 3.7 and 3.8, respectively) against all environmental variables also revealed no significant covariance between any of them. There was, however, an overall effect of moving the natural biofilm from the field into the laboratory: there was a decrease in live cell counts and the MDS plot from Bray-Curtis similarity indices between tanks on day 8 and the original assemblage (Figure 3.25) shows that there are no differences between the experimental treatments but a marked difference between all day 8 samples and original assemblage samples.

The only clear effect on MPB was that the final assemblages were different from the starting assemblages and this was likely a response to the shift to a sublittoral system, loss of light and/or change in temperature. Unfortunately, this suggests that laboratory conditions were not ideal for maintaining diatom assemblages for testing *C. volutator* engineering effects. The degree to which *C. volutator* reduced the light to the sediment bed in this experiment was relatively small ($< 250 \mu\text{mol m}^{-2} \text{s}^{-1}$ difference) compared to the light loss between emersion tide light to laboratory light in permanently emersed conditions ($> 750 \mu\text{mol m}^{-2} \text{s}^{-1}$ difference). This explains why the only big change in assemblage composition occurred between the original assemblage and all the laboratory incubated samples, regardless of experimental treatment. Temperatures in the laboratory were higher than they would have been in the field in late summer, varying between 14 – 18 °C rather than between 10 – 15

°C could have increased biomass and perhaps diversity (Defew *et al* 2004). However, only three taxa out of 64 (Appendix 2: Taxa 62, 63, and 64) disappeared entirely from the assemblage by day 8.

It has been suggested (Defew *et al* 2004 and references therein) that at higher temperatures and low light intensities cyanobacteria are more competitive than diatoms but this was certainly not the case in this experiment as starting cyanobacteria represented an average of 9 ± 2 (st.err) % in the original assemblage and 8 ± 3 , 9 ± 1 , 6 ± 1 , and 8 ± 3 % in the 0 – 2 g biomass treatments on day 8. Defew and colleagues (2002) also noted a shift from larger to smaller diatom species which was considered a normal response to a more nutrient and light limited environment, whereas Grover (1989) argues that for elongate diatoms (all pennate diatoms) larger cells are more competitive than smaller ones. In this experiment, the original assemblage the ‘live’ component contained 21 ± 2 % *Gyrosigma fasciola* (mean 85 μm length, mean 10 μm width) and 49 ± 4 % small *Navicula* spp. (< 30 μm length, < 10 μm width) whereas by day 8, biomass treatments 0 – 2 g contained 43 ± 3 , 42 ± 4 , 44 ± 5 , and 44 ± 4 % *G. fasciola* and 23 ± 3 , 20 ± 3 , 22 ± 3 , 21 ± 2 % small *Navicula* spp. Live: dead cell ratios were not consistent across taxa and smaller cells generally had lower live ratios than larger cells and this ratio generally decreased more for the small cells than the large. Smaller taxa (< 20 μm length) such as *Planothidium* spp., *Opephora* spp., *Cocconeis* spp. and *Navicula phyllepta* had initial live: dead ratios of 0.11, 0.34, 0.24, and 0.56, respectively, which dropped to 0.04, 0.08, 0.05, and 0.12, respectively, by day 8, whereas the largest taxa (> 50 μm length) *Cylindrotheca closterium*, *Cylindrotheca gracilis*, *Gyrosigma accuminatum*, *Gyrosigma baltica*, *G. fasciola*, and *Gyrosigma wansbecki* had initial live: dead ratios of 0.84, 0.94, 0.61, 0.86, 0.70, 0.68, respectively, and final ratios of 0.95, 0.94, 0.59, 0.85, 0.68, 0.64, respectively. This data is more in agreement with Grover’s prediction and also suggests that the more motile diatoms were most competitive.

It should also be noted that Defew and colleagues (2002) found that characterizing the whole assemblage from fixed sediment samples detected less change than characterizing just the epipellic portion from acid-cleaned lens tissue samples. However, lens tissue samples were not taken for two reasons: first, in a pilot experiment lens tissue samples were left for 2 hours but following acid-cleaning and mounting found not to contain any diatoms, therefore in this experiment the surface area used for lens tissues sampling was used instead to take multiple sediment samples, and second, lens tissue samples would not contain the epipsammic fraction of diatoms in the sediment. However, it turned out that the epipsammic fraction of the live assemblage was so small that in future, perhaps lens tissue samples left for more than 2 hours might be a more suitable sampling strategy.

3.4.4 General comments

A more appropriate design for this experiment would have been a tidal flow-through system instead of a sub-tidal cycling system. A passive flow of seawater over the bioturbated to the non-bioturbated tanks and then out of the system would have made for simpler, more clear-cut nutrient flux measurements in each treatment separately on each sampling day. Also, it would be a more realistic model for an intertidal system. As the *C. volutator* engineered variable affecting MPB biomass the most was turbidity, it would have been interesting to see whether this would still be an important variable in a tidal system where influence is limited to half the daylight hours.

It would appear from the results of this experiment that *C. volutator* was engaged in negative niche construction, i.e. their niche constructing activities were likely to change their environment in such a way as to reduce their own fitness (Odling-Smee *et al* 2003). Not only did they decimate the MPB population locally, but their water

column modification also imposed bottom-up controls on MPB population growth remotely. That said, many studies have found a positive flux of nutrients (Henriksen *et al* 1980; Henriksen *et al* 1983; Biles *et al* 2002; Emmerson *et al* 2001; Bulling *et al* 2010) and it is perhaps more due to the way in which flux measurements were made (as discussed above) that they could not be replicated. However, Gerdol and Hughes (1994b) argued that the prevention of biofilm accretion prevents salt marsh accretion in the long run and this could be seen as ultimately benefiting *C. volutator* for two reasons. First, salt marshes facilitate sediment deposition (Maynard *et al* 2011) and larger grain sizes are the first to deposit but *C. volutator* preferentially colonize silty habitats with very fine average grain sizes (Meadows 1964, 1967). Second, Pinkney and Zingmark (1993a) compared microalgal production in salt marshes, sandflats, mudflats, and sub-tidal habitats and found that mudflats are the most consistent and efficient microalgal communities. From that angle, *C. volutator* sediment resuspension and biofilm erosion could potentially be positive niche construction.

3.5 Conclusion

H₀2.1: *C. volutator* has no significant effect on the water column at any biomass.

This hypothesis must be rejected. *C. volutator*'s niche construction modifies the water column by significantly increasing sediment resuspension. Increased nutrient fluxes could not be demonstrated in this experiment.

H₀2.2: *C. volutator* has no significant effect on MPB biomass, locally or remotely.

This hypothesis must be rejected. The net effect of *C. volutator* resource modifications is a significant decrease in MPB biomass due to the increased water column turbidity.

H₀2.3: *C. volutator* has no significant effect on MPB assemblage composition, locally or remotely.

This hypothesis must be accepted. *C. volutator* did not affect MPB assemblage species richness, diversity or assemblage structure either locally or remotely. However, Larger diatoms were more competitive than smaller diatoms in the laboratory environment where both nutrient availability and light intensity were limiting.

Chapter 4: Ecosystem engineering effect of different bioturbators on microphytobenthic biomass and assemblage composition

Abstract

Corophium volutator (Pallas), *Hediste diversicolor* (Müller), and *Macoma balthica* (Linnaeus) are all common burrow-building, deposit- and suspension-feeding infauna of estuarine soft sediment in the North Atlantic. However, each species has a very different feeding and bioturbation style: *C. volutator* is both a biodiffuser and bioirrigator, *H. diversicolor* is considered a gallery-diffuser and *M. balthica* is a biodiffuser. As previous studies have shown that each species can have both deleterious and regenerative effects on MPB biomass, this experiment was designed to determine what net effect each feeding and bioturbation style has on MPB both locally and remotely.

Thirty-two mesocosms, containing homogenized mud (10 cm) and biofilm (~ 5 mm) and a seawater column (10 cm), were arranged into 16 experimental units in which one tank each contained either 2.0 g *C. volutator*, *H. diversicolor*, *M. balthica*, or no macrofauna, and water columns were circulated between two tanks (~ 1 hr turnover of tank water). Temperature, light intensity, turbidity, DIN, DIP, MPB bulk biomass (Chlorophyll-*a* in top 5 mm sediment), surface (fluorescing) biomass, and diatom counts were analysed after 6 days to determine whether *C. volutator*, *H. diversicolor*, and *M. balthica* had any effect on MPB biomass and diversity locally ('macrofauna present' tanks) or remotely ('macrofauna absent' tanks). Bulk MPB biomass was significantly ($p < 0.01$) reduced locally by the presence of feeding *C. volutator* and *H. diversicolor* but not by *M. balthica* ($p > 0.05$), but significantly in-

creased ($p = 0.001$) remotely, due to increased ammonium flux across macrofauna treatments. Surface biomass was significantly ($p < 0.05$) reduced locally by the presence of all feeding macrofauna and significantly ($p < 0.05$) reduced remotely by increased light attenuation which was approximately 5x, 5x, and 1.9x higher in the *C. volutator* treatment than in control, *M. balthica*, and *H. diversicolor* treatment. No differences were found between MPB diversities (Simpson's index) in control, *C. volutator*, *H. diversicolor*, and *M. balthica* treatments either locally or remotely. The results suggest that *C. volutator* may be more influential to MPB populations in the broad scale than other deposit-feeders.

Chapter 4: Ecosystem engineering effect of different bioturbators on microphytobenthic biomass and assemblage composition

4.1 Introduction

Bioturbation is a broad term which covers a multitude of different feeding and burrowing styles. Feeding and the creation, maintenance, and irrigation of a burrow can have biogeochemical, hydrological and sedimentological consequences (Thayer 1979; Henriksen *et al* 1980; Jones *et al* 1997; Emmerson *et al* 2001; Solan *et al* 2004; Michaud *et al* 2005, 2006; Meysman *et al* 2006; Dietrich & Perron 2006). The space and resource modifications that an organism imposes on in its environment are its ecosystem functions (Naeem *et al* 1999). These ecosystem functions have ramifications for all the organisms that share space and are dependent on or sensitive to those resources that are modified; therefore, bioturbators exert selective pressure on themselves and other species (Odling-Smee *et al* 2003). The more extreme, extensive, numerous, and permanent, those resource modifications are, the more pivotal the causal organism's role in the ecosystem (Jones *et al* 1997; Odling-Smee *et al* 2003).

Three common bioturbators in the muddier sediments of the Eden estuary are *Hediste diversicolor* Müller, *Corophium volutator* Pallas, and *Macoma balthica* Linnaeus. All three species spend almost their entire lives burrowed in the sediment and all three can both deposit and suspension feed, primarily on MPB or phytoplankton (Budd 2008; Budd & Rayment 2001; de Gooij & Luttikhuisen 1998; Green 1968; Meadows & Reid 1966; Møller & Riisgård 2006; Trevor 1977). However, they each have different feeding and burrowing styles. Whereas *Corophium* and *Hediste* both build and maintain burrows which they irrigate almost continuously during tidal immersion (Green 1968; Meadows & Reid 1966;

Møller & Riisgård 2006; Trevor 1977), *Macoma* does not build a burrow, it simply shuffles down into the sediment using its muscular foot and then sends its inhalant siphon up to the surface to breathe and deposit feed on MPB or phytoplankton. The exhalant siphon does not necessarily deposit waste on the sediment surface but often within the sediment matrix (de Gooij & Luttikhuisen 1998; Budd & Rayment 2001). *Corophium* and *Hediste* both generate irrigation currents, *Corophium* by beating its pleopods (Meadows & Reid 1966) and *Hediste* by muscular undulations along the body (Green 1968), which allows them to breathe and feed while remaining in their burrows. When suspension feeding, both species create a form of mesh to filter microalgae out of the water column, *Corophium* with the bristles on their gnathopods and *Hediste* by spinning a mucus web across the burrow which is reingested once it is full (Green 1968). Both species also gather biofilm (and scavenge dead and dying animals in the case of *Hediste*) from the sediment surface drag it into their burrows, resuspend it in the burrow water and ingest it as previously described. However, while it is well known that *Corophium* flings its waste sediment and excreta out of its burrow via the feeding current (Gerdol & Hughes 1994a; de Deckere *et al* 2000; Biles 2002), no such mechanism is described for *Hediste* and they are not observed to resuspend large amounts of sediment (Trevor 1977; Biles 2002) so presumably waste becomes part of the burrow wall.

These species perform various ecosystem functions. There are numerous studies that demonstrating that the trophic effects of these macrofauna are a general reduction in MPB biomass and primary productivity (Andersen & Kristensen 1988; Daborn *et al* 1993; Gerdol & Hughes 1994b; Smith *et al* 1996; Biles *et al* 2002; Hagerthey *et al* 2002; de Deckere *et al* 2000, 2003; Dyson *et al* 2007; Hicks 2010, Hicks *et al* 2011). However, there are very few studies that include the effect of *Hediste* and *Corophium* feeding on MPB assemblage composition (Smith *et al* 1996; Hagerthey *et al* 2002) and both concluded that these species feed relatively unselectively and therefore reduced dominant species the most. Smith and col-

leagues point out that while the diatom assemblages grazed upon by *Corophium* and *Hediste* were not different from each other (but different from the control assemblages), certain species were unaffected by grazing and this was more likely to be because they were better competitors in the new chemical environment created by the bioturbators rather than that they were rejected as food. Hagerthey and colleagues found that the MPB assemblages grazed upon by *Corophium* exhibited more diversity and evenness as the dominant species were reduced the most by non-specific grazing. No studies were found that investigated the effect of *Macoma* on MPB assemblage composition. Finally, another ecosystem function of MPB grazers is that as a consequence biofilm depletion, the loss of EPS increases the physical erodibility of the sediment (Daborn *et al* 1993; Gerdol & Hughes 1994b; de Deckere *et al* 2000; Wood & Widdows 2002; Underwood *et al* 2003).

One of the most important ecosystem functions of these bioturbators is the oxygenation the sediment. Infauna that build tunnel-like irrigated burrows, such as *Arenicola*, *Nereis*, *Hediste* and *Corophium*, increase the oxygen uptake of the sediment more than infauna that burrow into the sediment but use a siphon to feed and breathe, such as *Macoma*, *Mya* and *Cerastoderma* (Henriksen *et al* 1983; Pelegri & Blackburn 1995; Michaud *et al* 2005). An important consequence of increased sediment oxygenation and surface area by burrowers is a change in nutrient fluxes between the sediment and the overlying water column which are additional ecosystem functions. For marine systems, which are thought to be limited by inorganic nitrogen (Ryther & Dunstan 1971; Underwood *et al* 1998), the effect of sediment oxygenation enhances the microbially-mediated reduction-oxidation reactions of the nitrogen cycle so that ammonium flux into the overlying water often increases, especially in the dark and in flowing water, but nitrification of ammonium may also increase, and denitrification/remineralization of the overlying water column increases when light levels are low and nitrate levels are high (Henriksen *et al* 1980, 1983; Andersen & Kristensen 1988; Pelegri & Black-

burn 1994, 1995; Pelegri *et al* 1994; Rysgaard *et al* 1995; Mortimer *et al* 1999; Biles 2002; Mermillod-Blondin *et al* 2004; Ieno *et al* 2006; Michaud *et al* 2006; Bulling 2010). Burrowers with the greatest effect on the oxygen uptake are generally found to have the greatest effect on the nitrogen cycle (Henriksen *et al* 1980; Pelegri and Blackburn 1995; Michaud *et al* 2006) although in a field study in the Humber *Macoma* and *Hediste* were found to increase ammonia and nitrite release whereas no conclusive results were found for *Corophium* (Mortimer *et al* 1999). Some studies have also compared phosphate fluxes amongst sediments with different bioturbators or without bioturbation and found that phosphate release could be slightly enhanced by bio-irrigation (Mermillod-Blondin *et al* 2004; Bulling *et al* 2010) but the reverse has also been reported (Mortimer *et al* 1999). As with ammonium release, it has also been observed that phosphate release increases in the absence of light (Hylleberg & Henriksen 1980; Ieno *et al* 2006) due reduced interference by MPB photosynthesis.

Another consequence of increased oxygenation and turnover of the sediment is that it increases the biogenic mixing depth which has been shown to have important implications for smaller and less active infauna by creating suitable habitat (Solan *et al* 2004). A final important ecosystem function of bioturbators is that they can enhance physical sediment resuspension and deposition by actively adding or removing sediment from the water column: *Corophium* has been shown to be an important resuspender of sediment (Biles 2002; de Deckere *et al* 2003) and *Macoma* (and other bivalves) have been shown to increase deposition (Wood & Widdows 2002) but whether *Hediste* are generally bioresuspenders or biodepositors is still undefined.

The proliferation of burrowing invertebrates in the Phanerozoic coincided with a decline in immobile suspension feeders due to regular small-scale disturbance of the sediment (Thayer 1979). As estuarine sediments are dominated by motile bioturbators, it is likely that bioturbation also contributed to the diversification

of motile diatoms which now dominate fine grained sediment with high bioturbation and disturbance levels (Round *et al* 1981; van den Hoek 1995). It is possible that the other ecosystem functions of bioturbators discussed above could also exert selective pressure on MPB. Studies on freshwater benthic and pelagic communities and marine phytoplanktonic communities, which are far more numerous than benthic estuarine and marine studies, have shown that changing limiting nutrient and turbidity levels changes microalgal biomass and composition (Pan & Lowe 1994; Smith 1996; Naymik *et al* 2005; Passy 2007, 2008; Finkel *et al* 2009; Licurzi & Gomez 2009; Duarte *et al* 2000; Vidal & Duarte 2000).

Broadly speaking, estuarine-marine MPB biomass has been shown to increase with inorganic nitrogen supply (Hillebrand *et al* 2000; Hagerthey 2002) and decreased by infaunal grazing (Smith *et al* 1996; Hillebrand *et al* 2000; Hagerthey 2002), although the biomass response to grazing can vary with the grazer (Hagerthey *et al* 2000). The responses of estuarine-marine MPB biodiversity measurements to nitrogen enrichment and grazing are more complicated and no studies were found to determine the responses to water turbidities. While *Corophium* can feed selectively, it is able to consume most diatoms and *Hediste* is unlikely to feed unselectively (Smith *et al* 1996). Smith and colleagues (1996) showed that *Corophium* and *Hediste* significantly changed the MPB assemblage compared to ungrazed treatments but they did not have species specific effects on the resulting MPB assemblage. With the exception of two species, one highly silicified and one very large, they fed unselectively. As *Macoma* is also a deposit feeder and is also unlikely to feed selectively. However, simply by removing more dominant MPB species these infauna can favour the species more able to take advantage of the new physical and chemical conditions and reproduce more rapidly (Smith *et al* 1996). A marine study in the western Baltic (Hillebrand *et al* 2000), where gastropods were the dominant grazers, resulted in higher species richness and diversity (H') in the ungrazed assemblages because gastropods tended to remove upright species, leaving the prostrate species

(which can then benefit from the extra nutrients and light); these results corroborated findings from a similar study in freshwater (Pan & Lowe 1996). In the same study (Hillebrand *et al* 2000), species richness increased with low to mid-level nutrient (NPK) enrichment but declined with high level enrichment whereas species diversity (H') was significantly lower in the presence of grazers in the unenriched treatment and significantly higher in the presence of grazers in the maximally enriched treatment. Hagerthey and colleagues (2002) found that MPB assemblages grazed by *Hydrobia* were either no different or slightly more species rich than ungrazed assemblages and species richness did not increase in higher nutrient treatments. *Corophium* did not increase species richness either but did increase species evenness (E) and diversity (H'). With respect to nutrient levels, while diatoms have preferences for certain nutrient levels, they are quite flexible and can survive a wide range of conditions (Sundbäck & Snoeijs 1991; Underwood *et al* 1998; Underwood & Provot 2000) and with respect to light levels, diatoms have been shown to be able to last for well over a week in complete darkness due to their ability to horde nitrates and use them for nitrate respiration (Kamp *et al* 2011).

The aim of this experiment was to examine what effects the ecosystem functions of these species had on the water column, and what effects the water column characteristics had on the biomass and composition of MPB communities in the presence and absence of feeding bioturbators. In addition, it was an opportunity to observe whether there was a relationship between MPB diversity and biomass. More specifically, the following null hypotheses were tested:

H₀4.1: Bioturbation by *Corophium*, *Hediste*, and *Macoma* produces similar modifications to the overlying water column.

H₀4.2: *Corophium*, *Hediste*, and *Macoma* feeding and bioturbation only effects MPB biomass in the sediments in which they are present and cannot remotely affect MPB biomass remotely via resource modification in the water column.

H₀4.3: *Corophium*, *Hediste*, and *Macoma* feeding and bioturbation only effects MPB assemblage composition in the sediments in which they are present and cannot remotely affect MPB biomass remotely via resource modification in the water column.

H₀4.4: There is no relationship between MPB biomass and biodiversity.

4.2 Materials & Method

4.2.1 Experimental design

The experimental design was described in the previous chapter (see Chapter 3.2.1 and Figure 3.1) where each of 16 experimental units consisted of paired tanks in which one contained the bioturbation treatment and the other contained just MPB but the water columns were shared between them. The only change made here was that the tanks were transparent, rectangular, polyethylene containers (14.7 cm long x 12.7 cm wide x 23.5 cm high). Holes were punched into the centre of the end of each tank at 10 cm height and fitted O-rings and nylon tank connectors which allowed 32 tanks to be connected into 16 experimental units by the 16 peristaltic pumps (pumping at 35.4 ml min⁻¹). Experimental units were arranged 2 rows along the laboratory bench underneath banks of fluorescent daylight tubes (6500K colour temperature) delivering an average of 280 $\mu\text{mol photons m}^{-2} \text{s}^{-1}$ PAR (photosynthetically active radiation) to the tops of the tanks. Lights were set to a 14:10 hour light: dark cycle – lights came on at 8 am. The thermostat of the aquarium was set to 12 °C.

All 32 tanks contained sediment, MPB biofilm slurry, and seawater. The 16 units were divided into 4 macrofauna treatments with 4 replicates each: no macrofauna (control), *C. volutator*, *H. diversicolor*, and *M. balthica* (Figure 4.1). To avoid the confounding between light intensities and macrofauna treatments, as in the previous experiment, macrofaunal identity treatments were distributed so that each treatment had replicates in high and low light intensity areas. In addition

to the macrofauna identity treatments there was the macrofauna presence treatment: water was pumped from the tank containing macrofauna (MP: macrofauna present), includes the 0 g control treatments) to the tank containing no macrofauna (MA: macrofauna absent) from where it passively flowed back to the MP tank. To avoid confounding effects of macrofauna presence with temperature effects, 8 MP treatments were located in row 1 and 8 were in row 2 and the frame was pulled away from the wall to improve air circulation and heat convection away from row 1.

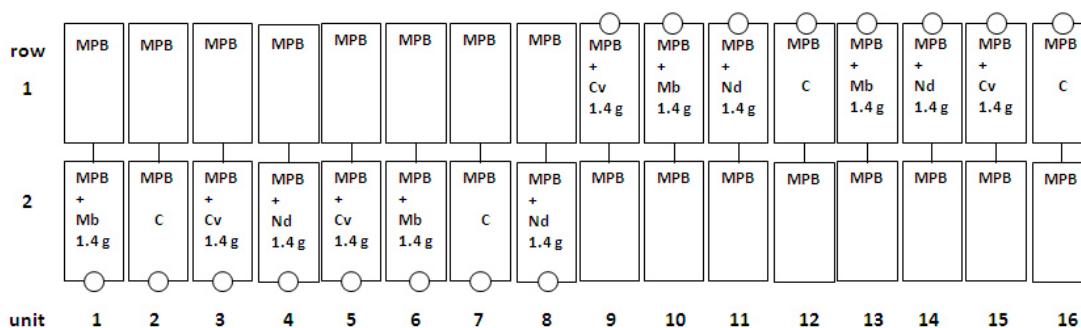


Figure 4.1: A total of 32 tanks, arranged as 16 units, distributed amongst 4 treatments: control (C) without macrofauna, 1.4 g *C. volutator* (Cv), 1.4 g *M. balthica* (Mb), 1.4 g *N. diversicolor* (Nd). All tanks contained 10 cm layer of sifted sediment and 0.5 cm layer of microphytobenthos (MPB). The pumps for units 1 – 8 are in row 1 and the pumps for units 9 – 16 are in row 2.

4.2.2 Set up and sampling

Mud was collected at the 400 m² quadrat on the North Shore of the Eden estuary at the Guardbridge paper mill (Chapter 2) in late July 2009. Mud was collected to about 15 cm depth and sifted through 0.5 mm² mesh into a mixture of filtered seawater and filtered tap water to salinity 22 which was the salinity of the pore water of the sediment. Macrofauna collected in the sieves were picked out and kept in aerated tanks with sifted mud microphytobenthic biofilm. At the start of the experiment (Figure 4.2, day 0) each tank was filled with 10 cm of sifted sediment after which microphytobenthic biofilm was scraped from the sediment surface just below the paper mill quadrat, sifted through a 0.5 mm mesh into a small amount of seawater (salinity 33), homogenized, and sampled. 140 ml of

the biofilm slurry was layered onto the sediment in each tank with a 50 ml syringe (approximately 5 mm deep).

The following morning (day 1), fluorescence measurements were made to account for variation in initial surface biomass. Macrofauna were then damp weighed into 4 batches of 1.4 g each, which corresponded to slightly more (0.2 g) than the *in situ* total macrofaunal biomass for 187 cm² sediment. *Macoma* and *Hediste* numbers were insufficient at the paper mill site at the time and so were collected from Kincapple flat (see map, Figure 2.1) and the Guardbridge site, respectively. Each tank was filled with 13 cm filtered and aerated coastal seawater (2.43 L, salinity 33) after which the animals were added and allowed to burrow in for the night. Turbidity was measured and pumps were switched on prior to lights-on the following morning (day 2). Animal activity in the tanks was monitored for the duration of the experiment and any dead animals were immediately removed, counted and replaced with similarly sized individuals. *Macoma* activity could only be monitored by observing siphons on the surface and they maintained activity until day 6 when they were fewer siphons visible in 3 out of 4 tanks. As they could not be removed without disrupting the sediment, the experiment was ended prematurely on day 7 instead of day 8.

On day 7, prior to lights-on, turbidity was measured in all tanks, 40 water ml water samples were taken for nutrient analysis and stored at -80 °C prior to analysis, and finally, the remaining ~ 2L of overlying water were collected for suspended sediment quantification. Minimum fluorescence measurements were made following lights on after 15 minutes of dark adaptation. Then, a double layer of 2 × 10 cm strips of lens tissue were placed across the centre of the sediment in each tank and left to trap migrating diatoms from the sediment surface for 6 hours. Finally, the top sheets of lens tissue were collected in 4 % glutaraldehyde in seawater solution at 8 °C and the bottom sheets discarded. Two con-

tact cores were collected from either side of where the lens tissue had lain and stored at -80°C for later chlorophyll a, water and organic content analysis.

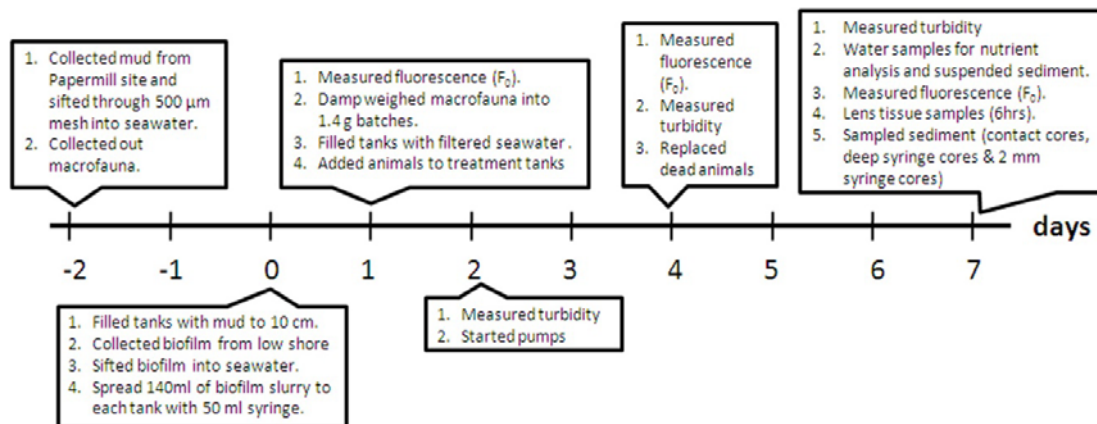


Figure 4.2: Timeline of the experiment.

4.2.3 Measurements

4.2.3.1 Temperature and light intensity

Temperature was measured in each tank on day 1 and 6 in the morning at lights-on and in the evening just prior to lights-off. Mean light intensity at the surface of each tank was recorded from two measurements per tank.

4.2.3.2 Turbidity, suspended sediment, light attenuation and nutrients in the overlying water

Turbidity was measured in nephelometric turbidity units (ntu) with a Eutech Instruments Turbidimeter TN100. The unit was calibrated using standards at 0.02, 100, and 800 ntu, followed by measurement of filtered seawater and then each tank's water was measured in triplicate and a mean taken; the unit was checked for drift with filtered seawater after every 4 tanks. In order to calibrate light attenuation to turbidity, the water collected from each tank was used to create a 13 cm water column in a glass beaker, which was raised to be at the same, fixed, height as the tops of the tanks from the experimental light, and light was measured with a LICOR 189 photometer fixed to the underside of the beaker. Light penetration through each water column was expressed as a proportion of light

penetration through a 13 cm column of filtered seawater. Following measurement of light attenuation, the sediment was allowed to settle for 48 hours, then the water column was gently siphoned off. The remaining sediment was rinsed into preweighed aluminium cups with tap water, baked until dry for 5 days at 60 °C, and reweighed to determine the weight of the sediment. The 40 ml water samples, which had been filtered through 0.45 Nalgene syringe-filters prior to storage at -80 °C, were analysed for $\text{NH}_4^+\text{-N}$, $\text{NO}_3^-\text{-N}$, and $\text{PO}_4^{3-}\text{-P}$ (Chapter 2.3) and quantities are reported in $\mu\text{mol L}^{-1}$.

4.2.3.3 Fluorescence measurements

Four minimum fluorescence (F_0) measurements were made in each tank following 15 minutes of dark ($< 4 \mu\text{mol m}^{-2} \text{s}^{-1}$) adaptation. Because the tanks measured later would have had a longer dark adaptation time, tanks were measured in randomized and recorded order. Measurements were made with a Hansatech FMS2 (settings detailed in Chapter 2.4.2.4).

4.2.3.4 Chlorophyll *a*, water, and organic content of sediment

The water contents of the contact cores was calculated (as detailed in Chapter 2.2.3) by placing each core in pre-weighed bags, reweighing, freeze-drying overnight, and reweighed the following morning. Dried sediment was then used for chlorophyll-*a* and organic content assays. Organic content was calculated (as detailed in Chapter 2.2.3) by putting approximately 2 g of the freeze-dried sediment into a preweighed aluminium boat, reweighing, combusting in a muffle furnace (450 °C) overnight and reweighing. Chlorophyll *a* analysis (detailed in Chapter 2.4.1) was modified by adding an acidification step following Lorenzen (1967) to account for pheo-pigments, chlorophyll-*a* degradation products. After measuring the absorbance at 664 nm wavelength, 60 μL of 1M HCl is added to each sample to acidify chlorophyll *a* but not pheopigments, and the sample was reread at 664 nm. Chlorophyll *a* g^{-1} of sample was then calculated by Equation

4.1 (modified from Lorenzen 1967) and chlorophyll a cm^{-2} was calculated by Equation 2.4.

$$\text{Chl } a \text{ } (\mu\text{g g}^{-1}) = \frac{A * K * (664_0 - 664_a) * v}{V_f * l}$$

Equation 4.1

Where

A = absorption coefficient of chlorophyll a = 11.0,

K = factor to equate the reduction in absorbency to initial chlorophyll concentration, = 2.43,

665₀ = absorbance before acidification,

665_a = absorbance after acidification,

v = volume of acetone used for extraction (ml),

V_f = grams of sediment in sample,

l = path length of cuvette (cm),

R = maximum ratio of 665₀ : 665_a in the absence of pheo-pigments = 1.7.

4.2.3.5 *Microphytobenthic assemblage*

Lens tissue samples were collected, oxidized, and mounted onto permanent slides (described in section 2.5.3) for examination under higher magnification (x 1,250) to make more refined taxonomic distinctions between the epipelagic species. Two hundred valves were identified per tank from which species richness (number of taxa per sample) and Simpson diversity (- ln transformed) indices were calculated. Taxa were classified by a two reference identification numbers but most could be identified to species (taxa descriptions presented in Appendix 1) using several published diatom catalogues (Barber & Haworth 1981, Hartley *et al* 1996, Hendey 1964, Kelly *et al* 2005, Round *et al* 1990, Snoeijs 1993, Snoeijs & Vilbaste 1994, Snoeijs & Potapova 1995, Snoeijs & Kasperoviciene 1996, Snoeijs & Balashova 1998, Van der Werff & Huls 1976, Wittkowski *et al* 2000, Ribeiro 2010, Bayer *et al* 2012).

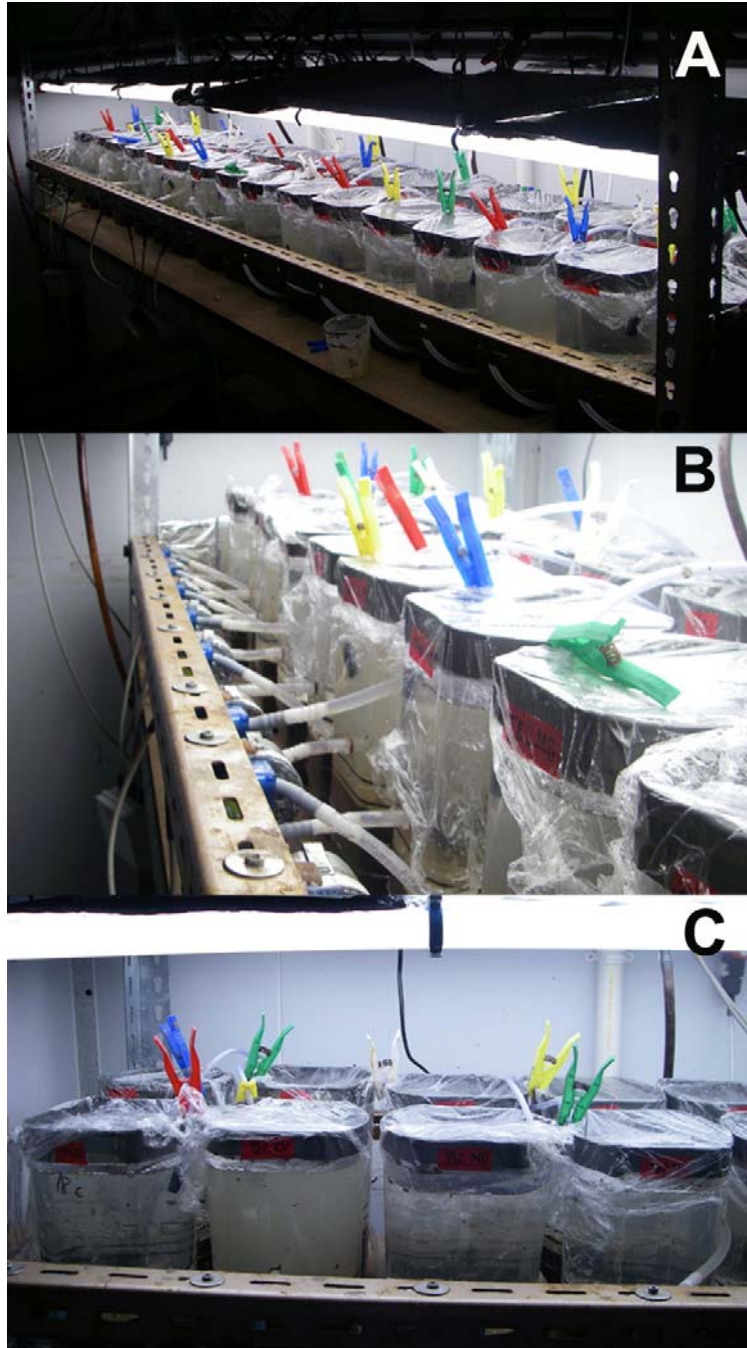


Figure 4.3: All tanks (A), pumps 1 – 7 in row 2 (B), units 1 – 4, ½ hr after adding animals (C), the 2nd tank from left is a *Corophium*/present treatment –the turbidity is already higher than in the *Macoma*/present and *Nereis*/present tanks to the left and right, respectively.

4.2.4 Analysis

All measurements made are presented graphically against treatment groups and group means are presented and reported with ± 1 standard error (Table 4.2).

Table 4.1: Summary of statistical models in Chapter 3: i = index for tank number; j = index for unit number; Y = the response variable; ID = macrofauna treatment; MP = the presence/absence treatment; fID = identity of macrofauna if present in tank; cPAR = centralised PAR; %LA = mean light attenuation ;. ε = errors; V = variance-covariance matrix

Model Nr	Response variable	Day	Fixed effects (maximum model)	Error
4.1.1	Turbidity (tanks)	2	$Y_i \sim \text{factor}(\text{ID}_i) * \text{factor}(\text{MP}) + \varepsilon_i$	$\varepsilon_i \sim N(\mu, \sigma^2 * V)$
4.1.2	Turbidity (tanks)	4	$Y_i \sim \text{factor}(\text{ID}_i) * \text{factor}(\text{MP}) + \varepsilon_i$	$\varepsilon_i \sim N(\mu, \sigma^2 * V)$
4.1.3	Turbidity (tanks)	7	$Y_i \sim \text{factor}(\text{ID}_i) * \text{factor}(\text{MP}) + \varepsilon_i$	$\varepsilon_i \sim N(\mu, \sigma^2 * V)$
4.1.4	Turbidity (unit)	4	$Y_j \sim \text{factor}(\text{ID}_i) * \text{factor}(\text{MP}) + \varepsilon_i$	$\varepsilon_i \sim N(\mu, \sigma^2 * V)$
4.1.5	Turbidity (unit)	7	$Y_j \sim \text{factor}(\text{ID}_i) * \text{factor}(\text{MP}) + \varepsilon_i$	$\varepsilon_i \sim N(\mu, \sigma^2 * V)$
4.2.1	Susp. Sed (tanks)	7	$Y_i \sim \text{factor}(\text{ID}_i) * \text{factor}(\text{MP}) + \varepsilon_i$	$\varepsilon_i \sim N(\mu, \sigma^2 * V)$
4.2.2	Light atten (tanks)	7	$Y_i \sim \text{factor}(\text{ID}_i) * \text{factor}(\text{MP}) + \varepsilon_i$	$\varepsilon_i \sim N(\mu, \sigma^2 * V)$
4.2.1a	ΔNH_4^+	1,7	$Y_i \sim \text{factor}(\text{ID}_i) * \text{factor}(\text{MP}) + \varepsilon_i$	$\varepsilon_i \sim N(\mu, \sigma^2 * V)$
4.2.1b	ΔPO_4^+	1,7	$Y_i \sim \text{factor}(\text{ID}_i) * \text{factor}(\text{MP}) + \varepsilon_i$	$\varepsilon_i \sim N(\mu, \sigma^2 * V)$
4.3.1	% water	7	$\text{anova}(Y_i \sim \text{factor}(\text{ID}_i) * \text{factor}(\text{MP}_i) + \varepsilon_i)$	$\varepsilon_i \sim N(\mu, \sigma^2)$
4.3.2	% organic	7	$\text{anova}(Y_i \sim \text{factor}(\text{ID}_i) * \text{factor}(\text{MP}_i) + \varepsilon_i)$	$\varepsilon_i \sim N(\mu, \sigma^2)$
4.4.1	% chlorophyll-a	7	$\text{anova}(Y_i \sim \text{factor}(\text{ID}_i) * \text{factor}(\text{MP}_i) + \varepsilon_i)$	$\varepsilon_i \sim N(\mu, \sigma^2 * V)$
4.4.2	F_0^{15}	7	$\text{anova}(Y_i \sim \text{factor}(\text{ID}_i) * \text{factor}(\text{MP}_i) + \varepsilon_i)$	$\varepsilon_i \sim N(\mu, \sigma^2 * V)$
4.4.3	Sp. Richness	7	$\text{anova}(Y_i \sim \text{factor}(\text{ID}_i) * \text{factor}(\text{MP}_i) + \varepsilon_i)$	$\varepsilon_i \sim N(\mu, \sigma^2)$
4.4.4	Simp. Div	7	$\text{anova}(Y_i \sim \text{factor}(\text{ID}_i) * \text{factor}(\text{MP}_i) + \varepsilon_i)$	$\varepsilon_i \sim N(\mu, \sigma^2)$
4.5.1	Chl- <i>a</i>	7	$Y_i \sim \text{factor}(\text{fID})_i + \text{cPAR}_i + \% \text{LA}_j + \Delta\text{NH}_4^+ + \Delta\text{PO}_4^{3+} + \text{cPAR}_j : \% \text{LA}_j + \text{factor}(\text{fID})_i : \% \text{LA}_j + \varepsilon_i$	$\varepsilon_i \sim N(\mu, \sigma^2 * V)$
4.5.2	F_0^{15}	7	$Y_i \sim \text{factor}(\text{fID})_i + \text{cPAR}_i + \% \text{LA}_j + \Delta\text{NH}_4^+ + \Delta\text{PO}_4^{3+} + \text{cPAR}_j : \% \text{LA}_j + \text{factor}(\text{fID})_i : \% \text{LA}_j + \varepsilon_i$	$\varepsilon_i \sim N(\mu, \sigma^2 * V)$
4.5.3	Sp. Richness	7	$Y_i \sim \text{factor}(\text{fID})_i + \text{cPAR}_i + \% \text{LA}_j + \Delta\text{NH}_4^+ + \Delta\text{PO}_4^{3+} + \text{cPAR}_j : \% \text{LA}_j + \text{factor}(\text{fID})_i : \% \text{LA}_j + \varepsilon_i$	$\varepsilon_i \sim N(\mu, \sigma^2 * V)$
4.5.4	Simp. Div	7	$Y_i \sim \text{factor}(\text{fID})_i + \text{cPAR}_i + \% \text{LA}_j + \Delta\text{NH}_4^+ + \Delta\text{PO}_4^{3+} + \text{cPAR}_j : \% \text{LA}_j + \text{factor}(\text{fID})_i : \% \text{LA}_j + \varepsilon_i$	$\varepsilon_i \sim N(\mu, \sigma^2 * V)$

Table 4.2: Mean measurements for all 8 treatment groups (± 1 standard error): incident light intensity (all days, $\mu\text{mol m}^{-2} \text{s}^{-1}$), turbidity (ntu), suspended sediment (day 7, g), light attenuation (day 7, %), NH_4^+-N flux ($\mu\text{mol L}^{-1}$), NO_3^--N flux ($\mu\text{mol L}^{-1}$), $\text{PO}_4^{3-}-\text{P}$ flux ($\mu\text{mol L}^{-1}$), sediment water and organic content (day 7, %), chlorophyll *a* (day 7, $\mu\text{g cm}^{-2}$), fluorescence (arbitrary units), species richness (day 7, # taxa), and negative log transformed Simpson diversity index (day 7, $-\ln D$).

Bioturbator	Control		<i>Corophium</i>		<i>Hediste</i>		<i>Macoma</i>	
Presence	MP	MA	MP	MA	MP	MA	MP	MA
Light int.	286 \pm 30	276 \pm 30	264 \pm 30	290 \pm 17	273 \pm 30	279 \pm 25	282 \pm 15	292 \pm 20
Turbidity								
day 2	2.79 \pm 0.2	3.32 \pm 0.2	14.6 \pm 1.9	2.8 \pm 0.34	4.20 \pm 0.4	2.39 \pm 0.3	3.56 \pm 0.6	3.50 \pm 0.7
day 4	2.13 \pm 0.3	2.01 \pm 0.3	12.8 \pm 1.5	13.4 \pm 1.85	3.33 \pm 0.4	3.80 \pm 0.3	2.17 \pm 0.3	2.20 \pm 0.3
day 7	2.05 \pm 0.4	1.91 \pm 0.3	52.5 \pm 5.0	55.8 \pm 9.26	2.30 \pm 0.3	2.80 \pm 0.7	2.25 \pm 0.3	2.84 \pm 0.7
Susp. sed	0.11 \pm 0.06	0.06 \pm 0.05	0.57 \pm 0.09	0.67 \pm 0.22	0.22 \pm 0.07	0.11 \pm 0.03	0.08 \pm 0.06	0.06 \pm 0.04
% Light	18.1 \pm 9.4	8.6 \pm 6.3	78.7 \pm 5.3	66.9 \pm 6.7	43.2 \pm 16.2	27.8 \pm 8.4	14.5 \pm 9.8	9.9 \pm 6.8
$\text{NH}_4^+ - \text{N}$	0.29 \pm 0.2	1.0 \pm 0.4	6.5 \pm 2.1	7.4 \pm 2.3	5.3 \pm 1.6	3.3 \pm 1.1	0.38 \pm 0.1	0.86 \pm 0.3
$\text{NO}_3^- - \text{N}$	0.0 \pm 0.0	0.0 \pm 0.0	0.2 \pm 0.2	0.1 \pm 0.1	0.02 \pm 0.02	0.05 \pm 0.05	0.0 \pm 0.0	0.0 \pm 0.0
$\text{PO}_4^{3+} - \text{P}$	1.8 \pm 0.1	1.9 \pm 0.2	2.8 \pm 0.1	2.7 \pm 0.1	2.6 \pm 0.3	2.2 \pm 0.1	3.3 \pm 0.5	3.3 \pm 0.5
% Water	63.7 \pm 0.7	61.4 \pm 1.2	63.0 \pm 1.6	64.4 \pm 0.7	60.6 \pm 2.2	66.0 \pm 0.6	64.2 \pm 0.6	57.8 \pm 4.5
% Organic	13.4 \pm 2.4	9.2 \pm 0.3	12.8 \pm 2.0	10.8 \pm 0.8	8.6 \pm 0.6	11.4 \pm 1.2	9.7 \pm 0.4	12.5 \pm 1.6
Chl- <i>a</i>	50.8 \pm 6.9	56.6 \pm 3.8	39.6 \pm 6.7	76.8 \pm 19.2	42.8 \pm 6.6	66.3 \pm 11.7	58.7 \pm 11.2	42.0 \pm 4.5
F_0^{15}								
day 1	413 \pm 15	453 \pm 22	372 \pm 39	404 \pm 26	392 \pm 15	389 \pm 6	413 \pm 36	370 \pm 25
day 4	412 \pm 16	429 \pm 24	194 \pm 9	329 \pm 21	309 \pm 44	418 \pm 12	316 \pm 21	434 \pm 23
day 7	416 \pm 44	433 \pm 16	187 \pm 12	264 \pm 36	129 \pm 42	310 \pm 90	240 \pm 42	394 \pm 30
# Taxa	33 \pm 3.9	27 \pm 2.4	30 \pm 3.6	25 \pm 3.9	22 \pm 1.7	31 \pm 0.9	30 \pm 2.1	28 \pm 1.8
Simpson D	0.14 \pm 3.9	0.13 \pm 2.6	0.13 \pm 3.6	0.20 \pm 3.9	0.18 \pm 1.7	0.11 \pm 0.9	0.12 \pm 2.1	0.16 \pm 1.8

Water column and MPB variables were analysed by GLS with macrofauna identity and presence as categorical variables; unit identity was added as categorical variance category to account for non-independence (if AICc with was lower than AICc without). MPB parameters were analysed by GLS regression with the identity of feeding macrofauna as a categorical variable and light intensity, and water column measurements as covariates; again, weights were fitted where necessary to accommodate non-independence or heteroscedasticity in the data. Details of model selection are described in Chapter 2.7. All maximum models (before selection) are presented in Table 4.1.

4.3 Results

4.3.1 Light and temperature

Temperature increased over the days of the experiment: on day 1 temperature increased from 12 °C in the morning to 20 °C by lights-out but by day 6 they started at 14 °C in the mornings and increased to 22 °C by lights-out. However, no temperature differences were found between tanks and treatments. While there were differences between incident light intensities to the tanks, spreading the treatments over areas of higher and lower light intensities ensured that mean light intensities between treatment groups were reasonably consistent (see Table 4.2; Figure 4.4).

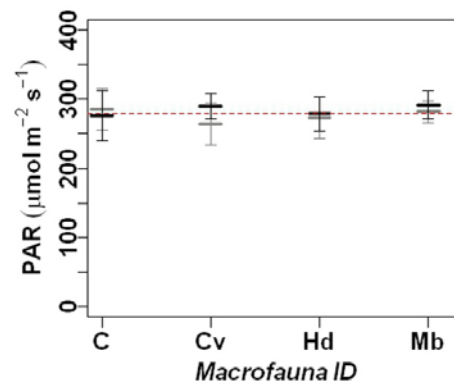


Figure 4.4: Mean light intensity (± 1 st. err.) in each treatment group: MP treatment (grey bars) and MA treatment (black bars) in each of the control (C), *Corophium* (Cv), *Hediste* (Hd), and *Macoma* (Mb) treatments.

4.3.2 Turbidity, suspended sediment, and light attenuation

4.3.2.1 Turbidity

The filtered seawater added to each tank on day 1 had a mean turbidity of 0.09 ntu (± 0.02). *Corophium* generated turbidity immediately upon burrowing the sediment and this did not occur as a consequence of *Nereis* and *Macoma* burrowing into the sediment (Figure 4.3 C). Turbidity in the control tanks (2.79 ± 0.2 ntu) was slightly higher than turbidity of seawater, presumably due to some suspension of sediment during set up but this sedimented out over the course of the experiment (see Table 4.2). By day 2, turbidity (see Figure 4.5; Table 4.3, Model 4.1.1) in the *Macoma*/present tanks (3.56 ± 0.6 ntu) the same as in the control/present tanks ($p = 0.288$) but turbidity in the *Hediste*/present tanks (4.20 ± 0.4 ntu) was slightly but significantly higher than in the control tanks ($p = 1.5 \times 10^{-4}$), and turbidities in *Corophium*/present tanks (14.6 ± 1.9 ntu) substantially and significantly higher than in the control tanks ($p = 6.8 \times 10^{-9}$). While there were no significant differences between MP/MA treatments (Table 4.3, Model 4.1.1) of the control ($p = 0.064$) and *Macoma* ($p = 0.561$) treatments on day 2 (prior to pumps being turned on), there were significant differences between the MP/MA treatments of the *Hediste* ($p = 1.5 \times 10^{-4}$) and *Corophium* ($p = 1.2 \times 10^{-6}$) treatments. However, differences in turbidity between the MP/MA treatments of all bioturbator treatments disappeared after the pumps were switched on (see Fig. 4.5 and Table 4.3: Models 4.1.2 and 4.1.3, where all Patch 2 $p > 0.05$). As turbidity is only generated in one tank per unit, for days 4 and 6, total unit turbidities rather than tank turbidities were compared between bioturbator treatments and control. The mean turbidity in the control and *Macoma* units on days 4 and 7 were approximately the same, but the mean turbidities in the *Hediste* unit were 1.7x and 1.9x higher than in the control units, and the mean turbidities in the *Corophium* units was 6x and 24x greater than in the control units (Figure 4.6). The differences in turbidities between the *Macoma* and control tanks were not significant ($p = 0.776$ and $p = 0.243$, respectively) on either days 4 and 7, the differences be-

tween the control and *Corophium* tanks were significant on both days ($p = 1.1 \times 10^{-5}$ and $p = 4.0 \times 10^{-6}$, respectively), whereas the difference between the *Hediste* and control tanks was only significant on day 7 ($p = 0.052$ and $p = 0.005$, respectively, Table 4.3: Model 4.1.4 & 4.1.5). Total unit turbidity increase over days was not linear but as this pattern was likely influenced by animal deaths (Figure 4.6).

In summary, *Macoma* generated no significant turbidity in the overlying water column, while *Hediste* generated a small but significant turbidity and *Corophium* generated a large and significant amount of turbidity. The pumps, which were switched on the morning after the animals were added, equalized the water column between the MP and MA treatments so that the biofilms were exposed to the same water column conditions for most of the experiment despite the presence or absence of macrofauna.

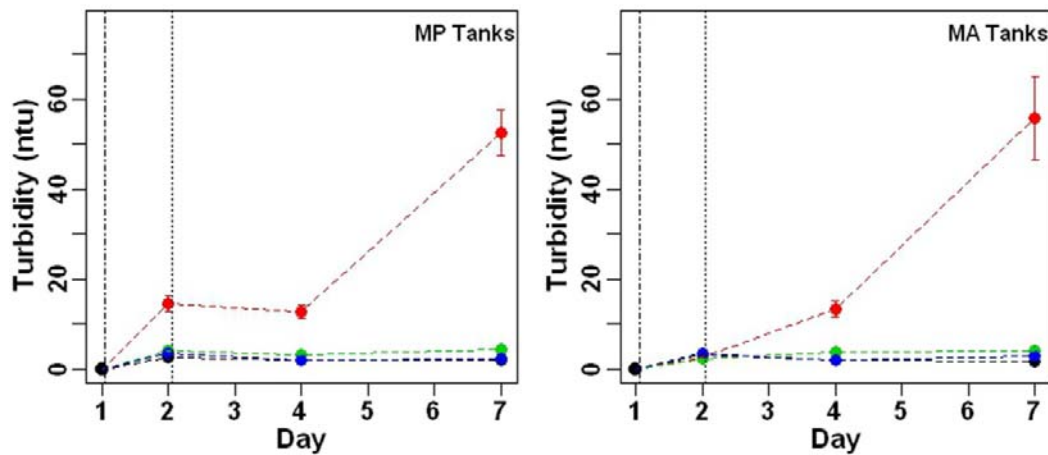


Figure 4.5: Mean turbidity (± 1 st. err.) in each macrofauna treatment over the 7 days of the experiment: control (black), *Corophium* (red), *Hediste* (green), and *Macoma* (blue). Filtered seawater and animals were added to the tanks on day 1 (dot-dashed line) and pumps were switched on the morning of day 2 (dotted line).

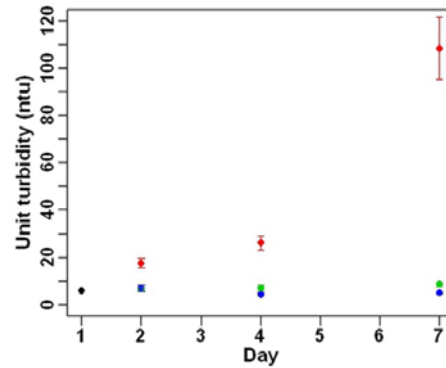


Figure 4.6: Total daily turbidity generated by each unit : control (black), *Macoma* (blue), *Hediste* (green), and *Corophium* (red).

Table 4.3: Regression results for models with turbidity as response variable.

Model Nr / Details	Res/Tot DF	Variable	Est	Standard error	p-value
4.1.1 Turbidity Day2, Tanks GLS with MF as variance category.	21/32	Intcpt (C, MP)	2.79	0.19	2.4×10^{-13}
		Cv	11.8	1.36	6.8×10^{-9}
		Hd	1.41	0.37	8.4×10^{-4}
		Mb	0.77	0.71	0.288
		MA	0.53	0.27	0.064
		Cv : MA	-12.4	1.92	1.2×10^{-6}
		Hd : MA	-2.34	0.52	1.5×10^{-4}
		Mb : MA	-0.59	1.01	0.561
4.1.2 Turbidity Day 4, Tanks LME with MF as variance category and unit as a random factor	20/32	Intcpt (C, MP)	2.12	0.31	1.7×10^{-5}
		Cv	10.7	1.69	3.8×10^{-5}
		Hd	1.21	0.67	0.099
		Mb	0.04	0.43	0.928
		MA	-0.11	0.11	0.335
		Cv : MA	0.65	2.31	0.784
		Hd : MA	0.56	0.74	0.466
		Mb : MA	0.15	0.15	0.368
4.1.3 Turbidity, Tank Day 7 LME with MF as variance category and unit as a random factor	20/32	Intcpt (C, MP)	2.0	0.43	4.5×10^{-4}
		Cv	50	7.42	1.9×10^{-5}
		Hd	2.47	0.61	1.7×10^{-3}
		Mb	0.20	0.83	0.813
		Patch 2	-0.14	0.17	0.435
		Cv : MA	3.46	10.5	0.747
		Hd : MA	-0.35	0.27	0.226
		Mb : MA	0.73	0.83	0.401
4.1.4 Turbidity Day 4, Unit GLS with MF as variance category.	9/16	Intcpt (C, MP)	4.13	0.51	3.6×10^{-6}
		Cv	22.02	3.06	1.1×10^{-5}
		Hd	2.98	1.38	0.052
		Mb	0.23	0.77	0.776
4.15 Turbidity Day 7, Unit GLS with MF as variance category.	9/16	Intcpt (C, MP)	3.96	0.70	0.0001
		Cv	104.4	13.1	4.0×10^{-6}
		Hd	4.59	1.32	0.005
		Mb	1.13	0.92	0.243

4.3.2.2 Suspended sediment

Suspended sediment collected in overlying water from MP and MA tanks at the end of the experiment was less than 1 g across the board but was lowest in the *Macoma* tanks, followed by the control tank and *Nereis* tanks, with *Corophium* tanks having by far the most (Table 4.2 and Figure 4.7). There were no significant differences between MP and MA treatments within any of the macrofauna treatments (Table 4.4, Model 4.2.1: all MA treatments $p > 0.05$) and neither *Hediste* nor *Macoma* treatments had suspended sediments significantly different from the control treatment (*Hediste* $p = 0.225$ and *Macoma* $p = 0.635$). The *Corophium* treatments, however, showed significantly greater amounts of suspended sediment than the control treatment ($p = 0.022$).

4.3.2.3 Light attenuation

Light penetration through the final water columns of each tank, expressed as a percentage of light penetrating a column of pure filtered seawater of the same height, was greatest through the columns of the control and *Macoma* treatments ($> 80\%$), followed by the *Hediste* treatments ($50\% - 80\%$) and was lowest ($< 40\%$) through the water columns of the *Corophium* treatments (Table 4.2 and Figure 4.7).

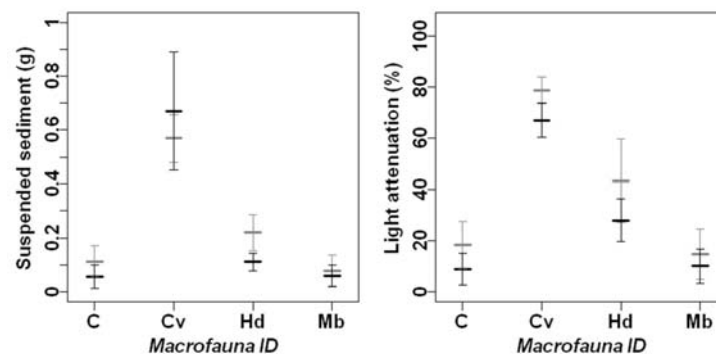


Figure 4.7: Mean suspended sediment (left) and light penetration (right) in each treatment group on day 7, where grey points and error bars represent the MP treatments and black points and error bars represent the MA treatments of the control (C), *Corophium* (Cv), *Hediste* (Hd), and *Macoma* (Mb) treatments.

There were no significant differences between MP and MA treatments within any of the macrofauna treatments (Table 4.4, Model 4.2.2: all MA treatments $p > 0.05$) and neither *Hediste* nor *Macoma* treatments had light losses significantly lower than the control treatment (*Hediste* $p = 0.772$ and *Macoma* $p = 0.549$) even though all of the MA treatments had slightly higher light than the MP treatments (Figure 4.7). The *Corophium* treatment, however, showed significantly less light penetration than the control treatment ($p = 0.0002$).

4.3.3 Nutrients

4.3.3.1 Ammonium

NH_4^+ ion levels in control and *Macoma* treatments were approximately the same ($0.6 \mu\text{mol L}^{-1}$) as the levels in seawater suggesting that there was no net flux into or out of the sediment from the overlying water column over the course of the experiment (Figure 4.8). However, NH_4^+ ions were substantially more abundant in *Hediste* (mean = $4.3 \mu\text{mol L}^{-1}$) and particularly *Corophium* (mean = $6.9 \mu\text{mol L}^{-1}$) treatments meaning there was a positive flux of NH_4^+ out of the sediment into the water column. In the MP treatments only *Corophium* and *Hediste* had a significantly higher NH_4^+ flux than the control (Table 4.4, Model 4.2.3: $p = 0.018$ and $p = 0.001$, respectively). There were no significant differences between MP and MA treatments within any of the macrofauna treatments (all MA treatments $p > 0.05$).

4.3.3.2 Nitrite + Nitrate

Final combined nitrite + nitrate (NO_x^-) levels were near 0 across all treatments. However, the seawater that the tanks were filled with contained $6.6 \mu\text{mol L}^{-1}$ NO_x^- . This means there was a negative flux of NO_x^- from the overlying water into the sediment in all tanks.

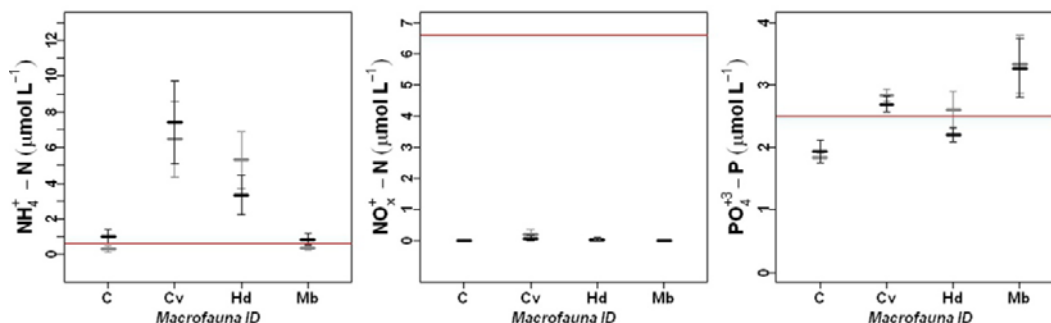


Figure 4.8: Mean quantity of nitrogen from ammonium ions ($\text{NH}_4^+\text{-N}$, left), combined nitrate and nitrite ions ($\text{NO}_x\text{-N}$, centre), and quantity of P from phosphate ions ($\text{PO}_4^{3+}\text{-P}$, right) in the overlying water columns on day 7. Grey points and error bars represent the MP treatments and black points and error bars represent the MA treatments of the control (C), *Corophium* (Cv), *Hediste* (Hd), and *Macoma* (Mb) treatments. The red lines represent the original levels in the filtered seawater with which the tanks were filled (on day 1). A final level > original level indicates a positive flux from the sediment into the overlying water and a final level < original level indicate a negative flux from the overlying water into the sediment).

4.3.3.3 Phosphate

The mean PO_4^{3+} fluxes in the control treatments and the *Hediste*-MA were negative: the most phosphate was absorbed from the overlying water column (seawater = $2.5 \mu\text{mol L}^{-1}$) into the sediment in the two control treatments followed by *Hediste*-MA (Figure 4.8). All other treatments had positive mean PO_4^{3+} fluxes, of which the two *Macoma* treatments were the highest, followed by both *Corophium* treatments, and finally the *Hediste*-MP treatment. The *Corophium*-MP and *Macoma*-MP were significantly different from the control-MP treatment (Table 4.4: Model 4.2.4: $p = 0.025$ and $p = 0.002$, respectively) but the *Hediste*-MP treatment was not ($p = 0.092$). Again, there were no significant differences between MP and MA treatments within any of the macrofauna treatments (all MA treatments $p > 0.05$), which, by logical extension, suggests that both the *Corophium*-MA and *Macoma*-MA were also significantly greater than the control-MA.

3.3.4 Sediment properties

The sediment grain size was bimodal with peaks at 20 and 40 μm with 100 % of the bed < 63 μm , i.e. silt or fine mud according to the Wentworth scale. The

mean water content of the surface sediment (≤ 2 mm) in the 8 treatments at the end of the experiment ranged from 57.8 % to 64.4 % (Table 4.2). While the in the *Corophium* and *Hediste* treatments the MP had lower water contents than the MA treatments the situation was reversed in the control and *Macoma* (Figure 4.9). There was no significant overall effect of macrofauna treatment (Table 4.4, Model 4.3.1: $p = 0.542$) or macrofauna presence ($p = 0.715$) on organic content but there was a significant interaction ($p = 0.027$) due to the opposite directions of increase in the MP and MA treatments over the MF treatments.

Mean sediment organic content ranged from 8.6 % to 13.4 % (Table 4.2). In the MP treatments the control treatments had the highest organic content, followed by *Corophium*, *Macoma*, and *Hediste*, whereas in the MA treatments the control treatments had the lowest organic content, followed by *Corophium*, *Hediste*, and *Macoma* (Figure 4.9). There was no significant overall effect of macrofauna treatment (Table 4.4, Model 4.3.2: $p = 0.075$) or macrofauna presence ($p = 0.191$) on organic content but there was a significant interaction ($p = 0.027$) due to the opposite directions of increase in the MP and MA treatments over the MF treatments.

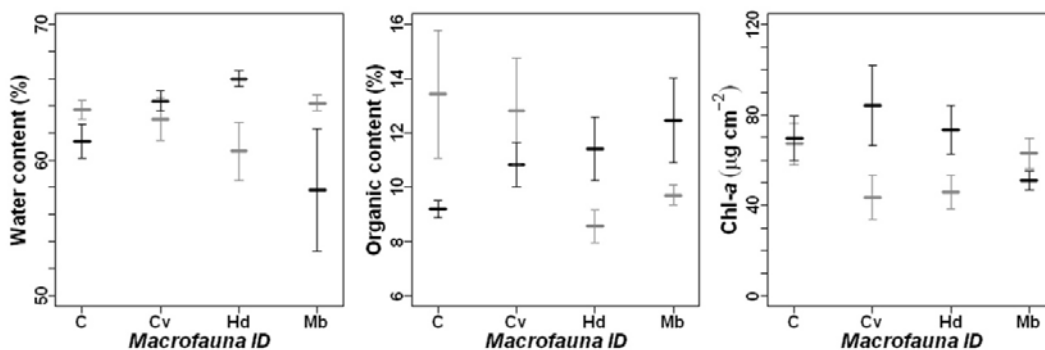


Figure 4.9: Mean water (left), organic (centre), and chlorophyll-*a* (right) content in the top 2 mm of sediment in each treatment group on day 7. Grey points and error bars represent the MP treatments and black points and error bars represent the MA treatments of the control (C), *Corophium* (Cv), *Hediste* (Hd), and *Macoma* (Mb) treatments.

Table 4.4: Regression results for models overlying water and sediment properties.

Model Nr / Details	Res/Tot DF	Variables	Est	Standard error	p-value
4.2.1 Susp. sed Day 7, Tanks LME with MF as vari- ance category and unit as a random factor	20/32	Intcpt (C, MP) Cv Hd Mb MA (C) Cv : MA Hd : MA Mb : MA	0.11 0.46 0.11 -0.03 -0.06 0.16 -0.05 0.04	0.55 0.17 0.08 0.07 0.05 0.23 0.09 0.06	0.065 0.022 0.225 0.635 0.302 0.503 0.563 0.521
4.2.2 Light atten Day 7, Tanks LME with MF as vari- ance category and unit as a random factor	20/32	Intcpt (C, MP) Cv Hd Mb MA (C) Cv : MA Hd : MA Mb : MA	18.1 60.5 25.2 -3.63 -9.45 -2.33 5.98 4.88	8.63 11.3 16.0 11.0 8.11 9.31 18.6 8.66	0.59 0.0002 0.142 0.748 0.267 0.807 0.753 0.584
4.2.3 $\Delta NH_4^+ - N$ Day 7, Tanks LME with MF as vari- ance category and unit as a random factor	20/32	Intcpt (C, MP) Cv Hd Mb MA (C) Cv : MA Hd : MA Mb : MA	-0.31 6.18 5.00 0.09 0.72 0.23 -2.68 -0.23	0.33 2.24 1.41 0.40 0.44 3.15 1.98 0.51	0.365 0.017 0.004 0.830 0.129 0.944 0.201 0.657
4.2.4 $\Delta PO_4^{3-} - P$ Day 4, Tanks LME with MF as vari- ance category and unit as a random factor	20/32	Intcpt (C, MP) Cv Hd Mb MA (C) Cv : MA Hd : MA Mb : MA	-0.67 1.00 0.77 1.50 0.11 -0.26 -0.51 -0.17	0.28 0.39 0.42 0.39 0.11 0.13 0.26 0.11	0.033 0.025 0.092 0.002 0.318 0.065 0.073 0.156
4.3.1 % Water content Day 7, Tanks ANOVA	24/32	MF [3] Pres [1] MF:Pres [3] Residuals [24]	11.4 2.11 50.7 15.5	0.733 0.136 3.28	0.542 0.715 0.038
4.3.2 % Organic content Day 7, Tanks ANOVA on GLS with fitted values as v-cv	23/32	Intcpt [1] MF [3] Pres [1] MF:Pres [3]		1331.7 2.61 1.81 3.65	$2.9 \cdot 10^{-6}$ 0.075 0.191 0.027

3.3.5 Sediment chlorophyll-*a* content

The mean chlorophyll-*a* content of the surface sediment (≤ 2 mm) in the 8 treatments at the end of the experiment ranged from 39.6 to 76.8 $\mu\text{g cm}^{-2}$ (Table 4.2). The two control treatments had approximately the same levels of chlorophyll-*a*, at about 53 $\mu\text{g cm}^{-2}$, whereas the *Corophium* and *Hediste* MP treatments had < 50 $\mu\text{g cm}^{-2}$ in the MP treatments but > 50 $\mu\text{g cm}^{-2}$ in the MA treatments (Figure 4.9). Conversely, in the *Macoma* treatments the MP tanks had higher mean chlorophyll-*a* concentration than the MA tanks. (Table 4.5, Model 4.4.1) Neither macrofauna identity nor macrofauna presence had a significant effect on Chlorophyll-*a* (ANOVA: $p = 0.672$ and $p = 0.602$, respectively) but there was a significant interaction ($p = 0.013$) due the reversal of MP:MA ratios of chlorophyll-*a* concentrations in the *Macoma* treatment (1.4) compared to the other three treatments (control = 0.897, *Corophium* = 0.515, *Hediste* = 0.645).

Chlorophyll-*a* concentrations did not respond to changes in light levels: there was no significant covariation between chlorophyll-*a* and either incident light (Fig. 4.12 D), turbidity (Fig. 4.13 D), suspended sediment (Fig. 4.12 E), or light attenuation (Fig. 4.12 F). In the regression of chlorophyll-*a* against light levels and OW properties (Table 4.6: Model 4.5.1) only the factors for the presence of *Corophium* and *Hediste* in tanks (fMF – Cv: $p = 0.0002$; fMF – HD: $p = 0.007$) and the variable for ammonium flux (ΔNH_4^+ , $p = 0.001$) covaried significantly. Bootstrapped means and confidence intervals (Fig 4.14) show that the presence of *Corophium* and *Hediste* in the sediment reduced chlorophyll-*a* concentrations whereas they increased the chlorophyll-*a* concentration in the second tank; conversely, the *Macoma* had no effect on sediment chlorophyll-*a* concentration either in the MP or the MA treatments. There was no correlation between chlorophyll-*a* and water and organic content of the sediment (cor = 0.170, DF = 30/32, $p = 0.352$, and cor = 0.04, DF = 30/32, $p = 0.827$).

Table 4.5: Regression results for models overlying water and sediment properties.

Model Nr / Details	Res/Tot DF	Variables	numDF/ denDF	F-value	p-value
4.4.1 Chl-a Day 7, Tanks ANOVA on LME with MF as variance category and unit as a random factor	20/32	Intcpt (C, MP)	1/12	326.4	0.00005
		factor(ID)	3/12	15.7	0.672
		factor(MP)	1/12	11.6	0.602
		factor(ID):factor(MP)	3/12	1.61	0.013
4.4.2 F_0^{15} Day 7, Tanks ANOVA on LME with MF as variance category and unit as a random factor	20/32	Intcpt (C, MP)	1/12	594.5	$2.9 \cdot 10^{-8}$
		factor(ID)	3/12	15.7	0.0002
		factor(MP)	1/12	11.6	0.005
		factor(ID):factor(MP)	3/12	1.61	0.238
4.4.3 Sp. Richness Day 7, Tanks ANOVA on LME with MF as variance category and unit as a random factor	20/32	Intcpt (C, MP)	1/12	871.1	$1.0 \cdot 10^{-9}$
		factor(ID)	3/12	0.560	0.652
		factor(MP)	1/12	0.304	0.591
		factor(ID):factor(MP)	3/12	7.31	0.005
4.4.4 Species Diversity Day 7, Tanks ANOVA on LME with MF as variance category and unit as a random factor	20/32	Intcpt (C, MP)	1/12	209.2	$2.8 \cdot 10^{-5}$
		factor(ID)	3/12	0.289	0.833
		factor(MP)	1/12	0.366	0.556
		factor(ID):factor(MP)	3/12	3.75	0.041

3.3.6 Surface biomass (F_0^{15})

Starting F_0^{15} values varied across treatment groups: the control-MA treatment had the highest mean starting values and the *Corophium*-MP treatment had the lowest mean starting values (Table 4.2). Neither of the control treatments changed substantially over the course of the experiment (MP = -4.11 ± 2.9 %; MA = $+0.27 \pm 8.8$ %) but biomass in tanks containing all 3 species declined substantially over the course of the experiment (Table 4.2 and Figure 4.10). By day 7, surface biofilms in the *Hediste*-MP tanks had declined the most (-67.1 ± 10.8 %), followed by the *Corophium*-MP tanks (-48.6 ± 4.8 %), and *Macoma*-MP tanks (-39.9 ± 12.6 %). However, in the MA treatments, the surface biofilms in the *Corophium*-MA declined the most (-32.5 ± 13.6 %), followed by *Hediste*-MA ($-21.2 \pm$

22.7 %), whereas the biofilms in *Macoma*-MA tanks hardly changed at all (-8.9 ± 14.0 %). Both macrofauna ID and macrofauna presence has a significant effect on F_0^{15} ($p = 0.0002$ and $p = 0.005$, respectively) but the interaction, i.e. the difference in F_0^{15} between MP-MA treatments across macrofauna treatments, was not significant (ANOVA, $p = 0.238$) (Table 4.5, Model 4.4.2).

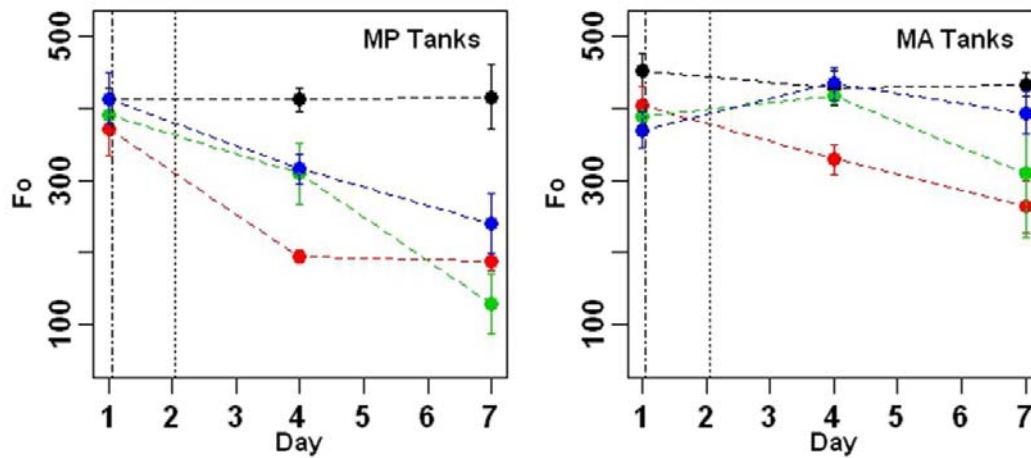


Figure 4.10: Mean F_0^{15} (arbitrary units, ± 1 st. err.) in each macrofauna treatment over the 7 days of the experiment: control (black), *Corophium* (red), *Hediste* (green), and *Macoma* (blue). Filtered seawater and animals were added to the tanks on day 1 (dot-dashed line) and pumps were switched on the morning of day 2 (dotted line).

Of the three different quantifications of water column optical condition, turbidity, suspended sediment and relative light attenuation (Fig. 4.13 A, B, C, respectively), relative light attenuation correlated best with final F_0^{15} and was therefore chosen as the covariate in the regression of MPB characteristics against light and overlying water characteristics. Differences in light levels to the tank surfaces did not covary significantly with final F_0^{15} values (Fig. 4.12A) and were therefore dropped from the regression of MPB characteristics against light and water properties (Table 4.6: Model 4.5.2). Mean unit ammonium and phosphate fluxes (Figures 4.12B and 4.12C, respectively) did not covary significantly with F_0^{15} and were also dropped from the final model. Only the presence and identity of macrofauna in each tank (fMF) and light attenuation covaried significantly with final F_0^{15} (Table 4.6: Model 4.5.2): surface biomass decreased with the presence of feeding macrofauna (*Nereis*, *Corophium*, *Hediste*) and with increasing light at-

tenuation. Final $F_{0.7}^{15}$ and model 4.10 residuals were checked for correlations with starting $F_{0.7}^{15}$ (cor = 0.19, DF = 30/32, $p = 0.308$), water content (cor = -0.07, DF = 30/32, $p = 0.719$), organic content (cor = 0.16, DF = 30/32, $p = 0.379$), or chlorophyll-*a* content (cor = 0.27, DF = 30/32, $p = 0.132$) and none were significant.

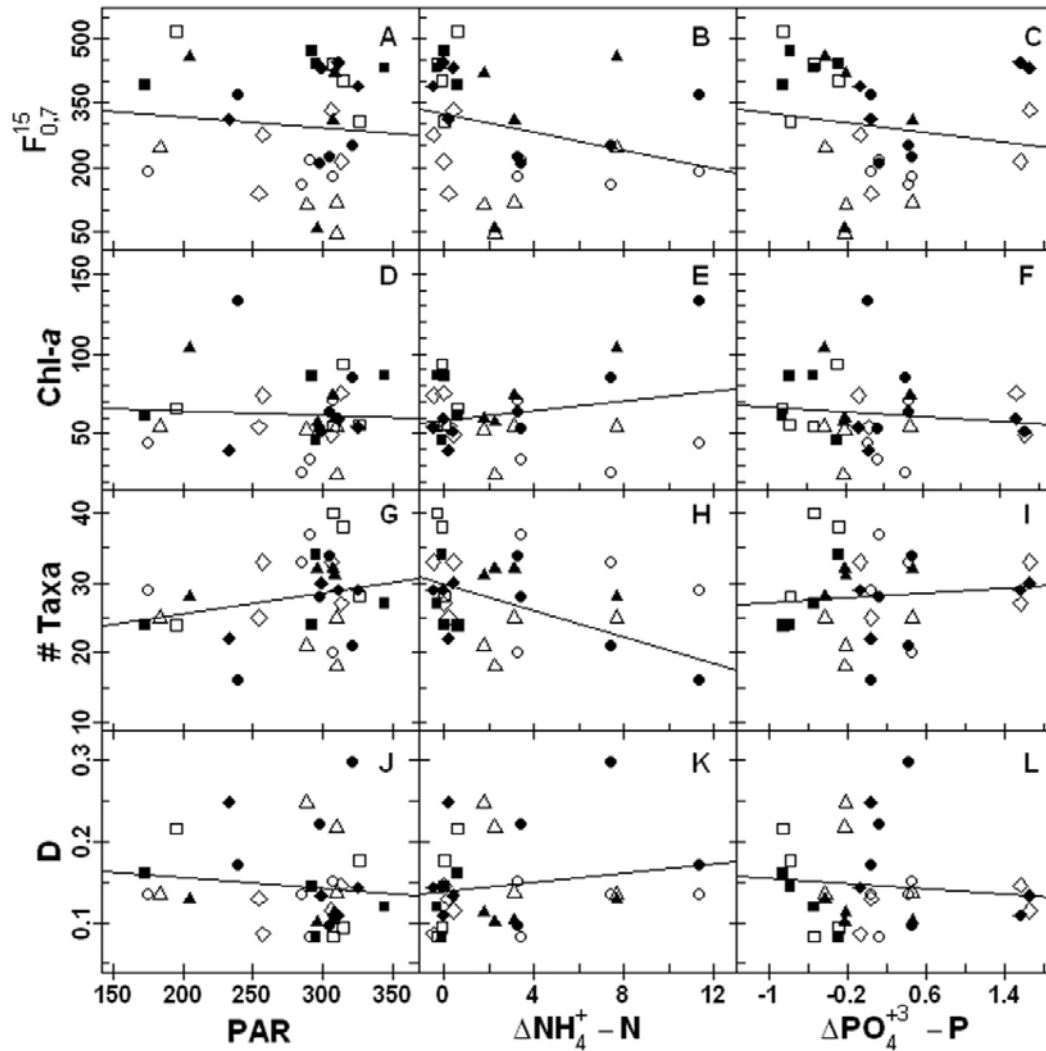


Figure 4.11: $F_{0.7}^{15}$, Chlorophyll-*a*, Species richness (# Taxa), and Simpson's Diversity index (D) in each tank against mean incident light (PAR, $\mu\text{mol m}^{-2} \text{s}^{-1}$), ammonium flux (ΔNH_4^+), and phosphate flux (ΔPO_4^{3+}) within each unit over the course of the experiment. Trend lines represent correlations, none of which are significant (all $p > 0.10$, all $R^2 < 0.10$). Open and closed symbols represent MP and MA tanks, respectively, and control, *Corophium*, *Hediste*, and *Macoma* treatments are represented by squares, circles, triangles, and diamonds, respectively.

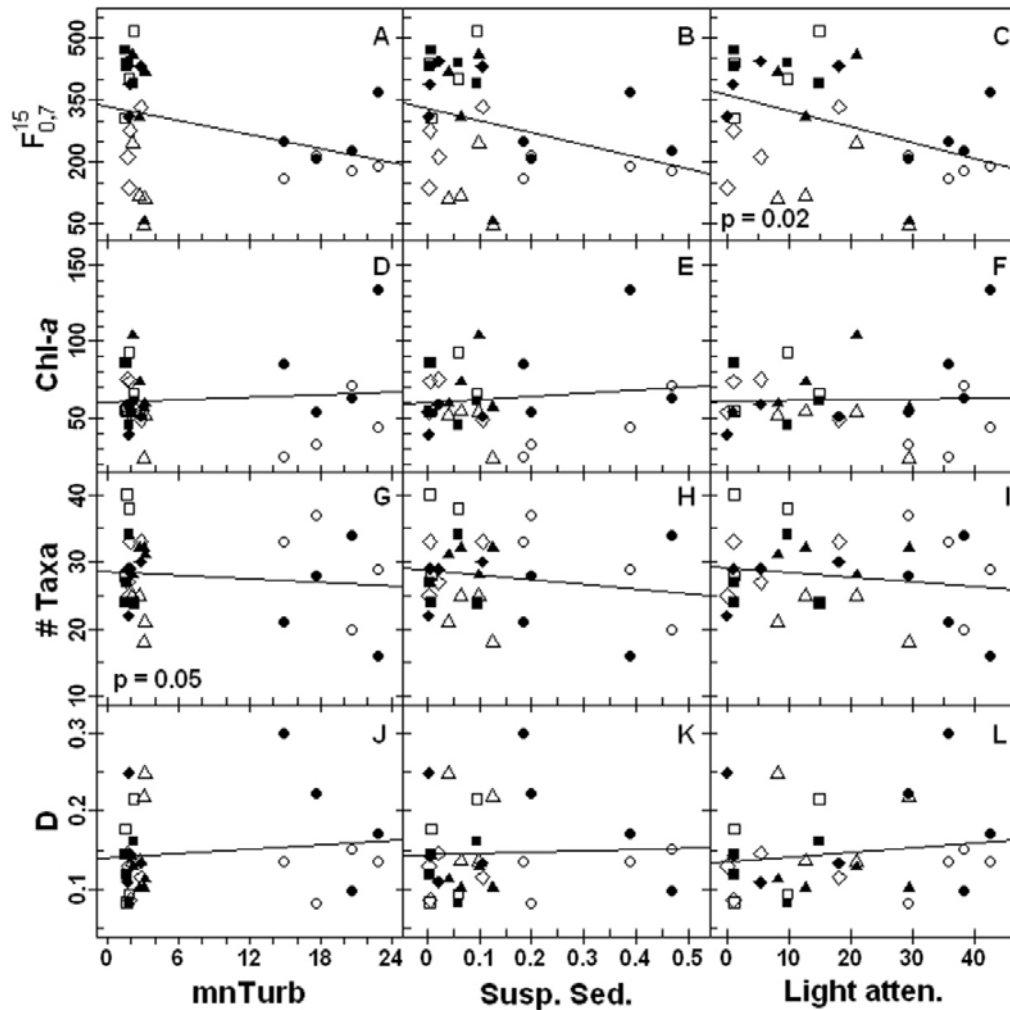


Figure 4.12: $F_{0.7}^{15}$, Chlorophyll-*a*, Species richness (# Taxa), and Simpson's Diversity index (D) in each tank against mean Turbidity (ntu), suspended sediment (g), and light penetration (%) within each unit over the course of the experiment. Trend lines represent correlations, none of which are significant (all $p > 0.10$, all $R^2 < 0.10$) with the exception of the correlation in C and G. Open and closed symbols represent MP and MA tanks, respectively, and control, *Corophium*, *Hediste*, and *Macoma* treatments are represented by squares, circles, triangles, and diamonds, respectively.

Table 4.6: Regression results for models with MPB biomass (Chlorophyll-*a* and $F_{0.7}^{15}$) and diversity (Species richness and Simpson diversity) measurements from day 7 as response variables.

Model Nr / Details	Res/Tot DF	Variables	Est	Standard error	p-value
4.5.1 Chl-a Day 7, Tanks LME with MF as variance category and unit as a random factor	23/32	Int (fMF = 0) Cv Hd Mb ΔNH_4^+	58.4 -42.2 -21.9 4.56 4.00	3.95 8.40 6.83 7.61 0.96	$6.18 \cdot 10^{-10}$ 0.0002 0.007 0.560 0.0010
4.5.2 $F_{0.7}^{15}$ Day 7, Tanks LME with MF as variance category and unit as a random factor	23/32	Int (fMF = 0) Cv Hd Mb %LA	414.9 -75.3 -228.8 -153.1 -4.03	37.9 30.8 35.6 27.8 1.75	$2.98 \cdot 10^{-8}$ 0.029 $2.28 \cdot 10^{-5}$ $1.02 \cdot 10^{-4}$ 0.037
4.5.3 Sp. Richness Day 7, Tanks GLS	31/32	Int (fMF = 0)	28.03	1.02	$2.7 \cdot 10^{-23}$
4.5.4 Species Diversity Day 7, Tanks GLS	31/32	Int (fMF = 0)	1.99	0.061	$1.7 \cdot 10^{-25}$

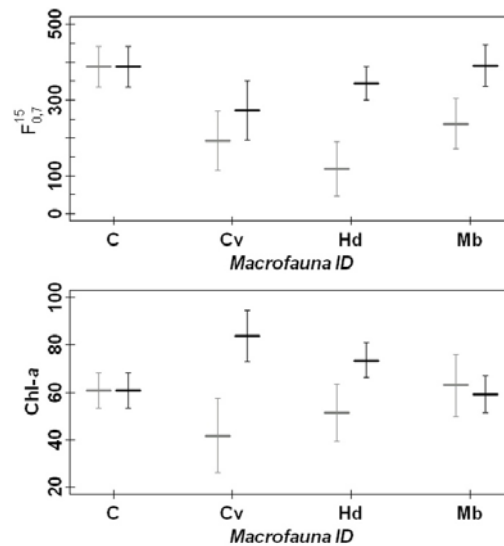


Figure 4.13: Model visualization: bootstrapped ($n = 10,000$) means and 95 % C.I.s from Models 4.5.1 (bottom) and 4.5.2 (top).

3.3.7 MPB assemblage

Of the 127 taxa found across all 32 tank assemblages, the dominant 3 species in each assemblage, in order of overall abundance, were *Navicula gregaria* Donkin, *Stauroneis dubitabilis* Hustedt, and *Navicula phyllepta* Kützing, which together made up just over 50% of the total cell count. However, in addition to those taxa *Gyrosigma fasciola* (Ehrenberg) Griffith et Henfrey, *Pleurosigma angulatum* (Quekett) Smith, and *Nitzschia cf. distans* Gregory (1857) were present in every tank and in > 1% total abundance. Finally, in order of overall abundance, *Achnanthes delicatula* (Kützing) Grunow (which in this thesis includes *Achnanthes hauckiana* according to van der Werff & Huls 1974, see Appendix 1), *Catenula adhaerens* Mereschkowsky, *Navicula digitatoradiata* (Gregory) Ralfs in Pritchard 1861, and *Plagiotropis vanheurckii* Grunow in Van Heurck 1880 also all made up > 1 % of total cells, and, together with the previous taxa, made up just over 80 % of total cell count.

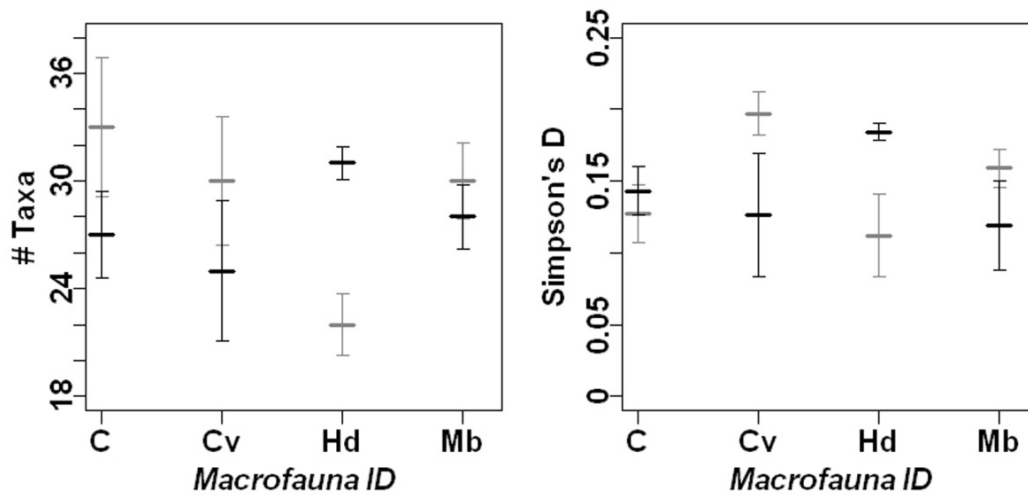


Figure 4.14: Mean Species richness (number of taxa per sample, left) and Simpson's diversity index (D, right) on day 7. Grey points and error bars represent the MP treatments and black points and error bars represent the MA treatments of the control (C), *Corophium* (Cv), *Hediste* (Hd), and *Macoma* (Mb) treatments.

3.3.7.1 *Taxa richness*

In addition to the 6 taxa present in all 32 assemblages, each assemblage contained between 10 and 32 other taxa. Mean species richness per treatment group varied between 22 and 33 taxa. Species richness was higher in the MP treatment than in the MA treatment of the control, *Corophium*, and *Macoma* treatments but the opposite was the case in the *Nereis* treatment where species richness was substantially lower in the grazed treatment than in the ungrazed treatment (Table 4.2 and Figure 4.11, left panel). Therefore, while there were no significant overall effects for macrofaunal identity and presence treatments (Table 4.5, Model 4.4.3 $p = 0.652$ and $p = 0.591$, respectively), the interaction was significant ($p = 0.005$). In the regression against the presence and identity of feeding macrofauna, light intensity (Figure 4.12 G), mean unit ammonium (Figure 4.12 H) and phosphate flux (Figure 4.12 I), and mean unit light attenuation (Figure 4.13 I), none of these variables significantly explained the variations in species richness (Table 4.6, Model 4.5.3).

3.3.7.2 *Assemblage diversity*

Simpson diversity index calculated from MPB taxa counts from each replicate did not vary much between treatment groups: the highest mean probability of two individuals being from the same species was 0.20 and the lowest was 0.11 (Table 4.2, Figure 4.11). In the control treatments the diversity was similar but in the *Corophium* and *Macoma* treatments the MP tanks had higher mean diversities than the MA tanks (Figure 0.13 vs. 0.20 and 0.12 vs. 0.16, respectively). Conversely, in the *Nereis* treatment the MA tanks had higher diversity than the MP tanks. The differences in species diversity by macrofauna identity or presences were not significant (Table 4.5, Model 4.4.4 $p = 0.833$ and $p = 0.556$, respectively) but there was a significant interaction ($p = 0.041$) due to the inverse relationship between MP-MA diversities in *Nereis* versus the other treatments. The variation that existed in species diversity was not explained by either the presence of feed-

ing macrofauna, light intensity (Figure 4.12 J), mean unit ammonium (Figure 4.12 K) or phosphate flux (Figure 4.12 L), or mean unit light attenuation (Figure 4.12 L; Table 4.6, Model 4.5.4). An MDS plot on Bray-Curtis similarity indices of log-transformed taxa counts (Figure 4.15) showed no within treatment groupings in assemblage composition.

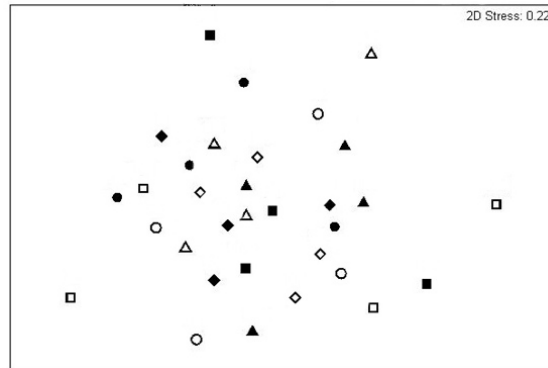


Figure 4.15: MDS plot from Bray-Curtis matrix of log-transformed diatom counts. Open and closed symbols represent MP and MA tanks, respectively, and control, *Corophium*, *Hediste*, and *Macoma* treatments are represented by squares, circles, triangles, and diamonds, respectively.

4.4 Discussion

4.4.1 The effects of *Corophium*, *Hediste*, and *Macoma* on sediment and overlying water column

The null hypothesis ($H_{04.1}$) that bioturbation by *Corophium*, *Hediste*, and *Macoma* produces similar effects on the overlying water column must be rejected in terms of sediment resuspension, turbidity in the water column, and the resulting attenuation of light to the sediment bed. Only *Corophium* resuspended significant amounts of sediment into the water column (Table 4.4, Model 4.2.1, $p = 0.022$) and, therefore, only *Corophium* treatments exhibited significant light attenuation through a 10 cm water column (Table 4.4, Model 4.2.2, $p = 0.0002$). However, *Hediste* did generate more suspended sediment than the control and *Macoma* treatments though this was statistically detected only in the turbidity measurements on days 2 and 7, which were significantly higher than those from control

treatments (Table 4.3: Model 4.1.1, $p = 8.4 \times 10^{-4}$; Model 4.1.3, $p = 1.7 \times 10^{-3}$). Turbidities in the *Macoma* treatments were never significantly different from those in the control treatments (Table 4.3: Model 4.1.1, $p = 0.228$; Model 4.1.2, $p = 0.928$; Model 4.1.3, $p = 0.813$) and turbidities in *Corophium* treatments were always significantly higher than in the control tank (Table 4.3: Model 4.1.1, $p = 6.8 \times 10^{-9}$; Model 4.1.2, $p = 3.8 \times 10^{-5}$; Model 4.1.3, $p = 1.9 \times 10^{-5}$), and the effects were visibly within 20 minutes of adding *Corophium* to the tanks (Figure 4.3 C). The pumps distributed the suspended sediment efficiently between test tanks so that no significant differences and only slightly lower turbidities (Table 4.3: Model 4.1.2 & 4.1.3 all MA p -values > 0.05), suspended sediment (Table 4.4: Model 4.2.1 all MA p -values > 0.05) and light attenuation (Table 4.4: Model 4.2.1 all MA p -values > 0.05) were found in the secondary (MA) tanks (compared to MP tanks). Therefore, it could be assumed that the MPB in the two treatments in each unit were subjected to the same conditions in the overlying water columns.

The differences in water column turbidity are most likely due to differences in waste disposal between *Corophium*, *Hediste* and *Macoma*. *Corophium* ejects its waste into the overlying water column by means of the irrigation current it maintains through its burrow (Meadows & Reid 1966a). *Hediste* also maintains an irrigation current through its burrow, which is presumably why some sediment inevitably becomes resuspended into the overlying water column although this does not appear to be the primary waste disposal method. Rather, waste and loose sediment probably becomes part of the burrow wall by the same undulating motion and parapodia wall-pressing by which the worm originally builds its burrow (Trevor 1977). *Macoma* uses its exhalant siphon to deposit waste somewhere within the sediment matrix away from the feeding area so it does not come into contact with the overlying water column (Green 1968).

Dissolved inorganic nitrogen levels in the coastal seawater used to fill tanks were very low ($NO_3^- = \sim 6.6 \mu\text{mol L}^{-1}$ or $93 \mu\text{g L}^{-1}$ and $NH_4^+ = 0.6 \mu\text{mol L}^{-1}$ or 9.0

$\mu\text{g L}^{-1}$). According to previous studies in the North Atlantic and Baltic, during summer, DIN levels in the water column are usually low, NO_x^- fluxes to the overlying water column are either low or negative, whereas NH_4^+ fluxes are often higher in late summer (Henriksen *et al* 1980; Rizzo 1990; Rysgaard *et al* 1995, Sundbäck *et al* 2000). In addition, both NO_x^- and NH_4^+ fluxes between sediment and water column are 'filtered' by MPB biofilms whose activities are modified by light (Henriksen *et al* 1980; Andersen & Kristensen 1988; Feuillet-Girard *et al* 1997; Rizzo 1990; Sundbäck *et al* 2000): in the dark, in the absence of photosynthesis, fluxes tend to be positive and in the light they tend to be low or negative. NO_x^- levels in the overlying water were nil across all treatments, indicating a negative flux into the sediment that was either sequestered by MPB or denitrifying bacteria in all treatments. NH_4^+ flux, however, did vary between treatments: fluxes were significantly higher in the *Corophium* and *Hediste* treatments (Table 4.4, Model 4.2.3, $p = 0.017$ and $p = 0.004$, respectively), than in control treatments. These results agree with the findings of previous studies in which either *Corophium*, *Hediste*, or both increased NH_4^+ flux from the sediment to the overlying water, particularly in the dark (Henriksen *et al* 1980, Andersen & Kristensen 1988, Mortimer *et al* 1999, Emmerson *et al* 2001, Biles *et al* 2002, Ieno *et al* 2006, Bulling *et al* 2010). Water samples for nutrient analysis were taken early in the morning prior to experimental daylight hours, following 9 hours of darkness, so while to some degree they represented cumulative effects of 6 days of flux, they were probably more representative of a "dark" flux than a "light" flux. A few studies have shown that *Macoma* increase NH_4^+ flux, partially due to excreted NH_4^+ (Henriksen *et al* 1983; Biles *et al* 2002; Mortimer *et al* 1999) but NH_4^+ flux in the *Macoma* treatments in this experiment did not differ significantly from the control treatments ($p = 0.830$). It is possible that the lack of effect in *Macoma* treatments was due to mortality. *Corophium* and *Hediste* died at the surface where they could be easily removed and then replaced with live individuals, *Macoma* did not surface so it was not possible to determine whether they were

alive or dead at the end of the experiment, but some siphons were still visible a day prior to the end of the experiment.

PO_4^{3+} fluxes to the overlying water were negative in the control treatments, negative and near zero in the *Hediste* treatments, low but positive in *Corophium* treatments and highest in the *Macoma* treatments (Figure 4.8). This means that in the control treatments PO_4^{3+} from the overlying water was absorbed into the sediment, whereas in the *Corophium* and *Nereis* treatments were relatively neutral suggesting neither uptake nor release. PO_4^{3+} fluxes in *Corophium* and *Macoma* treatments were significantly different from the control treatments (Table 4.4, Model 4.2.4, $p = 0.025$ and $p = 0.002$, respectively) whereas *Nereis* treatment was not ($p = 0.092$). It is unclear why *Macoma* should release more phosphate from the sediment than *Corophium* and *Hediste* who are far more active bioturbators.

4.4.2 The effects of *Corophium*, *Hediste*, and *Macoma* on MPB biomass

The two different measurement of MPB biomass, F_0^{15} and chlorophyll-*a*, did not respond uniformly to experimental treatments. In addition to the presence and identity of feeding macrofauna, which both measurements responded negatively to, F_0^{15} covaried only with the light attenuation by the overlying water column and chlorophyll-*a* covaried only with NH_4^+ fluxes. However, this result does not necessarily imply a contradiction as the two measurements are not replicate measurements of the exact same variable: F_0^{15} measures biomass at or within 100 μmol of the sediment surface (Consalvey *et al* 2004), whereas a chlorophyll-*a* assay of the top 2 mm contains > 90 % of the sediment microalgal content (Paterson 1986), not just the actively photosynthesizing proportion. The abundance of MPB at the sediment surface is highly changeable and responds very quickly to changes in light and/or tidal conditions due to the high motility of epipelagic diatoms that make up most of the MPB in silty sediments (Consalvey *et al* 2004). On the other hand, chlorophyll-*a* content in the sediment is far more resilient to change as diatoms can survive in the absence of light and in anoxic conditions

for well over a week (Kamp *et al* 2011). The increase in biomass with agrees with results from a 4 week experimental study of MPB assemblages in shallow water systems by Sundbäck & Snoeijs (1991) in which biomasses of MPB (and diatoms specifically) in nutrient enriched (DIN & IP) treatments were significantly higher than in unenriched treatments.

The bulk of MPB biomass in the sediment, quantified by chlorophyll-*a* concentration, was reduced significantly by the grazing and sediment turnover of *Corophium* and *Hediste* (Table 4.6, Model 4.5.2: $p = 0.0002$ and $p = 0.007$, respectively) but not by *Macoma* ($p = 0.560$). Neither variations in incident light levels nor increased light attenuation through the water column reduced bulk MPB biomass. As mentioned above, diatoms are resilient to the absence of light, and can survive by NO_3^- based respiration of organic compounds, which is hypothesized to be an adaptation to burial by bioturbating macrofauna in benthic organisms and SiO_2 -depletion related sinking in pelagic organisms (Admiraal & Peletier 1979; Kamp *et al* 2011). Highest chlorophyll-*a* concentrations in sediment were found in the MA treatments of the *Corophium* and *Hediste* and this coincided with increased NH_4^+ flux in these treatments, hence the model estimated a significant increase in chlorophyll-*a* content with increasing NH_4^+ flux (Table 4.6, Model 4.5.2: $p = 0.001$). The increased flux probably originated from the MP side of the unit (Henriksen *et al* 1980; Andersen & Kristensen 1988; Emmerson *et al* 2001; Biles *et al* 2002; Bulling *et al* 2010) but, due to pumping, made NH_4^+ more available in the MA side of these units. In the absence of grazers, the overnight increase in nutrients via the water column increased biomass (Figure 4.14 bottom). This relationship could be more effectively delineated with a one-way flow-through system where in each unit the secondary tank (MA) receives water from the primary tank (MP), which is supplied by a filtered seawater reservoir, but not vice versa. In this scenario, flux measurements could be made on the two tanks separately, to determine if and where the increased NH_4^+ flux originates, and would still enable an increase in biomass on the secondary side if indeed in-

creased NH_4^+ increased biomass. The previous experiment showed no increase in biomass with increased DIN, although this could have been due to poor chlorophyll-a data without phaeopigment correction, and Underwood and colleagues (1998) found no relationship between MPB biomass and DIN in either their enrichment experiment or in their field studies.

The presence of each species of macrofauna significantly reduced the photosynthetically active biomass (F_0^{15}) in the respective tank (Table 4.6, Model 4.5.2: $p = 0.029$, $p = 2.28 \times 10^{-5}$, $p = 1.02 \times 10^{-4}$ for *Corophium*, *Hediste*, *Macoma*, respectively) presumably due to grazing but also partially due to disruption of the sediment surface. However, of all the covariates in the original model (incident light to each tank, % light attenuation through the water column, ΔNH_4^+ , and ΔPO_4^{3+}) only the % light attenuation was significantly covaried with surface biomass. It should be noted that mean light attenuation over the experimental period is a mean between the pure seawater column that each tank was filled with (0%) and the final value measured from the water column from each tank on day 7 (max $78.7 \% \pm 5.3$ in *Corophium*-MP) and therefore is most certainly an underestimation because sediment resuspension occurred as the animals burrowed into the sediment, i.e. almost immediately after being added to the tanks (Figure 4.3 C). It is thought that benthic MPB adjust themselves in the sediment so as to maximize photosynthetic efficiency but minimize photoinhibition due to excess light, desiccation at the surface, and resuspension into the water column during tidal immersion (Consalvey *et al* 2004). As the assemblage in this experiment was removed from the intertidal and placed in a subtidal regime, it stands to reason that they would maximize the time spent at the surface to maximize photosynthetic window without suffering deleterious consequences from excess light or desiccation or resuspension (as there was very little flow in the water column). By that reasoning, the surface biomass in the tanks with higher light attenuation but absence of grazers (*Corophium*-MA, *Hediste*-MA) should be higher than in the control tanks and yet the reverse occurred. In fact, according to the model the

migratory response in the *Corophium* tanks is largely due to light attenuation rather than grazing (Figure 4.14 top). It would appear that light levels in these tanks were insufficient to keep MPB at the surface and they are responding by migrating down into the sediment (Fauvel & Bohn 1904; Perkins 1964; Hay 1983; Pinkney & Zingmark 1991; Consalvey 2002).

4.4.3 The effects of *Corophium*, *Hediste*, and *Macoma* on MPB assemblage composition

Only assemblages in the *Hediste* treatments showed a marked difference in species richness and were distinct from the other treatments because in this case and unlike the other treatments, the MP tank had lower species richness than the MA tank. In the *Corophium* and *Macoma* treatments, the presence of the grazer coincided with greater species richness. However, as this was also the case in the control treatment, where the “MP” treatment is simply the tank with the pump attached, and the errors on the counts were large, nothing can reasonably be concluded from these results. The presence of *Hediste* significantly reduced the diversity of the assemblage by approximately 10 taxa compared to the MA treatment (Figure 4.11; Table 4.5, Model 4.4.3: interaction $p = 0.005$). With the exception of *A. delicatula*, 90 % of the assemblage consisted of taxa that were epipelagic motile, large, or both. Noticeably absent was *Catenula adhaerens* Mereschkowsky which was abundant in the Hediste-MA treatment, suggesting that perhaps smaller epipsammic taxa are more likely to be consumed by *Hediste*. The dominant taxa (*Navicula gregaria* Donkin, *Stauroneis dubitabilis* Hustedt, and *Navicula phyllepta* Kützing) were consistent across all treatments and were not affected by ΔNH_4^+ . Underwood and colleagues (Underwood *et al* 1998; Underwood & Provot 2000) determined that *Navicula phyllepta* preferred low ΔNH_4^+ concentrations, however, in their system, low concentrations were $< 400 \mu\text{mol L}^{-1}$, so the additional NH_4^+ released from the sediment by *Hediste* and *Corophium* ($< 10 \mu\text{mol L}^{-1}$) was probably much too low to induce differences in reproductive rates amongst diatoms.

Characteristically for diatom assemblages, the frequency distributions were heavily skewed to the left, i.e. a very low mean from a few dominant taxa with a very long tail of infrequent taxa. Presumably the MDS plot of log transformed Bray-Curtis similarity indices (Figure 4.15) displayed no assemblage similarities (or differences) between treatment groups because the dominant taxa were consistent across treatments whereas the numbers of infrequent taxa, 10 to 32 in each sample distributed over 121 taxa, were completely different across all treatments. In addition, neither variation in species richness or Simpson diversity could be explained by the presence of grazers, even *Hediste*, or any of the covariates describing environmental conditions in each tank (Table 4.6, Model 4.5.3 & 4.5.4). Perhaps the lack of resolution between assemblages was due to insufficient counts per sample: a larger sample may have delineated greater differences in the large number of moderate to very rare species in each sample, making the distribution less skewed towards the extremely dominant taxa. Counts per sample for describing MPB assemblages in previous studies vary from 200 – 1000 and have detected distinct assemblages over a range of environmental conditions or experimental treatments (Sundbäck *et al* 1996; Underwood *et al* 1998; Hillebrand *et al* 2000; Thornton *et al* 2002; Hagerthey *et al* 2002; Forster *et al* 2006). It is possible that for samples coming from different field sites fewer counts may be required than for experimental treatments that all began with a similar assemblage as the differences are likely to be more extreme. An experimental study comparing natural succession of MPB assemblages between nutrient enriched and unenriched treatments found no substantial differences in dominance of major diatom and major taxonomic groups after counting 500 cells per sample (Sundbäck & Snoeijs 1991). Secondly, the assemblages were not described in terms of biovolume as commonly done by other diatom ecologists (Sundbäck *et al* 1996; Hillebrand *et al* 1999, 2000; Snoeijs *et al* 2002). Biovolumes might show important differences between assemblages as large species like those from *Gyrosigma*, *Pleurosigma*, and *Plagiotropis* (Appendix 1, taxa 94) are

rarer but more influential community components than small, frequent species like *Achnanthes delicatula* or *Navicula phyllepta* (Snoijes *et al* 2002). However, Ribeiro (2010) who analysed Tagus estuary diatom assemblages by environmental variables, biovolume and functional group found it laborious and not particularly informative. Using biovolumes effectively means assigning a volume (cm^3) taken from mean measurements to each species; for species with limited size ranges like *Navicula phyllepta* and *Gyrosigma fasciola* (see Appendix 1, taxa 14 and taxa 3) this could be very effective but for species like *Stauroneis dubitabilis* and *Pleurosigma angulatum* where there is large variation in sizes (see Appendix 1, taxa 4 and 94) it seems less intuitively useful (unless each individual is measured for length and a biovolume calculated from mean ratios of dimensions but this would be extremely laborious). Functional trait analysis as in Ribeiro (2010) was not carried out as not all taxa were identified to genus and species and some species have more than one lifestyle depending on morphotype (Appendix 1 and Ribeiro 2010 e.g. *Navicula gregaria*) but this would perhaps be a productive approach.

4.4.4 Biodiversity and ecosystem function of MPB

Considered as an ecosystem function of MPB, biomass (i.e. potential for primary productivity) was regressed against biodiversity (Figure 4.16) to establish whether there was any relationship as those described in examinations of various ecological systems (Tilman & Downing 1994; Naeem & Li 1997; Emmerson *et al* 2001; Solan *et al* 2004; Forster *et al* 2006, Bulling *et al* 2010, Hicks *et al* 2011). No significant relationships were found between either of the two measures of biomass with either of the two measurements of biodiversity.

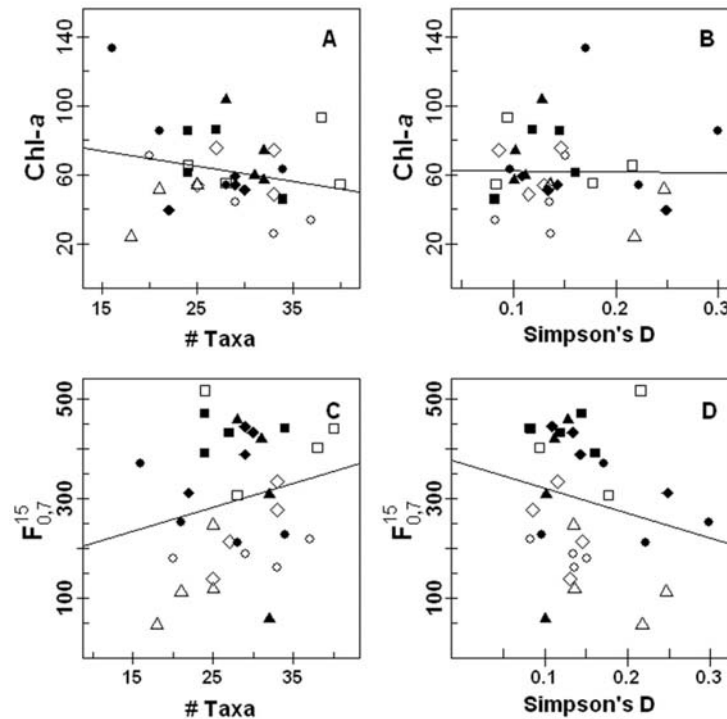


Figure 4.16: Correlations between Biodiversity and Ecosystem function (biomass) of MPB. Chlorophyll-*a* (A, by species richness, $p = 0.207$, and B, assemblage diversity, $p = 0.946$) or by $F_{0.7}^{15}$ (C, by species richness, $p = 0.243$ and D, assemblage diversity, $p = 0.256$). Open and closed symbols represent MP and MA tanks, respectively, and control, *Corophium*, *Hediste*, and *Macoma* treatments are represented by squares, circles, triangles, and diamonds, respectively.

The relationship between chlorophyll-*a* concentration and species richness (Figure 4.16 A) was negative but not significant ($\text{cor} = -0.229$, $p = 0.207$) and there was no relationship at all between chlorophyll-*a* concentration and Simpson's diversity (Figure 4.16 B). The relationship between photosynthetically active surface biomass ($F_{0.7}^{15}$) and species richness (Figure 4.16 C) was positive but not significant ($\text{cor} = 0.212$, $p = 0.243$) but the relationship with Simpson diversity was non-significant and negative ($\text{cor} = 0.207$, $p = 0.256$). In their examination of natural MPB assemblages compared to biomass in the Ems-Dollard estuary, Forster and colleagues (2006) found that there was a significant negative correlation between chlorophyll-*a* concentration and species richness of the assemblages. However, they found that there was a significant positive correlation

between net primary production (a short term variable) and both the species richness and Shannon index. While Colijn and Dijkema (1988) and Thornton and colleagues (2002) did not present a regression chlorophyll-a against species richness, the former reported that the highest biomasses were formed almost exclusively by single species and the latter reported that the highest biomass occurred in a sample in which a single species was very dominant (> 65%). These reported patterns of total biomass (and productivity) against species richness correspond to the overall patterns in this study so perhaps the non-significance here was due to the insufficient resolution in the MPB assemblage description (discussed above). However, why there should be a negative relationship between chlorophyll-a and species richness remains unclear but Forster and colleagues (2006) speculate that there are high occurrences of founder events and that once favourable conditions are stable, the more competitive species begins to monopolize the space.

Finally, as a useful follow up experiment would be to run the experiment in a flow-through system (as discussed in section 4.4.1) and measuring nutrient flux in each tank independently, as mentioned above, fluxes would have allowed them to be investigated as an ecosystem function and compared to diversity.

4.5 Conclusions

4.5.1 Null hypothesis H₀4.1 that bioturbation by *Corophium*, *Hediste*, and *Macoma* produces similar modifications to the overlying water column is false with respect to sediment resuspension. *Corophium* resuspends significantly more sediment which significantly increases turbidity in the overlying water column which reduces light penetration to the sediment bed. *Hediste* generates some turbidity and moderately reduces the light penetration to the sediment bed. *Macoma* generates hardly any suspended sediment and cannot be said to reduce light penetration to the sediment bed.

4.5.2 Null hypothesis H₀4.1 that bioturbation by *Corophium*, *Hediste*, and *Macoma* produces similar modifications to the overlying water column is false with respect to NH_4^+ flux which is significantly higher in *Corophium* and *Hediste* treatments than in the control and *Macoma* treatments.

4.5.3. Null hypothesis H₀4.2 that ecosystem engineering by *Corophium*, *Hediste*, and *Macoma* bioturbation cannot affect MPB biomass via resource modification is false with respect to chlorophyll-*a* concentration. Sediment chlorophyll-*a* concentration is estimated to increase with increased (dark) NH_4^+ fluxes in the *Corophium* and *Hediste* treatments.

4.5.4 Null hypothesis H₀4.3 that ecosystem engineering by *Corophium*, *Hediste*, and *Macoma* bioturbation cannot affect MPB biomass via resource modification is true. None of the modifications of the overlying water column in either the *Corophium* *Hediste* treatments affected either species richness or diversity (D) of the MPB assemblages.

4.5.5 Null hypothesis H₀4.4 that there is no relationship between MPB biomass and biodiversity is true: there was no relationship between either measure of biomass with either measure of biodiversity.

Chapter 5: Ecosystem engineering effect of *Corophium volutator* Pallas on the water column: daily and tidal time spans

Abstract

Previous experiments have demonstrated that *Corophium volutator* (Pallas) can substantially modify the biogeochemical environment of both the sediment and the overlying water column. However, many previous studies, including the ones in this thesis, examined these effects in sub-tidal systems. While *C. volutator* does inhabit sub-tidal soft sediment, it is most common and abundant in the intertidal sand- or mudflats. In the intertidal, its modification of the overlying water column is limited to the immersion period. This experiment was designed to determine whether significant changes to the overlying water column could be achieved within an average tidal immersion period and whether this effect changed with *C. volutator* residence time. Eighteen mesocosms were set up to contain homogenized mud (10 cm) from a *C. volutator* dominated habitat in Eden estuary and a seawater column (10 cm); 9 of these contained 1 g *C. volutator* (corresponding to an *in situ* biomass of 2000 ind m⁻²), the remaining 9 were control treatments. Mesocosms were sampled in a way that allowed both ongoing overlying water column changes to be measured every two days, and to allow measurement of a fresh seawater column after 3 and 6 hours on days 0, 2, 6 and 12, as well as enabling porewater and sediment measurements on those days. Overlying water was analysed for turbidity, suspended sediment, % light penetration through a 10 cm water column, deposited sediment, DIN and DIP, and sediment was sampled for water and organic content and porewater DIN and DIP. The experiment demonstrated that: (1) in the

absence of laminar flow, *C. volutator* can reduce light penetration to the sediment bed by about 50% within one tidal period; (2) that DIN fluxes within a tidal period are highly variable depending age of the sediment column but that generally there is more DIN release from *C. volutator* inhabited mud; (3) that *C. volutator* prevents the de-watering and compaction of sediment.

Chapter 5: Ecosystem engineering effect of *Corophium volutator* Pallas on the water column: daily and tidal time spans

5.1 Introduction

In the previous two experiments engineering effects of infaunal bioturbation were examined in subtidal mesocosms. However, both the MPB assemblages and the macrofauna used in those experiments came from intertidal areas of the estuary. The experimental systems were not 'flow-through' but rather water was cycled within units containing MPB and macrofauna for a week and this would have had 2 important ramifications. First of all, the effects that bioturbators had on the water column and sediment-water interface were able to accumulate over a week, and secondly, each experimental unit contained MPB as well as macrofauna, so the purely macrofaunally engineering effects on the water column would have been masked by MPB effects on the water column (Henriksen *et al* 1980; Andersen and Kristensen 1988; Sundbäck *et al* 2000). This would have been especially important for nutrient dynamics which differ radically not just in the presence and absence of MPB and macrofauna but also between day and night. In situ, ecosystem engineering effects on the overlying water column must be powerful enough to change the water column in a way that will have an effect on estuarine MPB within a single average tidal period (~ 6 hrs) because following that, modified estuarine waters will be diluted back to ambient coastal levels. Effectively, the clock is back to zero at the start of each tidal immersion.

Water column modifications potentially affecting MPB previously investigated were: changes in turbidity, increased DIN release from sediment, and increased phosphate release from sediment (see Chapter 3.1 and 4.1). The effect of benthic

fauna on sediment metabolism is best achieved using 'dark' systems to remove the effect of microalgae on O₂ and nutrient fluxes (Henriksen *et al* 1980; Andersen and Kristensen 1988; Ieno *et al* 2006). In Chapter 4, *Corophium volutator* Pallas was shown to have a greater engineering effect on MPB biomass than the other two species, so *C. volutator* was chosen as the model organism for this experiment. As light intensity has not previously been shown to change feeding and pumping behaviour of *C. volutator*, the resuspension of sediment was not assumed to be affected by the 'dark' ($< 4 \mu\text{mol photons m}^{-2} \text{s}^{-1}$) conditions required for nutrient flux measurements. Finally, another engineering effect of *C. volutator* which could not be properly examined in the previous experiments due to the presence of MPB biofilms is their effect on surface sediment compaction which is also examined here. Surface sediment compaction is important because it regulates light penetration into the sediment and therefore influences the thickness of the photic zone. Obviously, surface compaction does not need to act over a single tide. Hypotheses to be tested:

H₀5.1: Turbidity created by *C. volutator* in one average tidal period is not different from control groups and is a simple proportion (6/168 hrs) of what is generated over a week.

H₀5.2: DIN release from sediment modified by *C. volutator* in one average tidal period is not different from control groups and is a simple proportion (6/168 hrs) of what is released over a week.

H₀5.3: Phosphate release from sediment modified by *C. volutator* in one average tidal period is not different from what is released by control group and is a simple proportion (6/168 hrs) of what is released over a week.

H₀5.4: Surface sediment compaction is not modified by *C. volutator*.

5.2 Materials and Method

5.2.1 Set up

Surface sediment, containing *C. volutator* but without visible biofilm, was collected from the paper mill site of the Eden estuary (see Chapter 2.1) two days prior to starting the experiment. Sediment was sifted through 500 μm mesh into filtered seawater (1 μm) mixed with deionised water to a final salinity of 25 psu (*in situ* pore water salinity), homogenized, sampled, and distributed amongst 18 experimental tanks (clear Perspex tubes, i.d. 12.1 cm, 20.5 cm height) to a depth of 10 cm (~1150 ml). The tanks were randomly assigned to one of two treatments groups (*C. volutator* present or absent) and for examination on one of three final sampling days. *C. volutator* were collected from the sieves during sediment sifting and damp weighed into batches corresponding to the *in situ* macrofauna biomass per m^2 at the paper mill site scaled down to the area of the tanks (0.84 g or 200 – 230 individuals) and added to 9 tanks. Once all individuals had burrowed into the sediment the tanks were carefully filled with a 10 cm column of filtered seawater to (1150 ml). A 15 ml plastic centrifuge tube was inserted into the sediment in each tank to serve sediment trap; tubes protruded 1 cm above the sediment to prevent sediment from simply falling in from sediment surface. Tanks were kept at 10°C with the only illumination coming from overhead fluorescents ($< 4 \mu\text{mol m}^{-2} \text{s}^{-1}$) for 8 hours each day.

5.2.2 Sampling regime

The experiment lasted for 12 days following the addition of sediment and *C. volutator* to the tanks on 'day 0' (schematic presented in Figure 4.1). Prior to homogenizing and distributing the sediment amongst the tanks fluorescence measurements were made on the sediment surface using a Hansatech FMS2 and no chlorophyll-*a* signal was detected. Samples collected from sifted sediment were used to determine grain size and starting values of sediment water and or-

ganic content, pore water salinity, and nutrient levels. Filtered seawater was also sampled to determined starting turbidity, salinity, and nutrient levels. Overlying water in the tanks was then sampled at 3 and 6 hours to represent the half-way and end point of an average tidal immersion period.

Overlying water in the tanks was sampled for turbidity, suspended sediment and nutrients on the mornings of days 2, 4, 6, 8, 10, and 12. After very gentle stirring of the overlying water column a 50 ml sample was syringed from the middle of the column and salinity (Atago hand refractometer, ChemLab Scientific Products Ltd) and turbidity (in triplicate with a Eutech Instruments TN-100 turbidimeter) were measured before the sample was stored (in the dark at ~ 10°C) for suspended sediment quantification. In addition, a 12 ml sample for nutrient analysis was filtered through a 0.45 µm syringe filter (Nalgene) and stored at -80°C. In addition to the daily series of overlying water samples, to compare flux of nutrients and sediment from the sediment bed to the overlying water column within a tidal period 3 tanks from each treatment on days 2, 6, and 12 were drained, refilled with sampled filtered seawater and re-sampled after 3 and 6 hours; on days 2, 6, and 12 turbidity was also measured ½ hour after refilling the tank. Sediment traps were also collected on these days and replaced for the 6 hour tidal window.

Following sampling after the 6 hour 'tidal period', sediment traps from the 6 tanks (3 per treatment) were collected and pore water was extracted from the sediment with a Rhizon SMS 5 cm Soil Moisture Samplers (Rhizosphere Research Products) connected by microlance to a 9 ml untreated plastic vacuette (Becton-Dickson). The sampler was placed vertically so that it was sampling from the top 5 cm of sediment, which is the approximate burrowing depth of *C. volutator*.

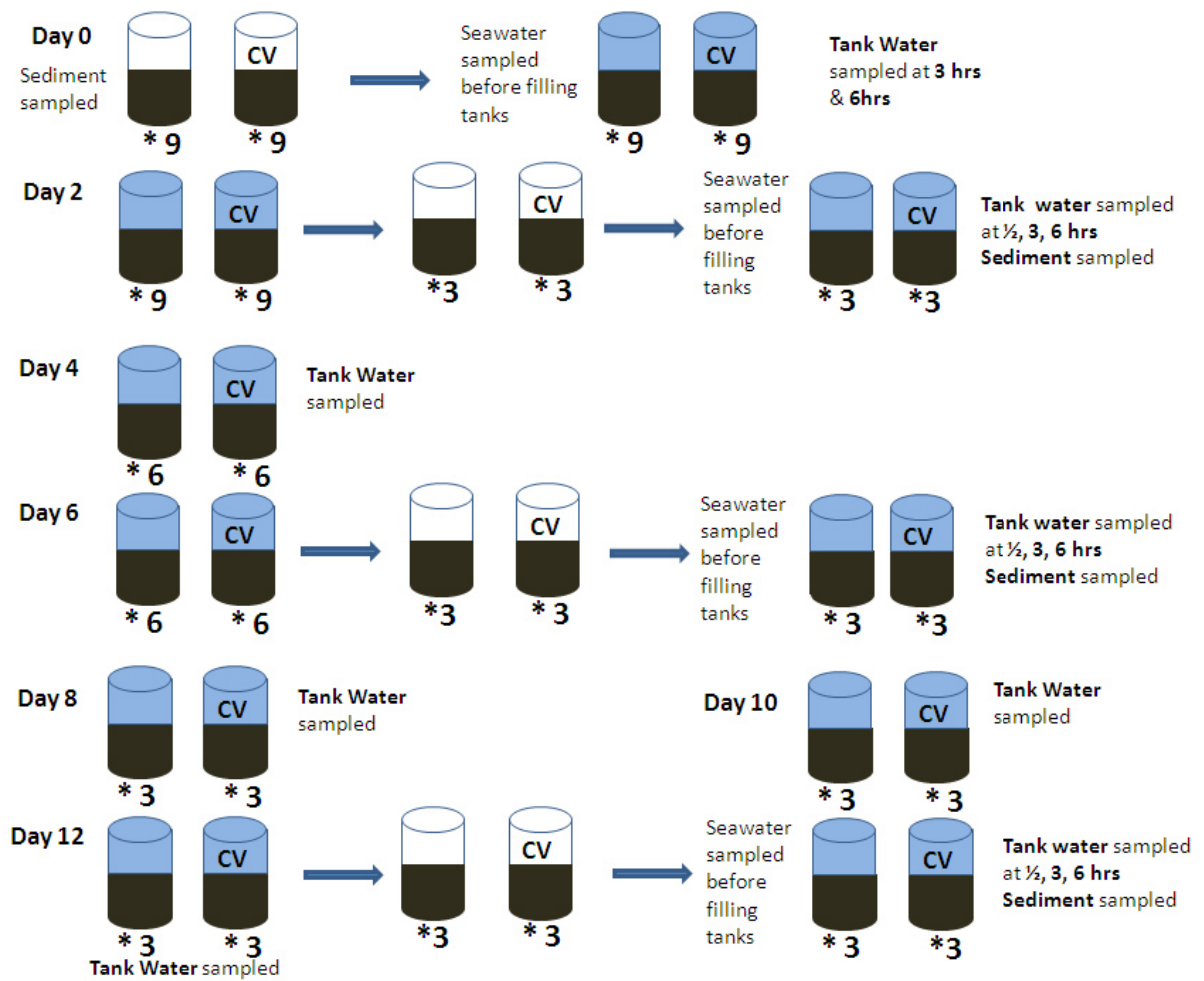


Figure 5.1: Schematic of Experiment

Salinity was measured for each sample and vacuettes were stored at -80°C prior to nutrient analysis. Finally, 3 sediment cores (i.d. 2 cm * 5 cm deep) were extracted to determine sediment water and organic content (2 frozen at -80°C) as well as total ammonium.

Total ammonium (dissolved in the pore water and adsorbed to the sediment particles) was extracted from the sediment following the method described by Henriksen and colleagues (1980). One of the sediment cores was expelled into a 50 ml centrifuge tube with 1M KCl at a 1:1 ratio to its own weight. Samples were shaken for an hour, centrifuged (1300 g, 10 minutes), and the supernatants were filtered through a $0.45\ \mu\text{m}$ disposable Nalgene filters into 9 ml untreated plastic

vacuettes, and, following salinity measurement, were stored at -80°C prior to $\text{NH}_4^+\text{-N}$ analysis.

5.2.3 Sample analysis

5.2.3.1 Nutrient analysis

Nutrient analysis was carried out as detailed in General Methods (Chapter 2.3). Bound $\text{NH}_4^+\text{-N}$ samples were run separately from as they required separate calibration solutions.

5.2.3.2 Sediment composition

The water and organic content of the top 3 cm of sediment were determined from duplicate cores from each tank and triplicate cores from the original sifted sediment in triplicate as detailed in General Methods (Chapter 2.3). Grain size of sifted sediment, and deposited sediment (from the sediment traps) were measured by a Coulter LS230 Laser Diffraction Particle Size Analyzer (Beckman).

5.2.3.3 Light attenuation through a 10 cm water column

Each of the 50 ml samples of the overlying water in the tanks and the filtered seawater samples were decanted in turn into a narrow glass beaker to create a 10 cm water column. The beaker was placed on top of a light sensor (Macam Quantum Photometer Q101-4, settings 400 – 700 nm at the 0 - 300 $\mu\text{mol m}^{-2} \text{s}^{-1}$ scale, Macam Photometrics Ltd) underneath a 175 $\mu\text{mol m}^{-2} \text{s}^{-1}$ light source and penetrating light levels recorded for later correlation against turbidity and suspended sediment values of each sample.

5.2.3.4 Suspended sediment

Overlying water samples from days 0, 2, 6 & 12 as well as seawater samples from those days were pumped through pre-combusted and pre-weighed Whatman GF/F glass fibre filters (0.7 μm mesh, 47 mm Φ) dried for 48 hours,

reweighed, and mean seawater weight subtracted off (to determine salt content) to determine total suspended sediment. Following that they were combusted in muffle furnace at 450°C to determine proportion of organic content in the sediment. Water samples from days 4, 8 & 10 were washed, dried and weighed for suspended sediment quantification

5.2.3.5 Deposition

Contents of the sediment traps were recorded by volume and by dry weight (washed) to compare to suspended sediment quantities. Following drying and weighing, samples were pooled to get a sample large enough to measure the grain size abundance in the Coulter Counter for comparison to the overall experimental sediment and suspended sediment. In still water a cylindrical sediment trap with should give a representative sample of the vertical sedimentation rate in the surrounding water (Hargrave & Burns 1979).

5.3 Results

Means and standard errors of all measurements within treatment group and sampling occasion (daily and hourly) are presented in Table 4.2.

5.3.1 Sediment

5.3.1.1 Sediment grain size, water and organic content

Grain size of the sifted sediment was all < 63 µm in diameter with a peak abundance of 20 µm in diameter particles. Starting sediment had a water content of 54 ± 0.7 % and remained thereabouts in the *C. volutator* treatments, ending at a final value of 52 ± 1.3 % on day 12 (Figure 5.2). However, in the control treatment water content of the sediment declined over the course of the experiment arriving at a final value of 46.7 ± 1.3 % by day 12.

Table 5.1: Treatment means (± 1 st. err) at each sampling occasion

Day	Start	0		2		4		6		8		10		12	
Treatment		con	Cvol	con	Cvol	con	Cvol	con	Cvol	con	Cvol	con	Cvol	con	Cvol
Sediment properties															
% Water		53.7 \pm 0.7			48.4 \pm 0.7	53.6 \pm 2.9			47.7 \pm 0.3	54.2 \pm 2.3				46.7 \pm 0.4	51.6 \pm 1.3
% Org		7.1 \pm 0.1			6.7 \pm 0.3	6.7 \pm 0.04			6.9 \pm 0.2	6.8 \pm 0.1				7.1 \pm 0.5	6.9 \pm 0.05
Deposition															
00:00	0. 9 \pm 0.9			12 \pm 3	511 \pm 222			71 \pm 15	440 \pm 69					263 \pm 124	885 \pm 630
06:00				86 \pm 57	44 \pm 8.5			23 \pm 6.9	55 \pm 24					24 \pm 6.5	35 \pm 15
NH ₄ ⁺ 06:00	169 \pm 11			260 \pm 12	253 \pm 15			201 \pm 34	111 \pm 13					283 \pm 5	171 \pm 6
tNH ₄ ⁺ 06:00	118 \pm 6			103 \pm 5	91 \pm 7			180 \pm 13	120 \pm 10					173 \pm 13	44 \pm 12
NO _x ⁻ 06:00	0.76 \pm 0.05			3.4 \pm 2.4	11.6 \pm 5.5			5.8 \pm 1.7	9.6 \pm 1.0					5.5 \pm 0.5	14.3 \pm 1.3
PO ₄ ³⁺ 06:00	4.9 \pm 0.6			3.8 \pm 0.8	2.8 \pm 0.3			8.0 \pm 4	1.4 \pm 0.1					11.4 \pm 0.5	10.7 \pm 7.6
Overlying water properties															
NH ₄ ⁺ 00:00	0.0 \pm 0.0			4.5 \pm 0.6	29.4 \pm 3.7	14.3 \pm 14	30.9 \pm 6.7	0.0 \pm 0.0	11.8 \pm 8.3	1.4 \pm 1.4	14.6 \pm 8.3	4.8 \pm 4.8	6.9 \pm 6.9	5.6 \pm 3.0	1.6 \pm 1.6
03:00		2.0 \pm 0.6	11.0 \pm 1.6	0.0 \pm 0.0	1.2 \pm 0.3			0.3 \pm 0.3	0.0 \pm 0.0					0.0 \pm 0.0	0.0 \pm 0.0
06:00		4.1 \pm 0.9	17.3 \pm 2.9	0.0 \pm 0.0	3.9 \pm 0.6			0.0 \pm 0.0	0.0 \pm 0.0					0.0 \pm 0.0	0.9 \pm 0.9
NO _x ⁻ 00:00	16.5 \pm 0.2			19.8 \pm 0.2	23.3 \pm 1.3	23.4 \pm 0.6	26.8 \pm 8.2	8.6 \pm 4.4	37.5 \pm 2.2	15.3 \pm 1.9	37.1 \pm 1.9	27.7 \pm 7.4	26.0 \pm 6.8	35.3 \pm 4.3	27.8 \pm 4.8
03:00		16.2 \pm 0.2	15.7 \pm 0.02	16.1 \pm 0.04	15.8 \pm 0.8			15.8 \pm 0.3	17.4 \pm 0.2					16.6 \pm 0.1	17.6 \pm 0.3
06:00		17.1 \pm 0.4	14.2 \pm 1.1	16.7 \pm 0.02	16.9 \pm 0.2			15.3 \pm 0.5	37.1 \pm 0.3					16.4 \pm 0.1	18.0 \pm 0.2
PO ₄ ³⁺ 00:00	3.9 \pm 0.04			2.7 \pm 0.7	1.3 \pm 0.2	1.5 \pm 0.3	1.2 \pm 0.1	0.7 \pm 0.1	1.4 \pm 0.2	0.9 \pm 0.05	1.5 \pm 0.03	1.4 \pm 0.2	2.3 \pm 0.9	1.9 \pm 0.2	1.6 \pm 0.05
03:00		4.0 \pm 0.7	3.1 \pm 0.1	3.7 \pm 0.04	3.1 \pm 0.05			3.3 \pm 0.01	3.0 \pm 0.1					3.7 \pm 0.02	3.3 \pm 0.04
06:00		3.4 \pm 0.04	2.7 \pm 0.04	3.3 \pm 0.17	2.5 \pm 0.06			3.1 \pm 0.1	2.5 \pm 0.1					3.6 \pm 0.02	3.0 \pm 0.1

Table 5.2 cont: Treatment means (± 1 st. err) at each sampling occasion

Day	Start	0		2		4		6		8		10		12	
Treatment		con	<i>Cvol</i>	con	<i>Cvol</i>	con	<i>Cvol</i>	con	<i>Cvol</i>	con	<i>Cvol</i>	con	<i>Cvol</i>	con	<i>Cvol</i>
Suspended sediment															
00:00	0.0 \pm 0.0			0.0 \pm 0.0	16 \pm 4.7	139 \pm 11	165 \pm 12	0.0 \pm 0.0	17 \pm 3.8	90 \pm 12	146 \pm 4	95 \pm 12	155 \pm 6.5	0.0 \pm 0.0	13 \pm 2.4
03:00		0.0 \pm 0.00	3.2 \pm 0.02	0.0 \pm 0.0	2.6 \pm 0.8			0.0 \pm 0.0	8.6 \pm 1.4					0.0 \pm 0.0	6.3 \pm 1.3
06:00		0.0 \pm 0.00	4.1 \pm 0.02	0.3 \pm 0.03	6.1 \pm 3.1			1.5 \pm 0.8	13 \pm 3.6					2.7 \pm 2.7	5.9 \pm 4.0
Turbidity															
00:00	0.02 \pm 0.01			4.5 \pm 1.6	277 \pm 19	4.2 \pm 1.7	149 \pm 23	4.2 \pm 7.2	221 \pm 18	2.1 \pm 0.5	181 \pm 46	1.5 \pm 0.6	164 \pm 16	3.4 \pm 1.4	227 \pm 8.4
00:30				19 \pm 4.3	53 \pm 15			25 \pm 4.7	72 \pm 19					6.5 \pm 2.7	65 \pm 2.8
03:00		7.9 \pm 2.6	87.1 \pm 13.4	11 \pm 3.2	89 \pm 14			13 \pm 1.2	121 \pm 22					4.6 \pm 2.1	120 \pm 10
06:00		6.8 \pm 1.8	110 \pm 27	11 \pm 1.0	124 \pm 16			8.6 \pm 0.7	151 \pm 29					4.1 \pm 1.5	139 \pm 15
% PAR															
00:00	100 \pm 0.2			86 \pm 3.1	23 \pm 0.9	95 \pm 0.6	43 \pm 4.3	93 \pm 0.1	50 \pm 21	95 \pm 0.4	39 \pm 9.1	96 \pm 1.3	39 \pm 2.7	73 \pm 23	75 \pm 24
03:00		93 \pm 2.3	58 \pm 5.3	90 \pm 1.1	53 \pm 4.4			89 \pm 1.0	43 \pm 4.3					96 \pm 1.1	46 \pm 3.1
06:00		92 \pm 1.0	49 \pm 8.1	85 \pm 1.5	43 \pm 2.8			92 \pm 0.6	38 \pm 6.3					95 \pm 1.1	41 \pm 3.2

Organic content of the original sediment was 7.1 ± 0.1 % and remained thereabouts for the duration of the experiment in both treatments (final values 7.1 ± 0.1 % and 6.9 ± 0.1 %, respectively).

5.3.1.2 Ammonium

The NH_4^+ content of the pore water from the sifted sediment (salinity 25 psu) absorbed by the sediment sippers was 169 ± 0.1 $\mu\text{mol L}^{-1}$ but the total NH_4^+ content of the sediment, adsorbed and dissolved, which ought to have been higher, was only 118 ± 6 $\mu\text{mol L}^{-1}$. Porewater salinity by day 2 had increased to 29 and 31 psu in the control and *C. volutator* treatment groups and dissolved NH_4^+ concentrations had increased to 260 ± 12 and 253 ± 15 $\mu\text{mol L}^{-1}$, respectively (Figure 5.3 top left). Thereafter, the pore water salinities continued to rise until, by day 12, they were approximately equal to the overlying seawater levels (24 vs. 35 psu) and whereas NH_4^+ concentrations increased to 283 ± 5 $\mu\text{mol L}^{-1}$ in the control treatments, they fell to 171 ± 6 $\mu\text{mol L}^{-1}$ in the *C. volutator* treatments.

5.3.1.3 Combined nitrite and nitrate

The original NO_x^- content of the porewater of the sifted sediment was 0.76 ± 0.1 $\mu\text{mol L}^{-1}$ but had increased in both treatments by day 2 (Figure 5.3 centre left). Control treatments rose from 3.4 ± 2.4 on day 2 to 5.5 ± 0.5 $\mu\text{mol L}^{-1}$ by day 12 but in the *C. volutator* treatments they rose from 11.6 ± 5.5 on day 2 to 14.3 ± 1.3 $\mu\text{mol L}^{-1}$ by day 12; i.e. the activity of *C. volutator* increased pore water NO_x^- levels approximately 3 fold.

5.3.1.4 Phosphates

Porewater PO_4^{3+} content of the sifted sediment was 4.9 ± 0.6 $\mu\text{mol L}^{-1}$ (Figure 5.3 bottom left). In the control treatments pore water PO_4^{3+} increased over the 12 days to

final value of $10.7 \pm 7.6 \mu\text{mol L}^{-1}$ on day 12. In the *C. volutator* treatments pore water decreased initially, to $1.41 \pm 7.6 \mu\text{mol L}^{-1}$, but ultimately reached 11.4 ± 0.05 by day 12.

5.3.2 Water column

5.3.2.1 Turbidity

Following addition of *C. volutator* to tanks, turbidity increased to 87 ± 13 ntu within 3 hours and 110 ± 27 ntu within the 6 hour tidal window, whereas turbidity in the control tanks had hardly changed (7.9 ± 2.7 and 6.8 ± 1.8 at 3 and 6 hours). By day 2 turbidities in the *C. volutator* tanks reached 277 ± 19 ntu (Figure 5.2, centre right) whereas turbidity in the control groups had declined to 4.5 ± 1.6 ntu. Turbidity in the *C. volutator* tanks declined after day 2 and fluctuated around 200 ntu until day 12 whereas control treatments fluctuated around 1.7 ntu. Turbidities reached within the tidal windows in the *C. volutator* treatments on days 2, 6 and 12 were approximately 19, 33, and 29 % of means on those days within $\frac{1}{2}$ hour, 32, 55, and 53 % within 3 hours, and 45, 68, and 61 % within 6 hours (Figure 5.5A). Increases in water column turbidities approximated a growth curve where > 80 % of full turbidity is achieved within the first half of the tide.

5.3.2.2 Suspended and deposited sediment

Suspended sediment in the water column, estimated from 50 ml samples, fluctuated substantially between 0 and 160 g m^{-2} in the *C. volutator* treatments and 0 and 152 g m^{-2} in the control treatments (Figure 5.2, top right). The fluctuations over days were consistent between control and *C. volutator* treatments but variations in the control treatments were so large that the difference in suspended sediment between the two treatments was not resolved. Mean organic content of the suspended sediment

in the *C. volutator* treatment (3.4 ± 0.1 %) was significantly higher ($t = 5.99$, $DF = 53$, $p = 1.9 \times 10^{-7}$) than in the control treatments (2.7 ± 0.05 %).

Sediment deposition over 2, 6, and 12 days was higher in the *C. volutator* treatments than in the control treatments (Figure 5.2, top left). Trapped sediment over the tidal periods on days 2, 6, and 12 was too small to detect differences between the two treatments. Organic content was not estimated from these samples as they were used to compare grain size suspended sediment to total sediment. Grain size did not differ from the grain size of the total sediment ($100\% < 63 \mu\text{m}$, with peak abundance of $20 \mu\text{m}$).

5.3.2.3 Light penetration through water column

Light penetration, measured as a % of light penetration through a 10 cm column of filtered seawater, was substantially and consistently greater in *C. volutator* than control treatments (Figure 5.2, bottom right). Within the tidal windows, light penetration in the control treatments never dropped below 80 %, whereas in the *C. volutator* treatments light penetrations were < 60 % by 3 hours and < 50 % by 6 hours. In the *C. volutator* treatment, loss of light at the sediment bed expressed as a proportion of the mean on the day reached by on days 2, 6, and 12 was 53 , 43, and 46 % within 3 hours, and 43, 38, and 41 % within 6 hours (Figure 5.4, row 4). Light penetration (%) declined exponentially with increasing turbidity (Figure 5.5B: $y = 95e^{-0.005x_i} + \epsilon_i$).

5.3.2.4 Ammonium

The filtered seawater with which the tanks were filled contained no NH_4^+ so all of the NH_4^+ released over the 12 days of the experiment came from the sediment. The difference in NH_4^+ released from sediment between the two treatments was greatest on day 2 where measurements in the overlying water column were approximately 6 fold higher in the *C. volutator* treatments than in the control treatments (Figure 5.3

top right). From then on the difference between the NH_4^+ released shrank but remained above $10 \mu\text{mol L}^{-1}$ (or 1 mmol m^{-2}) until day 10 where there was little difference between the two. By day 12 NH_4^+ levels in the overlying water column of the control treatments were 3x higher than in the *C. volutator* treatments.

NH_4^+ fluxes over the 6 hour tidal window were only noticeably different between the two treatments on days 0 and 2 (Figure 5.4 top row). On day 0 *C. volutator* treatments released 4 – 5 fold more NH_4^+ than the control treatments: NH_4^+ released from *C. volutator* treatments were $17.3 \mu\text{mol L}^{-1}$ (corresponding to as $288 \mu\text{mol hr}^{-1} \text{ m}^{-2}$). But by day 2, while total NH_4^+ released from *C. volutator* tanks was still $\sim 4 \times$ higher than that released by the control treatments, it was only $3.9 \mu\text{mol L}^{-1}$ (or $65 \mu\text{mol hr}^{-1} \text{ m}^{-2}$). By days 6 and 12 NH_4^+ released from the sediment over a 6 hour tidal window was too low to detect.

5.3.2.5 Combined nitrite + nitrate

NO_x^- levels in the filtered seawater used to fill the tanks was $16.5 \pm 0.8 \mu\text{mol L}^{-1}$ and these levels increased in both treatments over the following 4 days, more so in the *C. volutator* treatments than the control treatments, (Figure 5.3 centre right). Following day 4, NO_x^- levels in the overlying water of the *C. volutator* treatments continued to increase to a maximum of $\sim 37 \mu\text{mol L}^{-1}$ over days 6 and 8 and declined slightly thereafter. The control treatments on the other hand declined sharply on day 4 but then steadily rose thereafter reaching a maximum level of $28 \pm 5 \mu\text{mol L}^{-1}$ on day 12.

NO_x^- fluxes over the 6 hour tidal window varied over days and between treatment groups (Figure 5.4 2nd row). While fluxes in *C. volutator* started out negative and then became slightly positive over days 2 and 6, control treatments began with positive fluxes on the first 2 days and then became negative on days 6 and 12. How-

ever, both treatments showed maximum, and negative, fluxes by day 12: in *C. volutator* treatments the change in water column NO_x^- after 6 hours was $-6.1 \pm 0.2 \mu\text{mol L}^{-1}$ (corresponding to an hourly flux of $-10.1 \mu\text{mol hr}^{-1} \text{m}^{-2}$) and in control treatments it was slightly higher at $-7.7 \pm 0.1 \mu\text{mol L}^{-1}$ (corresponding to an hourly flux of $-12.8 \mu\text{mol hr}^{-1} \text{m}^{-2}$).

5.3.2.6 Phosphate

PO_4^{3+} in the filtered seawater used to fill the tanks ($3.9 \pm 0.2 \mu\text{mol L}^{-1}$) was slightly lower than in the pore water of the sifted sediment ($4.9 \pm 0.6 \mu\text{mol L}^{-1}$). Nevertheless, PO_4^{3+} fluxes in the first 6 days were negative (Figure 5.4, row 3) and in the control treatments PO_4^{3+} levels in the overlying water declined over the first 6 days (Figure 5.3, row 3). Negative PO_4^{3+} fluxes in the *C. volutator* treatments on days 0, 2, and 6 (-21.7 , -15 , $-13.7 \mu\text{mol hr}^{-1} \text{m}^{-2}$) were higher than in the control treatments (-8.5 , -10.5 , $-12.5 \mu\text{mol hr}^{-1} \text{m}^{-2}$). However, between days 6 and 12 PO_4^{3+} increased in the water column in both treatments, so that by day 12 levels in the control and *C. volutator* treatments were similar (1.9 ± 0.2 and $1.6 \pm 0.05 \mu\text{mol L}^{-1}$).

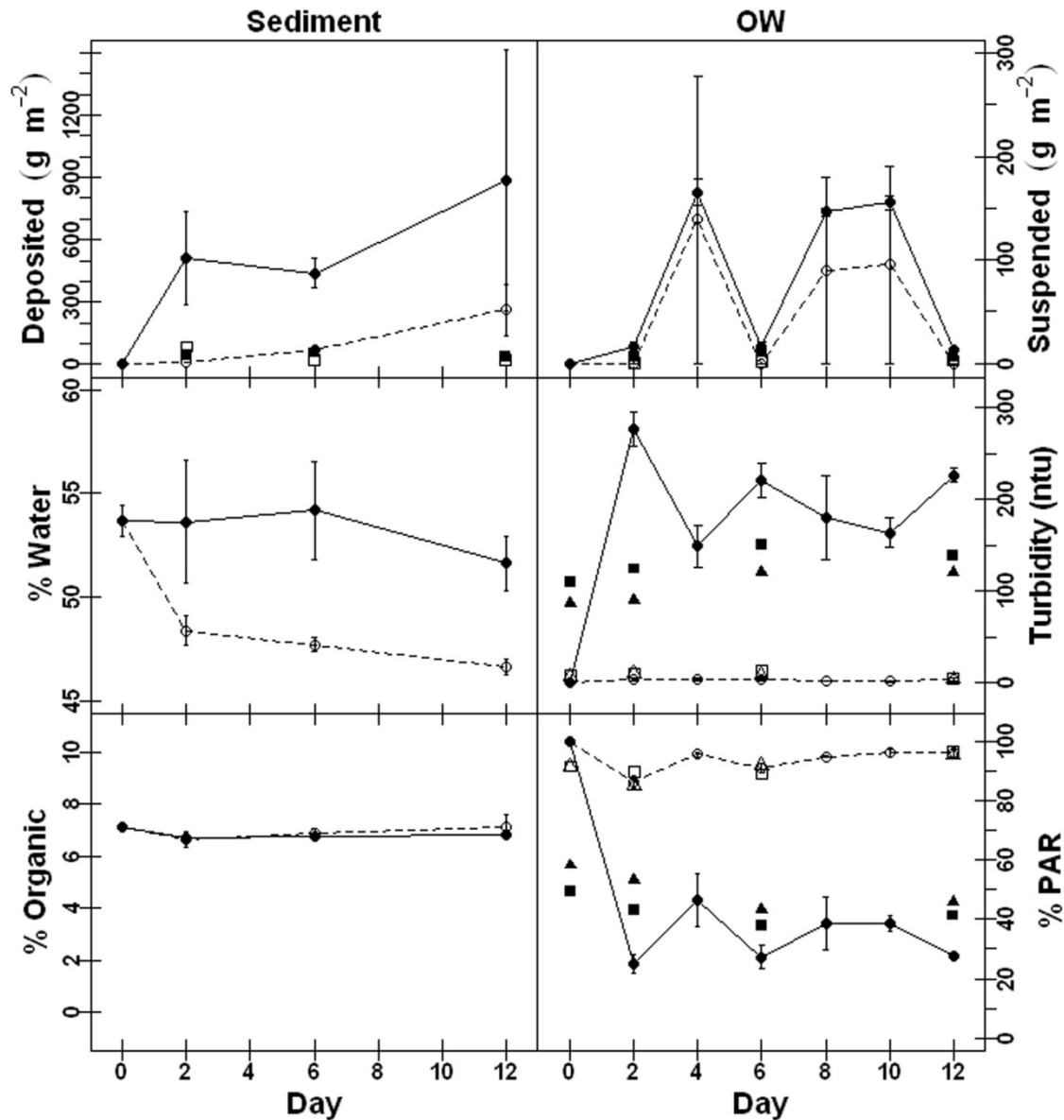


Figure 5.2: Sediment (left) and overlying water (right) characteristics in between treatments over the 12 days of the experiment. Open symbols represent control treatments and filled symbols represent *Corophium* treatments. Circles represent levels at each day and triangles and squares represent levels at 3 and 6 hours, respectively, following refilling with filtered seawater.

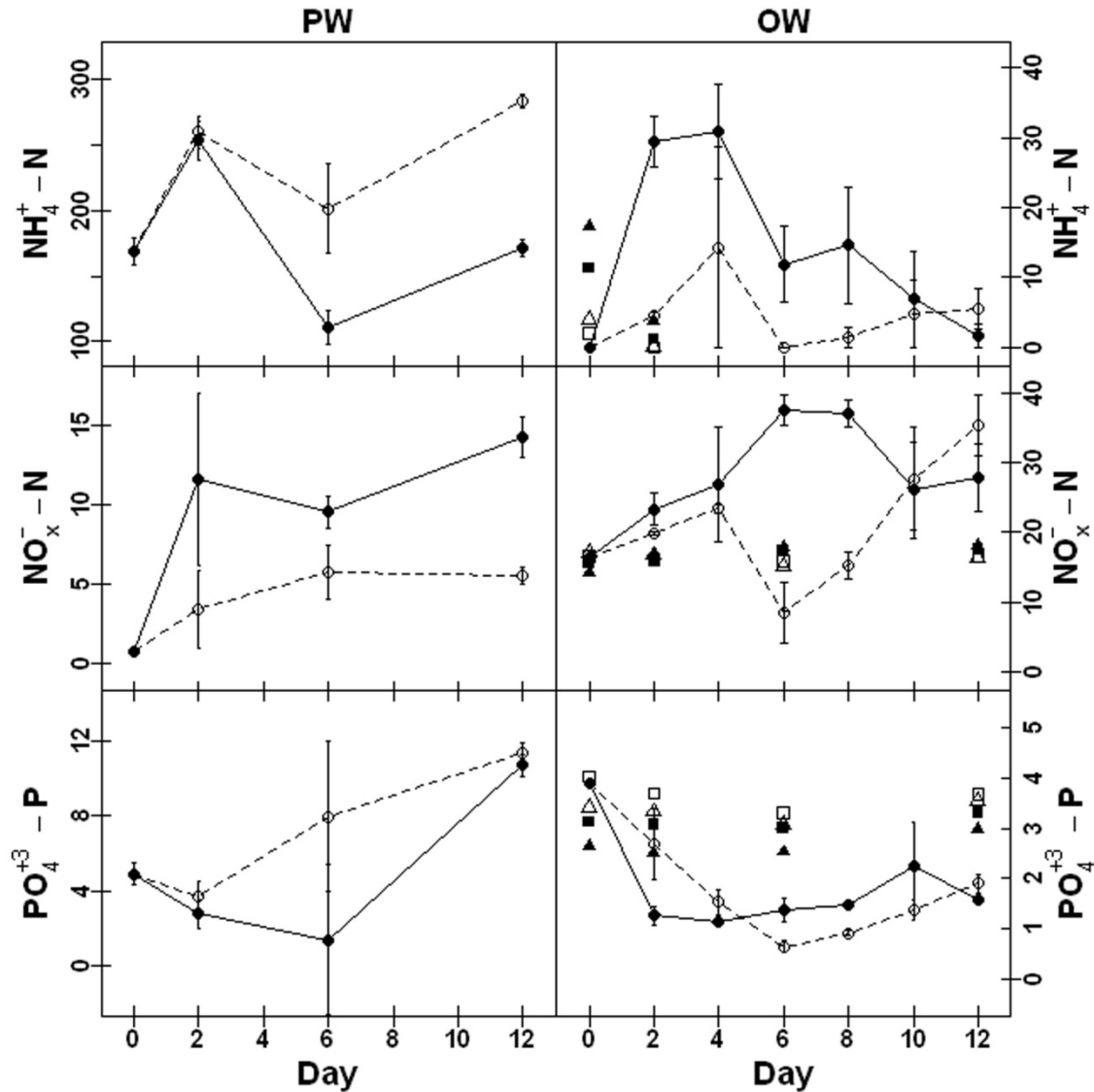


Figure 5.3: Nutrient levels ($\mu\text{mol L}^{-1}$) in the porewater (PW, top 5 mm of sediment) and overlying water column (OW). Open symbols represent control treatments and filled symbols represent *Corophium* treatments. Circles represent levels at each day and triangles and squares represent levels at 3 and 6 hours, respectively, following refilling with filtered seawater. Nutrient levels in filtered seawater did not change over the course of the experiment.

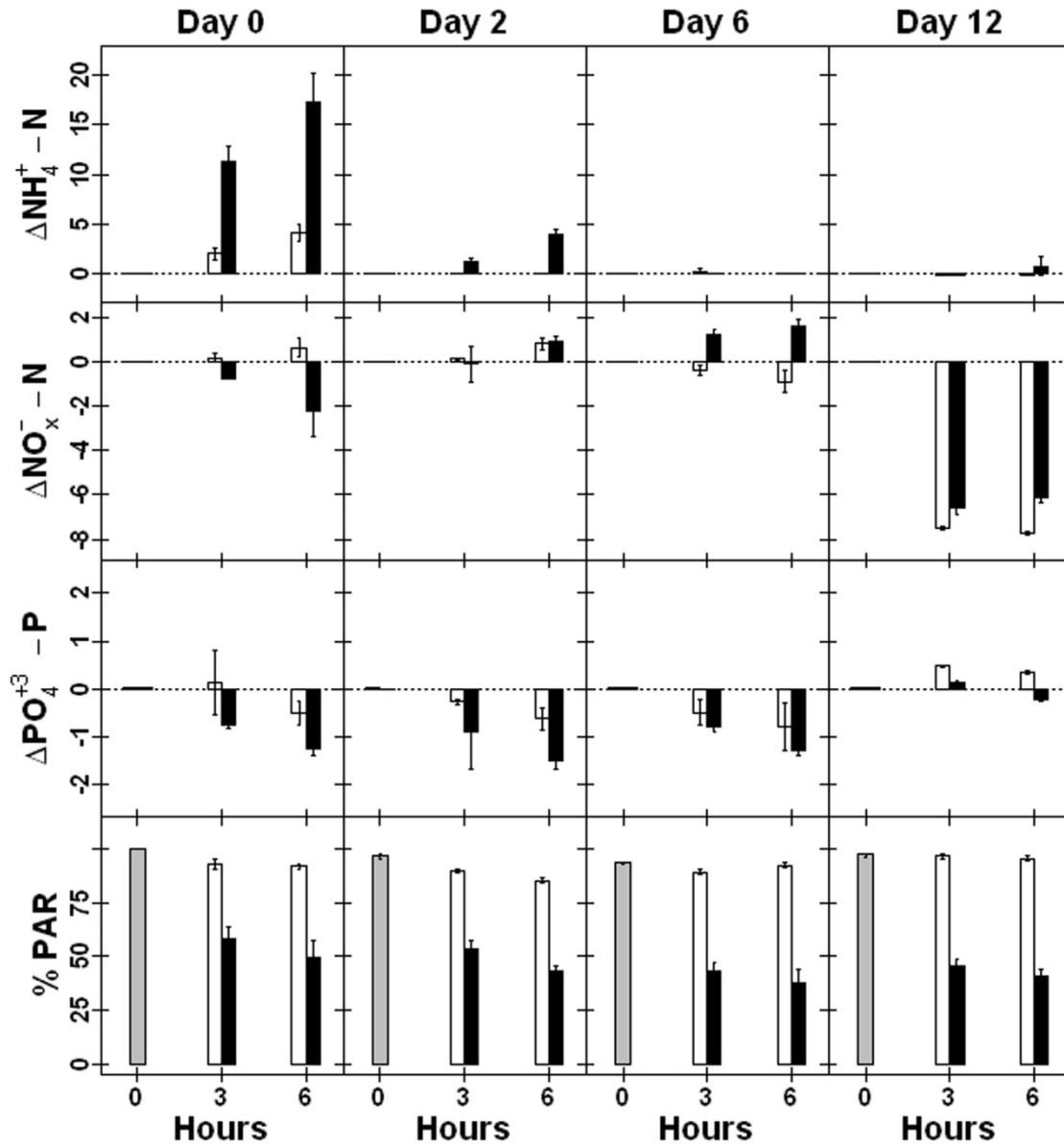


Figure 5.4: Nutrient fluxes ($\mu\text{mol L}^{-1}$) and on days 0, 2, 6, and 12. Dotted lines represent nutrient levels in the filtered seawater used to refill the tanks which did not vary much over the 12 days of the experiment. Fluxes out of the sediment into the overlying water are represented as positive values. Open bars represent control treatments and solid bars represent Corophium treatments. The amount of light penetration to the sediment bed is represented as a percent of light reaching the sediment through a 10 cm column of filtered seawater (% PAR). Grey bars represent the light penetration through the seawater used to refill the tanks on each day and did not vary substantially over the course of the experiment.

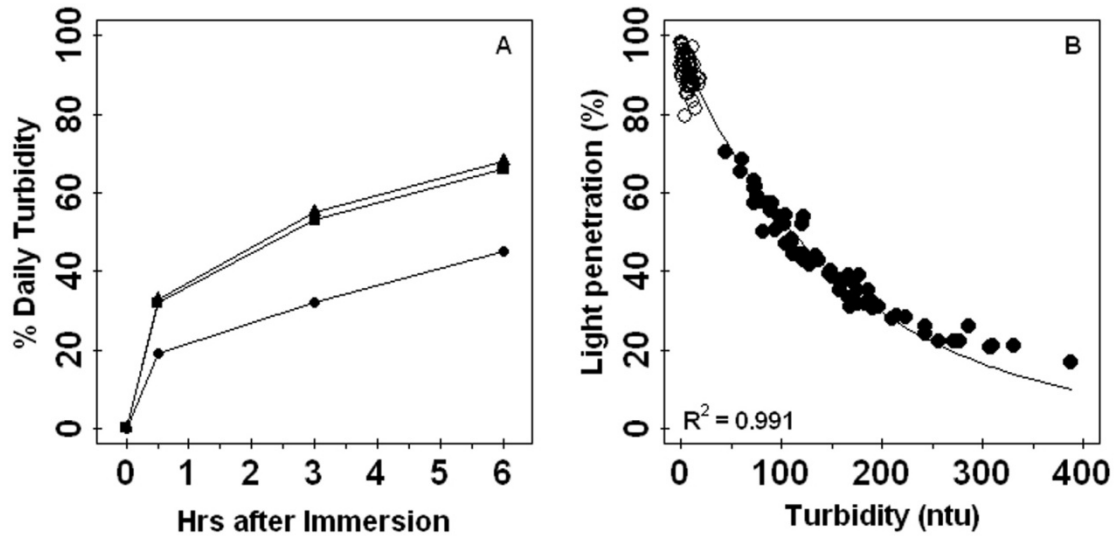


Figure 5.5: (A) Turbidity in *Corophium* treatments on days 2 (circles), 6 (triangles), 12 (squares) expressed as a percentage of total turbidity achieved by those days. (B) Light penetration (as a percent of light penetrating a 10 cm column of filtered seawater) against the turbidity of each sample. Light penetration decreased exponentially ($y_i = 95e^{-0.005x_i} + \varepsilon_i$) with increasing turbidity. Grain size of suspended sediment was 100% < 63 μm (mode = 20 μm). Open symbols represent control treatments and closed symbols represent *Corophium* treatments.

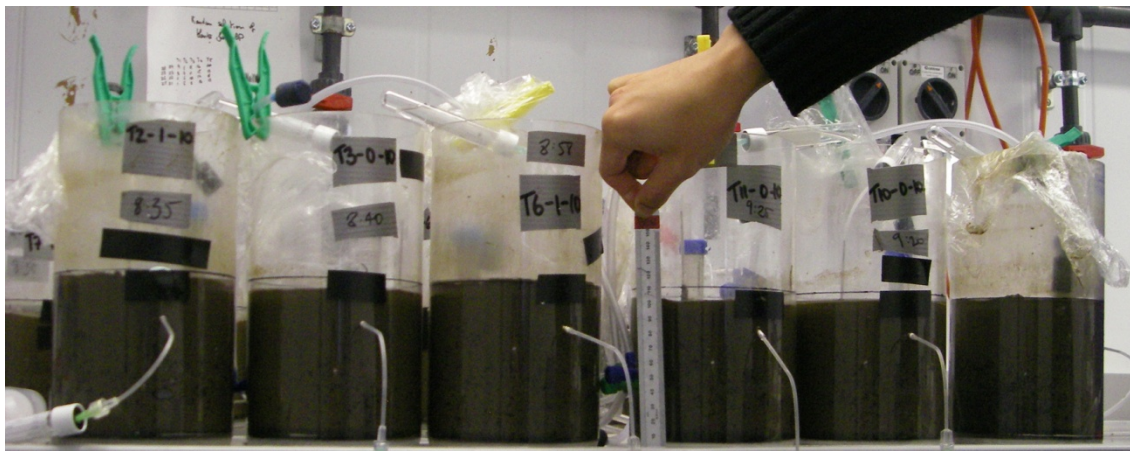


Figure 5.6: Compaction over 12 days in the control treatments (2nd, 4th and 5th tank from left) was approximately 5 mm whereas hardly any compaction was visible in *Corophium* treatments (1st, 3rd, 6th tank from left).

5.4 Discussion

5.4.1 Sediment grain size, water & organic content

Final sediment columns of the control treatments were compacted by approximately 5 mm by day 12 of the experiment whereas there was no substantial compaction in the sediment of the *C. volutator* treatments (Figure 5.6). The lack of compaction in the sediment of *C. volutator* treatments is reflected in the water content (%) of the top 5 cm of sediment (Figure 5.2, centre left) which was slightly () but significantly higher than in the control treatments (Treatment: $DF = 1/12$, $F = 16.7$, $p = 0.001$) from day 2 onward although they did not vary significantly between days 2, 6, and 12 (Day: $DF = 2/12$, $F = 6.6$, $p = 0.472$; no significant interaction). The evidence suggests that *C. volutator* prevents sediment compaction by maintaining high water content in the top 5 cm of sediment.

Organic content (%) of the top 5 cm of sediment did not vary over the course of the experiment or between treatment groups (Figure 5.2, bottom left). Mean organic content of suspended sediment ($\sim 3 \pm 0.1$ %) was much lower than in the sediment bed ($\sim 7 \pm 0.1$ %) in both treatments. However, this could simply have arisen from the very small suspended sediment quantities (< 1 g) for combustion increasing the chances of measurement error (HIMOM 2005). Grain size distribution of suspended sediment did not differ from grain size distribution of sifted sediment.

5.4.2 Sediment resuspension, turbidity, and light attenuation

Turbidities measured over the 12 days of this experiment were much greater than those measured in the previous two experiments (Figures 3.8 & 4.6) which suggests that perhaps the absence of biofilm increased resuspension of sediment. However, when raw maximum turbidities from each experiment were adjusted to biomass specific turbidity standardized to 1 L shows the maximum turbidity in this experi-

ment was 383 ntu g⁻¹ L⁻¹ compared to 87 and 387 ntu g⁻¹ L⁻¹ in the previous two experiments (grain size over the 3 experiments were more or less the same). So, in fact, the turbidities in the present and previous experiments were very similar although one contained biofilm and the other did not. Daily turbidities in the *C. volutator* treatments stabilized by day 4 and fluctuated around 200 ntu (230 ntu g⁻¹ L⁻¹) until the end of the experiment whereas in the control treatments they fluctuated around 3.7 ntu (4.25 ntu L⁻¹). Analysis of variance between turbidity in independent tanks from each treatment on days 6 and 12 results showed significant treatment effects (Tr: DF = 1/8, F = 64.4, p = 4.3*10⁻⁵) but no significant differences between days (Day: DF = 1/8, F = 0.73, p = 0.418; no significant interaction). Following 2 days of 'settling in' by *C. volutator*, the surface sediment was so disrupted that within ½ hour of refilling the tanks with clean seawater 33% of full daily turbidity levels (~200 ntu) were reached, ~50 % were reached halfway through the tidal immersion, and 60 % reached over the full immersion. In an actual tidal system turbidity would not accumulate statically over the same location but the laminar flow carrying sediment away would also increase sediment erosion and would therefore also increase turbidity. Turbidities in control treatment were slightly higher than daily turbidity levels as some resuspension occurred during refilling, however turbidity due to resuspension did not exceed 15 ntu.

Turbidity is a measure of light penetration through a water column but turbidity units do not give an intuitive sense of the loss of light at the sediment bed during immersion. According to the Lambert Law of Absorption light decreases exponentially with water column depth and according to the results here (Figure 5.5B) it also decreases exponentially with turbidity units (over a constant depth and grain size). From day 2 onward, by halfway through an average immersion period, mean light penetration through a 10 cm seawater column dropped by almost 50 % and

slightly more than that over the full immersion period whereas light penetration in the control tanks did not decrease beyond 90% during the tidal period.

The poor resolution in the suspended sediment between the two treatment groups and the large errors in the control groups (Figure 5.2, top right) was probably due to the measurement method. Instead of washing the salt out of the water samples prior to pumping them through the glass fibre filters and calculating sediment content by weight difference, the filtered seawater samples were from each day were also pumped and the weight of salt subtracted from the weight of the samples. A clearer signal of differences in suspended sediment between treatment groups came from the sediment traps (Figure 5.2, top left). Sediment traps with aspect ratios of at least 12:1 in relatively still water collect reasonably representative samples of sediment in the water column (Hargrave & Burns 1979). Analysis of variance determined that sediment trapped over days 2, 6, 12 in *C. volutator* treatments (mean = $570 \pm 188 \text{ g m}^{-2}$) was significantly higher (Treatment: DF = 1/12, F = 4.7, p = 0.049) than sediment trapped in control treatments (mean = $115 \pm 52 \text{ g m}^{-2}$). Trapped sediment was washed prior to drying and weighing and the removal of salt (rather than quantification) clearly improved quantification of sediment. However, even with salt removal, the amount of sediment deposited in a 1 cm^2 trap is very small (actual quantities trapped ranged from 1 to 374 mg) and several points indicate this is a likely source of measurement error. First, there was no significant difference in trapped sediment after 2, 6 and 12 days of *C. volutator* occupancy (Day: DF= 2/12, F = 0.85, p = 0.451). While this is a reasonable scenario for turbidity and suspended sediment in the water column (assuming a consistent pumping rate by *C. volutator*), trapped sediment would have accumulated over this time. In addition, the standard error on day 12 weights ($885 \pm 630 \text{ g m}^{-2}$) is so large that the mean value is virtually meaningless.

In conclusion, unless very large samples or numbers of replicates are collected/trapped, which is not practical in mesocosm experiments, turbidity measurements are a quicker, less invasive, more accurate and informative variable of sediment loading than measuring sediment weight per volume water. *C. volutator* assemblages are capable creating substantial water column turbidity within the first half of the tide and once settled into the sediment (and assuming no large population changes) the turbidity they generate is quite consistent over time.

5.4.3 Dissolved inorganic nitrogen dynamics

DIN levels in seawater, in the form of NO_x^- , in St Andrews Bay were noticeably higher ($16.5 \pm 0.2 \mu\text{mol L}^{-1}$) in November when this experiment was carried out, than in the summers ($6.6 \pm 6.4 \mu\text{mol L}^{-1}$), when the previous two experiments were carried out. A similar pattern in ambient levels of NO_x^- , i.e. much higher in winter than spring and summer, was also found at a silty coastal site in NE Kattegat (Sundbäck *et al* 2000) but not by other studies from the coastal North Atlantic (Rizzo 1990; Rysgaard *et al* 1995). During this experiment, there was no measurable NH_4^+ in the ambient seawater and there had also been very low the previous summer levels ($0.64 \pm 0.54 \mu\text{mol L}^{-1}$). In contrast, DIN in the sifted, homogenized sediment was mostly in the form of NH_4^+ ($168 \pm 11 \mu\text{mol L}^{-1}$) and NO_x^- levels were low ($0.76 \pm 0.05 \mu\text{mol L}^{-1}$) as expected. To extract total NH_4^+ from the sediment, cores were placed in KCl which has a higher salinity than the pore water and therefore is supposed to cause adsorbed NH_4^+ to become desorped and added to the NH_4^+ already dissolved in the pore water (Henriksen *et al* 1983; Rysgaard *et al* 1999; Pelegri & Blackburn 1994). It, therefore, ought to contain higher NH_4^+ levels than the pure porewater collected directly by the sediment sippers but this was not the case for any of the pore water samples but one (Table 5.1: sediment properties, NH_4^+ vs bNH_4^+). It is possible that there was not much NH_4^+ adsorbed to extract and that

during extraction, where some contact with air was unavoidable, some of it oxidized to NO_x^- (which was not measured in these samples) and this would not have happened in the sediment sipper samples as they were extracted directly from the sediment into vacuum tubes. Alternatively, as they were measured in separate runs of the autoanalyser because they required different blanking solutions, it is possible that error was introduced at this stage.

The increased in pore water NH_4^+ in both treatments upon addition of seawater to the mesocosms (Figure 5.3) is most likely caused by desorption due to higher salinity (Rysgaard *et al* 1999). The sediment had been sieved into seawater, diluted with deionised water to 25 psu, to match the *in situ* pore water salinity; upon adding the filtered seawater column on top, some diffusion would have taken place which increased the salinity of the pore water (to 29 and 31 psu in control and *C. volutator* treatments, respectively). The concurrent increase in NH_4^+ in the overlying water can be explained by positive NH_4^+ fluxes from sediment to water (Figure 5.4): 68 and 288 $\mu\text{mol hr}^{-1} \text{m}^{-2}$, in control and *C. volutator* treatments, respectively). The concurrent increase in pore water NO_x^- was probably due to nitrification of the NH_4^+ . Nitrification is facilitated by aerobic bacteria and can occur in aerobic areas of sediment and water column (Libes 1992). Because the NH_4^+ fluxes on days 0 and 2 were so much higher in the *C. volutator* treatments than in the control treatments, they are depleted more quickly by nitrification. In the control treatments there is a curious and dramatic decline in both DIN forms suggesting that a substantial amount of denitrification of seawater but not pore water DIN took place between days 4 and 6 which did not occur in the *C. volutator* treatments. Previous studies have shown that when levels in overlying water are high, overlying water will be denitrified prior to pore water (Pelegri *et al* 1994; Rysgaard *et al* 1995; Sundbäck *et al* 2000). However, the consensus so far on denitrification in coastal and estuarine sediment is that bioturbators, in particular gallery diffusers such as *C. volutator* and

various polychaetes, increase denitrification (Pelegri and Blackburn 1994, 1995; Pelegri *et al* 1994; Rysgaard *et al* 1995) because they increase the anaerobic-aerobic border area in the sediment that anaerobic denitrifying bacteria inhabit (Sørensen 1978). However, these previous studies were carried out either on intact sediment cores or by adding *C. volutator* to previously established sediment cores which presumably already had O_2 gradients. While there was no evidence of denitrification in the *C. volutator* treatments during this experiment, final NO_x^- fluxes was strongly negative (Figure 5.4 day 12, corresponding to -12.8 and $-10.1 \mu\text{mol hr}^{-1} \text{m}^{-2}$ in control and *C. volutator* treatments, respectively) and this was presumably because NO_x^- was beginning to be sequestered by denitrifying bacteria in the sediment. It would have taken denitrifiers longer to re-establish themselves in their preferential habitat from the sifted, aerated and homogenized sediment than it would have taken nitrifying bacteria and this process would have presumably been further delayed by *C. volutator* bioirrigation but had the experiment run longer the previously observed patterns may have arisen.

In conclusion, as found in previous studies (Henriksen & Blackburn 1980; Henriksen *et al* 1983; Pelegri & Blackburn 1994; Rysgaard *et al* 1995; Emmerson *et al* 2001; Biles *et al* 2002; Bulling *et al* 2010), DIN dynamics were more extreme in the *C. volutator* treatments than in control treatments: NH_4^+ release and nitrification were both enhanced by *C. volutator* presence. However, denitrification was more evident in the control treatments but this trend was on the brink of changing towards the end of the experiment. Previous studies, where flux measurements were performed on more established sediment cores with or where water columns were shallower, measured . However, in this study fluxes of DIN, with the exception of NH_4^+ on day 0 and NO_x^- on day 12, were very low in both treatments throughout most of the experiment, making it rather tenuous as to whether *C. volutator* exert much effect on water column DIN in the estuary within one tidal period.

5.4.3 Phosphate dynamics

In contrast to the previous two experiments (Figures 3.12 and 4.8) and other studies estuarine sediment (Hylleberg & Henriksen 1980; Rysgaard *et al* 1995; Bulling *et al* 2010; Ieno *et al* 2006), where PO_4^{3+} was released from sediment bioturbated by gallery diffusers, in this experiment PO_4^{3+} seemed to be absorbed from the overlying water into the sediment even though starting pore water had higher PO_4^{3+} than seawater. In the control treatments fluxes were negative and pore water PO_4^{3+} increased over the course of the experiment (Figures 5.3 and 5.4, row 3). However, in the *C. volutator* treatments, where fluxes were more negative than in the control treatments, pore water PO_4^{3+} decreased over the first half of the experiment but did increase dramatically to a similar level as the control treatments by day 12. Ultimately, PO_4^{3+} in the pore water was about 6 x higher in the pore water (11.38 & 10.7 $\mu\text{mol L}^{-1}$) than in the overlying water column (1.9 & 1.6 $\mu\text{mol L}^{-1}$) but at this point fluxes began to reverse to being positive (Figure 5.4). Given the general similarity in phosphate dynamics in control and *C. volutator* treatments it is unlikely the phosphate is a resource strongly modified by *C. volutator* engineering.

5.5 Conclusions

H_A5.1: Turbidity created by *C. volutator* in one average tidal period is **different** from control groups and is **not** a simple proportion (6/168 hrs = 7.2 ntu) of what is generated over a week.

Rather, it is 30 – 60 % (60 – 120 ntu) of the turbidity generated over a week. Light penetration is reduced by *C. volutator* (at 1.2 g m⁻² or ~ 300 ind m⁻² in muddy sediment) by approximately 50% of pure seawater levels over the course of one tide. In addition, turbidity is a far more accurate predictor of light attenuation to the sediment bed than quantification of suspended sediment.

H_A5.2: DIN release from sediment modified by *C. volutator* in one average tidal period is **different** from control groups and is **not** a simple proportion (6/168 hrs) of what is released over a week.

DIN fluxes in both treatments were different from each other and changed over the course of the experiment due to nitrification and denitrification. NH_4^+ fluxes in were positive and higher in *C. volutator* treatments and nitrification was higher in *C. volutator* treatments judging from rising levels of NO_x^- .

H₅.3: Phosphate release from sediment is not modified by *C. volutator* in one average tidal period but dynamics remain unclear.

H₅.4: Surface sediment compaction is modified by *C. volutator*: as measured by sediment depth where ~5 mm loss in surface level was coincided with the absence of *C. volutator* and ~0 mm in the presence of *C. volutator*. Water content of top 5 cm was ~ 5 % higher ($p = 0.001$) in sediment occupied by *C. volutator*.

In conclusion, modification of turbidity and subsequent light loss to the sediment bed is the most consistent and powerful ecosystem engineering effect that *C. volutator* exerts on the water column. DIN release from the sediment is increased by *C. volutator* but not necessarily consistently in magnitude due to dependence on nitrifying and denitrifying bacteria and ambient levels. Sediment compaction is prevented by *C. volutator* and it is, therefore, likely that *C. volutator* inhabited sediment has higher light penetration than sediment not inhabited by *C. volutator*.

Chapter 6: Investigating the effects of an overlying water column on microphytobenthic migration and productivity.

Abstract

Corophium volutator Pallas can create sufficient turbidity in an overlying water column to reduce light penetration to the sediment by 50 % during a single immersion tide. However, it has long been established that intertidal diatoms migrate vertically in the sediment and currently MPB productivity in estuaries is normally estimated for emersion periods only as there is no light limitation during this period. This experiment was designed to examine whether variable light penetration to the sediment during immersion would result in variability in photosynthetically active (surface) biomass and how this would affect biofilm productivity over the tidal cycle. Forty-four sediment cores containing biofilm slurry from the Eden estuary were transported to a laboratory environment in which the *in situ* tidal cycles were maintained by immersion/emersion of cores in filtered coastal seawater but light intensity to each core was manipulated for minimum variation between cores during emersion (435 to 628 $\mu\text{mol photons m}^{-2} \text{s}^{-1}$) and maximum variation (1 to 426 $\mu\text{mol photons m}^{-2} \text{s}^{-1}$) during immersion. Surface biomass (F_0^5) and maximum photosynthetic efficiency ($\frac{F_v}{F_m}$) were repeatedly measured over the *in situ* tidal cycle with a fluorometer. Rapid light curves (RLC) without previous dark adaptation were used to estimate actual productivity at ambient light levels prior to start and around mid-emersion and -immersion. The experiment was repeated over 3 different *in situ* daytime tidal cycles. Results clearly demonstrated that bulk migration was driven by *in situ* tidal patterns rather than opportunistically responding ambient light availability patterns. However, at the site the diatoms were collected

it was usual for MPB to be photosynthetically active during the immersion tide: surface biomass during immersion was at least as high or higher than during emersion regardless of when during the day they occurred. Variation in ambient light levels and dark adaptation times caused micro-cycling of diatoms within the photic zone but did not appear to drive bulk migration. In addition, bulk migration occurred prior to and during *in situ* sunrise and MPB did not re-emerge to the surface post *in situ* sunset regardless of laboratory light levels. Finally, ambient productivity (rETR) estimated from RLCs showed that productivity during immersion tide was a tiny proportion of emersion productivity regardless of increased surface biomass and photosynthetic efficiency which raises an interesting question as to why diatoms surface during immersion.

Chapter 6: Investigating the effects an overlying water column on microphytobenthic migration and productivity.

6.1 Introduction

6.1.1 Rationale

Previous chapters dealt with the effects that macrofauna can have on the water column and how this might affect microphytobenthic biomass and assemblage composition. However, it has long been established that intertidal diatoms migrate vertically in the sediment, following diurnal and tidal rhythms, and the general consensus is that microphytobenthic cells accumulate at the sediment surface during daylight tidal emersions to photosynthesize and then re-submerge into the sediment prior to tidal immersion or sunset (Round & Palmer 1966; Pinkney & Zingmark 1991; Hay 1993; Guarini *et al* 2000a; Serôdio *et al* 2001; Honeywill 2001; Consalvey 2002; Jesus 2006). If this is the case, then, in tidal systems, turbidity in the overlying water column is unlikely to exert selective pressure on microphytobenthic community composition or productivity because if cells have migrated out of the photic zone of the sediment anyway during immersion, then variation in light attenuation to the sediment bed cannot affect them. However, while diatoms from permanently submerged marine and freshwater systems often experience comparable irradiance levels to the intertidal at emersion due to the clarity of the water (Miles & Sundbäck 2000; Glud *et al* 2002), they will still photosynthesize at light intensities of ≤ 30 PAR (Sundbäck & Graneli 1988; Glud *et al* 2002; Longphuiert *et al* 2006; Du *et al* 2010; Spears 2010). As the species (such as *Navicula phyllepta*, *N. gregaria*, *Gyrosigma fasciola*, *G. balticum*, *Pleurosigma angulatum*, *Tryblionella apiculata*, and *Achnanthes delicatula*) commonly found in subtidal marine habitats (Sundbäck & Snoeijs 1991) and even freshwater habitats (Kelly *et al* 2005) are also commonly found in the estuarine intertidal assemblages of the Eden (Appendix 1), it is not unrea-

sonable to extrapolate that they could also photosynthesize during immersion in the intertidal if they were at the sediment surface and given sufficient irradiance (> 1 PAR). The benefits of remaining at the surface to photosynthesize during immersion are that cells can be more productive and are less likely to become photoinhibited, or become nutrient-limited (Miles & Sundbäck 2000; Perkins *et al* 2001). The deleterious effects of photosynthesizing under immersion are the increased likelihood of resuspension due to oxygen production (Sundbäck & Miles 2000) and an increased vulnerability to surface grazing. This study investigates whether cells automatically migrate downwards pre-immersion, regardless of irradiance, or whether downward migration during immersion is a function of irradiance. If cells do not automatically migrate downwards, then the influence of turbidity in the water column is possibly significant.

6.1.2 Previous migration studies

Fauvel and Bohn (1904) reported on the behaviour of diatoms in the intertidal sandflats on the Island of Tatihou: diatoms followed diurnal and tidal cycles, “exiting” the sediment during the daytime emersion and re-entering the sediment during the daytime immersion or prior to sunset. Another important observation made by Fauvel & Bohn (1904), was that when the biofilms were transported to the laboratory, the *in situ* rhythm observed prior to removal persisted, *ex situ*, regardless of the absence of light and tidal cues. Finally, Fauvel & Bohn (1904) observed that during neap tides, in calm weather conditions, diatoms could also be seen surfacing during the high tide, which suggested that while diatoms motility followed diurnal and tidal cycle rhythms, cells could respond opportunistically when environmental conditions allowed (e.g. when the light environment was favourable) and, presumably, extend their light dose. Subsequent investigations into cell motility patterns have been extensively reviewed by Consalvey and colleagues (2004). The main research questions raised by Fauvel & Bohn (1904) were whether cell migrations were triggered by

light cues, and if so whether the migrations were rhythmic, or 'entrained' by prevailing *in situ* conditions, or were they simply an opportunistic phototactic response to light availability as the reported observations gave evidence of both scenarios. Further investigations also generated evidence for both scenarios. Some field and experimental studies showed that diatoms migrated in response opportunistically to changes in irradiation which were modified by tidal immersion (Aleem 1950; Perkins 1960; Hopkins 1963, 1966) and were also driven to migrate downwards by disturbance due water flow (Hopkins 1966; Consalvey 2002) but could not migrate once water content of the sediment dropped below 66% during daytime emersion (Hopkins 1966). Perkins (1960) found that *in situ* diatoms in the Eden estuary immersed in up to 18 inches of water remained at the surface during daylight hours and, when transported to the laboratory, would migrate towards the surface at night if given artificial light and would migrate away from the surface in darkness regardless of time or day. Paterson (1986) found that cells could be drawn to the surface with the application of as little as $0.5 \mu\text{mol photons m}^{-2} \text{s}^{-1}$. On the other hand, other researchers found that cells accumulated at the surface prior to *in situ* daytime emersion migrated away from surface prior to immersion even in the absence of tidal stimulus in the laboratory for several days (Round & Palmer 1966; Happey-Wood & Jones 1988; Hay *et al* 1998; Kingston 1999; Guarini *et al* 2000). Since the 1980s a variety of methods have been employed to investigate the migration of micoralgal cells (also reviewed in Consalsvey *et al* 2005): LT-SEM (Paterson 1986; Hay *et al* 1993; Janssen *et al* 1999), EPS (extracellular polymeric saccharide mucilage) assays (Smith & Underwood 1998; Perkins *et al* 2001), pigment assays (Pinckney & Zingmark 1991, Hay *et al* 1993, Guarini *et al* 2000), Clarke-type O₂ electrode (Revsbech & Jorgensen 1986; Pinckney & Zingmark 1991, 1993 a, b, c; Serôdio 2001), spectral reflectance (Paterson *et al* 1998; Kromkamp *et al* 1998), and chlorophyll fluorescence (Serôdio 1997; Honeywill 2001; Perkins 2001, 2002, 2006, 2010; Consalvey 2002; Jesus 2005). Developments in fibre optics allowed the measurement of light attenuation through sed-

iment at a micron scale (Kühl & Jorgensen 1994 and references therein) and using this method Consalvey (2002) established that for Eden estuary intertidal mud (though organic & water content and grain size information were unfortunately not given) > 50% of light was attenuated by 100 μm sediment depth, 85% by 200 μm , and 99% of incident light was attenuated by 400 μm . LTSEM images and spectral reflectance measurements of biofilms over a tidal emersion period show that showed that once a biofilm had formed on the surface, almost all the cells were in the top 200 μm in a 2 – 3 cell layer (Paterson 1986; Kromkamp *et al* 1998). This layer of cells, from the surface to 400 μm depth, is often referred to as the ‘photosynthetically active biomass’ (PAB, Guarini *et al* 2000a, 2000b) or ‘productive biomass’ (Serôdio *et al* 2001). In addition to bulk migration cells “micro-cycle” within the photic zone, presumably to optimize light climate and productivity (Kromkamp *et al* 1998).

With the expansion of methods, the focus of migration studies shifted from the visual enumeration of microalgal biomass at the surface (colouring and cell counting), to the quantification of physiological and functional responses to environmental cues, i.e. photosynthetic and polymer production. Studying the functionality of biofilms in different estuarine habitats and under variable tidal rhythms was necessary for estimating large scale primary productivity of these systems, the fluctuations therein, and the relative importance of MPB assemblages to local and global carbon budgets. Pinkney & Zingmark (1991, 1993a) used Revsbech & Jorgensen’s (1986) O_2 microelectrode methods to generate P-E curves (see General Methods 2.4.2.2) in order to calculate maximum photosynthetic rate (P_{max}) of MPB over a range of tidal cycles and estuarine habitats. They devised a formula for estimating P_{max} based on a combination of ‘tide angles’ and ‘sun angles’ (time relative to peak high tide and sunrise) and found that their model predicted empirically measured productivity from their own and other studies reasonably accurately. Guarini and colleagues (2000a) similarly used pigment analysis from lens tissue samples taken at the start and end of the emersion tide to make ground truthing measurements to test their 2-

compartment model (photic and non-photic zone) for predicting the photosynthetically active (surface) biomass in Marennes-Oléron Bay. They used this data to develop a model of productivity of temperate intertidal MPB based on irradiance, temperature, and tidal patterns. In their model the immersion period were non-productive, presumably due to *in situ* turbidity and depth of water column. Finally, Serôdio and colleagues (2001) used a combination of fluorescence measurement (F_0) and P-E curves from O_2 microelectrode measurements to calculate total productive biomass and biomass specific productivity over a tidal cycle. They found that productivity peaked at emersion as did surface biomass as estimated by F_0 . From the analysis of O_2 levels at different depths they demonstrated that productivity at immersion shifted to lower sediment depths and that biomass corrected productivity was about 1.3 and 0.66 times the measured productivity at emersion and immersion, respectively. They concluded that short and mid-term variability in productivity could be explained by bulk migration over the spring-neap cycle.

Due to the relative difficulty of sampling biofilms in the field during immersion and maintaining tidal systems in the laboratory, studies tended to focus on either just the migration during emersion hours (Guarini 2000; Jesus 2005; Perkins 2001) or, given the convenient inertia of tidal rhythms demonstrated previously (Round & Palmer 1966; Happey-Wood & Jones 1988), during immersion hours but in the absence of immersion conditions (Pinckney & Zingmark 1991, 1993 a, b, c; Underwood *et al* 2005). The former studies simply assume that productivity during immersion is negligible and the latter studies assume that changing light levels due to actual immersion would not have any effect on PAB or productivity. Of the relatively few laboratory studies that did maintain cores in tidal systems (Hay 1993; Consalvey 2002; Defew *et al* 2002, 2004; Serôdio *et al* 2001) only Consalvey (2002) actually made biomass and photosynthetic rate measurements during the immersion period under immersed conditions. Using a fluorometer, Consalvey (2002) monitored surface biomass (F_0) in intact sediment cores placed in either light/exposed, light/immersed, dark/exposed, or

dark/emersed conditions in the laboratory over their *in situ* emersion period. By the end of the *in situ* emersion period, surface biomass in cores from the light/exposed treatments was twice as high as in the light/submerged treatment and about 9 times higher than in both the dark/exposed and dark/submerged treatment. In a second part to the experiment, Consalvey (2002) monitored another set of intact cores over their *in situ* emersion period but did not apply the experimental treatments (as above) until the start of the *in situ* immersion period. Surface biomasses dropped in all cores at the start of the immersion period and differences halfway through the immersion period when the experiment terminated were not as extreme as in the first part of the experiment. However, surface biomasses in light treatments were significantly higher than in both dark treatments and surface biomasses in both exposed treatments were higher than submerged treatments (biomasses at mid-immersion in descending order: light/exposed, light/immersed, dark/exposed and dark/emersed). Consalvey (2002) demonstrated that light was the most important factor in determining PAB and that actual, rather than entrained, immersion conditions also reduced PAB.

6.1.3 Using Fluorescence to monitor migration

Depending on the number of samples, cell enumeration by microscopy (light and LTSEM) and pigment analysis, can take days to weeks to process, so one great benefit of using O₂ microelectrodes (Revsbech and Jorgensen 1986, Glud 1992) and fluorescence methodology (Consalvey *et al* 2005) is that each measurement takes seconds (for F₀ and F_v/F_m measurement) or minutes (for a P-E curve) to carry out. Jesus *et al* (2005) made 100 F₀ measurements in 6 minutes. Another benefit is that these methods are non-destructive, allowing the same biofilm to be measured repeatedly over time and under different environmental cues. As discussed above, O₂ measurement has the advantage over fluorescence in that it measures gross O₂ production at known depths and, therefore, also measures depth of PAB whereas with fluorescence measurements the true

depth of PAB is unknown (Serôdio *et al* 2001; Perkins *et al.* 2002). Because true depth of PAB is unknown and photosynthetic efficiency is higher at lower irradiance, i.e. at lower sediment depths, the photosynthetic efficiency measured by fluorescence can be over- or underestimated (Perkins *et al* 2011). However, while an O₂ microelectrode can measure depth of PAB it cannot measure quantity of PAB, even in arbitrary, relative units as in F_0 , as the quantity of photosynthesizing units is confounded with photosynthetic efficiency in O₂ production (Glud 2008). Migration studies that used O₂ microelectrons to track migration over tidal cycles had to use secondary methods to measure surface biomass, which meant they were once again destructive (Pinckney & Zingmark 1991, 1993a; Serôdio *et al* 2001). Finally, fluorescence measuring equipment is far more robust and easy to use, both in the field and in the laboratory, than O₂ microelectrodes, which are extremely delicate and require far more expertise to make fast and accurate measurements. So, over a lengthy experiment there is much less scope for the introduction of error by the experimenter using fluorometry.

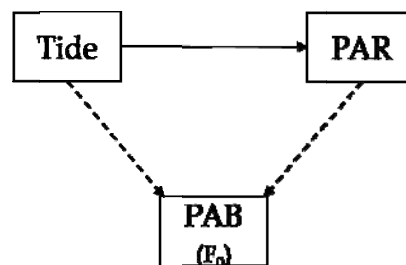
6.1.4 Hypotheses

The aims of this work were to test the following hypotheses:

H₀6.1: MPB bulk migration is triggered by changes in tidal state

H₀6.2: MPB bulk migration is triggered by changes in irradiance

H₀6.3: MPB productivity is negligible during emersion



6.2 Materials and Methods

6.2.1 Biofilm collection and treatment

Biofilm was scraped off the sediment surface from a site on the southeast shore and also from below Guardbridge on the Eden estuary (see Chapter 2.1). To remove macroinvertebrate grazers, the sediment slurry was then sieved through a 500 μm mesh into two plastic trays (internal dimensions: 36.5 x 26.5 x 11.6 cm) containing 4 cm depth of filtered (1 μm filter) seawater until the mixture reached 8 cm in depth. Experimental trays were placed outdoors to allow the sediment to settle and compact and for the MPB to migrate to the surface. Trays were then placed in a 10°C room overnight and surface seawater was siphoned off the following morning leaving an approximately 4 cm deep sediment bed with a biofilm at the surface.

Slurry samples were collected to measure grain size distribution by coulter counter (Chapter 2.2.2) and to describe the MPB community assemblage. For the MPB assemblage description, samples were fixed in 4 % glutaraldehyde solution and subsamples from these were acid-washed and permanently mounted with Naphrax (Chapter 2.5.3). Triplicate live-dead counts of 300 diatom frustules or cyanobacterial colonies (or total counted in 3 hours per replicate) were made on wet mounts under 788 \times magnification ($\times 63$ lens) for each run. Live:dead cell count ratios were classified by size and shape categories (presented in Appendix 2) and the categories which constituted ≥ 1 % of the combined live counts for each run were identified where possible (from 300 valves per run) on the permanent mounts under 1250 \times ($\times 100$ lens) magnification.

6.2.2 Experimental set up

Twenty-two corers (PVC pipe: i.d. 5.2 cm, e.d. 6.0 cm, depth 4.5 cm, with one rim tapered by sanding) were inserted into the mud of both trays to create 4 rows and 6 columns, where the 6th column contained only two cores. The experiments were run in a temperature-controlled room with the thermostat at

11°C (approximate shore water temperature 12°C). Illumination was provided by two low bay metal halide lights (400W HQI-T, Newey & Eyre/Hagemayer Ltd, Birmingham, UK). Metal halide lights provide high intensity photosynthetically active radiation (PAR; $\lambda = 400 - 700 \text{ nm}$). Variation and rise in temperature across the sediment, due to the proximity of lights to the sediment, was prevented by running a fan next to each tray to circulate the air and by placing the sediment trays on a stand within a larger tray of water which could be iced when necessary (Figure 6.1). Sediment temperature between cores was monitored throughout the experiment and maintained at $12 \pm 1 \text{ }^{\circ}\text{C}$. The positions of each tray were marked to ensure that the light intensity at each core was consistent over the three runs of the experiment.

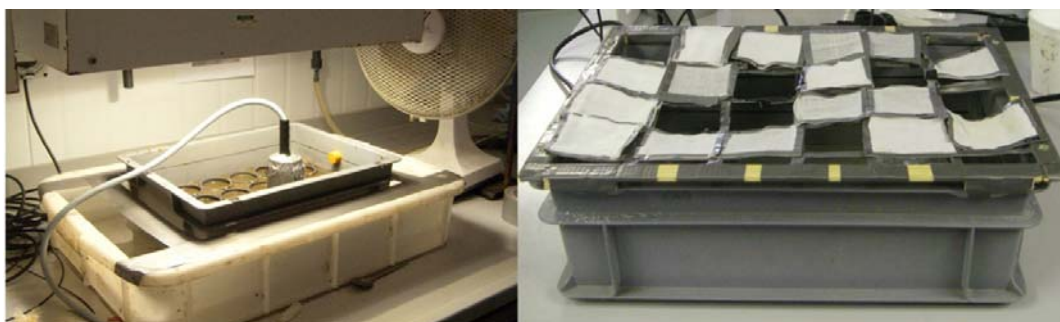


Figure 6.1 a (left) & b (right): (a) Tray 2 at emersion with PAM making RLC measurement. (b) The shading unit was held in position over the sediment tray with dowels. Each layered muslin square could be individually removed to allow access of PAM probe to individual core entry during RLC measurement at immersion without greatly affecting light levels whereas for the dark-adapted measurements the shading unit was removed entirely.

6.2.3 Light intensity at emersion and immersion

PAR during emersion hours in the field varies with season and cloud cover but on sunny summer days in Scotland it is generally in the vicinity of $1000 - 2000 \mu\text{mol PAR m}^{-2} \text{ s}^{-1}$ on a sunny day. While this level of irradiation could not be replicated in the laboratory, emersion light intensities of $400 - 500 \mu\text{mol PAR m}^{-2} \text{ s}^{-1}$ have previously been shown to be sufficient to saturate the photosynthetic activity of Eden estuary diatom biofilms at temperatures below 20°C (Defew *et*

al 2004, Jesus *et al* 2006) and irradiances higher than 600 $\mu\text{mol PAR m}^{-2} \text{s}^{-1}$ downward migration (Perkins *et al* 2010a).

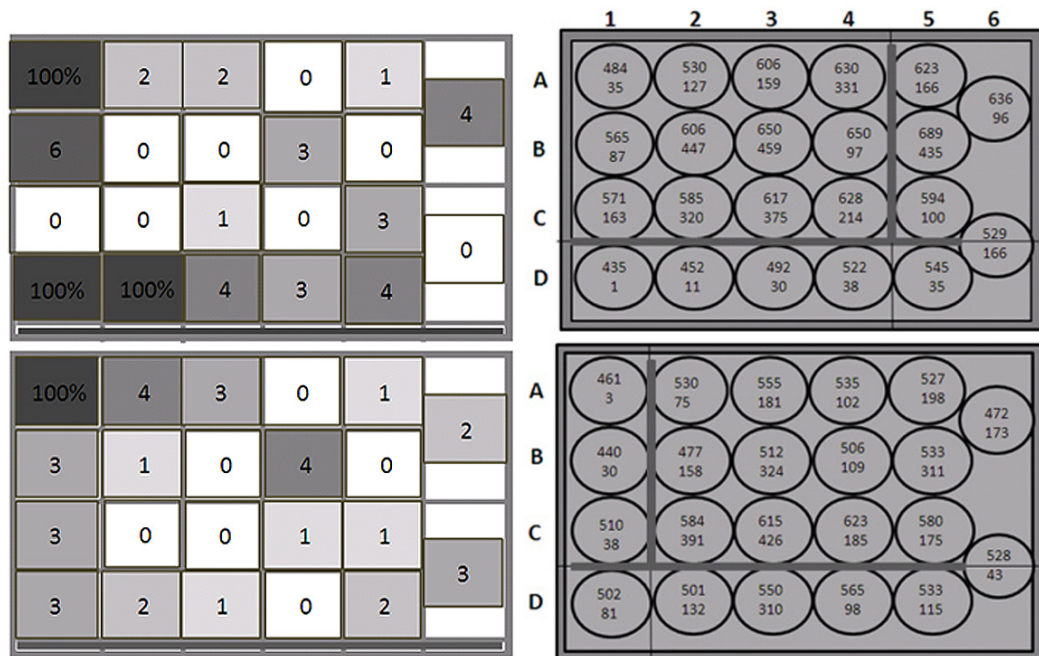


Figure 6.2: Schematic of shading units (left) and light level at the centre of each core position at emersion and immersion (right) for tray 1 (top) and tray 2 (bottom). The PAR values, in $\mu\text{mol photons m}^{-2} \text{s}^{-1}$, represent light intensity at the center of each core at emersion (top) and immersion (bottom). The wide beams represent internal barrier blocking horizontal light to cores to create very low light treatments. These were only in place, underneath the shading unit, during immersion. Light levels were measured *in situ* under immersion conditions with the 1mm diameter Diving-PAM light sensor.

High tide was simulated with a 6 cm seawater column depth and a shading structure for each tray that created a different level of immersion light level for each core. The shading structure had an outer frame constructed from wooden slats whose internal dimensions matched the internal dimensions of the sediment trays and an internal frame, constructed with duct tape, demarcated the rows and columns of the corers inside the tray. Squares of muslin were pinned to the inner frame to create differential shading levels for each core (Figures 6.1, right, and 6.4, left column). Higher shading levels were created simply by adding more layers of muslin. Muslin sheeting attenuates light but acts as a neutral density filter (Perkins 2010, personal communication). As the shading level of neighbouring cores affected light levels to any particular core, the shading lev-

els had to be assigned *in situ* under seawater immersion, using the PAM light sensor (30 x 3.5 mm, sensor diameter = 2.5 mm) to measure light intensity at the centre of each core in its experimental position. Light levels were highest in the central areas of the trays, nearest the bulb, and lowest around the edges. To get shading levels of $< 50 \mu\text{mol PAR m}^{-2} \text{ s}^{-1}$ lateral as well as downwelling irradiation had to be shaded. Lateral irradiation was blocked out entirely along 1 row and 1 column on the edges of both trays by opaque removable barriers within the water column but above the sediment (Figure 6.4, right column). Light intensity to the cores during emersion ranged from 435 to 628 $\mu\text{mol photons m}^{-2} \text{ s}^{-1}$ in tray 1 and 440 to 623 $\mu\text{mol photons m}^{-2} \text{ s}^{-1}$ in tray 2; during immersion light levels ranged from 1 to 459 and from 3 to 426 $\mu\text{mol photons m}^{-2} \text{ s}^{-1}$ in trays 1 and 2, respectively (Figure 6.4, left column). To keep light levels to each core consistent throughout, within and between runs of the experiment, the outer frame of the shading structure was locked into the edge of the sediment tray by dowels.

6.2.3 Measurements and tidal rhythms

Presence and photophysiology of microphytobenthic organisms at the surface of the sediment was monitored over consecutive tides by chlorophyll-a fluorescence measured with a Diving-PAM (Heinz Walz GmbH). Surface biomass proxy, F_0 , and maximum light utilization efficiency, F_v/F_m (Genty *et al* 1989), were monitored over the tidal period with a series of F_v/F_m measurements made following 5 minutes of low light ($< 4 \mu\text{mol PAR m}^{-2} \text{ s}^{-1}$) adaption (Chapter 2.3.2). Measurement order was randomized within trays for each measurement occasion to prevent covariation between measured parameters and core positions. To assess the impact of variation in dark adaptation times for each core, the starting time of the dark adaptation period for each tray was subtracted from the measurement time for each core in that tray and expressed as time in excess of 5 minutes (in seconds) and used as a covariate ('dark' adaptation time) in regressions against F_0 and F_v/F_m .

To evaluate photosynthetic potential, rapid light curves (RLCs, Chapter 2.3.2) were run on selected cores at the start of the experiment (before the lights were switched on) and near the peaks of the following tides without prior dark adaptation. RLCs were made using the Diving-PAM's 8 light-step protocol (0, 104, 186, 270, 368, 533, 752, 1133, 1660 $\mu\text{mol photons m}^{-2} \text{ s}^{-1}$ at 5 mm probe distance in air) with 20 s at each light step. Each RLC took approximately 3 minutes so could not be performed on each core. Therefore, 12 cores were selected to cover the broadest range of emersion/immersion light treatments. However, RLCs were only completed if the initial F' yield was greater than 130 (stipulated by the Walz GmbH Diving-PAM protocol) so in some cases cores were used simply because they had a high enough yield. In addition light curves were not used if NPQ induced during measurement resulted in a reduction of F yield below 130 units by the latter stages of each light curve. These light curves are used to extract photosynthetic parameters describing the maximum relative electron transport, $rETR_{\text{max}}$, maximum light use coefficient, α , and light utilization coefficient, E_k (for mathematical formulation and a fuller explanation see section 2.3.2).

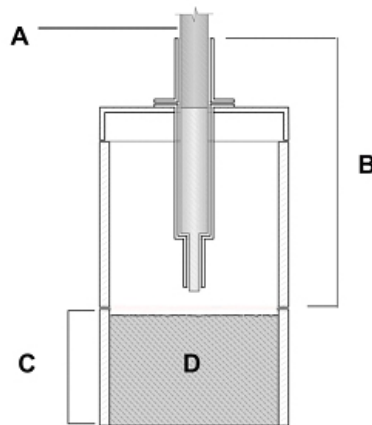


Figure 6.3: The Diving-PAM probe (A) was encased in a housing (B), constructed of the same PVC pipe as the corers (C) that ensured that the probe could always aligned at the same location over the sediment (D) in each core.

Diving PAM settings throughout this experiment were as follows (following the notation of Walz): AI-Fact = 1; RLC time step width = 20 sec; RLC starting in-

tensity level = 3; ETR FAC = 1; Sat Width = 4 sec; Saturating flash intensity level = 12 ($\sim 8600 \mu\text{mol photons m}^{-2} \text{ s}^{-1}$ at 5 mm probe height in air); Damping level = 2; Gain = 10; Measuring light intensity = 9 ($< 1 \mu\text{mol photons m}^{-2} \text{ s}^{-1}$ at 5 mm probe height in air). The Diving PAM probe was encased in the centre of a section of the same PVC pipe as the corers, so that it could be lined up with the rim of the corer and the probe would always measure the sediment in centre of each core where the light intensity measurements were made (see Figure 6.2).

The experiment was repeated three times in order to investigate MPB migration patterns under different tidal and diurnal regimes. The experimental tidal patterns followed the *in situ* patterns but experimental lights were switched on only after starting F_v/F_m and RLC measurements were made, but then remained on for the full length of the experiment, regardless of *in situ* sunrise and sunset. The *in situ* tidal immersion and emersion periods for each run were calculated from the UKHO Admiralty Tidal predictions for Anstruther Easter, Scotland, and the F_v/F_m measurement schedule was designed to measure surface biomass in all 44 cores over two consecutive tides and into a third tide (night time) if a surface signals remained strong enough. Four F_v/F_m measurements were made in each of the first two tides (MT = measurement time): halfway to peak tide (MT2 & MT6), peak tide (MT3 & MT7), halfway between peak tide and tidal change (MT4 & MT8) and just prior to tidal change (MT5 & MT9). RLCs were carried out on selected cores at the start of the experiments and as near to each peak (the mid-point) of each tide as possible. A list of all measurements is presented (Table 6.1) and *in situ* tidal and diurnal patterns with F_v/F_m measurement times are given in BST (GMT+1) (Figures 6.7 a – c, centre plots). Trays were flooded or drained halfway between peak high and peak low tide, which is approximately when the mid-shore of the south bank at Guardbridge begins to flood.

Table 6.1: List of Measurements in all 3 runs.

Measurement	MT	Tidal state	Run 1 (15 Sep)	Run 2 (21 Sep)	Run 3 (4 Oct)
F_v/F_m	1	Start	11:15	05:34	08:15
RLC	1	Start			
Experimental lights switched on					
F_v/F_m	2	1 st tide: halfway to peak tide	Emersion	Emersion	X
RLC	2	1 st tide : near peak tide	Emersion	Emersion	Immersion
F_v/F_m	3	1 st tide: peak tide	Emersion	Emersion	Immersion
RLC	2	1 st tide : near peak tide	Emersion	Emersion	Immersion
F_v/F_m	4	1 st tide: halfway to tide change	Emersion	Emersion	Immersion
F_v/F_m	5	1 st tide: just prior to tide change	Emersion	Emersion	Immersion
F_v/F_m	6	2 nd tide: halfway to peak tide	Immersion	Immersion	Emersion
RLC	3	2 nd tide : near peak tide	Immersion	Immersion	Emersion
F_v/F_m	7	2 nd tide: peak tide	Immersion	Immersion	Emersion
RLC	3	2 nd tide : near peak	Immersion	Immersion	Emersion
F_v/F_m	8	2 nd tide: halfway to tide change	Immersion	X	X
F_v/F_m	9	2 nd tide: just prior to tide change	Immersion	Immersion	Emersion
F_v/F_m	10	3 rd tide: halfway to peak	Emersion	Emersion	X
F_v/F_m	11	3 rd tide: peak tide	Emersion	Emersion	X
RLC	4	3 rd tide: near peak	Emersion	Emersion	X
F_v/F_m	12	3 rd tide: halfway to tide change	X	Emersion	X

6.2.5 Calibration measurements

Three sets of calibration measurements were made. First, the Diving-PAM light sensor was used to measure *in situ* light levels at the centre of each core because its small size enables measurement at small spatial scales. It was calibrated against the LICOR 189 cosine corrected light sensor (LI-COR Biosciences, USA) and found to be consistent (Figure 6.3).

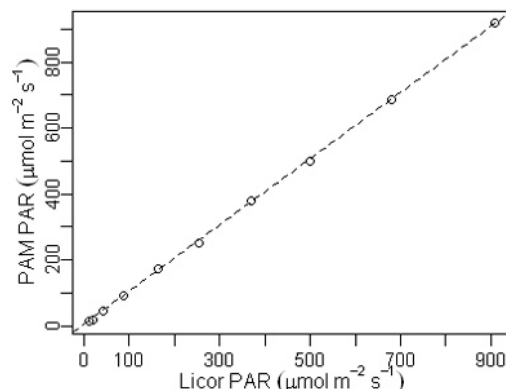


Figure 6.4: Calibration between the cosine corrected Licor LI-189 light meter Diving-PAM's own light sensor. The Diving PAM's 1mm diameter sensor was used to determine light intensity to the centre of each core at emersion and immersion.

The second calibration measured the effect of probe height and medium (air or seawater at emersion and immersion, respectively) on fluorescence yield using a fluorescence standard provided by Walz GmbH. The Diving-PAM probe was designed to be held at a fixed distance from the corer rims throughout a run (see Figure 6.2) but it is impossible to maintain an equal distance between sediment surface and corer rim across all corers, therefore, mm differences in probe height over the sediment arise between cores. The distance of the sediment surface from the rim of each core was recorded before beginning measurements in each run and the probe was fixed inside its housing so that probe height at all cores lay within 3 and 9 mm; this resulted in the majority of cores having a probe height of 5 mm. The fluorescence standard's signal strength was measured in triplicate at 1 to 10 mm probe heights in both air or seawater mediums using a stage micrometer. The relationships of mean ratios ($F_0^{x,m} : F_0^{5\text{mmair}}$, where

x is the probe height and m is the medium) to probe height (Figure 6.5) were used to standardize all F_0 measurement to 5 mm probe height in air.

A third calibration measurement accounted for variation in actinic light levels, during the RLCs, reaching the sediment surface due to different probe heights and mediums. RLCs were run at representative probe heights in air and sea-water with the PAM's own light sensor at substratum. Again, empirical relationships between measured proportions of light intensity ($PAR_{x,m}:PAR_{5mmair}$ 5 mm) and probe height and medium to provide correction factors for actinic light levels during an RLC at each core. During experiments, the Diving-PAM was run from a mains supply to ensure that battery degradation did not reduce light intensity from the internal actinic light source.

6.2.6 Analysis

All statistical tests were preceded by graphical examination of data and models were fitted using the "lm" ("stats" package), "nls"(stats package) and "gls" (nlme package) functions in R (v2.13.0). Model assumptions were investigated and error structures and fixed parameters were selected as described in Chapter 2.6. Full models to address each of the analytical questions (from section 6.1.6) are presented in Table 6.2.

As each core had a different starting F_0 , so to compare migration over the entire tidal period, statistical analysis was performed on (calibrated) surface biomass change, ΔF_0 (Equation 6.1), rather than raw F_0 .

$$\Delta F_0^{i,t} = \left(\frac{F_0^{i,t} - F_0^{i,1}}{F_0^{i,1}} \right) \times 100$$

(Equation 6.1)

where:

i = index for individual core (1,...,44)

t = Measurement time (1,...,n)

Photosynthetic efficiency is known to be a function of accumulated light dose. Accumulated light dose was calculated as

$$aLD_{t,i} = (PAR_{em,i} \times h_{em,t}) + (PAR_{im,i} \times h_{im,t})$$

Equation 6.2

Where:

 i = core index (1,...,44) t = measurement time (1,...,n) h = hours accumulated $PAR_{em/im}$ = $\mu\text{mol PAR m}^{-2} \text{ s}^{-1}$ at each core

For regressions against light intensity (Qu. 2 and 4), PAR values were centralised (cPAR) within tide (immersion mean = 171 ± 61 ; emersion mean = 552 ± 132) to prevent large errors on intercepts at emersion skewing the model. Dark adaptation times (DAT) were expressed as seconds in excess of 5 minutes dark adaptation also to bring them to the intercept. The 130 threshold is stipulated by Walz GmbH Diving-PAM as the minimum level for accurate F_v/F_m estimation; F_0 levels for biomass comparison within a study are much more flexible (Mouget 2010, personal communication; Perkins 2010 personal communication) but 100 was chosen so that variances would not be truncated. Therefore, response variables, F_0 and F_v/F_m , were dropped where F_0 was below 100 and 130, respectively. In addition, cores with damaged biofilms or erroneous measurements (see Appendix 4) were removed from data sets prior to analysis. Photosynthetically evolved oxygen bubbles sticking to the biofilm tend to cause biofilms to blister and peel away from the sediment at immersion due to their buoyancy. Floating pieces of biofilm were removed from the water surface to prevent them shading the sediment below.

The empirical RLC data was used to generate a P-E curve for each core by non-linear least squares estimation ("nls" function) using Eilers and Peeters (1988) 3-parameter model (described in section 2.4.2.2). The 3 estimated parameters from adequately fitting curves (parameters a , b , c had p - values ≤ 0.1) were subsequently used to calculate photosynthetic parameters $rETR_{max}$, α , and E_k

(section 2.4.2.2). Photosynthetic parameters were compared statistically between tidal periods (Model 6.5) and regressed against PAR.

Table 6.2: Statistical models for H₀6.1 – 6.3 where: “ β ” represents parameters to be estimated; $i = 1, \dots, m$ where m is the maximum core number at each measurement time or tide; $t = \text{index for measurement time } 1, \dots, n$ where n is the maximum measurement time in each run; $j = \text{index indicating tide}$; $p = 1, \dots, 8$ and is an index for each actinic light level in an RLC; cPAR represents centralized PAR ($\mu\text{mol photon m}^{-2} \text{s}^{-1}$) for each core prior to F_v/F_m measurement, DAT represents dark adaptation time (s) over 5 minutes; Prev represents the previous measurement ($t-1$) of the response variable at the same core; PAR represents each actinic light level in an RLC; $\varepsilon_{it} \sim N(\mu, \sigma^2)$ represents normally distributed errors structured by a variance-covariance matrix.

H ₀	Model Nr	R func	Response variable	Formula, fixed effects
6.1	6.1.1	gls	ΔF_0	$Y_{it} = \beta_i * MT_{it} + \varepsilon_{it}; \varepsilon_{it} \sim N(\mu, \sigma^2 * V)$
6.1	6.2.1	gls	ΔF_0	$Y_{itj} = \beta_j * Tide_{itj} + \varepsilon_{itj}; \varepsilon_{itj} \sim N(\mu, \sigma^2 * V)$
6.2	6.3	gls	F_0	$Y_{itj} = Tide_{itj} * Prev_i * cPAR_{itj} * DAT_{itj} + \varepsilon_{ij}; \varepsilon_{ij} \sim N(\mu, \sigma^2 * V)$
6.3	6.1.2	gls	F_v/F_m	$Y_{it} = \beta_i * MT_{it} + \varepsilon_{it}; \varepsilon_{it} \sim N(\mu, \sigma^2 * V)$
6.3	6.2.2	gls	F_v/F_m	$Y_{itj} = \beta_j * Tide_{itj} + \varepsilon_{itj}; \varepsilon_{itj} \sim N(\mu, \sigma^2 * V)$
6.3	6.4	nls	rETR	$Y_{ip} \sim PAR_{ip} / ((a * PAR_{ip}^2) + (b * PAR_{ip} + c)) + \varepsilon_{ip}; \varepsilon_{ij} \sim N(\mu, \sigma^2 * V)$
6.3	6.5.1 6.5.2 6.5.3	gls	rETR _{max} , α , E_k	$Y_{ij} = \beta_j * Tide_{ij} + \varepsilon_{ij}; \varepsilon_{ij} \sim N(\mu, \sigma^2 * V)$
6.3	6.6.1 6.6.2 6.6.3	gls	rETR _{max} , α , E_k	$Y_{ij} = \beta_{0j} * Tide_{ij} + \beta_{1j} * Run_{ij} + \beta_{2j} * cPAR_{ij}; \varepsilon_{ij} \sim N(\mu, \sigma^2 * V)$

All starting (maximum) models (Table 6.2) and final models are reported by giving either the model equation and the output table for the fixed portion (for covariate regressions) or by a table of estimates and confidence intervals (for factorial regression). For covariate regressions from Models 6.3 the estimated parameters from the final model were bootstrapped using the multivariate normal distribution (“rmvnorm” function, “MASS” package, 10000 replications) and predicted means and confidence intervals estimated over the range of previous values with dark adaptation time fixed at 1s and PAR fixed at the centralized values for 553 $\mu\text{mol PAR m}^{-2} \text{s}^{-1}$ (mean) at emersion and 50 and 500 $\mu\text{mol PAR m}^{-2} \text{s}^{-1}$ at immersion.

6.3 Results

6.3.1 Sediment grain size and microphytobenthic assemblage

Coulter counter analysis of the sediment slurry from runs 1 and 3 showed that both could be classified as “mud” with clay:silt ratios of 19:81 and 21:79, respectively, and mean grain sizes of 14.1 and 10.8 μm diameter, respectively.

Size-shape groups identified in live counts from the sediment slurry are listed in Appendix 3. In run 1, of the 3 (slides) \times 300 counts made, $89 \pm 0.05\%$ of cells or colonies (when cyanobacteria) were live (see General Methods) and cyanobacteria comprised only $0.38 \pm 0.02\%$ of the assemblage, and no chlorophytes were found. Of the live assemblage, 90% was comprised of 12 size-shape taxa and 40 taxa were represented in the live total. The 12 taxa were all solitary epipellic diatoms from genera *Navicula sensu lato*, *Gyrosigma*, and *Nitzschia* and possibly *Placoneis*. In run 3, there were noticeably fewer diatoms in the sediment and the slides did not yield 300 cells/colonies (144, 220, 202 cells were counted on 3 slides) and $79 \pm 0.05\%$ of those were live cells/colonies and all were diatoms. 90% of the assemblage came from 22 size-shape taxa and 44 taxa were represented in the live total. Of the 22 taxa 52% were solitary epipellic cells from genera *Navicula sensu lato*, *Nitzschia*, *Tryblionella*, *Gyrosigma*, *Fallacia*, and 39% were epipsammic, either semi-motile (pennate, monoraphid cells) or non-motile (pennate, araphid, colonial cells), dominated by *Achnanthes* cells.

6.3.2 Calibrations

The calibration of the Diving-PAM light sensor against the LICOR-189 cosine corrected light sensor (Figure 6.3) was near perfectly linear ($R^2=0.9999$).

The calibration of fluorescence signal strength through different mediums and at different probe heights (Figure 6.5) showed an exponential decay pattern of signal with increasing probe heights and that signal attenuation was less steep in seawater medium over these distances.

$$Y_i = \beta_{1j} * e^{\beta_{2j} * x_i} + \varepsilon_i ; \varepsilon_i \sim N(\mu, \sigma^2)$$

(Model 6.7)

Where

$i = 1, \dots, 10$, mm probe height

j = medium (air or seawater)

Y_i = Fluorescence signal strength (F),

X_i = Height of probe over the substrate,

β_1, β_2 = curve parameters to be estimated by non-linear regression.

ε_i = errors from non-linear regression follow a normal distribution

Parameters β_1 and β_2 estimated for fluorescence measurement in air (emersion) were $2.22 (\pm 0.009)$ and $-0.160 (\pm 0.001)$, respectively with $R^2 = 0.9998$, $p < 0.001$. Parameters β_1 and β_2 estimated for F measurement in seawater (immersion) were $1.68 (\pm 0.01)$ and $-0.120 (\pm 0.001)$, respectively and $R^2 = 0.9991$, $p < 0.001$.

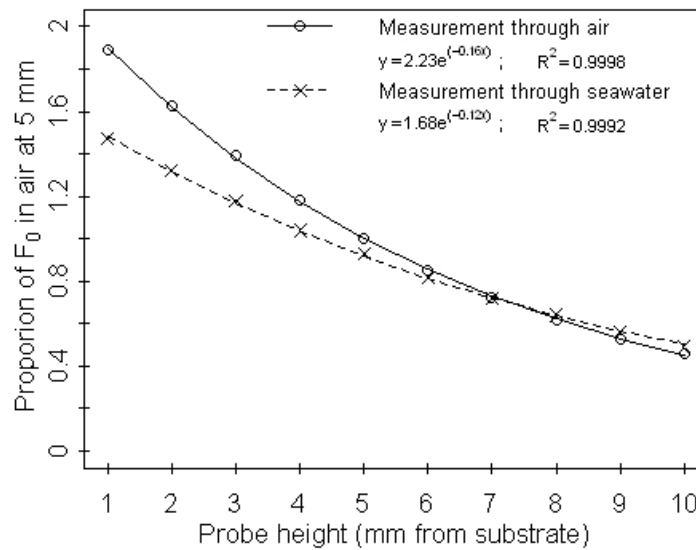


Figure 6.5: Ratios of $F_0:F_{0.5\text{mm}}$ in air and seawater plotted against probe height. Calibration curves were fitted according to Model 6.7. All F_0 values were subsequently adjusted to using these equations.

The calibration of RLC actinic light attenuation through different mediums and at different probe heights showed a linear attenuation of light with increasing probe heights and again signal attenuation was less steep in seawater medium over these distances (Figure 6.6).

$$Y_i = \beta_{0j} + \beta_{1j} * X_{ij} + \varepsilon_i; \varepsilon_i \sim N(\mu, \sigma^2)$$

(Model 6.8)

Where

i = height iteration 1,...,6

j = medium (air or seawater)

x = Height of probe over the substrate;

Y = ratio PAR:PAR_{5mm} ;

β_0 = intercept fixed so that regression for air and seawater passed through 1 and 0.78, respectively, at 5mm;

β_1 = estimated slope.

The linear regression was constrained so that 'air' measurements would pass through the ratio = 1.0 at 5 mm, and the regression for seawater would pass through the ratio = 0.78 at 5 mm. The intercepts (β_0) and slopes (β_1) for measurement in air ($R^2 = 0.979$, $p = 6.1 \times 10^{-5}$) were $1.451 (\pm 0.014)$ and $-0.083 (\pm 0.005)$, respectively, and $0.995 (\pm 0.11)$ with $-0.043 (\pm 0.003)$, respectively, for measurement in water ($R^2 = 0.962$, $p = 2.5 \times 10^{-4}$).

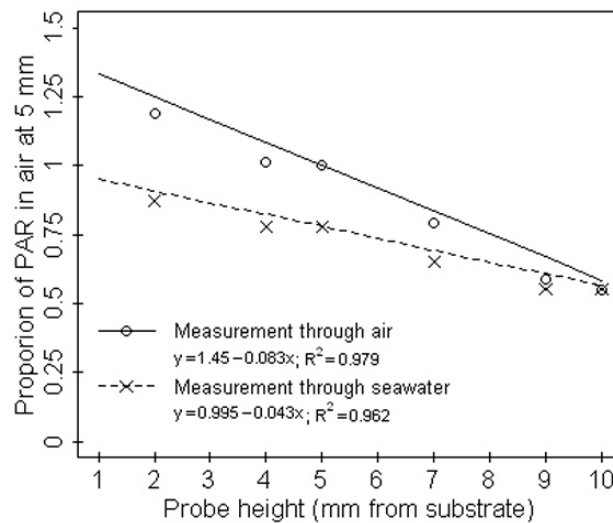


Figure 6.6: Mean ratios of PAR:PAR_{5mm} in air and seawater plotted against probe height. Calibration lines were fitted according to Model 6.8 constrained to pass through 1 and 0.78 at 5mm in air and seawater, respectively.

6.3.3 MPB bulk migration over tidal periods

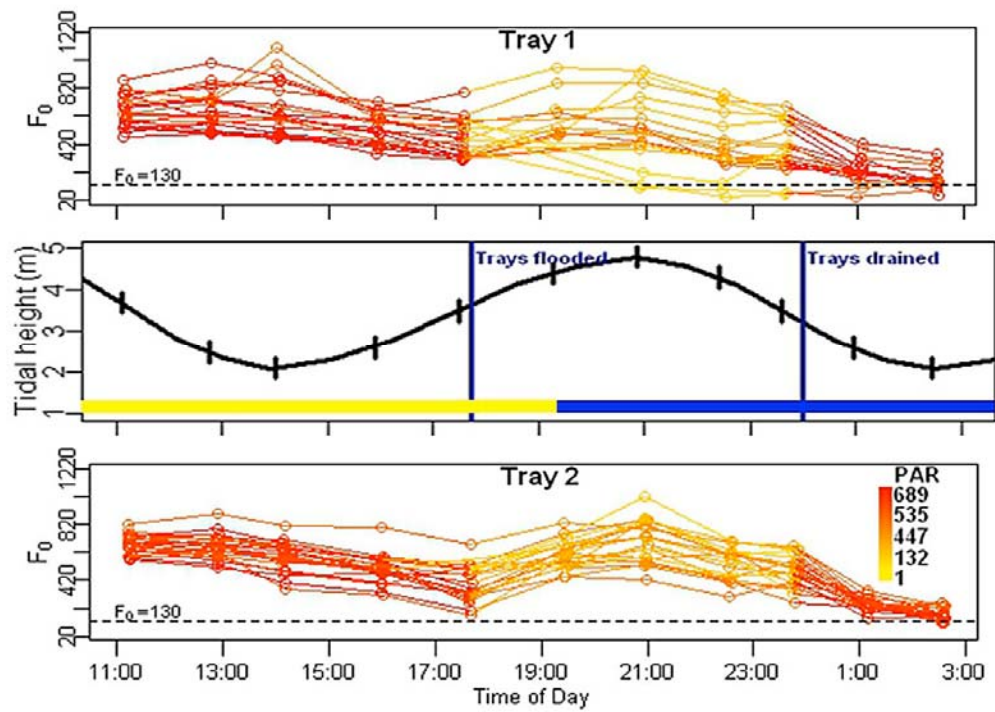
For visualisation of MPB bulk migration over the tidal cycle, calibrated F_0 for each core in both trays were plotted against time and *in situ* diurnal and tidal pattern for each of the three runs (Figures 6.7 a, b, c). For each run, the estimat-

ed means and confidence intervals for each measurement time (Model 6.1.1) are presented graphically (Figure 6.8 a, b & c) and estimated means and confidence for each tide (Model 6.2.1) are tabulated (Table 6.3).

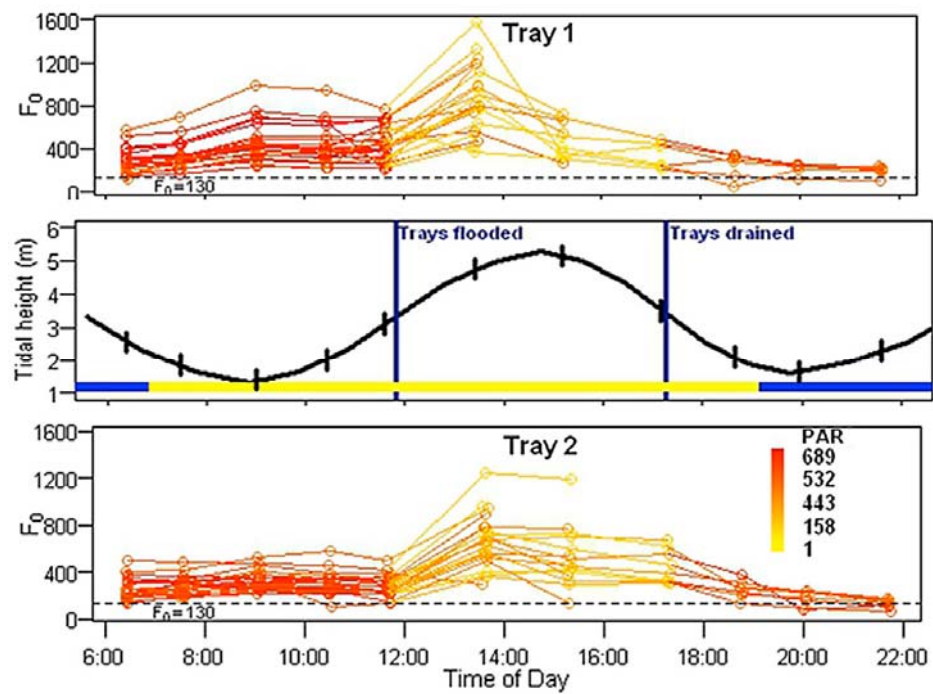
6.3.3.1 Run 1

The first run (Figures 6.7 a) took place on the 15 September 2010 and tidal periodicity lay between neap and spring tides. The shore would have become emersed at approximately 11:15, 4 hours after *in situ* sunrise. The peak of the emersion period was at approximately 14:00 and the subsequent immersion would have begun approximately 2 hours prior to *in situ* sunset at 19:30. The flood tide would have begun to reverse at approximately 21:00 and the sediment would have become re-emersed at approximately 23:30. The last measurement was made at the peak of the second emersion tide at 02:30. Average surface biomass at MT1 was quite high ($F_0 = 669 \pm 93$) and estimated mean ΔF_0 (Model 6.1.1) decreased very slightly in the first half and sharply in the second half of the emersion period (Figure 6.8 a). Following immersion, estimated mean ΔF_0 rose sharply so that by the peak of the immersion ΔF_0 was at the same level as at the peak of the daytime emersion (mean ΔF_0 were estimated at $-6.9 \pm 2.6\%$ and $-6.4 \pm 4.2\%$ of starting values at peak emersion and immersion, respectively). ΔF_0 also decreased dramatically in the second half of the tide and then dropped further during the second emersion that night (at peak mean ΔF_0 estimated at -73.9% starting values). Pooled factorial regression by tide (Model 6.2.1 results in Table 6.3) shows that overall ΔF_0 during immersion was actually slightly higher than during the first emersion ($\Delta F_0 = -11.0$ and -23.0 , $n = 145$ and 162 , respectively, $p < 0.0001$). Overall ΔF_0 during the second emersion was significantly lower than at both previous tides ($\Delta F_0 = -58.4$, $n = 73$, $p < 0.0001$, against both previous). However, 3 cores did show the “expected” downward migration pattern during the immersion tide (Figure 6.7 a, tray 1).

(a)



(b)



(c)

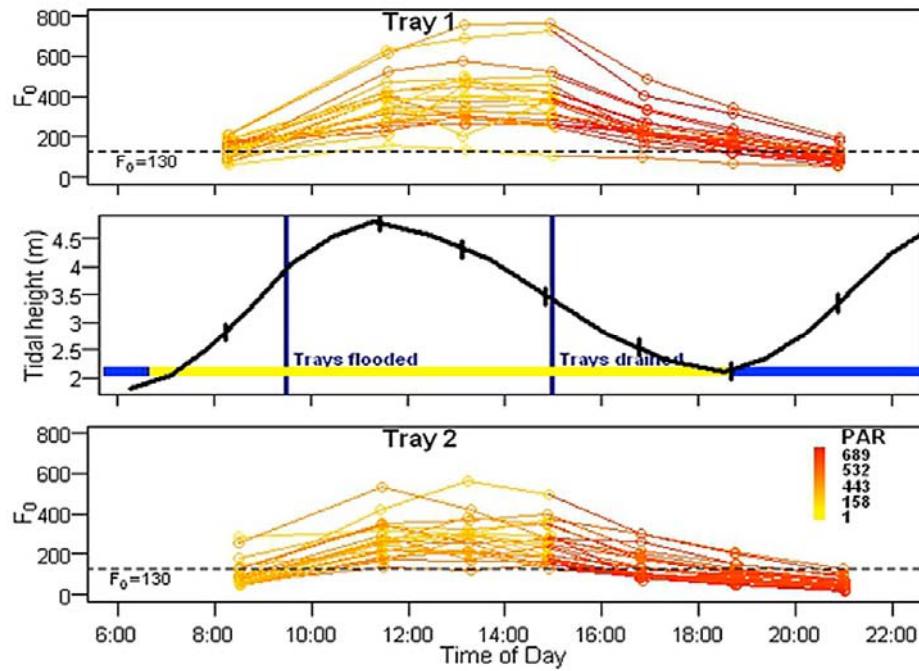


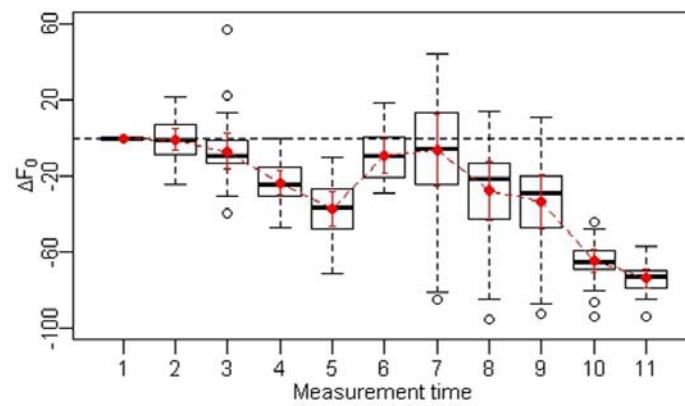
Figure 6.7 a, b, c: Calibrated F_0 data from each run (1,2,3, respectively) showing the surface biomass in each core over the tidal period. Incident light to cores is indicated by line colour. The central graph shows the *in situ* tidal cycle on the black line (with the cross-bars denoting F_v/F_m measurement times) and the *in situ* diurnal cycle as the bar across the bottom (day in yellow; night in blue).

Both Models 6.1.1 and 6.2.1 for run 1 contained a within-core continuous temporal autocorrelation structure and errors were categorically weighted by measurement time.

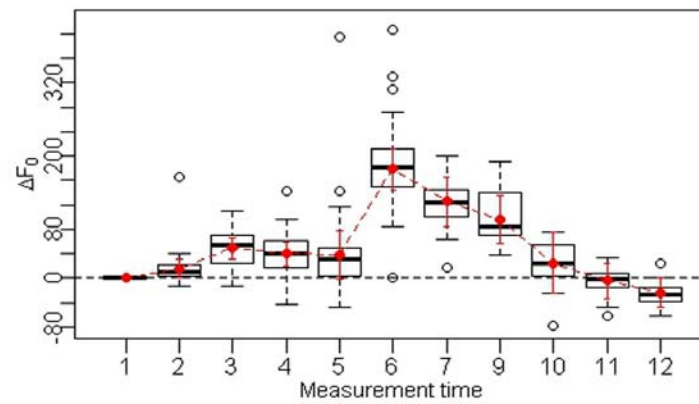
6.3.3.2 Run 2

The second run took place on the 21 September 2010 where tidal periodicity also lay between neap and spring tides. The first emersion period began at 05:34, approximately an hour before *in situ* sunrise (06:35), peaked at approximately 09:00 and ended just before midday (Figures 6.7 b). The afternoon immersion period lasted until 17:00, with its peak at 15:00. Many cores had to be dropped from this experiment due to extremely high O_2 production during immersion tearing off biofilms.

(a)



(b)



(c)

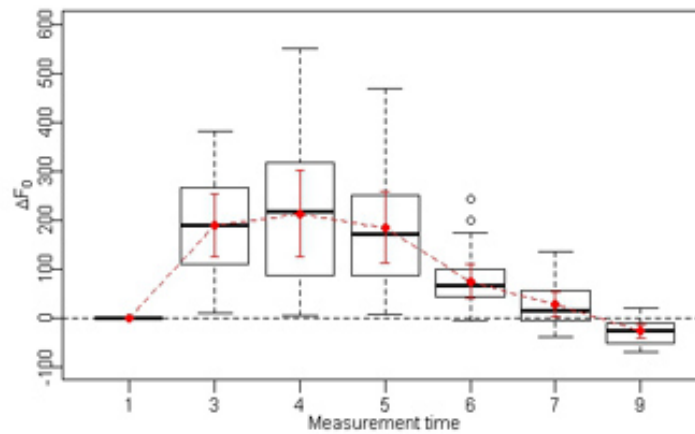


Figure 6.8 a, b, c: Boxplot displaying ΔF_0 at each MT overlaid (in red) with the estimated means and confidence intervals estimated by Model 6.1.1 for each run 1, 2, 3, respectively.

Table 6.3: Estimated means and confidence intervals for each tide (from Model 6.2.1) in each run. V represents a variance-covariance matrix; MT represents measurement time; DA time represents dark adaptation time. The p-values come from the t-tests within each model and the [†]p-values come from reparameterized models to test the difference between the immersion and 2nd emersion. The errors in all runs varied by MT (factor) and have continuous temporal autocorrelation within each core, run 2 additionally had DA time as variance covariate.

Run	DF (Res /Tot)	Tide	Lower 95% Confidence Interval	Estimated mean	Upper 95% Confidence Interval	t-test, p-value
1	$\Delta F_{0it} = \beta_j * Tide_{ij} + \varepsilon_{ij} ; \varepsilon_{ij} \sim N(\mu, \sigma^2 * V)$ V : a within-core continuous temporal autocorrelation structure and categorical weighting of errors by measurement time					
	386/	Emersion	-26.7	-23.0	-19.3	$1.2 * 10^{-29}$
	398	Immersion	-7.4	-12.0	-16.7	$4.5 * 10^{-7}$
		Emersion 2	-39.6	-35.3	-31.1	$5.4 * 10^{-46}$ [†] $8.5 * 10^{-77}$
2	$\Delta F_{0it} = \beta_j * Tide_{ij} + \varepsilon_{ij} ; \varepsilon_{ij} \sim N(\mu, \sigma^2 * V)$ V : a within-core continuous temporal autocorrelation structure and categorical weighting of errors by measurement time as well as DAT as fixed variance-covariate					
	293/	Emersion	21.3	28.1	34.8	$7.3 * 10^{-15}$
	279	Immersion	103.8	118.0	134.0	$6.5 * 10^{-40}$
		Emersion 2	-53.3	-39.8	26.3	$1.7 * 10^{-8}$ [†] $4.5 * 10^{-47}$
3	$\Delta F_{0it} = Tide_j * X_{ij} + \varepsilon_{ij} ; \varepsilon_{ij} \sim N(\mu, \sigma^2 * V)$ V : a within-core continuous temporal autocorrelation structure and categorical weighting of errors by measurement time as well as DAT as fixed variance-covariate					
	264/	Immersion	-2.1	16.7	35.6	
	255	Emersion	-65.7	-59.4	-53.1	p = 0.082

Most of the damage occurred between MT 6 and MT 7 which meant that RLCs were being made during this time took longer than anticipated, with the result that the MT 8 measurements were not taken. The second emersion tide began just under 2 h before *in situ* sunset (19:00) with its peak at 20:00.

Average starting surface biomass was 273 ± 105 (Figure 6.7 b) prior to emersion. During the first half of emersion period mean F_0 rose by an estimated 48.7 ± 4.3 % of starting values (Model 6.1) but values declined in the second half of the emersion towards the changing tide ending at 38.4 ± 10.0 % of starting values (Figure 6.8 b). Following immersion, ΔF_0 increased dramatically, peaking at

129.7 \pm 9.1 % but then decreased again prior to peak emersion (probably due to the loss of cores with intact biofilms). Regardless of biofilm losses, mean ΔF_0 at peak immersion was still significantly higher than at peak emersion (48.7 % \pm 4.3 % and 105.2 \pm 11.0 %, respectively, $p < 0.0001$). Following the peak of the immersion period, ΔF_0 dropped continuously until the last measurement ending at mean -24.5 \pm 6.1 % of starting values. Pooled factorial regression by tide (Model 6.2.1 results in Table 6.3) showed that overall ΔF_0 during immersion was higher than during the first emersion ($\Delta F_0 = 147.0 \pm 7.7$ and 28.1 ± 4.3 , $n = 176$ and 81 , respectively, $p < 0.0001$; and without 2 large outliers ($> +4$ standardized residuals) : $\Delta F_0 = 120.0 \pm 7.6$ and 8.5 ± 1.9 , $n = 174$ and 81 , respectively, $p < 0.0001$). Overall ΔF_0 during the second emersion was significantly lower than during both previous tides ($\Delta F_0 = -11.7 \pm 6.9$, $n = 36$, $p < 0.0001$, against both previous tides; without the 2 outliers: $\Delta F_0 = -12.5 \pm 9.6$, $n = 36$, $p < 0.0001$, against both previous tides).

The outliers came from a core which had a much higher ΔF_0 than expected at emersion (where emersion PAR = 492 $\mu\text{mol m}^{-2} \text{s}^{-1}$, slightly lower than mean 552 $\mu\text{mol m}^{-2} \text{s}^{-1}$). Both Models 6.1.1 and 6.2.1 from run 2 contained a within-core continuous temporal autocorrelation structure and had measurement as a variance category and dark adaptation time as fixed variance covariate.

6.3.3.3 Run 3

The final run took place on 4 October 2010 during a neap tide. The first daylight tide *in situ* was an immersion tide which began at approximately 08:45, 1 $\frac{1}{2}$ hours after sunrise, maximized just before noon, and ended before 15:00. The following emersion peaked at sunset, at about 18:30, and ended by 21:00 (Figure 6.7 c). Low surface biomasses (starting F_0 mean = 120 \pm 58.6), meant that RLCs had to be restarted repeatedly which meant experimental immersion was delayed by a half hour beyond *in situ* immersion, and there was insufficient time to make measurements at MT 2 and MT 8. Estimated ΔF_0 (Model 6.1.1) rose during most of the immersion tide and then declines towards the end of immer-

sion and continued to decline throughout the subsequent emersion (Figure 6.7 & 6.8 c). The estimated mean ΔF_0 at peak immersion (188 ± 16.2 %) was significantly larger ($p = 0.00005$) than the estimated mean ΔF_0 at peak emersion (26.4 ± 6.3 %). Also, none of the 95 % confidence intervals on the estimates between the two tides overlap (Figure 6.8 c). However, the large variation in ΔF_0 between cores and measurements resulted in Model 6.2.1 being unable to estimate reasonable mean values for immersion and emersion; estimated means for immersion and emersion are 16.7% and -59.4%, respectively, as compared to the actual means which are 195.4% and 24.3%, respectively. Consequently there was no significant difference ($p = 0.082$) between surface biomass during immersion and emersion (Table 6.3).

Both Models 6.1.1 and 6.2.1 applied to data from this run contained a within-core continuous temporal autocorrelation structure and had measurement as a variance category and dark adaptation time as fixed variance covariate. While neither model displayed any obvious outliers, heteroscedasticity, or skews in its residuals, both models estimated extremely large variances with 29% of measurements having an errors more than 12 standard deviations from their estimates.

6.3.3.4 Summary of results of bulk migration over tidal period

F_0 was at least as high or higher during tidal immersion as it was during tidal emersion. On run 1, where tidal emersion occurred several hours after sunrise, F_0 dropped slightly over the first half of emersion, but on run 2 where the emersion followed sunrise mean F_0 rose over the first half of the emersion tide. While there was some decrease in F_0 during the second half of the emersion tide in runs 1 and 2, F_0 levels increased again following *in situ* and laboratory immersion, with the exception of 3 cores in run 1. In the first run, the first half of tidal immersion occurred around dusk and mean surface biomass at mid-emersion and -immersion were similar but in the second run, where the first half of tidal immersion occurred well within daylight hours mean F_0 was 2 – 3 fold higher

during immersion than emersion. In both runs 1 and 2, F_0 declined following the mid-immersion and did not re-emerge during the second emersion which was after sunset in situ but not in the laboratory. In run 3, where immersion occurred just after sunrise and lasted until 15:00, F_0 increased almost two fold. The first half of the emersion tide occurred in the 2 hours prior to dusk and F_0 but declined throughout.

6.3.4 MPB migration over different levels of irradiation within tidal periods

If cells migrated as a response to light intensity at the surface then surface biomass should be explained by the surface biomass at the previous measurement and the light intensity in the interim, while accounting for differences in dark adaptation time. Calibrated F_0 measurements from $MT > 1$ ($F_{0,t}$) for each run were plotted, separately and pooled (Figure 6.9, rows 1 to 3 and row 4) against the previous measurements ($F_{0,t-1}$), cPAR, and dark adaptation time to determine overall trends in the data. The variation in the slopes and intercepts of $F_{0,t}$ against $F_{0,t-1}$ between each MT in each run reflected the degree to which surface biomass increased or decreased between measurements. However, the plots against $F_{0,t-1}$ (Figure 6.9, column 1) for individual runs do not show any clear differences in slopes within tides between runs, rather for run 2 there is much higher variance than for runs 1 and 3, and run 3 has a much smaller range of $F_{0,t-1}$ values than runs 1 and 2. The pooled plot shows that the slopes within tides have similar gradients and that there is a slight difference in gradient between tides, i.e. immersion values seem to have a higher gradient than emersion values. The plots against centralised PAR (Figure 6.9, column 2) show a convincing negative trend for immersion values in run 1, but much slighter gradients at runs 2 and 3; at emersion there is a shallower negative trend at run 1 and no trend at all in runs 2 and 3. The pooled data suggest an overall slightly decreasing gradient for both tides although there is a large amount of variation. Finally, the plots against dark adaptation time > 5 minutes (Figure 6.9, column 3) show a slightly declining trend in run 1 emersion and a less obvious declining

trend at immersion but there are no clearly discernable trends for either tides in runs 2 and 3. The pooled data also showed no clear trend presumably due to the large variation.

The minimum adequate regression model of F_0 against PAR between tides, while accounting for the previous level and slight differences in DA times (full model described in on Table 6.2, Model 6.3; minimum adequate model presented in Table 6.4), contained only the main effects, and three two-way interactions: Tide: $F_{0,t-1}$, $F_{0,t-1}$:DA time and Tide:DA time. The model estimated a slightly negative intercept for emersion time but this refers to a previous value of 0, which does not exist, and the actual intercept at the minimum previous measurement (48) is 21. The intercept for immersion was 108, reflecting increasing values with subsequent measurements at immersion but the rate of increase was lower at 0.633 than at emersion (+1). While overall there was a significant negative effect of irradiance (-0.149 ± 0.04 , $p = 0.0001$), cPAR, on surface biomass, the effect was very slight, only 15 points decrease (on a scale of 100 to ~1600) with 100 μmol increase in irradiance, and did not vary between immersion and emersion. The effect of dark adaptation time on the other hand did vary significantly between emersion and immersion ($p = 0.0007$): it was slightly, but not significantly negative at emersion (-0.09 , $p = 0.094$), but slightly positive (0.039) at immersion. In fact both effects were small: at emersion and immersion each additional minute means a 5.4 point decrease and a 2.4 point increase in F_0 , respectively. However, the significant interaction between previous measurement and dark adaptation time suggests that the relationship between the surface biomass and the previous surface biomass decreases slightly (-0.003 , $p = 0.001$) with increasing dark adaptation times.

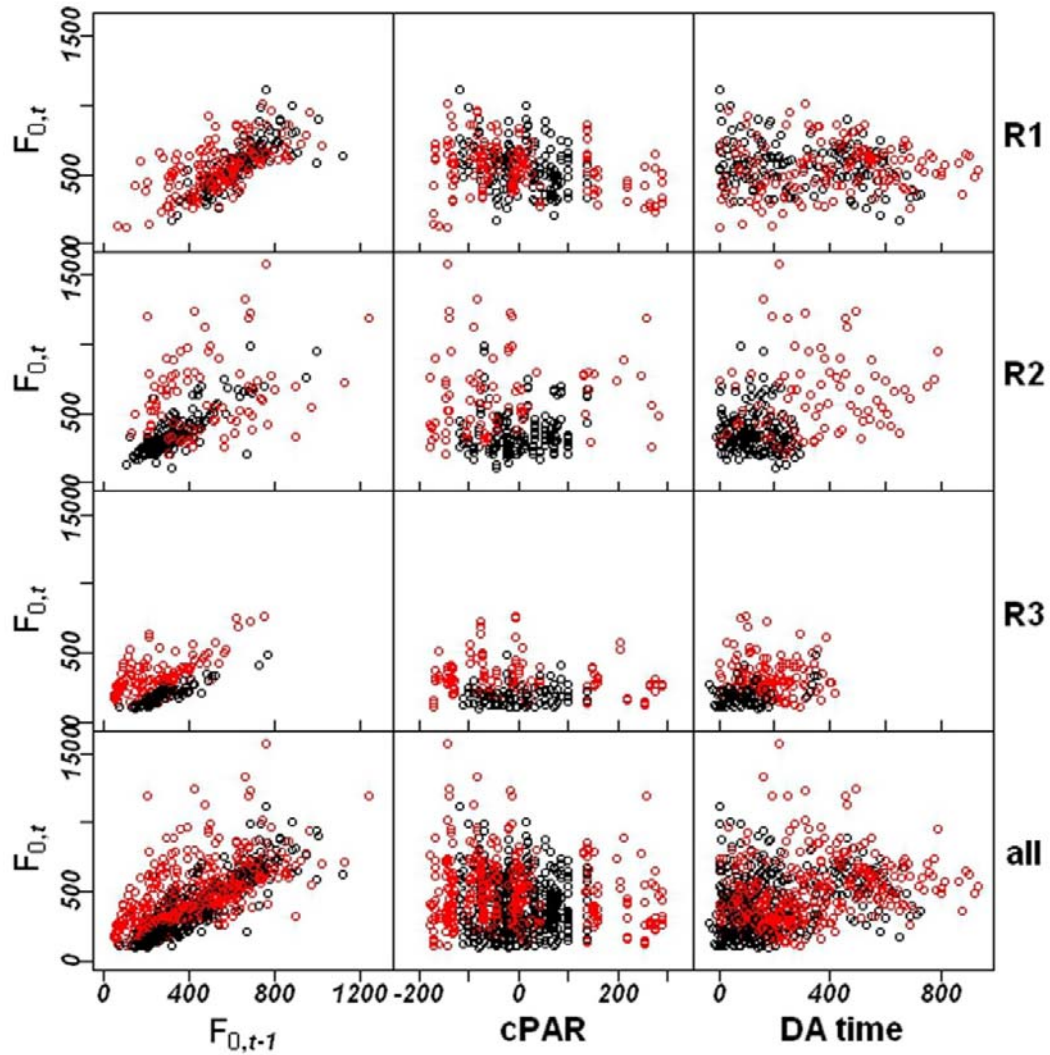


Figure 6.9: Calibrated F_0 values for emersion (o) and immersion (o) at $MT = t = 2, \dots, 9$ against calibrated F_0 values at time $t-1$ (column 1), cPAR at each core prior to that measurement (col 2, units = $\mu\text{mol m}^{-1} \text{s}^{-2}$), dark adaptation times at each measurement (col 3, units = seconds beyond 5 minutes) in run 1 (row 1), run 2 (row 1), run 3 (row 1), and with all the data combined (row 4). The second emersion is not included as run 3 did not have a third tide.

Table 6.4: Estimated intercepts and slopes of from Model 6.3 (gls) applied to calibrated $F_{0,t}$ value at each MT ($t= 2,...9$) with the value from previous measurement time ($F_{0,t-1}$), cPAR, and DA time, as explanatory variables.

AICc	resDF/ totDF	Parameter for	EST	Std Error	p-value
9530.2	743/781	$F_{0ij} = \text{Tide}_{ij} * \text{Prev}_{ij} * \text{cPAR}_{ij} * \text{DAT}_{ij} + \varepsilon_{ij}; \varepsilon_{ij} \sim N(\mu, \sigma^2 * V)$			
9522.5	751/781	$Y_{ij} = \beta_0 + \beta_{1j} * \text{Tide}_{ij} + \beta_{2j} * F_{0,t-1} + \beta_{3j} * \text{cPAR}_{ij} + \beta_{4j} * \text{DAT}_{ij} + \beta_{5j} * (\text{Tide}_{ij} * F_{0,t-1}) + \beta_{6j} * (\text{Tide}_{ij} * \text{DAT}_{ij}) + \beta_{7j} * (F_{0,t-1} * \text{DAT}_{ij}) + \varepsilon_{ij}; \varepsilon_{ij} \sim N(\mu, \sigma^2 * V)$ V = variance-covariance matrix (within core and run continuous temporal autocorrelations and errors to vary by run and MT			
		Intercept (Emersion)	-27.1	11.2	0.012
		Immersion	+135.2	17.3	$1.86 * 10^{-14}$
		$F_{0,t-1}$	+1.00	0.026	$1.64 * 10^{-178}$
		cPAR	-0.149	0.037	0.0001
		DAT	-0.09	0.059	0.0935
		$F_{0,t-1} : \text{Immersion}$	-0.367	0.037	$1.13 * 10^{-19}$
		DAT : Immersion	+0.129	0.038	0.0007
		$F_{0,t-1} : \text{DAT}$	-0.0003	0.0001	0.0011

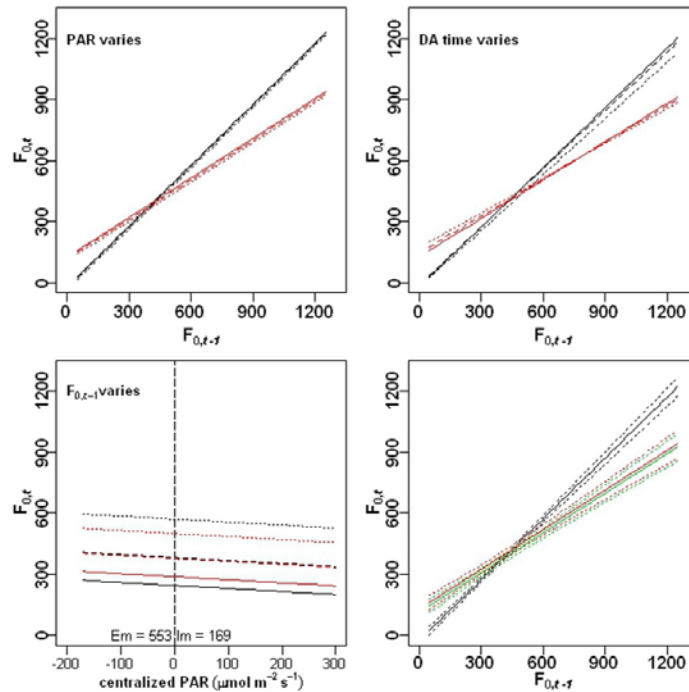


Figure 6.10: Estimated $F_{0,t}$ (Model 6.3) against $F_{0,t-1}$, where cPAR (top left) and DA time (top right) are represented in their 25th quantile (solid), 50th (dashed), and 75th quantile (dotted) and DA time (top left) and cPAR are at lowest (1s) and mean values (553 & 169), respectively. **Bottom left:** the estimated relationship between $F_{0,t}$ and cPAR, with $F_{0,t-1}$ at 25th (solid), 50th (dashed), and 75th quantile (dotted). **Bottom, right:** the estimated relationship between $F_{0,t}$ and $F_{0,t-1}$ (bottom right) between at emersion (black) and immersion with low (10 PAR) and high (450 PAR) irradiance (red and green, respectively) with bootstrapped (10000 draws) 95% confidence intervals.

In summary, pooled F_0 over all three runs was on average much greater during immersion than emersion (Figure 6.10, top plots, immersion intercept higher). F_0 decreased with increasing irradiance ($< 2\%$ decrease in F_0 per $100 \mu\text{mol PAR m}^{-2} \text{ s}^{-1}$) consistently in both tidal states (Figure 6.10, bottom left). Because emersion tides had higher irradiances than immersion tides, the estimated change from the previous measurement was steeper over emersion tides (Figure 6.10, top plots). The large difference between light levels during immersion tide ($458 \mu\text{mol PAR m}^{-2} \text{ s}^{-1}$) hardly affected the change in F_0 between consecutive measurements at all (Figure 6.10, bottom left). However, response to dark adaptation varied significantly ($p = 0.001$) between tidal states: with each minute of dark adaptation decreased F_0 slightly ($< 0.1\%$) during emersion, but increased F_0 slightly ($< 0.1\%$) during immersion.

6.3.5 Photosynthetic efficiency over the tidal cycle

Maximum light utilization efficiencies (F_v/F_m) at each MT and tide were estimated separately for each run (Model 6.1.2 & 6.2.2, where variance-covariance matrices, V , for all 3 runs had a within core continuous temporal autocorrelation structure and errors were categorically weighted by measurement time).

6.3.5.1 Run 1

Dark adapted maximum quantum efficiencies started at an estimated mean of 0.738 ± 0.002 and decreased to $0.673 (\pm 0.003)$ by the first measurement (Model 6.1.2, Figure 6.11a), where experimental lights had been on for ca. $1 \frac{1}{2}$ hours, and decreased further to $0.613 (\pm 0.003)$ by the end of emersion period. There was no further decrease during immersion and even a slight increase to $0.638 (\pm 0.006)$ by the third measurement (MT 8). At the start of the second emersion, the remaining biofilms had efficiencies just slightly lower (0.600 ± 0.008) than at the end of the first emersion. Overall (Model 6.2.2, Table 6.6), efficiencies during the 1st emersion (0.658 ± 0.002) were significantly lower than at the starting

efficiencies (0.733 ± 0.002 , $p = 1.2 \times 10^{-112}$), slightly higher than the immersion efficiencies (0.637 ± 0.006 , $p = 0.0003$), but much higher than the efficiencies at the 2nd emersion (0.604 ± 0.001 , $p = 4.8 \times 10^{-15}$).

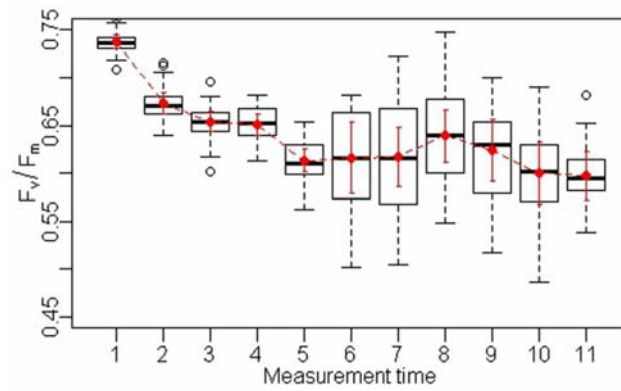
6.3.5.2 Run 2

Starting efficiencies were estimated at $0.732 (\pm 0.002)$ and dropped to $0.691 (\pm 0.004)$ by the first measurement, ca. an hour later. They continued to decrease reaching $0.632 (\pm 0.006)$ by the end of the first emersion (Figure 6.11b). During the immersion mean efficiencies increased from 0.631 ± 0.010 at the first measurement (MT 6) to $0.703 (\pm 0.007)$ at the last measurement (MT 9). By the first measurement of the subsequent emersion, mean efficiencies had returned to slightly lower levels than at the end of the first emersion $0.611 (\pm 0.012)$ and decreased further to $0.573 (\pm 0.015)$ by the last measurement (MT 12). Overall (Model 6.2.2, Table 6.6), efficiencies at the 1st emersion (0.653 ± 0.003) were significantly lower than the starting efficiencies (0.723 ± 0.003 , $p = 2.5 \times 10^{-63}$), slightly lower than the immersion efficiencies (0.683 ± 0.005 , $p = 6.7 \times 10^{-8}$), but much higher than the efficiencies at the 2nd emersion (0.585 ± 0.01 , $p = 1.6 \times 10^{-10}$).

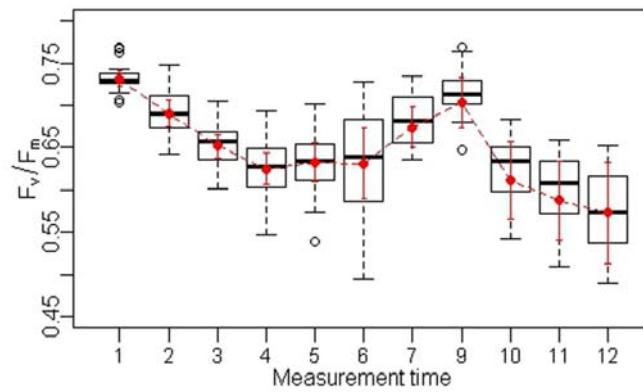
6.3.5.2 Run 3

Starting efficiencies were slightly lower than in the previous two runs at $0.724 (\pm 0.003)$. The initial decline after exposure to experimental lights but under immersion, ca. 3 h after starting time due to missed measurement (MT 2), was relatively small at $0.687 (\pm 0.005)$ and mean efficiency was still at $0.669 (\pm 0.006)$ at the end of the immersion tide (Figure 6.11 c). However, by first measurement of the subsequent emersion, ca. 2 h later, mean efficiency had dropped to $0.599 (\pm 0.006)$ and continued to decline thereafter to $0.551 (\pm 0.012)$ at the last measurement of the emersion. Overall (Model 6.2.2, Table 6.6), efficiencies at immersion (0.726 ± 0.003) were significantly higher than the starting efficiencies (0.616 ± 0.005 , $p = 1.8 \times 10^{-196}$) and the emersion efficiencies (0.684 ± 0.005 , $p = 5.1 \times 10^{-32}$).

(a)



(b)



(c)

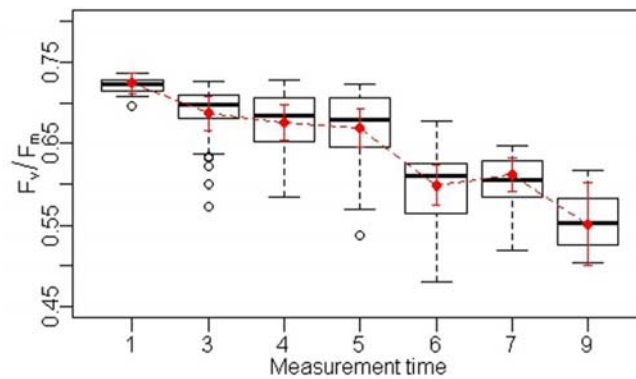


Figure 6.11 a, b, c: Boxplot comparing F_v/F_m at each measurement time for each run 1, 2, 3, respectively, with the red points, confidence intervals, and lines presenting the results of Model 6.1.2.

Table 6.5: Estimated means and confidence intervals of F_v/F_m for each tide (from Model 6.2.2) in each run. V represents a variance-covariance matrix in which errors vary by MT (factor) and have a continuous temporal autocorrelation (corCAR1) within each core; MT represents measurement time; DA time represents dark adaptation time. The p-values come from the t-tests within each model and the [†]p-values come from reparameterized models to test the difference between the 1st emersion and the immersion and 2nd emersion tides.

Run	DF (Res /Tot)	Tide	Lower 95% Confidence Interval	Estimated mean	Upper 95% Confidence Interval	t-test, p-value
1	$[F_v/F_m]_{it} = \beta_j * Tide_{ij} + \varepsilon_{ij} ; \varepsilon_{ij} \sim N(\mu, \sigma^2 * V)$					
	410/ 426	Start	0.730	0.733	0.737	0.000
		Emersion	0.653	0.658	0.663	$1.2 * 10^{-112}$
		Immersion	0.629	0.639	0.650	$7.9 * 10^{-51}$ [†] $2.8 * 10^{-4}$
		Emersion 2	0.593	0.604	0.615	$2.8 * 10^{-72}$ [†] $4.8 * 10^{-18}$
2	$[F_v/F_m]_{it} = \beta_j * Tide_{ij} + \varepsilon_{ij} ; \varepsilon_{ij} \sim N(\mu, \sigma^2 * V)$					
	310/ 326	Start	0.720	0.723	0.727	0.000
		Emersion	0.646	0.653	0.660	$2.5 * 10^{-63}$
		Immersion	0.673	0.683	0.694	$2.3 * 10^{-12}$ [†] $6.7 * 10^{-8}$
		Emersion 2	0.566	0.585	0.605	$2.1 * 10^{-33}$ [†] $1.6 * 10^{-10}$
3	$[F_v/F_m]_{it} = Tide_j * X_{ij} + \varepsilon_{ij} ; \varepsilon_{ij} \sim N(\mu, \sigma^2 * V)$					
	197/ 208	Start	0.717	0.723	0.729	$1.8 * 10^{-251}$
		Immersion	0.668	0.684	0.699	$1.2 * 10^{-14}$
		Emersion	0.599	0.614	0.631	$2.0 * 10^{-52}$ [†] $1.2 * 10^{-35}$

6.3.5.3 Summary of maximum photosynthetic efficiencies over tidal cycle

Starting (fully reduced PSII) efficiencies prior to sunrise were approximately 0.731 ± 0.002 and decreased over exposure time but less so during the immersion period (in runs 1 and 2 efficiency even recovered somewhat during the immersion). Maximum photosynthetic efficiencies followed the same declining trend with increasing light dose across all runs except for at low light levels during the immersion periods of runs 1 and 2 where maximum efficiencies were higher than expected (Figure 6.12).

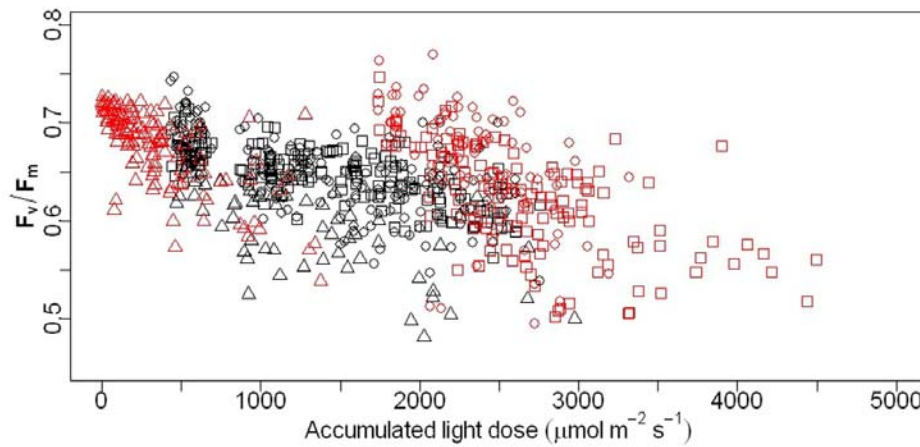


Figure 6.12: Photosynthetic efficiency by accumulated light dose in the first two tides (where emersion = black, immersion = red) of all three runs (run 1 = \square , run 2 = \circ , and run 3 = \triangle).

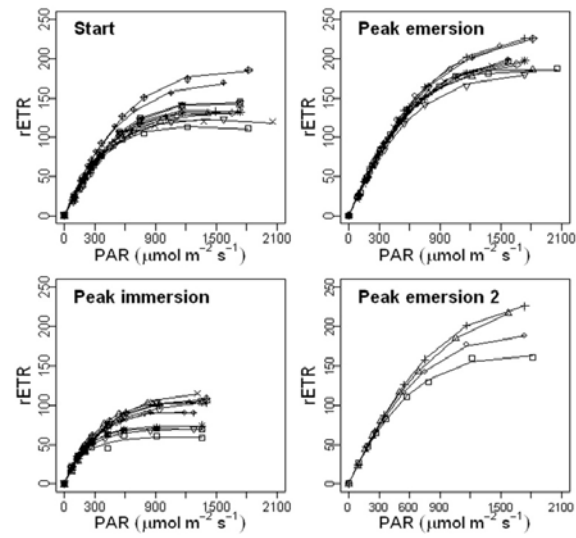
6.3.7 Are photosynthetic parameters ($rETR_{max}$, α , E_k) a response to tide, exposure time, or light intensity?

Rapid light curves from each tide for runs 1 – 3 (Figures 6.13 a, b, and c) show that while in the first two runs in most cores photosynthetic rates were reaching saturation within the maximum light step ($1660 \mu\text{mol PAR m}^{-2} \text{s}^{-1}$) at the start and during the immersion period, they were hardly reaching saturation during emersion, but this pattern was reversed in run 3 where immersion occurred first.

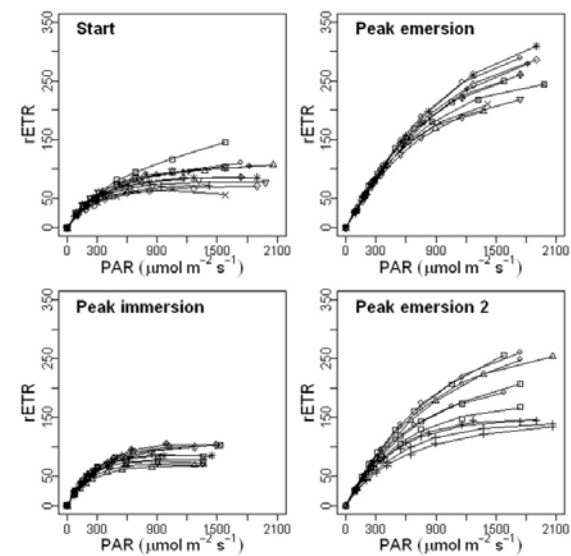
6.3.7.1 Maximum relative photosynthetic rate ($rETR_{max}$)

The RLCs of the first two runs (Fig. 6.13 a and b) clearly show that the maximum photosynthetic rate was much higher from the two emersions than from the immersion period. For run 1, mean estimated $rETR_{max}$ during the two emersions (Model 6.5.1 estimates in Table 6.6) were not significantly different from each other (res/tot DF = 36/40, $p = 0.810$) but were significantly higher than the immersion mean ($p = 5.5 \times 10^{-15}$) and the starting mean ($p = 1.4 \times 10^{-8}$). Maximum photosynthetic rate during the two emersion tides in run 2 (Table 6.6) were also not significantly different from each other (res/tot DF = 35/43, $p = 0.180$), but significantly higher than estimated mean at immersion ($p = 2.5 \times 10^{-15}$) and at the start ($p = 9.3 \times 10^{-15}$).

(a)



(b)



(c)

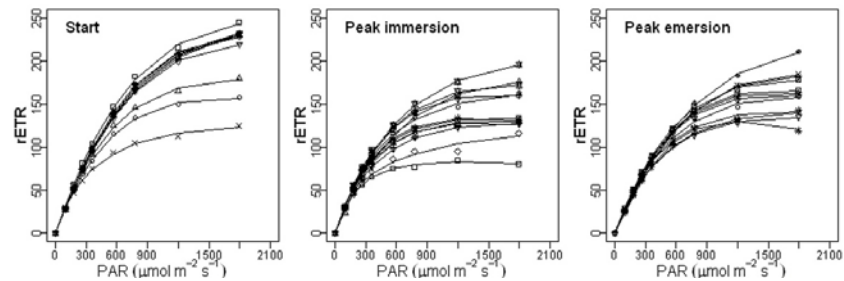


Figure 6.13a,b,c: Rapid Light Curves from runs 1 (a), 2 (b), and 3 (c) on selected cores at the start and near the peak of each subsequent tide.

Finally, RLC parameters from run 3 (Fig. 6.18 c) were not as different between starting, high and low tides as the first two runs (Table 6.6); estimated mean maximum photosynthetic rate at emersion was not significantly higher than at immersion (res/tot DF = 31/35, $p = 0.180$), but both were significantly lower than the starting mean ($p = 0.001$ for emersion and $p = 1 \times 10^{-17}$ for immersion).

The plot of pooled $rETR_{\max}$ from all runs against irradiance level suggests a slightly positive, linear correlation (Figure 6.14: top left). The final model (Table 6.7), estimated a single slope against irradiance (cPAR) but estimated a unique intercept for each run and tide. The overall effect of irradiance on maximum photosynthetic rate was estimated as $0.079 (\pm 0.023, p = 0.001)$: which means that with each $100 \mu\text{mol}$ increase in PAR maximum photosynthetic rate increases by only 8 points which means the full range of irradiance can only explain 52 points ($\sim 20.5\%$) where the full range of $rETR_{\max}$ values is 267.

Table 6.6: Estimated (Model 6.5) mean and 95% confidence intervals for photosynthetic parameters for each tide in each run. Means are in the centre with lower and upper confidence limits above and below. Variance-covariance matrices required in models were: categorical weighting of errors by measurement period for α in run 1, $rETR_{\max}$ in run 2, and E_k in run 2, as well as a within-core temporal autocorrelation in for α in runs 1

Tide	Start			Emersion			Immersion			Emersion2	
Run	1	2	3	1	2	3	1	2	3	1	2
$rETR_{\max}$	127	79	192	187	232	143	80	78	124	179	167
	139	90	212	200	258	163	92	87	143	198	219
	150	101	232	213	232	182	104	96	163	216	271
α	0.263	0.262	0.321	0.287	0.306	0.287	0.303	0.324	0.353	0.234	0.289
	0.284	0.283	0.331	0.309	0.315	0.302	0.324	0.345	0.373	0.266	0.306
	0.305	0.304	0.342	0.331	0.324	0.317	0.345	0.367	0.392	0.298	0.232
E_k	441	286	572	607	726	474	253	223	322	0.638	569
	487	318	645	655	822	544	299	256	392	0.638	702
	533	350	717	703	918	613	345	288	461	780	836

The intercepts for the tides between runs were significantly different in each run: the highest intercept at emersion was at run 2 (258 ± 10.9) which was significantly higher than that at run 1 (200.4 ± 5.0) and run 3 (164.5 ± 8.8). Immersion intercepts for runs 1 to 3 were $180.2 (\pm 7.0)$, $201.7 (\pm 15.7)$, and $254.7 (\pm 12.3)$, respectively. Most notably though, the ranges of the starting $rETR_{\max}$ values,

184.7, represents 69% of the range of values at subsequent two tides, 266.9 but as the same cores were not tested at each peak tide a correlation could not be fitted to account for it.

6.3.7.2 *Initial slope (α)*

In run 1, estimated (Model 6.5.2 estimates in Table 6.6) mean α in the first emersion and subsequent immersion were not significantly different (res/tot DF = 31/40, $p = 0.281$) but significantly higher than the starting mean ($p = 0.0001$) and final emersion ($p = 3.7 \times 10^{-7}$). In run 2, mean α at immersion was significantly higher than the both daytime emersions (res/tot DF = 35/43, $p = 0.021$), as the two emersion means were not significantly different from each other ($p = 0.180$), and significantly higher than mean α at the start ($p = 0.023$). In run 3, α during the immersion tide was significantly higher at the start ($p = 0.001$) but not significantly higher than at emersion ($p = 2.3 \times 10^{-7}$).

There is a negative linear trend between α and ambient PAR in the pooled data from the first 2 tides of all runs (Figure 19: top right). However, while no significant change in α with increasing PAR was estimated (Model 6.6) for emersion (Table 6.7, $cPAR_{em} = -0.0001$, $p = 0.099$), there was a significant estimated decline in α with increasing PAR at immersion ($cPAR_{im} = -0.0002$, $p = 0.019$).

6.3.7.3 *Saturation light coefficient (E_k)*

In run 1 mean estimated E_k at both emersions, were not significantly different from each other (res/tot DF = 36/40, $p = 0.21$), but were twice as high as at immersion ($p = 6.5 \times 10^{-13}$) (Model 6.5.3 estimates in Table 6.6). The starting value lay between emersion and immersion values and was significantly different from both of them ($p = 1.0 \times 10^{-5}$ and $p = 1.0 \times 10^{-6}$, respectively). In run 2 E_k followed the same pattern as in run 1, i.e. estimates for emersions 1 and 2 did not differ significantly ($p = 0.150$), but the estimated emersion mean was significantly higher than in the subsequent immersion ($p = 8.1 \times 10^{-14}$) and from the start ($p = 2.4 \times 10^{-12}$). During run 3 the estimated emersion mean was again significantly

higher ($p = 0.004$) than the immersion mean E_k (391.8 ± 34.2) but not significantly different ($p = 0.049$) from the mean starting E_k which was actually slightly higher (644.7 ± 35.7).

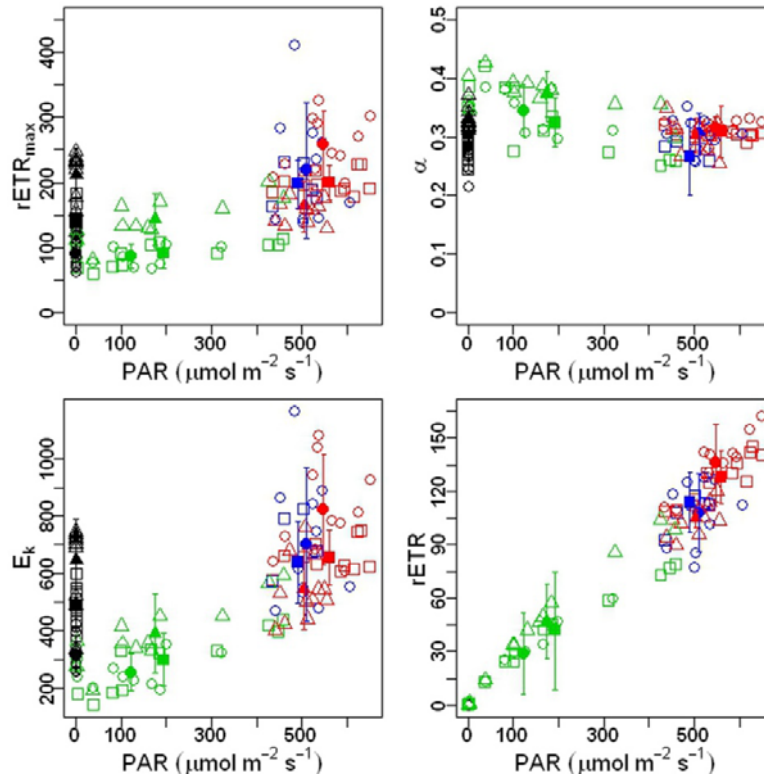


Figure 6.14 : Photosynthetic parameters (clockwise from top left: $rETR_{\text{max}}$, α , $rETR$, and E_k) against PAR at each core in runs 1 (\square), 2 (\circ), and 3 (Δ) showing starting values (black), 1st emersion (red), immersion (green), and 2nd emersion (red). Solid characters represent estimated means and 95 % confidence intervals for each tide and run.

There was a positive trend between pooled E_k from the all runs and tides against ambient PAR (Figure 6.14: bottom left). While there was a good deal of scatter at the top of the relationship, a single significant positive slope was estimated (Model 6.6.3) between E_k and PAR (Table 6.6, $\text{est} = 0.47$, $p < 0.0001$) for the first two tides across all runs. An increase in $100 \mu\text{mol PAR m}^{-2} \text{s}^{-1}$ light intensity increases E_k by 47, which means that over the full range of PAR E_k can vary by 305.5 which is 32.4% of the full variance of the observed E_k values (942).

Table 6.7: Estimated intercepts and slopes of from (Model 6.6) applied to each photosynthetic parameter with centralized PAR (cPAR) as covariate and runs and tide as a factor. V represents a variance-covariance matrix. Estimates are relative to intercept (ie. they are not independent values).

AICc	resDF/ totDF	Parameter for	EST	Std Error	p-value
646.7	53/68	$rETR_{maxij} = \text{Run} * \text{Tide}_{ij} * cPAR_{ij} + \varepsilon_{ij}; \varepsilon_{ij} \sim N(\mu, \sigma^2 * V)$ V = categorical weighting of errors by run			
634.8	58/68	$rETR_{maxij} = \beta_0 * \text{Run} + \beta_1 * \text{Tide}_{ij} + \beta_2 * cPAR_{ij} + \beta_3 * (\text{Run}_i * \text{Tide}_{ij}) + \varepsilon_{ij}; \varepsilon_{ij} \sim N(\mu, \sigma^2 * V)$			
		Intcpt (Run 1:em)	200.4	5.0	$2.9 * 10^{-35}$
		Run 2	57.3	10.9	$1.3 * 10^{-6}$
		Run 3	-35.9	8.8	0.001
		Run:Tide (1,im)	-110.4	7.0	$1.9 * 10^{-15}$
		Run:Tide (2,im)	-56.0	15.7	0.0006
		Run:Tide (3,im)	90.2	12.3	$5.6 * 10^{-8}$
		cPAR	0.079	0.023	0.001
-303.4	54/68	$\alpha_{ij} = \beta_0 * \text{Run} * \text{Tide}_{ij} * cPAR_{ij} + \varepsilon_{ij}; \varepsilon_{ij} \sim N(\mu, \sigma^2 * V)$ V = categorical weighting of errors by tide			
-302.8	58/68	$\alpha_{ij} = \beta_0 * \text{Run} + \beta_1 * \text{Tide}_{ij} + \beta_2 * cPAR_{ij} + \beta_3 * (\text{Run}_i * \text{Tide}_{ij}) + \varepsilon_{ij}; \varepsilon_{ij} \sim N(\mu, \sigma^2 * V)$			
		Intcpt (Run 1-em)	0.306	0.008	$8.2 * 10^{-54}$
		Run 2	0.01	0.011	0.213
		Run 3	-0.006	0.011	0.460
		Run:Tide (Run 1-im)	0.023	0.012	0.026
		Run 2:Tide	-0.003	0.016	0.760
		Run 3:Tide	0.051	0.015	0.002
		cPAR-em	-0.0001	0.00004	0.099
		cPAR-im	-0.0002	0.00006	0.019
814.7	54/68	$E_{k,ij} = \beta_0 * \text{Run} * \text{Tide}_{ij} * cPAR_{ij} + \varepsilon_{ij}; \varepsilon_{ij} \sim N(\mu, \sigma^2 * V)$ V = categorical weighting of errors by tide			
806.1	59/68	$E_{k,ij} = \beta_0 * \text{Run} + \beta_1 * \text{Tide}_{ij} + \beta_2 * cPAR_{ij} + \beta_3 * (\text{Run}_i * \text{Tide}_{ij}) + \varepsilon_{ij}; \varepsilon_{ij} \sim N(\mu, \sigma^2 * V)$			
	59/68	Run 1	656	34.5	$2.5 * 10^{-27}$
		Run 2	166	48.8	0.0012
		Run 3	-99.4	47.8	0.042
		Run 1-Tide:im	-367.9	38.5	$9.8 * 10^{-14}$
		Run 2- Tide:im	-173.5	55.2	0.0026
		Run 3- Tide:im	208.9	53.5	0.0002
		cPAR	0.47	0.07	$2 * 10^{-9}$

6.4 Discussion

6.4.1 Migratory response of MPB (F_0) to diurnal and tidal cycles and light variation.

The primary aim of this experiment was to determine whether MPB were active during immersion and whether different light levels under immersed conditions would modify their behaviour and physiology. The bulk of the previous literature on the subject suggested that surface biomass would decrease dramatically during the immersion tide due to entrained rhythms (Round & Palmer 1966; Pinkney & Zingmark 1991; Hay 1993; Guarini *et al* 2000a; Serôdio *et al* 2001; Honeywill 2001; Consalvey 2002; Jesus *et al* 2006). However, some studies did show that in shallow, relatively clear water MPB would remain at the surface throughout the tidal immersion, presumably as there is sufficient light for photosynthesis (Fauvel & Bohn 1904; Aleem 1950; Perkins 1960, Hopkins 1966), so it could be perhaps be quantified as continuous response with respect to irradiance. This experiment was designed to examine the natural migratory responses under different *in situ* tidal cycles so that migration could be attributed to *in situ* tidal pattern or laboratory light intensity. Hence, irradiance at emersion was kept as high as laboratory conditions would allow ($> 400, < 600 \mu\text{mol PAR m}^{-2} \text{ s}^{-1}$, still well below outdoor irradiance on a sunny day) and irradiance at immersion was designed to capture a range of conditions from almost no light ($1 \mu\text{mol PAR m}^{-2} \text{ s}^{-1}$) to approximately emersed light intensities ($> 400 \text{ m}^{-2} \text{ s}^{-1}$). *In situ* tidal cycles were maintained in the laboratory but *in situ* diurnal cycles were not in order to (1) monitor surface biomass by irradiance over a full emersion and immersion tide (which day length in September-October would not allow), and (2) compare surface biomass at daytime and night-time emersion. Over diurnal cycles night-time surfacing would occur given the same level of irradiance as during daytime emersion.

The unexpected result was that the surface biomass did, roughly, follow *in situ* tidal patterns but rather than reaching during maximum levels during emer-

sion, maximum levels were reached during immersion regardless of *in situ* diurnal cycles or experimental irradiance level (Figure 6.7 a – c and Figure 6.8 a – c). In all 3 runs, surface biomass was significantly higher during immersion than during emersion (Model 6.2.1, run 1 $p = 4.5 \times 10^{-7}$; Model 6.2.1, run 2: $p = 6.5 \times 10^{-40}$; Model 6.1.1 run 3: $p = 4.6 \times 10^{-5}$, details described in section 6.3.3.3). There are several possible explanations for this phenomenon. First, it is possible that this is an artefact of fluorescence methodology. At immersion there could be a slight resuspension of surface sediment meaning that F_0 readings are higher either because the photosynthetic biomass is effectively closer to the probe (Figure 6.5) or because measuring light can penetrate deeper into the sediment. There is some evidence for this possibility in run 3 which had extremely low starting biomass levels compared to the previous runs, and yet following immersion there was a 200% increase in surface biomass which then dramatically declined upon emersion, even though emersion started 4 hours prior to *in situ* sunset. The MPB assemblage in this run consisted of a much larger proportion (39 %) of semi-motile and non-motile epipsammic diatoms which may have only received light once the sediment layers were loosened at immersion. This could have been examined within the experiment had a subset of dark- and non-tidally-maintained cores been monitored alongside the experiment cores over the tidal cycle or had a second, night-time, immersion been monitored (just as in runs 1 and 2 a second emersion tide was monitored to elucidate diurnal cycles). Had the “control” cores not shown the same level of change in surface biomass at immersion, or had the measurements at the 2nd immersion 5 hours after sunset shown a dramatic increase in surface biomass, this would have been a good indication that high F_0 levels were not due to active migration to the surface but due slight resuspension of surface sediment. However, if this is the case, it does not necessarily negate all the experimental results; light attenuates much faster through a few mm of sediment than through a water column, so if the photic depth increases at immersion this would still result in more photosynthetically active biomass. Another possibility is that because all three

biofilm slurries were a mixture of diatoms from different microhabitats at the site (the open mudflat (unshaded), the sediment along the edges of rocks overhung with *Fucus* (partially shaded), and from underneath Guardbridge itself (shaded)), there was quite a large contingent of diatoms that were acclimated to low light intensities and hence would have preferred immersion conditions in the laboratory to emersed conditions. Finally, water depth the peak of spring immersion at the site was < 1 m, which, in combination with low flow rate and low turbidity (compared to the paper mill site) means that light levels may not be prohibitive and the diatoms at this site may be accustomed to photosynthesising during immersion.

Another unexpected result was that cells appeared to assemble at the surface prior to emersion and sunrise. In run 1, where *in situ* sunrise occurred several hours prior to the start of the experiment, mean surface biomass was higher at the starting measurement than over the rest of the emersion period. This means that cells were already at the surface during the sunrise immersion, and, when the experimental lights came on they migrated downwards to protect themselves from high irradiation (Perkins *et al* 2010). In run 2, where *in situ* sunrise occurred almost simultaneously with the start of the emersion period, surface biomass remained relatively consistent or increased somewhat over the emersion tide. Again, cells were already assembling at the surface at measurement time 1, prior to emersion (and sunrise). Assemblage of cells at the sediment surface at (or prior to) sunrise implies that this was either an extremely fast phototactic response or that there is an entrained rhythm that is specific to environmental conditions at the site (as described above). As measurements of vertical migration speed in diatoms range between $612 - 1,008 \mu\text{m h}^{-1}$ (Hopkins 1963; Harper 1977; Hay *et al* 1993), it is unlikely that they did not begin migrating until they sensed light. Therefore, it is more likely that there is a site-specific “expectation” of light and hydrodynamic conditions.

A final indicator of entrained tidal-diurnal rhythm was that cells did not migrate to the surface at the night-time emersion regardless of the availability of

light in the laboratory. In both runs 1 and 2 where there was a night-time emersion, cells migrated downward from the end of the evening immersion period onward and in both runs surface biomass at the second emersion was significantly lower than during the first emersion (Table 6.3: Model 6.2.1 run 1, $p = 5.4 \times 10^{-46}$; Model 6.2.1, run 2, $p = 1.7 \times 10^{-47}$). Aleem (1950) found that while in the field (Whitstable, UK) diatoms would not be coaxed to the surface by artificial light, in the laboratory they surfaced readily at night given sufficient light. His second observation was corroborated by Perkins (1960) with diatoms from the Eden estuary. However, according to Saburova and Polikarpov (2003) diatoms require a downward migration to more nutrient-rich depths in the sediment for cell division. If the diatoms at this site are accustomed to remaining at the surface throughout the daylight hours, regardless of tidal state, then they would require the night-time for cell division and reproduction. Interestingly, in run 1, where the first half of the immersion occurred around sunset, cells still maintained their surface positions and only started migrating away from the surface midway through the tide, when it would have been dark (Figure 6.7 a). In addition to entrained bulk migration, there was a small amount of migration in response to experimental variation in light levels. Not enough data on the really low (< 50) end of ambient light to give a clear pattern but as dark adaptation took place in < 4 PAR and responses varied.

F_0 measurements were made following five minute dark adaptation times as Serôdio *et al* (2001) found that it was a stable measurement over a large range of irradiances. However, as 88 measurements were made at each measurement time, the full extent of dark adaptation time by the final measurement could be as high as 900 seconds (15 minutes) over the initial 5 minutes dark adaptation time. As previously described by Jesus and colleagues (2006a, 2006b) surface biomass at emersion decreased with increasing dark adaptation time: each additional minute of dark adaptation reduced F_0 by ~ 5 units. The dark adaptation effect was less extreme at irradiance (an increase of 2.3 for each additional dark adaptation time), presumably because there was less of a difference between

ambient light and light levels during dark adaption ($\sim 4 \mu\text{mol m}^{-2} \text{s}^{-1}$). Jesus and colleagues 2000b recommend low light (5 % of ambient light) or far red adaptation to reduce diatom migratory response. To stagger each of the 88 measurements so that each only received only 5 minutes of dark adaptation would require an unreasonable effort given the relative smallness of the effect.

In conclusion, the overall migration patterns of MPB seemed to be determined by *in situ* conditions at the Guardbridge site. Cells migrated to the sediment surface prior to or at sunrise regardless of tidal state and remained at the surface for at least half of the tide but sometimes migrated downwards prior to tidal change. Cells were more abundant at the surface during immersion than emersion, which suggests that bulk migration is probably a site and species specific response. Cells remained at the surface prior to *in situ* sunset as long as there was light (even $1 \mu\text{mol PAR m}^{-2} \text{s}^{-1}$) and did not return to the surface following *in situ* sunset, regardless of light availability. However, there was a small but significant amount of migration away from the surface in response to increasing light intensity which was consistent between tidal states (15 ± 4 units per $100 \mu\text{mol PAR m}^{-2} \text{s}^{-1}$, $p = 0.0001$). This suggests that while variation in light levels during the day does not drive bulk migration but rather causes cells micro-cycle to find optimum light levels (Perkins *et al* 2010). However, while the general response to ambient light levels did not vary between tides, at very low light levels, such as during dark adaptation ($< 4 \mu\text{mol PAR m}^{-2} \text{s}^{-1}$) behaviour did vary between tidal state: at emersion exposure to very low light drove cells away from the surface as described previously (Jesus *et al* 2006a, 2006b) but at immersion it drove them upwards, which has not been previously reported.

6.4.2 Vertical migration and maximum light utilization efficiency

The maximum photosynthetic efficiency over measurement times (Figure 6.11) in each run decreased with duration of exposure. The decrease with increasing exposure time is clearly less steep during immersion tides compared to emersion tide, indeed in run 2 F_v/F_m actually increases within immersion tide. In

runs 1 and 2 where the first tide is emersion the mean F_v/F_m over these tides are significantly lower (10% drop, $p = 1.2 \times 10^{-112}$ and 2.5×10^{-63} , respectively) than the starting values, but over subsequent immersion, which is roughly the same amount of time, the change in F_v/F_m is only a 3 % decrease in run 1 ($p = 2.8 \times 10^{-4}$) and a 4 % increase ($p = 6.7 \times 10^{-8}$) in run 2. In run 3 where the immersion occurred first in the day the initial decrease from starting values was only 5.4% ($p = 1.2 \times 10^{-14}$) where as at the subsequent emersion (again approximately the same length of time) there was another 10% decrease ($p = 1.2 \times 10^{-35}$). The logical assumption, and indeed the assumption supported by the literature (Perkins *et al* 2011 and Consalvey *et al* 2005 and references therein) is that photosynthetic efficiency decreases with increased irradiance (due to the increase in NPQ) which is higher at emersion. However, the plot of F_v/F_m against irradiance (Figure 6.12, column 2) clearly shows that this is not the case at emersion in the first two run though it is the case in run 3. This means that at emersion, where there is less variation in irradiance, the decline in maximum efficiency is clearly a more a response to exposure time. At immersion in runs 1 and 2 there is a clear covariance between irradiance and maximum efficiency but less so at immersion in run 3. This clearly shows that the effect of irradiance level on efficiency increases with exposure time and is therefore a response to the total “light dose” a biofilm has received (Perkins *et al* 2010, 2011).

The regression of efficiencies against previous values, irradiance, and dark adaptation times (Model 6.3, Table 6.7) showed no significant effect of irradiance on efficiency at emersion ($+0.00002$, $p = 0.547$) but a much larger effect at immersion (-0.0001 , $p = 3.9 \times 10^{-7}$). While this effect is not particularly large over the 25th, 50th and 75th quantile of irradiance ranges at emersion and immersion (Figure 6.13, top left), it is more apparent in the plot against cPAR (Figure 6.13, bottom left) and (Figure 6.13, bottom right) the plot.

As discussed in the introduction, Serôdio *et al* (2001) found that at immersion biomass was distributed at lower depths so that the weak measuring light ($< 4 \mu\text{mol m}^{-2} \text{s}^{-1}$) did not penetrate to the biomass, hence the underestimation of bi-

omass by a factor of 0.66. However, the saturating flash is much more powerful ($\sim 8600 \mu\text{mol m}^{-2} \text{s}^{-1}$) and hence F_m measurement is integrated over deeper cell layers, and as a result maximum efficiency is overestimated (Perkins *et al* 2011). So it is possible that immersion efficiencies are simply inflated due to this overestimation. However, in these biofilms the reverse is the case, emersion has lower F_0 values and hence diatoms they are more are more likely present in lower layer of sediment, meaning that emersion efficiencies measured here are actually overestimations. Another reason, and the more likely one, for the shallower decrease and/or increase in efficiency during the immersion tide could be due to recovery from NPQ (Serôdio *et al* 2005; Perkins *et al* 2011). Non-photosynthetic quenching of fluorescence by xanthophyll cycling (see General Methods 2.4.2.2) increases over exposure to protect photosystems from excess light but can be reversed at low light conditions (Serôdio *et al* 2005; Jesus *et al* 2006).

6.4.3 Are photosynthetic parameters (rETR, rETR_{max}, α , E_k) a response to tide, exposure time or irradiance?

Ambient photosynthetic parameters were calculated from rapid light curves on selected cores without previous dark adaptation so the rETRs estimated are not maximum potentials but the actual rates of the biofilms. There are 4 parameters of interest in a P-E curve (see General Methods 2.4.2.2) which is an asymptotic growth curve: the initial, linear, rate of increase of photosynthetic rate per unit irradiance (α), the irradiance at which the linear increase ends (E_k), the maximum rETR (rETR_{max}) and the irradiance at saturation (E_s). The rETRmax is actually a function of the initial slope and saturation energy that is required to reach the maximum photosynthetic rate (E_s). However, in the Eilers and Peeters (1988) model the reverse approach is used: the 3 parameters estimated from empirically measured RLCs to calculate rETR_{max} and α , which are then used them to calculate E_k ; E_s is not used.

The RLCs (Figure 6.14a-c) show clearly that saturation energy and $rETR_{max}$ are much higher at emersion than immersion tides. These differences are mostly due to the fact that at emersion, higher irradiance activates xanthophyll cycles which increase NPQ resulting in more energy being diverted from photosynthetic pathway and therefore more energy is required to saturate the photosynthetic pathway (Falkowski & Raven 2007). However, as demonstrated by Perkins and colleagues (2006) acclimation of cells (increased NPQ) during RLCs with increasing light steps can mean overestimation of $rETR_{max}$ and E_k and underestimation of α . In addition, Jesus and colleagues (2006) found that the other adaptation to higher light level, downwards migration, can also occur during the RLC and will also cause overestimation of $rETR_{max}$ and E_k . RLC curves generated by decreasing lightsteps (as recommended by Perkins *et al* 2006) would probably have resulted in lower and more accurate $rETR_{max}$ and E_k estimates at emersion but these were not done as the automated RLC in the Diving-PAM allows choice in actinic light levels but not direction of application.

The effect of exposure time on photosynthetic parameters is best compared by comparisons of parameters between the first and second emersions in runs 1 and 2 which were about 12 hours apart but otherwise under the same conditions. $rETR_{max}$ were not significantly different between in either run (run 1: res/tot DF = 36/40, $p = 0.810$; run 2: res/tot DF = 35/43, $p = 0.180$) and neither are E_k (run 1: res/tot DF = 36/40, $p = 0.021$; run 2: res/tot DF = 35/43, $p = 0.150$). In the first run α was significantly lower in final emersion than in the first (res/tot DF = 36/40, $p = 3.7 \times 10^{-7}$) but not so in the 2nd run (res/tot DF = 35/43, $p = 0.150$). However, when the pooled photosynthetic parameters are compared graphically (Figure 6.15) the distributions of parameters at emersion 1 (red symbols) and emersion 2 (blue symbols) more or less completely overlap (with one high outlier from the 2nd emersion). This is somewhat suspicious as there should have been much higher NPQ during the 2nd emersion than in the first and, therefore, higher $rETR_{max}$ and E_k . This result is probably actually confounded by overes-

timation of these parameters (Serôdio 2005; Perkins *et al* 2011) because surface biomass was significantly lower in the second emersion (see Figure 6.8a & b and Table 6.3).

Regressions of photosynthetic parameters $rETR_{max}$, and E_k from the daytime tides against cPAR show that there is a universal and significant response to light intensity at each parameter ($rETR_{max}$: res/tot DF = 58/68, $p = 0.001$; E_k : res/tot DF = 59/68, $p = 2 \times 10^{-9}$) but that magnitude of the parameters vary by runs and tides. For α , the relationship to cPAR varied by tide and was only significant at immersion (res/tot DF = 58/68, $p = 0.10$ and $p = 0.02$ at emersion and immersion, respectively). Most interesting though is that almost all of the full variation of each parameter were already present in the cores at the start of each experiment (black symbols) before any differences in light regimes were applied. And yet the between tides tests within runs showed significant differences of parameters at each tide when compared to the start almost across the board (with the exception of the $rETR_{max}$ at immersion in run 2).

The regression of rETRs at each cores PAR intercept had to be constrained to 0 and the best fitting model as a result split the data along light intensities and irrespective of tide or runs (time along spring-neap cycle, tidal and diurnal cycle, MPB assemblage). At $\leq 200 \mu\text{mol m}^{-2} \text{s}^{-1}$ the rate of rETR increase with each additional μmol of light was $0.31 (\pm 0.01)$, and at $\text{PAR} > 200 \mu\text{mol m}^{-2} \text{s}^{-1}$ the rate of increase is $0.227 (\pm 0.003)$. Within this pattern run 1 and 2 residuals of immersion values are slightly lower and run 3 residuals are slightly higher reflecting the reduction in efficiency at higher exposure times, but adding tide or run to this model did not improve it. What is clear, is that during immersion rETRs are lower because incident light is lower, they are not qualitatively different from emersion. In this experiment there were no emersion cores at $\leq 200 \mu\text{mol m}^{-2} \text{s}^{-1}$, so they could not be compared but this could easily be carried out in future. Irradiances of $> 200 \mu\text{mol m}^{-2} \text{s}^{-1}$ at immersion are purely hypothetical though and are not likely to occur in anything deeper than a 5 cm water column. Some very rough calculations of photosynthetic output over a day (Day

P_{fluo}) assuming constant rETR (as estimated) over the full tide (unlikely), core mean immersion PAR values of 0, 10, 50, and 100 $\mu\text{mol m}^{-2} \text{s}^{-1}$, and constant mean F_0 at immersion and emersion (also unlikely) which are estimated from the data, multiplied up to an hourly rate and then summed over the full number of immersion and emersion hours in the tidal cycles represented in runs 1,2,3. The ratio of total daily gross photosynthetic production (per m^2) at each PAR value is then compared to the value when assuming that there is no production during immersion tides, as is predicted by the model of Guarini and colleagues (2000b). The ratios assuming 10 PAR at immersion are all more or less the same as at 0 PAR and, when the tidal cycles has emersion at midday (run 1) it also suggests that photosynthetic output during immersion is irrelevant regardless of PAR and F_0 at immersion. Only when PAR is ≥ 50 and peak daylight hours fall at immersion and F_0 is quite high by comparison to emersion F_0 at low tide, does their model underpredict photosynthetic output at the site (0.6x, 0.72x, 0.76x). So if most of the time irradiance at the sediment bed is < 50 PAR, which is probably the case, it begs the question of why are diatoms surfacing at these times?

Table 6.8: Rough calculations for total photosynthetic output (per m^2) at different tidal cycles and irradiances.

Run	Em PAR	Im PAR	Em hrs (day)	Im hrs (day)	Em F_0	Em F_0	Em rETR	Im rETR	Day P_{fluo}	as ratio of Im = 0
1	550	0	6.25	6.50	698	0	4.4×10^{-4}	0	9.8×10^{-8}	
	550	10	6.25	6.50	698	335	4.4×10^{-4}	5.1×10^{-2}	9.9×10^{-8}	0.99
	550	50	6.25	6.50	542	449	3.4×10^{-4}	3.4×10^{-3}	8.4×10^{-8}	1.16
	550	100	6.25	6.50	569	599	3.6×10^{-4}	9.2×10^{-3}	1.0×10^{-9}	0.97
2	550	0	7.00	5.50	285	0	1.8×10^{-4}	0	4.5×10^{-8}	
	550	10	7.00	5.50	285	466	1.8×10^{-4}	7.1×10^{-2}	4.6×10^{-8}	0.97
	550	50	7.00	5.50	429	519	2.7×10^{-4}	4.0×10^{-3}	7.5×10^{-8}	0.6
	550	100	7.00	5.50	317	409	2.0×10^{-4}	6.3×10^{-3}	6.2×10^{-8}	0.72
3	550	0	6.25	4.25	161	0	1.0×10^{-4}	0	2.3×10^{-8}	
	550	10	6.25	4.25	161	282	1.0×10^{-4}	4.3×10^{-2}	2.3×10^{-8}	0.97
	550	50	6.25	4.25	133	312	8.3×10^{-4}	2.4×10^3	2.2×10^{-8}	1.01
	550	100	6.25	4.25	150	366	9.4×10^{-4}	5.6×10^{-3}	3.0×10^{-8}	0.76

So it is necessary to determine whether the high surface biomass levels measured at immersion are simply an artefact of slightly 'looser' surface layers during immersion leading to deeper penetration of measuring light up- and downwelling, leading to an overestimation of biomass.

The above calculation could be made much more accurately by repeating the experiment without the RLCs but with 2 series of single saturating flash measurements at each core over the tidal cycle, once without dark adaptation ($\Delta F/F_m'$) to calculate actual rETR followed by a series with dark adaptation (F_v/F_m) to determine F_0 . The photosynthetic rate over the entire tidal period could then be monitored for each core using the fluorescence based index (developed by Serôdio, Perkins *et al* 2011)

$$P_{\text{fluo}} = F_0 \times \text{rETR}$$

P_{fluo} could then be integrated over the full tidal period and regressed against irradiance at each core to determine the effects of turbidity on productivity at a site (comparing sites as discussed above). It would have to be borne in mind that these would be based on instantaneous tidal and irradiance change whereas in fact change in irradiance is a gradual process as the tide ebbs and flows. These measurements could also be used to compare F_0 to F_0' and F_v/F_m to $\Delta F/F_m'$ to determine how much of an effect dark adaptation really has on biomass and efficiency estimation.

6.4.4 For further investigation

An interesting follow up to this experiment would be to compare migratory patterns over the same tidal cycle between diatoms from this site in one tray to those from a different site, more exposed during emersion, and with either deeper water during immersion or a macrofaunal assemblage dominated by *Corophium volutator*.

6.5 Conclusion

1. While migration patterns vary with tidal pattern for the populations of diatoms, it seems clear that they will surface during immersion. It is likely that this is not a result of experimental irradiance as it had a relatively small effect on surface biomass but due to *in situ* tidal patterns. The intertidal SE bank of the Eden at Guardbridge has a depth of $\sim 1 - 1.5$ meters at peak immersion, unknown (though probably low) flow rates, and the sediment is dominated by *Nereis diversicolor* rather than *Corophium volutator*, suggesting low turbidity at immersion (see Chapter 4).
2. Maximum photosynthetic efficiency is higher during immersion than emersion but overall is dependent on exposure hours.
3. In order to estimate daily photosynthetic output at this particular site, average PAR over the tidal cycle needs to be estimated more accurately as well as the accuracy of biomass estimates by fluorescence, F_0 , at immersion vs. emersion (by comparison to O_2 production over known depths at immersion vs. emersion).

Chapter 7: General Discussion

As stated at the outset, the primary aim of this thesis was to determine whether the engineering activities of *C. volutator* can modify resource flows to MPB, whether these modifications exert selective pressure which can change MPB biomass and assemblage composition and, ultimately, whether these modifications could potentially exert selective pressure on *C. volutator* themselves. The deleterious effects of infauna feeding on MPB are well established (Nielsen & Kofoed 1982; Daborn *et al* 1993; Gerdol & Hughes 1994a, 1994b; Hagerthey *et al* 2002; de Deckere *et al* 2001; de Deckere 2003; Dyson *et al* 2007; Hicks *et al* 2011). This implies that *C. volutator* are destroying their own habitat and reducing the survival chances of their offspring, i.e. a case of 'negative niche construction', which are "...activities that change environments in such a way as to reduce the fitness" (Odling-Smee *et al* 2003). Furthermore, several studies have demonstrated that active bioturbators can significantly alter water column turbidity (de Deckere *et al* 2000; Biles *et al* 2002), sediment – water nutrient fluxes (Henriksen *et al* 1980, 1983; Andersen & Kristensen 1988; Pelegri & Blackburn 1994; Pelegri *et al* 1994, 1995; Rysgaard *et al* 1995; Emmerson *et al* 2001; Mermillod-Blondin *et al* 2004; Michaud *et al* 2006; Ieno *et al* 2006; Bulling *et al* 2010), and microbial metabolism (Hargrave 1970; Sørensen 1978; Henriksen *et al* 1980; Pelegri & Blackburn 1994; Pelegri *et al* 1994, 1995; Rysgaard *et al* 1995; Aller & Aller 1998; Mermillod-Blondin *et al* 2004, 2005; Michaud *et al* 2006). However, whereas increased sediment resuspension and turbidity are likely to have further deleterious effects on MPB populations (further negative niche construction), increased availability of nutrients in the overlying water column could have regenerative effects on MPB populations (positive niche construction). The current study investigated what effects *C. volutator* engineering had on MPB assemblage bio-

mass and composition in comparison to their trophic effects and in comparison to other bioturbators.

7.1 Bioturbation modifies the overlying water column and resource flow to MPB

Experiments 1, 2 and 3 clearly demonstrated that *C. volutator* significantly increased the turbidity of the overlying water column by increasing the suspended sediment load and that this reduced light penetration to the substratum. Bioturbation also increased nutrient concentrations in the overlying water but less demonstrably and consistently so than turbidity.

7.1.1 Suspended sediment, turbidity and light attenuation

Turbidity was demonstrated to increase linearly and significantly ($p < 0.0001$) with increasing *C. volutator* biomass (Figure 3.8; Table 3.3, Model 3.12). This corroborates previous findings that suspended sediment in the water column increased with increasing *C. volutator* biomass (de Deckere *et al* 2000). It is likely that this increase would have become asymptotic had larger *C. volutator* biomasses been investigated (Biles *et al* 2002). As there was no significant water flow in these experiments, sediment resuspension occurred only by active resuspension and not by increased physical erosion due to biofilm consumption. After 6 days incubation in sediment columns containing a MPB biofilm, compared to the control treatments (Table 4.3, Model 4.15), *C. volutator* generated the most turbidity (104 ntu, $p < 0.0001$), *H. diversicolor* generated a small but significant amount of turbidity (4.6 ntu, $p = 0.005$) but *M. balthica* generated no significant turbidity (1.1 ntu, $p = 0.243$). Experiment 3 demonstrated that significant turbidity could be generated within a single immersion tide (> 100 ntu) and that it did not increase substantially with increased *C. volutator* residence time in the sediment (Figure 5.2). Biomass specific turbidity, standardized to the same surface area L^{-1} seawater, generated by *C. volutator* with and without biofilms was similar (383 and 387 ntu $g^{-1} L^{-1}$). Experiments 1 and 2 also demonstrated

that for sediment with low grain sizes ($100\% < 63 \mu\text{m}$) light penetration decreased exponentially with turbidity (Figure 5.5B: $y = 95e^{-0.005x_i} + \epsilon_i$) and that turbidity is the fastest and most accurate means of determining light attenuation potential of the overlying water column.

7.1.2 Nutrient release

Sediment – water DIN and DIP fluxes were less consistent with *C. volutator* biomass g^{-1} between experiments and between incubation times. This was to be expected because while nutrient fluxes are influenced by bioturbators (Henriksen *et al* 1980, 1983; Andersen & Kristensen 1988; Pelegri & Blackburn 1994; Pelegri *et al* 1994, 1995; Emmerson *et al* 2001; Biles *et al* 2002; Mermillod-Blondin *et al* 2004; Michaud *et al* 2006; Ieno *et al* 2006; Bulling *et al* 2010), they are also regulated by MPB photosynthetic activity (Henriksen *et al* 1980, 1983; Andersen & Kristensen 1988; Sundbäck & Graneli 1988; Rysgaard *et al* 1995; Rizzo 1990; Feuillet-Girard *et al* 1997) and microbial metabolism (Andersen & Kristensen 1988; Rysgaard *et al* 1995; Pelegri & Blackburn 1994; Pelegri *et al* 1994, 1995; Mermillod-Blondin *et al* 2004; Michaud *et al* 2006). In experiment 1, resolution in ΔNH_4^+ and ΔPO_4^{3+} was very poor: while there was a slight trend of increased flux out of the sediment for both nutrients with increased *C. volutator* biomass (Figures 3.11 and 3.13), neither were significant (Table 3.4, Model 3.2.2 a and b, $p > 0.1$). In experiment 2, NH_4^+ release from the sediment over 6 days (Figure 4.8) in *H. diversicolor* ($5.0 \mu\text{mol L}^{-1}$, $p < 0.05$) and *C. volutator* ($+6.18 \mu\text{mol L}^{-1}$, $p < 0.05$) treatments was significantly more positive than in the control ($-0.31 \mu\text{mol L}^{-1}$) and *M. balthica* ($0.09 \mu\text{mol L}^{-1}$, $p > 0.1$) treatments (Table 4.4, Model 4.2.3). Experiment 3 demonstrated that nutrient release varied over incubation time, which had more to do with microbial metabolism than *C. volutator* irrigation rate, which according to sediment resuspension data was quite consistent over the course of the experiment. However, more NH_4^+ was released in the *C. volutator* treatments than in the control treatments (Figure 5.3).

7.2 The effect of macrofaunal feeding and bioturbation on MPB biomass

Both feeding and engineering effects were found to affect MPB biomass. The effects of bioturbation on the water column can affect local MPB and MPB in areas where macrofauna are not physically present.

7.2.1 Trophic effect

Feeding *C. volutator* have been shown to reduce MPB bulk biomass in the sediment (Daborn *et al* 1993; Gerdol & Hughes 1994a, 1994b; Hagerthey *et al* 2002; de Deckere *et al* 2001). While this was not demonstrated very clearly in experiment 1 (Figure 3.16), the lack of resolution was possibly due to insufficient sample size and interference by chlorophyll-a degradation products (see section 3.4.2). However, it was demonstrated in experiment 2, where chlorophyll-a concentration assays (top 2 mm) were performed on homogenized sediment from larger surface area samples and chlorophyll-a degradation products were accounted for (Lorenzen 1967). Chlorophyll-a concentrations were lower in sediments where *H. diversicolor* or *C. volutator* were feeding than in control treatments or where *M. balthica* were feeding (Figure 4.9).

Surface biomass (F_0) declined significantly ($p < 0.001$) with increasing *C. volutator* biomass (Figure 3.17; Table 3.5, Model 3.5). In experiment 2, compared to control treatments ($F_0 = 415$) after 6 days incubation, F_0 declined significantly in the presence of *C. volutator* ($F_0 = 340$, $p < 0.05$), *H. diversicolor* ($F_0 = 186$, $p < 0.0001$), and *M. balthica* ($F_0 = 262$, $p < 0.001$) (Figure 4.10; Table 4.6, Model 4.5.1). This corroborates previous findings (Hagerthey *et al* 2002; Dyson *et al* 1997; Hicks *et al* 2011).

7.2.2 Effect of increased turbidity and nutrient release

Increased nutrient release due to bioturbation resulted in a significant increase in bulk biomass in experiments 1 and 2. Increasing *C. volutator* biomass did not

significantly increase PO_4^{3+} release from sediment but the slight positive trend had a significant ($p < 0.0001$) positive effect on chlorophyll-*a* concentration: chlorophyll-*a* concentration increased by $3.8 \mu\text{g cm}^{-1} \mu\text{mol}^{-1} \text{PO}_4^{3+}$ (Table 3.5, Model 3.4). However, due to the poor resolution in both PO_4^{3+} and chlorophyll-*a* concentrations in this experiment, bootstrapped predicted trend lines and confidence intervals are not convincing (Figure 3.21). In experiment 2 more NH_4^+ was released in *C. volutator* and *H. diversicolor* treatments and chlorophyll-*a* concentration significantly increased ($p < 0.01$) by $4 \mu\text{g cm}^{-1} \mu\text{mol}^{-1} \text{NH}_4^+$ (Table 4.6, Model 4.5.1). This corroborates previous findings that overall MPB biomass increases with increased nutrient availability (Sundbäck & Snoeijs 1991; Hillebrand & Sommer 1997; Agatz *et al* 1999; Hillebrand *et al* 2000).

Surface biomass (F_0) was most influenced by light intensity. F_0 significantly declined with increasing turbidity in both experiments 1 (Table 3.5, Model 3.5, $p < 0.01$) and 2 (Table 4.6, Model 4.5.2, $p < 0.05$). Model visualization (Figure 3.22) shows that at high turbidities *C. volutator* feeding becomes less influential on F_0 (Figure 3.22). In experiment 2, where *H. diversicolor* increased NH_4^+ release the most and *C. volutator* increased sediment resuspension the most, but the MA tanks showed only a decrease in F_0 and NH_4^+ did not have a significant effect on F_0 (Figure 4.10 & 4.14; Table 4.6, Model 4.5.2). It should be noted that while F_0 was consistently measured in the morning on all days in both experiments, these morning measurements would have been at different times within the *in situ* tidal cycles at the site from which the MPB were collected. So if MPB were vertically migrating following entrained tidal rhythms, as suggested in Chapter 6, they would have been at different stages of migration on different days. Chapter 3 measurements were made during *in situ* emersion on day 1 and during *in situ* immersion on day 8, and F_0 most in treatments where turbidity was highest. In experiment 2 whereas the reverse was the case in experiment 1, . Therefore whatever effect bulk vertical migration, due to entrained tidal patterns, had on

surface biomass the first two experiments suggested that this effect was overshadowed by the response to turbidity following 7 days in different regimes.

Assemblages for experiment 4 were collected from the Guardbridge site, which is different in hydrodynamics and sedimentology from the papermill site where organisms for experiments 1 and 2 were sourced (see 2.1). This occurred by chance, as no biofilm was found at the papermill site due to heavy rains prior to starting the experiment (Tolhurst *et al* 2008), whereas the bridge and rocks at the Guardbridge site must have provided some shelter from the rain as biofilms were abundant here. The site has very shallow water (< 1 m), low flow rates, and low turbidity. In all three runs, regardless of tidal patterns, diatoms migrated diurnally and to some degree tidally. However, the bulk downward tidal migration, as witnessed at the end of the emersion tide in so many previous studies (Round & Palmer 1966; Pinkney & Zingmark 1991; Hay 1993; Guarini *et al* 2000a; Serodio *et al* 2001; Honeywill 2001; Consalvey 2002; Jesus 2006), was temporary and was counteracted by a bulk upward migration during immersion (Figure 6.7). The importance of these findings are that (1) they suggest that bulk migration and productivity are determined by site-specific water column characteristics, and (2) models of estuarine MPB primary productivity, often disregarding the immersion periods as productive periods (Guarini *et al* 2000a, 2000b), could seriously underestimate intertidal MPB productivity in sheltered bar-built estuaries such as the Eden. If typical water column characteristics at a site determine general productivity patterns, then the proximity of populations of turbidity-generating *C. volutator* to the site are likely to be influential. From the literature, as well as from the experiments described here, it appears that *C. volutator* is the only macrofauna species, present in high concentrations in N. Atlantic estuarine mud- and sand-flats, which actively resuspends sediment and can generate significant turbidity within a single tidal immersion (Green 1968; McLusky 1968; Henriksen *et al* 1980; Hylleberg & Henriksen 1980; Murdoch *et al*

1986; Gerdol & Hughes 1994b; de Deckere *et al* 2001; Biles *et al* 2002; Møller & Riisgård 2006; Dyson *et al* 2007).

7.3 *C. volutator* feeding and bioturbation does not affect MPB assemblage composition

In experiments 1 and 2 no significant effects were found of *C. volutator* and *M. balthica* feeding or modification of the water column on the MPB assemblage species richness and diversity (Figures 3.23 and 4.11; Tables 3.6 and 4.6). As expected from previous findings (Smith *et al* 1996; Hagerthey *et al* 2002), *C. volutator* feeding increased overall species richness and diversity, presumably due to probabilistic reduction of the dominant taxa. The same pattern was found, only with less difference between the groups, for *M. balthica*. However, contrary to previous findings (Smith *et al* 1996), the reverse pattern was found in the *H. diversicolor* treatments in experiment 2: its trophic activity decreased species richness ($p < 0.01$) and diversity ($p < 0.05$) significantly (Table 4.5, Model 4.4.3 and 4.4.4), due to the complete removal of the chain forming diatom *Catenula adhaerans* Mereschowsky. However, MPB assemblage similarity as determined by an MDS plot using Bray-Curtis similarity index showed no groupings according to macrofaunal biomass or identity treatment in either experiment 1 (Figure 3.25) or experiment 2 (Figure 4.15).

7.4 Biodiversity and ecosystem function in MPB

If bulk MPB biomass is regarded as an ecosystem function, in this study there is no relationship between biomass and biodiversity (Figures 3.24 & 4.16). Previous findings have found either negative or no relationship between MPB bulk biomass of sediment and MPB biodiversity (Colijn & Dijkema 1988; Thornton *et al* 2002; Forster *et al* 2006). However, productivity, so actual primary production rates, have been shown to increase with biodiversity (Forster *et al* 2006) and this is likely to be the case but as biodiversity was not compared within runs at high

and low F_0 during experiment 4 this cannot be confirmed. However, a rough comparison of run 1 assemblage to run 3 assemblage, revealed that that while run 1 had a higher live cell percentage, more cells per slide, and overall higher maximum F_0 , the run 3 assemblage was more diverse (see 6.3.1) but contained more smaller, non-migratory epipsammic species.

7.5 Can *C. volutator* bioturbation be considered positive niche construction?

Estuarine morphology is the result of an eternal tug of war between land and sea (Dyer 1994; Brown *et al* 1999) where progradation processes leading to land accretion are countered by transgression processes leading to the sea encroachment. In this 'battle', *C. volutator* are important ecosystem engineers 'pulling for the marine side'. Previous studies have demonstrated that MPB are a stabilizing force in an otherwise very unstable environment (Paterson 1989; Paterson *et al* 1999, 2000; Gerdol & Hughes 1994; Dyer 1994; Daborn *et al* 1993; Tolhurst *et al* 1999, 2006, 2008; de Deckere *et al* 2001; Underwood *et al* 2003). Sediment stabilization by MPB enables plants like eel grass and salt marsh species to take root (Gerdol and Hughes 1994b; Chocholek 2011 personal communication). The establishment of these plants in the estuary further stabilizes the sediment stickiness and is thought to pave the way for grasses which further encourage sediment deposition and accretion by slowing flow near the sediment bed and attracting sediment particles and anchoring deposited sediment with their root systems (Maynard *et al* 2011; Wilkie 2011). The stabilizing of sediment dominated by primary producers increases the 'terrestrialization' of the estuary: once salt marsh has developed terrestrial animals such as insects begin to colonize the estuary (Boorman 2003). In opposition to this, bioturbators, which are marine species that have adapted to tolerate the salinity and exposure ranges of estuaries, have been shown to be a destabilizing force on soft sediment for several reasons: (1) they prevent sediment compaction (Rhoads 1974; Gerdol & Hughes

1994b; Chapter 5, Figure 5.6), (2) they increase sediment erosion by decreasing the critical shear velocity (Daborn *et al* 1993; Paterson *et al* 1999; de Deckere *et al* 2000) (3) they actively resuspend sediment into the water column (de Deckere *et al* 2000; Biles *et al* 2002; Chapters 3, 4, 5). This results in more erosion than would be caused solely by physical processes, (Widdows *et al* 2000, 2004; Wood & Widdows 2002). However, they can also increase bulk biomass by increasing nutrient availability. The deleterious engineering effect of *C. volutator* on surface biomass in conjunction with the facilitation of bulk biomass regeneration could mean that while the sediment is being destabilized by *C. volutator* is not necessarily being depleted of its primary productivity to the same degree. If this is the case, then *C. volutator* bioturbation can clearly be considered a case of positive niche construction as, while destroying surface biofilms, they are maintaining their portion of the estuary in the less stable, marine, state that they are adapted to, and preventing that portion's evolution into the more stable 'terrestrialized' state, that they are much less adapted to.

References

References

- Admiraal W & Peletier H (1979). "Influence of organic compounds and light limitation on the growth rate of estuarine benthic diatoms." *British Phycological Journal* **14**(3): 197-206.
- Admiraal W (1984). "The ecology of estuarine sediment-inhabiting diatoms." *Progress in Phycological Research* **3**: 267 - 315.
- Agatz M, Asmus RM & Deventer B (1999). "Structural changes in the benthic diatom community along a eutrophication gradient on a tidal flat." *Helgoland Marine Research* **53**(2): 92-101.
- Agrawal VP (1963). "Studies on the physiology of digestion in *Corophium volutator*." *Journal of Marine Biological Association UK* **43**: 125 - 128.
- Aleem AA (1950). "The community inhabiting the mudflats at Whitstable." *New Phytologist* **9**: 174 - 188.
- Allen JF, de Paula WBM, Puthiyaveetil S & Nield J (2011). "A structural phylogenetic map for chloroplast photosynthesis." *Trends in Plant Science* **16**(12).
- Aller RC & Aller JY (1998). "The effect of biogenic irrigation intensity and solute exchange on diagenetic reaction rates in marine sediments." *Journal of marine Research* **56**(4): 905-936.
- Andersen FØ & Kristensen E (1988). "The influence of macrofauna on estuarine benthic community metabolism: a microcosm study." *Marine Biology* **99**: 591 - 603.
- Andersen FO & Kristensen E (1991). Effects of burrowing macrofauna on organic matter decomposition in coastal marine sediments. *The Environmental*

impact of Burrowing Animals and Animal Burrows. P. S. Meadows and A. Meadows. Oxford Oxford University Press. **63**: 67 - 88.

Andersen FØ & Kristensen E (1992). "The importance of benthic macrofauna in decomposition of microalgae in a coastal marine sediment." *Limnology & Oceanography* **37**(7): 1392 -1403.

Armbrust EV (2009). "The life of diatoms in the world's oceans." *Nature* **459**(7244): 185-192.

Barber HG & Haworth EY (1981). A guide to the morphology of the diatom frustule, with a key to the British freshwater genera. Kendal, UK: Titus Wilson & Son Ltd.

Bärlocher F, Gordon J & Ireland RJ (1988). "Organic composition of seafoam and its digestion by *Corophium volutator* (Pallas)." *Journal of Experimental Marine Biology and Ecology* **115**: 179 - 186.

Bates CR, Moore CG, Malthus T, Mair JM & Karpouzli E (2004). Broad scale mapping of habitats in the Firth of Tay and Eden Estuary, Scotland, Scottish Natural Heritage. Commissioned Report No. 007 (ROAME No. F01AA401D).

Bayer M, Juggins S, Pullan M, Droop S, Mann D, Lewis M, Clarke A, Head R & Weckström K. "ADIAC Diatom Image Database." Retrieved 2012, from <<http://rbg-web2.rbge.org.uk/ADIAC/db/adiacdb.htm>>.

Bendall DS, Howe CJ, Nisbet EG & Nisbet RER (2008). "Introduction. Photosynthetic and atmospheric evolution." *Philosophic Transactions of the Royal Society B* **363**: 2625 - 2628.

Bennoun P (2002). "The present model for chlororespiration." *Photosynthesis Research* **73**(1): 273-277.

Berman T & Chava S (1999). "Algal growth on organic compounds as nitrogen sources." *J. Plankton Res.* **21**(8): 1423-1437.

Biles CL (2002). Marine benthic system function and biodiversity. *School of Biology*. St Andrews, University of St Andrews: 174.

Biles CL, Paterson DM, Ford RB, Solan M & Raffaelli DG (2002). "Bioturbation, ecosystem functioning and community structure." *Hydrology and Earth System Sciences* **6**(6): 999 - 1005.

Bolam SG, Whomersley P & Schratzberger M (2004). "Macrofaunal recolonization on intertidal mudflats: effect of sediment organic and sand content." *Journal of Experimental Marine Biology and Ecology* **306**(2): 157-180.

Boogert NJ, Paterson DM & Laland KN (2006). "The Implications of Niche Construction and Ecosystem Engineering for Conservation Biology." *BioScience* **56**(7): 570 - 578.

Boorman LA (2003). Saltmarsh Review. An overview of coastal saltmarshes, their dynamic and sensitivity characteristics for conservation and management. Peterborough, JNCC No. 334.

Brown E, Colling A, Park D, Phillips J, Rothery D & Wright J (1999). *Waves, Tides and Shallow-Water Processes*. Milton Keynes: Open University & Butterworth-Heinemann.

Budd G & Rayment W. (2001). "*Macoma baltica* (Baltic tellin)." *Marine Life Information Network: Biology and Sensitivity Key Information Sub-programme* [on-line] Retrieved 08/06/2012, from:
<<http://www.marlin.ac.uk/speciesfullreview.php?speciesID=3749>>.

Budd G. (2008). "*Hediste diversicolor* (Ragworm)." *Marine Life Information Network: Biology and Sensitivity Key Information Sub-programme* [on-line]

Retrieved 08/06/2012, from:

<<http://www.marlin.ac.uk/speciesfullreview.php?speciesID=3470>>.

Buick R (2008). "When did oxygenic photosynthesis evolve?" *Philosophical Transactions of the Royal Society B* **363**(1504): 2731 - 2743.

Bulling M, Hicks N, Murray L, Paterson DM, Raffaelli D, White PCL & Solan M (2010). "Marine biodiversity-ecosystem functions under uncertain environmental futures." *Phil. Trans. R. Soc. B* **365**: 2107 - 2116.

Burkholder JM (1996). Interaction of benthic algae with their substrata. *Algal Ecology: Freshwater Benthic Ecosystems*. R. J. Stevenson, M. L. Bothwell and R. L. Lowe. California, Academic Press: 753.

Campbell NA & Reece JB (2005). *Biology*. San Fransisco: Pearson Education Inc. as Benjamin Cummings.

Cartaxana P, Jesus B & Brotas V (2003). "Pheophorbide and pheophytin a-like pigments as useful markers for intertidal microphytobenthos grazing by *Hydrobia ulvae*." *Estuarine, Coastal and Shelf Science* **58**(2): 293-297.

Chocholek M (2012). The impact of climate change on estuarine ecosystems: a focus on the Eden estuary, Fife, Scotland. *School of Geoscience*. St Andrews, University of St Andrews. **PhD**: in preperation.

Christiansen T, Wiberg PL & Milligan TG (2000). "Flow and Sediment Transport on a Tidal Salt Marsh Surface." *Estuarine, Coastal and Shelf Science* **50**(3): 315-331.

Colodey AG & Wells PG (1992). "Effects of pulp and paper mill effluents on estuarine and marine ecosystems in Canada: a review." *Journal of Aquatic Ecosystem Health* **1**: 201 - 226.

Consalvey M (2002). The structure and function of microphytobenthic biofilms. *Biology*. St Andrews, University of St Andrews. **PhD**: 264.

- Consalvey M, Paterson DM & Underwood GJC (2004). "The ups and downs of life in a benthic biofilm: migration of benthic diatoms." *Diatom Research* **19**(2): 181 - 202.
- Consalvey M, Perkins RG, Paterson DM & Underwood GJC (2005). "PAM fluorescence: a beginners guide for benthic diatomists." *Diatom Research* **20**(1): 1 - 22.
- Cox EJ (1987). "Studies on the Diatom Genus *Navicula* Bory VI The identity structure and ecology of some freshwater species." *Diatom Research* **2**(2): 159 – 174.
- Cox EJ (1996). Identification of freshwater diatoms from live material. London: Chapman & Hall.
- Crawley MJ (2002). Statistical Computing: An Introduction to Data Analysis using S-Plus. Chichester, UK: John Wiley & Sons Ltd.
- Daborn GR, Amos CL, Brylinsky M, Christian H, Drapeau G, Faas RW, Grant J, Long B, Paterson DM, Perillo GME & Piccolo MC (1993). "An ecological cascade effect: Migratory birds affect stability of intertidal sediments." *Limnology & Oceanography* **38**(1): 225 - 231.
- Dawkins R (1982). *The Extended Phenotype: the long reach of the gene*. Oxford: Oxford University Press.
- Darwin C (1881). The Formation of Vegetable Mould through the action of worms, with observation on their habits. London: William Clowes and Sons, Ltd.
- de Deckere EMGT, van de Koppel J & Heip CHR (2000). "The influence of *Corophium volutator* abundance on resuspension." *Hydrobiologia* **426**: 37 - 42.

de Deckere EMGT, Tolhurst TJ & de Brouwer JFC (2001). "Destabilization of Cohesive Intertidal Sediments by Infauna." *Estuarine, Coastal and Shelf Science* **53**: 665 - 669.

de Deckere EMGT (2003). Faunal influence on sediment stability in intertidal mudflats. *Center for Estuarine and Coastal Ecology*. Yerseke, Rijksuniversiteit Groningen & Netherlands Institute of Ecology: 112.

Defew EC, Paterson DM & Hagerthey SE (2002). "The use of natural microphytobenthic assemblages as laboratory model systems." *Marine Ecology Progress Series* **237**: 15 - 25.

Defew EC (2003). Microphytobenthos: Ecophysiology and Community Dynamics in Estuarine Sediments. *School of Biology*. St Andrews, University of St Andrews. **PhD**: 191.

Defew EC, Perkins RG & Paterson DM (2004). "The influence of light and temperature interactions on a natural estuarine microphytobenthic assemblage." *Biofilms* **1**: 21 - 30.

de Goij P & Luttikhuisen P (1998). "Deep-burying reduces growth in intertidal bivalves: field and mesocosm experiments with *Macoma balthica*." *Journal of Experimental Marine Biology and Ecology* **228**: 327 - 337.

Dexter Dyer B (2003). *A Field Guide to Bacteria*. Ithaca: Comstock Publishing Associates, Cornell University Press.

Dietrich WE & Perron JT (2006). "The search for a topographic signature of life." *Nature* **439**(7075): 411-418.

Du GY, Oak JH, Li H & Chung IK (2010). "Effect of light and sediment grain size on the vertical migration of benthic diatoms." *Algae* **25**(3): 133 - 140.

- Duarte CM, Agusti S, Gasol JM, Vaquer D & Vazquez-Dominguez E (2000). "Effect of nutrient supply on the biomass structure of planktonic communities: an experimental test on a Mediterranean coastal community." *Marine Ecology Progress Series* **206**: 87-95.
- Dyer KR (1997). *Estuaries: A physical introduction*. Chichester, U.K.: John Wiley & Sons.
- Dyson KE, Bulling MT, Solan M, Hernandez-Milian G, Raffaelli DG, White PCL & Paterson DM (2007). "Influence of macrofaunal assemblages and environmental heterogeneity on microphytobenthic production in experimental systems." *Proceedings of the Royal Society B*. **274**: 2677 - 2684.
- Dyer KR (1997). *Estuaries: A physical introduction*. Chichester, U.K.: John Wiley & Sons.
- Eaton JW & Moss B (1966). "The estimation of numbers and pigment content in epipelagic algal populations." *Limnology and Oceanography* **11**(4): 584 - 595.
- Eilers PHC & Peeters JCH (1988). "A model of the relationship between light intensity and the rate of photosynthesis in phytoplankton." *Ecological Modelling* **42**: 199 - 215.
- Emmerson MC, Solan M, Emes C, Paterson DM & Raffaelli D (2001). "Consistent patterns and the idiosyncratic effects of biodiversity in marine ecosystems." *Nature* **411**(6833): 73-77.
- Falkowski PG & Raven JA (2007). *Aquatic Photosynthesis*. Princeton NJ, Princeton University Press.
- Falkowski PG & Godfrey LV (2008). "Electrons, life and the evolution of Earth's oxygen cycle." *Philosophical Transactions of the Royal Society B* **363**(1504): 2705 - 2716.

Falkowski PG, Fenchel T & Delong EF (2008). "The Microbial Engines That Drive Earth's Biogeochemical Cycles." *Science* **320**(5879): 1034-1039.

Fauvel P & Bohn G (1904). "Le rythme des marées chez les datomée litorales." *Compte Rendu des Seances de la Société Biologie* **62**: 121 - 123.

Feuillet-Girard M, Gouleau D, Blanchard GF & Joassard L (1997). "Nutrient fluxes on an intertidal mudflat in Marennes-Oléron Bay, and influence of the emersion period." *Aquat. Living Resour.* **10**(1): 49-58.

Field CB, Behrenfeld MJ, Randerson JT & Falkowski P (1998). "Primary Production of the Biosphere: Integrating Terrestrial and Oceanic Components." *Science* **281**(5374): 237-240.

Finkel ZV, Vaillancourt CJ, Irwin AJ, Reavie ED & Smol JP (2009). "Environmental control of diatom community size structure varies across aquatic ecosystems." *Proceedings of the Royal Society B: Biological Sciences* **276**(1662): 1627-1634.

Folk RL (1954). "The distinction between grain size and mineral composition in sedimentary rocks." *Journal of Geology* **62**: 344 - 359.

Ford RB & Honeywill C (2002). "Grazing on intertidal microphytobenthos by macrofauna: is pheophorbide a useful marker?" *Marine Ecology Progress Series* **229**: 33 - 42.

Gardner MRA, W. R. (1970). "Connectance of large dynamic (cybernetic) systems: critical values for stability. ." *Nature* **228**: 784

Gattuso J-P, Frankignoulle M & Wollast R (1998). "Carbon and carbonate metabolism in coastal aquatic ecosystems." *Annual Review of Ecology and Systematics* **29**: 405 - 434.

Gazeau F, Borges AV, Barrón C, Duarte CM, Iversen N, Middelburg JJ, Delille B, Pizay M-D, Frankignoulle M & Gattuso J-P (2005). "Net ecosystem metabolism in a micro-tidal estuary (Randers Fjord, Denmark): evaluation of methods." *Marine Ecology Progress Series* **301**: 23-41.

Genty B, Briantais J-M & Baker NR (1989). "The relationship between the quantum yield of photosynthetic electron transport and quenching of chlorophyll fluorescence." *Biochimica et Biophysica Acta (BBA) - General Subjects* **990**(1): 87-92.

Gerdol V & Hughes RG (1994a). "Feeding behaviour and diet of *Corophium volutator* in an estuary in southeastern England." *Marine Ecology Progress Series* **114**: 103 - 108.

Gerdol V & Hughes RG (1994b). "Effect of *Corophium volutator* on the abundance of benthic diatoms, bacteria and sediment stability in two estuaries in southeastern England " *Marine Ecology Progress Series* **114**: 109 - 115.

Glud R (2008). "Oxygen dynamics of marine sediments." *Marine Biology Research* **4**: 243 - 289.

Green J (1968). *The Biology of Estuarine Animals*. London: Sidgwick & Jackson Ltd.

Grover JP (1989). "Influence of cell shape and size on algal competitive ability." *Journal of Phycology* **25**: 402 - 405.

Guarini J-M, Blanchard GF, Gros P, Gouleau D & Bacher C (2000a). "Dynamic model of the short-term variability of microphytobenthic biomass on temperate intertidal mudflats." *Marine Ecology Progress Series* **195**: 291-303.

Guarini J-M, Blanchard GF & Gros P (2000b). "Quantification of the microphytobenthic primary production in European intertidal mudflats - a modelling approach." *Continental Shelf Research* **20**: 1771 - 1788.

- Hagerthey SE, Defew EC & Paterson DM (2002). "Influence of *Corophium volutator* and *Hydrobia ulvae* on intertidal benthic diatom assemblages under different nutrient and temperature regimes." *Marine Ecology Progress Series* **245**: 47 - 59.
- Happey-Wood CM & Jones P (1988). "Rhythms of vertical migration and motility in intertidal benthic diatoms with particular reference to *Pleurosigma angulatum*." *Diatom Research* **3**(1): 83 - 93.
- Hargrave BT (1970). "The effect of a deposit-feeding amphipod on the metabolism of benthic microflora." *Limnology and Oceanography* **15**(1): 21 - 30.
- Hargrave BT & Burns NM (1979). "Assessment of Sediment Trap Collection Efficiency." *Limnology and Oceanography* **24**(6): 1124 - 1136.
- Harper MA (1969). "Movement and migration of diatoms on sand grains." *British Phycology Journal* **4**(1): 97 - 103.
- Hartley B, Barber HG & Carter JR (1996). *An Atlas of British Diatoms*. Bristol: Biopress Ltd.
- Hay SI, Maitland TC & Paterson DM (1993). "The speed of diatom migration through natural and artificial substrata." *Diatom Research* **8**(2): 371 - 384.
- Hendey NI (1964). *An Introductory Account of the Smaller Algae of British Coastal Waters*. Koenigstein: Otto Koeltz Science Publishers.
- Henriksen K, Hansen JI & Blackburn TH (1980). "The influence of benthic infauna on exchange rates of inorganic nitrogen between sediment and water." *OPHELIA Suppl. 1*: 249 - 256.
- Henriksen K, Rasmussen MB & Jensen A (1983). "Effect of Bioturbation on Microbial Nitrogen Transformations in the Sediment and Fluxes of Ammonium and Nitrate to the Overlaying Water." *Ecological Bulletins* **35**: 193-205.

- Herbert RA (1982). Nitrate dissimilation in marine and estuarine sediments. *Sediment Microbiology*. D. B. Nedwell and C. M. Brown. London, Academic Press: 53 - 71.
- Hessen DO (1999). Catchment properties and the transport of major elements to estuaries. *Advances in Ecological Research*. D. B. Nedwell and D. G. Raffaelli. London, Academic Press Ltd. **29**.
- Hicks N, Bulling M, Solan M, Raffaelli D, White P & Paterson D (2011). "Impact of biodiversity-climate futures on primary production and metabolism in a model benthic estuarine system." *BMC Ecology* **11**(1): 7.
- Hillebrand H & Sommer U (1997). "Response of epilithic microphytobenthos of the Western Baltic Sea to in situ experiments with nutrient enrichment." *Marine Ecology Progress Series* **160**: 35 - 46.
- Hillebrand H, Dürselen C-D, Kirschtel D, Pollinger U & Zohary T (1999). "Biovolume calculation for pelagic and benthic microalgae." *Journal of Phycology* **35**(2): 403-424.
- Hillebrand H, Worm B & Lotze HK (2000). "Marine microbenthic community structure regulated by nitrogen loading and grazing pressure." *Marine Ecology Progress Series* **204**: 27-38.
- HIMOM (2005). Hierarchical Monitoring Methods for Intertidal Flats, European Commission's Fifth Framework Programme.
- Holland HD (2006). "The oxygenation of the atmosphere and oceans." *Philosophical Transactions of the Royal Society B* **361**(1470): 903 - 915.
- Holmén K (1992). The Global Carbon Cycle. *Global Biogeochemical Cycles*. S. S. Butcher, C. R. J., G. H.

- Hopkins JT (1963). Some light-induced changes in the behaviour and cytology of an estuarine mudflat diatom. *Light as an Ecological Factor*. R. Bainbridge. Oxford, Blackwell Scientific Publications: 335 - 358.
- Hopkins JT (1966). "The role of water in the behaviour of an estuarine mud-flat diatom." *Journal of the Marine Biological Association U.K.* **46**: 617 - 626.
- Honeywill C (2001). *In situ* Analysis of the biomass and distribution of microphytobenthos. *School of Biology*. St Andrews, University of St Andrews. **PhD**: 156.
- Howarth RW, Billen G, Swaney D, Townsend A, Jaworski N, Lajtha K, Downing JA, Elmgren R, Caraco N, Jordan T, Berendse F, Freney J, Kudeyarov V, Murdoch P & Zhao-Liang Z (1996). "Regional Nitrogen Budgets and Riverine N & P Fluxes for the Drainages to the North Atlantic Ocean: Natural and Human Influences." *Biogeochemistry* **35**(1): 75-139.
- Hylleberg J & Henriksen K (1980). "The central role of bioturbation in sediment mineralization and element re-cycling." *OPHELIA Suppl 1*: 1 - 16.
- Ieno EN, Solan M, Batty P & Pierce GJ (2006). "How biodiversity affects ecosystem functioning: roles of infaunal species richness, identity and density in the marine benthos." *Marine Ecology Progress Series* **311**: 263 - 271.
- Irlandi EA & Peterson CH (1991). "Modification of Animal Habitat by Large Plants: Mechanisms by Which Seagrasses Influence Clam Growth." *Oecologia* **87**(3): 307-318.
- Jesus B, Brotas V, Marani M & Paterson DM (2005). "Spatial dynamics of microphytobenthos determined by PAM fluorescence." *Estuarine, Coastal and Shelf Science* **65**(1-2): 30-42.

- Jesus B, Perkins RG, Consalvey M, Brotas V and Paterson DM (2006a). "Effects of vertical migrations by benthic microalgae on fluorescence measurements of photophysiology." *Marine Ecology Progress Series* **315**: 55-66.
- Jesus B, Perkins R, Mendes C, Brotas V & Paterson D (2006b). "Chlorophyll fluorescence as a proxy for microphytobenthic biomass: alternatives to the current methodology." *Marine Biology* **150**(1): 17-28.
- Jones CG & Shachak M (1990). "Fertilization of the desert by rock eating snails." *Nature* **346**: 839 - 841.
- Jones CG, Lawton JH & Shachak M (1997). "Positive and negative effects of organisms as physical ecosystem engineers." *Ecology* **78**(7): 1946 - 1957.
- Jones D & Frid CLJ (2009). "Altering intertidal sediment topography: effects on biodiversity and ecosystem functioning." *Marine Ecology* **30**(Supplement 1): 83 - 96.
- Jones SE & Jago CF (1993). "In situ assessment of modification of sediment properties by burrowing invertebrates." *Marine Biology* **115**(1): 133-142.
- Kamp A, de Beer D, Nitsch JL, Lavik G & Stief P (2011). "Diatoms respire nitrate to survive dark and anoxic conditions." *Proceedings of the National Academy of Sciences* **108**(14): 5649-5654.
- Kelly MG, Bennion H, Cox EJ, Goldsmith B, Jamieson J, Juggins S, Mann DG & Telford RJ. (2005). "Common freshwater diatoms of Britain and Ireland: an interactive key." From: <<http://craticula.ncl.ac.uk/EADiatomKey/html/>>.
- Kasting JF & Siefert JL (2002). "Life and the Evolution of Earth's Atmosphere." *Science* **296**(5570): 1066-1068.

- Kingston MB (1999). "Wave effects on the vertical migration of two benthic microalgae: *Nantzschia virgata* var. *intermedia* and *Euglena proxima* ." *Estuaries* **22**: 81 - 91.
- Krause GH & Weis E (1991). "Chlorophyll fluorescence and photosynthesis: the basics." *Annual Review of Plant Physiology and Plant Molecular Biology* **42**: 313 - 349.
- Kristensen E (1988). Benthic Fauna and Biogeochemical Processes in Marine Sediments: Microbial Activities and Fluxes. *Nitrogen Cycling in Coastal Marine Environments*. T. H. Blackburn and J. Sørensen. New York, John Wiley & Sons Ltd.
- Kristensen E (2000). "Organic matter diagenesis at the oxic/anoxic interface in coastal marine sediments, with emphasis on the role of burrowing animals." *Hydrobiologia* **426**: 1-24.
- Kylafis G & Loreau M (2008). "Ecological and evolutionary consequences of niche construction for its agent." *Ecology Letters* **11**(10): 1072-1081.
- Laland KN, Odling-Smee J & Feldman MW (1999). "Evolutionary consequences of niche construction and their implications for ecology." *Proc. Natl Acad. Sci. USA* **96**: 10242 - 10247.
- Lavaud J, Strzepek RF & Kroth PG (2007). "Photoprotection capacity differs among diatoms: Possible consequences on the spatial distribution of diatoms related to fluctuations in the underwater light climate." *Limnology and Oceanography* **52**(3): 1188 - 1194.
- Lawri SM & Raffaelli DG (1998). "In situ swimming behaviour of the amphipod *Corophium volutator* (Pallas)." *Journal of Experimental Marine Biology & Ecology* **224**: 238 - 251.

- Leterme SC, Ellis AV, Mitchell JG, Buscot M-J, Pollet T, Schapira M & Seuront L (2010). "Morphological flexibility of *Cocconeis placentula* (Bacillariophyceae) nanostructure to changing salinity levels." *Journal of Phycology* **46**: 715 - 719.
- Libes SM (1992). *Marine Biogeochemistry*. Hoboken NJ: John Wiley & Sons, Inc.
- Licursi M & Gómez N (2009). "Effects of dredging on benthic diatom assemblages in a lowland stream." *Journal of Environmental Management* **90**(2): 973-982.
- Lill JT & Marquis RJ (2003). "Ecosystem engineering by caterpillars increases insect herbivore diversity on white oak." *Ecology* **84**(3): 682 - 690.
- Lopez GR & Levinton JS (1987). "Ecology of Deposit-Feeding Animals in Marine Sediments." *The Quarterly Review of Biology* **62**(3): 235-260.
- Lorenzen C (1967). "Determination of chlorophyll and phaeo-pigments : Spectrophotometric equations." *Limnology & Oceanography* **12**: 343-346.
- Lubarsky HV (2011). The impact of microbial extracellular polymeric substances on sediment stability. *School of Biology*. St Andrews, University of St Andrews. **PhD**: 202.
- Lucas CH & Holligan PM (1999). "Nature and ecological implications of algal pigment diversity on the Molenplaat tidal flat (Westerschelde estuary, SW Netherlands)." *Marine Ecology Progress Series* **180**: 51-64.
- Luckenbach M (1986). "Sediment stability around animal tubes: The roles of hydrodynamic processes and biotic activity." *Limnology & Oceanography* **31**(4): 779 - 787.
- Mackenzie M, Donovan C, Photopoulou T, Borchers D, Scott-Hayward L & Thomas L (2011). Statistical Modelling Workshop. St Andrews, Fife, University of St Andrews.

Magurran AE (2004). *Measuring Biological Diversity*. Oxford, UK: Blackwell Science Ltd.

Malcolm SJ & Sivyer DB (1997). Nutrient recycling in intertidal sediments. *Biogeochemistry of intertidal sediments*. T. D. Jickels and J. E. Rae. Cambridge, Cambridge University Press: 15.

Martin W, Rotte C, Hoffmeister M, Theissen U, Gelius-Dietrich G, Ahr S & Henze K (2003). "Early Cell Evolution, Eukaryotes, Anoxia, Sulfide, Oxygen, Fungi First (?), and a Tree of Genomes Revisited." **55**: 193-204.

Maxwell K & Johnson GN (2000). "Chlorophyll fluorescence - a practical guide." *Journal of Experimental Botany* **51**(345): 659-668.

May RM (1972). "Will a large complex system be stable?" *Nature* **238**: 413 - 414.

Maynard C, McManus J, Crawford RMM & Paterson D (2011). "A comparison of short-term sediment deposition between natural and transplanted saltmarsh after saltmarsh restoration in the Eden Estuary (Scotland)." *Plant Ecology & Diversity* **4**(1): 103 - 113.

McCann KS (2000). "The diversity–stability debate." *Nature* **405**(11 May 2000): 228 - 233.

McLusky DS (1968). "Some effects of salinity on the distribution and abundance of *Corophium volutator* in the Ythan estuary." *Journal of the Marine Biological Association of the UK* **48**(02): 443-454.

McLusky DS (1970). "Salinity preference in *Corophium volutator*." *Journal of Marine Biological Association UK* **50** 747 - 752.

McLusky DS (1971). *Ecology of Estuaries*. London: Heinemann Educational Books.

- Meadows PS (1964). "Substrate Selection by Corophium Species: The Particle Size of Substrates." *Journal of Animal Ecology* **33**(3): 387-394.
- Meadows PS (1967). "Discrimination, previous experience and substrate selection by the amphipod Corophium." *Journal of Experimental Biology* **47**: 553 - 559.
- Meadows PS & Reid A (1966). "The behaviour of *Corophium volutator* (Crustacea: Amphipoda)." *Journal of Zoology, London* **150**: 387 - 399.
- Meadows PS & Tait J (1989). "Modification of sediment permeability and shear strength by two burrowing invertebrates." *Marine Biology* **101**: 75 - 82.
- Meadows PS, Tait J & Hussain SA (1990). "Effects of estuarine infauna on sediment stability and particle sedimentation." *Hydrobiologia* **190**: 263 - 266.
- Medlin L (2006). MINI REVIEW: The evolution of the diatoms and a report on the current status of their classification. *Functioning of microphytobenthos in estuaries*. J. C. Kromkamp, J. F. C. de Brouwer, G. F. Blanchard, R. M. Forster and V. Créach. Amsterdam, Royal Netherlands Academy of Arts and Sciences.
- Mermillod-Blondin F, Rosenberg R, François-Carcaillet F, Norling K & Mauclaire L (2004). "Influence of bioturbation by three benthic infaunal species on microbial communities and biogeochemical processes in marine sediment." *Aquatic Microbial Ecology* **36**: 271-284.
- Mermillod-Blondin F, François-Carcaillet F & Rosenberg R (2005). "Biodiversity of benthic invertebrates and organic matter processing in shallow marine sediments: an experimental study." *Journal of Experimental Marine Biology and Ecology* **315**(2): 187-209.
- Meysman FJR, Middelburg JJ & Heip CHR (2006). "Bioturbation: a fresh look at Darwin's last idea." *TRENDS in Ecology and Evolution*: 8.

Michaud E, Desrosiers G, Mermillod-Blondin F, Sundby B & Stora G (2005). "The functional group approach to bioturbation: The effects of biodiffusers and gallery-diffusers of the *Macoma balthica* community on sediment oxygen uptake." *Journal of Experimental Marine Biology and Ecology* **326**(1): 77-88.

Michaud E, Desrosiers G, Mermillod-Blondin F, Sundby B & Stora G (2006). "The functional group approach to bioturbation: II. The effects of the *Macoma balthica* community on fluxes of nutrients and dissolved organic carbon across the sediment-water interface." *Journal of Experimental Marine Biology and Ecology* **337**(2): 178-189.

Møller LF & Riisgård HU (2006). "Filter feeding in the burrowing amphipod *Corophium volutator*." *Marine Ecology Progress Series* **322**: 213 - 224.

Murdoch MH, Bärlocher F & Laltoo ML (1986). "Population dynamics and nutrition of *Corophium volutator* (Pallas) in the Cumberland Basin (Bay of Fundy)." *Journal of Experimental Marine Biology & Ecology* **103**: 235 - 249.

Mouget J-L & Tremblin G (2002). "Suitability of the Fluorescence Monitoring System (FMS, Hansatech) for measurement of photosynthetic characteristics in algae." *Aquatic Botany* **74**(3): 219-231.

Murdoch MH, Bärlocher F & Laltoo ML (1986). "Population dynamics and nutrition of *Corophium volutator* (Pallas) in the Cumberland Basin (Bay of Fundy)." *Journal of Experimental Marine Biology & Ecology* **103**: 235 - 249.

Murray JMH, Meadows A & Meadows PS (2002). "Biogeomorphological implications of microscale interactions between sediment geotechnics and marine benthos: a review." *Geomorphology* **47**: 15-30.

Naymik J, Pan Y & Ford J (2005). "Diatom Assemblages as Indicators of Timber Harvest Effects in Coastal Oregon Streams." *Journal of the North American Benthological Society* **24**(3): 569-584.

- Naeem S, Chapin FSI, Costanza R, Ehrlich PR, Golley FB, Hooper DU, Lawton JH, Neill RVO, Mooney HA, Sala OE, Symstad AJ & Tilman D (1999). "Biodiversity and Ecosystem Functioning: Maintaining Natural Life Support Processes." *Issues in Ecology* **4**: 2 -11.
- Neal K & Avant P. (2006). "Corophium volutator. A mud shrimp." *Marine Life Information Network: Biology and Sensitivity Key Information Sub-programme [online]* Retrieved 04/04/2010, 2010, from:
<<http://www.marlin.ac.uk/specieshabitats.php?speciesID=3052>>.
- Nealson KH (1997). "Sediment bacteria: Who's There, What Are They Doing, and What's New?" *Annual Review of Earth and Planetary Sciences* **25**: 403 -434.
- Nield J, Redding K & Hippler M (2004). "Remodeling of light-harvesting protein complexes in *Chlamydomonas* in response to environmental changes." *Eukaryotic Cell* **3**(6): 1370 - 1380.
- Nielsen MV & Kofoed LH (1982). "Selective Feeding and Epipsammic Browsing by the Deposit-Feeding Amphipod *Corophium volutator*." *Marine Ecology Progress Series* **10**: 81 - 88.
- Odling-Smee J, Laland K & Feldman MW (2003). *Niche Construction: The Neglected Process in Evolution*. Princeton: Princeton University Press.
- O'Connor MI, Violin CR, Anton A, Ladwig LM & Piehler MF (2011) "Salt marsh stabilization affects algal primary producers at the marsh edge." *Wetlands Ecology and Management* DOI: DOI 10.1007/s11273-010-9206-y.
- Orians and G. V. Wolfe. London, Academic Press Ltd: 239-262.
- Pan Y & Lowe RL (1994). "Independent and interactive effects of nutrients and grazers on benthic algal community structure." *Hydrobiologia* **291**: 201 - 209.

Passy SI (2007). "Diatom ecological guilds display distinct and predictable behavior along nutrient and disturbance gradients in running waters." *Aquatic Botany* **86**(2): 171-178.

Passy SI (2008). "Continental diatom biodiversity in stream benthos declines as more nutrients become limiting." *Proceedings of the National Academy of Sciences* **105**(28): 9663-9667.

Paterson DM (1986). "The migratory behaviour of diatom assemblages in a laboratory tidal micro-ecosystem examined by low temperature scanning electron microscopy." *Diatom Research* **1**: 227 - 239.

Paterson D (1989). "Short-term changes in the erodibility of intertidal cohesive sediments related to the migratory behaviour of epipelagic diatoms." *Limnology and Oceanography* **34**: 223 - 234.

Paterson DM, Wiltshire KH, Miles A, Blackburn J, Davidson I, Yates MG, McGrorty S & Eastwood JA (1989). "Microbiological mediation of spectral reflectance from intertidal cohesive sediments." *Limnology & Oceanography* **43**: 1207 - 1221.

Paterson DM, Black KS, Nedwell DB & Raffaelli DG (1999). Water Flow, Sediment Dynamics and Benthic Biology. *Advances in Ecological Research*, Academic Press. **Volume 29**: 155-193.

Paterson DM, Tolhurst TJ, Kelly JA, Honeywill C, de Deckere EMGT, Huet V, Shayler SA, Black KS, de Brouwer J & Davidson I (2000). "Variations in sediment properties, Skeffling mudflat, Humber Estuary, UK." *Continental Shelf Research* **20**(10-11): 1373-1396.

Paerl HW (2006). "Assessing and managing nutrient-enhanced eutrophication in estuarine and coastal waters: Interactive effects of human and climatic perturbations." *Ecological Engineering* **26**(1): 40-54.

Pelegri SP & Blackburn TH (1994). "Bioturbation effects of the amphipod *Corophium volutator* on microbial nitrogen transformations in marine sediments." *Marine Biology* **121**: 253 - 258.

Pelegri SP, Nielsen LP & Blackburn TH (1994). "Denitrification in estuarine sediment stimulated by the irrigation activity of the amphipod *Corophium volutator*." *Marine Ecology Progress Series* **105**(3 March): 285 - 290.

Pelegri SP & Blackburn TH (1995). "Effect of bioturbation by *Nereis* sp., *Mya arenaria* and *Cerastoderma* sp. on nitrification and denitrification in estuarine sediments." *OPHELIA* **42**: 289 - 299.

Peltier G & Cournac L (2002). "Chlororespiration." *Annual Review of Plant Biology* **53**(1): 523-550.

Perkins EJ (1960). "The diurnal rhythm of the littoral diatoms of the river Eden estuary, Fife." *Journal of Ecology* **48**: 725 - 728.

Perkins RG, Underwood GJC, Brotas V, Snow GC, Jesus B & Ribeiro L (2001). "Responses of microphytobenthos to light: primary production and carbohydrate allocation over an emersion period." *Marine Ecology Progress Series* **223**: 101-112.

Perkins RG, Mouget JL, Lefebvre S & Lavaud J (2006). "Light response curve methodology and possible implications in the application of chlorophyll fluorescence to benthic diatoms." *Marine Biology* **149**(4): 703-712.

Perkins RG, Lavaud J, Serôdio J, Mouget JL, Cartaxana P, Rosa P, Barille L, Brotas V & Jesus BM (2010). "Vertical cell movement is a primary response of intertidal benthic biofilms to increasing light dose." *Marine Ecology Progress Series* **416**: 93 - 103.

- Perkins RG, Kromkamp JC, Serôdio J, Lavaud J, Jesus B, Mouget J-L, Lefebvre S & Forster RM (2011). The application of variable chlorophyll fluorescence to microphytobenthic biofilms. *Chlorophyll a fluorescence in aquatic sciences: methods and applications*. D. Suggett, O. Prasi and M. Borowitzka, Springer, UK. 4.
- Pinheiro JC & Bates DM (2000). *Mixed-effects models in S and S-plus*. New York: Springer Verlag.
- Pinckney J & Zingmark R (1991). "The effect of the tidal stage and sun angles on intertidal benthic microalgal biomass and productivity." *Marine Ecology Progress Series* **76** 81 - 89.
- Pinckney J & Zingmark RG (1993a). "Biomass and production of benthic microalgal communities in estuarine habitats." *Estuaries* **16**(4): 887 - 897.
- Pinckney J & Zingmark RG (1993b). "Photophysiological responses of intertidal benthic microalgal communities to in situ light environments: methodological considerations." *Limnology and Oceanography* **38**(7): 1373 - 1383.
- Pinckney J & Zingmark RG (1993c). "Modeling the annual production of intertidal benthic microalgae in estuarine ecosystems." *Journal of Phycology* **29**: 396 - 407.
- Purves WK, Orians GH & Heller HC (1992). *Life: The Science of Biology*. Sunderland MA: Sinauer Associates, Inc.
- Raffaelli DG (2000). "Interactions between macro-algal mats and invertebrates in the Ythan estuary, Aberdeenshire, Scotland." *Helgoland Marine Research* **54**: 71 - 79.
- Register of Scotland, Scottish Executive. "Citation: Eden Estuary Site of Special Scientific Interest" Retrieved 16-11-2011, from:

<<https://www.eservices.ros.gov.uk/ros.sssi.presentation.ui/ros/sssi/presentation/ui/sssi/begin.do>>.

Rhoads DC (1974). "Organism-sediment relations on the muddy sea floor." *Oceanography and Marine Biology Annual Review* **12**: 263 - 300.

Ribeiro LLCS (2010). Intertidal benthic diatoms of the Tagus estuary: Taxonomic composition and spatial-temporal variation. *Departamento de Biologia Vegetal*. Lisbon, Universidade de Lisboa. **PhD**: 438.

Rizzo WM (1990). "Nutrient Exchanges between the Water Column and a Subtidal Benthic Microalgal Community." *Estuaries* **13**(3): 219 - 226.

Round FE & Haphey CM (1965). "Persistent, vertical-migration rhythms in benthic microflora. Part IV: a diurnal rhythm of the epipellic diatom association in non-tidal flowing water." *British Phycological Bulletin* **2**: 463-471.

Round FE & Palmer JD (1966). "Persistent, vertical-migration rhythms in benthic microflora. II. Field and laboratory studies on diatoms from the banks of the river Avon." *Journal of the Marine Biological Association of the United Kingdom* **46**: 191 - 214.

Round FE & Eaton JW (1966). "Persistent, Vertical-Migration Rhythms in Benthic Microflora: III. The Rhythm of Epipellic Algae in a Freshwater Pond." *Journal of Ecology* **54**(3): 609-615.

Round FE (1981). *The ecology of algae*. Cambridge: Cambridge University Press.

Round FE, Crawford RM & Mann DG (1990). *The Diatoms: Biology & Morphology of the Genera*. Cambridge: Cambridge University Press.

Ruddy G (1997). An overview of carbon and sulphur cycling in marine sediments. *Biogeochemistry of intertidal sediments*. T. D. Jickels and J. E. Rae. Cambridge, Cambridge University Press: 20.

- Rysgaard S, Christensen PB & Nielsen LP (1995). "Seasonal variation in nitrification and denitrification in estuarine sediment colonized by benthic microalgae and bioturbating infauna." *Marine Ecology Progress Series* **126**: 111-121.
- Rysgaard S, Thastum P, Dalgaard T, Christensen PB & Sloth NP (1999). "Effects of salinity on NH_4^+ adsorption capacity, nitrification, and denitrification in Danish estuarine sediments." *Estuaries* **22**(1): 21 - 30.
- Ryther JH & Dunstan WM (1971). "Nitrogen, Phosphorus, and Eutrophication in the Coastal Marine Environment." *Science* **171**(3975): 1008-1013.
- Scottish Natural Heritage (2006). Advice under Regulation 33(2) of The Conservation (Natural Habitats, & c.) Regulations 1994. S. N. Heritage.
- Saburova MA and Polikarpov IG (2003). "Diatom activity within soft sediments: behavioural and physiological processes." *Marine Ecology Progress Series* **251**: 115 - 126.
- Seabloom EW & Richards SA (2003). "Multiple stable equilibria in grasslands mediated by herbivore population dynamics and foraging behavior." *Ecology* **84**(11): 2891-2904.
- SEPA (2005). Eutrophication Assessment of Scottish Coastal, Estuarine and Inland Waters. SEPA. Stirling.
- SEPA (2006). Scotland's Water Environment Review 2000 - 2006.
- Serôdio J, da Silva JM & Catarino F (2001). "Use of in vivo chlorophyll a fluorescence to quantify short-term variations in the productive biomass of intertidal microphytobenthos." *Marine Ecology Progress Series* **218**: 45-61.
- Serôdio J, Cruz S, Vieira S & Brotas V (2005). "Non-photochemical quenching of chlorophyll fluorescence and operation of the xanthophyll cycle in estuarine

microphytobenthos." *Journal of Experimental Marine Biology and Ecology* **326**: 157 - 169.

Smith D, Hughes RG & Cox EJ (1996). "Predation of epipelagic diatoms by the amphipod *Corophium volutator* and polychaete *Nereis diversicolor* " *Marine Ecology Progress Series* **145**(31 Dec): 53 - 61.

Smith VH, Tilman GD & Nekola JC (1999). "Eutrophication: impacts of excess nutrient inputs on freshwater, marine, and terrestrial ecosystems." *Environmental Pollution* **100**(1-3): 179-196.

Snøeijs P (1993). Intercalibration and distribution of diatom species in the Baltic Sea, vol 1. *The Baltic Marine Biologists Publication*. P. Snøeijs. Uppsala, Opulus Press. **16c**: 129.

Snøeijs P & Vilbaste S, Eds. (1994). *Intercalibration and distribution of diatom species in the Baltic Sea, vol 2*. The Baltic Marine Biologists. Uppsala, Opulus Press.

Snøeijs P & Potapova M (1995). Intercalibration and distribution of diatom species in the Baltic Sea, vol 3. *The Baltic Marine Biologists Publication*. P. Snøeijs. Uppsala, Opulus Press. **16c**: 126.

Snøeijs P & Kasperoviciene J (1996). Intercalibration and distribution of diatom species in the Baltic Sea, vol 4. . *The Baltic Marine Biologists Publication*. Uppsala, Opulus Press. **16d**: 126.

Snøeijs P & Balashova N (1998). Intercalibration and distribution of diatom species in the Baltic Sea, vol 5. *The Baltic Marine Biologists Publications*. Uppsala, Opulus Press. **16e**: 144.

Snøeijs P, Busse S & Potapova M (2002). "The importance of diatom cell size in community analysis." *Journal of Phycology* **38**: 265 - 272.

Solan M, Cardinale BJ, Downing AL, Engelhardt KAM, Ruesink JL & Srivastava DS (2004). "Extinction and Ecosystem Function in the Marine Benthos." *Science* **306**(12 Nov): 1177 - 1180.

Sørensen J (1978). "Capacity for denitrification and reduction of nitrate to ammonia in coastal marine sediment." *Applied and Environmental Microbiology* **35**(2): 301 - 305.

Spears BM, Carvalho L, Perkins R, O'Malley MB & Paterson D (2010). "The contribution of epipelton to total sediment microalgae in a shallow temperate eutrophic loch (Loch Leven, Scotland)." *Hydrobiologia (online)*.

Stöcker FW & Dietrich G, Eds. (1996). *Concise Encyclopedia: Biology*. Berlin, Walter de Gruyter.

Strother PK, Servais T & Vecoli M (2010). "The effects of terrestrialization on marine ecosystems: the fall of CO₂." *Geological Society, London, Special Publications* **339**(1): 37-48.

Stuart V, Head EJH & Mann KH (1985). "Seasonal changes in the digestive enzyme levels of the amphipod *Corophium volutator* (Pallas) in relation to diet." *Journal of Experimental Marine Biology and Ecology* **88**: 243 - 256.

Sukenik A, Wyman KD, Bennet J & Falkowski PG (1987). "A novel mechanism for regulating the excitation of photosystem II in a green alga." *Nature* **327**(6124): 704 - 707.

Sundbäck K & Graneli W (1988). "Influence of microphytobenthos on the nutrient flux between sediment and water: a laboratory study." *Marine Ecology Progress Series* **43**: 63 - 69.

- Sundbäck K & Snoeijs P (1991). "Effects of nutrient enrichment on microalgal community composition in a coastal shallow-water sediment system - an experimental study." *Botanica Marina* **34**(4): 341-358.
- Sundbäck K, Nilsson P, Nilsson C & Jönsson B (1996). "Balance Between Autotrophic and Heterotrophic Components and Processes in Microbenthic Communities of Sandy Sediments: A Field Study." *Estuarine, Coastal and Shelf Science* **43**(6): 689-706.
- Sundbäck K, Miles A & Göransson E (2000). "Nitrogen fluxes, denitrification and the role of microphytobenthos in microtidal shallow-water sediments: an annual study." *Marine Ecology Progress Series* **200**: 59-76.
- Thayer CW (1979). "Biological Bulldozers and the Evolution of Marine Benthic Communities." *Science* **203**(4379): 458 -461.
- Thornton DCO, Dong LF, Underwood GJC & Nedwell DB (2002). "Factors affecting microphytobenthic biomass, species composition and production in the Colne Estuary (UK)." *Aquatic Microbial Ecology* **27**(3): 285-300.
- Tilman D & Downing JA (1994). "Biodiversity and stability in grasslands." *Nature* **367**(6461): 363-365.
- Tilman D, Reich PB & Knops JMH (2006). "Biodiversity and ecosystem stability in a decade-long grassland experiment." *Nature* **441**(7093): 629-632.
- Tolhurst TJ, Black KS, Shayler SA, Mather S, Black I, Baker K & Paterson DM (1999). "Measuring the in situ Erosion Shear Stress of Intertidal Sediments with the Cohesive Strength Meter (CSM)." *Estuarine, Coastal and Shelf Science* **49**(2): 281-294.
- Tolhurst TJ, Defew EC, de Brouwer JFC, Wolfstein K, Stal LJ & Paterson DM (2006). "Small-scale temporal and spatial variability in the erosion threshold and

properties of cohesive intertidal sediments." *Continental Shelf Research* **26**(3): 351-362.

Tolhurst TJ, Consalvey M & Paterson DM (2008). "Changes in cohesive sediment properties associated with the growth of a diatom biofilm." *Hydrobiologia* **596**: 225-239.

Townsend CR, Harper JL & Begon M (2000). *Essentials of Ecology*. London: Blackwell Science, Inc.

Trevor JH (1977). "The burrowing of *Nereis diversicolor* O.F. Müller, together with some observations on *Arenicola marina* (L.) (Annelida: Polychaeta)." *Journal of Experimental Marine Biology and Ecology* **30**(2): 129-145.

Underwood GJC, Phillips J & Saunders K (1998). "Distribution of estuarine benthic diatom species along salinity and nutrient gradients." *European Journal of Phycology* **33**(02): 173-183.

Underwood GJC & Kromkamp J (1999). Primary production by phytoplankton and microphytobenthos in estuaries. *Advances in Ecological Research: Estuaries*. D. B. Nedwell and D. G. Raffaelli. **29**: 93 - 153.

Underwood GJC & Provot L (2000). "Determining the environmental preferences of four estuarine epipelagic diatom taxa: growth across a range of salinity, nitrate and ammonium conditions " *European Journal of Phycology* **35**: 173 -182.

Vaccaro RF (1962). "The Oxidation of Ammonia in Sea Water." *ICES J. Mar. Sci.* **27**(1): 3-14.

Van den Hoek C, Mann DG & Jahns HM (1995). *Algae: an introduction to phycology*. Cambridge: Cambridge University Press.

Van der Werff A & Huls H (1976). *Diatomeeenflora van Nederland (Diatom Flora of the Netherlands)*. Koenigstein: Otto Koeltz Science Publishers.

Vidal M & Duarte CM (2000). "Nutrient accumulation at different supply rates in experimental Mediterranean planktonic communities." *Marine Ecology Progress Series* **207**: 1-11.

Wentworth CK (1922). "A scale of grade and class terms for clastic sediments." *Journal of Geology* **30**(5): 377 - 392.

Widdows J, Brinsley MD, Salkeld PN & Lucas CH (2000). "Influence of biota on spatial and temporal variation in sediment erodability and material flux on a tidal flat (Westerschelde, The Netherlands)." *Marine Ecology Progress Series* **194**: 23-37.

Widdows J & Brinsley M (2002). "Impact of biotic and abiotic processes on sediment dynamics and the consequences to the structure and functioning of the intertidal zone." *Journal of Sea Research* **48**(2): 143-156.

Widdows J, Blauw A, Heip CHR, Herman PMJ, Lucas CH, Middelburg JJ, Schmidt S, Brinsley MD, Twisk F & Verbeek H (2004). "Role of physical and biological processes in sediment dynamics of a tidal flat in Westerschelde Estuary, SW Netherlands." *Marine Ecology Progress Series* **274**: 41-56.

Whitmarsh J & Govindjee (1999). The photosynthetic process. *Concepts in Photobiology: Photosynthesis and Photomorphogenesis*. G. S. Singhal, G. Renger, S. K. Sopory, K.-D. Irrgang and Govindjee. Dordrecht and New Dehli, Kluwer Academic Publishers and Narosa Publishing House: 11 - 51.

Wilkie, L (2011) The role of intertidal seagrass *Zostera* spp. in sediment deposition and coastal stability in the Tay Estuary, Scotland. PhD Thesis, University of St Andrews.

Wittkowski A, Lange-Bertalot H & Metzeltin D (2000). *Diatom Flora of Marine Coasts I* A.R.G. Gantner Verlag K.G.

Wilson EO (1992). *The Diversity of Life*. New York: W.W. Norton & Company Inc./ Harvard University Press.

Wood R & Widdows J (2002). "A Model of Sediment Transport over an Intertidal Transect, Comparing the Influences of Biological and Physical Factors." *Limnology and Oceanography* **47**(3): 848 - 855.

Yoon HS, Hackett JD, Ciniglia C, Pinto G & Bhattacharya D (2004). "A Molecular Timeline for the Origin of Photosynthetic Eukaryotes." *Molecular Biology and Evolution* **21**(5): 809-818.

Zuur AF, Ieno EN & Smith GM (2007a). *Analysing ecological data*. New York: Springer.

Zuur (2007b) *Analysing Ecological Data using mixed modelling techniques and extensions*, Course handbook. Springer: pp164.

Zuur AF, Ieno EN, Walker NJ, Saveliev AA & Smith GM (2009). *Mixed Effects Models and Extension in Ecology with R*. New York: Springer Science + Business Media.

Zuur AF, Ieno EN & Elphick CS (2010). "A protocol for data exploration to avoid common statistical problems." *Methods in Ecology and Evolution* **1**: 3 - 14.

Glossary of terms

Glossary of terms

Ammonification

The breakdown of organic nitrogen (amino acids) by ammonifying bacteria under oxic conditions (Dexter Dyer 2003).

Benthic

Adj. describing organisms living in or on the substratum

Biodiffuser

Sediment infauna that move sediment around in a random directions and in small increments (e.g. *M.baltica*, *C. edule*, *C. volutator*). They oxygenate the sediment in small areas.

Bioirrigator

Sediment that actively irrigate their burrows by drawing surface water through it and expelling it at the surface (*C. volutator*).

Bioturbation

The reworking of sediment by organisms living in or on it which generally serves to mix, oxygenate, and irrigate the sediment (also see biodiffuser, bioirrigator, and gallery-diffuser).

Compaction

The sinking of sediment due to gravitational forces acting on it, generally serves to 'de-water' and solidify the sediment (Brown et al 1999).

Denitrification

The reduction of nitrates (NO_3^-) to atmospheric nitrogen (N_2) by anaerobic bacteria.

Deposition

The dropping of sediment and other particles out of the water column onto the substratum. Deposition is maximal in zero flow conditions and decreases (non-linearly) with increased flow and decreased grain size. Therefore, mudflats in estuaries can generally be assumed to be 'low-flow' areas (Brown et al 1999).

Ecosystem engineering

The process by which organismal activity creates or modifies the flow of biotic and abiotic resources in an ecosystem (Jones et al 1994, 1997).

Ecosystem function

Any process that naturally occurs in an ecosystem (e.g. primary production or slowing of water flow by plant, tube, or mussel beds and subsequent deposition of sediment), that connects two or more nodes (organisms or resources) of that system.

Ecosystem stability

This is a theoretical/mathematical concept that quantifies the recoverability or likelihood of return to a global or local equilibrium level of a process, resource or population after a slight perturbation (e.g. invasion of foreign species or physical destruction).

E_k

Energy (PAR) at which linear increase of photosynthetic output with PAR ceases (becomes non-linear).

E_s

Energy (PAR) at which photosynthetic output is maximized.

Epifauna

Fauna living on top of substratum (e.g. *Mytilus edulis*, *Hydrobia ulvae*).

Epipellic

Diatoms living free amongst sediment grains (motile).

Epiphytic

Diatoms (in this thesis, but otherwise any taxa) living on plants, attached by stalks, mucilage tubes, or valve face.

Epilithic

Diatoms (in this thesis, but otherwise any taxa) living on rocks, attached by stalks, mucilage tubes, or valve face.

Epipsammic

Diatoms living on sand grains, usually attached by valve face, semi-motile or non-motile.

Extended phenotype

Gallery-diffuser

Sediment infauna that actively irrigate a network of burrows by drawing surface water through it (e.g. *Hediste diversicolor*, Jones & Frid 2009).

Grain size

The widest diameter of a sediment grain by which sediment is classified as clay (< 2 μm), silt (2 – 63 μm), sand (63 μm – 2 mm), gravel (2 – 256 mm), and boulders (> 256 mm) (Wentworth 1922)

Infauna

Fauna living within of substratum, usually soft sediment (e.g. *Corophium volutator*, *Cerastoderma edule*, *Lumbricus terrestris*).

Inundation

The flooding of land by the sea.

Laminar flow

Single-directional flow that is parallel to the substratum (also see 'Turbulent flow')

Macrofauna

Any epi- or infauna that remains behind when sifted through a 500 μm mesh (not a biological definition, more a working definition).

Niche construction

The process by which organisms modify their habitats, thereby potentially modifying other resource flows, and create an ecological inheritance that interacts with genetic inheritance of the organism itself as well as other organisms which do not inherit the niche constructor's genes but do 'inherit' the ecological legacy.

Nitrification

The oxidation of ammonia (NH_4^+) to nitrite (NO_2^-) by aerobic bacteria.

Resuspension

The removal of particles from the substratum into the water column either by disturbance, increased flow, or biogenic erosion.

Sedimentation

The settling of sediment out of the water column (same as deposition).

Shear stress

Also, 'bed shear stress', 'critical shear stress'

Turbulent flow

Water flow which contains a vertical component which creates movement in multiple directions (in 3 dimensions) at multiple velocities within the net direction of flow (Brown et al 1999, also see 'Laminar flow')

Diatom morphology

Diatom morphology in Appendices I – II is described according to Hendey (1964), Barber & Haworth (1981), and Kelly *et al* (2005). Descriptions of "live" taxa in Appendices II and III are also described using Cox (1996) and Round *et al* (1990).

Aspect

The position in which the diatom frustule or valve is lying under the microscope and hence from what perspective it is observed from above: 'valve view' or 'girdle view' (Figure G1). The position in which the frustules (in case of unoxidized or "live" material) or valves (in case of oxidized material) tend to lie varies with taxa. Taxa where the valve width is similar to the girdle or mantle width will tend to fall in either girdle or valve view; taxa where the valve width is much larger than the girdle or mantle width, or the girdle mantle is convex, will tend to fall in valve view; taxa where the valve width is narrower than the girdle or mantle width or the valve face is strongly convex, will tend to fall in girdle view (Figure G3).

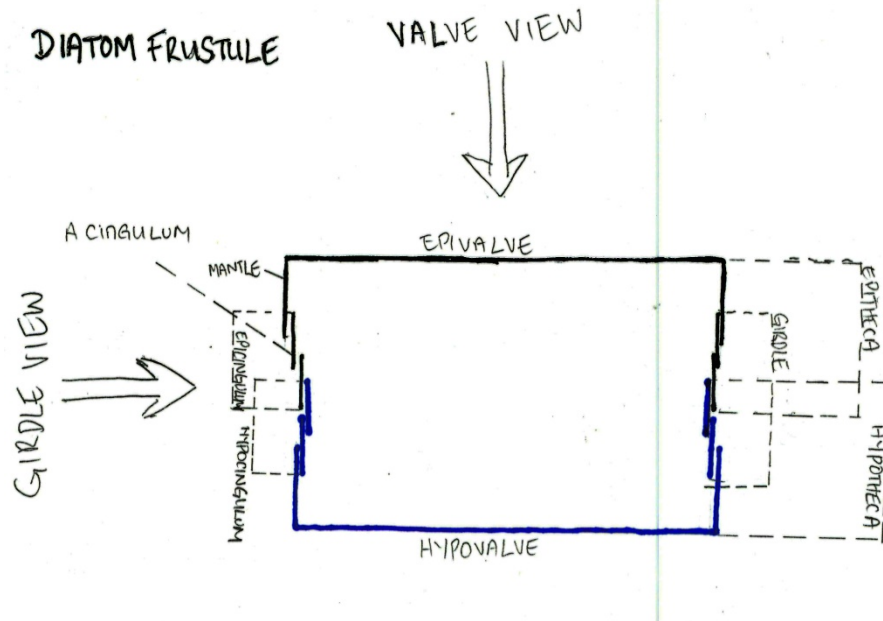


Figure G1: A standardized diatom frustule

Frustule

The siliceous cage that contains the diatom soft tissue. The frustule is composed of two valves (resembling the top and bottom half of a petri dish) which are connected by multiple girdle bands (Figure G1).

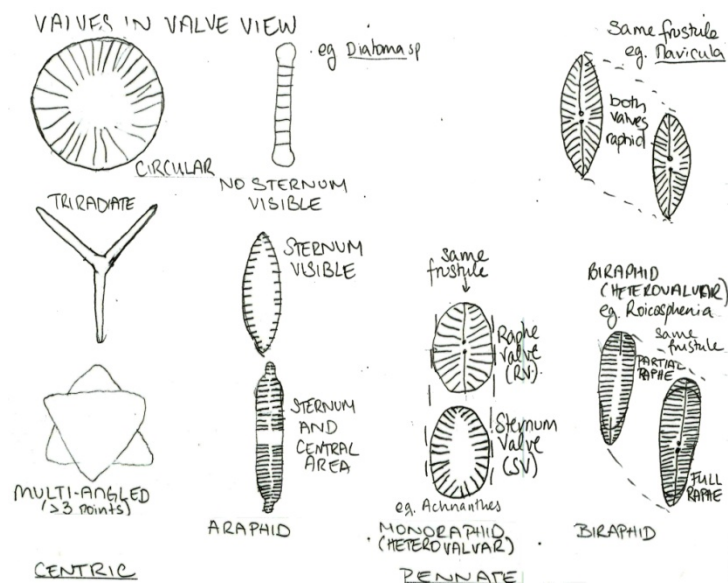


Figure G2: Valves view (centrics and pennates)

Araphid

Figure G3: Valve symmetry

Valve

A part of the siliceous skeleton of a diatom of which there are two: the large half is the epitheca and the smaller half is the hypotheca (Figure G1). Valves can be centric (circular) or pennate (elongate) and pelagic diatoms (marine and freshwater) are mostly centric and benthic valves are mostly pennate (Figure G2), although there are exceptions in each and, of course pelagic diatoms are found in the benthos because they are deposited and pennate diatoms are found in the water column because they are resuspended (Round et al 1990).

Symmetry

Apical: along the apical axis of a pennate diatom (from Kelly et al 2005).

Transapical: Symmetry along the transapical axis of a pennate diatom: can be isopolar (two ends are the same) or heteropolar (two ends are different) (from Kelly et al 2005).

Pervalvar: along pervalvar axis of diatom (from Kelly et al 2005).

Valve Features

Apex

The end of a pennate diatom: they are either inflected (distinct from 'body' of valve) or not (Figure G4).

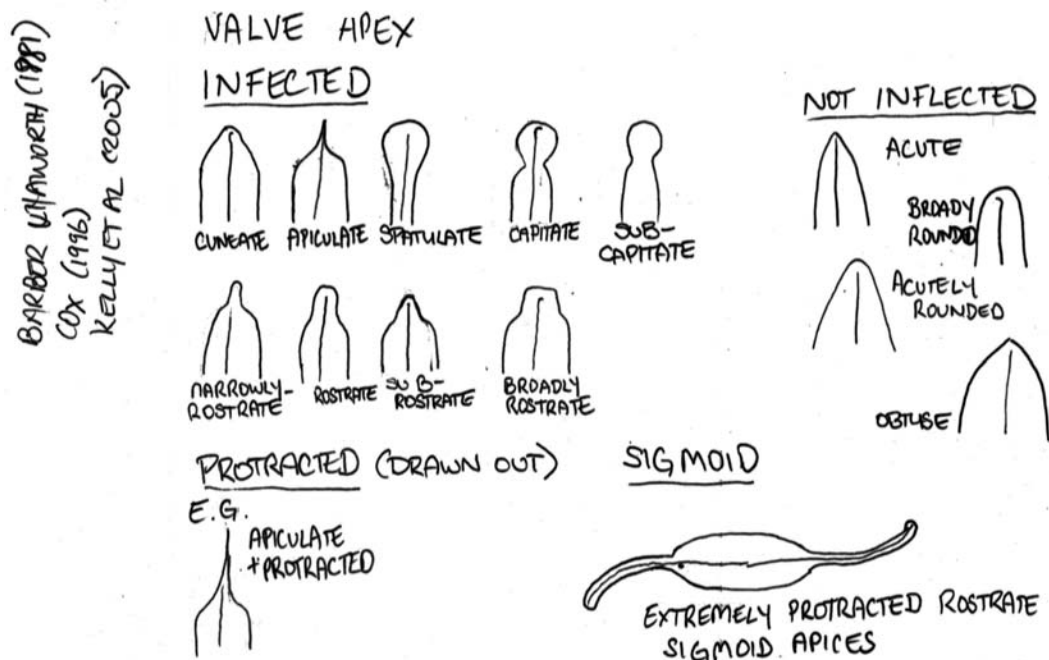


Figure G4: Valve apices

Central area

Fascia: hyaline running across transapical axis at centre of valve face.

Stauros: A transapical heavily silicified expansion of the sternum which looks like a bridge across the centre of the valve.

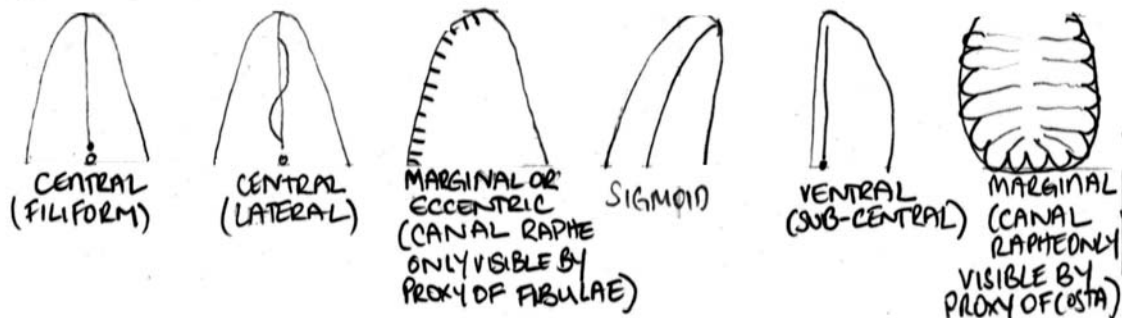
Hyaline area

An area with no ornamentation on the valve face. A **sternum** is the hyaline area along apical axis of a pennate valve, which may or may not contain a raphe. When longitudinal (as in *Cocconeis* spp.) hyaline areas appear like ribs separating striae, or lyre-shaped and longitudinal in *Fallacia*. A **central area** is common form of hyaline area at the centre of the valve face where striae stop well short of apical axis. A **polar area** is an unornamented area at the apices.

Raphe

A central slit running down the apical length of a pinnate diatom valve through which extracellular polymeric substances are exuded for protection of the cell and, most notably, movement within sediment. Raphes can be central (running along apical axis), lateral (off the apical axis but on valve face), or eccentric (running along the margin of the valve) (following Barber & Haworth 1981, Kelly et al 2005).

RAPHE



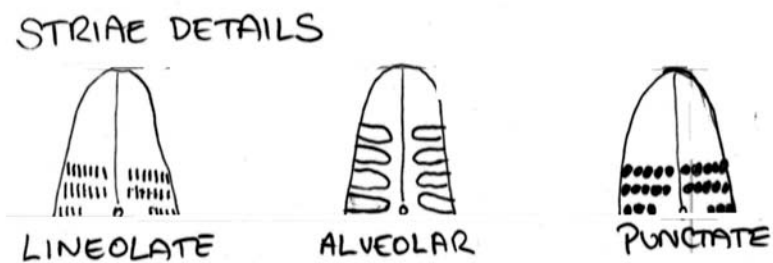
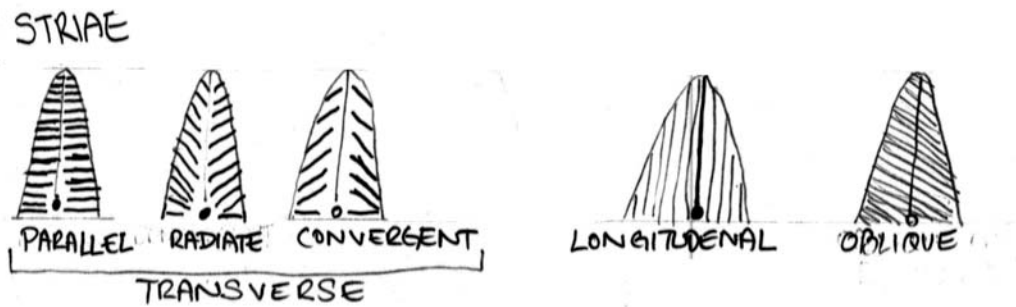
OTHER RAPHE FEATURES

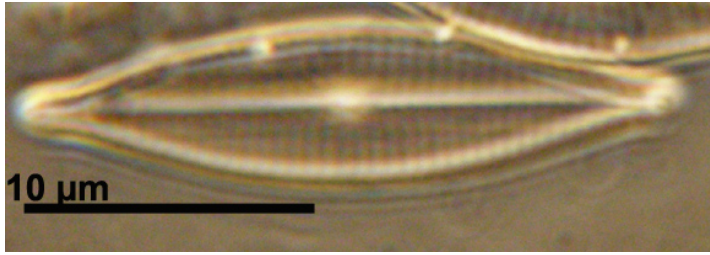


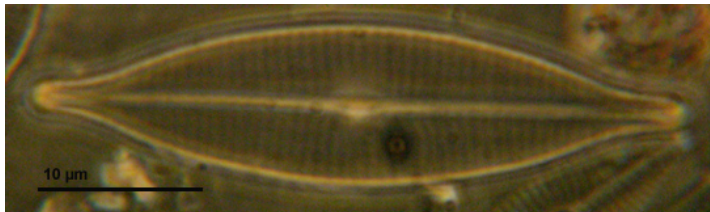
Central and terminal nodules are thickenings of silica at the central and terminal ending of a raphe that appear like a thick halo around these locations.

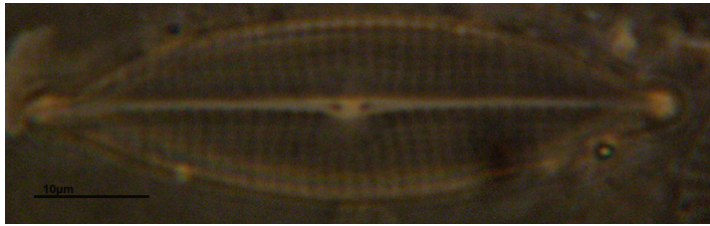
Striae

'Ornamentation' on the valve face in the form of channels or pores. Often the pores cannot be resolved in LM.

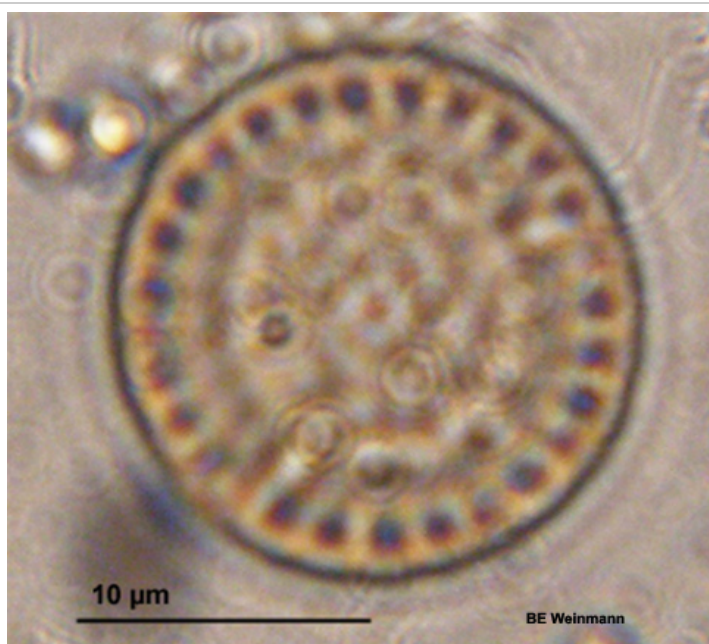


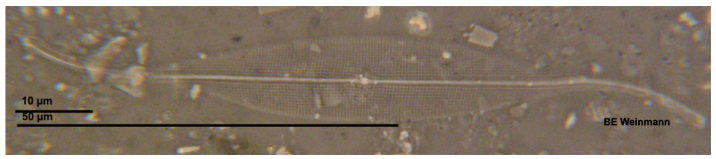
1_1	Navicula gregaria Donkin (type 1) [Cox 1987 p168-169 B?]
Specimens Measured:	20
Aspect:	Valve
Valve symmetry or shape:	Apical sym = Isobilateral, Transapical sym = Isopolar, Valve shape = Lanceolate, Valve curvature = none, Apex shape = inflection, Shape = 'Protracted, rostrate or sub-rostrate', Frustral shape = na
Dimensions µm [AA]:	16.3 - (23.8) - 34.5
Dimensions µm [TA]:	4.4 - (6.5) - 10.3
Raphe:	Raphe, location = Central, shape = 'linear, filiform', central endings = 'straight, slightly expanded', polar endings = 'not visible'
Striae:	17 - 20 per 10µm, orientation = 'parallel perhaps slightly radiate and becoming slightly convergent towards the poles', pores = 'not resolvable', na per 10µm
Fibulae or Costae:	
Axial area:	axial area = 'narrow, linear' , central area = Widened, round, unsymmetrical, central nodule = round and bright, terminal nodule = terminals just visible, other hyaline areas = na
Other Features:	Spines = None; Comments = 'gracile N. gregaria, lineolae not always visible, apex tending to sub-rostrate '; Other = 'na'
Image path:	Catalogue3\Cat3-Ref1\Cat3-Ref1-1_2008-11-19.jpg
	


1_2	Navicula gregaria Donkin [BMB2: #160; Witkowski 124: 8-25; Cox, 1987 p168-169 A?]
Specimens Measured:	22
Aspect:	Valve
Valve symmetry or shape:	Apical sym = Isobilateral, Transapical sym = Isopolar, Valve shape = Lanceolate, Valve curvature = none, Apex shape = inflection, Shape = 'Protracted, rostrate', Frustral shape = na
Dimensions µm [AA]:	23.7 - (32.3) - 57
Dimensions µm [TA]:	7.4 - (7.8) - 8.9
Raphe:	Raphe, location = Central, shape = 'linear', central endings = 'deflected to same side, slightly expanded', polar endings = 'not visible'
Striae:	per 10µm, orientation = 'transverse, slightly radiate becoming convergent towards poles', pores = 'lineolate', ~25 per 10µm
Fibulae or Costae:	
Axial area:	axial area = 'narrow, linear' , central area = irregular transverse expansion on both sides, not symmetrical, central nodule = large, irregular shape, terminal nodule = visible, other hyaline areas = none
Other Features:	Spines = None; Comments = 'larger, fatter N. gregaria, striae distinctly lineolate, apices distinctly rostrate'; Other = 'na'
Image path:	Catalogue3\Cat3-Ref1\Cat3-Ref1-2_E2-OA-c265.jpg
	

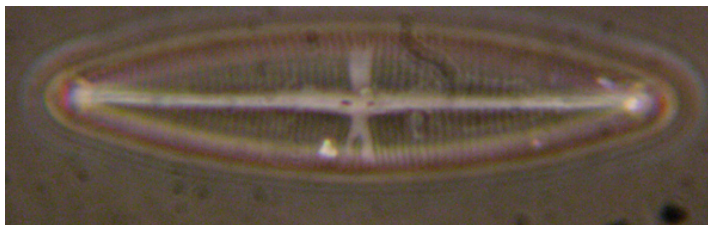
1_3	Navicula gregaria [Cox 1987 p168 - 169 C]
Specimens Measured:	10
Aspect:	Valve
Valve symmetry or shape:	Apical sym = Isobilateral, Transapical sym = Isopolar, Valve shape = Lanceolate, Valve curvature = none, Apex shape = inflection, Shape = 'Protracted, rostrate or sub-rostrate', Frustral shape = na
Dimensions µm [AA]:	23.5 - (30.1) - 55.9
Dimensions µm [TA]:	6.6 - (8.3) - 13.2
Raphe:	Raphe, location = Central, shape = 'linear, filiform', central endings = 'deflected to same side', polar endings = 'not visible'
Striae:	per 10µm, orientation = 'Transverse, parallel perhaps slightly convergent towards poles', pores = 'not resolvable', na per 10µm
Fibulae or Costae:	
Axial area:	axial area = 'broad and linear' , central area = slightly constricted, central nodule = large & bright, terminal nodule = visible (?), other hyaline areas = na
Other Features:	Spines = None; Comments = 'Slightly unsymmetric on AA, striae more parallel than straight, apices sub-rostrate, striae paler'; Other = 'na'
Image path:	Catalogue3\Cat3-Ref1\Cat3-Ref1-3_E2-OAc92.jpg
	


2_4	Cyclotella meneghiniana (Kützinger) 1844 [BMB1: #32 and Hartley et al pl. 58: Fig.17]
Specimens Measured:	na
Aspect:	Valve
Valve symmetry or shape:	Apical sym = na, Transapical sym = na, Valve shape = Round, Valve curvature = none, Frustral shape = na
Dimensions µm [AA]:	25.9 - (0) - na
Dimensions µm [TA]:	na - (0) - na
Raphe:	None, location = na, shape = 'na', central endings = 'na', polar endings = 'na'
Striae:	11 per 10µm, orientation = 'radiate from centre', pores = 'not resolvable', na per 10µm
Fibulae or Costae:	areolae
Axial area:	axial area = 'na', central area = na, central nodule = na, terminal nodule = na, other hyaline areas = large central (50% valve)
Other Features:	Spines = None; Comments = 'Outside ring of areolae, inside ring of striae, centre is bald.'; Other = 'na'
Image path:	Catalogue3\Cat3-Ref2\Cat3-Ref2-4_E2-T1.1-c3.jpg

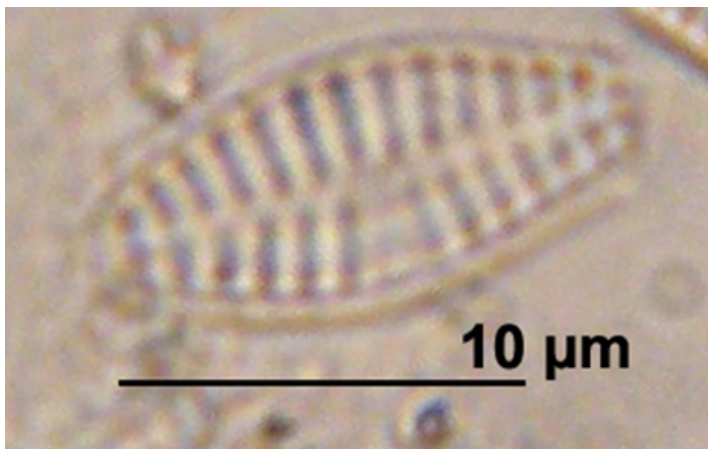


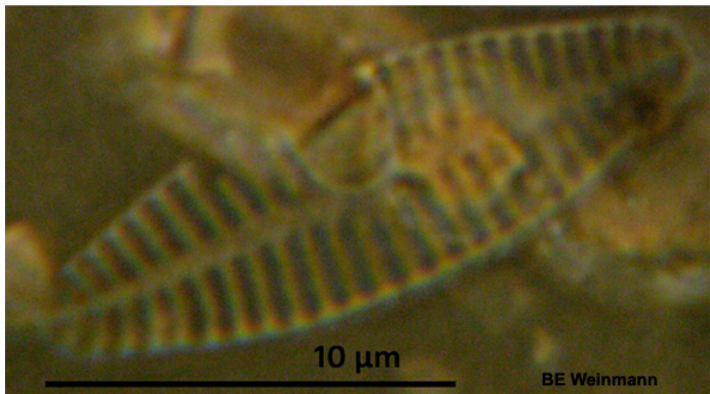
3_5	Gyrosigma fasciola (Ehrenberg) Griffith et Henfrey [BMB4: #347; Hartley pl. 113:3]
Specimens Measured:	na
Aspect:	Valve
Valve symmetry or shape:	Apical sym = Isobilateral, Transapical sym = Isopolar, Valve shape = Lanceolate-sigmoid, Valve curvature = none, Apex shape = inflection, Shape = 'Extremely protracted, rostrate, sigmoid', Frustral shape = na
Dimensions µm [AA]:	74 - (83) - 110
Dimensions µm [TA]:	8 - (11.2) - 17.3
Raphe:	Raphe, location = Central, shape = 'na', central endings = 'na', polar endings = 'na'
Striae:	na per 10µm, orientation = 'na', pores = 'na', na per 10µm
Fibulae or Costae:	
Axial area:	axial area = 'na' , central area = na, central nodule = na, terminal nodule = na, other hyaline areas = na
Other Features:	Spines = None; Comments = 'na'; Other = 'na'
Image path:	Catalogue3\Cat3-Ref3-5.jpg
	

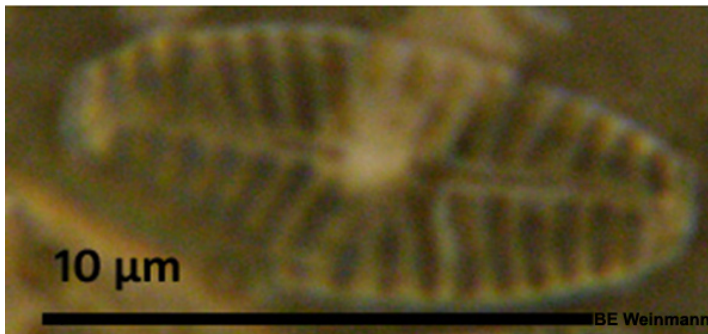
4_6	Stauroneis dubitabilis Hustedt [Witkowski pl. 149:1,2; pl. 151:18,19]
Specimens Measured:	na
Aspect:	Valve
Valve symmetry or shape:	Apical sym = Isobilateral, Transapical sym = Isopolar, Valve shape = Lanceolate, Valve curvature = none Apex shape = no inflection, Shape = 'Acute', Frustral shape = na
Dimensions µm [AA]:	48 - (49.1) - 50
Dimensions µm [TA]:	10.4 - (10.8) - 11.2
Raphe:	Raphe, location = Central, shape = 'linear, filiform', central endings = 'oval expansion', polar endings = 'hardly visible'
Striae:	per 10µm, orientation = 'Transverse, slightly radiate', pores = 'not resolvable', na per 10µm
Fibulae or Costae:	
Axial area:	axial area = 'linear' , central area = Stauros, slightly wider at margins, central nodule = not clear, terminal nodule = none, other hyaline areas = na
Other Features:	Spines = None; Comments = 'na'; Other = 'na'
Image path:	Catalogue3\Cat3-Ref4\Cat3-Ref4-6_2009-02-03.jpg
	

4_128	Stauroneis dubitabilis Hustedt [Witkowski pl. 149:1,2; pl. 151:18,19]
Specimens Measured:	na
Aspect:	Valve
Valve symmetry or shape:	Apical sym = Isobilateral, Transapical sym = Isopolar, Valve shape = Lanceolate, Valve curvature = None, Frustral shape = na
Dimensions µm [AA]:	na - (0) - na
Dimensions µm [TA]:	na - (0) - na
Raphe:	Raphe, location = Central, shape = 'Linear, straight', central endings = 'Straight, slightly inflated', polar endings = 'Not resolved'
Striae:	na per 10µm, orientation = 'Transverse, slightly radiate', pores = 'Punctate', Not resolved per 10µm
Fibulae or Costae:	
Axial area:	axial area = 'Linear, narrow' , central area = Narrowly lanceolate, central nodule = Very small, hardly visible, terminal nodule = Round, bright, other hyaline areas = Central fascia
Other Features:	Spines = None; Comments = 'I'm not sure this is distinct or a morphotype of Stauroneis dubitabilis. Haven't found a match in any of our catalogues'; Other = 'na'
Image path:	Catalogue3\Cat3-Ref4\Cat3-Ref4-128_2012-03-21-c128.jpg
	

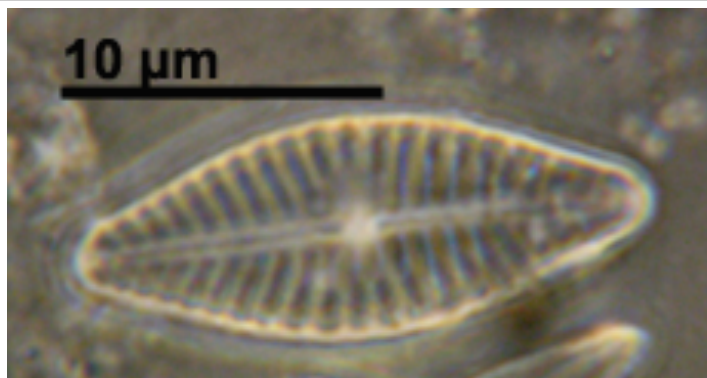
4_185	Stauroneis dubitabilis (?) [no ID]
Specimens Measured:	4
Aspect:	Girdle
Valve symmetry or shape:	
Dimensions µm [AA]:	40.4 - (43.4) - 46.3
Dimensions µm [PA]:	7.4 - (0) - 9.2
Raphe:	NA, location = NA, shape = 'NA', central endings = 'NA', polar endings = 'NA'
Striae:	16 - 19 per 10µm, orientation = 'Transverse, parallel', pores = 'Not resolved', 16 - 19 per 10µm
Fibulae or Costae:	
Axial area:	axial area = 'NA' , central area = NA, central nodule = Not visible, terminal nodule = Not visible, other hyaline areas = Stauros visible, with a few single striae in
Other Features:	Spines = None; Comments = 'na'; Other = 'na'
Image path:	Catalogue3\Cat3-Ref4\Cat3-Ref4-185_2012-04-18-c165.jpg
	

5_7	Achnanthes lanceolata (de Brébisson) Grunow (SV) [van der Werff & Huls PCFXV. 96] or Planothidium engelbrechtii Round & Buthyarova [Witkowski pl. 46:?]
Specimens Measured:	na
Aspect:	Valve
Valve symmetry or shape:	Apical sym = Isobilateral, Transapical sym = Isopolar, Valve shape = Broadly lanceolate, Valve curvature = none Apex shape = no inflection, Shape = 'Bluntly rounded', Frustral shape = na
Dimensions µm [AA]:	7 - (7.7) - 9.6
Dimensions µm [TA]:	3.7 - (4.7) - 5.2
Raphe:	Sternum, location = Central, shape = 'na', central endings = 'na', polar endings = 'na'
Striae:	na per 10µm, orientation = 'na', pores = 'na', na per 10µm
Fibulae or Costae:	
Axial area:	axial area = 'na' , central area = na, central nodule = na, terminal nodule = na, other hyaline areas = na
Other Features:	Spines = None; Comments = 'na'; Other = 'na'
Image path:	Catalogue3\Cat3-Ref5\Cat3-Ref5-7_2008-11-23.jpg
	

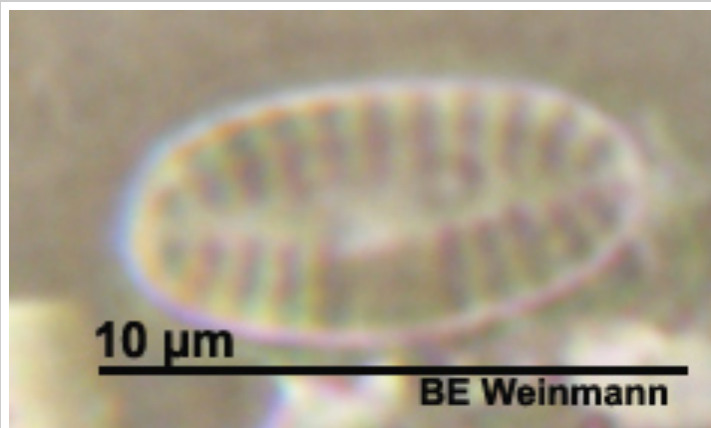
5_8	Achnanthes lanceolata (de Brébisson) Grunow (SV) [van der Werff & Huls PCFXV. 96]
Specimens Measured:	na
Aspect:	Valve
Valve symmetry or shape:	Apical sym = Isobilateral, Transapical sym = Isopolar, Valve shape = Broadly lanceolate, Valve curvature = none Apex shape = no inflection, Shape = 'Bluntly rounded', Frustral shape = na
Dimensions µm [AA]:	5.9 - (9.6) - 13.3
Dimensions µm [TA]:	3.7 - (4.8) - 4.7
Raphe:	Sternum, location = Central, shape = 'na', central endings = 'na', polar endings = 'na'
Striae:	15 per 10µm, orientation = 'Transverse, radiate becoming parallel', pores = 'not resolvable', na per 10µm
Fibulae or Costae:	
Axial area:	axial area = 'linear' , central area = One-sided, trapezoidal or horseshoe shaped, central nodule = none, terminal nodule = na, other hyaline areas = na
Other Features:	Spines = None; Comments = 'na'; Other = 'na'
Image path:	Catalogue3\Cat3-Ref5\Cat3-Ref5-8RLV_2008-12-02.jpg
	

5_9	Achnanthes lanceolata (de Brébisson) Grunow (RV) [van der Werff & Huls PCFXV. 96]
Specimens Measured:	na
Aspect:	Valve
Valve symmetry or shape:	Apical sym = Isobilateral, Transapical sym = Isopolar, Valve shape = Broadly lanceolate, Valve curvature = none Apex shape = no inflection, Shape = 'Bluntly rounded', Frustral shape = na
Dimensions µm [AA]:	5.9 - (9.6) - 13.3
Dimensions µm [TA]:	3.7 - (4.8) - 4.7
Raphe:	Raphe, location = Central, shape = 'linear, filiform', central endings = 'Distant, slightly expanded (pinhead)', polar endings = 'not expanded, bent to same side'
Striae:	13 - 14 per 10µm, orientation = 'Transverse, radiate becoming parallel', pores = 'not resolvable', na per 10µm
Fibulae or Costae:	
Axial area:	axial area = 'linear, narrow' , central area = One-sided, trapezoidal or horseshoe shaped, central nodule = Large, bright, terminal nodule = na, other hyaline areas = na
Other Features:	Spines = None; Comments = 'na'; Other = 'na'
Image path:	Catalogue3\Cat3-Ref5\Cat3-Ref5-9_E2-T1.1.jpg
	

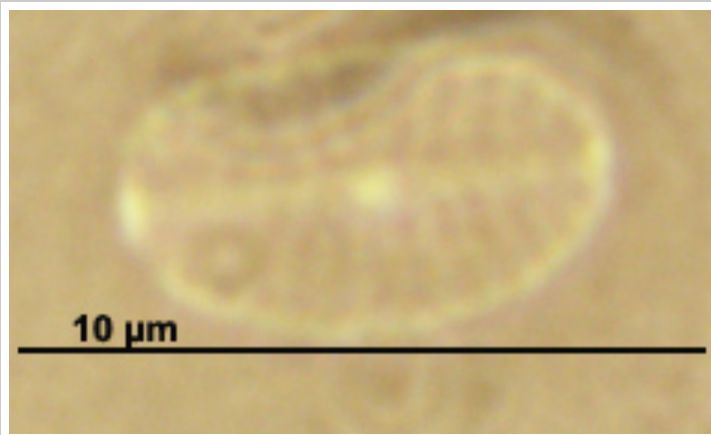
5_10	Achnanthes lanceolata (de Brébisson) Grunow (RV) [van der Werff & Huls PCFXV. 96]
Specimens Measured:	na
Aspect:	Valve
Valve symmetry or shape:	Apical sym = Isobilateral, Transapical sym = Isopolar, Valve shape = Broadly lanceolate, Valve curvature = none, Apex shape = inflection, Shape = 'Sub-rostrate', Frustral shape = na
Dimensions µm [AA]:	17 - (0) - na
Dimensions µm [TA]:	6.6 - (0) - na
Raphe:	Raphe, location = Central, shape = 'linear, filiform', central endings = 'Distant, slightly expanded (pinhead)', polar endings = 'not resolved (possibly hooked?)'
Striae:	13 - 14 per 10µm, orientation = 'Transverse, radiate', pores = 'not resolvable', na per 10µm
Fibulae or Costae:	
Axial area:	axial area = 'linear, narrow', central area = Unsymmetrical, trapezoidal on one side and elliptic on the other, central nodule = Large, bright, terminal nodule = Possibly, very small, other hyaline areas = na
Other Features:	Spines = None; Comments = 'Possibly P. deliculata (8-13)'; Other = 'na'
Image path:	Catalogue1\Cat1-ref92-121.bmp

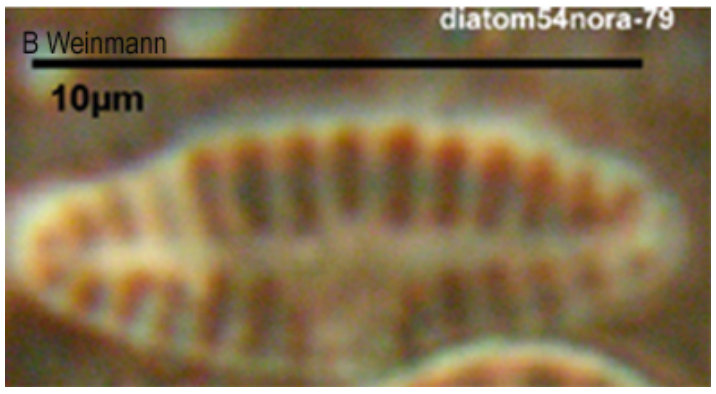


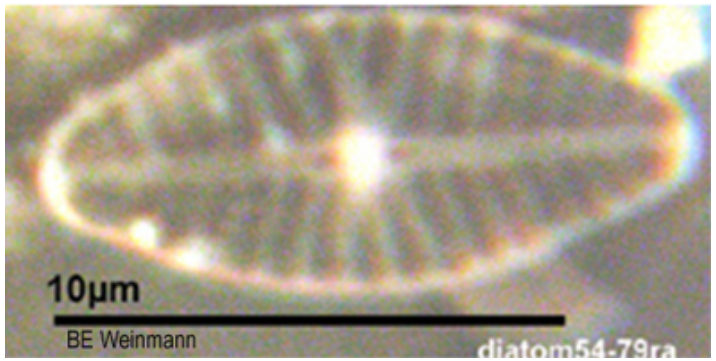
5_11	Achnanthes lanceolata var elliptica (SV) [van der Werff & Huls PCFXV. 96] or Achnanthes delicatula cf. m2 [Ribeiro 2010]
Specimens Measured:	na
Aspect:	Valve
Valve symmetry or shape:	Apical sym = Isobilateral, Transapical sym = Isopolar, Valve shape = Broadly lanceolate, Valve curvature = none Apex shape = no inflection, Shape = 'Broadly rounded', Frustral shape = na
Dimensions µm [AA]:	4.4 - (6.8) - 8.5
Dimensions µm [TA]:	1.5 - (4) - 5.4
Raphe:	Sternum, location = Central, shape = 'na', central endings = 'na', polar endings = 'na'
Striae:	13 - 14 per 10µm, orientation = 'Transverse, radiate', pores = 'not resolvable', na per 10µm
Fibulae or Costae:	
Axial area:	axial area = 'linear, narrow' , central area = Unsymmetrical, trapezoidal on one side, central nodule = none, terminal nodule = none, other hyaline areas = na
Other Features:	Spines = None; Comments = 'na'; Other = 'na'
Image path:	Catalogue3\Cat3-Ref5\Cat3-Ref5-11_2012-03-29-c26.jpg



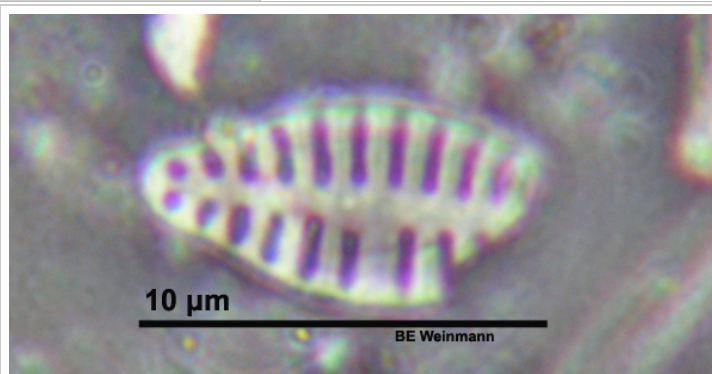
5_12	Achnanthes lanceolata var elliptica (RV) [van der Werff & Huls PCFXV. 96] or Achnanthes delicatula cf. m2 [Ribeiro 2010]
Specimens Measured:	na
Aspect:	Valve
Valve symmetry or shape:	Apical sym = Isobilateral, Transapical sym = Isopolar, Valve shape = Broadly lanceolate, Valve curvature = none Apex shape = no inflection, Shape = 'Broadly rounded', Frustral shape = na
Dimensions µm [AA]:	9.6 - (0) - na
Dimensions µm [TA]:	6 - (0) - na
Raphe:	Raphe, location = Central, shape = 'na', central endings = 'na', polar endings = 'na'
Striae:	10 per 10µm, orientation = 'Transverse, slightly radiate', pores = 'not resolvable', na per 10µm
Fibulae or Costae:	
Axial area:	axial area = 'linear, narrow' , central area = Symmetrical, rectangular TA expansion, central nodule = Large, bright, terminal nodule = small, very marginal, oval, other hyaline areas = na
Other Features:	Spines = None; Comments = 'na'; Other = 'na'
Image path:	Catalogue3\Cat3-Ref5\Cat3-Ref5-12_2012-03-24-c191.jpg



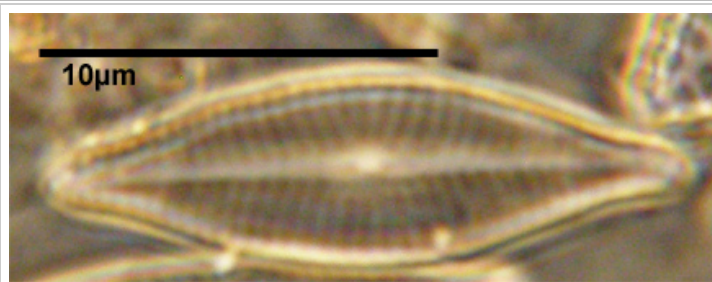
5_27	Achnanthes lanceolata (de Brébisson) Grunow (SV) [van der Werff & Huls PCFXV. 96]
Specimens Measured:	na
Aspect:	Valve
Valve symmetry or shape:	Apical sym = Isobilateral, Transapical sym = Isopolar, Valve shape = Broadly lanceolate, Valve curvature = none Apex shape = no inflection, Shape = 'Bluntly rounded', Frustral shape = na
Dimensions µm [AA]:	11.1 - (12.4) - 13.7
Dimensions µm [TA]:	4.4 - (2.8) - 4.4
Raphe:	Sternum, location = Central, shape = 'linear, filiform', central endings = 'na', polar endings = 'na'
Striae:	13 per 10µm, orientation = 'Transverse, parallel, becoming radiate', pores = 'not resolvable', na per 10µm
Fibulae or Costae:	
Axial area:	axial area = 'linear though slightly irregular' , central area = One-sided, trapezoidal, central nodule = na, terminal nodule = na, other hyaline areas = na
Other Features:	Spines = None; Comments = 'The lumpiness in the gap in striae could be thickening but found another photo and its actually an air bubble '; Other = 'na'
Image path:	Catalogue3\Cat3-Ref5\Cat3-Ref5-27_2009-01-20.jpg
	

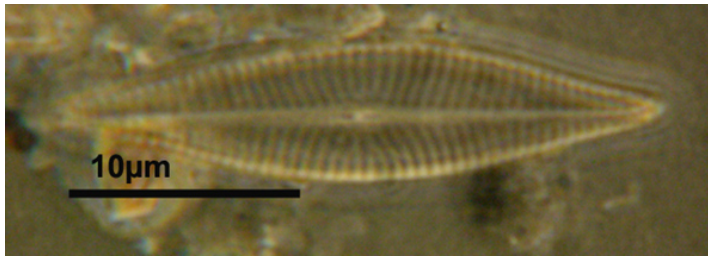
5_138	Achnanthes lanceolata (de Brébisson) Grunow (RV) [van der Werff & Huls PCFXV. 96]
Specimens Measured:	na
Aspect:	Valve
Valve symmetry or shape:	Apical sym = Isobilateral, Transapical sym = Isopolar, Valve shape = Broadly lanceolate, Valve curvature = none Apex shape = no inflection, Shape = 'Bluntly rounded', Frustral shape = na
Dimensions µm [AA]:	9.6 - (11.3) - 13
Dimensions µm [TA]:	5.1 - (5.5) - 5.9
Raphe:	Raphe, location = Central, shape = 'linear, filiform', central endings = 'Distant, slightly expanded (pinhead)', polar endings = 'Not resolved'
Striae:	13 per 10µm, orientation = 'Transverse, radiate', pores = 'not resolvable', na per 10µm
Fibulae or Costae:	
Axial area:	axial area = 'linear, quite narrow' , central area = One-sided, trapezoidal, central nodule = Large, bright, terminal nodule = not visible, other hyaline areas = na
Other Features:	Spines = None; Comments = 'na'; Other = 'na'
Image path:	Catalogue3\Cat3-Ref5\Cat3-Ref5-138_2009-01-20.jpg
	

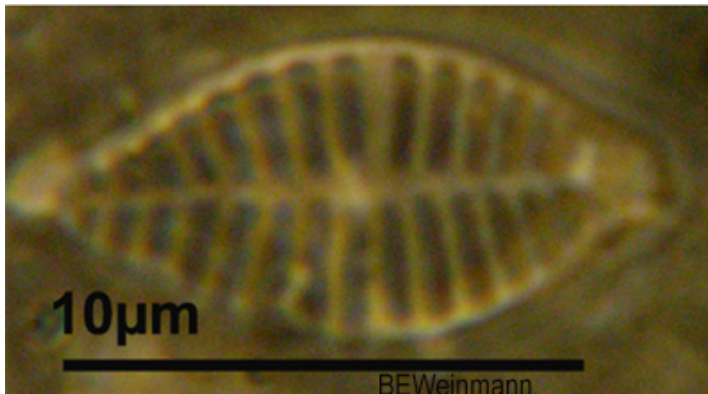
5_172	Achnanthes lanceolata var robusta SV [van der Werff & Huls 1974]
Specimens Measured:	1
Aspect:	Valve
Valve symmetry or shape:	Apical sym = na, Transapical sym = na, Valve shape = Lanceolate, Valve curvature = None, Apex shape = inflection, Shape = 'Protracted, broadly rostrate', Frustral shape = NA
Dimensions µm [AA]:	12.5 - (0) - na
Dimensions µm [TA]:	5.9 - (0) - na
Raphe:	Sternum, location = Central, shape = 'NA', central endings = 'NA', polar endings = 'NA'
Striae:	11 - 12 per 10µm, orientation = 'Transverse, parallel to slightly radiate', pores = 'Not resolved', na per 10µm
Fibulae or Costae:	
Axial area:	axial area = 'Linear' , central area = Slight TA expansion, central nodule = None, terminal nodule = None, other hyaline areas = None
Other Features:	Spines = None; Comments = 'I seperated these at the end, so I don't have any "5-172"s in my E3_DiatomIDs'; Other = 'na'
Image path:	Catalogue3\Cat3-Ref5\Cat2-Ref5-172_2012-04-13-c175.jpg

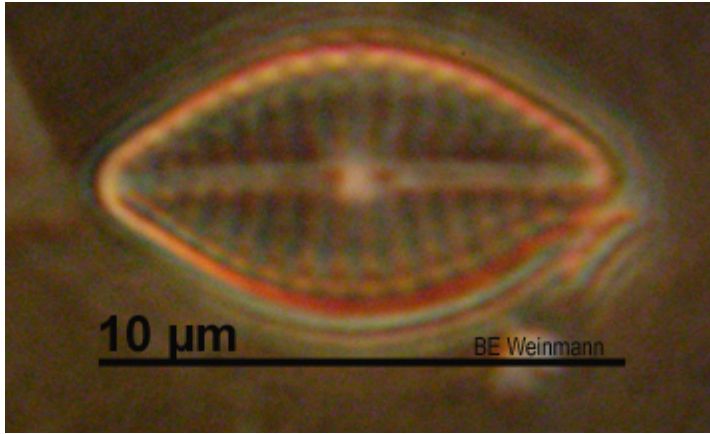


6_13	Navicula sp3 [?] or Navicula phyllepta (type II) [ADIAC 1-4]
Specimens Measured:	na
Aspect:	Valve
Valve symmetry or shape:	Apical sym = Isobilateral, Transapical sym = Isopolar, Valve shape = Lanceolate, Valve curvature = none, Apex shape = inflection, Shape = 'Protracted, sub-rostrate', Frustral shape = na
Dimensions µm [AA]:	14.7 - (0) - 25.9
Dimensions µm [TA]:	4.4 - (0) - 7.4
Raphe:	Raphe, location = Central, shape = 'linear, filiform', central endings = 'straight, slightly expanded', polar endings = 'not visible'
Striae:	20-22 per 10µm, orientation = 'transverse, radiate becoming parallel towards poles', pores = 'not resolvable', na per 10µm
Fibulae or Costae:	
Axial area:	axial area = 'narrow, linear' , central area = slightly widened, unsymmetrical, , central nodule = shape not disceranable, terminal nodule = visible, not resolvable, other hyaline areas = none
Other Features:	Spines = None; Comments = 'This was the one that was next to the N. gregaria that I decided was different due to the curvature in the striae and the pattern of the striae in the centre'; Other = 'na'
Image path:	Catalogue3\Cat3-Ref6\Cat3-Ref6-13_2008-11-24.jpg

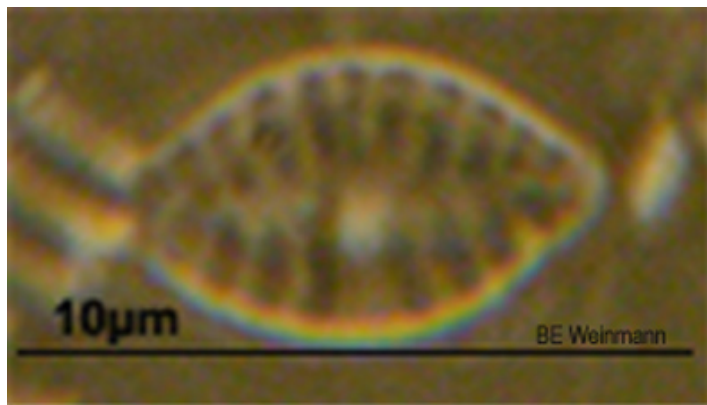



6_14	Navicula sp3 [?] or Navicula phyllepta (type II) [ADIAC 1-4]
Specimens Measured:	na
Aspect:	Valve
Valve symmetry or shape:	Apical sym = Isobilateral, Transapical sym = Isopolar, Valve shape = Lanceolate, Valve curvature = none, Apex shape = inflection, Shape = 'Protracted, sub-rostrate', Frustral shape = na
Dimensions µm [AA]:	na - (0) - 26.6
Dimensions µm [TA]:	5.9 - (0) - na
Raphe:	Raphe, location = Central, shape = 'linear, filiform', central endings = 'straight, slightly expanded', polar endings = 'not visible'
Striae:	16 - 18 per 10µm, orientation = 'transverse, radiate becoming parallel towards poles', pores = 'not resolved', na per 10µm
Fibulae or Costae:	
Axial area:	axial area = 'narrow, linear' , central area = slightly widened, not symmetrical, , central nodule = small, visible, terminal nodule = barely visible, other hyaline areas = none
Other Features:	Spines = None; Comments = 'na'; Other = 'na'
Image path:	Catalogue3\Cat3-Ref6\Cat3-Ref6-14_E2-T1.2-c216.jpg
	

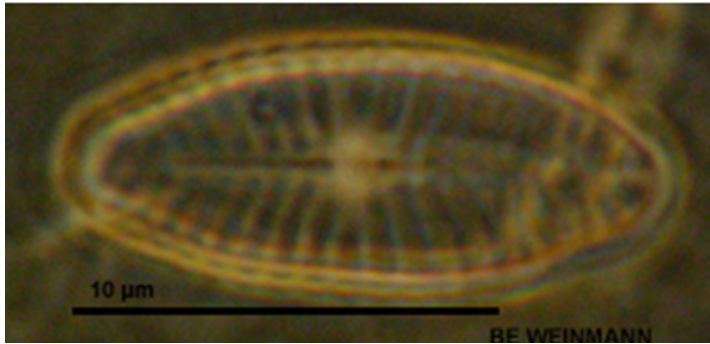
7_15	Achnanthes delicatula SV (Kützing) Grunow [BMB1: #3]
Specimens Measured:	na
Aspect:	Valve
Valve symmetry or shape:	Apical sym = Isobilateral, Transapical sym = Isopolar, Valve shape = Broadly lanceolate, Valve curvature = appears flat, Apex shape = inflection, Shape = 'Slightly protacted, sub-rostrate', Frustral shape = na
Dimensions µm [AA]:	9.6 - (12.5) - 17
Dimensions µm [TA]:	4.2 - (5.7) - 7.4
Raphe:	Sternum, location = Central, shape = 'na', central endings = 'na', polar endings = 'na'
Striae:	13 per 10µm, orientation = 'Transverse, parallel, becoming radiate', pores = 'not resolved', na per 10µm
Fibulae or Costae:	
Axial area:	axial area = 'narrow, linear' , central area = none, central nodule = na, terminal nodule = na, other hyaline areas = na
Other Features:	Spines = None; Comments = 'na'; Other = 'na'
Image path:	Catalogue3\Cat3-Ref7\Cat3-Ref7-15_2008-11.jpg
	

7_16	Achnanthes delicatula SV (Kützing) Grunow [BMB1: #3]
Specimens Measured:	na
Aspect:	Valve
Valve symmetry or shape:	Apical sym = Isobilateral, Transapical sym = Isopolar, Valve shape = Broadly lanceolate, Valve curvature = appears flat, Apex shape = inflection, Shape = 'Slightly protacted, sub-rostrate', Frustral shape = na
Dimensions μm [AA]:	16.3 - (13.6) - 11.1
Dimensions μm [TA]:	5.9 - (6.6) - 8.1
Raphe:	Raphe, location = Central, shape = 'linear, filiform', central endings = 'straight, slightly expanded (pinhead)', polar endings = 'not visible'
Striae:	15 per 10 μm , orientation = 'Transverse, parallel, becoming radiate', pores = 'not resolved', na per 10 μm
Fibulae or Costae:	
Axial area:	axial area = 'narrow, linear', central area = slight TA rectangular expansion, central nodule = round, bright, terminal nodule = not visible, other hyaline areas = na
Other Features:	Spines = None; Comments = 'na'; Other = 'na'
Image path:	Catalogue3\Cat3-Ref7\Cat3-Ref7-16_2009-01-19.jpg
	

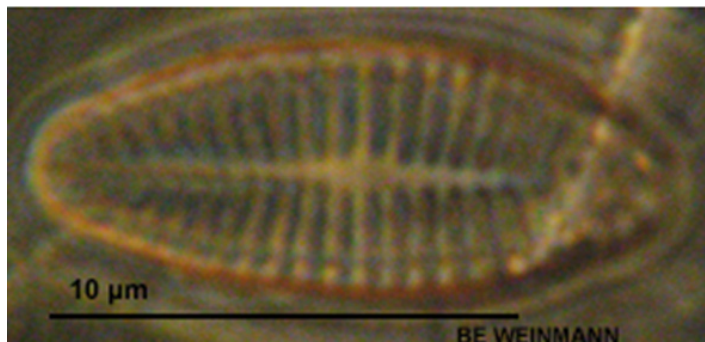
7_17	Achnanthes [?] hauckiana SV [van der Werff & Huls 1974]
Specimens Measured:	na
Aspect:	Valve
Valve symmetry or shape:	Apical sym = Isobilateral, Transapical sym = Isopolar, Valve shape = Broadly lanceolate, Valve curvature = appears flat, Apex shape = inflection, Shape = 'Slightly protacted, sub-rostrate', Frustral shape = na
Dimensions µm [AA]:	5.9 - (8.4) - 10.4
Dimensions µm [TA]:	3.7 - (4.9) - 5.9
Raphe:	Sternum, location = Central, shape = 'na', central endings = 'na', polar endings = 'na'
Striae:	12 per 10µm, orientation = 'Transverse, parallel, becoming radiate.', pores = 'not resolved', na per 10µm
Fibulae or Costae:	
Axial area:	axial area = 'narrow, linear' , central area = One-sided expansion to margin (fascia?), central nodule = na, terminal nodule = na, other hyaline areas = na
Other Features:	Spines = None; Comments = 'The SV of hauckiana has slightly darker and fatter striae than delicatula with bigger gaps between striae and more broadly lanceolate sternum'; Other = 'na'
Image path:	Catalogue3\Cat3-Ref7\Cat1-Ref7-17_2.jpg

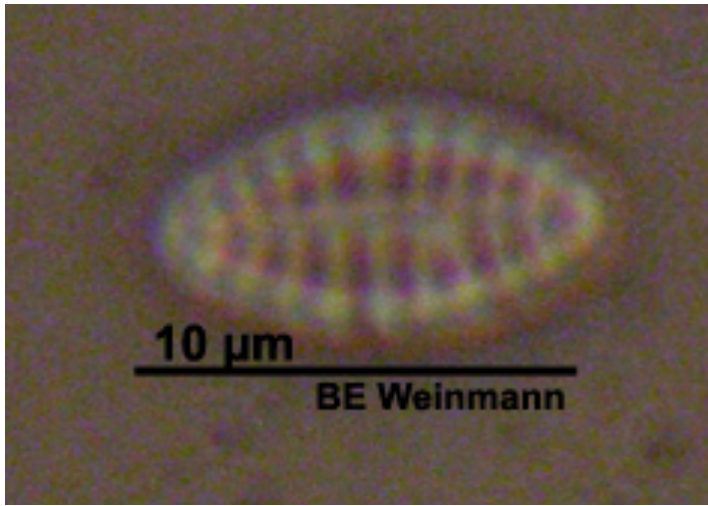


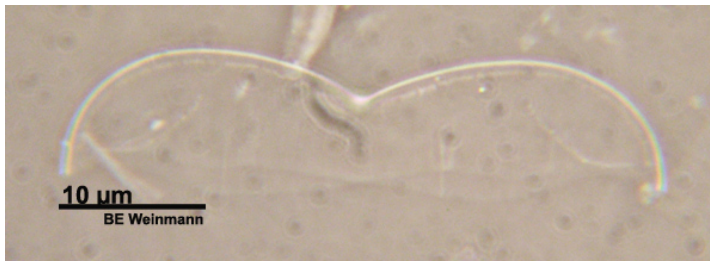
7_18	Achnanthes [delicatula var.] hauckiana RV [van der Werff & Huls 1974]
Specimens Measured:	na
Aspect:	Valve
Valve symmetry or shape:	Apical sym = Isobilateral, Transapical sym = Isopolar, Valve shape = Broadly lanceolate, Valve curvature = appears flat, Apex shape = inflection, Shape = 'Protacted, sub-rostrate', Frustral shape = na
Dimensions µm [AA]:	5.9 - (9.6) - 12.6
Dimensions µm [TA]:	4.4 - (5.3) - 5.9
Raphe:	Raphe, location = Central, shape = 'linear, filiform', central endings = 'straight, slightly expanded (pinhead)', polar endings = 'not visible'
Striae:	13 - 15 per 10µm, orientation = 'na', pores = 'na', na per 10µm
Fibulae or Costae:	
Axial area:	axial area = 'narrow, linear' , central area = slight TA rectangular expansion, central nodule = round, bright, terminal nodule = not visible, other hyaline areas = na
Other Features:	Spines = None; Comments = 'The RV of delicatula and hauckiana are virtually identical and no doubt frequently mixed up, its the SV that look different'; Other = 'na'
Image path:	Catalogue3\Cat3-Ref7\Cat3-Ref7-18_2009-01-19.jpg
	

7_19	Achnanthes delicatula (Kützing) RV [?] or Roicosphenia genuflexa CV [Witkowski ?]
Specimens Measured:	na
Aspect:	Valve
Valve symmetry or shape:	Apical sym = Isobilateral, Transapical sym = Isopolar, Valve shape = Broadly lanceolate, Valve curvature = Distinctly convex, Frustral shape = na
Dimensions µm [AA]:	14.1 - (0) - na
Dimensions µm [TA]:	5.1 - (0) - na
Raphe:	Raphe, location = Central, shape = 'Straight', central endings = 'Expanded (pinhead)', polar endings = 'Straight, end 2/3 before poles'
Striae:	13 per 10µm, orientation = 'Transverse, parallel in centre then radiate', pores = 'na', na per 10µm
Fibulae or Costae:	
Axial area:	axial area = 'Narrow, linear' , central area = Round, central nodule = large, bright, terminal nodule = not visible, other hyaline areas = na
Other Features:	Spines = None; Comments = 'These don't have the lemon shape of P. delicatula or hauckiana, though there are still slightly sub-rostrate apices, overall it is only the striae that look like this group and it totally blurs the distinctions between A. delicatula and A. lanceolata.'; Other = 'na'
Image path:	Catalogue3\Cat3-Ref7\Cat3-Ref7-19_2009-02-13.jpg
	

7_20	Achnanthes delicatula (Kützing) SV [?] or R. genuflexa CX [Witkowski ?]
Specimens Measured:	na
Aspect:	Valve
Valve symmetry or shape:	Apical sym = Isobilateral, Transapical sym = Isopolar, Valve shape = Broadly lanceolate, Valve curvature = Distinctly convex, Frustral shape = na
Dimensions µm [AA]:	14.1 - (0) - na
Dimensions µm [TA]:	5.1 - (0) - na
Raphe:	Sternum, location = Central, shape = 'Straight', central endings = 'na', polar endings = 'na'
Striae:	16 per 10µm, orientation = 'Transverse, parallel in centre then radiate', pores = 'na', na per 10µm
Fibulae or Costae:	
Axial area:	axial area = 'Narrow, linear' , central area = Small, narrowly lanceolate, central nodule = na, terminal nodule = na, other hyaline areas = na
Other Features:	Spines = None; Comments = 'These don't have the lemony shape thought there are still sub-rostrate apices, though they are wider than normal. The sternum valve does not have shortened raphes visible at poles but then poles are kind of twisted.'; Other = 'na'
Image path:	Catalogue3\Cat3-Ref7\Cat3-Ref7-20_2009-02-13.jpg

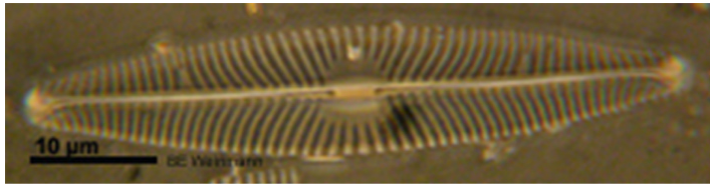


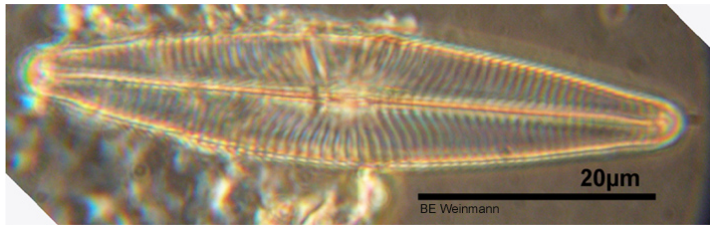
7_121	Achnanthes cf. delicatula [Ribeiro?]
Specimens Measured:	1
Aspect:	Valve
Valve symmetry or shape:	Apical sym = Isobilateral, Transapical sym = Isopolar, Valve shape = Lanceolate, Valve curvature = none, Frustral shape = na
Dimensions μm [AA]:	10.3 - (0) - na
Dimensions μm [TA]:	5.1 - (0) - na
Raphe:	Sternum, location = Central, shape = 'na', central endings = 'na', polar endings = 'na'
Striae:	10 - 12 per 10 μm , orientation = 'Transverse, radiate', pores = 'Punctate', Not resolved per 10 μm
Fibulae or Costae:	
Axial area:	axial area = 'Linear, narrow' , central area = Transapical expansion, rectangular, to margins, central nodule = na, terminal nodule = na, other hyaline areas = na
Other Features:	Spines = None; Comments = 'Not sure this isn't an Achnanthes or Planothidium'; Other = 'na'
Image path:	Catalogue3\Cat3-Ref7\Cat3-Ref7-121_2012-03-20-c30.jpg
	

8_21	Amphiprora angustata [Hendey 1964]
Specimens Measured:	na
Aspect:	Girdle
Valve symmetry or shape:	
Dimensions µm [AA]:	49 - (0) - 55
Dimensions µm [PA]:	17 - (0) - 29
Raphe:	Raphe, location = Central, shape = 'sigmoid', central endings = 'na', polar endings = 'na'
Striae:	24 per 10µm, orientation = 'parallel', pores = 'na', na per 10µm
Fibulae or Costae:	
Axial area:	axial area = 'na' , central area = na, central nodule = na, terminal nodule = na, other hyaline areas = na
Other Features:	Spines = None; Comments = 'na'; Other = 'na'
Image path:	Catalogue3\Cat3-Ref8\Cat3-Ref8-21_2012-03-24-c57.jpg
	

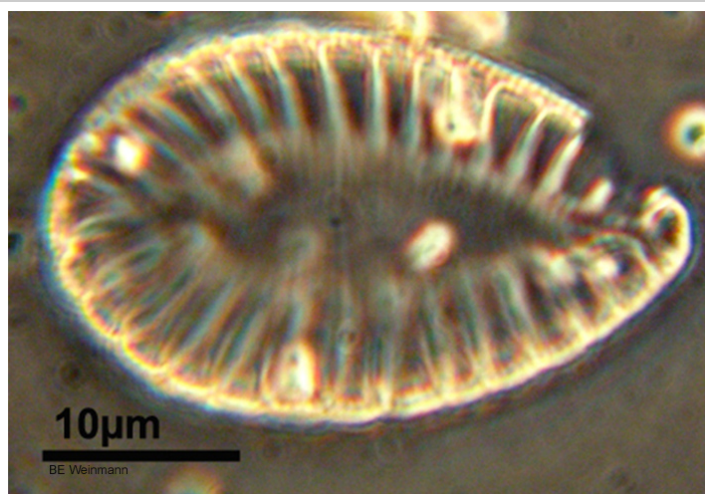
8_180	Amphiprora angustata [Hendey 1964, p254]
Specimens Measured:	2
Aspect:	Valve
Valve symmetry or shape:	Apical sym = Dorsiventral, Transapical sym = Isopolar, Valve shape = Linear-lanceolate, Valve curvature = None, Apex shape = inflection, Shape = 'Cuneate', Frustral shape = NA
Dimensions µm [AA]:	40.4 - (40.4) - 40.4
Dimensions µm [TA]:	10.3 - (11.1) - 11.8
Raphe:	Raphe, location = Central, shape = 'Sigmoid on wing-like projection', central endings = 'Inflated (?)', polar endings = 'not visible'
Striae:	Not resolved per 10µm, orientation = 'NA ', pores = 'NA ', na per 10µm
Fibulae or Costae:	
Axial area:	axial area = 'none' , central area = None, central nodule = None visible, terminal nodule = None , other hyaline areas = The entire valve is unstriated and hyaline
Other Features:	Spines = None; Comments = 'na'; Other = 'na'
Image path:	Catalogue3\Cat3-Ref8\Cat3-Ref8-180_2012-04-18-c82.jpg

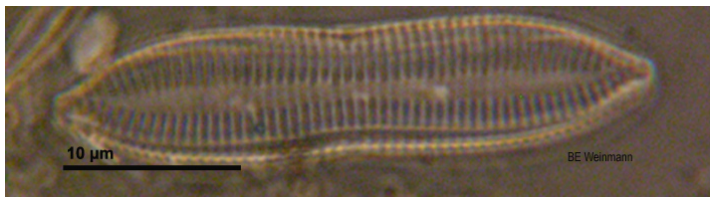


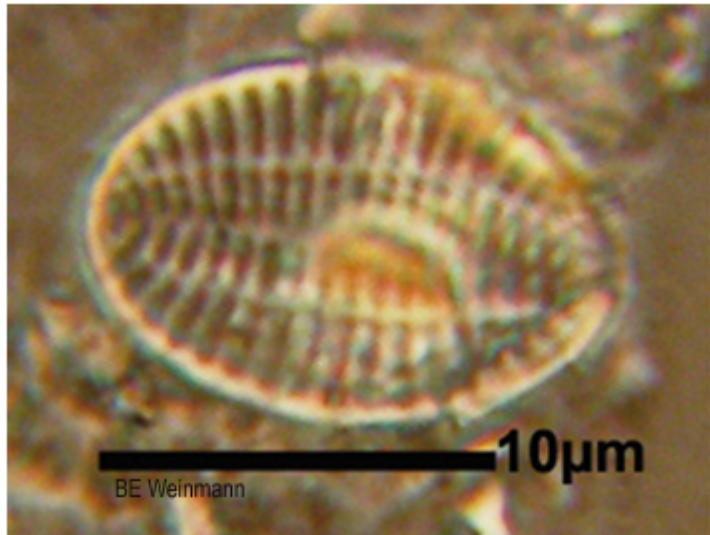
9_22	Navicula lanceolata (Agardh) Ehrenberg(1838) [BMB1: #66]
Specimens Measured:	na
Aspect:	Valve
Valve symmetry or shape:	Apical sym = Isobilateral, Transapical sym = Isopolar, Valve shape = Lanceolate, Valve curvature = none, Frustral shape = na
Dimensions µm [AA]:	26 - (47.5) - 59.9
Dimensions µm [TA]:	4.4 - (11.1) - 9.2
Raphe:	Raphe, location = Central, shape = 'linear', central endings = 'expanded, distant & straight', polar endings = 'bent to the same side'
Striae:	9 - 12 per 10µm, orientation = 'transverse, radiate becoming convergent towards poles', pores = 'not resolvable', na per 10µm
Fibulae or Costae:	
Axial area:	axial area = 'narrow, linear' , central area = Elliptic on one half and round on the other side, central nodule = No, terminal nodule = Possibly, other hyaline areas = na
Other Features:	Spines = None; Comments = 'This ID is very similar to Navicula radiosa (see BMB series 66 vs 366) but I think radiosa has more acute apices and bigger gaps between central striae'; Other = 'na'
Image path:	Catalogue3\Cat3-Ref9\Cat3-Ref9-22_2008-11-26.jpg
	

9_23	Navicula lanceolata (Agardh) Ehrenberg(1838) [BMB1: #66]
Specimens Measured:	na
Aspect:	Valve
Valve symmetry or shape:	Apical sym = Isobilateral, Transapical sym = Isopolar, Valve shape = Lanceolate, Valve curvature = none, Frustral shape = na
Dimensions µm [AA]:	43 - (48.2) - 53.3
Dimensions µm [TA]:	9.6 - (10) - 10.4
Raphe:	Raphe, location = Central, shape = 'linear', central endings = 'expanded, distant & straight', polar endings = 'bent to the same side'
Striae:	9 - 10 per 10µm, orientation = 'transverse, radiate becoming convergent towards poles', pores = 'not resolvable', na per 10µm
Fibulae or Costae:	
Axial area:	axial area = 'Narrow, linear' , central area = Elliptic on one half and round or triangular on the other side, central nodule = No, terminal nodule = Yes, other hyaline areas = na
Other Features:	Spines = None; Comments = 'This ID is very similar to Navicula radiosa (see BMB series 66 vs 366) but I think radiosa has more acute apices and bigger gaps between central striae'; Other = 'na'
Image path:	Catalogue3\Cat3-Ref9\Cat3-Ref9-23_2008-03-02.jpg
	

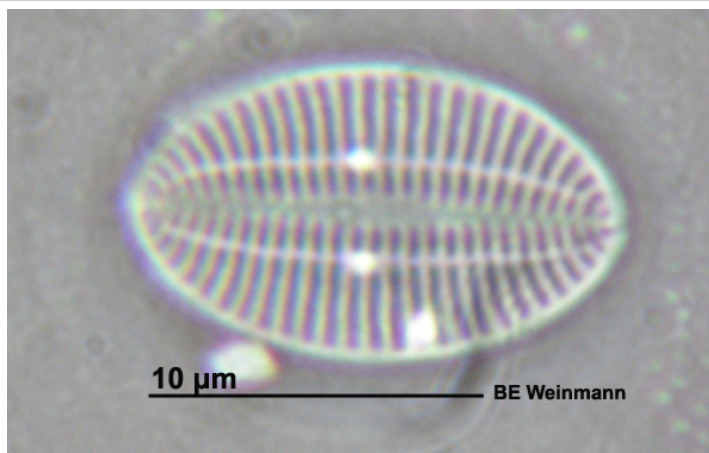
10_24	Surirella brebissonii Krammer & Lange-Bertalot [BMB1: #86]
Specimens Measured:	na
Aspect:	Valve
Valve symmetry or shape:	Apical sym = Isobilateral, Transapical sym = Heteropolar, Valve shape = Ovate, Valve curvature = na Apex shape = no inflection, Shape = 'Broadly rounded', Frustral shape = na
Dimensions µm [AA]:	33 - (31) - 29
Dimensions µm [TA]:	16 - (17) - 18.4
Raphe:	Raphe, location = Marginal (around each side) , shape = 'not visible', central endings = 'NA', polar endings = 'NA'
Striae:	12 - 15 per 10µm, orientation = 'Transverse, radiate', pores = 'not resolvable', na per 10µm
Fibulae or Costae:	costae = 5 per 10µm, Costae look like horse-shoe shapes ringing around around the margin
Axial area:	axial area = 'na' , central area = Narrowly ovate (cocentric to margin), central nodule = None, terminal nodule = None, other hyaline areas = na
Other Features:	Spines = None; Comments = 'na'; Other = 'na'
Image path:	Catalogue3\Cat3-Ref10\Cat3-Ref10-24_2008-11-25.jpg

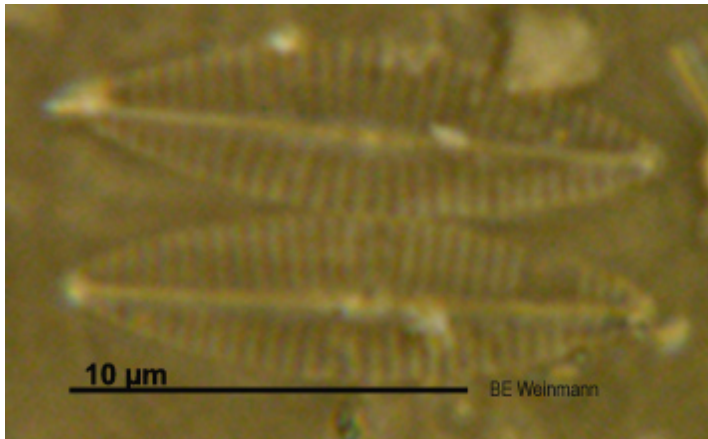


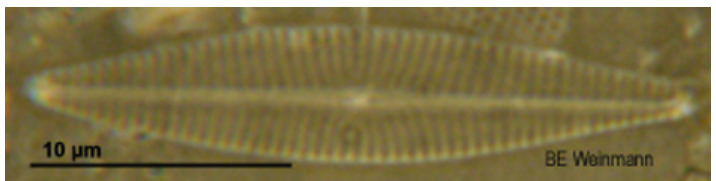
11_25	Tryblionella apiculata Gregory [BMB2: #196] (previously Nitzschia constricta (Kützinger) Ralfs)
Specimens Measured:	17
Aspect:	Valve
Valve symmetry or shape:	Apical sym = Isobilateral, Transapical sym = Heteropolar, Valve shape = Panduriform, Valve curvature = none, Apex shape = inflection, Shape = 'Sub-rostrate', Frustral shape = na
Dimensions µm [AA]:	26 - (35) - 54
Dimensions µm [TA]:	4.7 - (7.7) - 13.6
Raphe:	Raphe, location = Marginal (one side?), shape = 'not visible', central endings = 'NA', polar endings = 'NA'
Striae:	15 - 20 per 10µm, orientation = 'Transverse, parallel becoming slightly radiate', pores = 'not resolvable', na per 10µm
Fibulae or Costae:	
Axial area:	axial area = 'na' , central area = NA, central nodule = na, terminal nodule = na, other hyaline areas = Centre of valve face, narrow, linear or undulating following the valve margins
Other Features:	Spines = None; Comments = 'na'; Other = 'na'
Image path:	Catalogue3\Cat3-Ref11\Cat3-Ref11-25_2009-02-04.jpg
	

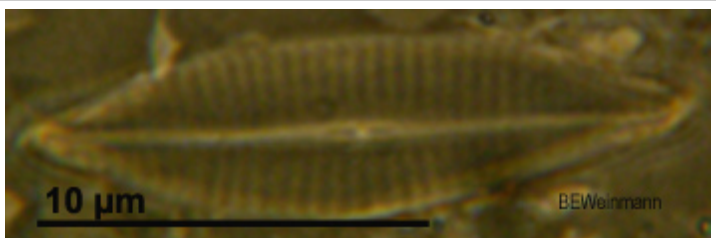
12_26	Cocconeis peltoides Hustedt 1939 (SV) [Witkowski pl. 38:1-9; Hartley pl. 53:1]
Specimens Measured:	12
Aspect:	Valve
Valve symmetry or shape:	Apical sym = Isobilateral, Transapical sym = Isopolar, Valve shape = Elliptic, Valve curvature = none Apex shape = no inflection, Shape = 'Broadly rounded', Frustral shape = na
Dimensions µm [AA]:	7.4 - (12.9) - 22.8
Dimensions µm [TA]:	5.1 - (8) - 10.3
Raphe:	Sternum, location = central, shape = 'na', central endings = 'na', polar endings = 'na'
Striae:	12 - 15 per 10µm, orientation = 'Transverse, parallel becoming slightly radiate', pores = 'Just visible, not resolved', na per 10µm
Fibulae or Costae:	
Axial area:	axial area = 'Linear, extremely narrow, hardly more than a seam' , central area = Diamond-shaped, central nodule = na, terminal nodule = na, other hyaline areas = One hyaline ridge running longitudinally down each transapical half at approximately at half width
Other Features:	Spines = None; Comments = 'na'; Other = 'na'
Image path:	Catalogue3\Cat3-Ref12\Cat3-Ref12-26_2008-11-26.jpg
	

12_178	Cocconeis peltoides Hustedt (SV) [Witkowski pl. 38:1-9; Hartley pl. 53:1]
Specimens Measured:	1
Aspect:	Valve
Valve symmetry or shape:	Apical sym = Dorsiventral, Transapical sym = Isopolar, Valve shape = Elliptic, Valve curvature = None, Frustral shape = NA
Dimensions µm [AA]:	14.7 - (0) - na
Dimensions µm [TA]:	4.4 - (0) - na
Raphe:	Sternum, location = Central, shape = 'NA', central endings = 'NA', polar endings = 'NA'
Striae:	15 - 16 per 10µm, orientation = 'Transverse, parallel becoming radiate', pores = 'Not resolved', na per 10µm
Fibulae or Costae:	
Axial area:	axial area = 'Arcuate' , central area = Round, central nodule = None, terminal nodule = None , other hyaline areas = Centre
Other Features:	Spines = None; Comments = 'I can't figure out what this is? At first I thought it was an Amphora frustule but there is no raphe visible'; Other = 'na'
Image path:	Catalogue3\Cat3-Ref12\Cat3-Ref12-178_2012-04-14-c140.jpg

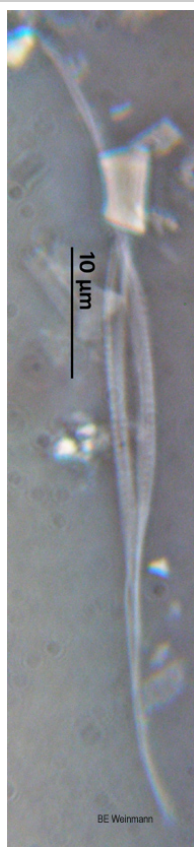


14_29	Navicula phyllepta Kützing (type I) [BMB3: #258 form 2]
Specimens Measured:	80
Aspect:	Valve
Valve symmetry or shape:	Apical sym = Isobilateral, Transapical sym = Isopolar, Valve shape = Lanceolate, Valve curvature = unknown Apex shape = no inflection, Shape = 'Acute, no inflexion', Frustral shape = na
Dimensions µm [AA]:	8.1 - (18.4) - 55.5
Dimensions µm [TA]:	3.7 - (3.5) - 5.3
Raphe:	Raphe, location = Central, shape = 'linear, filiform', central endings = 'straight, slightly expanded', polar endings = 'not visible'
Striae:	18 - 21 per 10µm, orientation = 'Slightly radiate to parallel towards the very end', pores = 'not resolvable', na per 10µm
Fibulae or Costae:	
Axial area:	axial area = 'narrow, linear' , central area = slight diamond shaped expansion, central nodule = small and bright, terminal nodule = sometimes visible, other hyaline areas = na
Other Features:	Spines = None; Comments = 'na'; Other = 'na'
Image path:	Catalogue3\Cat3-Ref14\Cat3-Ref14-29_2009-02-03.jpg
	

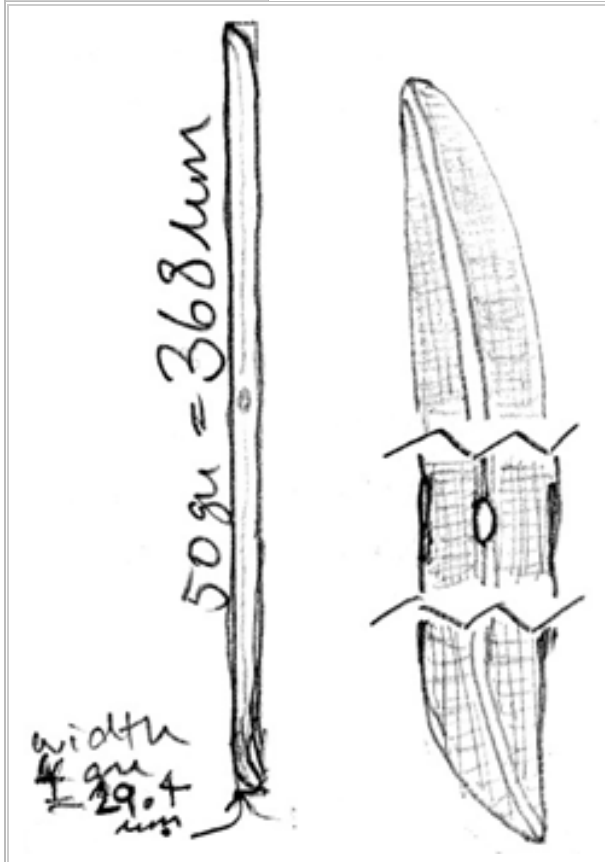
14_30	Navicula phyllepta Kützing (type I) [BMB3: #258 form 1]
Specimens Measured:	35
Aspect:	Valve
Valve symmetry or shape:	Apical sym = Isobilateral, Transapical sym = Isopolar, Valve shape = Lanceolate, Valve curvature = unknown, Frustral shape = na
Dimensions µm [AA]:	11.3 - (0) - 22.2
Dimensions µm [TA]:	3.7 - (0) - 6.9
Raphe:	Raphe, location = Central, shape = 'linear, filiform', central endings = 'straight, slightly expanded', polar endings = 'not visible'
Striae:	18 - 20 per 10µm, orientation = 'Radiate becoming parallel, possibly one or two convergent, towards the apices.', pores = 'not resolved in LM', na per 10µm
Fibulae or Costae:	
Axial area:	axial area = 'narrow, linear', central area = slight diamond shaped expansion, central nodule = small and bright, terminal nodule = sometimes visible, other hyaline areas = na
Other Features:	Spines = None; Comments = 'Intermediate form (btwn II and I)? Has slight concavity towards apex.'; Other = 'na'
Image path:	Catalogue3\Cat3-Ref14\Cat3-Ref14-30_2009-02-03.jpg
	

14_31	Navicula phyllepta Kützing [not matched by any published References but similar to others in this catalogue]
Specimens Measured:	5
Aspect:	Valve
Valve symmetry or shape:	Apical sym = Isobilateral, Transapical sym = Isopolar, Valve shape = Lanceolate, Valve curvature = unknown, Frustral shape = na
Dimensions µm [AA]:	16.3 - (18.9) - 22.2
Dimensions µm [TA]:	4.4 - (5) - 5.1
Raphe:	Raphe, location = Central, shape = 'linear, filiform', central endings = 'straight, slightly expanded', polar endings = 'not visible'
Striae:	17 -21 per 10µm, orientation = 'Transverse, parallel though slightly bent at the tips, towards the very end', pores = 'not resolved in LM', na per 10µm
Fibulae or Costae:	
Axial area:	axial area = 'narrow, linear', central area = There is hardly any central area, slightly triangular on one side, central nodule = small and bright, terminal nodule = sometimes visible, other hyaline areas = na
Other Features:	Spines = None; Comments = 'This one is like a cross between 29-30 and 103-131, so much so that I'm not sure they are separate and I'm sure I've misIDed many cells by confounding this group and 103-131.'; Other = 'na'
Image path:	Catalogue3\Cat3-Ref14\Cat3-Ref14-31_2009-02-04.jpg
	

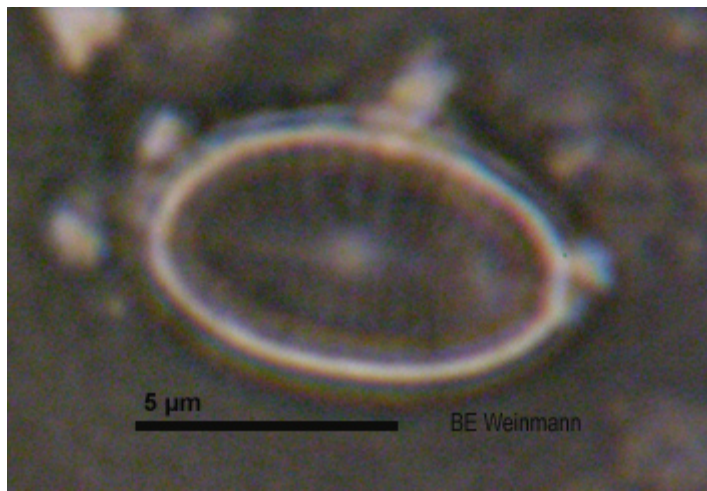
15_32	Cylindrotheca closterium (Ehrenberg) Reimann & Lewin [BMB1: #33]
Specimens Measured:	10
Aspect:	Valve
Valve symmetry or shape:	Apical sym = Isobilateral, Transapical sym = Isopolar, Valve shape = Lanceolate, Valve curvature = unknown, Apex shape = inflection, Shape = 'Extremely protracted, sigmoid', Frustral shape = na
Dimensions μm [AA]:	59 - (75.4) - 91.9
Dimensions μm [TA]:	1.8 - (2.7) - 6
Raphe:	Raphe, location = marginal (if fibulae visible then on both sides), shape = 'na', central endings = 'na', polar endings = 'na'
Striae:	not resolved in LM per 10 μm , orientation = 'na', pores = 'not resolved in LM', na per 10 μm
Fibulae or Costae:	fibulae = > 30 per 10 μm , Fibulae can be seen on both sides but too small and plentiful to count
Axial area:	axial area = 'na', central area = na, central nodule = na, terminal nodule = na, other hyaline areas = Almost the entire valve face as striae not visible
Other Features:	Spines = None; Comments = 'na'; Other = 'na'
Image path:	Catalogue3\Cat3-Ref15\Cat3-Ref15-32_2008-03-12.jpg

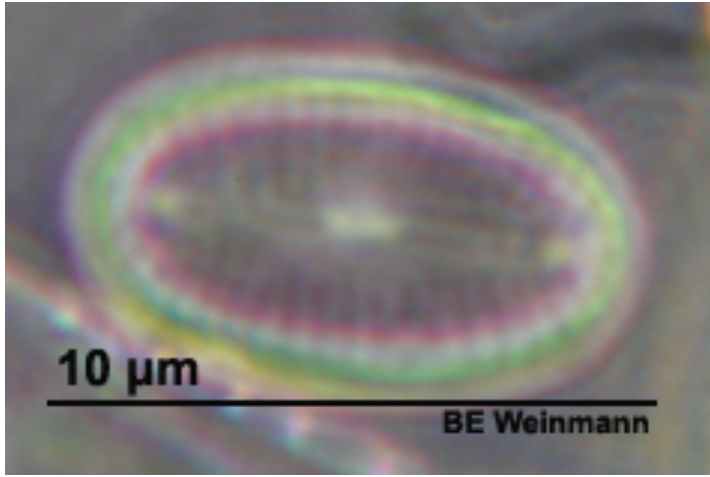


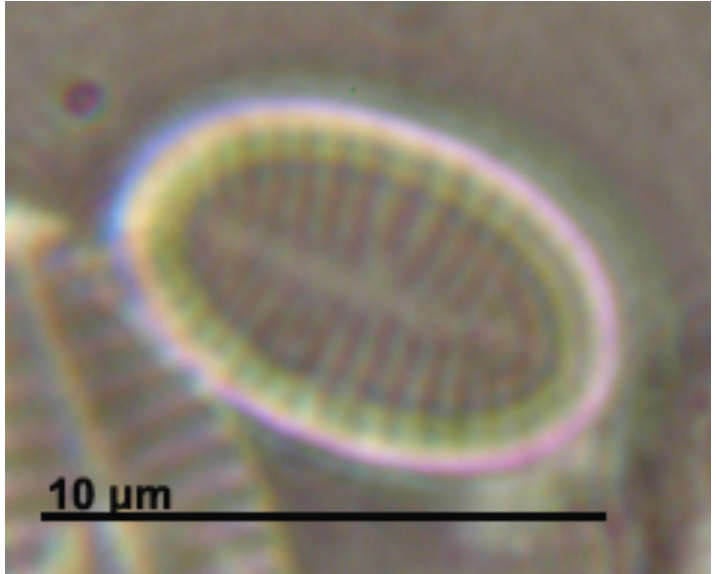
16_33	Gyrosigma balticum (Ehrenberg) Rabenhorst 1853 [BMB2: #144]
Specimens Measured:	9
Aspect:	Valve
Valve symmetry or shape:	Apical sym = Isobilateral, Transapical sym = Isopolar, Valve shape = linear with sigmoid apices, Valve curvature = unknown Apex shape = no inflection, Shape = 'Acutely rounded', Frustral shape = na
Dimensions μm [AA]:	292 - (401.6) - 470
Dimensions μm [TA]:	27.2 - (29.8) - 34.5
Raphe:	Raphe, location = Central, shape = 'sigmoid', central endings = 'straight (maybe slightly deflected in opposite directions ?)', polar endings = 'reaches margin'
Striae:	11 per $10\mu\text{m}$, orientation = 'Transverse & longitudinal', pores = 'Not resolved', na per $10\mu\text{m}$
Fibulae or Costae:	
Axial area:	axial area = 'narrow, sigmoid', central area = elliptic (on apical axis), central nodule = small, oval, terminal nodule = not visible, other hyaline areas = na
Other Features:	Spines = None; Comments = 'na'; Other = 'na'
Image path:	Catalogue3\Cat3-Ref16-33_2008-11-27.bmp

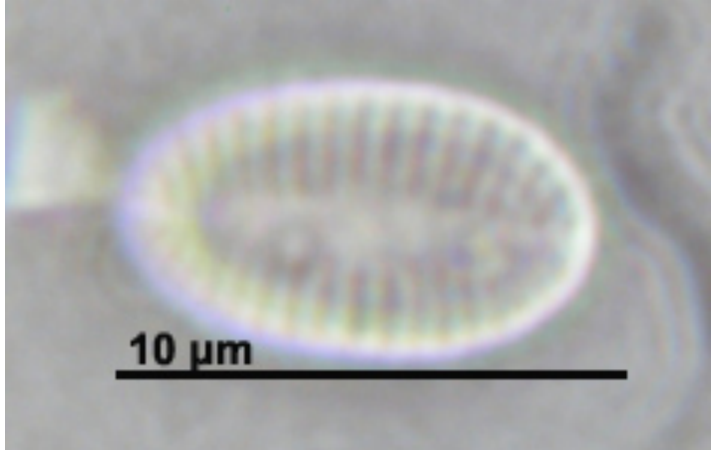


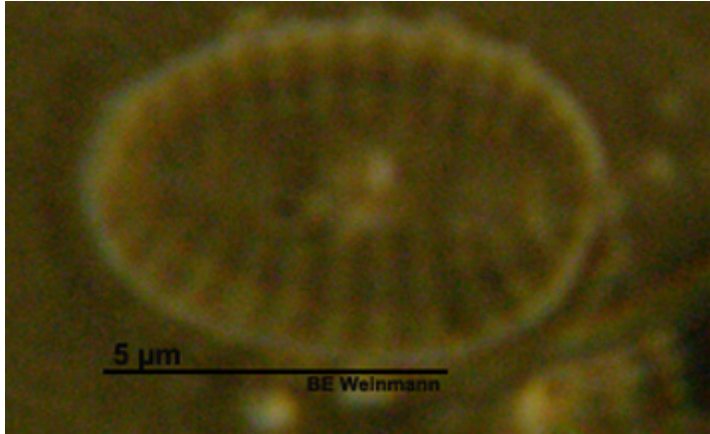
17_34	Cocconeis sp. 1 RV [Ribeiro p181, pl9: 8-10]
Specimens Measured:	24
Aspect:	Valve
Valve symmetry or shape:	Apical sym = Isobilateral, Transapical sym = Isopolar, Valve shape = Elliptic, Valve curvature = Convex maybe Apex shape = no inflection, Shape = 'Broadly rounded', Frustral shape = na
Dimensions μm [AA]:	15.9 - (0) - na
Dimensions μm [TA]:	9.1 - (0) - na
Raphe:	Sternum, location = Central, shape = 'na', central endings = 'na', polar endings = 'na'
Striae:	20 - 24 per 10 μm , orientation = 'Transverse, radiate', pores = 'Not resolved', na per 10 μm
Fibulae or Costae:	
Axial area:	axial area = 'Lanceolate' , central area = Not differentiated from sternum, central nodule = Maybe (unless its from the other side), terminal nodule = No, other hyaline areas = na
Other Features:	Spines = None; Comments = 'I originally treated the striated and "blank" ones the same bc I thought it was blank and realised later, upon seeing the image that faint striae could be seen, so I figured they simply couldn't always be seen depending on illumination. I'm still not sure of this which is why I'm maintaining them in the same overall group but with different Ref2s '; Other = 'na'
Image path:	Catalogue3\Cat3-Ref17\Cat3-Ref17-34_2009-01-29.jpg

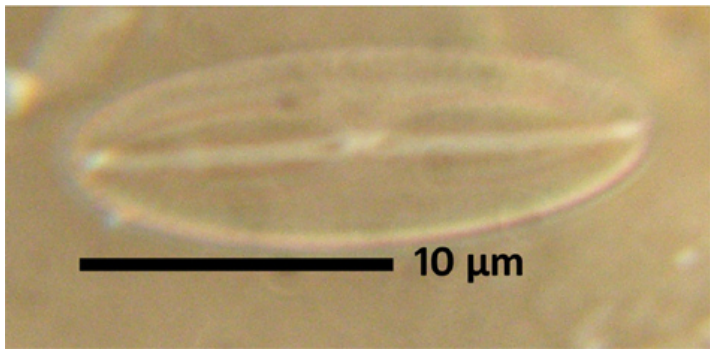


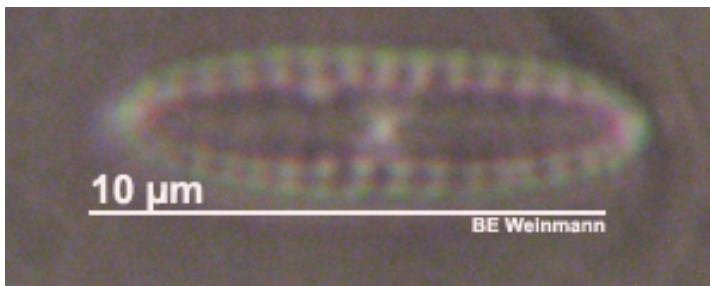
17_147	Cocconeis sp. 1 RV [?]
Specimens Measured:	3
Aspect:	Valve
Valve symmetry or shape:	Apical sym = Isobilateral, Transapical sym = Isopolar, Valve shape = Linear, very slightly rhombic, Valve curvature = Not visible, Frustral shape = na
Dimensions μm [AA]:	8.1 - (8.5) - 8.8
Dimensions μm [TA]:	4.4 - (4.4) - 4.4
Raphe:	Raphe, location = Central, shape = 'Straight', central endings = 'Elongated inflation, distant', polar endings = 'Not resolved'
Striae:	20 -22 per $10\mu\text{m}$, orientation = 'Transverse, radiate', pores = 'Not resolved', na per $10\mu\text{m}$
Fibulae or Costae:	
Axial area:	axial area = 'Linear, moderately narrow' , central area = TA widened but uneven central area, central nodule = Elongate, narrowly elliptic, bright, terminal nodule = Small, well in from apex, other hyaline areas = None
Other Features:	Spines = None; Comments = 'This could possibly be Cocconeis cf. Discrepans Schmidt RSV [Ribeiro p174, p19: 17 - 18]'; Other = 'na'
Image path:	Catalogue3\Cat3-Ref17\Cat3-Ref17-147_2012-03-30-c18.jpg
	

17_148	Cocconeis sp. 1 SV [?]
Specimens Measured:	3
Aspect:	Valve
Valve symmetry or shape:	Apical sym = Isobilateral, Transapical sym = Isopolar, Valve shape = Elliptic, Valve curvature = Not visible, Frustral shape = na
Dimensions µm [AA]:	7.4 - (7.6) - 8.1
Dimensions µm [TA]:	4 - (4.4) - 4.8
Raphe:	Sternum, location = Central, shape = 'na', central endings = 'na', polar endings = 'na'
Striae:	18 - 20 per 10µm, orientation = 'Transverse, radiate', pores = 'Not resolved', na per 10µm
Fibulae or Costae:	
Axial area:	axial area = 'Linear, moderately narrow' , central area = Very slight one-sided expansion, central nodule = None, terminal nodule = None, other hyaline areas = None
Other Features:	Spines = None; Comments = 'na'; Other = 'na'
Image path:	Catalogue3\Cat3-Ref17\Cat3-Ref17-148_2012-03-30-c55.jpg
	

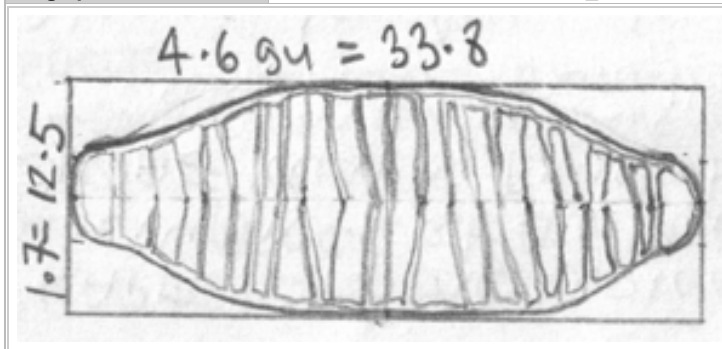
17_149	Cocconeis sp. 1 SV [?]
Specimens Measured:	2
Aspect:	Valve
Valve symmetry or shape:	Apical sym = Isobilateral, Transapical sym = Isopolar, Valve shape = Elliptic, Valve curvature = Not visible, Frustral shape = na
Dimensions µm [AA]:	7.4 - (7.4) - 7.4
Dimensions µm [TA]:	4.4 - (4.8) - 5.1
Raphe:	Sternum, location = Central, shape = 'na', central endings = 'na', polar endings = 'na'
Striae:	18 - 20 per 10µm, orientation = 'Transverse, radiate', pores = 'Not resolved', na per 10µm
Fibulae or Costae:	
Axial area:	axial area = 'Narrowly lanceolate' , central area = TA expansion, central nodule = None, terminal nodule = None, other hyaline areas = None
Other Features:	Spines = None; Comments = 'na'; Other = 'na'
Image path:	Catalogue3\Cat3-Ref17\Cat3-Ref17-149_2012-03-30-c56.jpg
	

18_35	Cocconeis sp. 1 SV [Ribeiro p181, pl9: 8-10]
Specimens Measured:	1
Aspect:	Valve
Valve symmetry or shape:	Apical sym = Isobilateral, Transapical sym = Isopolar, Valve shape = Elliptic, Valve curvature = None Apex shape = no inflection, Shape = 'Broadly rounded', Frustral shape = na
Dimensions μm [AA]:	7.4 - (0) - na
Dimensions μm [TA]:	3.7 - (0) - na
Raphe:	Sternum, location = Central, shape = 'na', central endings = 'na', polar endings = 'na'
Striae:	16 -18 per 10 μm , orientation = 'Transverse, parallel becoming radiate', pores = 'Not resolved', na per 10 μm
Fibulae or Costae:	
Axial area:	axial area = 'Lanceolate' , central area = none, central nodule = None, terminal nodule = None, other hyaline areas = None
Other Features:	Spines = None; Comments = 'na'; Other = 'na'
Image path:	Catalogue3\Cat3-Ref18-35_2009-03-13.jpg
	

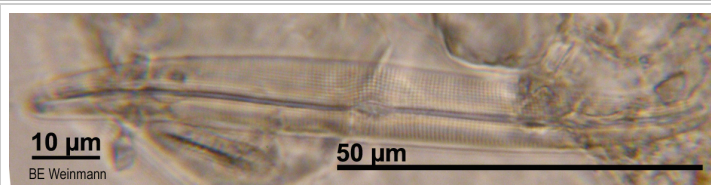
19_36	Fallacia sp. 1 [?]
Specimens Measured:	3
Aspect:	Valve
Valve symmetry or shape:	Apical sym = Isobilateral, Transapical sym = Isopolar, Valve shape = Elliptic, Valve curvature = None Apex shape = no inflection, Shape = 'Broadly rounded', Frustral shape = na
Dimensions µm [AA]:	11.1 - (12.5) - 13.3
Dimensions µm [TA]:	5 - (5.7) - 7
Raphe:	Sternum, location = Central, shape = 'linear', central endings = 'Inflated, straight', polar endings = 'Not resolved'
Striae:	Not resolved per 10µm, orientation = 'Transverse, parallel or radiate', pores = 'Not resolved', na per 10µm
Fibulae or Costae:	
Axial area:	axial area = 'linear, narrow' , central area = Rectangular? , central nodule = Bright, rectangular, terminal nodule = Bright, rectangular, other hyaline areas = Lyre-shaped hyaline slits halfway between raphe and margins?
Other Features:	Spines = None; Comments = 'The hyaline areas are not really visible under LM, didn't see them until I magnified them in photoshop'; Other = 'na'
Image path:	Catalogue3\Cat3-Ref19-36_2008-12-02.jpg
	

20_37	Biremis lucens (Hustedt) Sabbe, Witkowski & Vyverman 1995 [BMB4: #324]
Specimens Measured:	1
Aspect:	Valve
Valve symmetry or shape:	Apical sym = Isobilateral, Transapical sym = Isopolar, Valve shape = Linear, Valve curvature = na, Apex shape = inflection, Shape = 'Cuneate', Frustral shape = na
Dimensions µm [AA]:	9.6 - (9.9) - 10.3
Dimensions µm [TA]:	2.2 - (3.2) - 3.7
Raphe:	Raphe, location = Central, shape = 'linear, filiform', central endings = 'not resolvable', polar endings = 'Not resolved'
Striae:	13 - 16 per 10µm, orientation = 'Transverse, parallel', pores = 'not resolvable', na per 10µm
Fibulae or Costae:	
Axial area:	axial area = 'linear, narrow' , central area = Square?, central nodule = Round & bright, terminal nodule = Round & bright, other hyaline areas = Linear - lanceolate, does not reach apices
Other Features:	Spines = None; Comments = 'na'; Other = 'na'
Image path:	Catalogue3\Cat3-Ref20\Cat3-Ref20-37_2012-03-21-c47.jpg
	

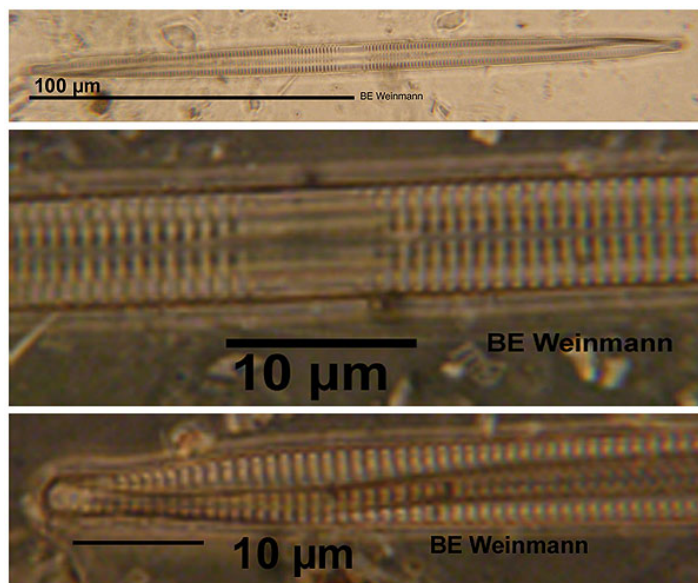
21_38	Diatoma vulgare Bory (1824) [BMB1: #38]
Specimens Measured:	na
Aspect:	Valve
Valve symmetry or shape:	Apical sym = Isobilateral, Transapical sym = Isopolar, Valve shape = Linear, Valve curvature = na, Apex shape = inflection, Shape = 'Broad, protracted, rostrate or sub-rostrate', Frustral shape = na
Dimensions µm [AA]:	34 - (0) - na
Dimensions µm [TA]:	12.5 - (0) - na
Raphe:	Sternum, location = Central, shape = 'na', central endings = 'na', polar endings = 'na'
Striae:	not resolvable per 10µm, orientation = 'na', pores = 'na', na per 10µm
Fibulae or Costae:	costae = 6 per 10µm, transverse, irregular angles, irregularly spaced, axial area = 'extremely narrow, almost not visible', central area = none, central nodule = na, terminal nodule = na, other hyaline areas = na
Other Features:	Spines = None; Comments = 'na'; Other = 'na'
Image path:	Catalogue3\Cat3-Ref21-38_2008-12.bmp

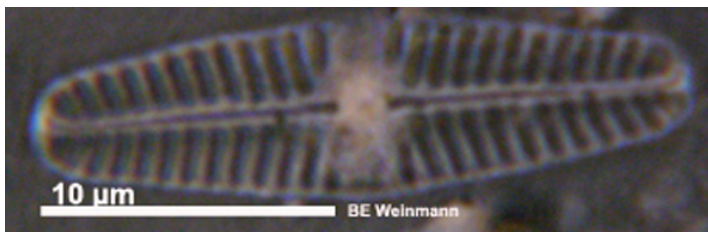


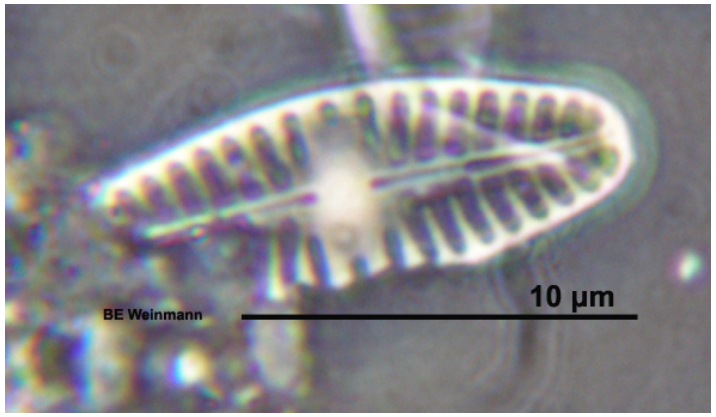
22_39	Gyrosigma spencerii (W. Smith) Cleve [Hartley pl. 115:2]
Specimens Measured:	4
Aspect:	Valve
Valve symmetry or shape:	Apical sym = Isobilateral, Transapical sym = Isopolar, Valve shape = Linear- sigmoid, Valve curvature = na Apex shape = no inflection, Shape = 'Acutely rounded', Frustral shape = na
Dimensions µm [AA]:	66.9 - (82.9) - 94.5
Dimensions µm [TA]:	10.5 - (11.3) - 125.5
Raphe:	Raphe, location = Central, shape = 'sigmoid', central endings = 'not resolvable', polar endings = 'reaches margin, not resolvable'
Striae:	fine (22 - 25 longitudinal, 17 - 23 transverse) per 10µm, orientation = 'Transverse & longitudinal', pores = 'not resolvable', na per 10µm
Fibulae or Costae:	
Axial area:	axial area = 'very narrow', central area = tiny elliptical, barely visible, central nodule = visible, terminal nodule = not visible, other hyaline areas = na
Other Features:	Spines = None; Comments = 'na'; Other = 'na'
Image path:	Catalogue3\Cat3-Ref22-39_2009-01-21.jpg

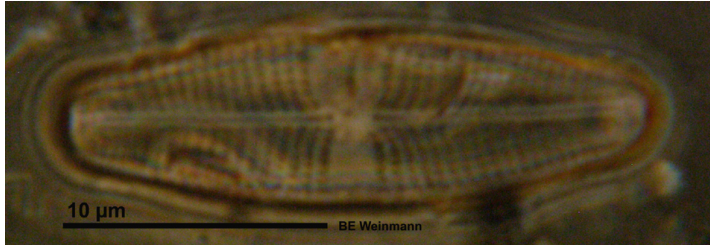


23_40	Synedra ulna (Nitzsch) Ehrenberg var. amphirhynchus (Ehrenberg) Grunow [BMB3: #295]
Specimens Measured:	na
Aspect:	Valve
Valve symmetry or shape:	Apical sym = Isobilateral, Transapical sym = Isopolar, Valve shape = Linear, Valve curvature = na, Apex shape = inflection, Shape = 'Protracted, rostrate or sub-capitate', Frustral shape = na
Dimensions μm [AA]:	na - (0) - 200.5
Dimensions μm [TA]:	7.3 - (0) - na
Raphe:	Sternum, location = Central, shape = 'na', central endings = 'na', polar endings = 'na'
Striae:	9 \pm 1 per 10 μm , orientation = 'transverse, parallel', pores = 'not resolvable', na per 10 μm
Fibulae or Costae:	
Axial area:	axial area = 'narrow, linear' , central area = rectangular, reaching all the way to valve margin, central nodule = na, terminal nodule = na, other hyaline areas = na
Other Features:	Spines = None; Comments = 'na'; Other = 'na'
Image path:	Catalogue3\Cat3-Ref23\Cat3-Ref23-40_2009-02-15-c300_combined.jpg

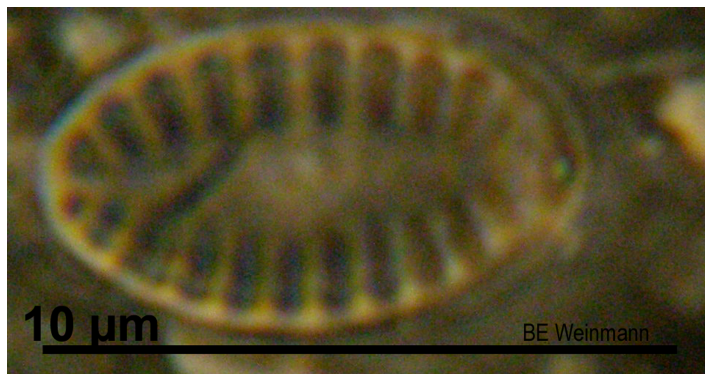


24_41	Pinnularia sp. 1 [?]
Specimens Measured:	1
Aspect:	Valve
Valve symmetry or shape:	Apical sym = Isobilateral, Transapical sym = Isopolar, Valve shape = Linear-lanceolate, Valve curvature = none Apex shape = no inflection, Shape = 'Broadly rounded', Frustral shape = na
Dimensions µm [AA]:	21.5 - (0) - na
Dimensions µm [TA]:	6 - (0) - na
Raphe:	Raphe, location = Central, shape = 'linear, thick', central endings = 'large & distant, inflated, porelike', polar endings = 'bent to the same side'
Striae:	13 - 14 per 10µm, orientation = 'Transverse, radiate', pores = 'not resolvable', na per 10µm
Fibulae or Costae:	
Axial area:	axial area = 'narrow' , central area = Transversely expanded to the margins, central nodule = large, undefined edges, terminal nodule = small, other hyaline areas = na
Other Features:	Spines = None; Comments = 'na'; Other = 'na'
Image path:	Catalogue3\Cat3-Ref24\Cat3-Ref24-41_2009-03-02.jpg
	

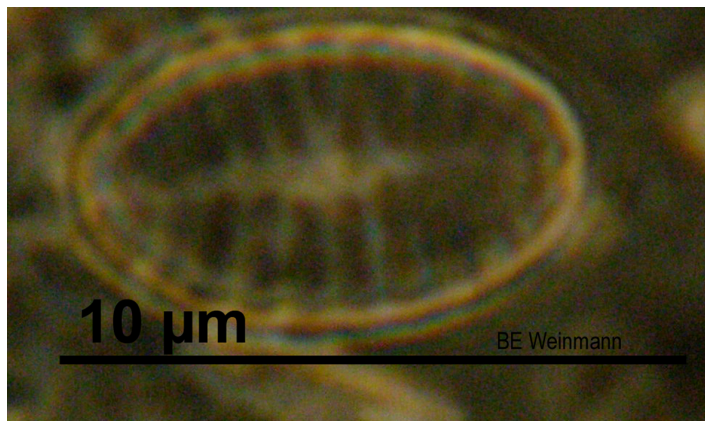
24_171	Pinnularia sp. 1 [?]
Specimens Measured:	1
Aspect:	Valve
Valve symmetry or shape:	Apical sym = Isobilateral, Transapical sym = Isopolar, Valve shape = Linear-lanceolate, Valve curvature = None, Frustral shape = NA
Dimensions µm [AA]:	17.6 - (0) - na
Dimensions µm [TA]:	5.9 - (0) - na
Raphe:	Raphe, location = Central, shape = 'Linear', central endings = 'Distant, straight, inflated (pinhead)', polar endings = 'Very slightly bent to same side'
Striae:	13 per 10µm, orientation = 'Transverse, radiate', pores = 'Not resolved', na per 10µm
Fibulae or Costae:	
Axial area:	axial area = 'NA' , central area = NA, central nodule = NA, terminal nodule = NA, other hyaline areas = NA
Other Features:	Spines = None; Comments = 'Not sure its the same but the only difference is the lack of "ghost striae"'; Other = 'na'
Image path:	Catalogue3\Cat3-Ref24\Cat3-Ref24-171_2012-04-13-c92.jpg
	

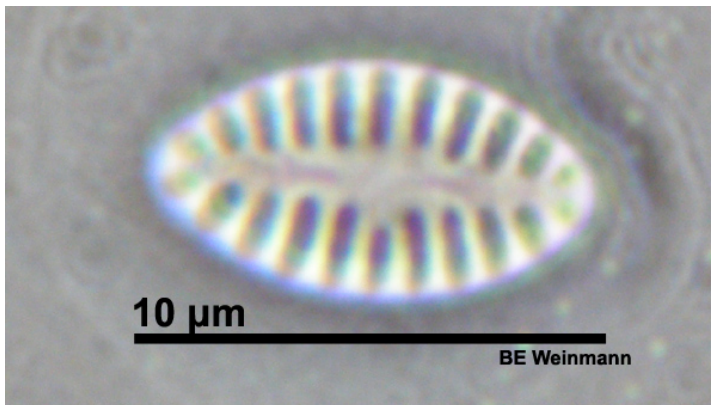
25_42	Dickieia subinflata (Grunow) Mann [BMB2: #169; Witkowski pl. 169]
Specimens Measured:	3
Aspect:	Valve
Valve symmetry or shape:	Apical sym = Isobilateral, Transapical sym = Isopolar, Valve shape = Linear-lanceolate, Valve curvature = none, Frustral shape = na
Dimensions µm [AA]:	11 - (15.3) - 22.2
Dimensions µm [TA]:	2.7 - (4.2) - 6.6
Raphe:	Raphe, location = Central, shape = 'linear, filiform', central endings = 'slightly inflated and very slightly inflected to the same side', polar endings = 'bent to the same side'
Striae:	18 - 19 per 10µm, orientation = 'Transverse, radiate', pores = 'punctate', 22 - 23 per 10µm
Fibulae or Costae:	
Axial area:	axial area = 'narrow, linear' , central area = Transversely expanded to the margins; unsymmetrical, side with odd striae slightly wider than the other, central nodule = large, undefined edges, terminal nodule = just visible, other hyaline areas = na
Other Features:	Spines = None; Comments = 'na'; Other = 'na'
Image path:	Catalogue3\Cat3-Ref25-42_2009-03-13.jpg
	

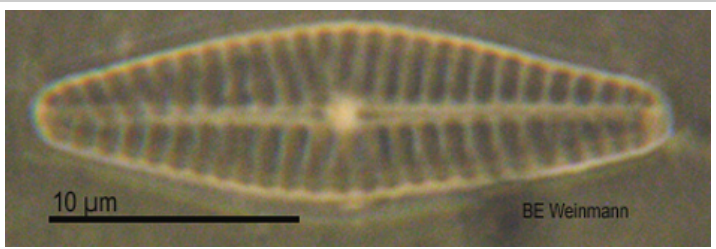
26_28	Achnanthes conspicua SV Mayer [BMB ?]
Specimens Measured:	na
Aspect:	Valve
Valve symmetry or shape:	Apical sym = Isobilateral, Transapical sym = Isopolar, Valve shape = Elliptic, Valve curvature = Slight convex Apex shape = no inflection, Shape = 'Broadly rounded', Frustral shape = na
Dimensions μm [AA]:	8.1 - (8.8) - 9.6
Dimensions μm [TA]:	4.4 - (5.1) - 5.9
Raphe:	Sternum, location = Central, shape = 'NA', central endings = 'NA', polar endings = 'NA'
Striae:	13 - 15 per 10 μm , orientation = 'Transverse, radiate', pores = 'Not resolved', na per 10 μm
Fibulae or Costae:	
Axial area:	axial area = 'Broadly lanceolate' , central area = Not distinct from sternum, central nodule = None, terminal nodule = None, other hyaline areas = na
Other Features:	Spines = None; Comments = 'The two valves were still attached hence I could see both. The raphe was not clearly visible so its possible I made a mistake but there aren't any heterovalvar araphid diatoms as far as i know and this one is clearly araphid.'; Other = 'na'
Image path:	Catalogue3\Cat3-Ref26\Cat3-Ref26-28_2009-03-05-c92.jpg

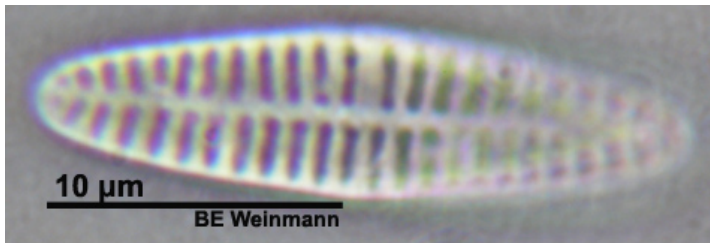


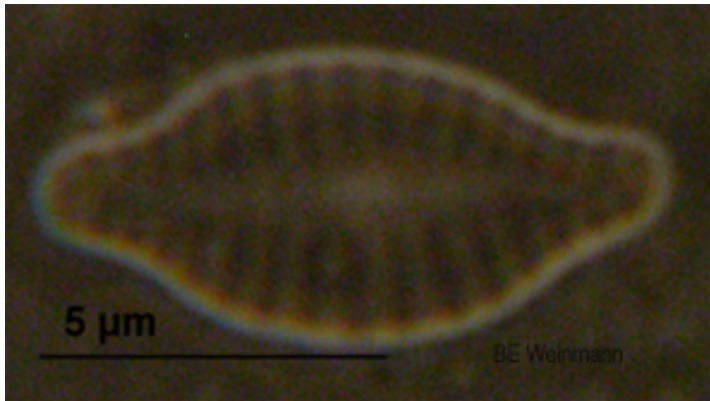
26_43	Achnanthes conspicua RV Mayer [BMB ?]
Specimens Measured:	na
Aspect:	Valve
Valve symmetry or shape:	Apical sym = Isobilateral, Transapical sym = Isopolar, Valve shape = Linear-lanceolate, Valve curvature = none Apex shape = no inflection, Shape = 'Broadly rounded', Frustral shape = slight curvature
Dimensions μm [AA]:	8.1 - (0) - na
Dimensions μm [TA]:	5.1 - (0) - na
Raphe:	Raphe, location = Central, shape = 'linear, filiform', central endings = 'Not resolved', polar endings = 'Resolved'
Striae:	12 per 10 μm , orientation = 'Transverse, becoming slightly radiate', pores = 'Not resolved', na per 10 μm
Fibulae or Costae:	
Axial area:	axial area = 'Linear or narrowly lanceolate' , central area = One-sided, central nodule = Not distinct, terminal nodule = not visible, other hyaline areas = na
Other Features:	Spines = None; Comments = 'The two valves were still attached hence I could see both. The raphe was not clearly visible so its possible I made a mistake but there aren't any heterovalvar araphid diatoms as far as i know'; Other = 'na'
Image path:	Catalogue3\Cat3-Ref26\Cat3-Ref26-43_2009-03-05.jpg



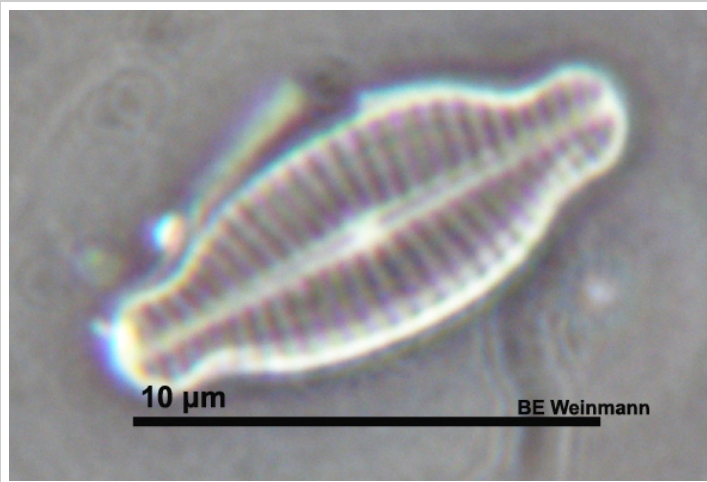
26_183	Achnanthes conspicua SV [BMB ?]
Specimens Measured:	1
Aspect:	Valve
Valve symmetry or shape:	Apical sym = Isobilateral, Transapical sym = Isopolar, Valve shape = Broadly lanceolate, Valve curvature = None, Frustral shape = NA
Dimensions µm [AA]:	9.6 - (0) - na
Dimensions µm [TA]:	5.1 - (0) - na
Raphe:	Sternum, location = Central, shape = 'NA', central endings = 'NA', polar endings = 'NA'
Striae:	11 - 12 per 10µm, orientation = 'Transverse, parallel becoming radiate', pores = 'Not resolved', na per 10µm
Fibulae or Costae:	
Axial area:	axial area = 'Lanceolate' , central area = Not distinct from axial area, central nodule = None, terminal nodule = None, other hyaline areas = None
Other Features:	Spines = None; Comments = 'Not sure this is actually the same as A. conspicua but they look similar its just different shape (less elliptic) more pointy'; Other = 'na'
Image path:	Catalogue3\Cat3-Ref26\Cat3-Ref26-183_2012-04-18-c73.jpg
	

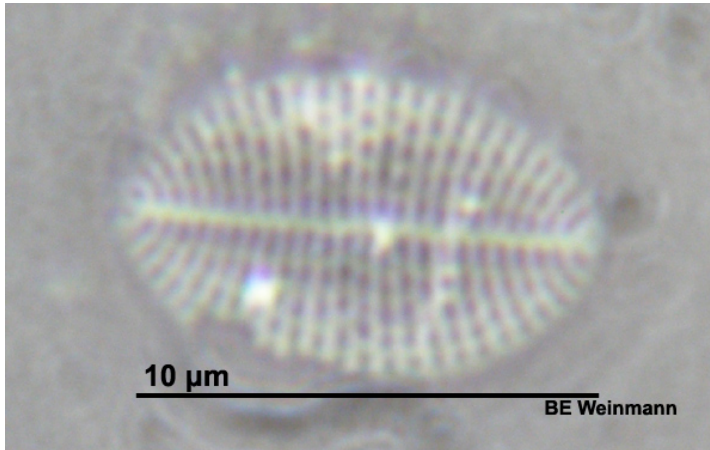
27_44	Achnanthes pericava (RV) Carter 1966 [BMB5: #404]
Specimens Measured:	na
Aspect:	Valve
Valve symmetry or shape:	Apical sym = Isobilateral, Transapical sym = Isopolar, Valve shape = Linear-lanceolate, Valve curvature = none Apex shape = no inflection, Shape = 'Bluntly rounded', Frustral shape = na
Dimensions µm [AA]:	24.4 - (0) - na
Dimensions µm [TA]:	5.1 - (0) - na
Raphe:	Raphe, location = Central, shape = 'linear, filiform', central endings = 'Expanded (pinhead), distant', polar endings = 'not visible'
Striae:	2 per 10µm, orientation = 'Transverse, radiate', pores = 'na', na per 10µm
Fibulae or Costae:	
Axial area:	axial area = 'Narrow, linear' , central area = slight transverse expansion, trapezoidal on the one side, central nodule = Large and bright, terminal nodule = Very fine, bent to one side, other hyaline areas = na
Other Features:	Spines = None; Comments = 'The 2nd valve was attached but not clearly visible, but the striae must be different from the top valve as the shadows.'; Other = 'na'
Image path:	Catalogue3\Cat3-Ref27\Cat3-Ref27-44_E2-T8.2-c13.jpg
	

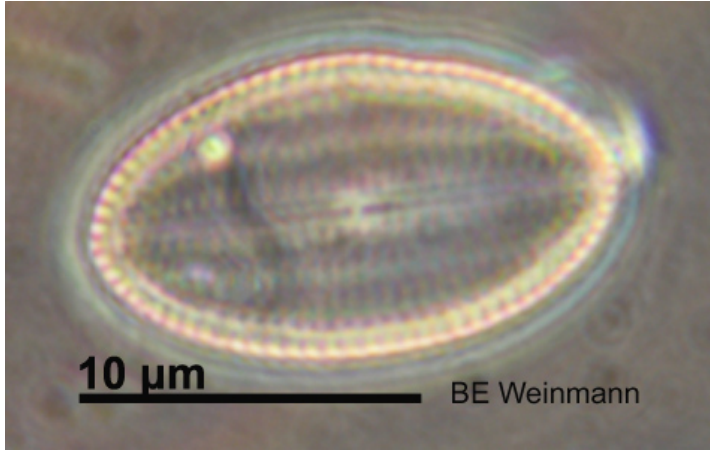
27_146	Achnanthes pericava (SV) Carter 1966 [BMB5: #404]
Specimens Measured:	na
Aspect:	Valve
Valve symmetry or shape:	Apical sym = Isobilateral, Transapical sym = Isopolar, Valve shape = Linear, Valve curvature = Strongly convex (like boomerang), Frustral shape = NA
Dimensions µm [AA]:	na - (0) - na
Dimensions µm [TA]:	na - (0) - na
Raphe:	Sternum, location = Central, shape = 'Straight', central endings = 'na', polar endings = 'na'
Striae:	13 - 14 per 10µm, orientation = 'Transverse', pores = 'Not resolved', na per 10µm
Fibulae or Costae:	
Axial area:	axial area = 'Linear, narrow' , central area = None, central nodule = None, terminal nodule = None, other hyaline areas = None
Other Features:	Spines = None; Comments = 'na'; Other = 'na'
Image path:	Catalogue3\Cat3-Ref27\Cat3-Ref27-146_2012-03-30-c12.jpg
	

28_45	Achnanthes lemmermannii SV Hustedt [BMB4: #305; Witkowski pl. 48:135-41] or Staurosira construens var. Binodis (Ehrenberg) Hamilton 1992
Specimens Measured:	7
Aspect:	Valve
Valve symmetry or shape:	Apical sym = Isobilateral, Transapical sym = Isopolar, Valve shape = Linear-lanceolate, Valve curvature = none, Apex shape = inflection, Shape = 'Rostrate, protracted', Frustral shape = na
Dimensions µm [AA]:	7.4 - (9.6) - 12.5
Dimensions µm [TA]:	3.1 - (4) - 5.1
Raphe:	Sternum, location = Central, shape = 'na', central endings = 'na', polar endings = 'na'
Striae:	15 - 18 per 10µm, orientation = 'Transverse, slightly radiate', pores = 'na', na per 10µm
Fibulae or Costae:	
Axial area:	axial area = 'lanceolate' , central area = none, central nodule = None, terminal nodule = None, other hyaline areas = na
Other Features:	Spines = None; Comments = 'Never found the raphid valve'; Other = 'na'
Image path:	Catalogue3\Cat3-Ref28\Cat3-Ref28-45_2009-02-04.jpg
	

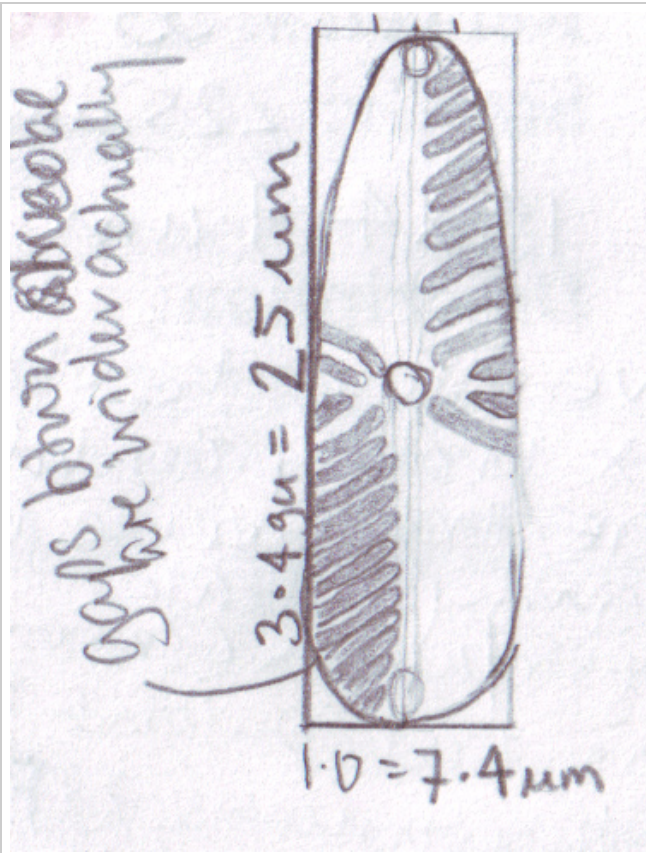
28_169	Achnanthes lemmermannii RV Hustedt [BMB4: #305; Witkowski pl. 48:135-41]
Specimens Measured:	4
Aspect:	Valve
Valve symmetry or shape:	Apical sym = Isobilateral, Transapical sym = Isopolar, Valve shape = Lanceolate, Valve curvature = None, Apex shape = inflection, Shape = 'Protracted, rostrate', Frustral shape = NA
Dimensions µm [AA]:	7.4 - (9.8) - 12.5
Dimensions µm [TA]:	3.7 - (4.2) - 4.4
Raphe:	Raphe, location = Central, shape = 'Linear', central endings = 'Straight, distant but not inflated', polar endings = 'Straight and distant from apices'
Striae:	22 per 10µm, orientation = 'Transverse, radiate', pores = 'Not resolved', na per 10µm
Fibulae or Costae:	
Axial area:	axial area = 'Narrow, Linear' , central area = Not really distinct from axial area, central nodule = Yes but with vague borders, terminal nodule = Not distinct, other hyaline areas = NA
Other Features:	Spines = None; Comments = 'na'; Other = 'na'
Image path:	Catalogue3\Cat3-Ref28\Cat3-Ref28-169_2012-04-14-c76.jpg



29_46	Cocconeis placentula var euglypta SV (Ehrenberg) Grunow [BMB5: #425 & ADIAC] (similar to Cocconeis neothumensis)
Specimens Measured:	7
Aspect:	Valve
Valve symmetry or shape:	Apical sym = Isobilateral, Transapical sym = Isopolar, Valve shape = Elliptic, Valve curvature = none Apex shape = no inflection, Shape = 'Broadly rounded', Frustral shape = na
Dimensions µm [AA]:	6.6 - (12.3) - 28.0894736842105
Dimensions µm [TA]:	3.5 - (5.6) - 7.4
Raphe:	Sternum, location = Central, shape = 'NA', central endings = 'NA', polar endings = 'NA'
Striae:	20 per 10µm, orientation = 'Transverse, parallel becoming radiate towards the poles', pores = 'Dashes', 8 - 9 per 10µm
Fibulae or Costae:	
Axial area:	axial area = 'Narrow, linear' , central area = Not distinguished from sternum, central nodule = Visible, terminal nodule = Not visible, other hyaline areas = longitudinal hyaline "seams" created by punctate striae
Other Features:	Spines = None; Comments = 'saw 4, they were not seperate so I know they belong together (....????)'; Other = 'na'
Image path:	Catalogue3\Cat3-Ref29\Cat3-Ref29-46_2012-04-18-c178.jpg
	

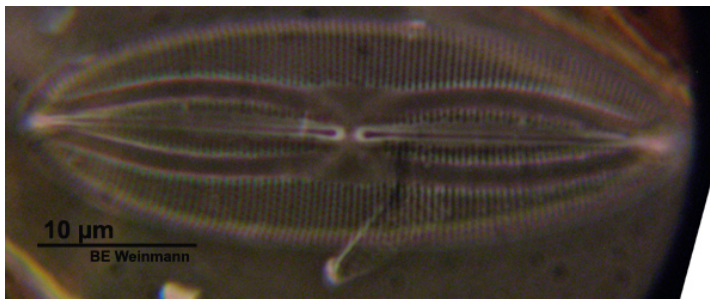
29_47	Cocconeis placentula var euglypta RV(Ehrenberg) Grunow [BMB5: #425]
Specimens Measured:	4
Aspect:	Valve
Valve symmetry or shape:	Apical sym = Isobilateral, Transapical sym = Isopolar, Valve shape = Elliptic, Valve curvature = none Apex shape = no inflection, Shape = 'Broadly rounded', Frustral shape = na
Dimensions µm [AA]:	10.4 - (10.9) - 11.1
Dimensions µm [TA]:	5.9 - (6.8) - 7.4
Raphe:	Raphe, location = Central, shape = 'Linear', central endings = 'Longitudinally inflated, slightly approximate', polar endings = 'Straight'
Striae:	19 - 20 per 10µm, orientation = 'Transverse, parallel becoming radiate towards the poles', pores = 'Dashes', Not resolved per 10µm
Fibulae or Costae:	
Axial area:	axial area = 'Narrow, linear' , central area = Not distinguished from sternum, central nodule = Large, round, terminal nodule = not visible, other hyaline areas = longitudinal hyaline "seams" created by punctate striae
Other Features:	Spines = None; Comments = 'looks like longitudinally striped egg'; Other = 'na'
Image path:	Catalogue3\Cat3-Ref29\Cat3-Ref29-47_2012-04-01-c124.jpg
	


30_48	Gomphonema olivaceum (Hornemann) Brebisson [BMB1: #49]
Specimens Measured:	1
Aspect:	Valve
Valve symmetry or shape:	Apical sym = Isobilateral, Transapical sym = Heteropolar, Valve shape = Skittle-shaped, Valve curvature = none Apex shape = no inflection, Shape = 'Broadly rounded', Frustral shape = na
Dimensions μm [AA]:	24 - (0) - na
Dimensions μm [TA]:	7.4 - (0) - na
Raphe:	Raphe, location = Central, shape = 'linear', central endings = 'Straight, slightly inflated', polar endings = 'not visible'
Striae:	11 per $10\mu\text{m}$, orientation = 'Transverse', pores = 'not visible ', not resolvable per $10\mu\text{m}$
Fibulae or Costae:	
Axial area:	axial area = 'Narrow, linear' , central area = na, central nodule = large, terminal nodule = visible, other hyaline areas = Narrow, rectangular transapical expansion
Other Features:	Spines = None; Comments = 'na'; Other = 'na'
Image path:	Catalogue3\Cat3-Ref30-48_2008-12-.bmp



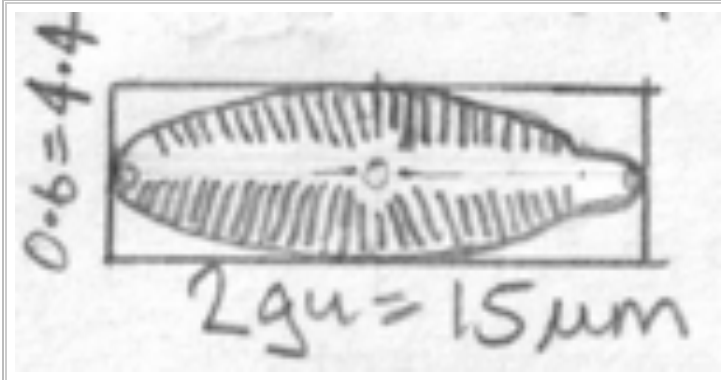
31_49	Amphora coffeaeformis (Agardh) Kützing [BMB3: #20]
Specimens Measured:	4
Aspect:	Valve
Valve symmetry or shape:	Apical sym = Dorsiventral, Transapical sym = Isopolar, Valve shape = Arcuate, Valve curvature = none, Apex shape = inflection, Shape = 'Protracted, rostrate or sub-capitate', Frustral shape = na
Dimensions μm [AA]:	11 - (19) - 25.9
Dimensions μm [TA]:	2.9 - (4.2) - 6
Raphe:	Raphe, location = Ventral, shape = 'linear', central endings = 'not recorded but look straight', polar endings = 'not visible'
Striae:	21 - 24 per 10 μm , orientation = 'Transverse, becoming slightly radiate', pores = 'not resolved', not resolvable per 10 μm
Fibulae or Costae:	
Axial area:	axial area = 'narrow, linear' , central area = slight transverse expansion, central nodule = yes, terminal nodule = yes, at very end of apex, other hyaline areas = na
Other Features:	Spines = None; Comments = 'na'; Other = 'na'
Image path:	Catalogue3\Cat3-Ref31\Cat3-Ref31-49_2008-12-02.jpg



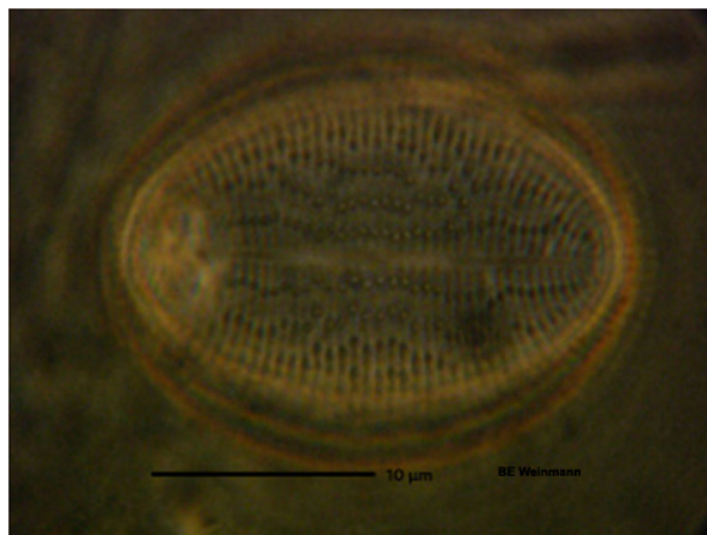
32_84	Fallacia oculiformis (Hustedt) Mann in Round et al 1990 [BMB4: #343; Witkowski pl. 71:23-30]
Specimens Measured:	1
Aspect:	Valve
Valve symmetry or shape:	Apical sym = Isobilateral, Transapical sym = Isopolar, Valve shape = Elliptic, Valve curvature = Slight convex Apex shape = no inflection, Shape = 'Broadly rounded', Frustral shape = na
Dimensions µm [AA]:	16.3 - (0) - na
Dimensions µm [TA]:	8.1 - (0) - na
Raphe:	Raphe, location = Central, shape = 'Linear', central endings = 'Inflated, straight, distant', polar endings = 'Not visible'
Striae:	27 per 10µm, orientation = 'Transverse, parallel then radiate', pores = 'na', na per 10µm
Fibulae or Costae:	
Axial area:	axial area = 'Narrow, linear' , central area = na, central nodule = None, terminal nodule = Not visible, other hyaline areas = Broad (1/3 TA), slightly rounded-H shaped
Other Features:	Spines = None; Comments = 'na'; Other = 'na'
Image path:	Catalogue3\Cat3-Ref63\Cat2-Ref63-125_2012-03-21-c95.jpg
	

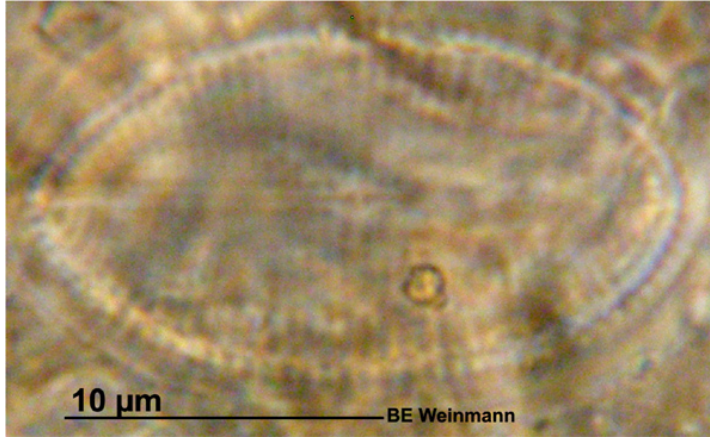
33_51	Hantzschia petitiiana Grunow in Cleve & Möller [Witkowski ?]
Specimens Measured:	1
Aspect:	Valve
Valve symmetry or shape:	Apical sym = Dorsiventral, Transapical sym = Isopolar, Valve shape = arcuate, Valve curvature = none, Apex shape = inflection, Shape = 'Protracted, cuneate or sub-rostrate', Frustral shape = na
Dimensions µm [AA]:	40 - (0) - na
Dimensions µm [TA]:	na - (0) - na
Raphe:	Raphe, location = Ventral, shape = 'eccentric', central endings = 'na', polar endings = 'na'
Striae:	not resolved per 10µm, orientation = 'Presumably transverse', pores = 'not resolved', not resolved per 10µm
Fibulae or Costae:	fibulae = 10 - 15 per 10µm, not evenly spaced
Axial area:	axial area = 'na' , central area = na, central nodule = na, terminal nodule = na, other hyaline areas = na
Other Features:	Spines = None; Comments = 'na'; Other = 'na'
Image path:	Catalogue3\Cat3-Ref33-51_2008-12-03.jpg
	

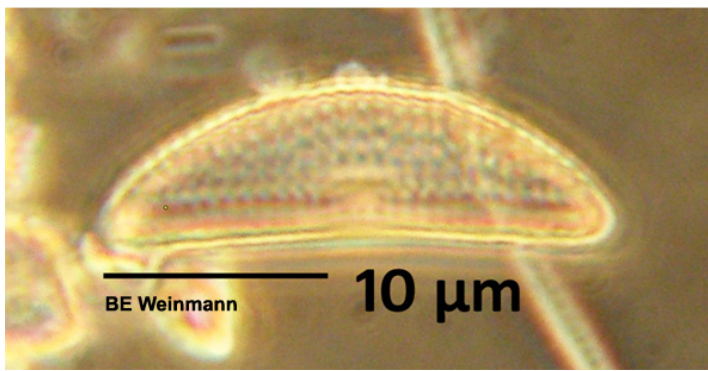
34_52	Gomphonema olivaceum var minutissima Agardh (Agardh) [Simonsen pl. 95:8-11; ADIAC #15]
Specimens Measured:	2
Aspect:	Valve
Valve symmetry or shape:	Apical sym = Isobilateral, Transapical sym = Heteropolar, Valve shape = Cuneate - skittle shaped, Valve curvature = none, Frustral shape = na
Dimensions μm [AA]:	15 - (0) - na
Dimensions μm [TA]:	na - (0) - na
Raphe:	Raphe, location = Central, shape = 'linear', central endings = 'Straight, slightly inflated', polar endings = 'not visible'
Striae:	15-18 per $10\mu\text{m}$, orientation = 'Slightly transverse', pores = 'not resolved', not resolved per $10\mu\text{m}$
Fibulae or Costae:	
Axial area:	axial area = '1/4 TA, linear' , central area = slight transverse expansion, central nodule = yes, terminal nodule = yes, other hyaline areas = na
Other Features:	Spines = None; Comments = 'na'; Other = 'na'
Image path:	Catalogue3\Cat3-Ref34-52_2008-12-03.bmp

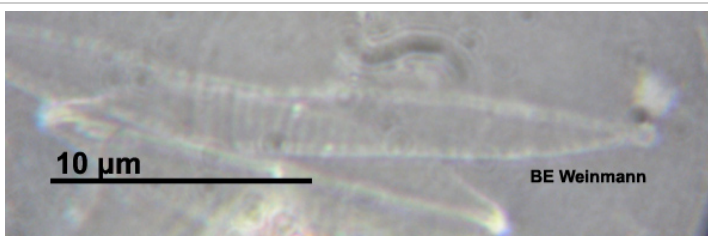


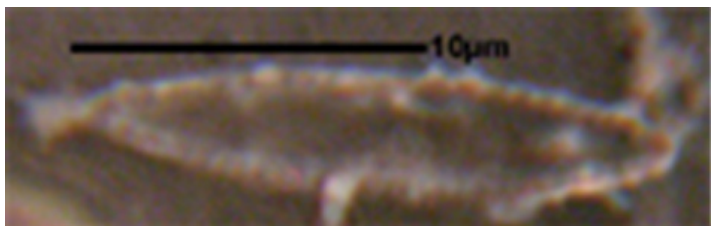
35_53	Cocconeis pediculous SV Ehrenberg 1838 [BMB1: #23]
Specimens Measured:	2
Aspect:	Valve
Valve symmetry or shape:	Apical sym = Isobilateral, Transapical sym = Isopolar, Valve shape = Linear - elliptic, Valve curvature = yes (convex?) Apex shape = no inflection, Shape = 'Broadly rounded', Frustral shape = na
Dimensions µm [AA]:	11.1 - (18.9) - 26
Dimensions µm [TA]:	7.4 - (13.2) - 19
Raphe:	Sternum, location = Central, shape = 'na', central endings = 'na', polar endings = 'na'
Striae:	17 - 23 per 10µm, orientation = 'Transverse, parallel becoming radiate towards the poles', pores = 'visible', > 7 per 10µm
Fibulae or Costae:	
Axial area:	axial area = 'narrow, linear' , central area = na, central nodule = no, terminal nodule = no, other hyaline areas = Longitudinal, bimodal curve between striae punctae
Other Features:	Spines = None; Comments = 'na'; Other = 'na'
Image path:	Catalogue3\Cat3-Ref35-53_2008-12-03.jpg



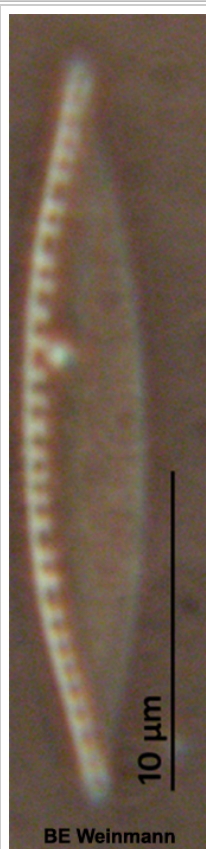
35_54	Cocconeis pediculous RV Ehrenberg 1838 [BMB1: #23]
Specimens Measured:	1
Aspect:	Valve
Valve symmetry or shape:	Apical sym = Isobilateral, Transapical sym = Isopolar, Valve shape = Linear, elliptic, Valve curvature = Not distinctly Apex shape = no inflection, Shape = 'Broadly rounded or Obtuse', Frustral shape = na
Dimensions µm [AA]:	22.5 - (0) - na
Dimensions µm [TA]:	15 - (0) - na
Raphe:	Raphe, location = Central, shape = 'Linear', central endings = 'Inflated, pinheads, straight, close together', polar endings = 'Not resolved'
Striae:	17 - 20 per 10µm, orientation = 'Transverse, parallel becoming radiate', pores = 'Punctate', Not resolved per 10µm
Fibulae or Costae:	
Axial area:	axial area = 'Narrow, linear' , central area = Small and round and distinct, central nodule = Not visible, terminal nodule = Not visible, other hyaline areas = none
Other Features:	Spines = None; Comments = 'na'; Other = 'na'
Image path:	Catalogue3\Cat3-Ref35-54_2009-03-14.jpg
	

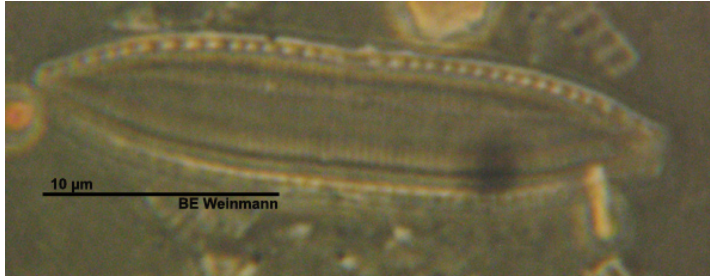
36_55	Amphora sp. 1 [?]
Specimens Measured:	2
Aspect:	Valve
Valve symmetry or shape:	Apical sym = Dorsiventral, Transapical sym = Isopolar, Valve shape = Cymbiform-lunate, Valve curvature = none Apex shape = no inflection, Shape = 'Acutely rounded', Frustral shape = na
Dimensions µm [AA]:	20.6 - (0) - 22
Dimensions µm [TA]:	4.4 - (0) - 5.9
Raphe:	Raphe, location = Ventral, shape = 'linear', central endings = 'slightly inflated and very slightly inflected to the same side', polar endings = 'not resolved'
Striae:	10 - 14 per 10µm, orientation = 'Transverse, parallel', pores = 'visible', > 5 per 10µm
Fibulae or Costae:	
Axial area:	axial area = 'linear' , central area = rectangular, central nodule = yes, terminal nodule = not visible, other hyaline areas = longitudinal, following dorsal curve, between striae punctae
Other Features:	Spines = None; Comments = 'na'; Other = 'na'
Image path:	Catalogue3\Cat3-Ref36-55_2008-12-03.jpg
	

37_56	Nitzschia palea (Kützinger) W. Smith(1856) (?) [EA Diatomkey: #13540980]
Specimens Measured:	1
Aspect:	Valve
Valve symmetry or shape:	Apical sym = Isobilateral, Transapical sym = Isopolar, Valve shape = Narrowly lanceolate, Valve curvature = none, Apex shape = inflection, Shape = 'Protracted rostrate or sub-capitate', Frustral shape = na
Dimensions µm [AA]:	68 - (0) - na
Dimensions µm [TA]:	4.4 - (0) - na
Raphe:	Raphe, location = Eccentric, shape = 'marginal', central endings = 'na', polar endings = 'na'
Striae:	not resolved per 10µm, orientation = 'na', pores = 'na', na per 10µm
Fibulae or Costae:	fibulae = 10 - 13 per 10µm, Gap between central fibulae
Axial area:	axial area = 'na' , central area = na, central nodule = na, terminal nodule = na, other hyaline areas = na
Other Features:	Spines = None; Comments = 'na'; Other = 'na'
Image path:	Catalogue3\Cat3-Ref37-56_2012-04-18-c9.jpg
	

38_50	Nitzschia aqueora Hustedt [Witkowski pl. 210:14-15]
Specimens Measured:	7
Aspect:	Valve
Valve symmetry or shape:	Apical sym = Isobilateral, Transapical sym = Isopolar, Valve shape = Narrowly lanceolate, Valve curvature = none, Apex shape = inflection, Shape = 'Protracted rostrate or sub-capitate', Frustral shape = na
Dimensions μm [AA]:	18.5 - (19.8) - 22.1
Dimensions μm [TA]:	2.9 - (3.5) - 3.7
Raphe:	Raphe, location = Eccentric, shape = 'marginal', central endings = 'na', polar endings = 'na'
Striae:	not resolved per 10 μm , orientation = 'Transverse, parallel presumably', pores = 'na', na per 10 μm
Fibulae or Costae:	fibulae = 16 - 18 per 10 μm , Gap between central fibulae
Axial area:	axial area = 'na', central area = na, central nodule = na, terminal nodule = na, other hyaline areas = na
Other Features:	Spines = None; Comments = 'This is very similar to Hantzschia petitiana but the fibulae are just not as regular?'; Other = 'Apices is full with fibulae'
Image path:	Catalogue3\Cat3-Ref38\Cat3-Ref38-50_2008-12.jpg
	

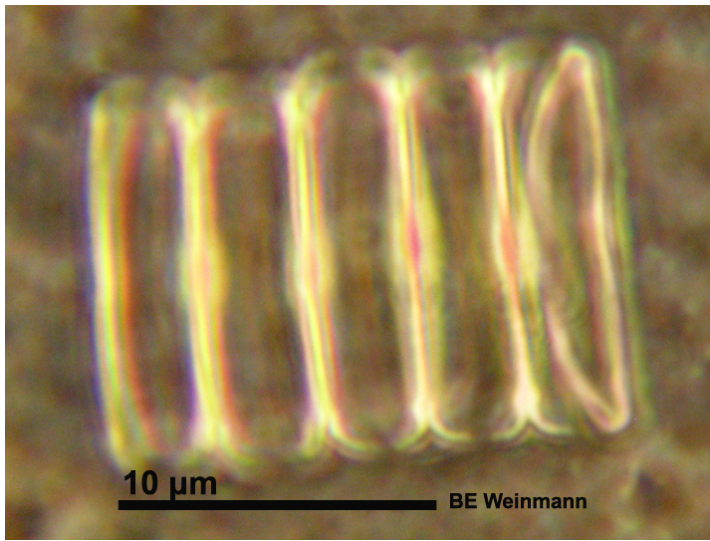
38_57	Nitzschia aqueora Hustedt [Witkowski p367 & Rib pl33:15]
Specimens Measured:	16
Aspect:	Valve
Valve symmetry or shape:	Apical sym = Isobilateral, Transapical sym = Isopolar, Valve shape = Narrowly lanceolate, Valve curvature = none Apex shape = no inflection, Shape = 'acute', Frustral shape = na
Dimensions µm [AA]:	8.1 - (14.7) - 23.7
Dimensions µm [TA]:	2.2 - (3.7) - 5.9
Raphe:	Raphe, location = Eccentric, shape = 'marginal', central endings = 'na', polar endings = 'na '
Striae:	not resolved per 10µm, orientation = 'not resolved', pores = 'na', na per 10µm
Fibulae or Costae:	fibulae = 10 - 16 per 10µm, very short
Axial area:	axial area = 'na' , central area = na, central nodule = no, terminal nodule = no, other hyaline areas = na
Other Features:	Spines = None; Comments = 'I think this might just be N. aqueora where the valves have not separated'; Other = 'na'
Image path:	Catalogue3\Cat3-Ref38\Cat3-Ref38-57_2008-12.jpg

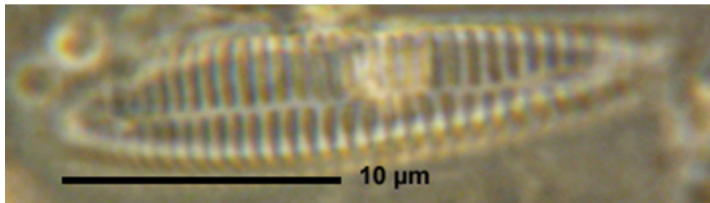


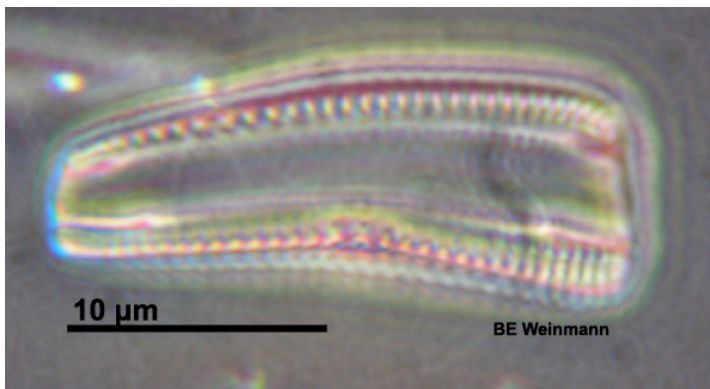
39_58	Nitzschia salinicola Aleem & Hustedt 1951 [BMB5-466]
Specimens Measured:	3
Aspect:	Valve
Valve symmetry or shape:	Apical sym = Isobilateral, Transapical sym = Isopolar, Valve shape = Panduriform, Valve curvature = none, Apex shape = inflection, Shape = 'Slightly protracted, short sub-rostrate', Frustral shape = na
Dimensions µm [AA]:	25 - (26.9) - 29
Dimensions µm [TA]:	5.9 - (7.2) - 9.6
Raphe:	Raphe, location = Eccentric, shape = 'marginal', central endings = 'na', polar endings = 'na '
Striae:	45 + per 10µm, orientation = 'Transverse, parallel', pores = 'Not resolved', na per 10µm
Fibulae or Costae:	fibulae = 12 - 15 per 10µm, Gap in central fibulae
Axial area:	axial area = 'NA' , central area = NA, central nodule = NA, terminal nodule = NA, other hyaline areas = NA
Other Features:	Spines = None; Comments = 'na'; Other = 'na'
Image path:	Catalogue3\Cat3-Ref39\Cat1-Ref39-58_2009-03-12.jpg
	

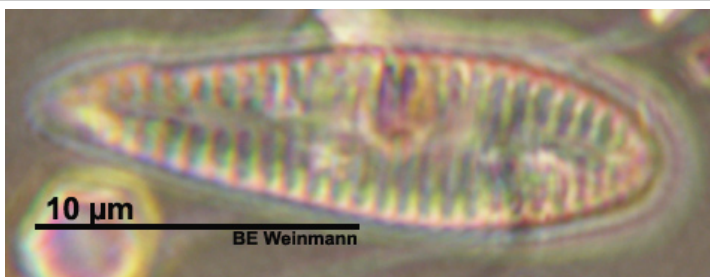
40_59	Catenula adhaerens Mereschkowsky [BMB1: 19]
Specimens Measured:	11
Aspect:	Valve
Valve symmetry or shape:	Apical sym = Dorsiventral, Transapical sym = Isopolar, Valve shape = Lunate with slight constriction in centre, Valve curvature = none Apex shape = no inflection, Shape = 'acute', Frustral shape = na
Dimensions µm [AA]:	5.9 - (10.6) - 12.9
Dimensions µm [TA]:	2 - (2.5) - 3.7
Raphe:	Yes but not visible, location = Ventral, shape = 'na', central endings = 'not resolved', polar endings = 'not resolved'
Striae:	not resolved per 10µm, orientation = 'not resolved', pores = 'not resolvable', na per 10µm
Fibulae or Costae:	
Axial area:	axial area = 'na' , central area = na, central nodule = Yes, bright, terminal nodule = Yes, bright, other hyaline areas = center from ventral to dorsal margin
Other Features:	Spines = None; Comments = 'na'; Other = 'na'
Image path:	Catalogue3\Cat3-Ref40\Cat3-Ref40-59_2009-01-29.jpg

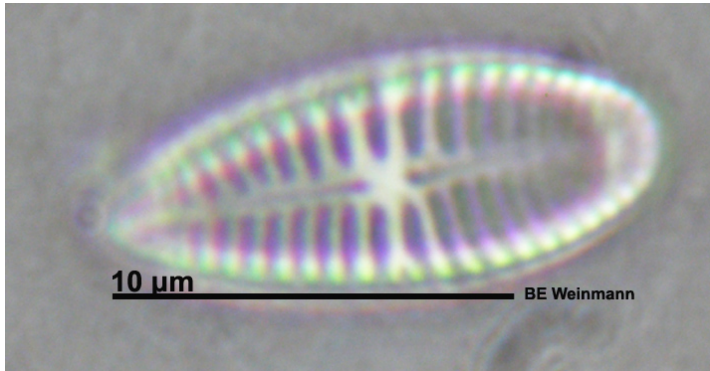


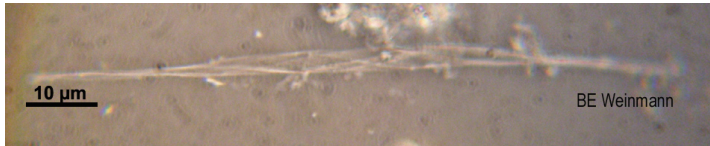
40_158	Catenula adherens Girdle [Weinmann]
Specimens Measured:	2
Aspect:	Girdle
Valve symmetry or shape:	
Dimensions µm [AA]:	8.1 - (10.7) - 13.2
Dimensions µm [PA]:	0.4 - (1.7) - 2.9
Raphe:	na, location = na, shape = 'na', central endings = 'na', polar endings = 'na'
Striae:	na per 10µm, orientation = 'na', pores = 'na', na per 10µm
Fibulae or Costae:	
Axial area:	axial area = 'na' , central area = na, central nodule = na, terminal nodule = na, other hyaline areas = na
Other Features:	Spines = na; Comments = 'na'; Other = 'na'
Image path:	Catalogue3\Cat3-Ref40\Cat2-Ref40-158_2012-04-08-c109.jpg
	

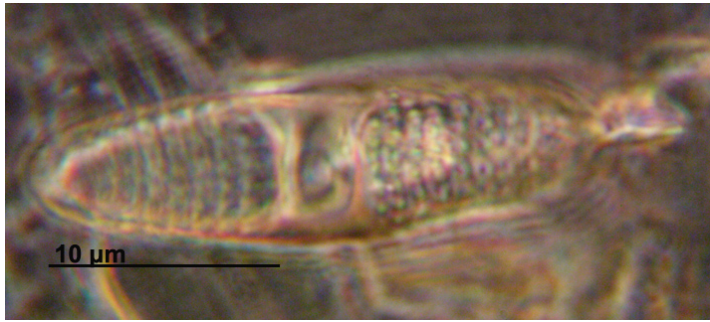
41_60	Rhoicosphenia marina CX (W. Smith) Schmidt [Witkowski pl. 58:8-18]
Specimens Measured:	3
Aspect:	Valve
Valve symmetry or shape:	Apical sym = Isobilateral, Transapical sym = Heteropolar, Valve shape = Curved, Valve curvature = Yes Apex shape = no inflection, Shape = 'Broadly rounded', Frustral shape = na
Dimensions µm [AA]:	22.2 - (23.4) - 25.9
Dimensions µm [TA]:	4.8 - (4.9) - 5.1
Raphe:	Raphe, location = Central, shape = 'Partial (1/5 valve)', central endings = 'Straight', polar endings = 'Not resolved'
Striae:	18 - 20 per 10µm, orientation = 'Transverse, parallel', pores = 'na', na per 10µm
Fibulae or Costae:	
Axial area:	axial area = 'Narrow, linear' , central area = None, central nodule = None, terminal nodule = None, other hyaline areas = na
Other Features:	Spines = None; Comments = 'na'; Other = 'NA'
Image path:	Catalogue3\Cat3-Ref41\Cat3-Ref41-60_2009-02-05.jpg
	

42_61	Rhoicosphenia curvata or abbreviata Girdle (Kützing) Grunow 1860 [BMB1: 81; Witk. et al 2000, p345]
Specimens Measured:	3
Aspect:	Girdle
Valve symmetry or shape:	
Dimensions µm [AA]:	11.8 - (16.5) - 20
Dimensions µm [PA]:	5.9 - (6.6) - 7.4
Raphe:	na, location = na, shape = 'na', central endings = 'na', polar endings = 'na'
Striae:	10 - 15 per 10µm, orientation = 'Transverse, parallel', pores = '>10', na per 10µm
Fibulae or Costae:	
Axial area:	axial area = 'na', central area = na, central nodule = na, terminal nodule = na, other hyaline areas = na
Other Features:	Spines = None; Comments = 'This sketch may be innacurate....I didn't notice that the striae on the two sides were different (perhaps they were not ?). Also called Roicosphenia sp.1 abbreviata (C.A.Agardh) Lange-Bertalot 1980'; Other = 'NA'
Image path:	Catalogue3\Cat3-Ref42\Cat3-Ref42-61_2012-04-18-c102.jpg
	

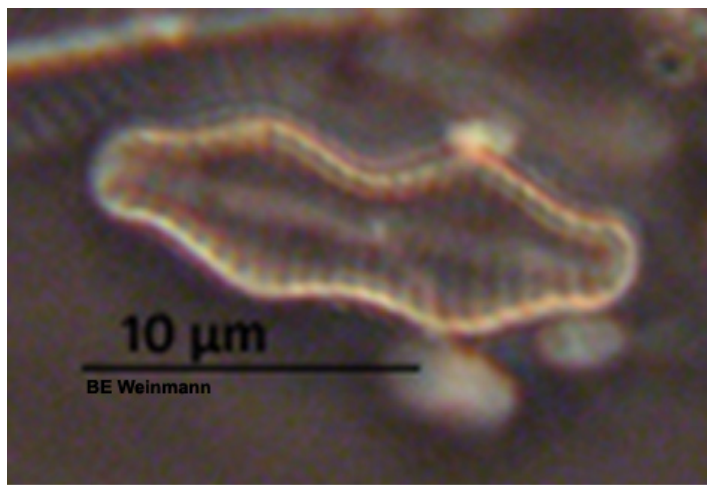
42_132	Rhoicosphenia curvata or abbreviata CVV (partial raphe) (Kützing) Grunow 1860 [ADIAC p1: #5; Witk. et al 2000, p345]
Specimens Measured:	2
Aspect:	Valve
Valve symmetry or shape:	Apical sym = Isobilateral, Transapical sym = Heteropolar, Valve shape = club-shaped and curved, Valve curvature = Yes, concave Apex shape = no inflection, Shape = 'Broadly rounded', Frustral shape = na
Dimensions µm [AA]:	16.9 - (18) - 19.1
Dimensions µm [TA]:	5.1 - (5.5) - 5.9
Raphe:	Raphe (partial), location = Central, shape = 'Partial (only visible on one side)', central endings = 'Straight', polar endings = 'Straight'
Striae:	13 - 15 per 10µm, orientation = 'Transverse, parallel', pores = 'Not resolved', na per 10µm
Fibulae or Costae:	
Axial area:	axial area = 'Narrow, linear', central area = None, central nodule = None, terminal nodule = None, other hyaline areas = NA
Other Features:	Spines = None; Comments = 'na'; Other = 'NA'
Image path:	Catalogue3\Cat3-Ref42\Cat3-Ref42-132_2012-03-29-c13.jpg
	

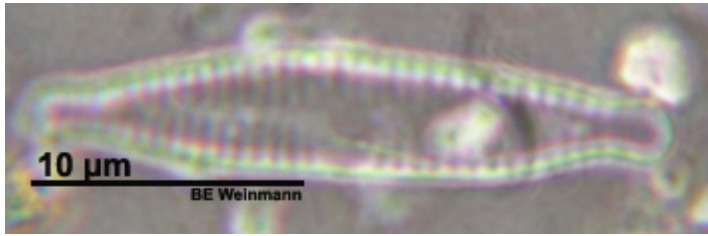
42_165	Rhoicosphenia curvata CXV (full raphe) (Kützting) Grunow 1860 [BMB1: 81]
Specimens Measured:	1
Aspect:	Valve
Valve symmetry or shape:	Apical sym = Isobilateral, Transapical sym = Heteropolar, Valve shape = Club-shaped, Valve curvature = Convex, Frustral shape = na
Dimensions µm [AA]:	14 - (0) - na
Dimensions µm [TA]:	5.9 - (0) - na
Raphe:	Sternum, location = Central, shape = 'Straight', central endings = 'Distant, inflated (golf T)', polar endings = 'Curving to one side'
Striae:	13 - 15 per 10µm, orientation = 'Transverse, slightly radiate', pores = 'Not resolved', na per 10µm
Fibulae or Costae:	
Axial area:	axial area = 'Linear or very narrowly lanceolate', central area = Not distinct from axial area, central nodule = None visible, terminal nodule = None visible, other hyaline areas = na
Other Features:	Spines = None; Comments = 'na'; Other = 'na'
Image path:	Catalogue3\Cat3-Ref42\Cat3-Ref42-165_2012-04-12-c15.jpg
	

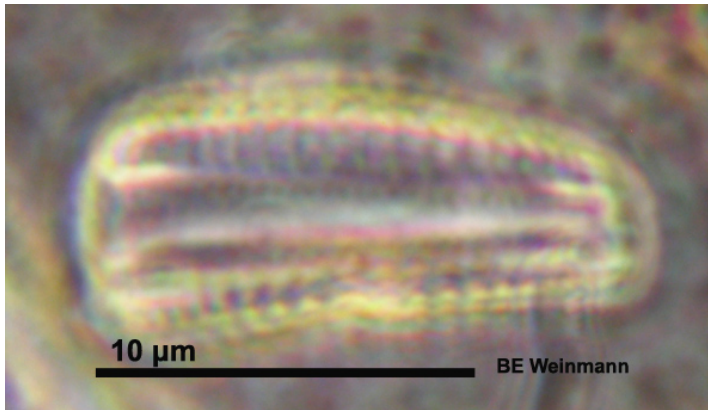
43_62	Cylindrotheca gracilis (de Brebisson) Grunow ex van Heurck [Witkowski pl. 212:7]
Specimens Measured:	6
Aspect:	Valve
Valve symmetry or shape:	Apical sym = Isobilateral, Transapical sym = Isopolar, Valve shape = Acicular (spindle-shaped), Valve curvature = maybe, Apex shape = inflection, Shape = 'very produced, apiculate, curved to the same size', Frustral shape = na
Dimensions µm [AA]:	62.2 - (76.6) - 88
Dimensions µm [TA]:	2.2 - (3.6) - 4.4
Raphe:	Raphe, location = Eccentric, shape = 'Spiral', central endings = 'na', polar endings = 'na'
Striae:	not resolved per 10µm, orientation = 'na', pores = 'na', na per 10µm
Fibulae or Costae:	
Axial area:	axial area = 'na', central area = na, central nodule = na, terminal nodule = na, other hyaline areas = na
Other Features:	Spines = None; Comments = 'na'; Other = 'na'
Image path:	Catalogue3\Cat3-Ref43\Cat3-Ref43-62_2009-01-12.jpg
	

44_63	Plagiogramma staurophorum (Gregory) Heiberg 1863 [BMB3: 279]
Specimens Measured:	2
Aspect:	Valve
Valve symmetry or shape:	Apical sym = Isobilateral, Transapical sym = Isopolar, Valve shape = Lanceolate, Valve curvature = none Apex shape = no inflection, Shape = 'Obtusely rounded', Frustral shape = na
Dimensions μm [AA]:	8 - (16.2) - 24.3
Dimensions μm [TA]:	2.9 - (4.8) - 6.6
Raphe:	Sternum, location = Central, shape = 'na', central endings = 'na', polar endings = 'na'
Striae:	10 per $10\mu\text{m}$, orientation = 'Transverse, parallel', pores = 'punctate', 21 per $10\mu\text{m}$
Fibulae or Costae:	
Axial area:	axial area = 'none ', central area = Broad rectangular hyaline area all the way to margin, central nodule = na, terminal nodule = na, other hyaline areas = na
Other Features:	Spines = None; Comments = 'There is no sternum visible, the gap between the punctae of opposite striae is the same as the gap between punctae within striae'; Other = 'na'
Image path:	Catalogue3\Cat3-Ref44\Cat3-Ref44-63_2012-04-12-c126.jpg
	

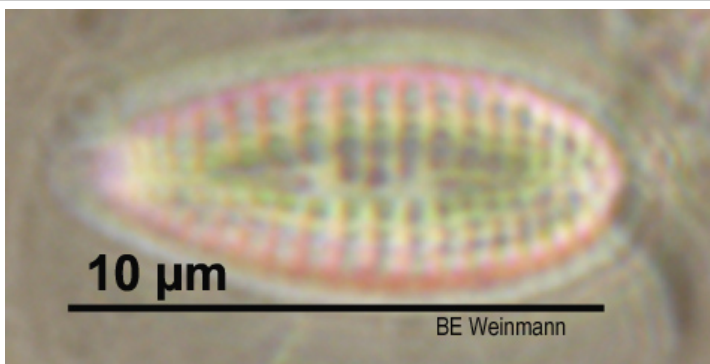
45_64	Staurosira construens var. binodis (Ehrenberg) Hamilton [BMB5: #489, ADIAC, Kelly et al 2005]
Specimens Measured:	1
Aspect:	Valve
Valve symmetry or shape:	Apical sym = Isobilateral, Transapical sym = Isopolar, Valve shape = Panduriform, Valve curvature = none, Apex shape = inflection, Shape = 'Protracted, broadly rostrate', Frustral shape = na
Dimensions μm [AA]:	15.8 - (0) - na
Dimensions μm [TA]:	5.9 - (0) - na
Raphe:	Sternum, location = Central, shape = 'na', central endings = 'na', polar endings = 'na'
Striae:	16 per 10 μm , orientation = 'Transverse, parallel', pores = 'punctate', not resolved per 10 μm
Fibulae or Costae:	
Axial area:	axial area = 'Narrowly linear' , central area = none, central nodule = ? Could just be debris, terminal nodule = none, other hyaline areas = na
Other Features:	Spines = None; Comments = 'na'; Other = 'na'
Image path:	Catalogue3\Cat3-Ref45\Cat3-Ref45-64_2008-12.jpg



45_143	Staurosira construens var. binodis (Ehrenberg) Hamilton [BMB5: #489, ADIAC, Kelly et al 2005]
Specimens Measured:	1
Aspect:	Valve
Valve symmetry or shape:	Apical sym = Isobilateral, Transapical sym = Isopolar, Valve shape = Linear-undulate, Valve curvature = None, Apex shape = inflection, Shape = 'Protracted, capitate', Frustral shape = na
Dimensions µm [AA]:	22.8 - (0) - na
Dimensions µm [TA]:	na - (4.4) - na
Raphe:	Sternum, location = Central, shape = 'na', central endings = 'na', polar endings = 'na'
Striae:	15 - 17 per 10µm, orientation = 'Transverse, parallel', pores = 'Not resolved', na per 10µm
Fibulae or Costae:	
Axial area:	axial area = 'NA' , central area = NA, central nodule = NA, terminal nodule = NA, other hyaline areas = na
Other Features:	Spines = None; Comments = 'IF there is a central gap on one side I think it might not be Fragilaria construens but another taxa'; Other = 'na'
Image path:	Catalogue3\Cat3-Ref45\Cat3-Ref45-143_2012-03-29-c153.jpg
	

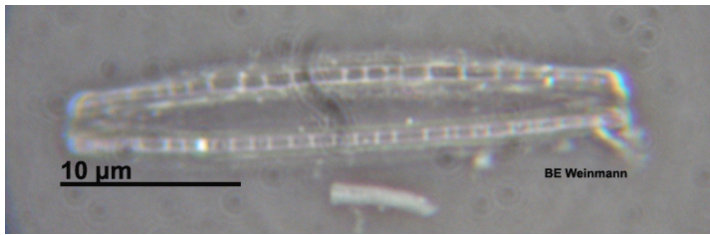
46_65	Roicosphenia genuflexa Girdle (Kützing) Medlin [Witk et al 2000 p.346]
Specimens Measured:	7
Aspect:	Girdle
Valve symmetry or shape:	
Dimensions µm [AA]:	6.7 - (12) - 14
Dimensions µm [PA]:	na - (0) - na
Raphe:	na, location = na, shape = 'na', central endings = 'na', polar endings = 'na'
Striae:	10 per 10µm, orientation = 'Transverse, parallel', pores = 'not resolved', na per 10µm
Fibulae or Costae:	
Axial area:	axial area = 'na' , central area = na, central nodule = not visible, terminal nodule = not visible, other hyaline areas = na
Other Features:	Spines = None; Comments = 'na'; Other = 'na'
Image path:	Catalogue3\Cat3-Ref46\Cat3-Ref46-65_2012-04-07-c65.jpg
	

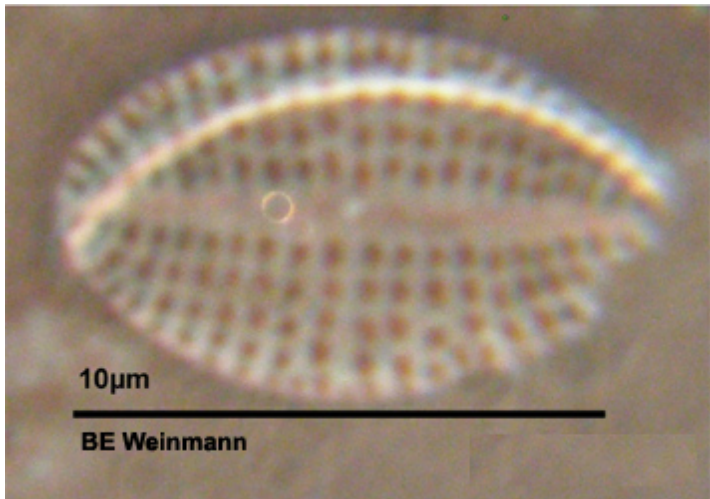
46_90	Roicosphenia genuflexa CV/full raphe (Kützing) Medlin [Witk et al 2000 p.346]
Specimens Measured:	4
Aspect:	Valve
Valve symmetry or shape:	Apical sym = Isobilateral, Transapical sym = Isopolar, Valve shape = Club-shaped, curved, Valve curvature = Concave Apex shape = no inflection, Shape = 'Broadly rounded', Frustral shape = na
Dimensions µm [AA]:	11.8 - (13.1) - 15.5
Dimensions µm [TA]:	3.7 - (4.2) - 4.4
Raphe:	Raphe, location = Central, shape = 'linear', central endings = 'Straight, very inflated, slightly distant', polar endings = 'Not resolved (straight?)'
Striae:	11 - 14 per 10µm, orientation = 'Transverse, parallel to radiate', pores = 'Not resolved', na per 10µm
Fibulae or Costae:	
Axial area:	axial area = 'Linear, 1/5 TA width', central area = TA expansion, square or rectangular (maybe butterfly-shaped), central nodule = Large, terminal nodule = Not visible, other hyaline areas = None
Other Features:	Spines = None; Comments = 'na'; Other = 'na'
Image path:	Catalogue3\Cat3-Ref46\Cat3-Ref46-90_2009-02-04.jpg
	

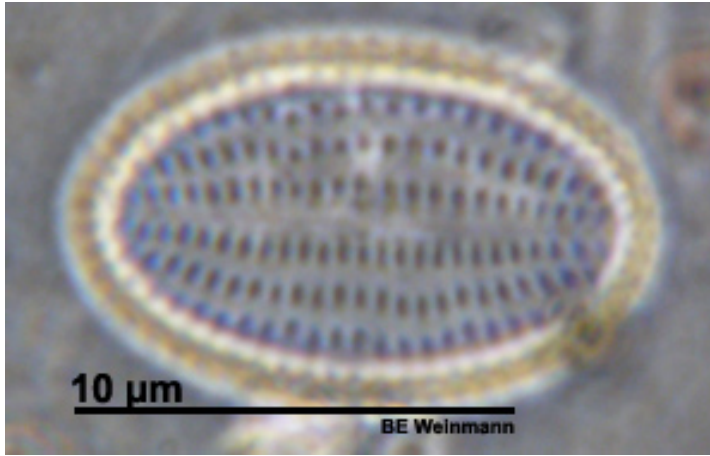
46_141	Roicosphenia genuflexa CX/short raphe [Witk et al 2000 p345, pl58: 19 - 22]
Specimens Measured:	1
Aspect:	Valve
Valve symmetry or shape:	Apical sym = Isobilateral, Transapical sym = Heteropolar, Valve shape = Club-shaped, Valve curvature = Convex, Apex shape = inflection, Shape = 'Broadly rounded', Frustral shape = na
Dimensions µm [AA]:	10.3 - (0) - na
Dimensions µm [TA]:	4 - (0) - na
Raphe:	Raphe (1/2 length), location = Central, shape = 'Straight', central endings = 'Straight', polar endings = 'Not visible'
Striae:	18 - 20 per 10µm, orientation = 'Transverse parallel', pores = 'Punctate', 20 - 22 per 10µm
Fibulae or Costae:	
Axial area:	axial area = 'NA', central area = NA, central nodule = NA, terminal nodule = NA, other hyaline areas = na
Other Features:	Spines = None; Comments = 'There is not the gap with the shortened striae as there is in the CV fully raphid valve'; Other = 'na'
Image path:	Catalogue3\Cat3-Ref46\Cat3-Ref46-141_2012-03-29-c56.jpg
	

47_66	Nitzschia cf. distans Gregory (1857) [BMB4: #370]
Specimens Measured:	22
Aspect:	Valve
Valve symmetry or shape:	Apical sym = Isobilateral, Transapical sym = Isopolar, Valve shape = Narrowly lanceolate, Valve curvature = none, Apex shape = inflection, Shape = 'Protracted, rostrate', Frustral shape = na
Dimensions µm [AA]:	35.3 - (46.2) - 73.5
Dimensions µm [TA]:	2.9 - (4.8) - 7.4
Raphe:	Raphe, location = Subcentral, shape = 'linear', central endings = 'not visible', polar endings = 'not visible'
Striae:	not resolved per 10µm, orientation = 'na', pores = 'na', na per 10µm
Fibulae or Costae:	fibulae = 5 - 12 per 10µm, irregularly spaced, no bigger gap in centre
Axial area:	axial area = 'na' , central area = na, central nodule = no, terminal nodule = no, other hyaline areas = na
Other Features:	Spines = None; Comments = 'na'; Other = 'na'
Image path:	Catalogue3\Cat3-Ref47\Cat3-Ref47-66_2012-03-20-c23.jpg

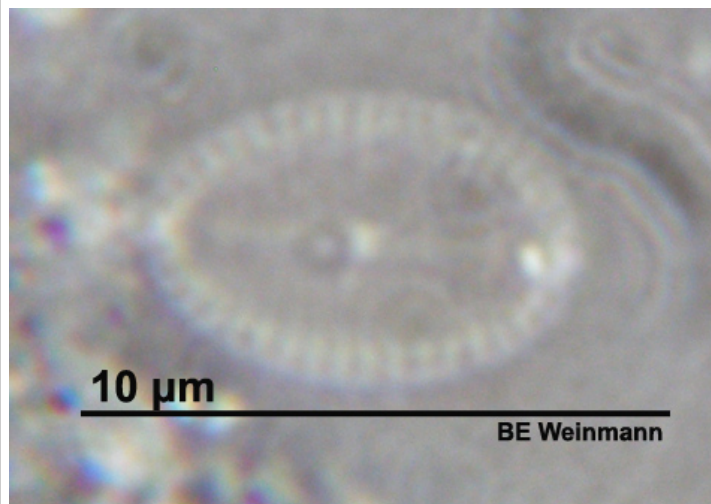


47_173	Nitzschia cf. distans Gregory (1857) [BMB4: #370]
Specimens Measured:	4
Aspect:	Girdle
Valve symmetry or shape:	
Dimensions µm [AA]:	30.9 - (35) - 39
Dimensions µm [PA]:	na - (0) - na
Raphe:	Raphe, location = na, shape = 'na', central endings = 'na', polar endings = 'na'
Striae:	na per 10µm, orientation = 'na', pores = 'na', na per 10µm
Fibulae or Costae:	
Axial area:	axial area = 'na' , central area = na, central nodule = na, terminal nodule = na, other hyaline areas = na
Other Features:	Spines = na; Comments = 'na'; Other = 'na'
Image path:	Catalogue3\Cat3-Ref47\Cat3-Ref47-173_2012-04-14-c79.jpg
	

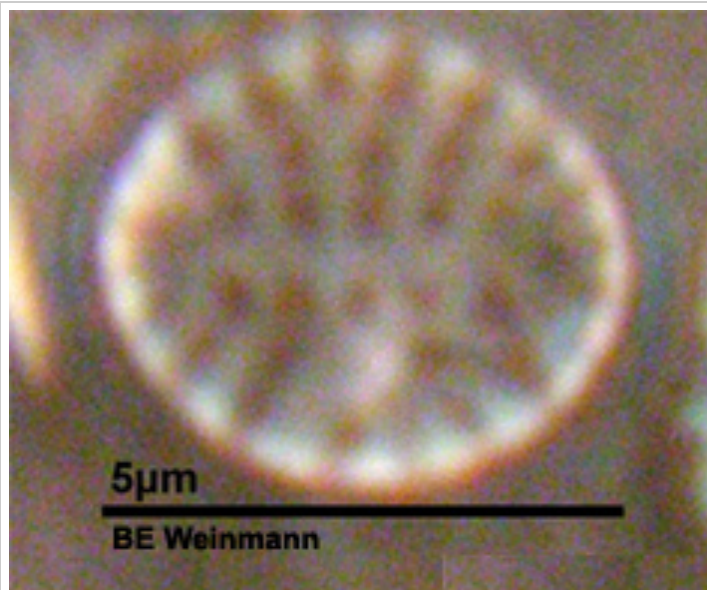
48_67	Cocconeis neothumensis Krammer SV [ADIAC]
Specimens Measured:	2
Aspect:	Valve
Valve symmetry or shape:	Apical sym = Isobilateral, Transapical sym = Isopolar, Valve shape = Elliptic, Valve curvature = none Apex shape = no inflection, Shape = 'Broadly rounded', Frustral shape = na
Dimensions µm [AA]:	8.5 - (10.2) - 11.8
Dimensions µm [TA]:	5.1 - (6.3) - 7.4
Raphe:	Sternum, location = Central, shape = 'Linear', central endings = 'Straight, slightly inflated', polar endings = 'not visible (unless it is ver short and ends about 1/3 to pole.'
Striae:	20 per 10µm, orientation = 'Transverse parallel becoming radiate', pores = 'Punctate, rectangular punctae', 15 per 10µm
Fibulae or Costae:	
Axial area:	axial area = 'Lanceolate' , central area = na, central nodule = Yes, small bright, terminal nodule = not visible, other hyaline areas = na
Other Features:	Spines = None; Comments = 'This could be a mistake, the raphe is by no means clearly visible so it is possible that it is the RLV, it certainly matches Cocconeis spp. Ehrenb.(1837) '; Other = 'na'
Image path:	Catalogue3\Cat3-Ref48\Cat3-Ref48-67_2009-01-19.jpg
	

48_68	Cocconeis neothumensis SV Krammer [ADIAC]
Specimens Measured:	1
Aspect:	Valve
Valve symmetry or shape:	Apical sym = Isobilateral, Transapical sym = Isopolar, Valve shape = Elliptic, Valve curvature = Possibly convex Apex shape = no inflection, Shape = 'Broadly rounded', Frustral shape = na
Dimensions μm [AA]:	14.7 - (0) - na
Dimensions μm [TA]:	8.1 - (0) - na
Raphe:	Sternum, location = Central, shape = 'na', central endings = 'na', polar endings = 'na'
Striae:	19 - 21 per 10 μm , orientation = 'Transverse, parallel to radiate', pores = 'Punctate, rectangular punctae', 8 - 11 per 10 μm
Fibulae or Costae:	
Axial area:	axial area = 'Narrowly, lanceolate', central area = none, central nodule = None, terminal nodule = None, other hyaline areas = 3 longitudinal columns in between striae
Other Features:	Spines = None; Comments = 'I cannot find the RV match for this. I cant see it being the other Cocconeis (picture before this one) '; Other = 'na'
Image path:	Catalogue3\Cat3-Ref48\Cat3-Ref48-68_2009-03-12.jpg
	

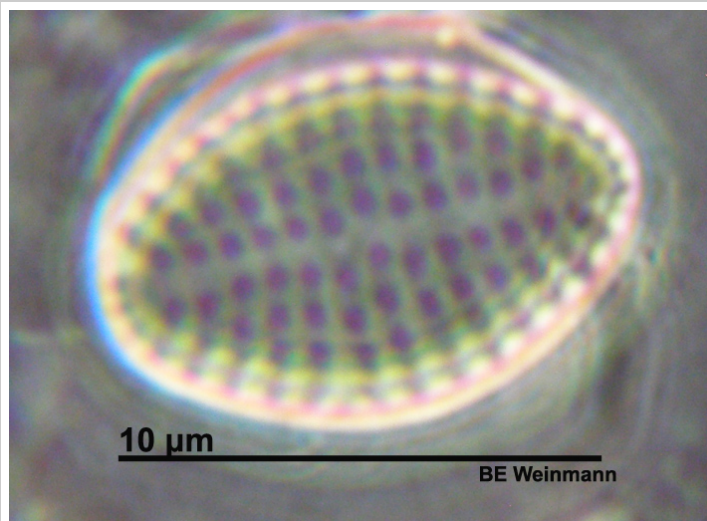
48_126	Cocconeis neothumensis RV [, though not sure as the RV does have striae, check Witkowski]
Specimens Measured:	8
Aspect:	Valve
Valve symmetry or shape:	Apical sym = Isobilateral, Transapical sym = Isopolar, Valve shape = Elliptic, Valve curvature = None, Frustral shape = na
Dimensions µm [AA]:	7.4 - (8.1) - 10.3
Dimensions µm [TA]:	3.7 - (4.6) - 6.6
Raphe:	Raphe (though not visible), location = Central, shape = 'Not resolved', central endings = 'Not resolved', polar endings = 'Not resolved'
Striae:	25 - 27 per 10µm, orientation = 'Transverse, parallel becoming radiate', pores = 'Not resolved', na per 10µm
Fibulae or Costae:	
Axial area:	axial area = 'Linear, narrow' , central area = Not distinct from sternum, central nodule = Small, round and very bright, terminal nodule = Small, round and very bright, other hyaline areas = Broadly lanceolate hyaline area covers 4/5 of the valve face
Other Features:	Spines = None; Comments = 'I've had this before but it was confounded with others in 23 - 30'; Other = 'na'
Image path:	Catalogue3\Cat3-Ref48\Cat3-Ref48-126_2012-04-13-c114.jpg

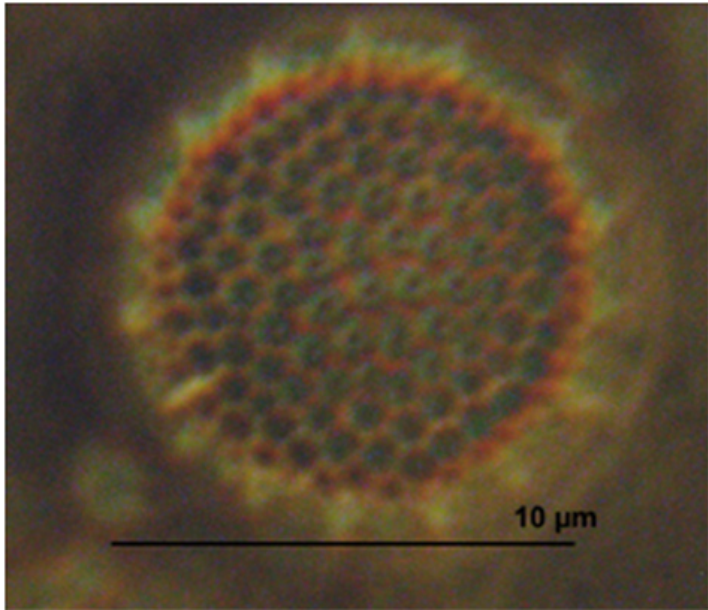


49_69	Delphineis minutissima (Hustedt) Simonsen [Witkowski pl. 22:11]
Specimens Measured:	4
Aspect:	Valve
Valve symmetry or shape:	Apical sym = Isobilateral, Transapical sym = Isopolar, Valve shape = Elliptic, Valve curvature = none Apex shape = no inflection, Shape = 'Broadly rounded', Frustral shape = na
Dimensions μm [AA]:	5.1 - (6.4) - 8.1
Dimensions μm [TA]:	4.4 - (5.5) - 6.6
Raphe:	Sternum, location = Central, shape = 'na', central endings = 'na', polar endings = 'na'
Striae:	14 per 10 μm , orientation = 'Transverse, radiate', pores = 'Punctate, square punctae', 16 - 17 per 10 μm
Fibulae or Costae:	
Axial area:	axial area = 'Linear' , central area = na, central nodule = No, terminal nodule = No, other hyaline areas = na
Other Features:	Spines = None; Comments = 'na'; Other = 'na'
Image path:	Catalogue3\Cat3-Ref49\Cat3-Ref49-69_2009-01-19.jpg

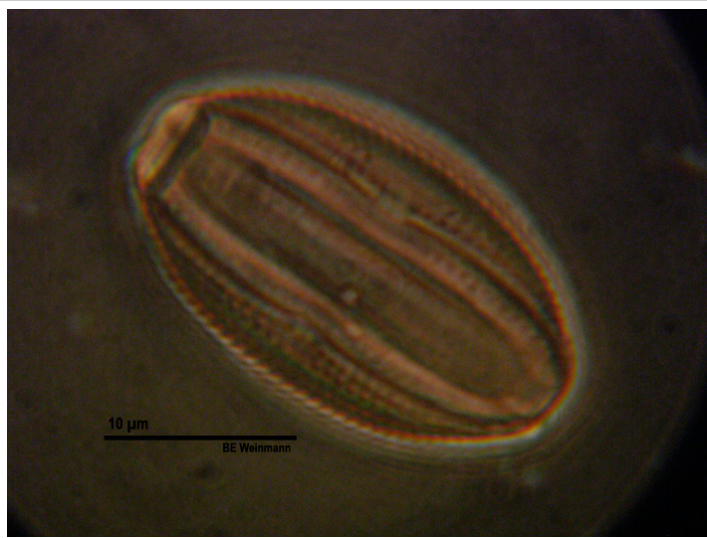


49_134	Delphineis minutissima (Hustedt) Simonsen [ADIAC]
Specimens Measured:	1
Aspect:	Valve
Valve symmetry or shape:	Apical sym = Isobilateral, Transapical sym = Isopolar, Valve shape = Rhombic, Valve curvature = None, Frustral shape = na
Dimensions µm [AA]:	11 - (0) - na
Dimensions µm [TA]:	7.4 - (0) - na
Raphe:	Sternum, location = Central, shape = 'NA', central endings = 'NA', polar endings = 'NA'
Striae:	13 per 10µm, orientation = 'Transverse, parallel becoming radiate', pores = 'Punctate', 12 per 10µm
Fibulae or Costae:	
Axial area:	axial area = 'Linear, narrow' , central area = None, central nodule = None, terminal nodule = None, other hyaline areas = na
Other Features:	Spines = None; Comments = 'na'; Other = 'na'
Image path:	Catalogue3\Cat3-Ref49\Cat3-Ref49-134_2012-04-12-c110.jpg

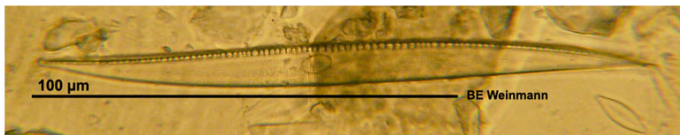
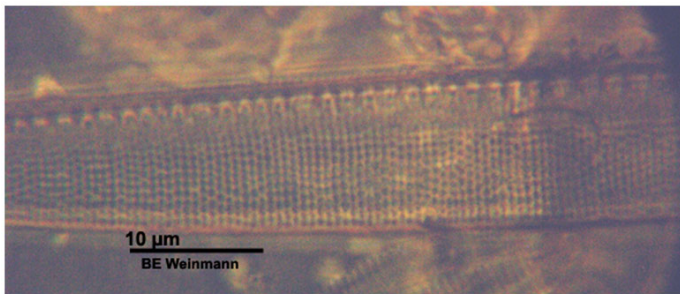
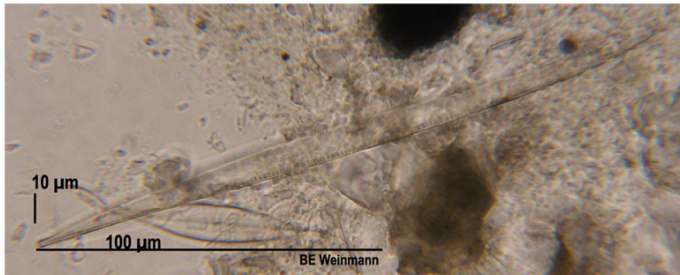


50_70	Thallasiosira sp.1 [Ribeiro 2010: pl. 2]
Specimens Measured:	3
Aspect:	Valve
Valve symmetry or shape:	Apical sym = Circular, Transapical sym = na, Valve shape = Circular, Valve curvature = none, Frustral shape = na
Dimensions μm [AA]:	10.3 - (11.8) - 14.7
Dimensions μm [TA]:	na - (0) - na
Raphe:	na, location = na, shape = 'na', central endings = 'na', polar endings = 'na'
Striae:	na per 10 μm , orientation = 'na', pores = 'na', na per 10 μm
Fibulae or Costae:	
Axial area:	axial area = 'na' , central area = na, central nodule = na, terminal nodule = na, other hyaline areas = na
Other Features:	Spines = na; Comments = 'na'; Other = 'na'
Image path:	Catalogue3\Cat3-Ref50\Cat3-Ref50-70_2009-01-19.jpg
	

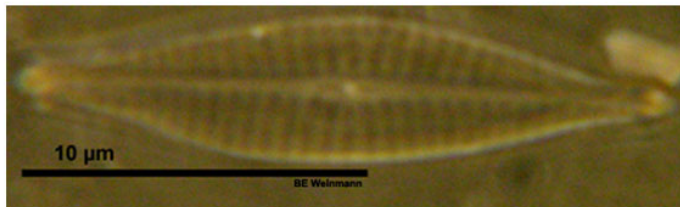
51_71	Amphora sp. 2 [?]
Specimens Measured:	6
Aspect:	Valve
Valve symmetry or shape:	Apical sym = Dorsiventral, Transapical sym = Isopolar, Valve shape = Arcuate, Valve curvature = na Apex shape = no inflection, Shape = 'na', Frustral shape = Elliptic with blunt ends
Dimensions μm [AA]:	22.1 - (30) - 47
Dimensions μm [TA]:	5.1 - (6.2) - 6.7
Raphe:	Raphe, location = Ventral, shape = 'Arcuate', central endings = 'curved to same side', polar endings = 'curved to same side'
Striae:	8 - 10 per 10 μm , orientation = 'Transverse, parallel to radiate', pores = 'Punctate', not resolved per 10 μm
Fibulae or Costae:	
Axial area:	axial area = 'Follows raphe (arcuate), relatively evenly' , central area = large hyaline area, not quite reaching the margins, central nodule = na, terminal nodule = not visible, other hyaline areas = na
Other Features:	Spines = None; Comments = 'na'; Other = 'na'
Image path:	Catalogue3\Cat3-Ref51\Cat3-Ref51-71_2009-01-20.jpg



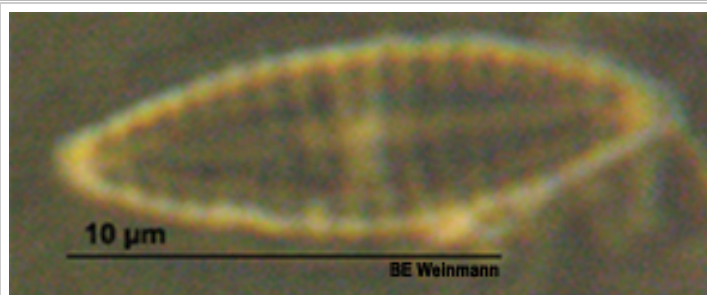
52_72	Nitzschia sigma (Kützting) W. Smith 1853 [BMB2: #173]
Specimens Measured:	6
Aspect:	Valve
Valve symmetry or shape:	Apical sym = Sigmoid, Transapical sym = Isopolar, Valve shape = Linear, sigmoid, Valve curvature = possibly, Apex shape = inflection, Shape = 'Sub-capitate or sub-rostrate', Frustral shape = na
Dimensions µm [AA]:	47.8 - (113.8) - 196.4
Dimensions µm [TA]:	5.1 - (8.9) - 10.4
Raphe:	Raphe, location = Eccentric, shape = 'marginal', central endings = 'na', polar endings = 'na'
Striae:	20 + per 10µm, orientation = 'Transverse, parallel', pores = 'not resolved', 14 - 15 per 10µm
Fibulae or Costae:	
Axial area:	axial area = 'na' , central area = na, central nodule = No, terminal nodule = No, other hyaline areas = na
Other Features:	Spines = None; Comments = 'na'; Other = 'na'
Image path:	Catalogue3\Cat3-Ref52\Cat3-Ref52-72_2009-01-20_combined.jpg

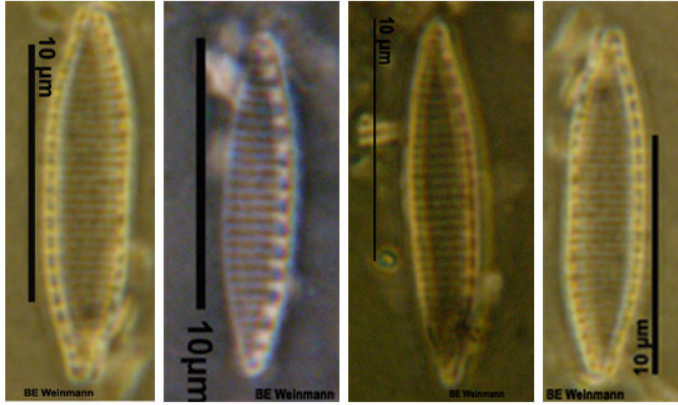


53_73	Navicula vandamii Schoeman& Archibald [Witk. et al 2000 p313] or Navicula vandamii var. mertensiae Schoeman& Archibald [Witk. et al 2000 p313]
Specimens Measured:	12
Aspect:	Valve
Valve symmetry or shape:	Apical sym = Isobilateral, Transapical sym = Isopolar, Valve shape = Lanceolate, Valve curvature = none, Frustral shape = na
Dimensions µm [AA]:	16.3 - (23.4) - 31.1
Dimensions µm [TA]:	4 - (5.3) - 7.4
Raphe:	Raphe, location = Central, deflected to secondary half, shape = 'straight', central endings = 'Slightly inflated and straight', polar endings = 'hooked (only one visible)'
Striae:	13 - 17 per 10µm, orientation = 'Transverse, radiate becoming parallel to convergent', pores = 'Punctate', > 20 per 10µm
Fibulae or Costae:	
Axial area:	axial area = 'Narrow, linear' , central area = Narrowly lanceolate, though more pronounced on primary side, central nodule = small, round, terminal nodule = Not clear, other hyaline areas = na
Other Features:	Spines = None; Comments = 'This was originally 63 - 88'; Other = 'na'
Image path:	Catalogue3\Cat3-Ref53\Cat3-Ref53-73_2009-01-30_combined.jpg

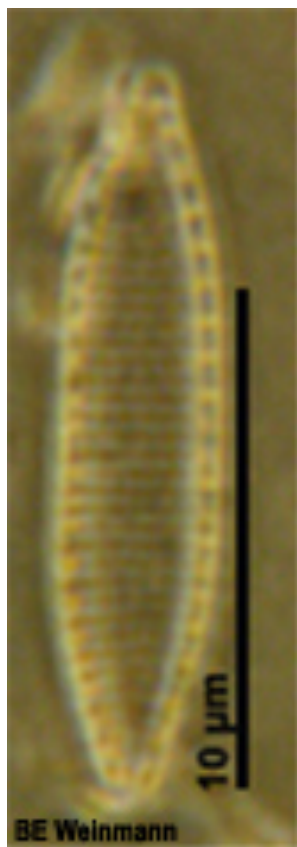


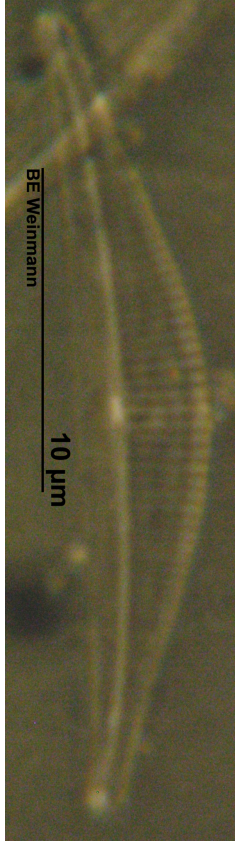
54_74	Navicula perminuta Grunow in van Heurck 1880 [BMB1:69]
Specimens Measured:	15
Aspect:	Valve
Valve symmetry or shape:	Apical sym = Isobilateral, Transapical sym = Isopolar, Valve shape = Lanceolate, Valve curvature = none Apex shape = no inflection, Shape = 'Acute', Frustral shape = na
Dimensions µm [AA]:	7.4 - (9.4) - 14.1
Dimensions µm [TA]:	2.2 - (3.2) - 5.9
Raphe:	Raphe, location = Central, shape = 'Linear', central endings = 'Not resolved', polar endings = 'Not resolved'
Striae:	17 - 19 per 10µm, orientation = 'Transverse, parallel', pores = 'Not resolved', na per 10µm
Fibulae or Costae:	
Axial area:	axial area = 'Narrow, linear' , central area = Expanded and symmetrical, central nodule = Yes, small and round, terminal nodule = Not visible, other hyaline areas = Fascia to the margins, interrupted by single central short striae
Other Features:	Spines = None; Comments = 'na'; Other = 'na'
Image path:	Catalogue3\Cat3-Ref54\Cat3-Ref54-74_2009-01-29.jpg

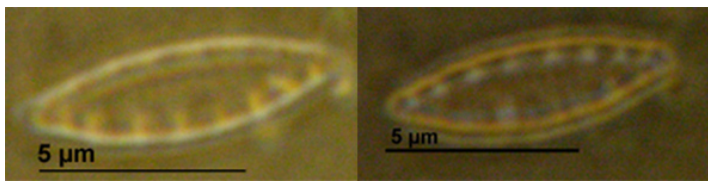


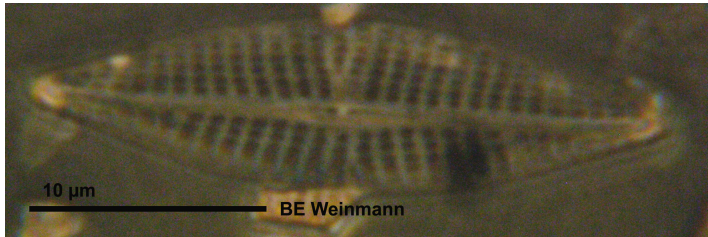
55_75	Nitzschia frustulum (Kützting) Grunow 1880 [BMB1: #76; ADIAC] or Nitzschia liebetruthii Rabenhorst [Witkowski pl. 209: # 11, 21 - 23]
Specimens Measured:	12
Aspect:	Valve
Valve symmetry or shape:	Apical sym = Isobilateral, Transapical sym = Isopolar, Valve shape = Lanceolate, Valve curvature = none Apex shape = no inflection, Shape = 'Acute', Frustral shape = na
Dimensions µm [AA]:	7.4 - (12.1) - 26.6
Dimensions µm [TA]:	2.2 - (3) - 4.4
Raphe:	Raphe, location = Eccentric, shape = 'marginal', central endings = 'na', polar endings = 'na'
Striae:	18 - 22 per 10µm, orientation = 'Transverse, parallel', pores = 'Punctate', 16 - 18 per 10µm
Fibulae or Costae:	fibulae = 11 - 13 per 10µm, Triangular, relatively regularly spaced
Axial area:	axial area = 'na' , central area = na, central nodule = No, terminal nodule = No, other hyaline areas = na
Other Features:	Spines = None; Comments = 'na'; Other = 'na'
Image path:	Catalogue3\Cat3-Ref55\Cat3-Ref55-75_2009-02-04_combined.jpg
	

55_76	Nitzschia frustulum (Kützting) Grunow 1880 [BMB1: #76; ADIAC] or Nitzschia liebetruthii Rabenhorst [Witkowski pl. 209: # 11, 21 - 23]
Specimens Measured:	1
Aspect:	Valve
Valve symmetry or shape:	Apical sym = Isobilateral, Transapical sym = Isopolar, Valve shape = Lanceolate, Valve curvature = none Apex shape = no inflection, Shape = 'Acute', Frustral shape = na
Dimensions µm [AA]:	14.7 - (0) - na
Dimensions µm [TA]:	3.7 - (0) - na
Raphe:	Raphe, location = Eccentric, shape = 'marginal', central endings = 'na', polar endings = 'na'
Striae:	26 per 10µm, orientation = 'Transverse, parallel', pores = 'Punctate', not resolved per 10µm
Fibulae or Costae:	fibulae = 14 -16 per 10µm, Irregularly spaced
Axial area:	axial area = 'na' , central area = na, central nodule = No, terminal nodule = No, other hyaline areas = na
Other Features:	Spines = None; Comments = 'Frustulum still intact'; Other = 'na'
Image path:	Catalogue3\Cat3-Ref55\Cat3-Ref55-76_2009-01-29.jpg

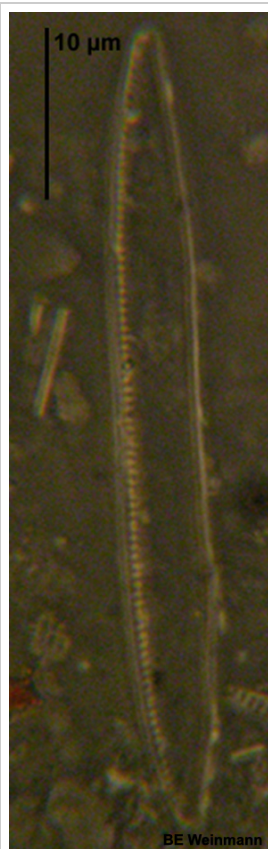


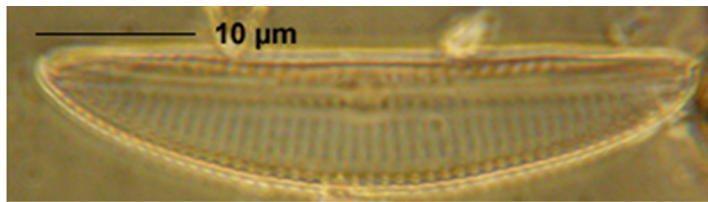
56_77	Amphora cf. tenerrima Aleem & Hustedt 1951 [BMB5: #414]
Specimens Measured:	7
Aspect:	Valve
Valve symmetry or shape:	Apical sym = Dorsiventral, Transapical sym = Isopolar, Valve shape = Arcuate, Valve curvature = none, Frustral shape = na
Dimensions µm [AA]:	11.7 - (13.8) - 18.4
Dimensions µm [TA]:	2.2 - (3) - 3.7
Raphe:	Raphe, location = Slightly ventral, shape = 'arcuate', central endings = 'Straight', polar endings = 'not resolved'
Striae:	22 - 26 per 10µm, orientation = 'Transverse parallel', pores = 'Not resolved', na per 10µm
Fibulae or Costae:	
Axial area:	axial area = 'regular, arcuate' , central area = None on dorsal side, on ventral side, takes up 1/2 length, central nodule = bright,narrow oval, terminal nodule = round bright, other hyaline areas = na
Other Features:	Spines = None; Comments = 'na'; Other = 'na'
Image path:	Catalogue3\Cat3-Ref56\Cat3-Ref56-77_2009-01-29.jpg
	

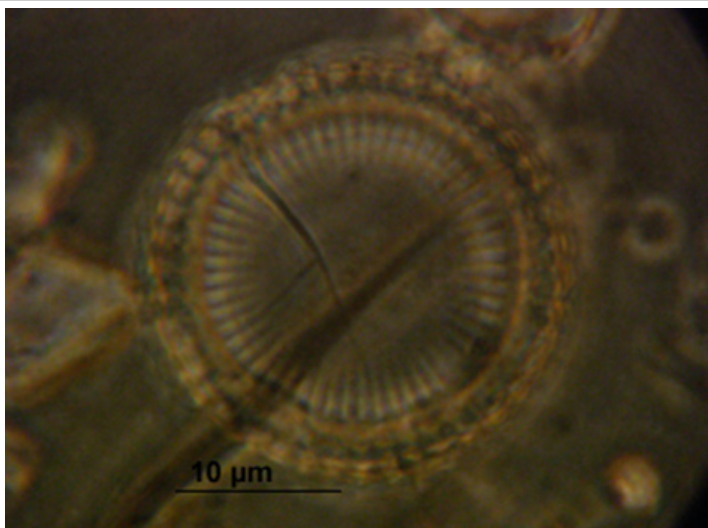
57_78	Nitzschia sp. 1 [?]
Specimens Measured:	7
Aspect:	Valve
Valve symmetry or shape:	Apical sym = Isobilateral, Transapical sym = Isopolar, Valve shape = Lanceolate, Valve curvature = none, Apex shape = inflection, Shape = 'Protracted, cuneate or sub-rostrate', Frustral shape = na
Dimensions µm [AA]:	7.4 - (7.6) - 8.1
Dimensions µm [TA]:	2.2 - (2.3) - 2.6
Raphe:	Raphe, location = Eccentric, shape = 'marginal', central endings = 'na', polar endings = 'na'
Striae:	not resolved per 10µm, orientation = 'na', pores = 'na', na per 10µm
Fibulae or Costae:	fibulae = 10 per 10µm, Relatively narrow and irregular, quite widely spaced
Axial area:	axial area = 'na' , central area = na, central nodule = None, terminal nodule = None, other hyaline areas = na
Other Features:	Spines = None; Comments = 'I'm pretty sure this is different from 59-84 as the striae are not visible and the fibulae are more widely spaced.'; Other = 'na'
Image path:	Catalogue3\Cat3-Ref57\Cat3-Ref57-78_2009-02-03.jpg
	

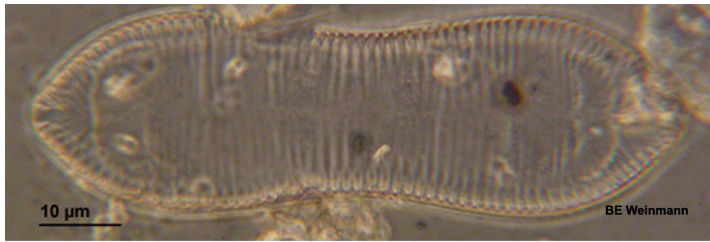
58_79	Navicula eidrigiana Carter 1979 [BMB4: #358 & Witk121: 1-6] or Navicula cf. pseudolanceolata Lange-Bertalot [ADIAC]
Specimens Measured:	10
Aspect:	Valve
Valve symmetry or shape:	Apical sym = Isobilateral, Transapical sym = Isopolar, Valve shape = Lanceolate, Valve curvature = none, Frustral shape = na
Dimensions µm [AA]:	24.3 - (39.2) - 62.5
Dimensions µm [TA]:	5.9 - (8.4) - 11.8
Raphe:	Raphe, location = Central, though very slightly deflected to secondary half, shape = 'straight', central endings = 'Slightly inflated and straight', polar endings = 'na'
Striae:	12 - 13 per 10µm, orientation = 'Transverse, radiate becoming parallel to convergent', pores = 'Punctate', 19 - 20 per 10µm
Fibulae or Costae:	
Axial area:	axial area = 'Narrow, linear' , central area = Narrowly lanceolate, though more pronounced on primary side, central nodule = small, round, terminal nodule = Not clear, other hyaline areas = na
Other Features:	Spines = None; Comments = 'This was originally 63 - 152'; Other = 'na'
Image path:	Catalogue3\Cat3-Ref58\Cat3-Ref58-79_2009-02-13.jpg
	

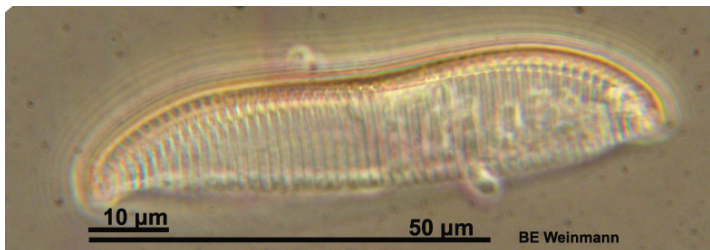
59_80	Nitzschia recta Hantzsch in Rabenhorst [BMB3: #268]
Specimens Measured:	1
Aspect:	Valve
Valve symmetry or shape:	Apical sym = Isobilateral, Transapical sym = Isopolar, Valve shape = Linear, Valve curvature = none, Apex shape = inflection, Shape = 'Cuneate', Frustral shape = na
Dimensions µm [AA]:	48.1 - (0) - na
Dimensions µm [TA]:	4.4 - (0) - na
Raphe:	Raphe, location = Eccentric, shape = 'marginal', central endings = 'Not visible', polar endings = 'Not visible'
Striae:	not resolved per 10µm, orientation = 'na', pores = 'na', na per 10µm
Fibulae or Costae:	
Axial area:	axial area = 'na' , central area = na, central nodule = None, terminal nodule = None, other hyaline areas = na
Other Features:	Spines = None; Comments = 'Very rare, only encountered once in E2 but more so in the live counts. So possibly the frustule is fragile?'; Other = 'na'
Image path:	Catalogue3\Cat3-Ref59\Cat3-Ref59-80_2009-02-04.jpg

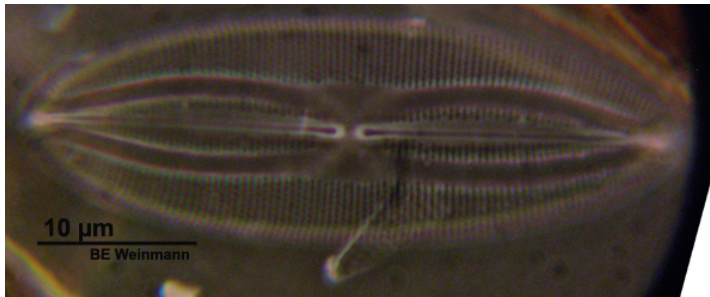


60_81	Amphora sp. 3 [?]
Specimens Measured:	1
Aspect:	Valve
Valve symmetry or shape:	Apical sym = Dorsiventral, Transapical sym = Isopolar, Valve shape = Lunate, Valve curvature = none Apex shape = no inflection, Shape = 'Acutely rounded', Frustral shape = na
Dimensions µm [AA]:	40.7 - (0) - na
Dimensions µm [TA]:	8.1 - (0) - na
Raphe:	Raphe, location = Ventral, shape = 'straight', central endings = 'Inflated, straight', polar endings = 'Straight'
Striae:	12 per 10µm, orientation = 'Transverse, parallel', pores = 'Punctate', not resolved per 10µm
Fibulae or Costae:	
Axial area:	axial area = 'Narrow' , central area = gap on both sides in striae, central nodule = Just visible, terminal nodule = Not visible, other hyaline areas = narrow hyaline area in dorsal striae
Other Features:	Spines = None; Comments = 'Very rare, only encountered once in E2 (formerly Cat1-Ref66-91)'; Other = 'na'
Image path:	Catalogue3\Cat3-Ref60\Cat3-Ref60-81_2009-02-04.jpg
	

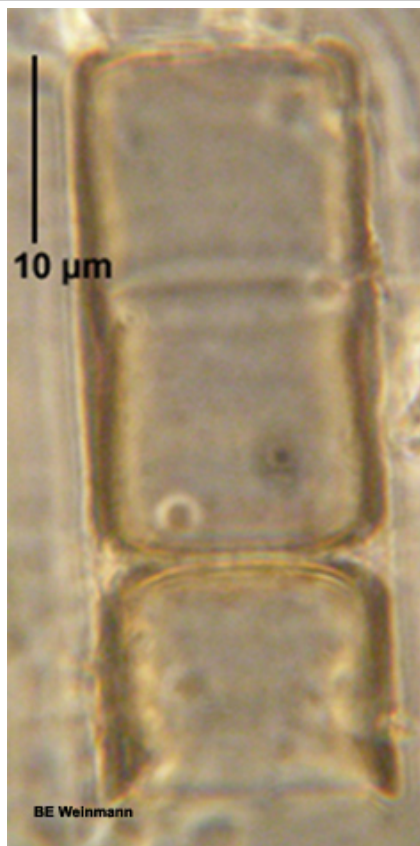
61_82	Paralia sulcata [BMB2: #175]
Specimens Measured:	2
Aspect:	Valve
Valve symmetry or shape:	Apical sym = Circular, Transapical sym = na, Valve shape = Circular, Valve curvature = na, Frustral shape = na
Dimensions µm [AA]:	19.8 - (22.4) - 25
Dimensions µm [TA]:	na - (0) - na
Raphe:	na, location = na, shape = 'na', central endings = 'na', polar endings = 'na'
Striae:	11 per 10µm, orientation = 'Radiate', pores = 'na', na per 10µm
Fibulae or Costae:	costae = 6 - 7 per 10µm, Radial
Axial area:	axial area = 'na' , central area = Half of cell from center hyaline, central nodule = na, terminal nodule = na, other hyaline areas = na
Other Features:	Spines = Not resolved; Comments = 'Was Cat1-Ref67-92'; Other = 'na'
Image path:	Catalogue3\Cat3-Ref61\Cat3-Ref61-82_2009-02-04.jpg
	

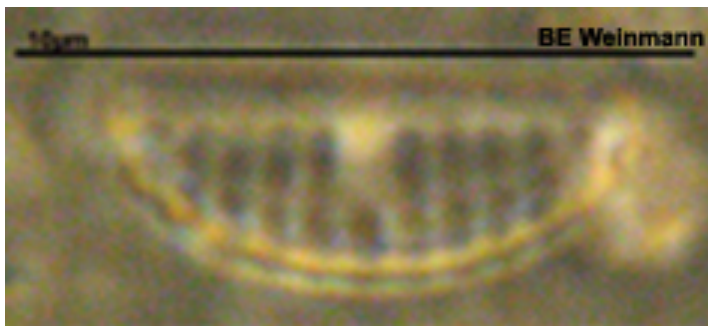
62_83	Surirella smithii Ralfs [Van der Werff & Huls 1976 P.DJ XXII. 141]
Specimens Measured:	3
Aspect:	Valve
Valve symmetry or shape:	Apical sym = Isobilateral, Transapical sym = Isopolar, Valve shape = Panduriform, Valve curvature = none Apex shape = no inflection, Shape = 'Blunt', Frustral shape = na
Dimensions µm [AA]:	36.8 - (61.9) - 79.9
Dimensions µm [TA]:	12.6 - (17.2) - 23.7
Raphe:	Sternum, location = Central, shape = 'Linear', central endings = 'na', polar endings = 'na'
Striae:	6 - 8 per 10µm, orientation = 'Transverse, parallel', pores = 'na', na per 10µm
Fibulae or Costae:	costae = 6 - 8 per 10µm, In line with striae
Axial area:	axial area = 'Narrow, linear' , central area = None, central nodule = None, terminal nodule = None, other hyaline areas = na
Other Features:	Spines = None; Comments = 'Was Cat1-Ref70-96'; Other = 'na'
Image path:	Catalogue3\Cat3-Ref62\Cat3-Ref62-83_2009-02-05.jpg
	

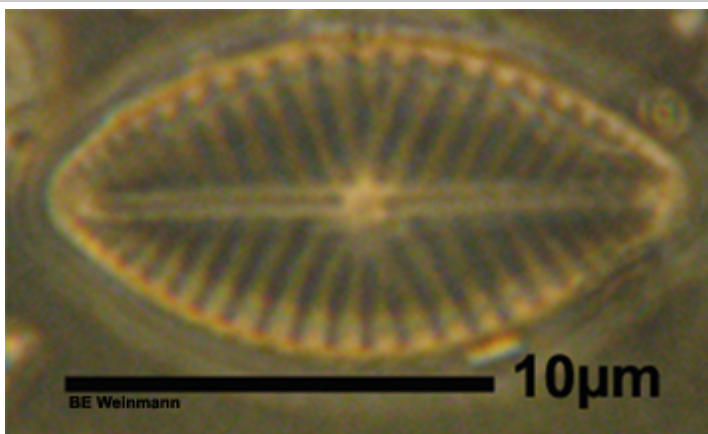
62_167	Surirella smithii Ralfs [Van der Werff & Huls 1976 P.DJ XXII. 141]
Specimens Measured:	1
Aspect:	Valve
Valve symmetry or shape:	Apical sym = Dorsiventral, Transapical sym = Isopolar, Valve shape = Semi-panduriform, Valve curvature = Possibly, Frustral shape = NA
Dimensions µm [AA]:	69.1 - (0) - na
Dimensions µm [TA]:	15.4 - (0) - na
Raphe:	Raphe (by proxy of fibulae?), location = Eccentric, shape = 'Marginal', central endings = 'NA', polar endings = 'NA'
Striae:	7 - 8 per 10µm, orientation = 'Transverse, parallel', pores = 'na', na per 10µm
Fibulae or Costae:	
Axial area:	axial area = 'na' , central area = na, central nodule = na, terminal nodule = na, other hyaline areas = na
Other Features:	Spines = na; Comments = 'na'; Other = 'na'
Image path:	Catalogue3\Cat3-Ref62\Cat3-Ref62-167_2012-04-13-c7.jpg
	

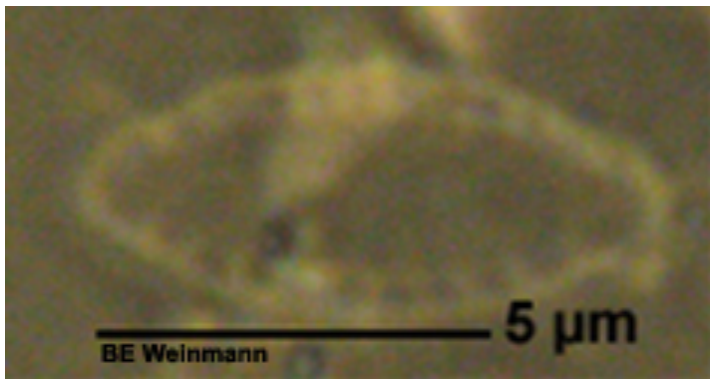
63_125	Fallacia pygmaea (Kützing) Stickle & Mann 1990 [EA Diatomkey: #13360150]
Specimens Measured:	5
Aspect:	Valve
Valve symmetry or shape:	Apical sym = Isobilateral, Transapical sym = Isopolar, Valve shape = Elliptic, Valve curvature = None, Frustral shape = na
Dimensions µm [AA]:	25.7 - (36.4) - 44.1
Dimensions µm [TA]:	12.5 - (13.8) - 14.7
Raphe:	Raphe, location = Central, shape = 'Linear, straight', central endings = 'Straight, slightly distant, slightly inflated', polar endings = 'Hooked, same side'
Striae:	21 - 23 per 10µm, orientation = 'Transverse, parallel becoming radiate', pores = 'Punctate', na per 10µm
Fibulae or Costae:	
Axial area:	axial area = 'Narrow, linear (though slightly panduriform on one side)', central area = Triangular on both sides (pointing to central area), central nodule = Not visible, terminal nodule = not visible, other hyaline areas = Lyre-shaped quite \nevenly broad hyaline area mid-way btwn raphe and each margin
Other Features:	Spines = None; Comments = 'Possibly the same as 63-84'; Other = 'na'
Image path:	Catalogue3\Cat3-Ref63\Cat2-Ref63-125_2012-03-21-c95.jpg
	

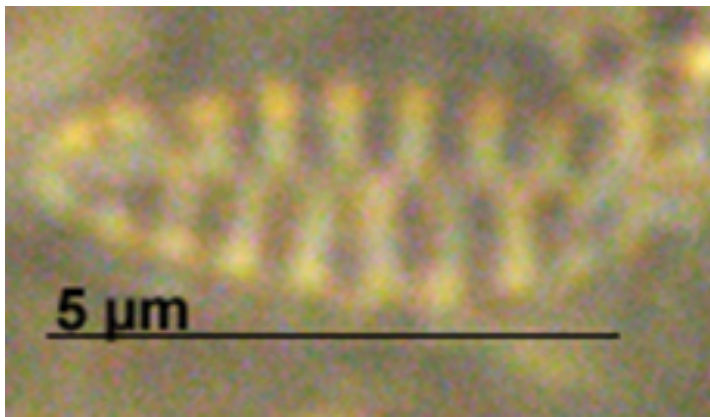
64_85	Melosira varians Agardh [BMB1: #64]
Specimens Measured:	4
Aspect:	Girdle
Valve symmetry or shape:	
Dimensions μm [AA]:	12.6 - (23.4) - 23.4
Dimensions μm [PA]:	12.7 - (15.1) - 18.5
Raphe:	na, location = na, shape = 'na', central endings = 'na', polar endings = 'na'
Striae:	na per 10 μm , orientation = 'na', pores = 'na', na per 10 μm
Fibulae or Costae:	
Axial area:	axial area = 'na' , central area = na, central nodule = na, terminal nodule = na, other hyaline areas = na
Other Features:	Spines = Tiny spicules along edge of valve face; Comments = 'There seems to be some sort of crease in the centre of the cylinder'; Other = 'na'
Image path:	Catalogue3\Cat3-Ref64-85_2009-02-05.jpg

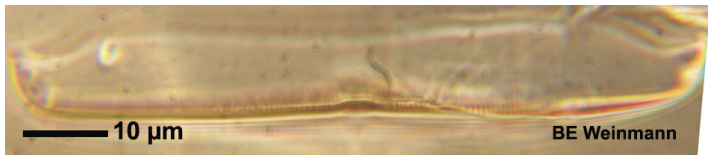


65_86	Amphora pediculus (Kützinger) Grunow in Schmidt et al 1875 [BMB1: #10]
Specimens Measured:	9
Aspect:	Valve
Valve symmetry or shape:	Apical sym = na, Transapical sym = Dorsiventral, Valve shape = Lunate, Valve curvature = None Apex shape = no inflection, Shape = 'Obtusely rounded', Frustral shape = na
Dimensions µm [AA]:	4.4 - (7.7) - 11.1
Dimensions µm [TA]:	2.2 - (2.7) - 3.1
Raphe:	Raphe, probably, location = Ventral, shape = 'Isopolar', central endings = 'Marginal', polar endings = 'na'
Striae:	na per 10µm, orientation = '41609', pores = 'Transverse, parallel', Not resolved per 10µm
Fibulae or Costae:	
Axial area:	axial area = 'na' , central area = na, central nodule = Longitudinal hyaline crescent mid-valve, terminal nodule = Large and bright, other hyaline areas = Rectangular
Other Features:	Spines = na; Comments = 'Previously Cat1-Ref75-102'; Other = 'Yes, smaller and bright'
Image path:	Catalogue3\Cat3-Ref65\Cat3-Ref65-86_2009-02-09.jpg
	

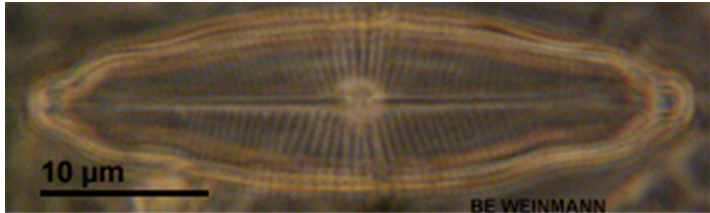
66_87	Placoneis clementis (Grunow) Cox 1987 [BMB2: #183]
Specimens Measured:	2
Aspect:	Valve
Valve symmetry or shape:	Apical sym = Isobilateral, Transapical sym = Isopolar, Valve shape = Broadly lanceolate, Valve curvature = Maybe slightly convex, Frustral shape = na
Dimensions µm [AA]:	14.8 - (18.8) - 22.8
Dimensions µm [TA]:	7.4 - (8.5) - 9.6
Raphe:	Raphe, location = Central, shape = 'Linear', central endings = 'Slightly inflated, straight, distant', polar endings = 'Not resolved'
Striae:	12 - 14 per 10µm, orientation = 'Transverse, radiate', pores = 'Not resolved', na per 10µm
Fibulae or Costae:	
Axial area:	axial area = 'Narrow, linear' , central area = Irregular, rounded on one side, more triangular on the other, central nodule = Large, bright, terminal nodule = Not distinct, other hyaline areas = na
Other Features:	Spines = None; Comments = 'Rare. Only 2 found, one in E2 and E3. Previously Cat1-Ref76-103'; Other = 'na'
Image path:	Catalogue3\Cat3-Ref66-87_2009-02-09.jpg
	

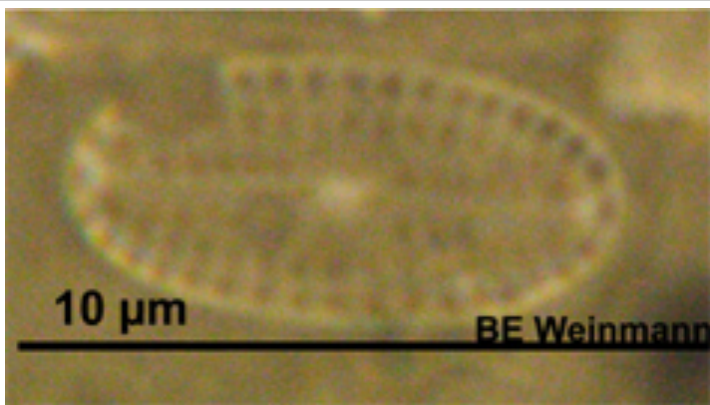
67_88	Mastogloia sp.1 [Witkowski ?]
Specimens Measured:	1
Aspect:	Valve
Valve symmetry or shape:	Apical sym = Isobilateral, Transapical sym = Isopolar, Valve shape = Lanceolate, Valve curvature = None, Frustral shape = na
Dimensions µm [AA]:	7.4 - (0) - na
Dimensions µm [TA]:	2.9 - (0) - na
Raphe:	Not visible, location = na, shape = 'na', central endings = 'na', polar endings = 'na'
Striae:	na per 10µm, orientation = 'na', pores = 'na', n per 10µm
Fibulae or Costae:	costae = 18 per 10µm, Square chambers
Axial area:	axial area = 'na' , central area = na, central nodule = na, terminal nodule = na, other hyaline areas = The whole centre of the valve
Other Features:	Spines = na; Comments = 'Very rare and I'm not sure this isn't an unseparated frustule of . Nitzschia sp.1 (). Previously Cat1-Ref77-104'; Other = 'na'
Image path:	Catalogue3\Cat1-Ref67-88_2009-02-09.jpg
	

68_89	Opephora olsenii Møller 1950 [BMBI: #79]
Specimens Measured:	12
Aspect:	Valve
Valve symmetry or shape:	Apical sym = Isobilateral, Transapical sym = Heteropolar, Valve shape = Club-shaped, Valve curvature = none, Frustral shape = na
Dimensions µm [AA]:	3.7 - (5.6) - 8.1
Dimensions µm [TA]:	1.5 - (2.1) - 2.2
Raphe:	Sternum, location = Central, shape = 'na', central endings = 'na', polar endings = 'na'
Striae:	18 per 10µm, orientation = 'Transverse, parallel', pores = 'Not resolved', na per 10µm
Fibulae or Costae:	
Axial area:	axial area = 'Very narrow, hardly there' , central area = None, central nodule = None, terminal nodule = None, other hyaline areas = na
Other Features:	Spines = None; Comments = 'Previously Cat1-Ref78-105'; Other = 'na'
Image path:	Catalogue3\Cat3-Ref68-89_2009-02-09.jpg
	

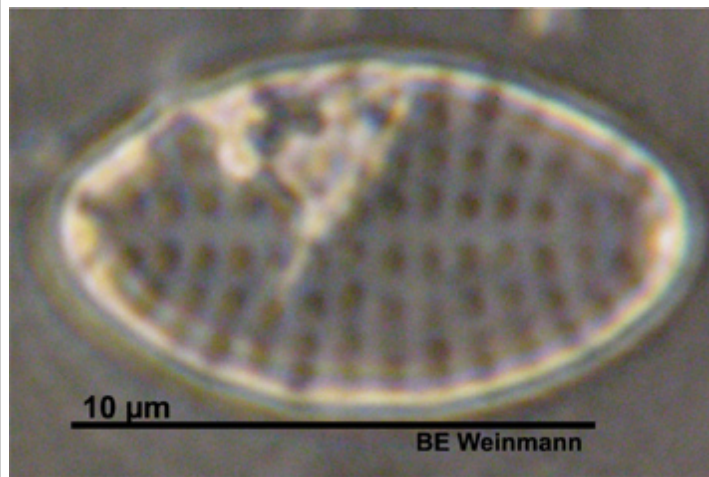
69_101	Unkown sp. [?]
Specimens Measured:	na
Aspect:	Girdle
Valve symmetry or shape:	
Dimensions µm [AA]:	na - (0) - na
Dimensions µm [PA]:	na - (0) - na
Raphe:	na, location = na, shape = 'na', central endings = 'na', polar endings = 'na'
Striae:	19? per 10µm, orientation = 'Transverse, parallel', pores = 'Punctate', Not resolved per 10µm
Fibulae or Costae:	
Axial area:	axial area = 'na' , central area = na, central nodule = Small depression, terminal nodule = Small depression, other hyaline areas = na
Other Features:	Spines = None; Comments = 'Very shallow valve, hardly any margin, very narrow stria but with gap in centre'; Other = 'na'
Image path:	Catalogue3\Cat3-Ref69-101_2012-03-24-c129.jpg
	

70_91	Navicula tripunctata (Möller) Bory 1822 [BMB3: #260]
Specimens Measured:	7
Aspect:	Valve
Valve symmetry or shape:	Apical sym = Isobilateral, Transapical sym = Isopolar, Valve shape = Linear-lanceolate, Valve curvature = none, Frustral shape = na
Dimensions µm [AA]:	36.8 - (51) - 69.1
Dimensions µm [TA]:	7.4 - (9.3) - 11
Raphe:	Raphe, location = Central, shape = 'straight', central endings = 'Distant, pinhead inflation, slight downward slope away from centre', polar endings = 'Forked'
Striae:	11 - 13 per 10µm, orientation = 'Transverse, radiate becoming parallel to convergent', pores = 'Not resolved', na per 10µm
Fibulae or Costae:	
Axial area:	axial area = 'Narrow, linear' , central area = Trapezoidal butterfly-shaped expansion, central nodule = Not distinct from sternum, terminal nodule = Slight expansion of sternum, other hyaline areas = na
Other Features:	Spines = None; Comments = 'Previously Cat1-Ref81-108'; Other = 'na'
Image path:	Catalogue3\Cat3-Ref70\Cat3-Ref70-91_2009-02-11.jpg
	

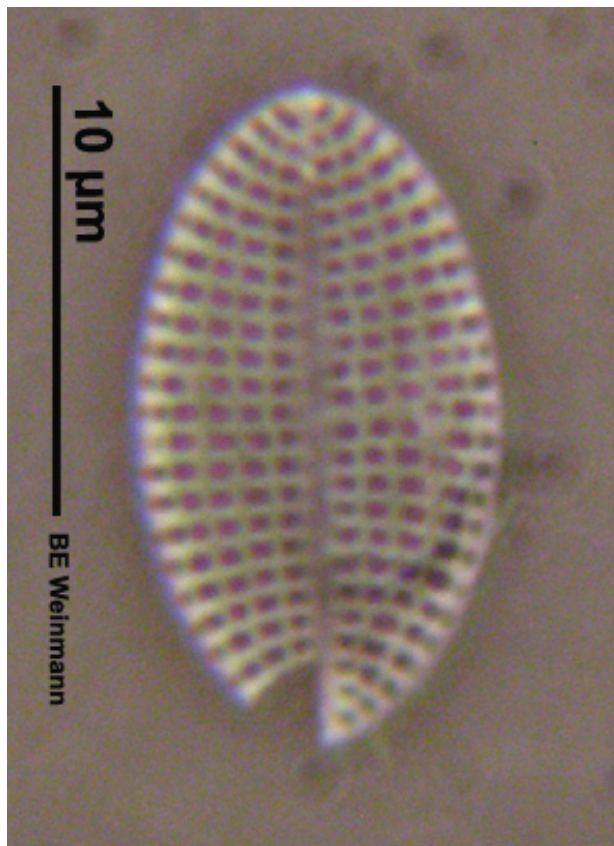
71_92	Navicula integra (Smith) Ralfs in Pritchard 1861 [BMB4: #360]
Specimens Measured:	1
Aspect:	Valve
Valve symmetry or shape:	Apical sym = Isobilateral, Transapical sym = Isopolar, Valve shape = Lanceolate-undulate, Valve curvature = Possibly convex, Apex shape = inflection, Shape = 'Protracted, rostrate or sub-rostrate', Frustral shape = na
Dimensions µm [AA]:	39.2 - (0) - na
Dimensions µm [TA]:	10.4 - (0) - na
Raphe:	Raphe, location = Central, shape = 'straight', central endings = 'Distant, straight and slightly expanded', polar endings = 'Not resolved'
Striae:	17 - 22 per 10µm, orientation = 'Transverse, radiate', pores = 'Not resolved', na per 10µm
Fibulae or Costae:	
Axial area:	axial area = 'Narrow, linear' , central area = Large and round, central nodule = not distinguishable from central area, terminal nodule = Not resolved, other hyaline areas = na
Other Features:	Spines = None; Comments = 'Previously Cat1-Ref85-113'; Other = 'na'
Image path:	Catalogue3\Cat3-Ref71-92_2009-02-13.jpg
	

72_93	Fallacia tenera [BMB3: #242] (or Cocconeis sp. 2 RV?)
Specimens Measured:	7
Aspect:	Valve
Valve symmetry or shape:	Apical sym = Isobilateral, Transapical sym = Isopolar, Valve shape = Elliptic, Valve curvature = Possibly convex Apex shape = no inflection, Shape = 'Broadly rounded', Frustral shape = na
Dimensions µm [AA]:	6.6 - (8.2) - 9.6
Dimensions µm [TA]:	3.7 - (4.2) - 4.4
Raphe:	Raphe, location = Central, shape = 'Linear', central endings = 'Straight, distant', polar endings = 'Not resolved'
Striae:	19 - 24 per 10µm, orientation = 'Transverse, parallel to radiate', pores = 'Punctate, rectangular punctae', 13 - 16 per 10µm
Fibulae or Costae:	
Axial area:	axial area = 'Narrow, linear' , central area = Transapical expansion, rectangular or butterfly, central nodule = Elliptic, bright, terminal nodule = Small round, bright, other hyaline areas = 3 longitudinal columns in between striae
Other Features:	Spines = None; Comments = 'Previously Cat1-Ref88-137'; Other = 'na'
Image path:	Catalogue3\Cat3-Ref72\Cat3-Ref72-93_2009-03-11.jpg
	

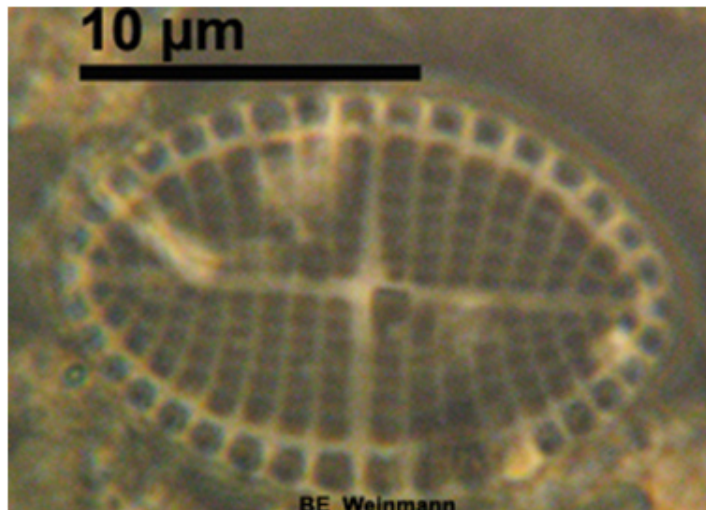
73_94	Cocconeis sp. 3 SV [?]
Specimens Measured:	1
Aspect:	Valve
Valve symmetry or shape:	Apical sym = Isobilateral, Transapical sym = Isopolar, Valve shape = Elliptic, Valve curvature = None Apex shape = no inflection, Shape = 'Broadly rounded', Frustral shape = na
Dimensions µm [AA]:	13.6 - (0) - na
Dimensions µm [TA]:	6.6 - (0) - na
Raphe:	Sternum, location = Central, shape = 'na', central endings = 'na', polar endings = 'na'
Striae:	12 - 14 per 10µm, orientation = 'Transverse, parallel to radiate', pores = 'Punctate, rectangular punctae', 10 - 14 per 10µm
Fibulae or Costae:	
Axial area:	axial area = 'narrow, linear' , central area = none, central nodule = None, terminal nodule = None, other hyaline areas = 2 - 3 longitudinal columns in between striae
Other Features:	Spines = None; Comments = 'Previously 88-141, this looks similar to 88-117 but it is slightly different because the sternum is narrow and distinctly linear rather than lanceolate and it seems to have much fewer striae and more punctae in 10 µm.'; Other = 'na'
Image path:	Catalogue3\Cat3-Ref73\Cat3-Ref73-94_2009-03-12.jpg

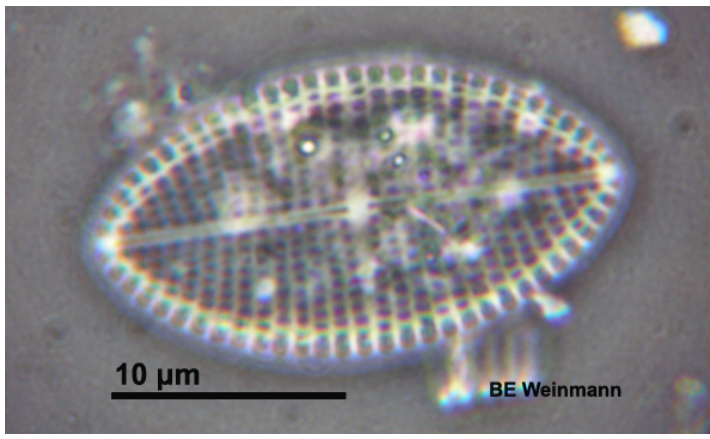


73_129	Cocconeis sp. 3 SV [?]
Specimens Measured:	na
Aspect:	Valve
Valve symmetry or shape:	Apical sym = Isobilateral, Transapical sym = Isopolar, Valve shape = Elliptic, Valve curvature = None, Frustral shape = na
Dimensions µm [AA]:	na - (0) - na
Dimensions µm [TA]:	na - (0) - na
Raphe:	Sternum, location = Central, shape = 'na', central endings = 'na', polar endings = 'na'
Striae:	13 - 14 per 10µm, orientation = 'Transverse, parallel becoming radiate', pores = 'Punctate', 14 - 15 per 10µm
Fibulae or Costae:	
Axial area:	axial area = 'Narrow, linear or very narrowly lanceolate' , central area = Not distinct from sternum, central nodule = Not visible, terminal nodule = Not visible, other hyaline areas = Longitudinal lines (between striae punctae)
Other Features:	Spines = None; Comments = 'Not sure about this ID, did have it as ref 48, but prob more lik esp. 3'; Other = 'na'
Image path:	Catalogue3\Cat3-Ref73\Cat3-Ref73-129_2012-03-21-c133.jpg

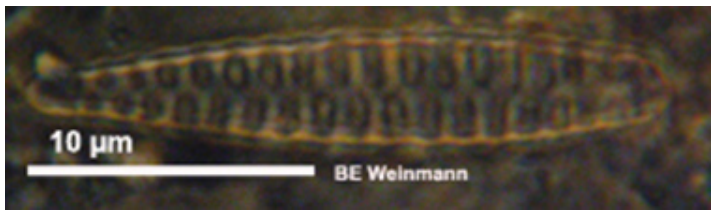


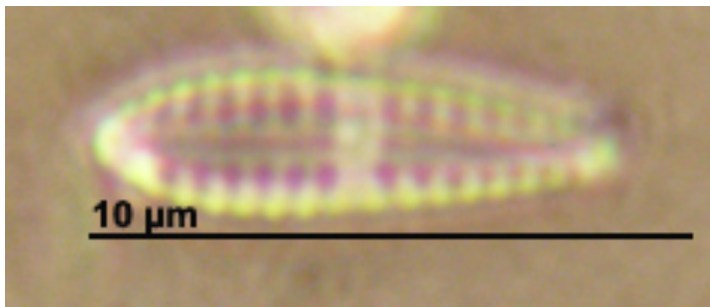
74_95	Cocconeis cf. stauroneiformis SV [Witkowski et al 2000 pl.38: 25] or Cocconeis costata var. costata SV [Witkowski et al 2000 p. 104, pl33: 17 - 22]
Specimens Measured:	1
Aspect:	Valve
Valve symmetry or shape:	Apical sym = Isobilateral, Transapical sym = Isopolar, Valve shape = Elliptic, Valve curvature = None Apex shape = no inflection, Shape = 'Obtusely rounded', Frustral shape = na
Dimensions µm [AA]:	17.8 - (0) - na
Dimensions µm [TA]:	11.1 - (0) - na
Raphe:	Sternum (or possibly raphid?), location = Central, shape = 'not resolved', central endings = 'not resolved', polar endings = 'not resolved'
Striae:	10 - 12 per 10µm, orientation = 'Transverse, parallel to radiate', pores = 'Punctate, rectangular punctae', 15 - 19 per 10µm
Fibulae or Costae:	costae = 9 - 10 per 10µm, Square chambers
Axial area:	axial area = 'Narrow, linear' , central area = Narrow transverse expansion to margin, central nodule = na, terminal nodule = na, other hyaline areas = na
Other Features:	Spines = na; Comments = 'Previously Cat1-Ref90-119. Cocconeis costata var. costata [BMB4: #334] has this striae pattern on the RV'; Other = 'na'
Image path:	Catalogue3\Cat3-Ref74\Cat3-Ref74-95_209-02-17.jpg



74_152	Cocconeis cf. stauroneiformis RV [Witkowski et al 2000 pl38: 19] or Cocconeis costata var. costata RV [Witkowski et al 2000 p. 104, pl33: 17 - 22]
Specimens Measured:	2
Aspect:	Valve
Valve symmetry or shape:	Apical sym = Isobilateral, Transapical sym = Isopolar, Valve shape = Elliptic, Valve curvature = None Apex shape = no inflection, Shape = 'Obtusely rounded', Frustral shape = na
Dimensions µm [AA]:	12.1 - (17.8) - 23.5
Dimensions µm [TA]:	7.4 - (6.7) - 5.9
Raphe:	Raphe, location = Central, shape = 'Straight', central endings = 'Very slight slit-like expansion', polar endings = 'straight'
Striae:	12 - 14 per 10µm, orientation = 'Transverse, parallel becoming radiate', pores = 'Punctate', 13 - 14 per 10µm
Fibulae or Costae:	
Axial area:	axial area = 'NA' , central area = NA, central nodule = NA, terminal nodule = NA, other hyaline areas = NA
Other Features:	Spines = None; Comments = 'Cocconeis costata var. Costata has this striae pattern on the SV'; Other = 'na'
Image path:	Catalogue3\Cat3-Ref74\Cat3-Ref74-152_2012-04-14-c137.jpg
	

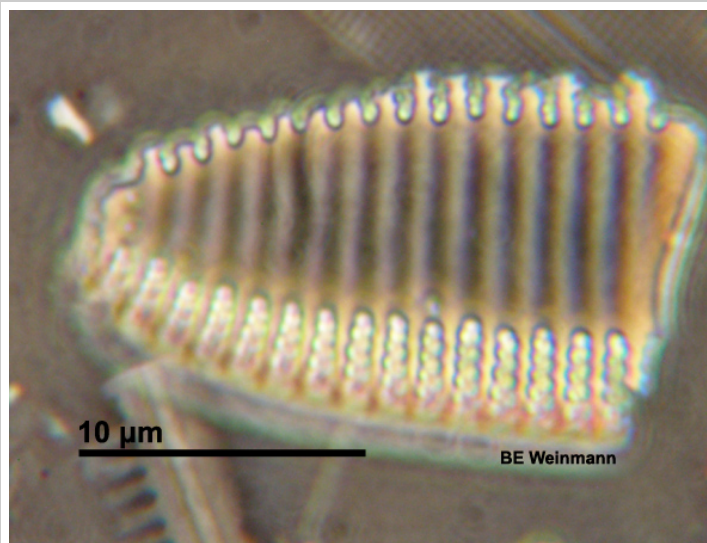
75_96	Navicula palpebralis Brébisson ex Smith [BMB1: #67]
Specimens Measured:	1
Aspect:	Valve
Valve symmetry or shape:	Apical sym = Isobilateral, Transapical sym = Isopolar, Valve shape = Elliptic, Valve curvature = None Apex shape = no inflection, Shape = 'Acute', Frustral shape = na
Dimensions µm [AA]:	45.9 - (0) - na
Dimensions µm [TA]:	18.5 - (0) - na
Raphe:	Raphe, location = Central, shape = 'Linear', central endings = 'Circular', polar endings = 'bent to the same side'
Striae:	11 - 13 per 10µm, orientation = 'Transverse, radiate', pores = 'Not resolved', na per 10µm
Fibulae or Costae:	
Axial area:	axial area = 'Trapezoidal' , central area = not differentiated from trapezoidal sternum, central nodule = large round, terminal nodule = not visible, other hyaline areas = na
Other Features:	Spines = None; Comments = 'Previously Cat1-Ref94-123'; Other = 'na'
Image path:	Catalogue3\Cat3-Ref75-96_2009-02-27.jpg
	

77_98	Opephora mutabilis (Grunow) Sabbe & Vyverman [Witkowski pl. 25:10 - 17]
Specimens Measured:	5
Aspect:	Valve
Valve symmetry or shape:	Apical sym = Isobilateral, Transapical sym = Heteropolar, Valve shape = Skittle-shaped, Valve curvature = None, Frustral shape = na
Dimensions µm [AA]:	7.4 - (16.8) - 25.7
Dimensions µm [TA]:	1.5 - (3.1) - 5.1
Raphe:	Sternum, location = Central, shape = 'na', central endings = 'na', polar endings = 'na'
Striae:	8 - 10 per 10µm, orientation = 'Transverse, parallel', pores = 'Vague', not resolved per 10µm
Fibulae or Costae:	
Axial area:	axial area = 'Extremely narrow, linear ' , central area = none, central nodule = None, terminal nodule = None, other hyaline areas = None
Other Features:	Spines = None; Comments = 'Previously Cat1-Ref99-130'; Other = 'na'
Image path:	Catalogue3\Cat3-Ref77\Cat3-Ref77-98_2009-03-4.jpg
	

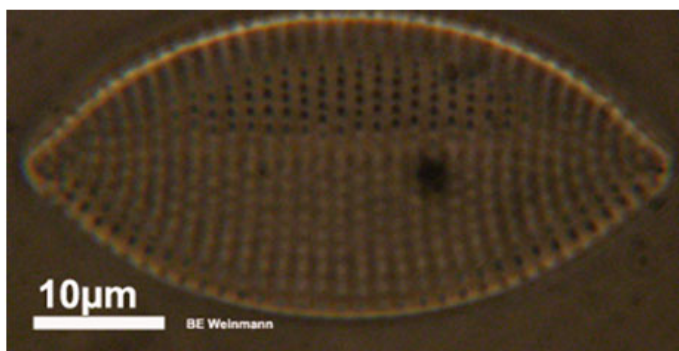
78_99	Gomphonemeopsis pseudoexigua (Simonsen) Medlin [BMB2: 140]
Specimens Measured:	2
Aspect:	Valve
Valve symmetry or shape:	Apical sym = Isobilateral, Transapical sym = Heteropolar, Valve shape = Club-shaped, Valve curvature = None Apex shape = no inflection, Shape = 'Broadly or obtusely rounded', Frustral shape = na
Dimensions µm [AA]:	8.8 - (9.2) - 9.6
Dimensions µm [TA]:	2.6 - (2.8) - 2.9
Raphe:	Raphe, location = Central, shape = 'Linear', central endings = 'Straight, very slight inflation, quite distance', polar endings = 'Not resolved'
Striae:	16 per 10µm, orientation = 'Transverse, parallel or slightly radiate', pores = 'Not resolved', na per 10µm
Fibulae or Costae:	
Axial area:	axial area = 'Linear, 1/2 TA width', central area = Rectangular expansion to margin (fascia?), central nodule = None visible, terminal nodule = Slight bright spots right on margin, other hyaline areas = na
Other Features:	Spines = None; Comments = 'Previously Cat1-Ref100-131. This is different from Rhoicosphenia genuflexa, firstly its flat secondly the striae are much shorter'; Other = 'na'
Image path:	Catalogue3\Cat3-Ref78\Cat3-Ref78-99_2012-03-24-c154.jpg
	

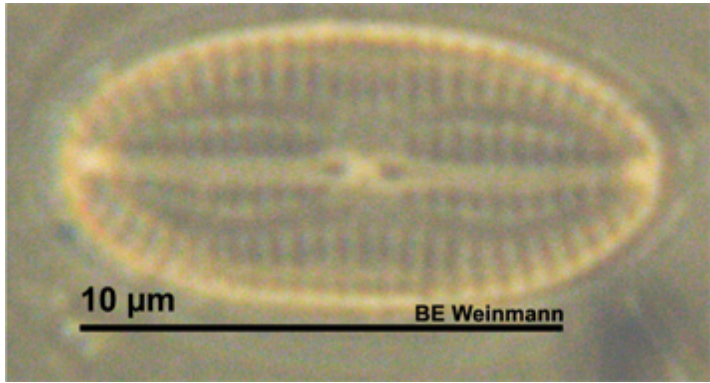
79_100	Opephora minuta (Cleve-Euler) stat. Nov. [Witkowski 25: 39 - 42]
Specimens Measured:	6
Aspect:	Valve
Valve symmetry or shape:	Apical sym = Isobilateral, Transapical sym = Heteropolar, Valve shape = Skittle-shaped, Valve curvature = None, Frustral shape = na
Dimensions µm [AA]:	5.1 - (8.6) - 11.1
Dimensions µm [TA]:	1.5 - (2.8) - 5.1
Raphe:	Sternum, location = Central, shape = 'na', central endings = 'na', polar endings = 'na'
Striae:	19 - 21 per 10µm, orientation = 'Transverse, parallel or slightly radiate', pores = 'Not resolved', na per 10µm
Fibulae or Costae:	
Axial area:	axial area = 'Lanceolate', central area = No differentiation from sternum, central nodule = None, terminal nodule = None, other hyaline areas = na
Other Features:	Spines = None; Comments = 'Previously Cat1-Ref102-133.'; Other = 'na'
Image path:	Catalogue3\Cat3-Ref79\Cat3-Ref79-100_2009-03-04.jpg
	

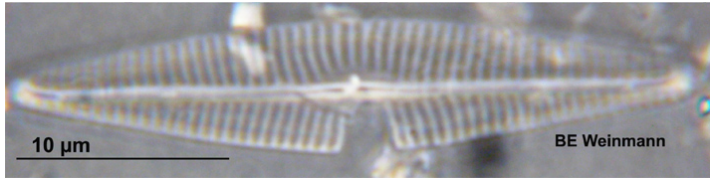
80_102	Tryblionella navicularis (Brébisson) Ralfs in Pritchard 1861 [BMB5: #498]
Specimens Measured:	1
Aspect:	Valve
Valve symmetry or shape:	Apical sym = Isobilateral, Transapical sym = Isopolar, Valve shape = Lanceolate, Valve curvature = None Apex shape = no inflection, Shape = 'Acute', Frustral shape = na
Dimensions µm [AA]:	35.5 - (0) - na
Dimensions µm [TA]:	14.8 - (0) - na
Raphe:	Neither visible, location = NA, shape = 'na', central endings = 'na', polar endings = 'na'
Striae:	7 per 10µm, orientation = 'Transverse, parallel', pores = 'Punctate', not resolved per 10µm
Fibulae or Costae:	fibulae = 7 per 10µm, They are wide (but not "filled in" like striae) there are nodules up inside margins with areolae 4 per side = 8 - 10
Axial area:	axial area = 'none' , central area = none, central nodule = none, terminal nodule = none, other hyaline areas = none
Other Features:	Spines = None; Comments = 'Previously Cat1-Ref104-136.'; Other = 'na'
Image path:	Catalogue3\Cat3-Ref80\Cat3-Ref80-102_2012-04-18-c90.jpg

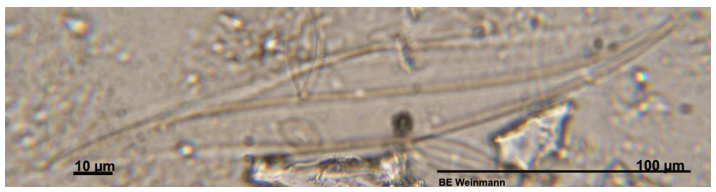


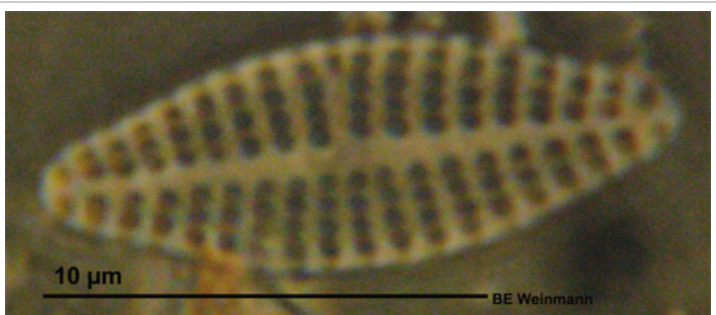
81_103	Tryblionella punctata Smith 1853 [BMB2: #200]
Specimens Measured:	7
Aspect:	Valve
Valve symmetry or shape:	Apical sym = Isobilateral, Transapical sym = Isopolar, Valve shape = Linear, broadly lanceolate, Valve curvature = None, Apex shape = inflection, Shape = 'Small protracted sub-rostrate nubs', Frustral shape = na
Dimensions μm [AA]:	40.4 - (50.8) - 55.1
Dimensions μm [TA]:	22.1 - (23) - 24.3
Raphe:	Neither, location = na, shape = 'na', central endings = 'na', polar endings = 'na'
Striae:	na per 10 μm , orientation = 'Transverse, parallel', pores = 'Punctate', 10 per 10 μm
Fibulae or Costae:	
Axial area:	axial area = 'na', central area = na, central nodule = na, terminal nodule = na, other hyaline areas = na
Other Features:	Spines = None; Comments = 'Previously Cat1-Ref107-139.'; Other = 'na'
Image path:	Catalogue3\Cat3-Ref81\Cat3-Ref81-103_2009-03-09_combined.jpg

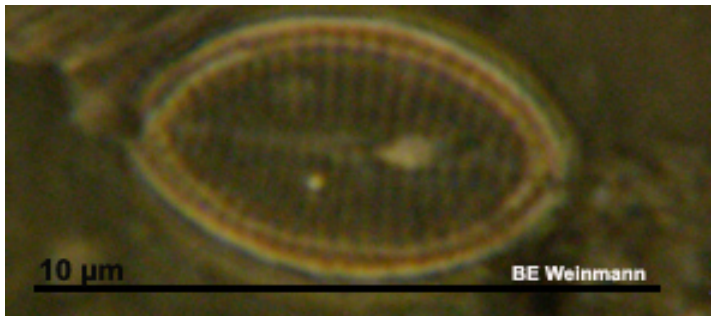


82_104	Fallacia suspirii (Cholnoky) comb. nov. [Witkowski pl. 71:4] or Fallacia clepsidroides [BMB3: #239; Witkowski pl. 70:31-34]
Specimens Measured:	3
Aspect:	Valve
Valve symmetry or shape:	Apical sym = Isobilateral, Transapical sym = Isopolar, Valve shape = Elliptic, Valve curvature = None Apex shape = no inflection, Shape = 'Broadly rounded', Frustral shape = na
Dimensions µm [AA]:	8.8 - (10.8) - 12.6
Dimensions µm [TA]:	5.9 - (5.9) - 5.9
Raphe:	Raphe, location = Central, shape = 'Linear', central endings = 'Largely inflated, round, Straight, distant', polar endings = 'Not resolved'
Striae:	22 per 10µm, orientation = 'Transverse, parallel becoming radiate', pores = 'Not resolved', na per 10µm
Fibulae or Costae:	
Axial area:	axial area = 'Linear, 1/5 TA' , central area = Rectangular, halfway to margin, central nodule = Small, terminal nodule = Small, other hyaline areas = Lyre-shaped hyaline slits halfway between raphe and margins
Other Features:	Spines = None; Comments = 'The sternum curves around the ends of the striae, like two q-tips head to head'; Other = 'na'
Image path:	Catalogue3\Cat3-Ref82\Cat3-Ref82-104_2009-03-13.jpg
	

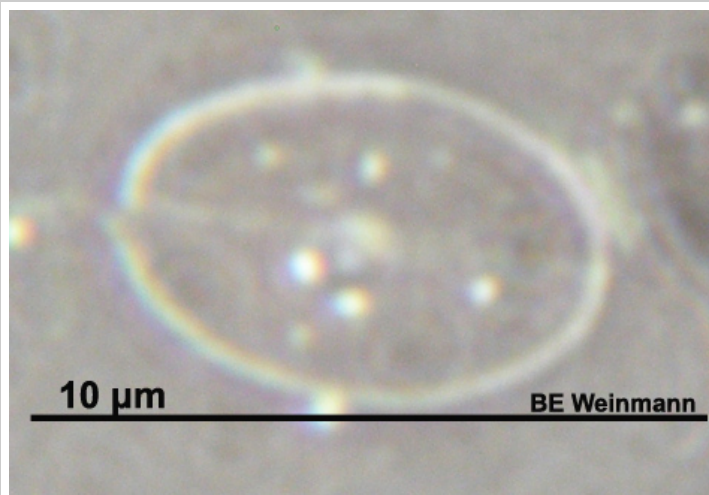
83_105	Navicula areneria Donkin 1861 [BMB5: #452]
Specimens Measured:	1
Aspect:	Valve
Valve symmetry or shape:	Apical sym = Isobilateral, Transapical sym = Isopolar, Valve shape = Lanceolate, Valve curvature = None Apex shape = no inflection, Shape = 'Acute', Frustral shape = na
Dimensions µm [AA]:	31.82 - (0) - na
Dimensions µm [TA]:	6.7 - (0) - na
Raphe:	Raphe, location = Central, shape = 'Linear', central endings = 'Slight linear inflation and bent slightly to secondary side', polar endings = 'Bent to same side or possibly hooked (ie bent then curving back down)'
Striae:	15 - 18 per 10µm, orientation = 'Transverse, radiate and possibly possibly parallel or convergent athe poles', pores = 'Not resolved', na per 10µm
Fibulae or Costae:	
Axial area:	axial area = 'Narrow, linear and distinct' , central area = Elliptical, central nodule = Not distinct from sternum, terminal nodule = Yes, but not very distinct from sternum, other hyaline areas = Sternum expands at poles
Other Features:	Spines = None; Comments = 'This is very similar to 13-19, apparantly Navicula areneria is a synonym of Navicula lanceolata var. arenaria (Donkin) Van Heurck 1885, but the raphe central endings are not at all distant and the central area is much shallower elliptical whereas in 13 - 19 its almost elliptical along TA. This specimen is smaller than the BMB specification (AA = 43 - (48) -55 and TA = 9 - (12.8) - 10)'; Other = 'na'
Image path:	Catalogue3\Cat3-Ref83\Cat3-Ref83-105_2009-03-12.jpg
	

84_106	Gyrosigma accuminata (Kützing) Rabenhorst [BMB2: #142]
Specimens Measured:	1
Aspect:	Valve
Valve symmetry or shape:	Apical sym = Sigmoid, Transapical sym = Isopolar, Valve shape = Rhombic-sigmoid, Valve curvature = Yes Apex shape = no inflection, Shape = 'Acute', Frustral shape = na
Dimensions µm [AA]:	164.4 - (0) - na
Dimensions µm [TA]:	25.5 - (0) - na
Raphe:	Raphe, location = Central, shape = 'Sigmoid', central endings = 'Straight, with slight linear inflation', polar endings = 'Not resolved'
Striae:	25 - 35 per 10µm, orientation = 'Transverse and longitudinal', pores = 'Not resolved', na per 10µm
Fibulae or Costae:	
Axial area:	axial area = 'Narrow, sigmoid', central area = Very slightly elliptical, central nodule = Small, round, bright, terminal nodule = Not visible, other hyaline areas = none
Other Features:	Spines = None; Comments = 'Previously Cat1-Ref109-145'; Other = 'na'
Image path:	Catalogue3\Cat3-Ref84\Cat3-Ref84-106_2009-03-12.jpg
	

85_107	Achnanthes sp. 1 [ADIAC sp. p.8]
Specimens Measured:	1
Aspect:	Valve
Valve symmetry or shape:	Apical sym = Isobilateral, Transapical sym = Isopolar, Valve shape = Lanceolate, Valve curvature = None, Frustral shape = NA
Dimensions µm [AA]:	14.7 - (0) - na
Dimensions µm [TA]:	5.1 - (0) - na
Raphe:	Sternum, location = Central, shape = 'na', central endings = 'na', polar endings = 'na'
Striae:	13 - 15 per 10µm, orientation = 'Transverse, parallel and radiate', pores = 'Punctate', 16 - 20 per 10µm
Fibulae or Costae:	
Axial area:	axial area = 'Linear 1/5 TA', central area = Not distinct from sternum, central nodule = Possibly, terminal nodule = none, other hyaline areas = None
Other Features:	Spines = None; Comments = 'Previously Cat1-Ref110-146'; Other = 'na'
Image path:	Catalogue3\Cat3-Ref85\Cat3-Ref85-107_2009-03-13.jpg
	

86_109	Cocconeis hauniensis SV Witkowski emend. Witkowski [Witkowski ?]
Specimens Measured:	1
Aspect:	Valve
Valve symmetry or shape:	Apical sym = Isobilateral, Transapical sym = Isopolar, Valve shape = Elliptic, Valve curvature = None Apex shape = no inflection, Shape = 'Obtuse', Frustral shape = na
Dimensions μm [AA]:	6.6 - (0) - na
Dimensions μm [TA]:	3.7 - (0) - na
Raphe:	Sternum, location = Central, shape = 'na', central endings = 'na', polar endings = 'na'
Striae:	30 - 35 per 10 μm , orientation = 'Transverse, parallel becoming radiate', pores = 'Not resolved', na per 10 μm
Fibulae or Costae:	
Axial area:	axial area = 'Narrow, linear' , central area = none, central nodule = None, terminal nodule = None, other hyaline areas = none
Other Features:	Spines = None; Comments = 'It looks like the other but there are way more striae so not sure'; Other = 'na'
Image path:	Catalogue3\Cat3-Ref86\Cat3-Ref86-109_2009-03-13.jpg
	

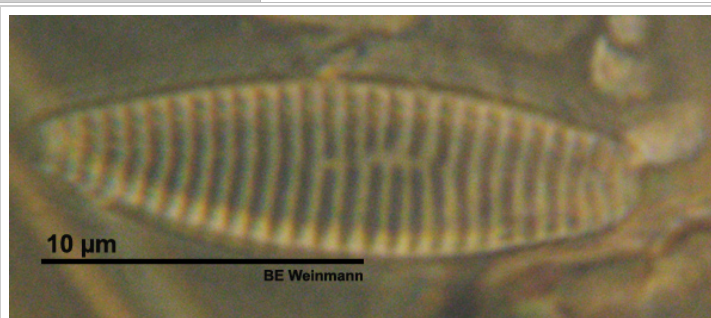
86_157	Cocconeis hauniensis RV Witkowski emend. Witkowski [Ribeiro 2010, Vol 2, p. 176, pl10: 1] Or Navicula sp. # 98 (ADIAC, p10)
Specimens Measured:	1
Aspect:	Valve
Valve symmetry or shape:	Apical sym = Isobilateral, Transapical sym = Isopolar, Valve shape = Elliptic, Valve curvature = None, Frustral shape = na
Dimensions µm [AA]:	7.4 - (0) - na
Dimensions µm [TA]:	4.4 - (0) - na
Raphe:	Raphe, location = Central, shape = 'linear', central endings = 'Not resolved', polar endings = 'Not resolved'
Striae:	not resolved per 10µm, orientation = 'Not resolved', pores = 'Not resolved', na per 10µm
Fibulae or Costae:	
Axial area:	axial area = 'Linear, narrow' , central area = Not resolved, central nodule = Large, bright, terminal nodule = Not visible, other hyaline areas = Valve face appears hyaline
Other Features:	Spines = None; Comments = 'Not sure about the C. hauniensis ID bc there is a faint trace of the placental submarginal ring, which hauniensis does not have.'; Other = 'na'
Image path:	Catalogue3\Cat3-Ref86\Cat3-Ref86-157_2012-04-08-c34.jpg



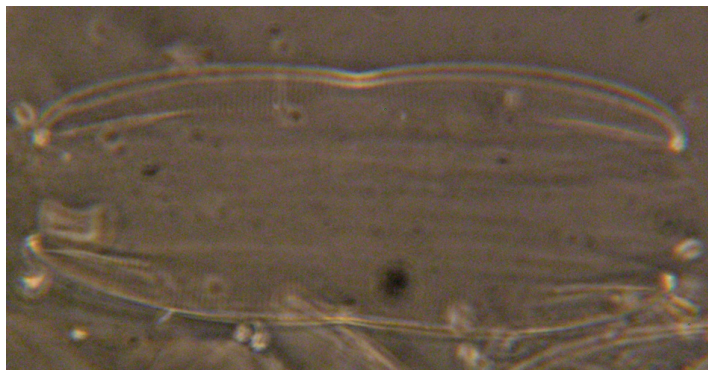
87_110	Nitzschia microcephala Grunow in Cleve & Möller 1878 [BMB2: #171]
Specimens Measured:	1
Aspect:	Valve
Valve symmetry or shape:	Apical sym = Isobilateral, Transapical sym = Isopolar, Valve shape = Linear-lanceolate, Valve curvature = None, Apex shape = inflection, Shape = 'Protracted, rostrate or sub-rostrate', Frustral shape = NA
Dimensions µm [AA]:	12.6 - (0) - na
Dimensions µm [TA]:	3.7 - (0) - na
Raphe:	Raphe, location = Eccentric, shape = 'marginal', central endings = 'NA', polar endings = 'NA'
Striae:	Not resolved per 10µm, orientation = 'na', pores = 'na', na per 10µm
Fibulae or Costae:	
Axial area:	axial area = 'None' , central area = None, central nodule = None, terminal nodule = None, other hyaline areas = None
Other Features:	Spines = None; Comments = 'Previously Cat1-Ref114-151'; Other = 'na'
Image path:	Catalogue3\Cat3-Ref87-110_2009-03-13.jpg



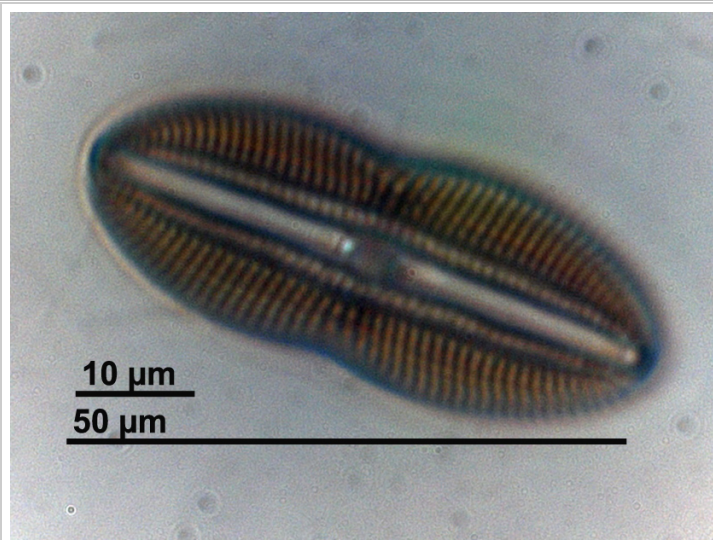
88_111	Fragilaria schulzii Brockmann [Witkowski pl. 24: 7 - 12]
Specimens Measured:	1
Aspect:	Valve
Valve symmetry or shape:	Apical sym = Isobilateral, Transapical sym = Isopolar, Valve shape = Club-shaped, curved, Valve curvature = Slight Apex shape = no inflection, Shape = 'Broadly rounded', Frustral shape = na
Dimensions µm [AA]:	18.5 - (0) - 19.8
Dimensions µm [TA]:	5.9 - (0) - 7.4
Raphe:	Sternum, only very slight, location = Central, shape = 'na', central endings = 'na', polar endings = 'na'
Striae:	14 - 15 per 10µm, orientation = 'Transverse, parallel', pores = 'Not resolved', na per 10µm
Fibulae or Costae:	
Axial area:	axial area = 'Hardly visible' , central area = None, central nodule = None, terminal nodule = None, other hyaline areas = None
Other Features:	Spines = None; Comments = 'Very rare'; Other = 'na'
Image path:	Catalogue3\Cat3-Ref88-111_2009-03-14.jpg

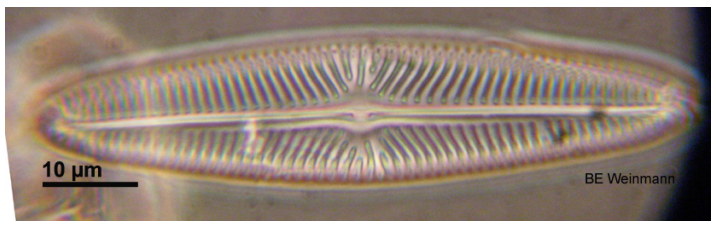


89_112	Plagiotropis vanheurckii Grunow in Van Heurck 1880 [BMB4: #381]
Specimens Measured:	10
Aspect:	Girdle
Valve symmetry or shape:	
Dimensions μm [AA]:	27.2 - (58.3) - 79.4
Dimensions μm [PA]:	5.9 - (9.9) - 13.2
Raphe:	na, location = na, shape = 'na', central endings = 'na', polar endings = 'na'
Striae:	na per 10 μm , orientation = '20 - 23', pores = 'Transverse, parallel', Not resolved per 10 μm
Fibulae or Costae:	
Axial area:	axial area = 'na' , central area = na, central nodule = na, terminal nodule = Yes, bright, other hyaline areas = na
Other Features:	Spines = na; Comments = 'Previously Cat1-Ref117-156'; Other = 'Yes, right at margin'
Image path:	Catalogue3\Cat3-Ref89-112_2009-03-14.jpg

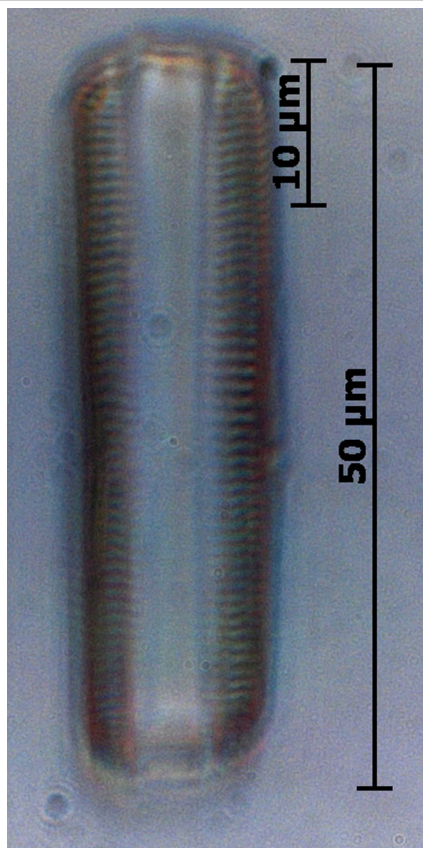


90_113	Diploneis sp. 1 [?]
Specimens Measured:	2
Aspect:	Valve
Valve symmetry or shape:	Apical sym = Isobilateral, Transapical sym = Isopolar, Valve shape = Broadly lanceolate, Valve curvature = None Apex shape = no inflection, Shape = 'Obtusely rounded', Frustral shape = na
Dimensions μm [AA]:	50 - (51.5) - 53
Dimensions μm [TA]:	20 - (20.5) - 21
Raphe:	Raphe, location = Central, shape = 'Linear, possibly undulating', central endings = 'Very inflated, large and round', polar endings = 'Not resolved'
Striae:	9 - 11 per $10\mu\text{m}$, orientation = 'Transverse, radiate', pores = 'Not resolved', na per $10\mu\text{m}$
Fibulae or Costae:	
Axial area:	axial area = 'Narrow, bright, linear' , central area = Square with slightly rounded sides, central nodule = Not visible, terminal nodule = Not visible, other hyaline areas = na
Other Features:	Spines = None; Comments = 'na'; Other = 'Narrow furrows along the sternum and the canals are more or less parallel 1/5 way to the margin.'
Image path:	Catalogue3\Cat3-Ref90\Cat3-Ref90-113_2011-01-31-c1.jpg



91_114	Navicula digitatoradiata (Gregory) Ralfs in Pritchard 1861 [BMB2: #158]
Specimens Measured:	21
Aspect:	Valve
Valve symmetry or shape:	Apical sym = Isobilateral, Transapical sym = Isopolar, Valve shape = Narrowly lanceolate, Valve curvature = None, Frustral shape = na
Dimensions µm [AA]:	34.5 - (55.7) - 68.4
Dimensions µm [TA]:	10 - (12.5) - 16.2
Raphe:	Raphe, location = Central, shape = 'Central', central endings = 'Inflate, slightly deflected to same size', polar endings = 'Bent to same side'
Striae:	10 - 12 per 10µm, orientation = 'Transverse, radiate becoming parallel and slight convergent at poles', pores = 'Not resolved', na per 10µm
Fibulae or Costae:	
Axial area:	axial area = 'Looks one-sided (primary), slightly lanceolate in each TA half' , central area = Not symmetrical and irregular TA expansion on both side, central nodule = Not visible, terminal nodule = Not visible, other hyaline areas = na
Other Features:	Spines = None; Comments = 'na'; Other = 'na'
Image path:	Catalogue3\Cat3-Ref91\Cat3-Ref91-114_2012-03-21-c98.jpg
	

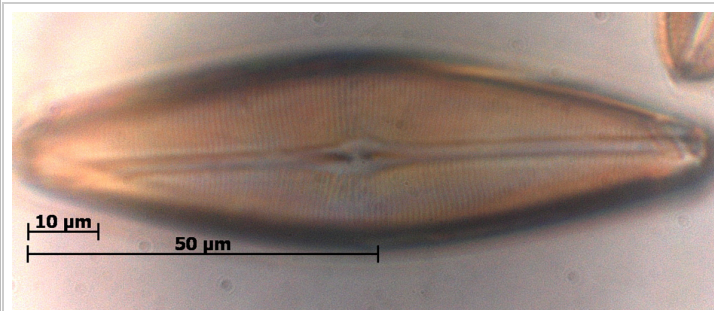
91_115	Navicula digitatoradiata (Gregory) Ralfs in Pritchard 1861 [BMB2: #158]
Specimens Measured:	2
Aspect:	Girdle
Valve symmetry or shape:	
Dimensions μm [AA]:	51 - (55.5) - 60
Dimensions μm [PA]:	11 - (12) - 13
Raphe:	na, location = na, shape = 'na', central endings = 'na', polar endings = 'na'
Striae:	10 - 12 per 10 μm , orientation = 'Transverse, parallel on margins', pores = 'Not resolved', na per 10 μm
Fibulae or Costae:	
Axial area:	axial area = 'na' , central area = na, central nodule = Not visible, terminal nodule = Not visible, other hyaline areas = na
Other Features:	Spines = None; Comments = 'Not sure this is Cryptocephala....'; Other = 'na'
Image path:	Catalogue3\Cat3-Ref91\Cat3-Ref91-115_2011-01-31-c22.jpg



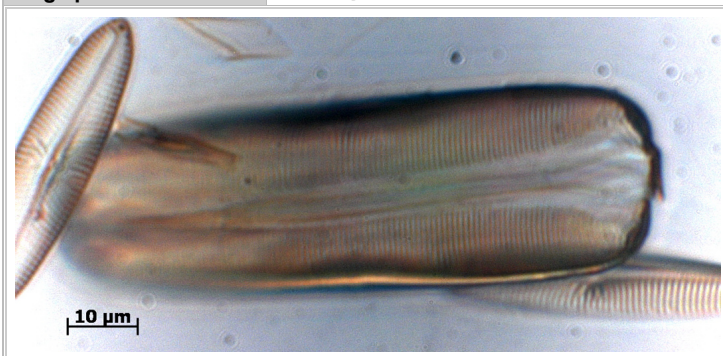
91_160	Navicula digitatoradiata (really small one...?) [BMB2: #158]
Specimens Measured:	1
Aspect:	Valve
Valve symmetry or shape:	Apical sym = Isobilateral, Transapical sym = Isopolar, Valve shape = Linear, Valve curvature = None, Frustral shape = na
Dimensions µm [AA]:	34.5 - (0) - na
Dimensions µm [TA]:	11 - (0) - na
Raphe:	Raphe, location = Central, shape = 'Straight', central endings = 'Very slightly deflected to same side and slightly inflated', polar endings = 'na'
Striae:	na per 10µm, orientation = 'na', pores = 'na', na per 10µm
Fibulae or Costae:	
Axial area:	axial area = 'na' , central area = na, central nodule = na, terminal nodule = na, other hyaline areas = na
Other Features:	Spines = na; Comments = 'This is a good deal smaller than the other N. digitatoradiata, thought it was other maybe Navicula bipistulata Mann 1925)'; Other = 'na'
Image path:	Catalogue3\Cat3-Ref91\Cat3-Ref91-160_2012-04-08-c124.jpg



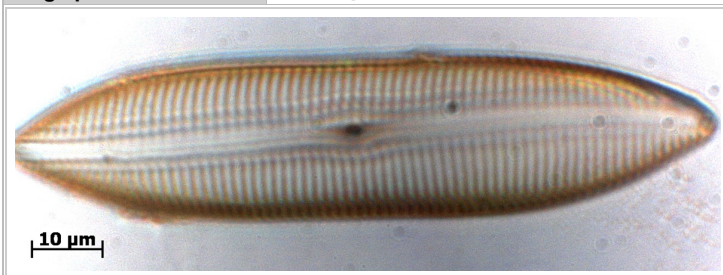
92_108	Parlibellus sp.1 [Round et al 516]
Specimens Measured:	2
Aspect:	Valve
Valve symmetry or shape:	Apical sym = Isobilateral, Transapical sym = Isopolar, Valve shape = Lanceolate, Valve curvature = None Apex shape = no inflection, Shape = 'Acute', Frustral shape = na
Dimensions µm [AA]:	89 - (93.5) - 98
Dimensions µm [TA]:	26 - (26) - 26
Raphe:	Raphe, location = Central, very slightly oblique, shape = 'Linear', central endings = 'Straight, with elongate inflation and slightly darkened ', polar endings = 'na'
Striae:	13 - 15 per 10µm, orientation = 'Transverse, parallel to radiate', pores = 'Not resolved', na per 10µm
Fibulae or Costae:	
Axial area:	axial area = 'Linear, narrow' , central area = Unsymmetrical, round and lanceolate, central nodule = Not visible, terminal nodule = Not visible, other hyaline areas = na
Other Features:	Spines = na; Comments = 'na'; Other = 'na'
Image path:	Catalogue3\Cat3-Ref92\Cat3-Ref92-118_2009-03-31-c11.jpg

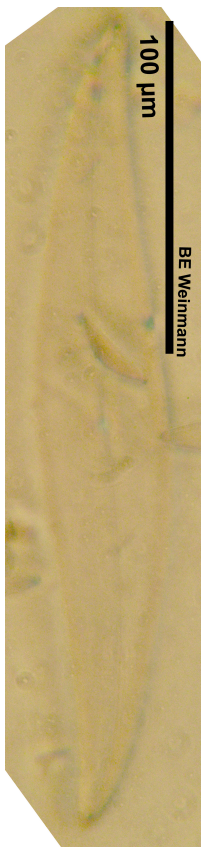


92_116	Parlibellus sp.1 [Round et al 516; Ribeiro pl. 13:9 - 10]
Specimens Measured:	3
Aspect:	Girdle
Valve symmetry or shape:	
Dimensions µm [AA]:	86 - (94.2) - 96
Dimensions µm [PA]:	24 - (30.5) - 41
Raphe:	na, location = na, shape = 'na', central endings = 'na', polar endings = 'na'
Striae:	13 - 14 per 10µm, orientation = 'Transverse, parallel on margins', pores = 'Not resolved', na per 10µm
Fibulae or Costae:	
Axial area:	axial area = 'na' , central area = na, central nodule = Not visible, terminal nodule = Not visible, other hyaline areas = na
Other Features:	Spines = None; Comments = 'na'; Other = 'na'
Image path:	Catalogue3\Cat3-Ref92\Cat3-Ref92-116_2009-03-31-c10.jpg

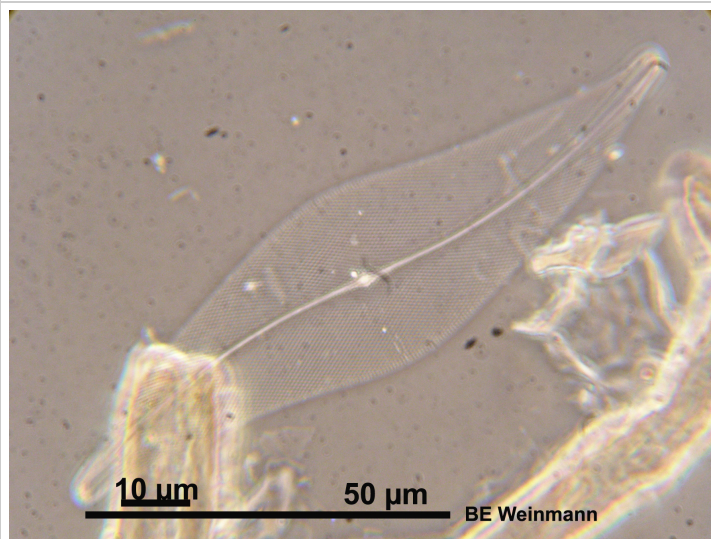


93_117	Scolioneis latestriata (Brebisson in Kützing) Cleve 1894 [BMB4, Round et al 546]
Specimens Measured:	2
Aspect:	Valve
Valve symmetry or shape:	Apical sym = Isobilateral, Transapical sym = Isopolar, Valve shape = Linear, Valve curvature = None, Apex shape = inflection, Shape = 'Cuneate', Frustral shape = na
Dimensions µm [AA]:	96 - (97.5) - 99
Dimensions µm [TA]:	19 - (20.5) - 22
Raphe:	Raphe, location = Central, oblique, shape = 'Linear, oblique', central endings = 'Elongate inflation, very approximate (hard to tell they are separate), straight', polar endings = 'Maybe curved in opposite directions (not clearly resolved)'
Striae:	7 -9 per 10µm, orientation = 'Transverse, parallel, slightly oblique', pores = 'Not resolved', na per 10µm
Fibulae or Costae:	
Axial area:	axial area = 'Linear' , central area = Not distinct from sternum, central nodule = Maybe, terminal nodule = Not visible, other hyaline areas = na
Other Features:	Spines = None; Comments = 'na'; Other = 'There are one or two longitudinal ridges running alongside the sternum creating a ripple effect in the striae'
Image path:	Catalogue3\Cat3-Ref93\Cat2-Ref93-117_2011-01-31-c14.jpg

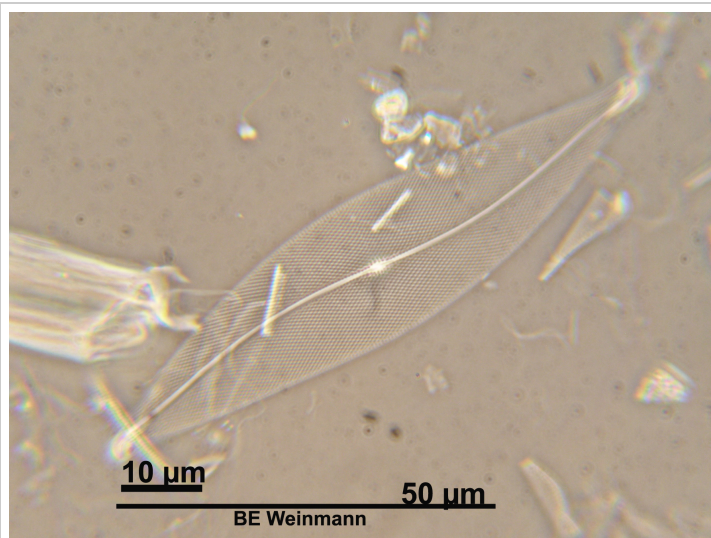


94_118	Pleurosigma angulatum (Quekett) Smith [BMB4: #384, van der Werff & Huls]
Specimens Measured:	12
Aspect:	Valve
Valve symmetry or shape:	Apical sym = Isobilateral, Transapical sym = Sigmoid, Valve shape = Rhombic, sigmoid Sigmoid, rhombic to lanceolate , Valve curvature = None Apex shape = no inflection, Shape = 'Acute', Frustral shape = na
Dimensions µm [AA]:	213.2 - (248.8) - 271.9
Dimensions µm [TA]:	36.8 - (39.7) - 41.9
Raphe:	Raphe, location = Central, shape = 'sigmoid', central endings = 'deflected to same side, slightly inflated', polar endings = 'Not inflated, sigmoid'
Striae:	16 - 19 per 10µm, orientation = 'Oblique in each direction', pores = 'Punctate', 7 per 10µm
Fibulae or Costae:	
Axial area:	axial area = 'Narrow, linear' , central area = Small and broadly lanceolate, central nodule = small and round, terminal nodule = not visible, other hyaline areas = na
Other Features:	Spines = None; Comments = 'na'; Other = 'na'
Image path:	Catalogue3\Cat3-Ref94\Cat3-Ref94-118_2012-03-20-c21.jpg
	

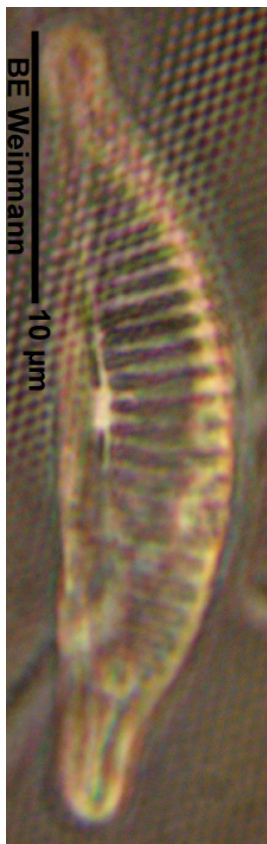
94_135	Pleurosigma angulatum (Quekett) Smith [BMB4: #384, van der Werff & Huls]
Specimens Measured:	10
Aspect:	Valve
Valve symmetry or shape:	Apical sym = Isobilateral, Transapical sym = Sigmoid, Valve shape = Rhombic, sigmoid, Valve curvature = None, Frustral shape = na
Dimensions µm [AA]:	75 - (102.3) - 114.7
Dimensions µm [TA]:	22.1 - (27.2) - 34.5
Raphe:	Raphe, location = Central, shape = 'Sigmoid', central endings = 'Slightly deflected to same side', polar endings = 'Not resolved'
Striae:	16 - 19 per 10µm, orientation = 'Oblique in each direction', pores = 'Punctate', 7 per 10µm
Fibulae or Costae:	
Axial area:	axial area = 'Narrow, linear' , central area = Small and broadly lanceolate, central nodule = small and round, terminal nodule = not visible, other hyaline areas = na
Other Features:	Spines = None; Comments = 'This is much smaller than the P. angulatum range....so either its a "baby" Pleurosigma or its P. estuarii (?) which is more lanceolate than rhombic according to most catalogues (BMB, Hendey, Hartley, but the french catalogue has a rhombic specimen'; Other = 'na'
Image path:	Catalogue3\Cat3-Ref94\Cat3-Ref94-135_2012-03-24-c72.jpg

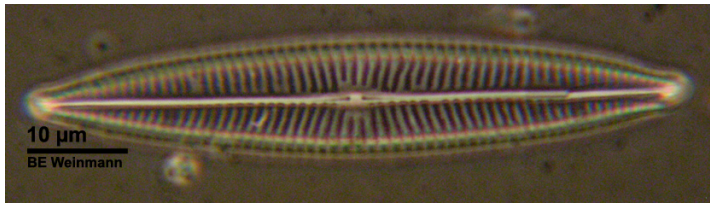


94_136	Pleurosigma angulatum (Quekett) Smith [BMB4: #384, van der Werff & Huls]
Specimens Measured:	7
Aspect:	Valve
Valve symmetry or shape:	Apical sym = Isobilateral, Transapical sym = Sigmoid, Valve shape = Lanceolate, slightly sigmoid, Valve curvature = None, Frustral shape = na
Dimensions µm [AA]:	88.2 - (116.9) - 220.5
Dimensions µm [TA]:	19.1 - (28.1) - 40.4
Raphe:	Raphe, location = Central, shape = 'sigmoid', central endings = 'Straight?', polar endings = 'Not resolved'
Striae:	16 - 19 per 10µm, orientation = 'Oblique in each direction', pores = 'Punctate', 7 per 10µm
Fibulae or Costae:	
Axial area:	axial area = 'Narrow, linear' , central area = Small and broadly lanceolate, central nodule = small and round, terminal nodule = not visible, other hyaline areas = na
Other Features:	Spines = None; Comments = 'na'; Other = 'na'
Image path:	Catalogue3\Cat3-Ref94\Cat3-Ref94-136_2012-03-24-c158.jpg

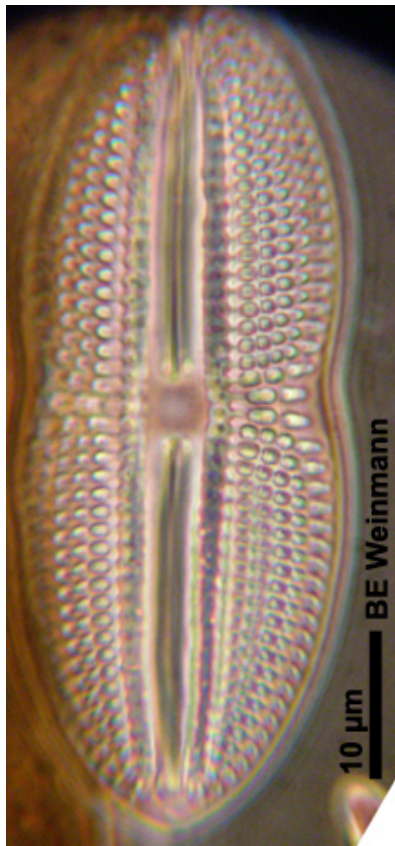


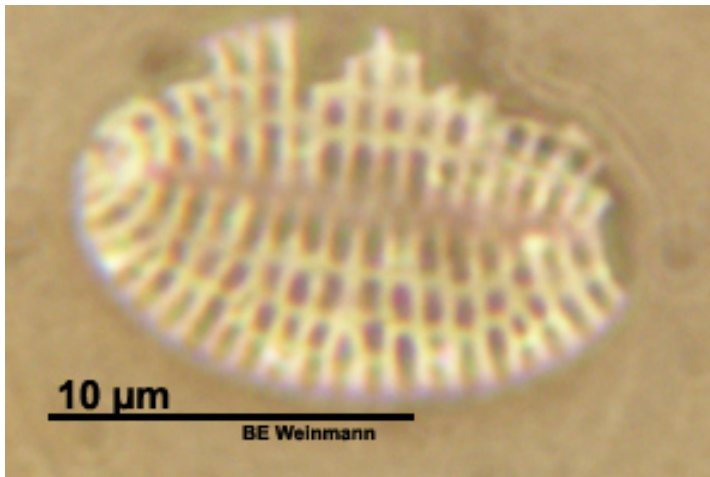
95_119	Amphora cf. exigua Gregory 1857 [BMB ?]
Specimens Measured:	5
Aspect:	Valve
Valve symmetry or shape:	Apical sym = Isobilateral, Transapical sym = Dorsiventral, Valve shape = Lunate, Valve curvature = None, Apex shape = inflection, Shape = 'Protracted, rostrate or sub-rostrate', Frustral shape = na
Dimensions μm [AA]:	15.4 - (20.3) - 29.4
Dimensions μm [TA]:	3.8 - (5) - 7.4
Raphe:	Raphe, location = Ventral, shape = 'Linear', central endings = 'Slightly distant, slightly deflected to dorsal side', polar endings = 'Not resolved'
Striae:	9 - 12 per $10\mu\text{m}$, orientation = 'Transverse, parallel becoming radiate', pores = 'Punctate', 21 - 22 per $10\mu\text{m}$
Fibulae or Costae:	
Axial area:	axial area = 'Linear, narrow' , central area = Not distinct from sternum, central nodule = Not visible, terminal nodule = Not visible, other hyaline areas = na
Other Features:	Spines = None; Comments = 'na'; Other = 'na'
Image path:	Catalogue3\Cat3-Ref95\Cat3-Ref95-119_2012-03-20-c24.jpg

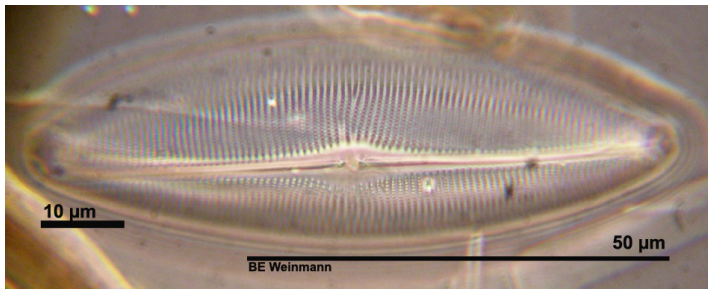


96_120	Navicula peregrina Ehrenberg (Kützinger) 1844 [BMB2: 163] or perhaps Navicula cf. recens [Ribeiro 2000]
Specimens Measured:	21
Aspect:	Valve
Valve symmetry or shape:	Apical sym = Isobilateral, Transapical sym = Isopolar, Valve shape = Narrowly lanceolate, Valve curvature = None, Frustral shape = na
Dimensions µm [AA]:	36 - (60.3) - 117.6
Dimensions µm [TA]:	2.2 - (9.4) - 12.5
Raphe:	Raphe, location = Central, shape = 'Linear', central endings = 'Slightly inflated (pinheads), straight, slightly distant', polar endings = 'Not resolved'
Striae:	10 - 12 per 10µm, orientation = 'Transverse, radiate', pores = 'Lineolate', 25 - 28 per 10µm
Fibulae or Costae:	
Axial area:	axial area = 'Linear, narrow' , central area = Not symmetrical and irregular TA expansion on both sides, central nodule = Narrow, rectangular , terminal nodule = Round (?), other hyaline areas = na
Other Features:	Spines = None; Comments = 'These specimens are larger than those described by either Ribeiro (2010) or Witkowski et al (2000) but other than that they are the closest fit I found.'; Other = 'na'
Image path:	Catalogue3\Cat3-Ref96\Cat3-Ref96-120_2012-03-20-c22.jpg
	

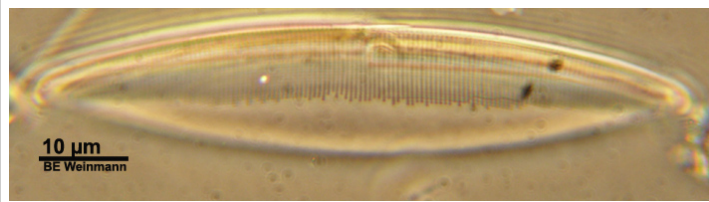
97_122	Diploneis didyma (Ehrenberg) Ehrenberg 1854 [BMB1: 39]
Specimens Measured:	10
Aspect:	Valve
Valve symmetry or shape:	Apical sym = Isobilateral, Transapical sym = Isopolar, Valve shape = Panduriform, Valve curvature = none, Frustral shape = na
Dimensions μm [AA]:	33.1 - (44.9) - 52.2
Dimensions μm [TA]:	13.2 - (18.1) - 21.3
Raphe:	Sternum, location = Central, shape = 'Linear', central endings = 'Slightly longitudinally expanded', polar endings = 'Slightly bent to the same side'
Striae:	8 - 10 per $10\mu\text{m}$, orientation = 'Transverse, slightly radiate', pores = 'Punctate', 8 - 10 per $10\mu\text{m}$
Fibulae or Costae:	
Axial area:	axial area = 'Linear, moderately narrow (1/5 TA)', central area = Slight undulation facing primary half, central nodule = Not visible, terminal nodule = Not visible, other hyaline areas = Narrow longitudinal hyaline area between 1st and 2nd row of punctae (from sternum)
Other Features:	Spines = None; Comments = 'na'; Other = 'na'
Image path:	Catalogue3\Cat3-Ref97\Cat3-Ref97-122_2012-03-20-c43.jpg



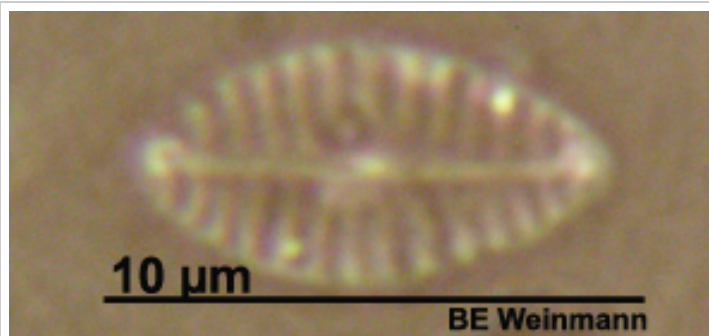
98_123	Cocconeis disculus SV (Schumann) Cleve in Cleve & Jentzsch 1882 [BMB3: 222]
Specimens Measured:	3
Aspect:	Valve
Valve symmetry or shape:	Apical sym = Isobilateral, Transapical sym = Isopolar, Valve shape = Elliptic, Valve curvature = None, Frustral shape = na
Dimensions µm [AA]:	15.4 - (15.9) - 16.9
Dimensions µm [TA]:	8.1 - (9.3) - 11
Raphe:	Sternum, location = Central, shape = 'na', central endings = 'na', polar endings = 'na'
Striae:	13 - 14 per 10µm, orientation = 'Transverse, radiate', pores = 'Punctate', 8 per 10µm
Fibulae or Costae:	
Axial area:	axial area = 'Linear, narrow' , central area = Not distinct from sternum, central nodule = Not visible, terminal nodule = not visible, other hyaline areas = 3 - 4 narrow hyaline areas running longitudinally between striae
Other Features:	Spines = None; Comments = 'na'; Other = 'na'
Image path:	Catalogue3\Cat3-Ref98\Cat3-Ref98-123_2012-03-20-c46.jpg
 <p>10 µm BE Weinmann</p>	

99_124	Parlibellus sp. 2 [?]
Specimens Measured:	10
Aspect:	Valve
Valve symmetry or shape:	Apical sym = Isobilateral, Transapical sym = Isopolar, Valve shape = Elliptic, Valve curvature = Maybe (convex?), Frustral shape = na
Dimensions µm [AA]:	58.8 - (74.9) - 96.6
Dimensions µm [TA]:	8.8 - (19.1) - 26.5
Raphe:	Raphe, location = Subcentral, shape = 'Linear, slightly deflected and slight curvature', central endings = 'Only slightly longitudinally inflated', polar endings = 'Not resolved'
Striae:	13 - 15 per 10µm, orientation = 'Transverse, slightly radiate', pores = 'Punctate', 22 - 28 per 10µm
Fibulae or Costae:	
Axial area:	axial area = 'Linear, moderately narrow (1/5 TA)', central area = Lanceolate, central nodule = Not visible, terminal nodule = Not visible, other hyaline areas = None
Other Features:	Spines = None; Comments = 'na'; Other = 'na'
Image path:	Catalogue3\Cat3-Ref99\Cat3-Ref99-124_2012-03-21-c68.jpg
	

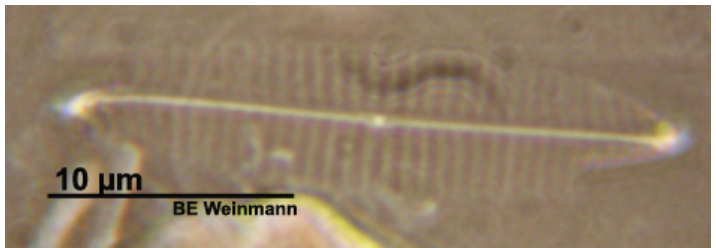
99_145	Parlibellus sp. 2 [?]
Specimens Measured:	5
Aspect:	Girdle
Valve symmetry or shape:	
Dimensions µm [AA]:	58.8 - (70.7) - 84.5
Dimensions µm [PA]:	na - (0) - na
Raphe:	na, location = na, shape = 'na', central endings = 'na', polar endings = 'na'
Striae:	20 per 10µm, orientation = 'Transverse', pores = 'Punctate', Not resolved per 10µm
Fibulae or Costae:	
Axial area:	axial area = 'na' , central area = na, central nodule = Not visible, terminal nodule = Not visible, other hyaline areas = na
Other Features:	Spines = None; Comments = 'na'; Other = 'na'
Image path:	Catalogue3\Cat3-Ref99\Cat9-Ref99-145_2012-03-29-c111.jpg

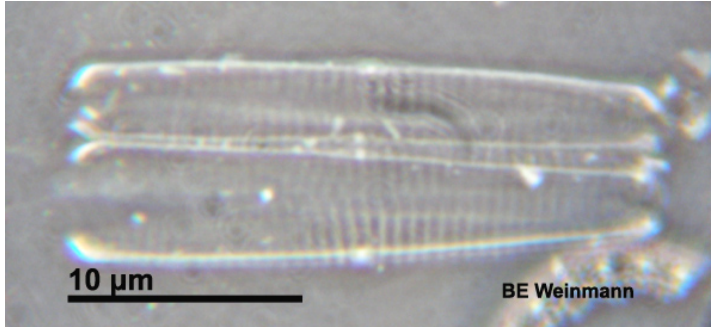


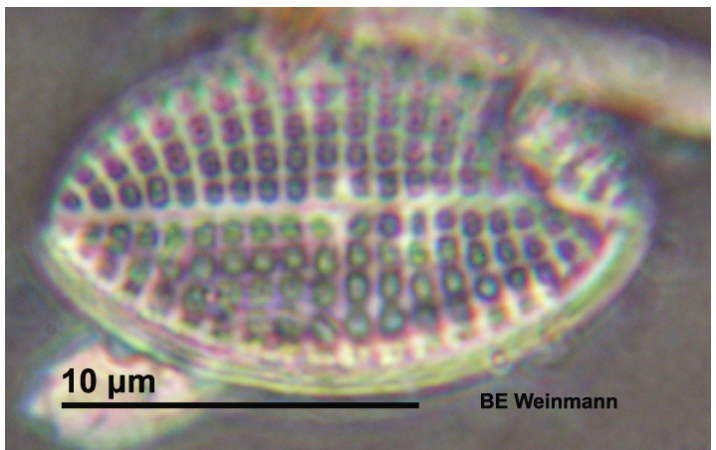
101_127	Navicula viminoides Giffen 1975 [Ribeiro ?]
Specimens Measured:	10
Aspect:	Valve
Valve symmetry or shape:	Apical sym = Isobilateral, Transapical sym = Isopolar, Valve shape = Broadly lanceolate, Valve curvature = None, Frustral shape = na
Dimensions µm [AA]:	7.4 - (9.3) - 13.2
Dimensions µm [TA]:	3.7 - (4.7) - 6.6
Raphe:	Raphe, location = Central, shape = 'Linear, straight', central endings = 'Straight, slightly inflated', polar endings = 'Not resolved'
Striae:	13 - 15 per 10µm, orientation = 'Transverse, parallel or slightly radiate', pores = 'Punctate', Not resolved per 10µm
Fibulae or Costae:	
Axial area:	axial area = 'Linear, narrow' , central area = Round (though one side slightly angular), central nodule = Small and bright, terminal nodule = Small and bright, other hyaline areas = none
Other Features:	Spines = None; Comments = 'I'm not entirely sure about this but its the best match'; Other = 'na'
Image path:	Catalogue3\Cat3-Ref101\Cat3-Ref101-127_2012-03-21-c103.jpg



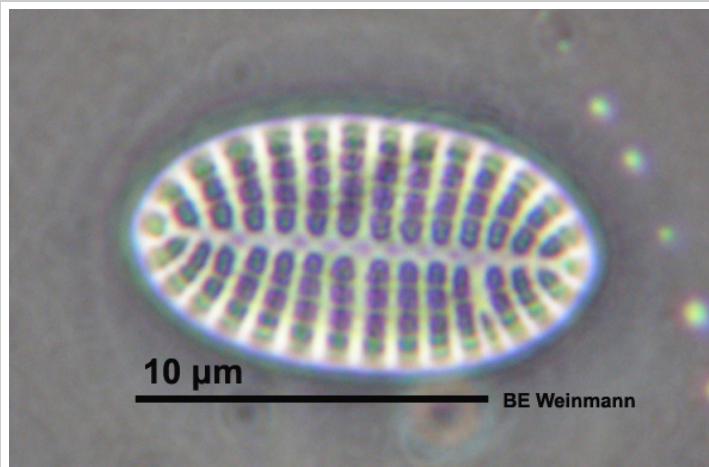
102_130	Scolioneis sp2 cf. brunkseiensis [Witkowski et al 2000]
Specimens Measured:	4
Aspect:	Valve
Valve symmetry or shape:	Apical sym = Isobilateral, Transapical sym = Isopolar, Valve shape = Lanceolate, Valve curvature = Perhaps slight convex, Frustral shape = na
Dimensions µm [AA]:	36.8 - (43.2) - 61
Dimensions µm [TA]:	9.6 - (12.5) - 18.4
Raphe:	Raphe, location = Central, shape = 'Linear, oblique', central endings = 'Not resolved', polar endings = 'Not resolved'
Striae:	16 - 19 per 10µm, orientation = 'Transverse, parallel and slightly radiate', pores = 'Punctate', Not resolved per 10µm
Fibulae or Costae:	
Axial area:	axial area = 'Narrow, linear, oblique' , central area = Rectangular or butterfly-shaped expansion to margins (as Stauroneis), central nodule = Not visible, terminal nodule = not visible, other hyaline areas = na
Other Features:	Spines = None; Comments = 'na'; Other = 'na'
Image path:	Catalogue3\Cat3-Ref102\Cat3-Ref102-130_2012-03-24-c200.jpg
	

103_131	Navicula abscondita Hustedt 1939 [Ribeiro 206, pl.17: 4 - 10]
Specimens Measured:	19
Aspect:	Valve
Valve symmetry or shape:	Apical sym = Isobilateral, Transapical sym = Isopolar, Valve shape = Lanceolate, Valve curvature = None, Frustral shape = na
Dimensions µm [AA]:	22.1 - (26.3) - 39.7
Dimensions µm [TA]:	1.47 - (6.2) - 7.4
Raphe:	Raphe, location = Central, shape = 'Linear', central endings = 'Straight, tiny pinhead inflation', polar endings = 'Not resolved'
Striae:	14 - 17 per 10µm, orientation = 'Transverse, parallel', pores = 'Not resolved', Not resolved per 10µm
Fibulae or Costae:	
Axial area:	axial area = 'Narrow, linear' , central area = Very small rounded, central nodule = Small, round and very bright, terminal nodule = Small, round and very bright, other hyaline areas = None
Other Features:	Spines = None; Comments = 'na'; Other = 'na'
Image path:	Catalogue3\Cat3-Ref103\Cat3-Ref103-131_2012-03-24-c44.jpg
	

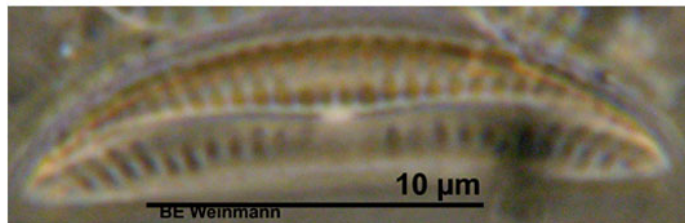
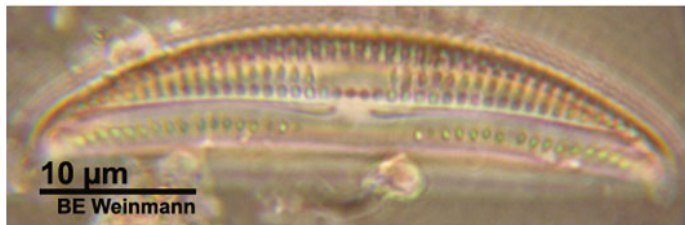
103_159	Navicula abscondita (Girdle) Hustedt 1939 [Ribeiro 206, pl.17: 4 - 10]
Specimens Measured:	4
Aspect:	Girdle
Valve symmetry or shape:	
Dimensions µm [AA]:	25.7 - (25.7) - 25.7
Dimensions µm [PA]:	1.47 - (1.5) - 1.47
Raphe:	NA, location = NA, shape = 'NA', central endings = 'NA', polar endings = 'NA'
Striae:	16 - 18 per 10µm, orientation = 'Transverse, parallel', pores = 'Not resolved', na per 10µm
Fibulae or Costae:	
Axial area:	axial area = 'NA' , central area = NA, central nodule = Visible, bright, terminal nodule = Slight marginal thickening , other hyaline areas = NA
Other Features:	Spines = None; Comments = 'na'; Other = 'na'
Image path:	Catalogue3\Cat3-Ref103\Cat3-Ref103-159_2012-04-14-c178.jpg
	

104_133	Cocconeis scutellum var. parva SV (Grunow) Cleve in Van Heurck [ADIAC, p. 3 # 24 - 26]
Specimens Measured:	1
Aspect:	Valve
Valve symmetry or shape:	Apical sym = Isobilateral, Transapical sym = Isopolar, Valve shape = Elliptic, Valve curvature = Slight curvature so edges not visible, Frustral shape = na
Dimensions µm [AA]:	16.9 - (0) - na
Dimensions µm [TA]:	11 - (0) - na
Raphe:	Sternum, location = Central, shape = 'NA', central endings = 'NA', polar endings = 'NA'
Striae:	11 - 12 per 10µm, orientation = 'Transverse, parallel becoming radiate', pores = 'Punctate', 10 per 10µm
Fibulae or Costae:	
Axial area:	axial area = 'Linear, narrow' , central area = None, central nodule = None, terminal nodule = None, other hyaline areas = na
Other Features:	Spines = None; Comments = 'na'; Other = 'na'
Image path:	Catalogue3\Cat3-Ref104\Cat3-Ref104-133_2012-04-12-c120.jpg
	

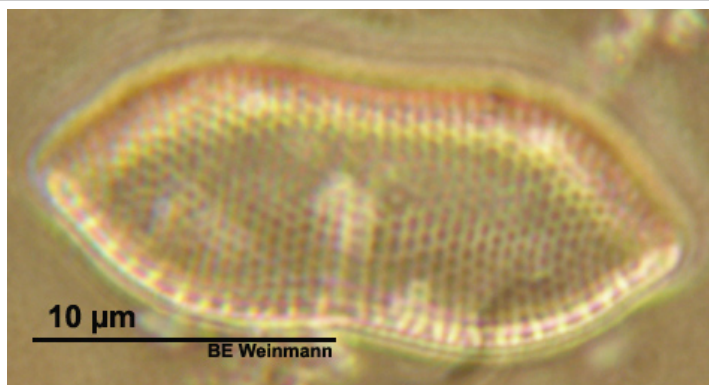
104_150	Cocconeis scutellum var. parva SV (Grunow) Cleve in Van Heurck [ADIAC, p. 3 # 24 - 26]
Specimens Measured:	1
Aspect:	Valve
Valve symmetry or shape:	Apical sym = na, Transapical sym = na, Valve shape = Elliptic, Valve curvature = None, Frustral shape = NA
Dimensions µm [AA]:	13.2 - (0) - na
Dimensions µm [TA]:	7.4 - (0) - na
Raphe:	Sternum, location = Central, shape = 'NA', central endings = 'NA', polar endings = 'NA'
Striae:	10 - 12 per 10µm, orientation = 'Transverse, parallel becoming transverse', pores = 'Clearly punctate', 10 - 14 per 10µm
Fibulae or Costae:	
Axial area:	axial area = 'Linear, narrow' , central area = None, central nodule = None, terminal nodule = None, other hyaline areas = None
Other Features:	Spines = None; Comments = 'na'; Other = 'na'
Image path:	Catalogue3\Cat3-Ref104\Cat3-Ref104-150_2012-04-14-c147.jpg



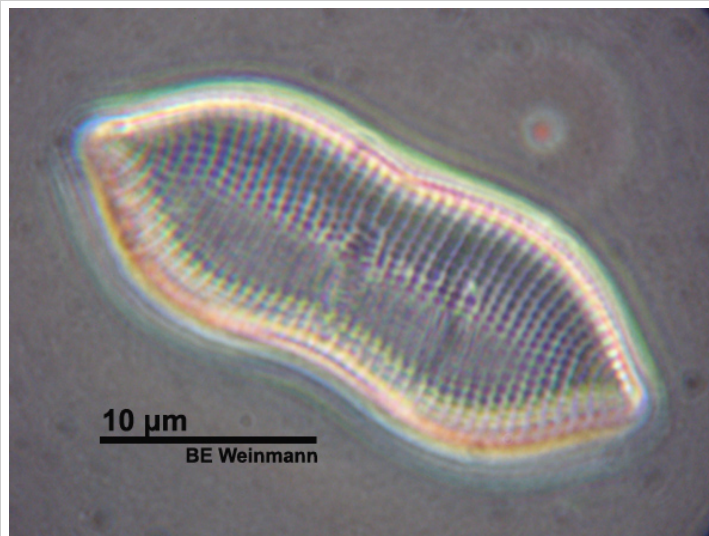
105_139	Amphora helenensis [?]
Specimens Measured:	8
Aspect:	Valve
Valve symmetry or shape:	Apical sym = Dorsiventral, Transapical sym = Isopolar, Valve shape = Lunate, Valve curvature = Somewhat along TA, Frustral shape = na
Dimensions µm [AA]:	22.1 - (30.6) - 39.7
Dimensions µm [TA]:	4.4 - (7) - 8.8
Raphe:	Raphe, location = Central, shape = 'Arcuate', central endings = 'Central endings curve to ventral side and then curl back up to dorsal side (like a Poirot moustache) to distant, inflated endings ', polar endings = 'Curve to ventral side'
Striae:	12 - 16 per 10µm, orientation = 'Transverse, slightly radiate', pores = 'Punctate', 10 - 12 per 10µm
Fibulae or Costae:	
Axial area:	axial area = 'Arcuate' , central area = One sided rounded or lanceolate TA expansion, central nodule = Rectangular or elliptic, terminal nodule = Not visible, other hyaline areas = Half of the ventral area is clear except for a central strip of stria. There is also a rectangular hyaline area central on AA and TA on the dorsal side.
Other Features:	Spines = None; Comments = 'na'; Other = 'na'
Image path:	Catalogue3\Cat3-Ref105\Cat3-Ref105-139_2012-03-29-c102_combined.jpg

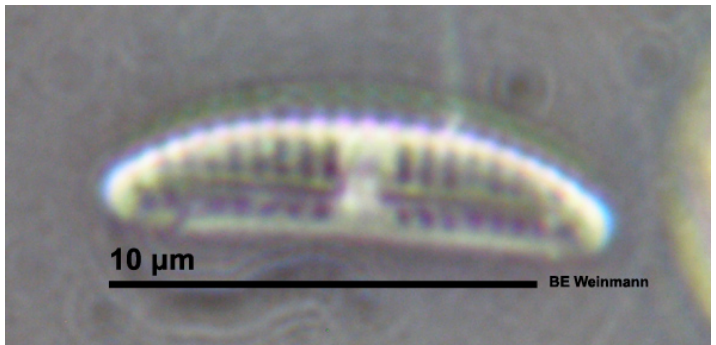


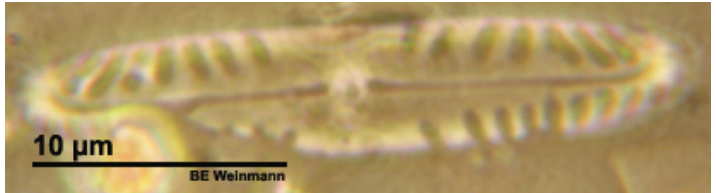
106_140	Nitzschia coarctata [Witk. et al 183: 11 - 12, 186: 4 - 13]
Specimens Measured:	7
Aspect:	Valve
Valve symmetry or shape:	Apical sym = Isobilateral, Transapical sym = Isopolar, Valve shape = Panduriform, Valve curvature = None, Apex shape = inflection, Shape = 'Very slightly protracted sub-rostrate', Frustral shape = NA
Dimensions µm [AA]:	19.1 - (24.8) - 33.1
Dimensions µm [TA]:	5.1 - (8.3) - 9.6
Raphe:	Raphe (by proxy of fibulae), location = Eccentric, shape = 'Marginal', central endings = 'NA', polar endings = 'NA'
Striae:	20 - 22 per 10µm, orientation = 'Transverse, parallel', pores = 'Clearly punctate', 18 - 20 per 10µm
Fibulae or Costae:	fibulae = 13 - 15 per 10µm, Irregular, some crooked, bright
Axial area:	axial area = 'NA' , central area = NA, central nodule = NA, terminal nodule = NA, other hyaline areas = na
Other Features:	Spines = None; Comments = 'There is one in Witkowski which is unnamed and undescribed, just picture pl183: 11 - 12.'; Other = 'na'
Image path:	Catalogue3\Cat3-Ref106\Cat3-Ref106-140_2012-03-29-c19.jpg

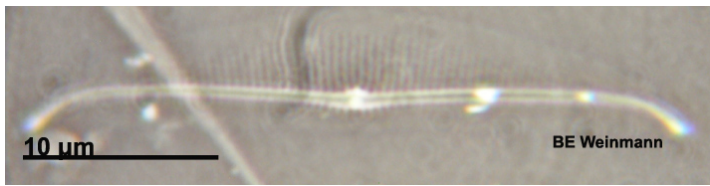



106_176	Tryblionella coarctata (Grunow) Mann in Round et al 1990 [BMB5: 496]
Specimens Measured:	3
Aspect:	Valve
Valve symmetry or shape:	Apical sym = Isobilateral, Transapical sym = Isopolar, Valve shape = Panduriform, Valve curvature = Possibly, parts of valve on different plane of focus, Frustral shape = NA
Dimensions μm [AA]:	22 - (25.2) - 29.4
Dimensions μm [TA]:	9.6 - (10.1) - 11
Raphe:	None visible, location = NA, shape = 'Marginal', central endings = 'NA', polar endings = 'NA'
Striae:	16 - 18 per 10 μm , orientation = 'Transverse, parallel', pores = 'Clearly punctate', 18 per 10 μm
Fibulae or Costae:	
Axial area:	axial area = 'None' , central area = None, central nodule = None, terminal nodule = None, other hyaline areas = None
Other Features:	Spines = None; Comments = 'Not sure whether this is the same as Nitzschia coarctata (106-140) as their is no marginal fibulae visible and the unfocused portion of the valve makes it look more like a Tryblionella. However, ADIAC Tryblionella and Nitzschia coarctata are the same (then again, it wasn't N. coarctata but something similar in Witkowski)'; Other = 'na'
Image path:	Catalogue3\Cat3-Ref106\Cat3-Ref106-176_2012-04-14-c117.jpg

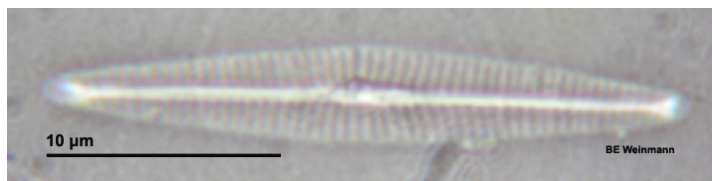


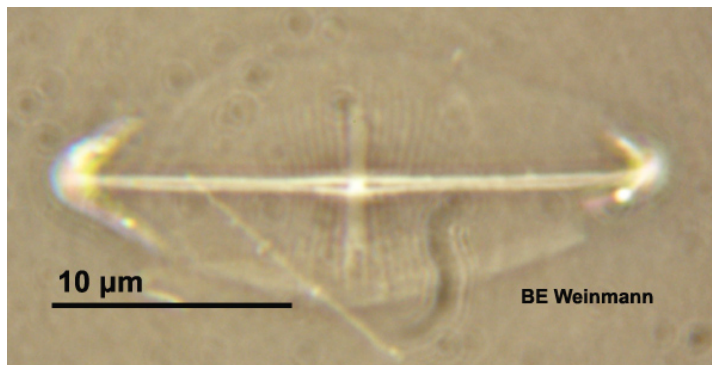
107_142	Amphora sp. 5 [?]
Specimens Measured:	2
Aspect:	Valve
Valve symmetry or shape:	Apical sym = Dorsiventral, Transapical sym = Isopolar, Valve shape = Lunate, Valve curvature = Semi-lunate, Frustral shape = na
Dimensions µm [AA]:	11 - (11.4) - 11.8
Dimensions µm [TA]:	5.1 - (8.7) - 11
Raphe:	Raphe, location = Central, shape = 'Arcuate (ends toward ventral)', central endings = 'Straight, slightly inflated, slightly distant', polar endings = 'Not visible'
Striae:	17 - 19 per 10µm, orientation = 'Transverse, parallel or slightly radiate', pores = 'Not resolved', na per 10µm
Fibulae or Costae:	
Axial area:	axial area = 'NA' , central area = NA, central nodule = NA, terminal nodule = NA, other hyaline areas = None
Other Features:	Spines = None; Comments = 'Pretty sure this is different from A. pediculus as the striae are thinner and paler'; Other = 'na'
Image path:	Catalogue3\Cat3-Ref107\Cat3-Ref107-142_2012-04-18-c30.jpg
	

108_144	Pinnularia sp. 2 [?]
Specimens Measured:	1
Aspect:	Valve
Valve symmetry or shape:	Apical sym = Isobilateral, Transapical sym = Isopolar, Valve shape = Linear, Valve curvature = None, Frustral shape = na
Dimensions µm [AA]:	25 - (0) - na
Dimensions µm [TA]:	5.1 - (0) - na
Raphe:	Raphe, location = Central, shape = 'Straight', central endings = 'Inflation to same side and distant', polar endings = 'Curved to same side'
Striae:	9 - 11 per 10µm, orientation = 'Transverse, radiate then convergent', pores = 'Not resolved', na per 10µm
Fibulae or Costae:	
Axial area:	axial area = 'NA' , central area = NA, central nodule = NA, terminal nodule = NA, other hyaline areas = None
Other Features:	Spines = None; Comments = 'na'; Other = 'na'
Image path:	Catalogue3\Cat3-Ref108\Cat3-Ref108-144_2012-03-29-c195.jpg
	

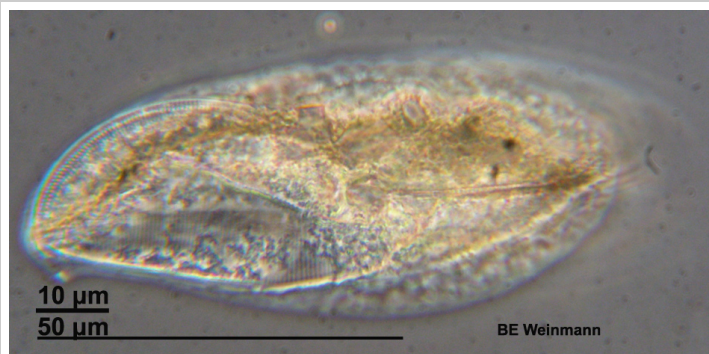
109_154	Amphora lineolata Ehrenberg 1838 [BMB2: #108]
Specimens Measured:	4
Aspect:	Valve
Valve symmetry or shape:	Apical sym = Dorsiventral, Transapical sym = Isopolar, Valve shape = Arcuate, Valve curvature = None, Frustral shape = na
Dimensions µm [AA]:	29.4 - (31.1) - 33.1
Dimensions µm [TA]:	4.4 - (4.9) - 5.1
Raphe:	Raphe, location = Ventral, shape = 'Arcuate', central endings = 'Very slightly deflected to one side and slightly inflated (pinhead)', polar endings = 'Curving to same side'
Striae:	26 - 28 per 10µm, orientation = 'Transverse, parallel becoming radiate', pores = 'Punctate', Not resolved per 10µm
Fibulae or Costae:	
Axial area:	axial area = 'NA' , central area = NA, central nodule = NA, terminal nodule = NA, other hyaline areas = NA
Other Features:	Spines = None; Comments = 'na'; Other = 'na'
Image path:	Catalogue3\Cat3-Ref109\Cat3-Ref109-154_2012-04-07-c28.jpg
	

110_155	Nitzschia dubia Smith 1853 [BMB3: #264]
Specimens Measured:	3
Aspect:	Valve
Valve symmetry or shape:	Apical sym = Isobilateral, Transapical sym = Isopolar, Valve shape = Linear-panduriform, Valve curvature = None, Apex shape = inflection, Shape = 'Slightly protracted, sub-rostrate', Frustral shape = NA
Dimensions µm [AA]:	23.5 - (41.2) - 73.5
Dimensions µm [TA]:	4.4 - (7.1) - 11.8
Raphe:	Raphe (by proxy of fibulae), location = Eccentric, shape = 'Marginal', central endings = 'NA', polar endings = 'NA'
Striae:	19 - 25 per 10µm, orientation = 'Transverse, parallel', pores = 'Punctate', Not resolved per 10µm
Fibulae or Costae:	fibulae = 12 - 14 per 10µm, Moderately long (1/10 TA), irregularly spaced
Axial area:	axial area = 'NA' , central area = NA, central nodule = NA, terminal nodule = NA, other hyaline areas = NA
Other Features:	Spines = None; Comments = 'na'; Other = 'na'
Image path:	Catalogue3\Cat3-Ref110\Cat3-Ref110-155_2012-04-07-c66.jpg
	

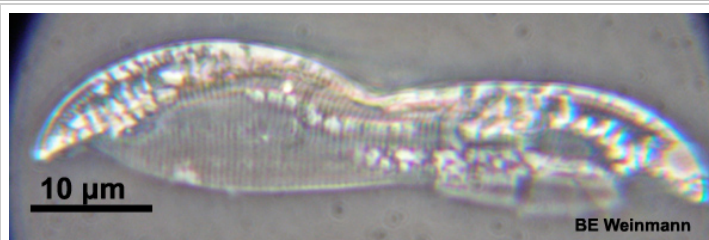
111_156	Navicula duerrenbergiana Hustedt in Schmidt Atlas [Witkowski et al 2000: p276, pl. 116: 8 - 14]
Specimens Measured:	1
Aspect:	Valve
Valve symmetry or shape:	Apical sym = Isobilateral, Transapical sym = Isopolar, Valve shape = Linear-narrowly lanceolate, Valve curvature = None, Frustral shape = na
Dimensions µm [AA]:	16.9 - (0) - 26.5
Dimensions µm [TA]:	4.4 - (0) - 4.4
Raphe:	Raphe, location = Central, shape = 'linear', central endings = 'Straight, very slightly inflated', polar endings = 'Not resolved'
Striae:	19 per 10µm, orientation = 'Transverse, radiate then parallel to perhaps convergent', pores = 'Not resolved', na per 10µm
Fibulae or Costae:	
Axial area:	axial area = 'Very narrow' , central area = Narrowly lanceolate, central nodule = Small, slightly elongated, terminal nodule = Visible, other hyaline areas = na
Other Features:	Spines = None; Comments = 'Very similar to Navicula lanceolata but the central endings are not distant'; Other = 'na'
Image path:	Catalogue3\Cat3-Ref111\Cat3-Ref111-156_2012-04-07-c28.jpg
	

112_161	Navicula sp.4 [?]
Specimens Measured:	1
Aspect:	Valve
Valve symmetry or shape:	Apical sym = Isobilateral, Transapical sym = Isopolar, Valve shape = Linear, Valve curvature = None, Frustral shape = na
Dimensions µm [AA]:	25.7 - (0) - na
Dimensions µm [TA]:	11 - (0) - na
Raphe:	Raphe, location = Central, shape = 'Straight', central endings = 'Straight, slightly longitudinally inflated', polar endings = 'Not visible'
Striae:	na per 10µm, orientation = 'na', pores = 'na', na per 10µm
Fibulae or Costae:	
Axial area:	axial area = 'na' , central area = na, central nodule = na, terminal nodule = na, other hyaline areas = na
Other Features:	Spines = na; Comments = 'na'; Other = 'na'
Image path:	Catalogue3\Cat3-Ref112\Cat3-Ref112-161_2012-04-08-c9.jpg
	

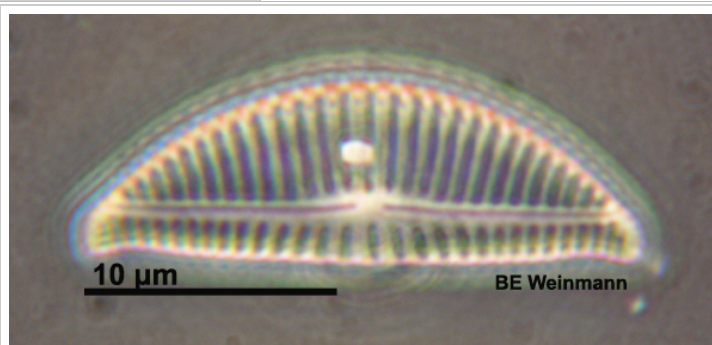
113_162	Amphiprora alata (Ehrenberg) Kützing [Hendey p253, pl XXXIX: 14 - 16]
Specimens Measured:	2
Aspect:	Valve
Valve symmetry or shape:	Apical sym = Isobilateral, Transapical sym = Isopolar, Valve shape = Linear-lanceolate, Valve curvature = Yes, Frustral shape = na
Dimensions µm [AA]:	80.9 - (81.6) - 82.3
Dimensions µm [TA]:	22.1 - (24.7) - 27.2
Raphe:	Raphe, location = Central, sigmoid wing, shape = 'Sigmoid on wing', central endings = 'Not visible', polar endings = 'Not visible'
Striae:	15 - 19 per 10µm, orientation = 'Transverse, parallel', pores = 'Puntate', 30 - 33 per 10µm
Fibulae or Costae:	
Axial area:	axial area = 'None' , central area = None, central nodule = None visible, terminal nodule = None visible, other hyaline areas = na
Other Features:	Spines = None; Comments = 'na'; Other = 'na'
Image path:	Catalogue3\Cat3-Ref113\Cat3-Ref113-162_2012-04-08-c55.jpg



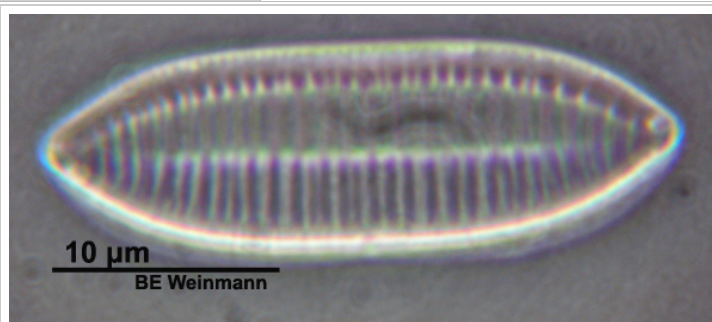
113_182	Amphiprora alata Girdle (Ehrenberg) Kützing [Hendey p253, pl. XXXIX: 14 - 16]
Specimens Measured:	1
Aspect:	Girdle
Valve symmetry or shape:	
Dimensions µm [AA]:	53.7 - (0) - na
Dimensions µm [PA]:	5.9 - (0) - na
Raphe:	Raphe, location = Central, shape = 'Wing', central endings = 'NA', polar endings = 'NA'
Striae:	20 per 10µm, orientation = 'Transverse, parallel', pores = 'Punctate', Not resolved per 10µm
Fibulae or Costae:	
Axial area:	axial area = 'NA' , central area = NA, central nodule = NA, terminal nodule = NA, other hyaline areas = None
Other Features:	Spines = None; Comments = 'na'; Other = 'na'
Image path:	Catalogue3\Cat3-Ref113\Cat2-Ref113-182_2012-04-18-c133.jpg

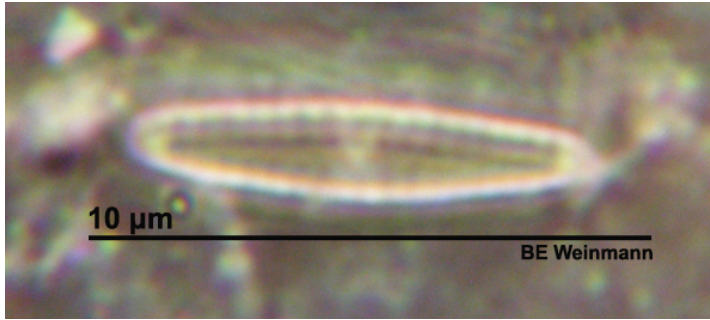


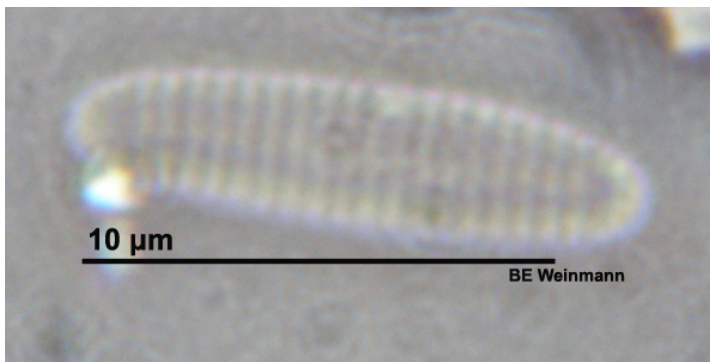
114_163	Encyonema caespitosum Kützinger 1849 [BMB1: #42, EAD]
Specimens Measured:	1
Aspect:	Valve
Valve symmetry or shape:	Apical sym = Dorsiventral , Transapical sym = Isopolar, Valve shape = Lunate, Valve curvature = None, Apex shape = inflection, Shape = 'Protracted, sub-rostrate, bent towards ventral ', Frustral shape = na
Dimensions µm [AA]:	22.1 - (0) - na
Dimensions µm [TA]:	7.4 - (0) - na
Raphe:	Raphe, location = Ventral, shape = 'Straight', central endings = 'Distant, slightly curved to dorsal side', polar endings = 'Straight'
Striae:	12 - 14 per 10µm, orientation = 'Transverse, parallel becoming radiate central striae ', pores = 'Not resolved', na per 10µm
Fibulae or Costae:	
Axial area:	axial area = 'Linear, narrow' , central area = Very slightly elliptic, central nodule = Easily visible, bright, terminal nodule = Very small but bright, other hyaline areas = na
Other Features:	Spines = None; Comments = 'na'; Other = 'na'
Image path:	Catalogue3\Cat3-Ref114\Cat3-Ref114-163_2012-04-10-c65.jpg

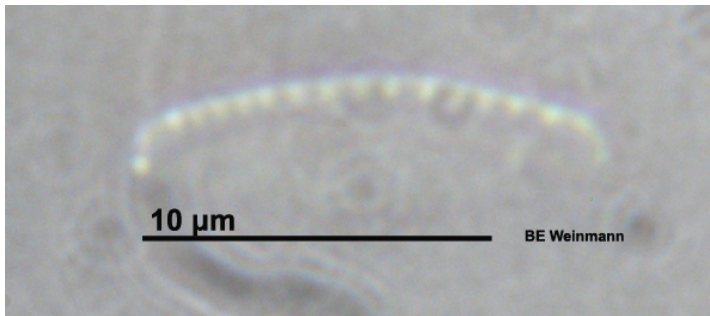


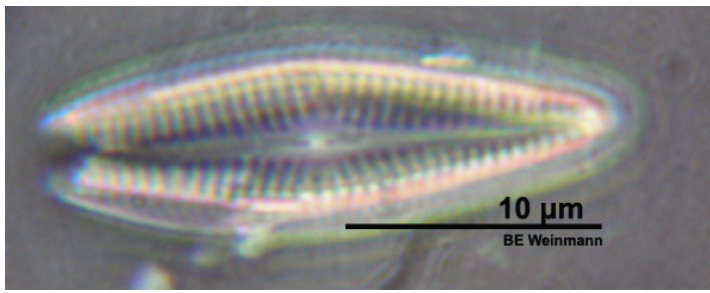
115_164	Tryblionella salinarum (Grunow in Cleve & Grunow) Pelletan 1889 [BMB3: #299]
Specimens Measured:	1
Aspect:	Valve
Valve symmetry or shape:	Apical sym = Isobilateral, Transapical sym = Isopolar, Valve shape = Linear, very slightly cinching at centre, Valve curvature = None, Apex shape = inflection, Shape = 'Very slightly protracted, sub-rostrate', Frustral shape = na
Dimensions µm [AA]:	27.2 - (0) - na
Dimensions µm [TA]:	8.8 - (0) - na
Raphe:	Sternum, location = na, shape = 'NA', central endings = 'NA', polar endings = 'NA'
Striae:	12 - 14 per 10µm, orientation = 'Transverse, parallel', pores = 'Not resolved', na per 10µm
Fibulae or Costae:	
Axial area:	axial area = 'Linear, narrow' , central area = None, central nodule = None visible, terminal nodule = None visible, other hyaline areas = na
Other Features:	Spines = None; Comments = 'na'; Other = 'na'
Image path:	Catalogue3\Cat3-Ref115\Cat3-Ref115-164_2012-04-10-cl15.jpg



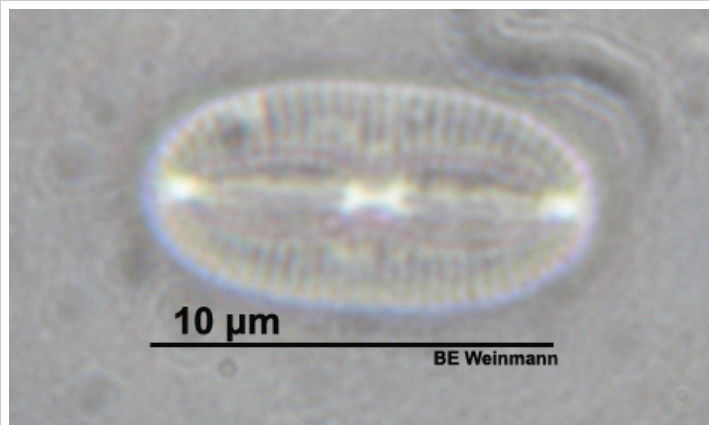
116_166	Navicula starmachioides [BMB5: #458]
Specimens Measured:	5
Aspect:	Valve
Valve symmetry or shape:	Apical sym = Isobilateral, Transapical sym = Isopolar, Valve shape = Linear or very narrowly lanceolate, Valve curvature = Possibly slightly folded along AA, Frustral shape = NA
Dimensions µm [AA]:	7.4 - (9.4) - 12.5
Dimensions µm [TA]:	1.5 - (2) - 2.2
Raphe:	Raphe, location = Central, shape = 'Linear', central endings = 'Not resolved', polar endings = 'Not resolved'
Striae:	16 - 19 per 10µm, orientation = 'Transverse, slightly radiate', pores = 'Not resolved', na per 10µm
Fibulae or Costae:	
Axial area:	axial area = 'Linear' , central area = H - shaped hyaline reaching margins, central nodule = Small and bright, terminal nodule = Small and bright, other hyaline areas = Apices appear hyaline (ie final striae distant from apices)
Other Features:	Spines = None; Comments = 'The specimen was hard to see clearly but appeared to linear to be Navicula perminuta'; Other = 'na'
Image path:	Catalogue3\Cat3-Ref116\Cat3-Ref116-166_2012-04-12-cl16.jpg
	

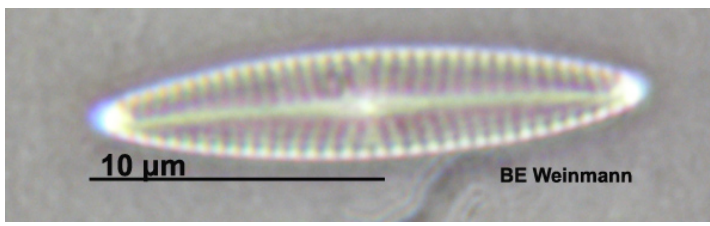
117_151	Fragilariopsis cylindricus (Grunow) Krieger in Helmcke & Krieger 1954 [Witkowski ?; BMB ?]
Specimens Measured:	2
Aspect:	Valve
Valve symmetry or shape:	Apical sym = na, Transapical sym = na, Valve shape = Cylindrical, Valve curvature = None, Frustral shape = NA
Dimensions µm [AA]:	12.1 - (12.3) - 12.5
Dimensions µm [TA]:	2.9 - (3.1) - 3.3
Raphe:	Neither visible, location = NA, shape = 'NA', central endings = 'NA', polar endings = 'NA'
Striae:	17 - 20 per 10µm, orientation = 'Transverse, parallel', pores = 'Not resolved', na per 10µm
Fibulae or Costae:	
Axial area:	axial area = 'None' , central area = None, central nodule = None, terminal nodule = None, other hyaline areas = None
Other Features:	Spines = none; Comments = 'na'; Other = 'na'
Image path:	Catalogue3\Cat3-Ref117\Cat3-Ref117-151_2012-04-14-c29.jpg
	


118_168	Nitzschia sp.2 [?]
Specimens Measured:	2
Aspect:	Valve
Valve symmetry or shape:	Apical sym = Isobilateral, Transapical sym = Isopolar, Valve shape = Lanceolate, Valve curvature = None, Frustral shape = NA
Dimensions µm [AA]:	7.4 - (10.3) - 13.2
Dimensions µm [TA]:	2.9 - (2.9) - 2.9
Raphe:	Raphe (by proxy of fibulae), location = Eccentric, shape = 'Marginal', central endings = 'NA', polar endings = 'NA'
Striae:	Not resolved per 10µm, orientation = 'NA', pores = 'NA', na per 10µm
Fibulae or Costae:	fibulae = 12 per 10µm, Short, regularly spaced
Axial area:	axial area = 'NA' , central area = NA, central nodule = NA, terminal nodule = NA, other hyaline areas = NA
Other Features:	Spines = None; Comments = 'na'; Other = 'na'
Image path:	Catalogue3\Cat3-Ref118\Cat3-Ref118-168_2012-04-13-c30.jpg
	

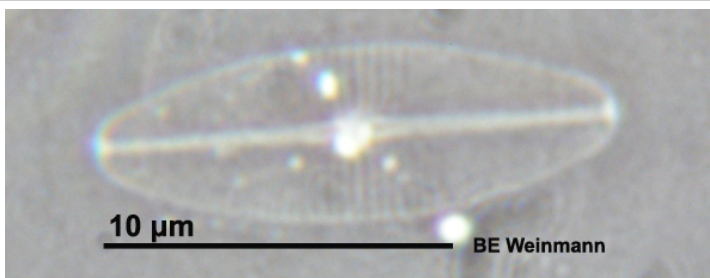
119_174	Navicula sensu lato sp. 5 [?]
Specimens Measured:	1
Aspect:	Valve
Valve symmetry or shape:	Apical sym = na, Transapical sym = na, Valve shape = Diamond, Valve curvature = Convex, Frustral shape = NA
Dimensions µm [AA]:	22.1 - (0) - na
Dimensions µm [TA]:	5.9 - (0) - na
Raphe:	Raphe, location = Central, shape = 'Linear', central endings = 'Slightly deflected to same side and slightly inflated', polar endings = 'Not resolved'
Striae:	16 - 19 per 10µm, orientation = 'Transverse, radiate', pores = 'Not resolved', na per 10µm
Fibulae or Costae:	
Axial area:	axial area = 'Diamond shaped' , central area = Not distinct from axial area, central nodule = Small, elliptic, terminal nodule = Not visible, other hyaline areas = None
Other Features:	Spines = none; Comments = 'na'; Other = 'na'
Image path:	Catalogue3\Cat3-Ref119\Cat3-Ref119-174_2012-04-14-c81.jpg
	

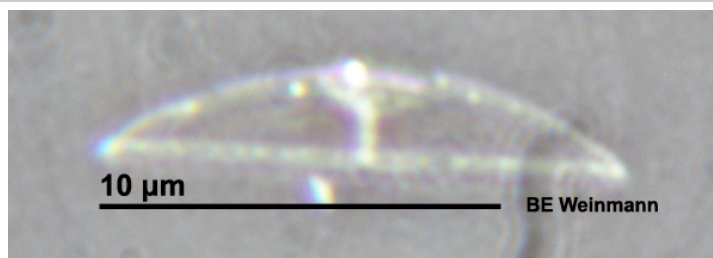
120_175	Fallacia sp. 2 [?]
Specimens Measured:	2
Aspect:	Valve
Valve symmetry or shape:	Apical sym = na, Transapical sym = na, Valve shape = Elliptic, Valve curvature = None, Frustral shape = NA
Dimensions µm [AA]:	11 - (0) - na
Dimensions µm [TA]:	5.9 - (0) - na
Raphe:	Raphe, location = Central, shape = 'Linear', central endings = 'Distant, straight, slightly inflated (pinheads)', polar endings = 'Not resolved (appear to terminate straight and well before margin)'
Striae:	26 - 28 per 10µm, orientation = 'Transverse, parallel becoming radiate', pores = 'Not resolved', na per 10µm
Fibulae or Costae:	
Axial area:	axial area = 'Linear, narrow' , central area = Rectangular expansion covering central 1/3 of TA width, central nodule = Central nodules connected by bridge (like spectacles), terminal nodule = Quite large, irregularly shaped, bright, and well in from margin of cell, other hyaline areas = Striae interrupted by hyaline fingers extending from central area creating a lyre-shape (or curved H shaped) centred in centre of cell
Other Features:	Spines = none; Comments = 'This is definitely not Fallacia susprii, striae are finer and central endings of raphe much more distant.'; Other = 'na'
Image path:	Catalogue3\Cat3-Ref120\Cat3-Ref120-175_2012-04-14-c84.jpg

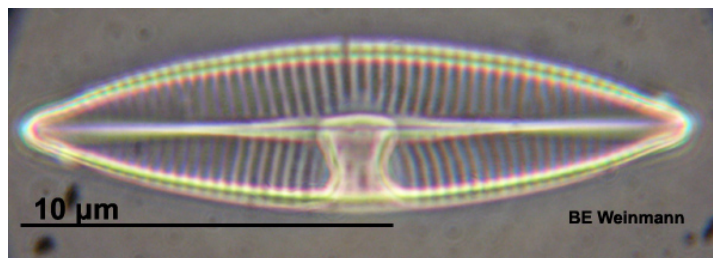


122_170	Navicula microdigitatoradiata Lange-Bertalot [witkowski et al 2000, p.290, pl. 126: 1 - 7]
Specimens Measured:	1
Aspect:	Valve
Valve symmetry or shape:	Apical sym = Isobilateral, Transapical sym = Isopolar, Valve shape = Narrowly lanceolate, Valve curvature = None, Frustral shape = NA
Dimensions µm [AA]:	18.4 - (0) - na
Dimensions µm [TA]:	3.7 - (0) - na
Raphe:	Raphe, location = Central, shape = 'Linear', central endings = 'Straight, slightly inflated ', polar endings = 'Not resolved'
Striae:	18 per 10µm, orientation = 'Transverse, radiate becoming parallel to convergent', pores = 'Punctate', 28 - 30 per 10µm
Fibulae or Costae:	
Axial area:	axial area = 'Linear' , central area = Narrowly lanceolate, central nodule = Small and round, terminal nodule = Large, appears to cover entire apex, other hyaline areas = None
Other Features:	Spines = None; Comments = 'Initially wasn't sure whether this wasn't just Navicula phyllepta (14 - 29) but the central striae seem more distant and clearly punctate (thicker)'; Other = 'na'
Image path:	Catalogue3\Cat3-Ref122\Cat3-Ref122-170_2012-04-14-c40.jpg
	

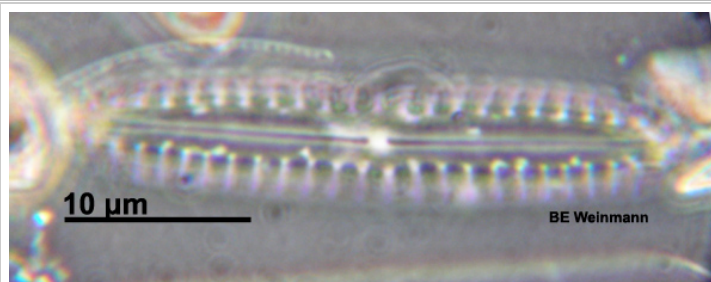
122_179	Navicula microdigitatoradiata Lange-Bertalot [Witkowski et al 2000, p.290, pl. 126: 1 - 7]
Specimens Measured:	1
Aspect:	Valve
Valve symmetry or shape:	Apical sym = Isobilateral, Transapical sym = Isopolar, Valve shape = Narrowly lanceolate, Valve curvature = None, Frustral shape = NA
Dimensions µm [AA]:	29.4 - (0) - na
Dimensions µm [TA]:	5.9 - (0) - na
Raphe:	Raphe, location = Central, shape = 'Linear', central endings = 'Straight, Inflated longitudinally', polar endings = 'Not resolved'
Striae:	17 - 19 per 10µm, orientation = 'Transverse, radiate becoming parallel', pores = 'Not resolved', na per 10µm
Fibulae or Costae:	
Axial area:	axial area = 'Linear, narrow' , central area = Narrowly lanceolate, central nodule = Small, not bright, rectangular or elliptic, terminal nodule = Bright and seems to fill apices, other hyaline areas = None
Other Features:	Spines = None; Comments = 'Navicula microdigitatoradiata?'; Other = 'na'
Image path:	Catalogue3\Cat3-Ref122\Cat3-Ref122-179_2012-04-18-c198.jpg
	

123_177	Achnanthes bremeyeri RV Lange-Bertalot 1989 [BMB4: #301]
Specimens Measured:	3
Aspect:	Valve
Valve symmetry or shape:	Apical sym = Isobilateral, Transapical sym = Isopolar, Valve shape = Lanceolate or Elliptic, Valve curvature = None, Frustral shape = NA
Dimensions µm [AA]:	13.2 - (0) - na
Dimensions µm [TA]:	5.1 - (0) - na
Raphe:	Raphe, location = Central, shape = 'Linear', central endings = 'Straight, slightly distant and inflated ', polar endings = 'Not resolved'
Striae:	28 - 29 per 10µm, orientation = 'Transverse, Parallel', pores = 'Not resolved', na per 10µm
Fibulae or Costae:	
Axial area:	axial area = 'Linear' , central area = Narrowly lanceolate, central nodule = Large and irregular, terminal nodule = Small and marginal , other hyaline areas = Most of cell
Other Features:	Spines = None; Comments = 'This is similar to the Fallacia (19-36) except in that there's hint of lyre-shaped hyaline areas and no striae'; Other = 'na'
Image path:	Catalogue3\Cat3-Ref123\Cat3-Ref123-177_2012-04-14-c106.jpg
	

124_181	Amphora staurophora Juhlin-Dannfelt 1882 [BMB4: #318]
Specimens Measured:	2
Aspect:	Valve
Valve symmetry or shape:	Apical sym = Dorsiventral, Transapical sym = Isopolar, Valve shape = Lunate, Valve curvature = None, Frustral shape = NA
Dimensions µm [AA]:	13.2 - (13.6) - 14
Dimensions µm [TA]:	2.9 - (3.3) - 3.7
Raphe:	Raphe, location = Ventral, shape = 'Straight', central endings = 'Straight, inflated', polar endings = 'Straight'
Striae:	Not resolved per 10µm, orientation = 'NA ', pores = 'NA ', na per 10µm
Fibulae or Costae:	
Axial area:	axial area = 'Narrow' , central area = Hyaline are expands all the way to the dorsal margin, central nodule = Small and round, terminal nodule = Small and round, other hyaline areas = Hyaline area expands before dorsal edge, thats what makes it look similar to Catenula adherans
Other Features:	Spines = None; Comments = '2nd Nodule midway between raphe and dorsal edge'; Other = 'na'
Image path:	Catalogue3\Cat3-Ref124\Cat3-Ref124-181_2012-04-18-c92.jpg
	

125_184	Navicula sensu lato sp. 6 [?]
Specimens Measured:	1
Aspect:	Valve
Valve symmetry or shape:	Apical sym = Isobilateral, Transapical sym = Isopolar, Valve shape = Narrowly lanceolate, Valve curvature = None, Frustral shape = NA
Dimensions µm [AA]:	17.6 - (0) - na
Dimensions µm [TA]:	7.4 - (0) - na
Raphe:	Raphe, location = Central, shape = 'Linear', central endings = 'Strongly approximate', polar endings = 'Not resolved'
Striae:	29 per 10µm, orientation = 'Transverse, radiate becoming convergent near poles', pores = 'Not resolved', na per 10µm
Fibulae or Costae:	
Axial area:	axial area = 'Narrow and linear but expands towards poles and centre' , central area = Asymmetric (one-sided), rounded, central nodule = None, terminal nodule = None, other hyaline areas = Thickened, transverse hyaline area on one side (reaches just beyond raphe) with a distinct outline, a weakly convex top and strongly concave sides.
Other Features:	Spines = None; Comments = 'na'; Other = 'na'
Image path:	Catalogue3\Cat3-Ref125\Cat3-Ref125-184_2012-04-18-c97.jpg
	

126_186	<i>Biremis ambigua</i> (Cleve) Mann [Witk. et al 2000, p158, pl155: 2 -6] or <i>Biremis</i> sp. 154 [Witk. Et al 2000, pl154: 9 - 10]
Specimens Measured:	1
Aspect:	Valve (and margin)
Valve symmetry or shape:	
Dimensions µm [AA]:	35.3 - (0) - na
Dimensions µm [PA]:	na - (0) - na
Raphe:	Raphe, location = Central, shape = 'Linear', central endings = 'Very short, inflated and slightly bent section at end', polar endings = 'Not resolved'
Striae:	8 per 10µm, orientation = 'Transverse, parallel or slightly radiate', pores = 'Not resolved', Not resolved per 10µm
Fibulae or Costae:	
Axial area:	axial area = 'Broad and linear' , central area = Not distinct from axial area, central nodule = Round and bright, terminal nodule = Not visible, other hyaline areas = None
Other Features:	Spines = None; Comments = 'na'; Other = 'na'
Image path:	Catalogue3\Cat3-Ref126\Cat3-Ref126-186_2012-04-18-c146.jpg



127_137	<i>Achnanthes rossi</i> RV Hustedt 1954 [BMB4: #310]
Specimens Measured:	1
Aspect:	Valve
Valve symmetry or shape:	Apical sym = Isobilateral, Transapical sym = Isopolar, Valve shape = Lanceolate, Valve curvature = None, Apex shape = inflection, Shape = 'Protracted sub-rostrate', Frustral shape = NA
Dimensions µm [AA]:	15.4 - (0) - na
Dimensions µm [TA]:	6.6 - (0) - na
Raphe:	Raphe, location = Central, shape = 'Linear', central endings = 'Straight, inflated, slightly distant', polar endings = 'Not resolved'
Striae:	18 - 20 per 10µm, orientation = 'Transverse, radiate', pores = 'Not resolved', na per 10µm
Fibulae or Costae:	
Axial area:	axial area = 'Linear, narrow' , central area = Butterfly-shaped, central nodule = Large and bright, terminal nodule = Appear to cover the entire apex, other hyaline areas = na
Other Features:	Spines = None; Comments = 'na'; Other = 'na'
Image path:	Catalogue3\Cat3-Ref127\Cat3-Ref127-137_2012-04-12-c120.jpg



1_1	Merismopodea
Type:	Cyano1-chain&sheet
Desc:	Beaded chains (trichomes), the tip of them are rounded. What looks like a cell is pinched in the middle (pretty sure this is the normal taxonomy of the cell not the cells dividing as they are all the same) or sheets of loosely packed rounded cells (otherwise just like chains)
Aspect:	NA
Image:	

2_2	Lyngbya or Oscillatoria [http://www.dr-ralf-wagner.de/index-englisch.htm]
Type:	Cyano2
Desc:	like a green ladder
Aspect:	NA
Image:	

3_3	Possibly Oscillatoria [as above] but this is thinner more gracile and with pointed ends
Type:	Cyano3
Desc:	Like a blade of grass but rounded (some are pointed) at both ends. You can see demarcations inside the blade but they do not have "width", rather than being like a ladder, its more like pencil lines drawn across a blade
Aspect:	NA
Image:	

4_4	Cyanobacteria [?]
Type:	Cyano4
Desc:	Spiral, nothing else recorded
Aspect:	NA
Image:	

5_5	Achnanthes spp.
Type:	Achn?20
Desc:	"Achnanthoid" by which I mean, isopolar and isobilateral, broadly lanceolate usually with protracted apex and AA ?20, plasmids follow Cox (1996).
Aspect:	NA
Image:	

6_6	Achnanthes spp. or Cocconeis spp.
Type:	AchCoc?20
Desc:	Cell is small and elliptical AA ?20, plasmids follow Cox (1996)
Aspect:	Valve
Image:	

7_7	Actinoptychus [ADIAC]
Type:	Actinop
Desc:	Centric diatom (definitely phytoplankton), looks like pie with different topping alternating slices.
Aspect:	Valve
Image:	

8_8	Hantzschia?
Type:	ArcPrA>30
Desc:	Cymbiform, ventral raphe, arcuate with protracted apex
Aspect:	Valve
Image:	

9_9	Aulacoseira [Cox 1996; ADIAC]
Type:	Aulaco
Desc:	centric diatom, mostly seen in girdle view, rectangular chains with jagged edges
Aspect:	Girdle
Image:	

10_10	Roicosphenia spp., Gomphonemeopsis spp. or Opephora spp.
Type:	Clavate?20
Desc:	Valve skittle shaped (heteropolar, isobilateral). AA ? 20
Aspect:	Valve
Image:	

11_11	Roicosphenia marina or abbreviata
Type:	Clavate>20
Desc:	Valve skittle shaped (heteropolar, isobilateral). AA > 20
Aspect:	Valve
Image:	

12_12	Cocconeis spp., Fallacia spp., or Diploneis spp.
Type:	Cocc>20
Desc:	linear, elliptical > 20
Aspect:	Valve
Image:	

13_13	Ctenophora [ADIAC; Cox 1996]
Type:	Cteno>200
Desc:	Linear, non-raphid >200, hyaline centre
Aspect:	Girdle
Image:	

14_14	Cylindrotheca closterium
Type:	CylClo
Desc:	Linear, raphes lateral but not always visible, apex extremely protracted with neck 1/3 of width of "body" and slightly inflated head. Two cup-shaped plastids lying lengthwise, transapically symmetrical (i.e. Clear area centre of transapical axis)
Aspect:	Valve
Image:	

15_15	Cylindrotheca gracilis
Type:	CylGrac
Desc:	Linear, raphes not visible but spiral striations visible. Apex is extremely protracted with neck 1/3 of width of "body" and slightly inflated head. Plastids are small round globules lying all along the cell.
Aspect:	Valve
Image:	

16_16	Amphora spp., Cymbella spp.
Type:	Cymb?20
Desc:	Cymbiform, ventral raphe, arcuate with protracted apex
Aspect:	Valve
Image:	

17_17	Amphora spp.
Type:	Cymb>20
Desc:	From the shape I thought this was a cymbiform cell in girdle view but the plastids don't tally with Cox group J (Amphora, Cymbella, Encyonema, Reimera), p55 fig.18 girdle views. The plastids look like Nitzschia, Cox Fig.31p, r & s (perminuta, communis & palea), and interestingly, these diagrams show no fibulae... This is a Amphora (from French diatom images).
Aspect:	Girdle
Image:	

18_18	Diatoma vulgare
Type:	Diavul
Desc:	NA
Aspect:	Valve
Image:	

19_19	Fallacia spp, Diploneis spp., or Lyrella spp.
Type:	DipLyr
Desc:	Fallacia, Diploneis, or Lyrella. Have lyre shaped hyaline area. Distinguishable from Cocconeis when dead by striae, when live by plasmids: these have 2 lying along sides of valve like Navicula, Cocconeis have single blob with invaginations.
Aspect:	Valve
Image:	

20_20	Fragilaria spp., Catenula spp.
Type:	Fragil
Desc:	Fragilariophyceae, Fragilaria (Eileen Cox p 20, Fig.9e) Or something colonial that forms long chains (Diadsmis), the greatest difficulty is distinguishing this from the ladder-like CB2 but I was working on the assumption that dead CB would not be visible (i.e there's no remnants once the cell is dead, unlike silica skeleton). Cox group C, Fig 12q but these are attached long-side instead of short side.
Aspect:	Girdle, colonial
Image:	

21_21	Gyrosigma accuminata
Type:	Gyracc
Desc:	NA
Aspect:	Valve
Image:	

22_22	Gyrosigma baltica
Type:	Gyrbal
Desc:	NA
Aspect:	Valve
Image:	

23_23	Gyrosigma fasciola
Type:	Gyrfas
Desc:	NA
Aspect:	Valve
Image:	

24_24	Gyrosigma wansbecki
Type:	Gyrwan
Desc:	NA
Aspect:	Valve
Image:	

25_25	Dickiea subinflata
Type:	LinBrApPr?20
Desc:	Valve isobilateral and isopolar, broadly linear with a rostrate protracted apex. AA ? 20
Aspect:	Valve
Image:	

26_26	Navicula starmachiodes
Type:	LinNaApPr?20
Desc:	Valve isobilateral and isopolar, narrowly linear with a rostrate protracted apex. AA ? 20
Aspect:	Valve
Image:	

27_27	?
Type:	LinApNPr?20
Desc:	Valve isobilateral and isopolar and narrowly linear with with a acute apex. AA ? 20
Aspect:	Valve
Image:	

28_28	?
Type:	LinApNPr?30
Desc:	Valve isobilateral and isopolar and narrowly linear with with a acute apex. 20 > AA ? 30
Aspect:	Valve
Image:	

29_29	?
Type:	LinApNPr>30
Desc:	Valve isobilateral and isopolar and narrowly linear with with a acute apex. AA > 30
Aspect:	Valve
Image:	

30_30	Melosira varians
Type:	Melol
Desc:	NA
Aspect:	Girdle
Image:	

31_31	Melosira spp.
Type:	Melo2
Desc:	Similar to Melo 1 but less girdle (shorter)
Aspect:	Girdle
Image:	

32_32	Melosira spp.
Type:	Melo3
Desc:	Similar to Melo 1 but convex valves
Aspect:	Girdle
Image:	

33_33	Navicula phyllepta (type II) or small Navicula gregaria.
Type:	NavApPr?20
Desc:	small gracile linear lanceolate cell with inflected apices, central raphe and (not usually visible) transverse striae. AA ? 20
Aspect:	Valve
Image:	

34_34	Navicula phyllepta (type II) or Navicula gregaria.
Type:	NavApPr?30
Desc:	small gracile linear lanceolate cell with inflected apices, central raphe and (not usually visible) transverse striae. 20 > AA ? 30
Aspect:	Valve
Image:	

35_35	Navicula phyllepta (type II) or Navicula gregaria.
Type:	NavApPr>30
Desc:	small gracile linear lanceolate cell with inflected apices, central raphe and (not usually visible) transverse striae. AA > 30
Aspect:	Valve
Image:	

36_36	Navicula phyllepta (type I)
Type:	NavApNPr?20
Desc:	small gracile linear lanceolate cell with acute apices, central raphe and (not usually visible) transverse striae. AA ? 20
Aspect:	Valve
Image:	

37_37	Navicula phyllepta (type I)?
Type:	NavApNPr?30
Desc:	small gracile linear lanceolate cell with acute apices, central raphe and (not usually visible) transverse striae. 20 > AA ? 30
Aspect:	Valve
Image:	

38_38	Navicula phyllepta (type I)?
Type:	NavApNPr>30
Desc:	small gracile linear lanceolate cell with acute apices, central raphe and (not usually visible) transverse striae. AA > 30
Aspect:	Valve
Image:	

39_39	?
Type:	NavBrApPr?20
Desc:	A thick Naviculoid with the apex rostrate. In some scribbles there is a slight neck (2/3 the body width), but i marked it as rostrate in T3.2 so this is probably just the way i drew it at the time.
Aspect:	Valve
Image:	

40_40	?
Type:	NavBrApPr?30
Desc:	A thick Naviculoid with the apex rostrate. In some scribbles there is a slight neck (2/3 the body width), but i marked it as rostrate in T3.2 so this is probably just the way i drew it at the time.
Aspect:	Valve
Image:	

41_41	Triblionella apiculata
Type:	Trybapic
Desc:	NA
Aspect:	Valve
Image:	

42_42	Nitzschia spp. or Hantzshia spp.
Type:	NitLinLan?30
Desc:	Linear or narrowly lanceolate Nitzschoid, apex inflected, protracted, plastids nitzschoid (Cox 1996). AA ? 30
Aspect:	Valve
Image:	

43_43	Nitzschia spp. or Hantzshia spp.
Type:	NitLinLan>30
Desc:	Linear or narrowly lanceolate Nitzschoid, apex inflected, protracted, plastids nitzschoid (Cox 1996). AA > 30
Aspect:	Valve
Image:	

44_44	Nitzschia sigma
Type:	Nitsig
Desc:	NA
Aspect:	Both
Image:	

45_45	Nitzschia spp.
Type:	NitApPrLong>30
Desc:	Linear, lanceolate with a protracted, extremely produced sub-capitate apex. Their are two plastids, sort of triangular, lying end to end, broad-ends in the centre. I did comment that it looked like dissipata on the dead section, when the raphe/fibulae is visible, suggesting that the raphe/fibulae is central, but dissipata doesn't have the extended apices.
Aspect:	Valve
Image:	

46_46	Paralia sulcata or Cyclotella meneghiana
Type:	Paralia
Desc:	NA
Aspect:	Valve
Image:	

47_47	Pleurosigma angulatum
Type:	Pleuro
Desc:	NA
Aspect:	Valve
Image:	

48_48	?
Type:	Rhombic?20
Desc:	Rhombic cell without protracted apex, acute, central raphe, striae not described. AA ? 20
Aspect:	Valve
Image:	

49_49	?
Type:	Rhombic?30
Desc:	Rhombic cell without protracted apex, acute, central raphe, striae not described. AA ? 30
Aspect:	Valve
Image:	

50_50	Roicosphenia spp.
Type:	Roicos
Desc:	NA
Aspect:	Girdle
Image:	

51_51	Stauroneis dubitabilis
Type:	Stauro
Desc:	I'm a bit puzzled bc you normally can't see the striae of the live cells under the light microscope, but I have live as well as dead Stauroneis so it must have been possible.
Aspect:	Valve
Image:	

52_52	Surirella brightwelli
Type:	Surbri
Desc:	NA
Aspect:	Valve
Image:	

53_53	Surirella brightwelli
Type:	Sursmi
Desc:	NA
Aspect:	Valve
Image:	

54_54	Tryblionella navicularis
Type:	Trynav
Desc:	NA
Aspect:	Valve
Image:	

55_55	?
Type:	unIDT7.2
Desc:	NA
Aspect:	Valve
Image:	

56_56	?
Type:	unIDT9.1
Desc:	NA
Aspect:	Valve
Image:	

57_57	?
Type:	unID12.2
Desc:	NA
Aspect:	Valve
Image:	

58_58	?
Type:	unIDbrLan-ArcApNPr>30
Desc:	Its basically like a Pleurosigma but instead of sigmoidal apices curve to the same side
Aspect:	Valve
Image:	

59_59	Euglenid
Type:	Euglenid
Desc:	NA
Aspect:	NA
Image:	

60_60	Nitzschia spp.
Type:	Nitgirdle?20,?60
Desc:	Nitzshiod cell in girdle view with nitzshiod plastids
Aspect:	Girdle
Image:	

61_61	Astrionella
Type:	Astrio
Desc:	colonial, snowflake morphology
Aspect:	Valve
Image:	

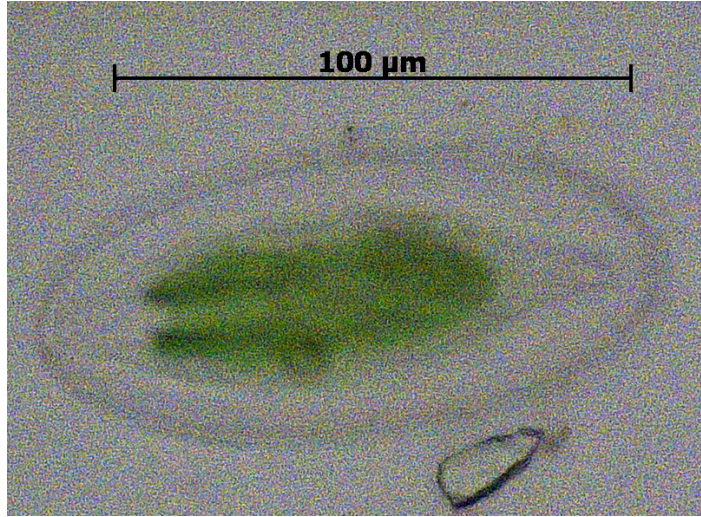
62_62	?
Type:	GirdRect<100
Desc:	Large rectangular cell in girdle view, large plastid
Aspect:	Girdle
Image:	

63_63	?
Type:	GirdCinchLgPlas
Desc:	Large rectangular cell in girdle view with cinched centre (probably raphid with node), large plastid
Aspect:	Girdle
Image:	

64_64	Nitzschia salinicola
Type:	Nitsal
Desc:	NA
Aspect:	Valve
Image:	

1_1	Oscillatora
Name:	CB_Oscil
Desc:	Oscillatora
Aspect:	na
Image:	LiveDead_images\E5r1tr1sl1\E5Lr1_CB3_10x.jpg
 A light micrograph showing a long, thin, green, curved filament of Oscillatora. A scale bar above the filament indicates 500 µm. The background is light pinkish-grey with some small dark spots.	

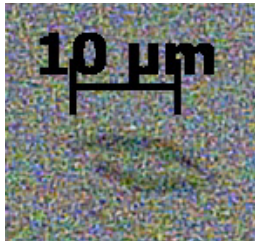
2_2	?
Name:	GirdleRect >40
Desc:	Girdle view, rectangular
Aspect:	Girdle
Image:	LiveDead_images\E5r1tr1sl1\E5Lr2_GirdleRect_40x.jpg
 A light micrograph showing a rectangular, green, girdle-like structure. A scale bar below the structure indicates 100 µm. The background is light pinkish-grey with some small dark spots.	


3_3	Surirella
Name:	ovoid >100
Desc:	large elliptic >100 μm ? Channels visible along the perimeter and lanceolate central area suggesting this is Surirella. Plastid lies in middle of cell against valve face, irregular edges
Aspect:	Valve
Image:	LiveDead_images\E5r1tr1sl1\E5Lr3-2_Suril_40x.jpg
	

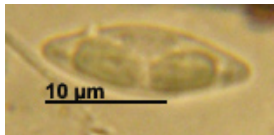
4_4	Navicula digitatoradiata
Name:	LinLanApBrR>50
Desc:	valve view, linear, linear-lanceolate, apex broadly rounded? Navicula digitatoradiata?
Aspect:	Valve
Image:	LiveDead_images\E5r1tr1sl1\E5Lr4_40x.jpg
	

5_5	Melosira varians
Name:	Melosira1
Desc:	Girdle view, colonial, chain, both valves convex
Aspect:	Girdle
Image:	LiveDead_images\E5r1tr1sl1\E5Lr4&5_20x.jpg
	

6_6	Gyrosigma fasciola
Name:	Gfasc
Desc:	NA
Aspect:	Valve
Image:	LiveDead_images\E5r1sl1\E5Lr6_GyrFasc_x63.jpg
	

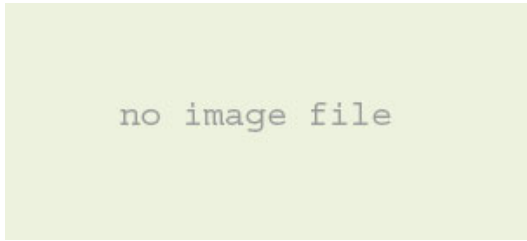
7_7	Navicula phyllepta (I)
Name:	NavApAc <20
Desc:	Naviculoid, ie linear-lanceolate with acute apices and pale striae <20µm. Assumed to be N.phyllepta but there are three types of plastids for the same cell shape.
Aspect:	Valve
Image:	LiveDead_images\E5r1tr1sl1\E5Lr7_40x_cropped.jpg
	

7_8	Navicula phyllepta (I)
Name:	NavApAc <20
Desc:	Naviculoid, ie linear-lanceolate with acute apices and pale striae <20µm. Both have plastids lying against the girdle on both sides. Type 1 is the one with even plastids and Type 2 has Z shaped plastids.
Aspect:	Valve
Image:	LiveDead_images\E5r1tr1sl1\E5Lr7-1&2_NavAPAc_63x.jpg
	

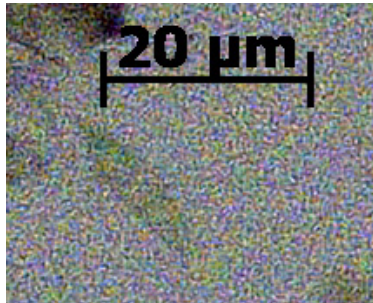
7_9	Nitzschia spp.
Name:	NavApAc <20
Desc:	Naviculoid, ie linear-lanceolate with acute apices <20µm. Plastids are in a more Nitzschoid formation, lying more to one side.
Aspect:	Valve
Image:	LiveDead_images\E5r1tr1sl1\E5Lr7-3_NavApPr_63x.jpg
	

8_10	Navicula gregaria
Name:	NavApPr>20
Desc:	Naviculoid, ie linear-lanceolate, apex protracted rostrate, with pale striae, probably N.gregaria
Aspect:	Valve
Image:	LiveDead_images\E5r1tr1sl1\E5Lr8_40x.jpg
	

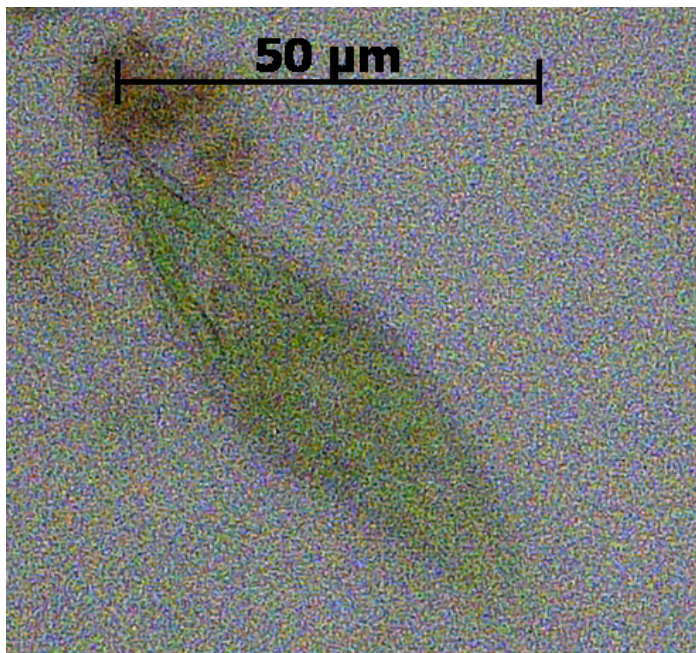
8_11	Navicula gregaria
Name:	NavApPr>20
Desc:	Naviculoid, ie linear-lanceolate, apex protracted rostrate, with pale striae, probably N.gregaria
Aspect:	Valve
Image:	LiveDead_Images\noimage.jpg
	

9_12	?
Name:	Girdle_rect <40
Desc:	Not sure about this, this one is very slight convex and one large plastid is against the girdle covering 3/4 of AA (E5Lr9_Girdle2_40x.jpg -> add this to r15, most of the ones in this group were as Gr 2, AA:TA 3:1, with striae just visible along edges but the marginal striae are very shallow 1/10 PA. This one was IDed at x40 which is not enough magnification for something this small but as the r15 was created on the same slide, I'm pretty sure that most of the ones that looked like this were put into r15).
Aspect:	Girdle
Image:	LiveDead_Images\noimage.jpg
	

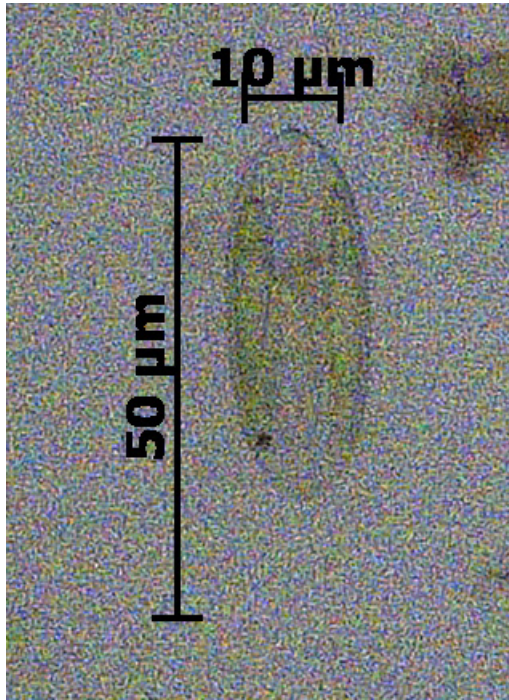
10_13	Stauroneis?
Name:	NitzApPr<20
Desc:	Cell linear lanceolate apex protracted, plastids Nitzschoid, ie 2 plastids lying against valve face towards the two poles creating a clear transverse gap at the centre.
Aspect:	Valve
Image:	LiveDead_images\E5r1tr1sl1\E5Lr10_40x_cropped.jpg



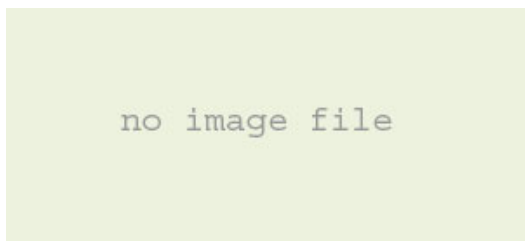
11_14	?
Name:	RhomSigm >50
Desc:	Cells rhombic-sigmoid apex acutely rounded >100 μm. Chloroplast takes up the entire valve face apart from narrow margin.
Aspect:	Valve
Image:	LiveDead_images\E5r1tr1sl1\E5Lr11_40x.jpg



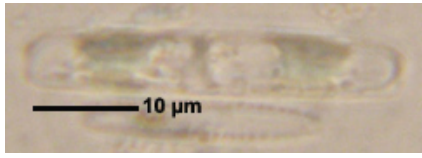
12_15	Amphora sp.
Name:	GirdEllip<50
Desc:	Frustules elliptical. Initially presumed valve view as the apex is obtusely pointed rather than blunt, >50 x 10 µm. Striae transverse (?) and an H-shaped plastid, 2 plastid lying against the valve connected by a bridge lying against the girdle. Then (E5r3sl3) found two specimens attached to sand particle I'm sure are Amphora in girdle view as I can see the striae, raphe and hyaline, rectangular central area on both sides . Its possible i've confounded two or more types, one elliptic in valve view one elliptic in girdle view but more likely that I misinterpreted the first ones. Type 2: only found in E5r1tr2sl3 (E5r12typeII_lgEllipGirdl_x63.jpg) and looks to be girdle view, cymbiform, araphid (no sternum), possibly Campylosira, see Hendey & Witk.
Aspect:	Girdle
Image:	LiveDead_images\E5r1tr1sl1\E5Lr12_40x_2.jpg



13_16	?
Name:	BrLanApPr<15
Desc:	Cells in valve view, linear, broadly lanceolate, apex protracted sub- or rostrate
Aspect:	Valve
Image:	LiveDead_Images\noimage.jpg

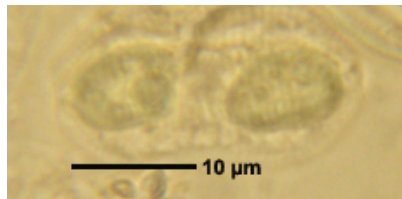


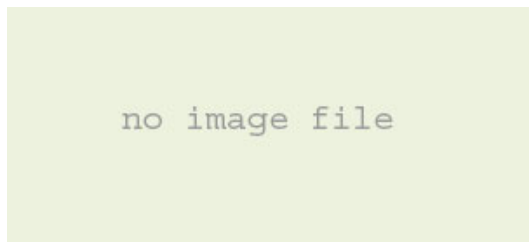
14_17	Nitzschia spp.
Name:	Nitzschiod
Desc:	not adequately visible to describe....not even sure if its girdle or valve view, 2 cup-shaped plastids lying against the poles suggesting Nitzschia, Hantzschia, Tryblionella.
Aspect:	Girdle
Image:	LiveDead_images\E5r1tr1s11\E5Lr14_blob_40x.jpg
	


15_18	?
Name:	GirdNarRect
Desc:	Type 1: Girdle view, narrowly rectangular, AA:PA > 5:1, with slightly rounded apices. Appearance of divider in the middle, so might be 2 cells? 2 plastids, one approximately in the centre of each half, spanning the PA, with concave sides; . If this is a colony rather than a single cell they are attached end to end. However it is unlikely because if it were a colony it would be found in multiples of more than 2, so i think this is a solitary cell and that the 'divider' in the centre is something structural within the cell. Dave agrees and thinks that it would be relatively narrow TA valve and probably lanceolate (just bc most are) but he reckons that the plastid lies against the valve and wraps around to the girdle but I cannot find a genus with this plastid shape-position (maybe same as E5Lr22_NavApPr?). Type 2: Girdle view narrowly rectangular, AA:PA = 5:1, slightly rounded apices. Striae just visible along the edge. One Plastid approximately in the centre spanning PA width with concave sides, this should probably be a different group if I go with the notion that type 1 is neither colonial nor a dividing cell.
Aspect:	Girdle
Image:	LiveDead_images\E5r1tr1s11\E5Lr15_GirdNarRect_63x.jpg
	

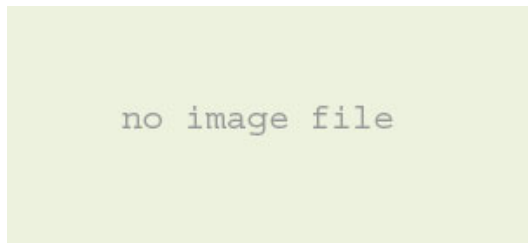
16_19	Nitzschia spp.
Name:	NitzApPr>20
Desc:	Linear, narrowly lanceolate, apex protracted, 5020. Plasmids nitzschiod.
Aspect:	Valve
Image:	LiveDead_Images\noimage.jpg
	


17_20	Roicosphenia
Name:	ClavCurv
Desc:	Clavate, curved, horn-shaped
Aspect:	Girdle
Image:	LiveDead_Images\noimage.jpg
	

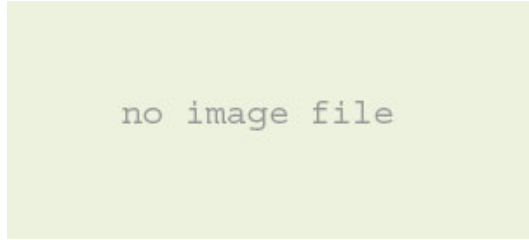
18_21	Surirella brightwelli or Tryblionella coarctica
Name:	EllipConstrApPr
Desc:	Elliptic with constriction in the centre and protracted apices <50.
Aspect:	Valve
Image:	LiveDead_images\E5r1tr1sl2\E5r18_EllipConstr_x63.jpg
	

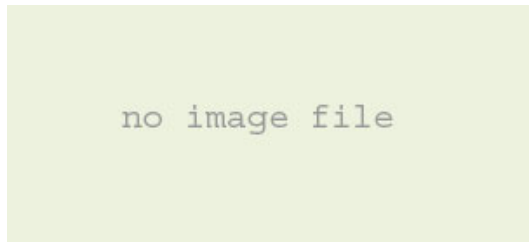
19_22	Pleurosigma angulatum
Name:	PleuroIg
Desc:	Large Pleurosigma (able to see oblique striae). Lanceolate, sigmoid. Plasmid covers the whole face 100
Aspect:	Valve
Image:	LiveDead_Images\noimage.jpg
	

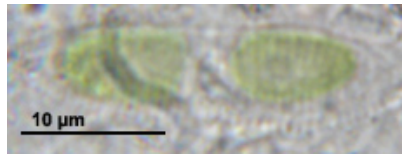
20_23	Achnanthes delicatula
Name:	P.delic
Desc:	Planothidium delicatulum shape: Broadly lanceolate, protracted, rostrate or sub-rostrate apices. Striae quite visible.
Aspect:	Valve
Image:	LiveDead_images\E5r3sl1\E5Lr20-2_Pdelic_x63.jpg
	

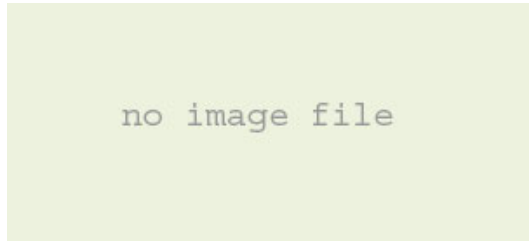
21_24	Achnanthes lanceolata or delicatula
Name:	P.lanceo
Desc:	Planothidium lanceolatum shape: Broadly lanceolate, blunt apices. Striae visible.
Aspect:	Valve
Image:	LiveDead_Images\noimage.jpg
	

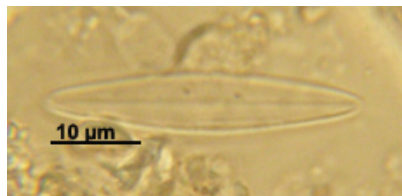
22_25	Navicula phyllepta (II) or small Navicula gregaria
Name:	NavApPr<20
Desc:	Naviculoid (linear, lanceolate) with protracted apex, < 20 µm
Aspect:	Valve
Image:	LiveDead_images\E5r1tr1sl1\E5Lr22_NavApPr_63x.jpg
	

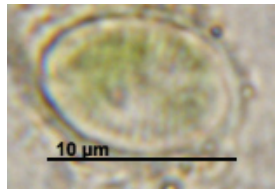
23_26	Navicula lanceolata.
Name:	Nlanceo
Desc:	Valve view, linear, linear or narrowly lanceolate, apex is rounded or very slightly rostrate, AA = 36.
Aspect:	Valve
Image:	LiveDead_Images\noimage.jpg
	

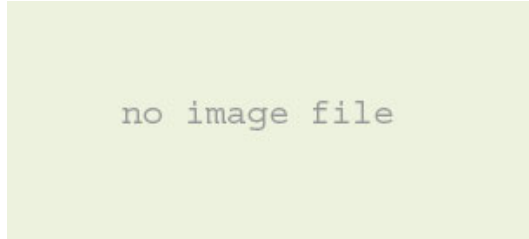
24_27	Cocconeis spp. or Achnanthes spp. or Navicula viminoides
Name:	BrEllipApAc<20
Desc:	broadly elliptical, apex obtusely pointed, < 20 µm, probably Cocconeis
Aspect:	Valve
Image:	LiveDead_Images\noimage.jpg
	

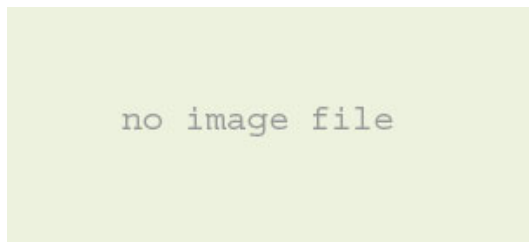
25_28	Tryblionella apiculata
Name:	TrybApic
Desc:	Linear, lin-elliptical, short apiculate apices, > 20 µm, striae clearly visible transverse.
Aspect:	Valve
Image:	LiveDead_images\E5r3sl2\E5Lr25_TrybApic_x63.jpg
	

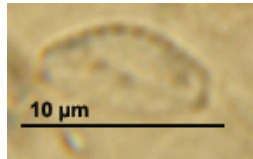
26_29	Plagiotropis sp.
Name:	Plagiotropis
Desc:	Large cell ~50, smooth margin on one side, other side indistinct edge.
Aspect:	Valve
Image:	LiveDead_Images\noimage.jpg
	

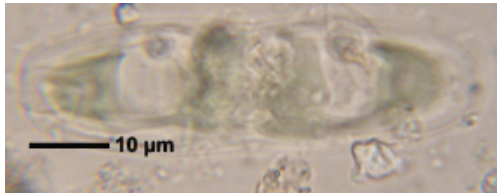
27_30	Navicula vandammi, N. duerrenbergiana
Name:	NavApAc>20
Desc:	Cells in valve view, linear, narrowly lanceolate, apex acute, >20 μm (4-5:1). Plastids lying against girdle on both sides, slightly off centre.
Aspect:	Valve
Image:	LiveDead_images\E5r1tr1s11\E5Lr27_NarLanApAc_63x.jpg
	


28_31	Cocconeis spp. or Achnanthes spp. or Fallacia spp.
Name:	BrEllipApBr<20
Desc:	Broadly elliptical, with broadly rounded apex < 20 μm , probably Cocconeis or Planothidium. Raphe? Striae?
Aspect:	Valve
Image:	LiveDead_images\E5r3s13\E5Lr28_EllApBr_x63.jpg
	


29_32	Nitzschia sigma
Name:	NitzSigma ~100
Desc:	Cells lie in valve view, fibulae visible on both sides, linear-sigmoid shape, apex acute, > 30 μ m
Aspect:	Valve
Image:	LiveDead_Images\noimage.jpg
	

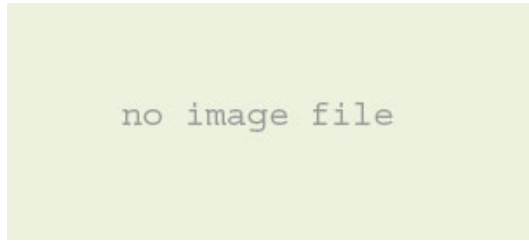
30_33	Gomphonema spp. or Opephora spp.
Name:	ClavNoCurve<20
Desc:	Cells lie in valve and girdle view, wedge shaped in girdle view, in valve view head and foot poles both broadly rounded the former wider than the latter, can see curve of other valve above the foot (?).
Aspect:	Valve
Image:	LiveDead_Images\noimage.jpg
	

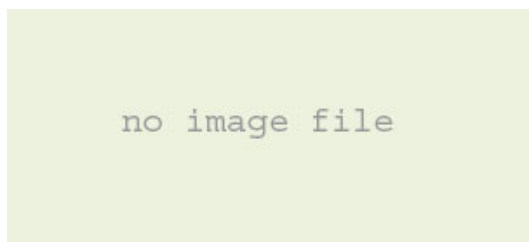
31_34	?
Name:	GirdwStr<15
Desc:	Girdle view, small (<15) various types. I've lumped together the ones where one valve is convex (possibly planothidium?) with the ones that are both flat (ie box) with striae quite dark and distinct (Opephora, see Round et al p382) and ones that are slight wedge-shaped.
Aspect:	Girdle
Image:	LiveDead_images\E5r1tr1sl2\E5r31_PlanoGirdl_x63.jpg
	

32_35	Donkinia [french diatom website]
Name:	GirdLanConstr
Desc:	Girdle view, elliptic with depression in the centre (of valve). The valve margins appear narrow, striae not visible, the cingulum approximately twice the width. The plastids are irregularly shaped mostly "nitzschioid", lying against the poles, but have extension along one valve face and then expanding again towards the centre.
Aspect:	Girdle
Image:	LiveDead_images\E5r1tr1sl1\E5Lr32_Girdle4_63x.jpg
	

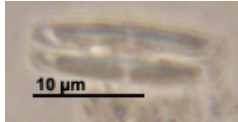
33_36	Amphora sp.
Name:	Cymb1
Desc:	Cell in valve view, cymbiform, Amphora? (36 x 12)
Aspect:	Valve
Image:	LiveDead_images\E5r1tr1sl1\E5Lr33_Cymbi1_63x.jpg
	

34_37	Catenula adhaerens
Name:	ColDial
Desc:	Looks like a green ladder. Cell width <10 µm, chain length variable (image ~120 µm). In E2 had this down as a cyanobacteria, but I now doubt it is one, seems to have too much solid structure, more likely to be small diatom chain, though haven't been able to find an ID for either
Aspect:	Girdle
Image:	LiveDead_images\E5r1tr1sl1\E5Lr34_ColDial_63x.jpg
	

35_38	Amphora spp.
Name:	Cymb2
Desc:	valve view, Cell cymbiform, ventral edge straight, dorsal curve, apices protracted, rostrate and bent to the dorsal side. Small (didn't measure) TA:AA = ~3
Aspect:	Valve
Image:	LiveDead_Images\noimage.jpg
	

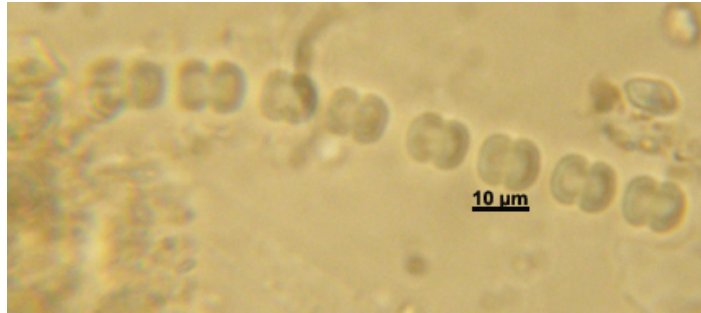
36_39	Cylindrotheca closterium
Name:	Cylclos
Desc:	valve narrowly lanceolate with very drawn out narrow apices, deflected to opposite or same side, plastids nitzschiod
Aspect:	Valve
Image:	LiveDead_Images\noimage.jpg
	

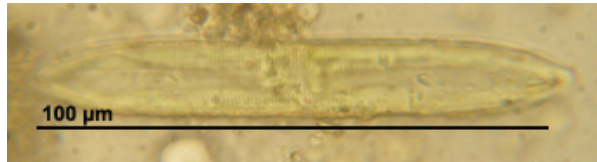
37_40	Amphora spp.
Name:	GirdEllipApBl
Desc:	Large cell in girdle view, elliptic with blunt ends, plastids lying against girdle
Aspect:	Girdle
Image:	LiveDead_images\E5r1tr1sl1\E5Lr37_girdle5_63x.jpg
	

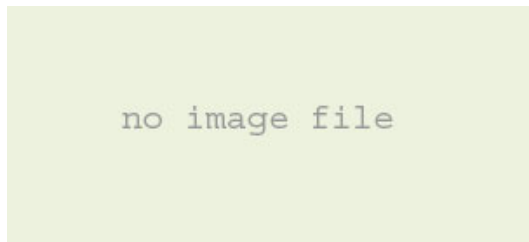
38_41	Nitzschia spp.
Name:	GirdNitz
Desc:	Presumably a Nitzschia in girdle view as plastids are Nitzshoid and to the one side of the . Species with a broad cingulum (AA:PA = 2.6 - 2.8)
Aspect:	Girdle
Image:	LiveDead_images\E5r1tr1sl1\E5Lr38_NitzGird_63x.jpg
	


39_42	Placoneis clementis
Name:	BrLanApr>20
Desc:	Valve view. Looks like Placoneis, striae just visible
Aspect:	valve
Image:	LiveDead_Images\noimage.jpg
	

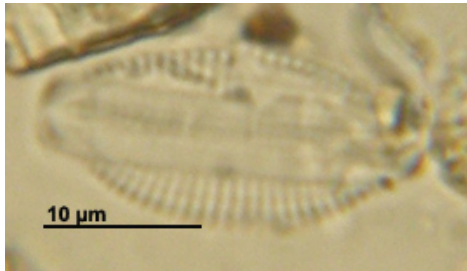
40_43	Cyclotella meneghiana
Name:	Centric1
Desc:	valve view. Centric with detail around the outer circumference
Aspect:	valve
Image:	LiveDead_images\E5r1tr1sl2\E5r40_centric1_x63.jpg
	

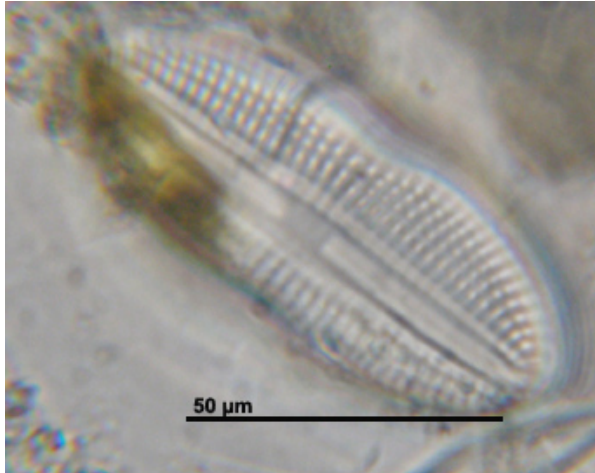
41_44	Merismopedia spp.
Name:	CB1chain
Desc:	Cyanobacteria, looks like Merismopedia, in chain, indiv cells about 4-5 μm
Aspect:	na
Image:	LiveDead_images\E5r1tr1sl2\E5r41_CB1chain_x63.jpg
	

42_45	Tryblionella apiculata
Name:	LinEllApPrLg
Desc:	Valve view. Linear, elliptic rectangle with protracted, short cuneate apex, dense transverse striae just visible, seems wide central area. Plastids: 2 or 4 lying along the margins (possibly pressed against the girdle?), hard to tell if each side is continuous or whether there is a break in them, more likely continuous.
Aspect:	valve
Image:	LiveDead_images\E5r1tr1sl2\E5r42_LinEllApPr_63x.jpg
	

43_46	Navicula starmachiodes
Name:	LinApAc<20
Desc:	Presumably valve view, narrow linear with a acute apex
Aspect:	valve
Image:	LiveDead_Images\noimage.jpg
	

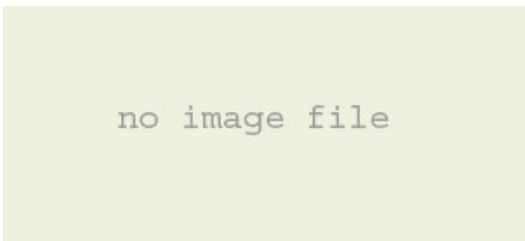
44_47	?
Name:	LinLanApRos<50
Desc:	Narrowly lanceolate to linear with rostrate apex that are 4/5 TA width. Plastids lie against the margins opposite off-centre of each other. Type specimen AA~30.
Aspect:	valve
Image:	LiveDead_images\E5r1tr1sl3\E5r44_LinLanApRos_x63.jpg
	

45_48	Amphora ?
Name:	Amph2Girdl
Desc:	Amphora girdle view. Type specimen AA = 24.
Aspect:	Girdle
Image:	LiveDead_images\E5r1tr1sl3\E5r45_AmphGirdle_x63.jpg
	

46_49	Diploneis sp.1
Name:	DiplLg
Desc:	Large Diploneis, linear, elliptic with constricted centre, broadly rounded apex. Raphe distant, sternum linear, striae interrupted ~ 8 in 10 µm.
Aspect:	valve
Image:	LiveDead_images\E5r1tr1sl3\E5r46_DiploLg_x63.jpg
	


47_50	?
Name:	GirdOblConstrThStr
Desc:	Girdle view, the girdle band is approximately the depth of the valve. Margins deep and coarsely striated. Plastids sit as 2 round "port holes" against the girdle, seem to small for such a large cell, > 50 μ
Aspect:	Girdle
Image:	LiveDead_images\E5r1tr2s11\E5Lr47_GirdOblStr_x63.jpg
	

48_51	Thallasiosira sp.1
Name:	Centric2
Desc:	Centric diatom of the Thallasiosira type, ie the entire cell is covered in aereolae
Aspect:	valve
Image:	LiveDead_Images\noimage.jpg
	

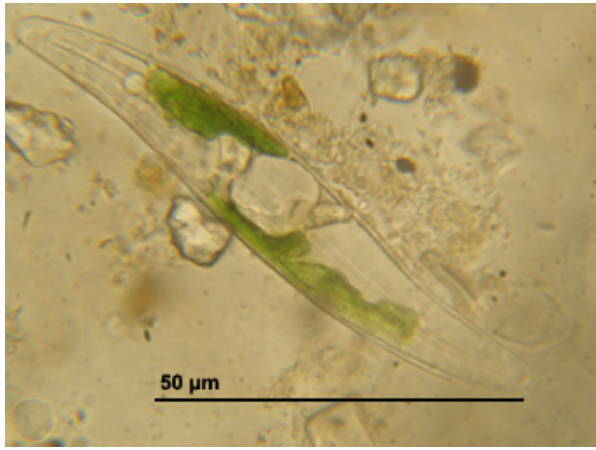
49_52	Gyrosigma balticum
Name:	G. balticum
Desc:	Valve view, very large G. Balticum, ~500 μ m, linear, sigmoidal with cuneate apices
Aspect:	valve
Image:	LiveDead_Images\noimage.jpg
	

50_53	?
Name:	Unkown
Desc:	Can't figure out if this is a diatom or something else. Its like a flat disc with a twist in it. If it is a diatom I reckon its something centric but it could be a Euglenid
Aspect:	na
Image:	LiveDead_images\E5r1tr2sl2\E5Lr50_unknown_x63.jpg
	

51_54	Cyanobacteria?
Name:	CB3
Desc:	Cyanobacteria, colony of mostly circular to oval but irregularly shaped cells, entirely full of plastid and no other distinguishing features
Aspect:	na
Image:	LiveDead_images\E5r1tr2sl3\E5Lr50_CB3_x63.jpg
	

52_55	Navicula eidrigina or Navicula digitatoradiata
Name:	BrLanApAc
Desc:	Valve view, broadly lanceolate apex acute, > 30 µm
Aspect:	valve
Image:	LiveDead_images\E5r3sl1\E5Lr52_BrLanApAc_x63.jpg
	

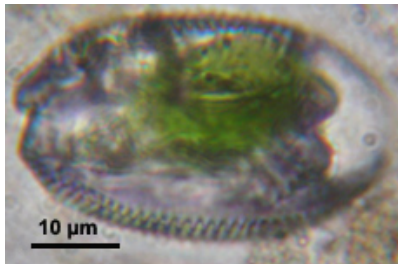
53_56	Melosira sp. 2
Name:	Melosira2
Desc:	Melosira, more rectangular
Aspect:	
Image:	LiveDead_images\E5r3sl1\E5Lr53_Melo2_x63.jpg
	

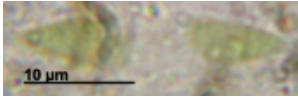
54_57	Pleurosigma angulatum (lanceolate morphotype)
Name:	Gyrosigma
Desc:	Lanceolate and large with large plastid
Aspect:	
Image:	LiveDead_images\E5r3sl1\E5Lr54_Gyro_x63.jpg
	

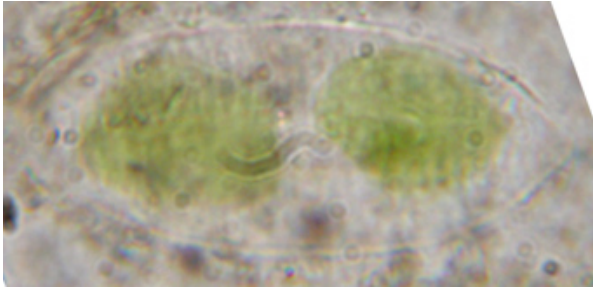
55_58	?
Name:	LinEllipConstrApBr
Desc:	Not sure if its valve or girdle view, looks like it could have costae along the edges and hint of a raphe in centre surrounded by hyaline area. Could be a Surrirella or something in girdle view and the 'raphe' is edge of girdle band. Need to see more.
Aspect:	?
Image:	LiveDead_images\E5r3sl1\E5Lr55_LinEllipConstrApBr_x63.jpg
	

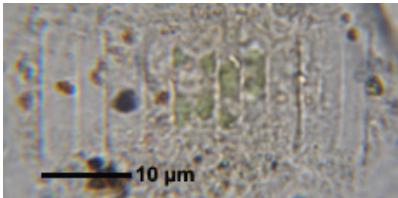
56_60	Diatoma?
Name:	LanApAc?40
Desc:	Valve view, valve lanceolate with acutely rounded apices. Striae visible, cross the valve face, no raphe or pseudoraphe. Looks like a Diatoma but without the midline.
Aspect:	valve
Image:	LiveDead_images\E5r3sl1\E5Lr72_Diatoma_x63.jpg
	

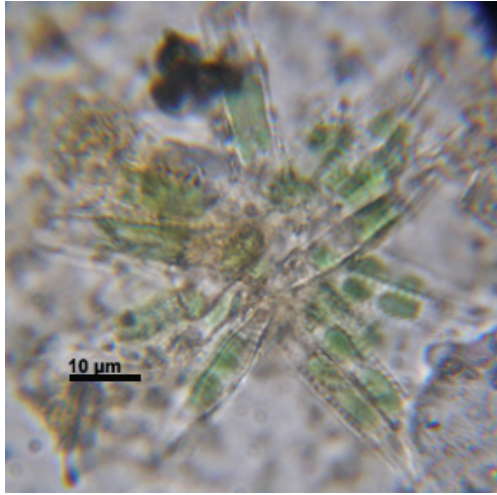
57_59	?
Name:	GirdleClav
Desc:	Girdle view I think (unlikely to be araphid due to blunt apices), striae quite thick and dark and clearly becoming narrower at the 'foot' end. The second one I think is probably different, it is more wedge-shaped and the striae don't seem as . But they aren't distinctive enough to put them in separate categories. 2nd one has 9 striae/10 μm.
Aspect:	Girdle
Image:	LiveDead_images\E5r3sl1\E5Lr57_GirdClav_x63.jpg
	

58_62	?
Name:	GirdBrEllipStr
Desc:	Frustule in girdle view elliptical. Striae do not appear to extend the length of the valve margin and are alveolar and punctated, 8 - 10 in 10 μm. Cingulum broad.
Aspect:	Girdle
Image:	LiveDead_images\E5r3sl1\E5Lr58_GirdEllipStrAlv_x63.jpg
	

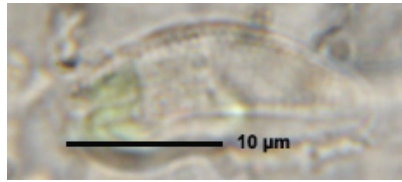
59_63	Nitzschia spp.
Name:	NitzApAc
Desc:	Frustule in valve view, striae or more likely fibulae just visible along the margins (I noted both margins so probably Nitzschia). Plastids lying against valve-face at poles.
Aspect:	Valve
Image:	LiveDead_images\E5r3sl1\E5Lr59_NitzApAc_x63.jpg
	

60_64	Tryblionella navicularis or gracilis
Name:	BrLanApAc
Desc:	Frustule lying in valve view. Valve shape lanceolate, quite broad, apex acute or perhaps very short apiculate. Striae faintly visible, transverse & parallel. Two plastids, approximately round, one towards each pole. Likely Tryblionella, maybe gracilis.
Aspect:	Valve
Image:	LiveDead_images\E5r3sl1\E5LrNS_BrLanTrybl_x63.jpg
	

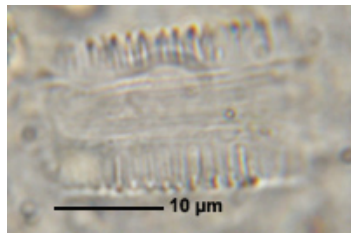
61_65	Catenula adhaerens
Name:	GirdNarRectCol
Desc:	Colonial Diatoms, narrowly rectangular in girdle view, attached by valve face, striae only just visible, not countable. Plastids against girdle irregularly shaped but span the frustule. It may be same as r15 but AA:PA > 4:1 and attachment different if r15 is head to head and plastids regular, maybe same as r9, its plastids seem smaller, r9 like r2? So all in all more likely to confound dead cells and non-colonial than live or colonial ones.
Aspect:	Valve
Image:	LiveDead_images\E5r3sl2\E5Lr61_GirdNarRectCol_x63.jpg
	

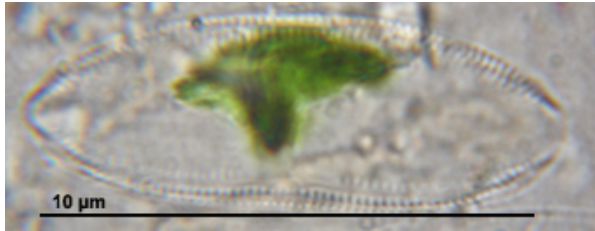
62_66	?
Name:	GirdNarRectStr
Desc:	Frustules narrowly rectangular in girdle view, with striae clearly visible, $\sim 7 \pm 1$ in $10 \mu\text{m}$, perhaps with gap in centre. Some appear to be lying in valve view and look araphid with sternum; appear linear with tapered rounded apices in valve view with pseudoraphe (see oblique at 6 o'clock), and gap in striae. Colonial Diatoms, seem to be attached by stalk rather than valve face and most have two irregularly shaped plastids lying against the girdle. Perhaps there are more than two species here as some have one large plastid (they may be same as r15).
Aspect:	Girdle
Image:	LiveDead_images\E5r3sl2\E5Lr62_GirdNarRectStr_x63.jpg
	


63_67	Amphora spp.
Name:	CymbLunRCen
Desc:	Valve view, Cymbiform, lunate, with rounded apices, raphe central. For some reason I didn't photograph, probably couldn't get clear focus on one plane. Small
Aspect:	valve
Image:	LiveDead_Images\noimage.jpg
	


64_68	Cymbella spp.
Name:	CymbiLun
Desc:	Valve view, probably a frustule as it seems to have several focal depths, like an orange wedge (so definitely not Amphora as I think their valves are joined at ventral edge. Cymbiform, lunate, raphe ventral or none? Around 20 μm . Not sure it isn't the same as r63 but the raphe here is definitely not central.
Aspect:	Valve
Image:	LiveDead_images\E5r3sl3\E5Lr64_CymbLun_x63.jpg
	

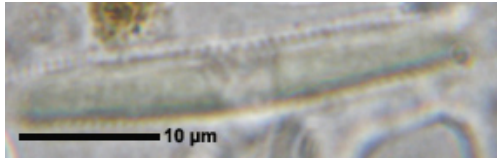
65_69	Surirella brebissoni
Name:	OvoidSuri<50
Desc:	Surirella, ovoid, valve view ? 50. couldn't get good focus on it.
Aspect:	Valve
Image:	LiveDead_Images\noimage.jpg
	


66_71	?
Name:	GirdSquCost
Desc:	Girdle view of frustule, square, the cingulum the width of two valve depths. The valve margins have costae or fibulae (same side). Small ~24 μm .
Aspect:	Girdle
Image:	LiveDead_images\E5r3sl3\E5Lr66_Gird_x63.jpg
	

67_72	?
Name:	Amph2Girdl
Desc:	I think the reason i got confused is that it looks raphid in one focal plane and araphid in the other, think the other is the much broader dorsal margin
Aspect:	Girdle
Image:	LiveDead_images\E5r3sl3\E5Lr67_GirdAmph3_x63.jpg
	

68_73	Opephora spp. or Fragilaria spp.
Name:	RhomSmApAcR
Desc:	Frustule in valve view, Rhombic Apices bluntly rounded. Striae thick & dark, 8 in 10 μm, and alternate on opposite sides, pseudoraphe. I think this is probably on Opephora or Fragilaria.
Aspect:	Valve
Image:	LiveDead_images\E5r3sl3\E5Lr68_RhomSmApBl_x63.jpg
	

69_74	?
Name:	MucSheath?
Desc:	Frustule perhaps in valve view and lanceolate in shape but is surrounded by a rectangular mucilage sheath. I'm not sure i've always had these and lumped them into rl5type1 or whether this is the first instance.
Aspect:	Valve
Image:	LiveDead_images\E5r1sl1\E5Lr69_unsure_x63.jpg
	

70_75	?
Name:	RectGirdBent
Desc:	Girdle view of valve rectangular but slightly bent in the centre. Approximately 14 ± 2 striae in 10 μm .
Aspect:	Girdle
Image:	LiveDead_images\E5r1sl2\E5lr70_GirdRectBent_x63.jpg
	

71_76	Nitzschia recta
Name:	NitzLg
Desc:	Very lg Nitzschia probably valve view, narrowly linear attenuating to protracted apices possibly sub-capitate. Fibulae visible, but not countable, on one side.
Aspect:	Valve
Image:	LiveDead_images\E5r1sl2\E5lr71_NitzLg_x63.jpg
	

72_70	Diatoma vulgare
Name:	DiatVulg
Desc:	NA
Aspect:	
Image:	LiveDead_images\noimage.jpg
	

73_61	Diatoma?
Name:	ClavApBrR
Desc:	Valve view, valve club-shaped with broadly rounded apices. Striae visible, cross the valve face, no raphe or pseudoraphe. Looks like a Diatoma, hint of a midline.
Aspect:	Valve
Image:	LiveDead_images\E5r3sl1\E5Lr73_ClavDiatoma_x63.jpg
